

Vivek K. Patel · Vimal J. Savsani ·  
Mohamed A. Tawhid

# Thermal System Optimization

A Population-Based Metaheuristic  
Approach



Springer

# Thermal System Optimization

Vivek K. Patel · Vimal J. Savsani ·  
Mohamed A. Tawhid

# Thermal System Optimization

A Population-Based Metaheuristic Approach



Springer

Vivek K. Patel  
Department of Mechanical Engineering,  
School of Technology  
Pandit Deendayal Petroleum University  
Raisan, Gandhinagar, Gujarat, India

Vimal J. Savsani  
Department of Mechanical Engineering  
Pandit Deendayal Petroleum University  
Raisan, Gandhinagar, Gujarat, India

Mohamed A. Tawhid  
Department of Mathematics and Statistics  
Thompson Rivers University  
Kamloops, BC, Canada

ISBN 978-3-030-10476-4      ISBN 978-3-030-10477-1 (eBook)  
<https://doi.org/10.1007/978-3-030-10477-1>

Library of Congress Control Number: 2018965429

MATLAB® is a registered trademark of The MathWorks, Inc., 1 Apple Hill Drive, Natick, MA 01760-2098, USA, <http://www.mathworks.com>.

© Springer Nature Switzerland AG 2019

This work is subject to copyright. All rights are reserved by the Publisher, whether the whole or part of the material is concerned, specifically the rights of translation, reprinting, reuse of illustrations, recitation, broadcasting, reproduction on microfilms or in any other physical way, and transmission or information storage and retrieval, electronic adaptation, computer software, or by similar or dissimilar methodology now known or hereafter developed.

The use of general descriptive names, registered names, trademarks, service marks, etc. in this publication does not imply, even in the absence of a specific statement, that such names are exempt from the relevant protective laws and regulations and therefore free for general use.

The publisher, the authors and the editors are safe to assume that the advice and information in this book are believed to be true and accurate at the date of publication. Neither the publisher nor the authors or the editors give a warranty, express or implied, with respect to the material contained herein or for any errors or omissions that may have been made. The publisher remains neutral with regard to jurisdictional claims in published maps and institutional affiliations.

This Springer imprint is published by the registered company Springer Nature Switzerland AG  
The registered company address is: Gewerbestrasse 11, 6330 Cham, Switzerland

*Dedicated to almighty God*

# Preface

Any system which converts the thermal energy into mechanical energy or any other forms of energy is known as a thermal system. Modeling of a thermal system always required the integrated knowledge of thermodynamics, heat transfer, fluid dynamics, and cost evaluation. The effective modeling of thermal systems includes an optimization process in which designers always consider certain objectives such as heat transfer, effectiveness, cooling capacity, pressure drop, etc. depending on the requirements. While achieving the objectives mentioned above, it is also desirable to minimize the total cost of the system. Further, the design optimization of a complete thermal system assembly leads to a large number of design variables and constraints. The conventional methods of thermal system design optimization apply an iterative procedure. Typically, the use of this approach results in oversize equipment and complicated design procedure. On the other hand, the application of population-based metaheuristic algorithms makes the design-optimization process of thermal systems simplified and accurate. Thus, the applications of such algorithms for the optimization of thermal systems attract the attention of researchers.

In this book, 36 different thermal systems which include different types of heat exchangers, heat engines, heat pumps, power cycles, refrigerating systems, and few other solar energy-based systems are considered for the modeling and optimization. All the 36 thermal systems are very important systems as far as real-life application and usefulness are concerned. A detailed thermal modeling of each system is presented step by step. The important objective function of each thermal system is derived precisely. Further, the associated design variables and constraints involved in the design of each of the thermal system are explained carefully.

The population-based metaheuristic algorithms simulate different natural phenomena (because the phenomenon takes place in nature is always optimized). Based on the natural phenomenon simulated by metaheuristic algorithms, it may be considered as evolutionary algorithms or swarm intelligence-based algorithms. This book covers 11 metaheuristic algorithms. These algorithms consist of very well-known and well-established techniques such as genetic algorithm (GA),

particle swarm optimization (PSO), and differential evolution (DE). There are some algorithms which are developed in the last decade and have shown their effectiveness on several engineering applications. These algorithms are artificial bee colony (ABC), cuckoo search algorithm (CSA), and teaching–learning-based optimization (TLBO). The rest of the algorithms are recently developed ones and yet not addressed to solve thermal system design problems. These algorithms include symbiotic organism search (SOS), water wave optimization (WWO), heat transfer search (HTS), passing vehicle search (PVS), and sine cosine algorithm (SCA). Further, the tuning of the control parameters of each algorithm is carried out before implementing for the optimization of thermal systems. As of today, the applications of all these metaheuristic methods are found in almost all the fields of engineering and science. A large number of publications based on the application of these metaheuristic algorithms are found in the various international journals published by the reputed publishers like Springer, Elsevier, IEEE, ASME, and Taylor and Francis.

This book provides a detailed understanding of thermal modeling, metaheuristic algorithms, and implementation of these algorithms to optimize various thermal systems. In particular, this book covers 11 metaheuristic algorithms and 36 thermal systems. Each algorithm implemented for the optimization of the all the 36 thermal systems is considered in this book. The search characteristic of each metaheuristic algorithm is different from each other (as it simulates different natural phenomena). Hence, the performance of each algorithm is varied based on the class of problems on which it was implemented. So, a detailed performance comparison of all algorithms for the optimization of each thermal system is also provided. Statistical analysis of the results is also included in this book to provide a ranking of the various metaheuristic algorithms for the optimization of each thermal system.

The book is expected to be useful to undergraduate and postgraduate students and research scholar of mechanical engineering as it provides a detailed understanding of the thermal modeling and optimization aspects of various thermal systems. This book is expected to become a valuable reference for those wishing to do research in the area of metaheuristic algorithms and their application to optimize the real-life problems. This book is also useful to engineers, managers, institutes involved in the applied optimization works, and graduate students of various engineering disciplines who want to pursue their carrier in the applied optimization.

We would like to thank our publisher Springer for the continuous support and interest in our project. In particular, we would like to thank Oliver Jackson, Meertinus Faber, and Ram Prasad Chandrasekar for their commitment and engagement with regard to this book project. We are gratefully acknowledging the support of our past and present M.Tech and Ph.D. students and postdoctoral fellows. We are also thankful to various researchers and the international journal publishers for giving us the permission to reuse certain parts of their research work. Finally, our special thanks to our family members for supporting us during the preparation of the entire book.

On the whole, we had put the wholehearted efforts to ensure that no errors (printing or another kind) remain in the book. However, the possibility of such an error in the book is always there. So, we will be thankful to the readers if they point out any such errors which may remain in the book.

Gandhinagar, India  
Gandhinagar, India  
Kamloops, Canada

Vivek K. Patel  
Vimal J. Savsani  
Mohamed A. Tawhid

# Contents

<b>1</b>	<b>Introduction</b>	<b>1</b>
	References . . . . .	4
<b>2</b>	<b>Metaheuristic Methods</b>	<b>7</b>
2.1	Genetic Algorithm (GA) . . . . .	8
2.1.1	Reproduction . . . . .	8
2.1.2	Crossover . . . . .	9
2.1.3	Mutation . . . . .	9
2.2	Particle Swarm Optimization (PSO) Algorithm . . . . .	10
2.3	Differential Evolution (DE) Algorithm . . . . .	12
2.4	Artificial Bee Colony (ABC) Algorithm . . . . .	14
2.5	Cuckoo Search Algorithm (CSA) . . . . .	16
2.6	Teaching–Learning-Based Optimization (TLBO) Algorithm . . . . .	17
2.6.1	Teacher Phase . . . . .	18
2.6.2	Learner Phase . . . . .	18
2.7	Symbiotic Organism Search (SOS) Algorithm . . . . .	19
2.7.1	Mutualism Phase . . . . .	20
2.7.2	Commensalism Phase . . . . .	20
2.7.3	Parasitism Phase . . . . .	21
2.8	Water Wave Optimization (WWO) Algorithm . . . . .	22
2.8.1	Propagation Operator . . . . .	22
2.8.2	Refraction Operator . . . . .	23
2.8.3	Breaking Operator . . . . .	23
2.9	Heat Transfer Search (HTS) Algorithm . . . . .	24
2.10	Passing Vehicle Search (PVS) Algorithm . . . . .	27
2.11	Sine Cosine Algorithm (SCA) . . . . .	29
2.12	Parameter Tuning of Algorithms . . . . .	30
	References . . . . .	32

<b>3 Thermal Design and Optimization of Heat Exchangers . . . . .</b>	<b>33</b>
3.1 Shell and Tube Heat Exchanger (STHE) . . . . .	33
3.1.1 Thermal Model . . . . .	37
3.1.2 Case Study, Objective Function Description, and Constraints . . . . .	45
3.1.3 Results and Discussion . . . . .	47
3.2 Plate-Fin Heat Exchanger (PFHE) . . . . .	49
3.2.1 Thermal Model . . . . .	53
3.2.2 Case Study, Objective Function Description, and Constraints . . . . .	57
3.2.3 Results and Discussion . . . . .	59
3.3 Fin and Tube Heat Exchanger (FTHE) . . . . .	62
3.3.1 Thermal Model . . . . .	64
3.3.2 Case Study, Objective Function Description, and Constraints . . . . .	68
3.3.3 Results and Discussion . . . . .	70
3.4 Regenerative Heat Exchanger (Rotary Regenerator) . . . . .	72
3.4.1 Thermal Model . . . . .	74
3.4.2 Case Study, Objective Function Description, and Constraints . . . . .	78
3.4.3 Results and Discussion . . . . .	79
3.5 Plate Heat Exchanger (PHE) . . . . .	82
3.5.1 Thermal Model . . . . .	84
3.5.2 Case Study, Objective Function Description, and Constraints . . . . .	89
3.5.3 Results and Discussion . . . . .	90
References . . . . .	92
<b>4 Thermal Design and Optimization of Heat Engines and Heat Pumps . . . . .</b>	<b>99</b>
4.1 Carnot Heat Engine . . . . .	100
4.1.1 Thermal Model . . . . .	103
4.1.2 Case Study, Objective Function Description, and Constraints . . . . .	105
4.1.3 Results and Discussion . . . . .	106
4.2 Rankine Heat Engine . . . . .	108
4.2.1 Thermal Model . . . . .	111
4.2.2 Case Study, Objective Function Description, and Constraints . . . . .	114
4.2.3 Results and Discussion . . . . .	115
4.3 Stirling Heat Engine . . . . .	118
4.3.1 Thermal Model . . . . .	120
4.3.2 Case Study, Objective Function Description, and Constraints . . . . .	124
4.3.3 Results and Discussion . . . . .	125

4.4	Brayton Heat Engine . . . . .	128
4.4.1	Thermal Model . . . . .	131
4.4.2	Case Study, Objective Function Description, and Constraints . . . . .	135
4.4.3	Results and Discussion . . . . .	136
4.5	Ericsson Heat Engine . . . . .	139
4.5.1	Thermal Model . . . . .	141
4.5.2	Case Study, Objective Function Description, and Constraints . . . . .	144
4.5.3	Results and Discussion . . . . .	145
4.6	Diesel Heat Engine . . . . .	147
4.6.1	Thermal Model . . . . .	150
4.6.2	Case Study, Objective Function Description, and Constraints . . . . .	153
4.6.3	Results and Discussion . . . . .	154
4.7	Radiative-Type Heat Engine . . . . .	156
4.7.1	Thermal Model . . . . .	158
4.7.2	Case Study, Objective Function Description, and Constraints . . . . .	161
4.7.3	Results and Discussion . . . . .	162
4.8	Stirling Heat Pump . . . . .	164
4.8.1	Thermal Model . . . . .	167
4.8.2	Case Study, Objective Function Description, and Constraints . . . . .	170
4.8.3	Results and Discussion . . . . .	171
4.9	Heat Pump Working on Reverse Brayton Cycle . . . . .	174
4.9.1	Thermal Model . . . . .	176
4.9.2	Case Study, Objective Function Description, and Constraints . . . . .	179
4.9.3	Results and Discussion . . . . .	180
4.10	Absorption Heat Pump . . . . .	182
4.10.1	Thermal Model . . . . .	185
4.10.2	Case Study, Objective Function Description, and Constraints . . . . .	188
4.10.3	Results and Discussion . . . . .	189
	References . . . . .	191
<b>5</b>	<b>Thermal Design and Optimization of Refrigeration Systems . . . . .</b>	<b>199</b>
5.1	Carnot Refrigerator . . . . .	200
5.1.1	Thermal Model . . . . .	203
5.1.2	Case Study, Objective Function Description, and Constraints . . . . .	207
5.1.3	Results and Discussion . . . . .	208

5.2	Single-Effect Vapor Absorption Refrigerator . . . . .	210
5.2.1	Thermal Model . . . . .	213
5.2.2	Case Study, Objective Function Description, and Constraints . . . . .	216
5.2.3	Results and Discussion . . . . .	217
5.3	Multi-temperature Vapor Absorption Refrigerator . . . . .	219
5.3.1	Thermal Model . . . . .	222
5.3.2	Case Study, Objective Function Description, and Constraints . . . . .	226
5.3.3	Results and Discussion . . . . .	227
5.4	Cascade Refrigerator . . . . .	229
5.4.1	Thermal Model . . . . .	233
5.4.2	Case Study, Objective Function Description, and Constraints . . . . .	237
5.4.3	Results and Discussion . . . . .	239
5.5	Ejector Refrigerator . . . . .	241
5.5.1	Thermal Model . . . . .	244
5.5.2	Case Study, Objective Function Description, and Constraints . . . . .	249
5.5.3	Results and Discussion . . . . .	250
5.6	Thermo-Electric Refrigerator . . . . .	252
5.6.1	Thermal Model . . . . .	254
5.6.2	Case Study, Objective Function Description, and Constraints . . . . .	257
5.6.3	Results and Discussion . . . . .	258
5.7	Stirling Cryogenic Refrigerator . . . . .	261
5.7.1	Thermal Model . . . . .	264
5.7.2	Case Study, Objective Function Description, and Constraints . . . . .	267
5.7.3	Results and Discussion . . . . .	268
5.8	Ericsson Cryogenic Refrigerator . . . . .	270
5.8.1	Thermal Model . . . . .	273
5.8.2	Case Study, Objective Function Description, and Constraints . . . . .	277
5.8.3	Results and Discussion . . . . .	278
	References . . . . .	280
<b>6</b>	<b>Thermal Design and Optimization of Power Cycles . . . . .</b>	<b>287</b>
6.1	Rankine Power Cycle . . . . .	288
6.1.1	Thermal Model . . . . .	291
6.1.2	Case Study, Objective Function Description, and Constraints . . . . .	294
6.1.3	Results and Discussion . . . . .	296

6.2	Brayton Power Cycle . . . . .	299
6.2.1	Thermal Model . . . . .	301
6.2.2	Case Study, Objective Function Description, and Constraints . . . . .	305
6.2.3	Results and Discussion . . . . .	306
6.3	Braysson Power Cycle . . . . .	308
6.3.1	Thermal Model . . . . .	310
6.3.2	Case Study, Objective Function Description, and Constraints . . . . .	313
6.3.3	Results and Discussion . . . . .	314
6.4	Kalina Power Cycle . . . . .	316
6.4.1	Thermal Model . . . . .	319
6.4.2	Case Study, Objective Function Description, and Constraints . . . . .	322
6.4.3	Results and Discussion . . . . .	323
6.5	Combined Brayton and Inverse Brayton Power Cycle . . . . .	325
6.5.1	Thermal Model . . . . .	327
6.5.2	Case Study, Objective Function Description, and Constraints . . . . .	329
6.5.3	Results and Discussion . . . . .	330
6.6	Atkinson Power Cycle Optimization . . . . .	333
6.6.1	Thermal Model . . . . .	335
6.6.2	Case Study, Objective Function Description, and Constraints . . . . .	337
6.6.3	Results and Discussion . . . . .	338
	References . . . . .	340
7	<b>Thermal Design and Optimization of Few Miscellaneous Systems . . . . .</b>	345
7.1	Cooling Tower . . . . .	345
7.1.1	Thermal Model . . . . .	348
7.1.2	Case Study, Objective Function Description, and Constraints . . . . .	354
7.1.3	Results and Discussion . . . . .	355
7.2	Heat Pipe . . . . .	357
7.2.1	Thermal Model . . . . .	360
7.2.2	Case Study, Objective Function Description, and Constraints . . . . .	364
7.2.3	Results and Discussion . . . . .	365
7.3	Micro-channel Heat Sink . . . . .	368
7.3.1	Thermal Model . . . . .	370
7.3.2	Case Study, Objective Function Description, and Constraints . . . . .	374
7.3.3	Results and Discussion . . . . .	375

7.4	Solar Air Heater . . . . .	378
7.4.1	Thermal Model . . . . .	380
7.4.2	Case Study, Objective Function Description, and Constraints . . . . .	382
7.4.3	Results and Discussion . . . . .	383
7.5	Solar Water Heater . . . . .	385
7.5.1	Thermal Model . . . . .	387
7.5.2	Case Study, Objective Function Description, and Constraints . . . . .	390
7.5.3	Results and Discussion . . . . .	391
7.6	Solar Chimney Power Plant . . . . .	394
7.6.1	Thermal Model . . . . .	396
7.6.2	Case Study, Objective Function Description, and Constraints . . . . .	398
7.6.3	Results and Discussion . . . . .	398
7.7	Turbojet Engine . . . . .	400
7.7.1	Thermal Model . . . . .	402
7.7.2	Case Study, Objective Function Description, and Constraints . . . . .	403
7.7.3	Results and Discussion . . . . .	404
	References . . . . .	407
	<b>MATLAB Code of Optimization Algorithms</b> . . . . .	415
	<b>Index</b> . . . . .	471

# Chapter 1

## Introduction



**Abstract** Thermal systems deal with the conversion of thermal energy (i.e., heat energy) into mechanical energy, which is further converted into electric energy. Design optimization of thermal systems involves a large number of design variables and constraints. The conventional methods of the thermal system design optimization apply an iterative procedure which may trap in local optimum. Advanced optimization algorithms offer solutions to the problems, because they find a solution nearer to the global optimum within reasonable time and computational costs.

Any system that converts the thermal energy into mechanical energy or any other forms of energy is known as thermal system. The thermal energy is available to the system due to fuel combustion, from solar energy, from geothermal energy, or from any such other sources. The thermal energy is then supplied to the working media (i.e., working fluid) of the system, which undergoes a series of processes before converted into other forms of energy. All these conversion processes take place in the different components of the thermal systems. Further, the pressure, temperature, volume, as well as other thermo-physical properties of the working fluid like density, viscosity, thermal conductivity, etc. continuously change as the working fluid passes through different components of the thermal systems. Thus, the modeling and design of each component of the thermal systems are very important for the proper working of the entire system.

Thermal system design includes an optimization process in which designers always consider certain objectives such as heat transfer, effectiveness, cooling capacity, pressure drop, etc. depending on the requirements. While achieving the objectives mentioned above, it is also desirable to minimize the total cost of the system. Thus, the design optimization for a complete thermal system assembly leads to a complicated objective function with a large number of design variables and constraints. The conventional methods of the thermal system design optimization apply an iterative procedure based on the design specification and assuming design variables for several configurations until one is found that meets the system requirements within given set of constraints. Typically, the use of this approach results in oversize equipment and complicated design procedure.

Analytical or numerical methods for calculating the extreme values of a function have been applied to engineering computations for a long time. Although these methods may perform well in many practical cases, they may fail in more complex design situations. In real design problems, the number of design parameters can be very large, and their influence on the value to be optimized (the objective function) can be very complicated, having nonlinear characteristics. The objective function may have many local optima, whereas the designer is interested in the global optima. Such problems cannot be handled by classical methods (e.g., gradient methods) as they only compute local optima. In these complex cases, advanced optimization algorithms offer solutions to the problems, because they find a solution nearer to the global optimum within a reasonable time and computational costs.

The optimization techniques can be classified into two distinct types as given below:

- (a) **Traditional optimization techniques:** These are deterministic algorithms with specific rules for moving from one solution to the other. These algorithms have been in use for quite some time and have been successfully applied to many engineering design problems. The techniques include linear programming (Kantorovich 1940), nonlinear programming (Zoutendijk 1960), quadratic programming (Wolfe 1959), dynamic programming (Bellman 1957), geometric programming (Duffin et al. 1967), generalized reduced gradient method (Gabriele and Ragsdell 1977), etc.
- (b) **Advanced optimization techniques:** These techniques are stochastic in nature with probabilistic transition rules. These techniques are comparatively new and gaining popularity due to certain properties that the deterministic algorithms do not have. These techniques can be classified into different groups depending on the criteria being considered. Depending on the nature of the phenomenon simulated by these techniques, the advanced optimization techniques have two important groups: evolutionary algorithms (EA) and swarm intelligence-based algorithms. The general framework of the optimization techniques is shown in Fig. 1.1 .

Although traditional optimization techniques had been employed to solve optimization problems in thermal system design, these techniques have the following limitations:

- Traditional techniques do not fare well over a broad spectrum of problem domains.
- Traditional techniques are not suitable for solving multi-modal problems as they tend to obtain a local optimal solution.
- Traditional techniques are not ideal for solving multi-objective optimization problems.
- Traditional techniques are not suitable for solving problems involving a large number of constraints.

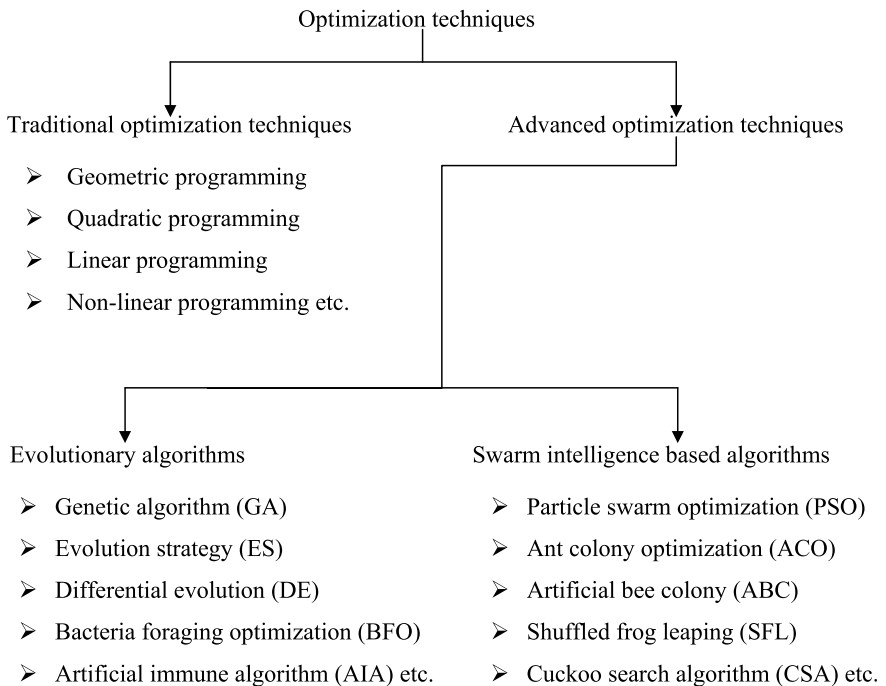


**Fig. 1.1** The general framework of optimization techniques

Considering the drawbacks of traditional optimization techniques, attempts are being made to optimize the thermal system design optimization problems by using evolutionary optimization techniques.

Some of the well-known population-based optimization techniques developed during last three decades are: genetic algorithm (Holland 1975), which works on the principle of the Darwinian theory of the survival of the fittest and the theory of evolution of the living beings; artificial immune algorithm (Farmer et al. 1986), which works on the principle of immune system of the human being; ant colony optimization (Dorigo et al. 1991), which works on the principle of foraging behavior of the ant in search of food sources; Particle swarm optimization (Eberhart and Kennedy 1997), which works on the principle of foraging behavior of the swarm of birds; differential evolution (Storn and Price 1997), which is similar to genetic algorithm with specialized mutation strategies; harmony search (Geem et al. 2001), which works on the principle of music improvisation in a music player; Bacteria foraging optimization (Passino 2002), which works on the principle of behavior of bacteria; shuffled frog leaping (Eusuff and Lansey 2003), which works on the principle of communication among the frogs; artificial bee colony (Karaboga 2005), which works on the principle of foraging behavior of a honey bee; biogeography-based optimization (Simon 2008), which works on the principle of immigration and emigration of the species from one place to the other; gravitational

search algorithm (GSA) (Rashedi et al. 2009), which works on the principle of gravitational force acting between the bodies; grenade explosion method (Ahrari and Atai 2010), which works on the principle of explosion of grenade; league championship algorithm (Kashan 2011), which mimics the sporting competition in a sport league; cuckoo search algorithm (Yang and Deb 2009) inspired by the obligate brood parasitism of some cuckoo species by laying their eggs in the nests of other host birds teaching–learning-based optimization (Rao et al. 2011) mimic the traditional teaching–learning behavior of the class room; symbiotic organisms search algorithm (Cheng and Prayogo 2014) analogous to the interactive behavior among organisms in nature; water wave optimization (Zheng 2015) works on the phenomena of water waves, such as propagation, refraction, and breaking; heat transfer search (Patel and Savsani 2015), which mimics the heat transfer behavior between the system and surrounding to reach the equilibrium condition; passing vehicle search (Savsani and Savsani 2016), which works based on the mathematics of vehicle passing on a two-lane highway; and sine cosine algorithm (Mirjalili 2016), which works using a mathematical model based on sine and cosine functions. These algorithms have been applied to many engineering optimization problems and proved their effectiveness to solve some specific kinds of problems.

This work demonstrates the application of a few recently developed metaheuristic algorithms for the thermal system design optimization. This book is organized as follows: Chap. 2 covers the details of metaheuristic methods considered in this work. Chapter 3 describes the thermal design and optimization of heat exchangers. Chapter 4 explains the thermal design and optimization of heat engines and heat pumps. Chapter 5 discusses the thermal design and optimization of refrigerators. Chapter 6 provides the thermal design and optimization of power cycles. Chapter 7 presents the thermal design and optimization of a few miscellaneous systems.

## References

- Ahrari A., Atai A.A. (2010) ‘Grenade explosion method-a novel tool for optimization of multimodal functions’, *Applied Soft Computing*, vol. 10, 1132–1140.
- Bellman, R. E. (1957) *Dynamic Programming*, Princeton University Press, Princeton, NJ.
- Dorigo M., Maniezzo V., Colorni A. (1991) *Positive feedback as a search strategy*, Technical Report 91–016, Politecnico di Milano, Italy.
- Duffin R. J., Peterson E., Zener C. (1967) *Geometric Programming*, John Wiley, New York.
- Eberhart R., Kennedy J. (1997) ‘A new optimizer using particle swarm theory’, In: *Proceedings of IEEE Symposium on Micro Machine and Human Science*, Nagoya, Japan, pp. 39–43.
- Eusuff M., Lansey E. (2003) ‘Optimization of water distribution network design using the shuffled frog leaping algorithm’, *Journal of Water Resources Planning and Management*, vol. 129, 210–225.
- Farmer J.D., Packard N., Perelson A. (1986) ‘The immune system, adaptation and machine learning’, *Physica D*, vol. 22, 187–204.
- Gabriele G. A., Ragsdell K. M. (1977) ‘The generalized reduced gradient method: a reliable tool for optimal design’, *ASME Journal of Engineering for Industry*, vol. 99, 384–400.

- Geem Z.W., Kim J.H., Loganathan G.V. (2001) ‘A new heuristic optimization algorithm: harmony search’, *Simulation*, vol. 76, 60–70.
- Holland J. (1975) *Adaptation in Natural and Artificial Systems*. University of Michigan Press, Ann Arbor.
- Kantorovich L.V. (1940) ‘A new method of solving some classes of extrema problems’, *Doklady Akad Science USSR*, vol. 28, 211–214.
- Karaboga D. (2005) ‘An idea based on honey bee swarm for numerical optimization’, Technical report-TR06, Erciyes University, Engineering Faculty, Computer Engineering Department.
- Kashan A. H. (2011) ‘An efficient algorithm for constrained global optimization and application to mechanical engineering design: League championship algorithm (LCA)’, *Computer Aided Design*, vol. 43, 1769–1792.
- Min-Yuan Cheng, Doddy Prayogo (2014) ‘Symbiotic Organisms Search: A new metaheuristic optimization algorithm’, *Computers & Structures*, vol. 139, 98–112.
- Mirjalili S. (2016) ‘SCA: a sine-cosine algorithm for solving optimization problems. *Knowledge-Based Systems*’, vol. 96, pp. 120–133.
- Passino K.M. (2002) ‘Biomimicry of Bacterial Foraging for Distributed Optimization and Control’, *IEEE Control Systems Magazine*, vol. 22, 52–67.
- Patel V.K. and Savsani V.J. (2015) ‘Heat transfer search (HTS): a novel optimization algorithm’, *Information Sciences*, vol. 324, pp. 217–246.
- Rao R.V., Savsani V.J. and Vakharia D.P. (2011) ‘Teaching–learning-based optimization: a novel method for constrained mechanical design optimization problems’, *Computer- Aided Design*, vol. 43(3), pp. 303–315.
- Rashedi E., Nezamabadi-pour H., Saryazdi S. (2009) ‘GSA: A gravitational search algorithm’, *Information Sciences*, vol. 179, 2232–2248.
- Savsani P. and Savsani V. (2016) ‘Passing vehicle search (PVS): A novel metaheuristic algorithm’, *Applied Mathematical Modelling*, vol. 40(5–6), pp. 3951–3978.
- Simon D. (2008) ‘Biogeography-based optimization’, *IEEE Transactions on Evolutionary Computation*, vol. 12(6), 702–713.
- Storn R., Price K. (1997) ‘Differential evolution – a simple and efficient heuristic for global optimization over continuous spaces’, *Journal of Global Optimization*, vol. 11, 341–359.
- Wolfe P. (1959) ‘The simplex method for quadratic programming’, *Econometrica*, vol. 27, 382–398.
- Yang X.-S., Deb S. (2009) ‘Cuckoo search via Lévy flights. World Congress on nature & Biologically Inspired Computing (NaBIC 2009)’, *IEEE Publications*, pp. 210–214.
- Zheng Y.J. (2015) ‘Water wave optimization: a new nature-inspired metaheuristic. *Computers & Operations Research*’, vol. 55, pp. 1–11.
- Zoutendijk G. (1960) *Methods of Feasible Directions*, Elsevier, Amsterdam.

# Chapter 2

## Metaheuristic Methods



**Abstract** Optimization problems of thermal systems are multi-model, multi-dimensional, nonlinear, and implicit in nature. Analytical methods are not suitable to optimize such thermal systems as these methods trap into a local optimum. Metaheuristic techniques are often considered as the best choice for the optimization of such thermal systems. A large number of metaheuristics have been developed and used significantly since last two decades. These metaheuristics have proved their effectiveness to solve many real and challenging practical optimization problems. Eleven different metaheuristic algorithms are described in this chapter in detail with their pseudo code. These algorithms are further used to optimize the various thermal systems, which are discussed in subsequent chapters. The MATLAB code of these algorithms is also given in this book.

Optimization problems of thermal system design applications can be of large search space, nonlinear, nonconvex, multi-modal, multi-dimensional, and implicit. Such functions may not provide gradient-based information. Therefore, analytical methods become insignificant and usually trap into a local optimum. To optimize such complex thermal systems, metaheuristic techniques are often considered as the best choice to find near global optimum solution with less computational efforts. A large number of metaheuristics have been developed and used significantly since last two decades. These metaheuristics have proved their effectiveness to solve many real and challenging practical optimization problems. However, according to the no free lunch (NFL) theorem (Wolpert and Macready 1997), there is no metaheuristic best suited for optimizing all types of problems. Therefore, one algorithm can be expected to outperform another in solving one set of challenges, but it may be a poor performer on a different set of problems. This was the foundation of many works in this field. So, in this work, 11 different metaheuristics algorithms are considered in this book. These algorithms include very well-known and developed algorithms such as genetic algorithm (GA), particle swarm optimization (PSO), and differential evolution (DE). Some algorithms that are developed in the last decade and prove their effectiveness on several engineering applications. These algorithms are artificial bee colony (ABC), cuckoo search algorithm (CSA), and teaching–learning-based

optimization (TLBO). The rest of the algorithms are recently developed ones and are not yet addressed to solve thermal system design problems. These algorithms include symbiotic organism search (SOS), water wave optimization (WWO), heat transfer search (HTS), passing vehicle search (PVS), and sine cosine algorithm (SCA). All the considered metaheuristics are population-based algorithms. The metaheuristics initiate with a randomly generated population of the optimization problem. The population of an algorithm is then updated by using a succession of different mathematical formulas, which are primarily inspired by nature. The considered algorithms are briefly summarized in the subsequent sections.

## 2.1 Genetic Algorithm (GA)

Genetic algorithm (GA) works on Darwin's theory of evolution and the survival of the fittest (Holland 1975). Genetic algorithms guide the search through the solution space by using natural selection and genetic operators, such as crossover, mutation, and reproduction. GA encodes the decision variables or input parameters of the problem into solution strings of a finite length. While traditional optimization techniques work directly with the decision variables or input parameters, genetic algorithms usually work with the coding. Genetic algorithms start to search from a population of encoded solutions instead of from a single point in the solution space. The initial population of individuals is created at random. Genetic algorithms use genetic operators to obtain global optimum solutions based on the solutions in the current population (Rao 2009). These genetic operators are (1) reproduction, (2) crossover, and (3) mutation. The newly generated individuals replace the old population, and the evolution process proceeds until certain termination criteria are satisfied.

### 2.1.1 *Reproduction*

Reproduction is the first operation applied to the population to select good strings (designs) of the population to form a mating pool. The reproduction operator is also called the selection operator because it selects good strings of the population. The reproduction operator is used to pick average strings from the current population and inserts their multiple copies in the mating pool based on a probabilistic procedure. In a commonly used reproduction operator, a string is selected from the mating pool with a probability proportional to its fitness. Thus, if  $F_i$  denotes the fitness of the  $i$ th string in the population of size  $n$ , the probability for selecting the  $i$ th string for the mating pool ( $p_i$ ) is given by

$$p_i = \frac{F_i}{\sum_{j=1}^n F_j} i = 1, 2, \dots, n \quad (2.1)$$

The implementation of the selection process given by above equation can be understood by imagining a roulette wheel with its circumference divided into segments, one for each string of the population, with the segment lengths proportional to the fitness of the strings. By this process, the string with a higher (lower) fitness value will be selected more (less) frequently. Thus, strings with high fitness values in the population, probabilistically, get more copies in the mating pool. It is to be noted that no new strings are formed in the reproduction stage; only the existing strings in the population get copied to the mating pool. The reproduction stage ensures that highly fit individuals (strings) live and reproduce, and less fit individuals (strings) die. Thus, the GA simulates the principle of the ‘survival of the fittest’ of nature.

### **2.1.2 *Crossover***

After reproduction, the crossover operator is implemented. The purpose of crossover is to create new strings by exchanging information among strings of the mating pool. Many crossover operators have been used in the literature of GAs. In most crossover operators, two individual strings (designs) are picked (or selected) at random from the mating pool generated by the reproduction operator, and some portions of the strings are exchanged between the strings. In the commonly used process, known as a single-point crossover operator, a crossover site is selected at random along the string length, and the binary digits lying on the right side of the crossover site are swapped (exchanged) between the two strings. Since the crossover operator combines substrings from parent strings (which have good fitness values), the resulting child strings are expected to have better fitness values provided an appropriate (suitable) crossover site be selected. However, the suitable or appropriate crossover site is not known beforehand. Hence, the crossover site is usually chosen randomly with crossover probability  $p_c$ .

### **2.1.3 *Mutation***

The crossover is the main operator by which new strings with better fitness values are created for the new generations. The mutation operator is applied to the new strings with a specific small mutation probability,  $p_m$ . The mutation operator changes the binary digit 1–0 and vice versa. Several methods can be used for

implementing the mutation operator. In the single-point mutation, a mutation site is selected at random along the string length, and the binary digit at that site is then changed from 1 to 0 or 0 to 1 with a probability of  $p_m$ . The purpose of mutation is (1) to generate a string (design point) in the neighborhood of the current string, thereby accomplishing a local search around the current solution, (2) to safeguard against a premature loss of important genetic material at a particular position, and (3) to maintain diversity in the population. The pseudocode of the genetic algorithm is given below.

START

    Initialize algorithm parameters: population size ( $N$ ), number of function evaluation ( $F$ ), number of design variables ( $D$ ), upper and lower limits for the design variables ( $x_{max}$ ,  $x_{min}$ ), crossover rate, mutation rate

    Generate a random population of  $n$  chromosomes and obtain the fitness value (i.e., objective function value)

    For  $i=1$  to  $F$

        Select two parent chromosomes from a population according to their fitness (the better fitness, the bigger chance to be selected)

        With a crossover probability cross over the parents to form a new offspring (children) and evaluate them

        With a mutation, probability mutate new offspring at each locus (position in the chromosome) and evaluate them

        Replace new solution if it is better than the previous one (i.e., Apply greedy selection process)

    Use new generated population for a further run of the algorithm

End

STOP

## 2.2 Particle Swarm Optimization (PSO) Algorithm

Particle swarm optimization (PSO) is an evolutionary computational technique for solving global optimization problems developed by Kennedy and Eberhart (1995, 1997). It is a computational technique working through individual improvement plus population cooperation and competition, which are based on the simulation of simplified social models, such as bird flocking, fish schooling, and the swarm theory. Researchers found that the synchrony of animal's behavior was through maintaining optimal distances between individual members and their neighbors. Thus, velocity plays an important role in adjusting each other for optimal distances. Furthermore, researchers simulated the scenario in which birds search for food and observe their social behavior. They perceived that in order to find food, the individual members determine their velocities by two factors: their own best previous experience and the best experience of all other members.

It exhibits common evolutionary computational attributes including initialization with a population of random solutions and searching for optima by updating generations. Potential solutions, called ‘birds’ or ‘particles,’ are then ‘flown’ through the problem space by following the current optimum particles. The particle swarm concept was originated as a simulation of a simplified social system. The original intent was to graphically simulate the graceful but unpredictable choreography of a bird flock. Each particle keeps track of its coordinates in the problem space, which is associated with the best solution (fitness) it has achieved so far. This value is called ‘*pBest*.’ Another ‘best’ value that is tracked by the global version of the particle swarm optimization is the overall best value, and its location is obtained so far by any particle in the population. This location is called ‘*gBest*.’

The particle swarm optimization concept consists of, at each step, changing the velocity (i.e., accelerating) of each particle toward its ‘*pBest*’ and ‘*gBest*’ locations (the global version of PSO). Acceleration is weighted by a random term with separate random numbers being generated for acceleration toward ‘*pBest*’ and ‘*gBest*’ locations. The updates of the particles are accomplished as per the following equations.

$$V_{i+1} = wV_i + c_1r_1(pBest_i - X_i) + c_2r_2(gBest_i - X_i) \quad (2.2)$$

$$X_{i+1} = X_i + V_i \quad (2.3)$$

Equation 2.2 calculates a new velocity ( $V_{i+1}$ ) for each particle (potential solution) based on its previous velocity, the best location it has achieved (‘*pBest*’) so far, and the global best location (‘*gBest*’) that the population has achieved. Equation 2.3 updates the individual particle’s position ( $X_i$ ) in solution hyperspace. The two random numbers ‘ $r_1$ ’ and ‘ $r_2$ ’ in Eq. 2.2 are independently generated in the range [0, 1].

The acceleration constants ‘ $c_1$ ’ and ‘ $c_2$ ’ in Eq. 2.2 represent the weighting of the stochastic acceleration terms that pull each particle toward ‘*pBest*’ and ‘*gBest*’ positions. ‘ $c_1$ ’ represents the confidence the particle has in itself (cognitive parameter) and ‘ $c_2$ ’ represents the confidence the particle has in swarm (social parameter). Thus, the adjustment of these constants changes the amount of tension in the system. The inertia weight ‘ $w$ ’ plays an essential role in the PSO convergence behavior since it is employed to control the exploration abilities of the swarm. The large inertia weights allow wide velocity updates to globally explore the design space, while small inertia weights concentrate the velocity updates to nearby regions of the design space. The pseudocode of the PSO algorithm is given below.

**START**

Initialize algorithm parameters: population size ( $N$ ), Number of function evaluation ( $F$ ), Number of design variables ( $D$ ), upper and lower limits for the design variables ( $x_{max}$ ,  $x_{min}$ ), inertia weight, social and cognitive parameters.

Initialize a swarm with random positions and velocities

Evaluate the objective function values (i.e., fitness values) of all particles.

For  $i=1$  to  $F$

    For each particle set ' $pBest$ ' (best position each particle ever meet) and its corresponding fitness value

    For entire swarm set ' $gBest$ ' (best global position) and its corresponding fitness value attained by the swarm

    Update the velocity and position of each particle according to Eqs. (2.2) moreover, (2.3)

    Evaluate the fitness values of all particles for the updated position.

    For each particle, compare its current fitness value with the best fitness value it attained so far (' $pBest$ '). If the current value is better, then set the update position as ' $pBest$ '

    Determine the best particle of the current population. If the current fitness value is better than the fitness value of ' $gBest$ ' then set updated position as ' $gBest$ '

    Use new generated population for a further run of the algorithm

End

At termination, ' $gBest$ ' and its fitness value is the optimum value of the considered problem

**STOP**

## 2.3 Differential Evolution (DE) Algorithm

Differential evolution (DE) is a population-based algorithm proposed by Storn and Price (1997). The DE algorithm used similar operators like genetic algorithm, i.e., crossover, mutation, and selection. However, the difference between the genetic algorithm and DE is the selection process and the mutation scheme. In DE, all solutions have the same chance of being selected as parents without dependence on their fitness value. DE employs a greedy selection process: The better one of the new solution and its parent wins the competition, providing a significant advantage of converging performance over genetic algorithm. Further, the GA relies on crossover for producing a better solution while DE relies on mutation operation.

The DE algorithm uses mutation operation as a search mechanism (exploration) and selection operation to direct the search toward the prospective regions (exploitation) in the search space. The DE algorithm also uses a nonuniform crossover that can take child vector parameters from one parent more often than it does from others. By using the components of the existing population members to construct

trial vectors, the crossover operator efficiently shuffles information about successful combinations, enabling the search for a better solution space.

The mutation vector ( $v_{i,j}$ ) of the DE algorithm is updated based on the target vector ( $x_{i,j}$ ) as below:

$$v_{i,j+1} = x_{i,j} + K(x_{r_1,j} - x_{i,j}) + F(x_{r_2,j} - x_{r_3,j}) \quad (2.4)$$

where  $i$ ,  $r_1$ ,  $r_2$ , and  $r_3$  are the randomly selected individuals from the population and are different from each other.  $K$  is the combination factor while  $F$  is the scaling factor.

After mutation, the crossover is performed to increase the diversity of the perturbed parameter vectors. In the crossover operation of the DE algorithm, the parent vector is mixed with the mutated vector to produce a trial vector as below:

$$u_{g_i,j+1} = \begin{cases} v_{g_i,j+1} & \text{if } (\text{rand}_j \leq \text{CR}) \text{ or } g = \text{rnbr}_i \\ x_{g_i,j} & \text{if } (\text{rand}_j > \text{CR}) \text{ or } g \neq \text{rnbr}_i \end{cases} \quad (2.5)$$

where  $\text{rand}_j$  is the  $j$ th evaluation of a uniform random number generator and varies between 0 and 1;  $g$  is the number of design variables;  $\text{rnbr}_i$  is the randomly chosen index, and it depends on the number of design variables; and CR is the crossover constant.

Crossover step of the DE algorithm is followed by the selection. In the selection process, trial vector  $u_{i,j+1}$  is compared with the target vector  $x_{i,j}$ . If the trial vector produced better fitness value than the target vector, then the trial vector is set as a target vector; otherwise, previous target vector is retained. The pseudocode of the PSO algorithm is given below.

#### START

Initialize algorithm parameters: population size ( $N$ ), number of function evaluation ( $F$ ), number of design variables ( $D$ ), upper and lower limits for the design variables ( $x_{\max}$ ,  $x_{\min}$ ), crossover rate, mutation rate

Generate a random population of  $n$  chromosomes and obtain the fitness value (i.e., objective function value)

For  $i=1$  to  $F$

    Generate the random indices  $r_1$ ,  $r_2$  and  $r_3$  with  $r_1 \neq r_2 \neq r_3$  to produce the mutation vector using Equation 2.4

    Generate the trial vector based on the crossover operation using Equation 2.5

    Evaluate the fitness value of mutation vector and trial vector

    Apply the greedy selection between mutation vector and trial vector based on the fitness value produced by both the vector

    Use new generated population for a further run of the algorithm

End

#### STOP

## 2.4 Artificial Bee Colony (ABC) Algorithm

ABC algorithm proposed by Karaboga (2005) and further developed by Karaboga and Basturk (2007a, b) is a nature-inspired algorithm based on the intelligent foraging behavior of honeybee swarm. The algorithm mimics insect's food-searching ability. The ABC algorithm describes the foraging behavior, learning, memorizing, and information-sharing characteristics of honeybees. The honeybee swarms consist of two essential components (i.e., food sources and foragers) and define two leading modes of the behavior (i.e., recruitment to a nectar source and abandonment of a source).

The colony of artificial bees consists of three groups of bees: employed bees, onlookers, and scouts. The colony of the artificial bees is divided into two groups: the first half of the colony consists of the employed artificial bees and the second half includes the onlooker bees. Scout bees are the employed bees whose food source has been abandoned. In the ABC algorithm, the position of a food source represents a possible solution to the optimization problem (value of design variables), and the nectar amount of a food source corresponds to the quality of the associated solution (i.e., fitness value). At the first step, the ABC generates a randomly distributed initial population  $P_{\text{initial}}$  of  $N$  solutions, where  $N$  denotes the size of the population. Each solution  $x_i$  ( $i = 1, 2, \dots, N$ ) is a  $S$ -dimensional vector where  $S$  is the number of optimization parameters (design variables). After initialization, the population of the solutions is subjected to repeated cycles,  $C = 1, 2, \dots, G$ , of the search processes of the employed bees, the onlooker bees, and scout bees. An employed bee produces a modification of the solution in her memory depending on the local information. If the objective function value (fitness) of the new solution is better than that of the previous one, the bee memorizes the new position and forgets the old one. Otherwise, she keeps the position of the previous one in her memory. After all employed bees complete the search process, they share the nectar information of the food sources and their position information with the onlooker bees on the dance area. An onlooker bee evaluates the fitness information taken from all employed bees and chooses a food source with a probability related to its fitness value. An onlooker bee also produces a new solution, and it memorizes the new position if its fitness value is better than the previous position. An artificial onlooker bee chooses a food source depending on the probability value associated with that food source,  $p_i$ , calculated by the following expression:

$$p_i = \frac{F_i}{\sum_{n=1}^{N_b} F_n} \quad (2.6)$$

where  $F_i$  is the fitness value of the solution  $i$  which is proportional to the nectar amount of the food source in the position  $i$  and  $N_b$  is the number of food sources

which is equal to the number of employed bees. In order to produce a candidate food position from the old one in memory, the ABC uses the following expression:

$$v_{ij} = x_{ij} + r_{ij}(x_{ij} - x_{kj}) \quad (2.7)$$

where  $k \in \{1, 2, \dots, N\}$  and  $j \in \{1, 2, \dots, D\}$  are randomly chosen indices. Although  $k$  is determined randomly, it has to be different from  $i$ .  $r_{ij}$  is a random number between  $-1$  and  $1$ .

If the position of the food source cannot be improved for some predetermined number of cycles, then that food source is abandoned. The abandoned food source is replaced with a new food source by the scouts. In the ABC, this is simulated by producing a position randomly and replacing it with the abandoned one. The value of the predetermined number of cycles is an important control parameter of the ABC algorithm, which is called ‘limit’ for abandonment. The value of the limit is generally taken as  $N*S$ . Assume that the abandoned source is  $x_i$  and  $j \in \{1, 2, \dots, D\}$ , then the scout discovers a new food source to be replaced with  $x_i$ . This operation can be expressed as

$$x_i^j = x_{\min}^j + \text{rand}(0, 1)(x_{\max}^j - x_{\min}^j) \quad (2.8)$$

So, from the above explanation, it is clear that control parameters used in the ABC are the number of food sources which are equal to the number of employed bees, the number of onlookers and scout bees, the value of ‘limit,’ and the maximum cycles number. The detailed pseudocode of the ABC algorithm is given below.

**START**

    Initialize algorithm parameters: population size ( $N$ ), number of function evaluation ( $F$ ), number of design variables ( $D$ ), upper and lower limits for the design variables ( $x_{\max}$ ,  $x_{\min}$ ), the limit value

    Evaluate the initial population and obtain the fitness value (i.e., objective function value)

    For  $i=1$  to  $F$

        Produce new solutions  $v_{ij}$  for the employed bees by using Equation (2.7) and evaluate them

        Replace new solution if it is better than the previous one (i.e., Apply greedy selection process)

        Calculate the probability values  $p_{ij}$  for the solutions  $x_{ij}$  by using Equation (2.6)

        Select solutions  $x_{ij}$  based on probability values  $p_{ij}$  and produce the new solutions  $v_{ij}$  for the onlookers and evaluate them.

        Replace new solution if it is better than the previous one (i.e., Apply greedy selection process for the onlooker)

        Determine the abandoned solution for the scout, if exists, and replace it with a new randomly produced solution  $x_{ij}$  by using Equation (2.8)

    End

**STOP**

## 2.5 Cuckoo Search Algorithm (CSA)

Cuckoo search (CS) is a population-oriented stochastic algorithm proposed by Yang and Deb (2009, 2010). The CSA is inspired by the lifestyle of a bird family called cuckoo. The CSA is a nature-inspired metaheuristic algorithm, which is based on the obligate brood parasitic behavior of some cuckoo species in combination with Lévy flight distribution of some birds and fruit flies (Payne et al. 2005). Cuckoos are fascinating birds having aggressive reproduction strategy. Cuckoo engages the obligate brood parasitism by laying their eggs in the nests of other host birds (often other species). There are three basic types of brood parasitism: intraspecific brood parasitism, cooperative breeding, and nest takeover. Cuckoos can engage in direct conflict with the host birds. Host birds can either throw the alien eggs out of the nest or abandon the nest and make new ones.

In Lévy flight distribution, it is found that animals and birds search for food in a random or quasi-random manner, and mainly follow a random walk because the next step is based on the current place and the transition probability to the next state. Such behavior has been applied in cuckoo search optimization by Yang and Deb (2010) and has demonstrated its superiority over other distribution-based random walk problems. This type of behavior can be modeled mathematically. Usually, Lévy flight distribution is expressed by taking its Fourier transform. Further, there are many ways of implementing this, but one of the easiest ways (Yang 2010) is Mantegna algorithm for a symmetric Lévy stable distribution.

There are three idealized rules in the cuckoo search algorithm proposed by Yang and Deb (2009, 2010). The underlying idealized rules as an optimization tool of CS algorithm are:

- Each cuckoo lays one egg at a time and dumps it in a randomly chosen nest.
- The best nests with the high quality of eggs will carry over to the next generation.
- The number of available host nest is fixed, and the egg laid by a cuckoo is discovered by the host bird with a probability of  $p_a \in [0, 1]$ . In this case, the host bird can either throw the egg away or abandon the nest to build an entirely new nest in a new location.

For maximization or minimization problems, the fitness function is chosen as the objective function itself. For generating a new solution,  $X_{ij}^{\text{new}}$  for cuckoo  $j$ , a Lévy flight is performed as

$$X_{i,j}^{\text{new}} = X_{i,j}^{\text{old}} + \alpha \oplus \text{Lévy}(\lambda) \quad (2.9)$$

where  $\alpha$  is the step size, generally  $\alpha \geq 1$ . The product  $\oplus$  deals with entry-wise multiplications process. However, Lévy flights provide a random walk, whereas their random step lengths are drawn from a Lévy distribution for large steps defined by

$$\text{Lévy} \sim u = i^{-\lambda} \quad 1 \leq \alpha \leq 3 \quad (2.10)$$

Lévy function can be changed according to the application. Further, if a cuckoo's egg is very similar to a host's eggs, then this cuckoo's egg is less likely to be discovered; thus, the fitness should be related to the difference in solutions. Therefore, it is a good practice to perform a random walk in a biased way with some random step sizes. The detailed pseudocode of the cuckoo search algorithm is given below.

START

    Initialize algorithm parameters: population size ( $n$ ), number of function evaluation ( $F$ ), number of design variables ( $D$ ), upper and lower limits for the design variables ( $x_{max}$ ,  $x_{min}$ ), the limit value

    Evaluate the initial population (i.e., host nests) and obtain the fitness value (i.e., objective function value)

        For  $i=1$  to  $F$

            Generate the cuckoo  $j$  randomly by Lévy flights

            Evaluate the fitness value  $F_j$

            Choose a nest among  $n$  (say  $i$ ) randomly

                If  $F_j > F_i$

                    Replace  $i$  with a new solution

                End

            Abandon a fraction  $p_a$  of worse nests and build new ones at new locations via Lévy flights

            Keep the best solutions (i.e., nests with quality solutions)

            Rank the solutions and find the current best

        End

    STOP

## 2.6 Teaching–Learning-Based Optimization (TLBO) Algorithm

Teaching–learning method is the core of any education system. Inspired by the idea of teaching and learning, Rao et al. (2011) introduced an innovative approach called teaching–learning-based optimization (TLBO) algorithm. The TLBO algorithm simulates the traditional teaching–learning phenomenon of the classroom. The algorithm simulates two fundamental modes of learning: (i) through teacher and (ii) through interacting with the other learners. The TLBO is a population-based algorithm where a group of students (i.e., learners) is considered as population, and the different subjects offered to the learners are analogous with the different design variables of the optimization problem. The grades of a learner in each subject represent a possible solution to the optimization problem (value of design variables), and the mean result of a learner considering all subjects corresponds to the quality of the associated solution (fitness value). The best solution in the entire population is considered as the teacher.

At the first step, the TLBO generates a randomly distributed initial population  $P_{\text{initial}}$  of  $n$  solutions, where  $n$  denotes the size of the population. Each solution  $X^k$  ( $k = 1, 2, \dots, n$ ) is an  $m$ -dimensional vector where  $m$  is the number of optimization parameters (design variables). After initialization, the population of the solutions is subjected to repeated cycles,  $i = 1, 2, \dots, g$ , of the teacher phase and learner phase. The working principle of the TLBO algorithm is explained below with the teacher phase and learner phase.

### 2.6.1 Teacher Phase

This phase of the algorithm simulates the learning of the students (i.e., learners) through the teacher. During this phase, a teacher conveys knowledge among the learners and put efforts to increase the mean result of the class. Suppose that ‘ $m$ ’ is the number of subjects (i.e., design variables) offered to ‘ $n$ ’ number of learners (i.e., population size,  $k = 1, 2, \dots, n$ ). At any sequential teaching–learning cycle  $i$ ,  $M_{j,i}$  is the mean result of the learners in a particular subject ‘ $j$ ’ ( $j = 1, 2, \dots, m$ ). Since a teacher is the most experienced and knowledgeable person on a subject, the best learner in the entire population is considered as a teacher in the algorithm. Let  $X_{j,i}^b$  is the grades of the best learner and  $f(X^b)$  is the result of the best learner considering all the subjects, who is identified as a teacher for that cycle. Teacher will put maximum effort to increase the knowledge level of the whole class, but learners will gain knowledge according to the quality of teaching delivered by a teacher and the quality of learners present in the class. Considering this fact, the existing solution ‘ $k$ ’ is updated in the teacher phase according to the following expression:

$$X_{j,i}^{t_k} = X_{j,i}^k + r_i \left( X_{j,i}^b - T_F M_{j,i} \right) \quad (2.11)$$

where  $X_{j,i}^{t_k}$  is the updated value of  $X_{j,i}^k$ ,  $X_{j,i}^b$  is the grade of the teacher (i.e., best learner) in subject  $j$ ,  $r_i$  is the random number in the range  $[0, 1]$ , and  $T_F$  is the teaching factor. Value of  $T_F$  can be either 1 or 2, which is again a heuristic step, and so it is decided randomly with equal probability as

$$T_F = \text{round}[1 + \text{rand}] \quad (2.12)$$

where  $\text{rand}$  is the random number in the range  $[0, 1]$ .

### 2.6.2 Learner Phase

This phase of the algorithm simulates the learning of the students (i.e., learners) through interaction among themselves. The students can also gain knowledge by

discussing and interacting with the other students. The learning phenomenon of this phase is expressed below.

Randomly select two learners  $p$  and  $q$  such that  $f(X^p) \neq f(X^q)$  (where  $f(X^p)$  and  $f(X^q)$  are the updated result of the learner  $p$  and  $q$  at the end of teacher phase):

$$X_{j,i}''^p = \begin{cases} X_{j,i}'^p + r_i(X_{j,i}'^p - X_{j,i}'^q), & \text{If } f(X^p) < f(X^q) \\ X_{j,i}'^p + r_i(X_{j,i}'^q - X_{j,i}'^p), & \text{If } f(X^q) < f(X^p) \end{cases} \quad (2.13)$$

where  $X_{j,i}''^p$  is the updated value of  $X_{j,i}'^p$ . Accept  $X_{j,i}''^p$  if it gives a better function value. The detailed pseudocode of the TLBO algorithm is given below.

START

    Initialize algorithm parameters: population size ( $n$ ), number of function evaluation ( $F$ ), number of design variables ( $m$ ), upper and lower limits for the design variables ( $x_{max}$ ,  $x_{min}$ ),

    Evaluate the initial population and obtain the fitness value (i.e., objective function value)

    For  $i=1$  to  $F$

        Calculate the mean of learners in each subject (i.e.,  $M_j$ ) and the difference between the current mean and the corresponding result of the teacher by utilizing the teaching factor

        Update the learners' knowledge as per the teacher phase of the TLBO algorithm using Equations (2.11) and (2.12).

        Apply greedy selection process to preserve the modified solutions.

        Update the learners' knowledge as per the learner phase of the TLBO algorithm using Equation (2.13).

        Apply greedy selection process to preserve the modified solutions.

    End

STOP

## 2.7 Symbiotic Organism Search (SOS) Algorithm

The SOS algorithm, proposed by Cheng and Prayogo (2014), is a simple and powerful metaheuristic algorithm. The SOS algorithm works on the cooperative behavior seen among organisms in nature. Some organisms do not live alone because they are interdependent on other species for survival and food. The interdependency between two discrete species is known as symbiotic. In this context, mutualism, commensalism, and parasitism are the most common symbiotic relations found in nature. Interdependency between two different species that results in mutual benefit is called mutualism. A relationship between two different species that offers benefits to only one of them (without the affecting other) is called commensalism. Finally, a relationship between two different species that offers benefits to one and cause harm to the other is called parasitism.

The SOS algorithm initiates with a randomly generated population, where the system has ' $n$ ' number of organisms (i.e., population size) in the ecosystem. In the next

stage, the population is updated in each generation ‘ $g$ ’ by ‘the mutualism phase,’ ‘the commensalism phase,’ and ‘the parasitism phase,’ respectively. Moreover, the updated solution in each phase is accepted only if it has a better functional value. The course of optimization is repeated until the termination criterion is satisfied. In this optimization method, a better solution can be achieved by the symbiotic relations between the current solution and either of other random solution and the best solution from the population. The detailed description of all three phases and modification of the SOS algorithm is explained in the subsequent sections.

### 2.7.1 Mutualism Phase

A relationship between two organisms of different species resulting in individual benefits of the symbiotic interaction is called mutualism. This symbiotic association benefits both individuals from the exchange. Therefore, this relationship is called a mutually beneficial symbiotic. In this phase, the design vector ( $X_i$ ) of the organism ‘ $i$ ’ (i.e., population) interacts with another design vector ( $X_k$ ) of a randomly selected organism ‘ $k$ ’ of the ecosystem (where  $k \neq i$ ). The interaction between these organisms results in a mutualistic relationship, which improves individual functional values of the organisms in the ecosystem. The organism with the best functional value is considered as the best organism ( $X_{\text{best}}$ ) of the ecosystem. In this phase, organisms ‘ $X_i$ ’ and ‘ $X_k$ ’ also interact with the best organism. The mathematical formulations of the new solutions are given below:

$$X'_i = X_i + \text{rand} \times (X_{\text{best}} - \text{MV} \times \text{BF}_1) \quad (2.14)$$

$$X'_k = X_k + \text{rand} \times (X_{\text{best}} - \text{MV} * \text{BF}_2) \quad (2.15)$$

$$\text{MV} = \frac{X_i + X_k}{2} \quad (2.16)$$

$$\text{BF}_1 = 1 + \text{round}(\text{rand}) \quad (2.17)$$

$$\text{BF}_2 = 1 + \text{round}(\text{rand}) \quad (2.18)$$

where  $i = 1, 2, \dots, k$  is a randomly selected population;  $k \neq i, k \in 1, 2, \dots, n$  and rand is a random number between 0 and 1.

### 2.7.2 Commensalism Phase

When a relationship established by an organism with another organism of a different species results in benefits to this organism while having no influence on the

other organism, such symbiotic interaction is called commensalism. In this phase, the design vector ( $X_i$ ) of the organism ‘ $i$ ’ (i.e., population) interacts with another design vector ( $X_k$ ) of a randomly selected organism ‘ $k$ ’ of the ecosystem (where  $k \neq i$ ). The interaction between these organisms results in a commensalism relationship, which improves the functional value of the organism ‘ $i$ ’. The mathematical formulation of the new population is given by

$$X'_i = X_i + \text{rand} \times (X_{\text{best}} - X_i) \quad (2.19)$$

where rand is the random number between  $-1$  and  $1$ .

### 2.7.3 Parasitism Phase

A relationship established by an organism with another organism of a different species either benefits or harms the other organism; such symbiotic phenomenon is called parasitism. This symbiotic association benefits or harms another organism from the exchange. In this phase, the design vector ( $X_i$ ) of the organism ‘ $i$ ’ (i.e., population) interacts with another design vector ( $X_k$ ) of a randomly selected organism ‘ $k$ ’ of the ecosystem (where  $k \neq i$ ). This vector  $X_k$  is a fusion of design variable of the organism ‘ $i$ ’ and randomly generated design variables. The highly random nature of the phase allows the search to jump into nonvisited regions to escape premature convergence and also permits the local search of visited regions to improve convergence rate. The detailed pseudocode of the cuckoo search algorithm is given below.

START

    Initialize algorithm parameters: population size ( $n$ ), number of function evaluation ( $F$ ), number of design variables ( $m$ ), upper and lower limits for the design variables ( $x_{\text{max}}$ ,  $x_{\text{min}}$ ),

    Evaluate the initial population and obtain the fitness value (i.e., objective function value)

        For  $i=1$  to  $F$

            Identify the best solution of the populations

            Evaluate the mutation vector and update the solution based on the mutation vector using Equations (2.14) to (2.18).

            Apply greedy selection process to preserve the modified solutions.

            Update the solution based on the commensalism phase using Equations (2.19).

            Apply greedy selection process to preserve the modified solutions.

            Update the solution based on the Parasitism phase

            Apply greedy selection process to preserve the modified solutions.

    End

STOP

## 2.8 Water Wave Optimization (WWO) Algorithm

The WWO algorithm, proposed by Zheng (2015), is a metaheuristic inspired by the shallow water wave theory. The WWO algorithm mimics phenomena of water wave moves, such as propagation, refraction, and breakage. In this algorithm, low-energy water waves have large wavelengths that allow making exploration capability stronger during short life cycles, whereas high-energy waves have small wavelengths that allow making exploration capability stronger during long life cycles. Moreover, the progression of the WWO algorithm is controlled by various parameters viz. wavelength ( $\lambda$ ), maximum wave height ( $h_{\max}$ ), wavelength reduction coefficient ( $\alpha$ ), breaking coefficients ( $\beta_{\max}$  and  $\beta_{\min}$ ), and the maximum number of breaking directions ( $k_{\max}$ ).

The WWO algorithm initiates with a randomly generated population (i.e., waves). In the next stage, the population is updated in each generation by ‘propagation operator,’ ‘refraction operator,’ and ‘breaking operator,’ respectively. The process is repeated until the termination criterion is satisfied. The description of each of the operator is explained below.

### 2.8.1 Propagation Operator

At each generation, each wave needs to be propagated exactly once. The propagation operator creates a new wave  $X^{\text{new}}$  by shifting each dimension  $D$  of the original wave  $X$  as

$$X_{i,j}^{\text{new}} = X_{i,j} + \text{rand} \times \lambda L_D \quad (2.20)$$

where rand is the random number in the range of  $-1$  to  $1$ ,  $L_D$  is the length of the  $D$ th dimension of the search space, and  $\lambda$  is the wavelength of each wave and updated as per below equation:

$$\lambda = \lambda \alpha^{\frac{-(f(X) - f_{\min} + \epsilon)}{(f_{\max} - f_{\min} + \epsilon)}} \quad (2.21)$$

where  $f_{\max}$  and  $f_{\min}$  are the maximum and minimum fitness values, respectively; among the current population,  $\alpha$  is the wavelength reduction coefficient, and  $\epsilon$  is a very small positive number to avoid division by zero.

### 2.8.2 Refraction Operator

In wave propagation, if the wave ray is not perpendicular to the isobaths, its direction will be deflected. It is observed that the rays converge in shallow regions while diverging in deep regions. In the WWO, refraction is performed on the waves whose heights decrease to zero based on the following equation:

$$X_{i,j}^{\text{new}} = N\left(\frac{X_{i,j}^{\text{best}} + X_{i,j}}{2}, \frac{|X_{i,j}^{\text{best}} - X_{i,j}|}{2}\right) \quad (2.22)$$

where  $X_{i,j}^{\text{best}}$  is the best solution found so far, and  $N(\mu, \sigma)$  is a Gaussian random number with mean  $\mu$  and standard deviation  $\sigma$ . That is, the new position is a random number centered halfway between the original position and the known best position, and the standard deviation equal to the absolute value of their difference.

After refraction, the wave height of  $X_{i,j}^{\text{new}}$  is also reset to  $h_{\max}$ , and its wavelength is set as

$$\lambda^{\text{new}} = \lambda \frac{f(X^{\text{old}})}{f(X^{\text{new}})} \quad (2.23)$$

### 2.8.3 Breaking Operator

When a wave moves to a position where the water depth is below a threshold value, the wave crest velocity exceeds the wave celerity. Consequently, the crest becomes steeper and steeper, and finally, the wave breaks into a train of solitary waves. In the WWO, the breaking operation is performed as per the below equation:

$$X_{i,j}^{\text{new}} = X_{i,j} + N(0, 1)\beta L_D \quad (2.24)$$

where  $\beta$  is the breaking coefficient. The detailed pseudocode of the WWO algorithm is given below.

START

Initialize algorithm parameters: population size ( $n$ ), number of function evaluation ( $F$ ), number of design variables ( $m$ ), upper and lower limits for the design variables ( $x_{max}$ ,  $x_{min}$ ),

Evaluate the initial population and obtain the fitness value (i.e., objective function value)

For  $i=1$  to  $F$

    Propagate wave  $X$  to obtained wave  $X^{new}$  using Equations (2.20) and (2.21)

    If  $f(X^{new}) > f(X)$

        Set  $X=X^{new}$  and  $f(X)=f(X^{new})$

        Update the wave height

    Else If  $f(X^{new}) > f(X^{best})$

        Perform the breaking operator on  $X^{new}$  using Equation (2.24) and update  $X^{best}$  with  $X^{new}$

    Else

        Perform refraction on wave  $X$  to a  $X^{new}$  using Equation (2.22)

    End

    Update the wave length using Equation (2.23)

End

STOP

## 2.9 Heat Transfer Search (HTS) Algorithm

Heat transfer search (HTS) is a recently developed population-based algorithm proposed by Patel and Savsani (2015). The HTS algorithm inspired from the law of thermodynamics and heat transfer. The fundamental law of thermodynamics states that any system always tries to achieve thermal equilibrium with its surroundings. Therefore, any system lagging thermal equilibrium always tries to achieve thermal equilibrium by conducting heat transfer with surrounding as well as within the different parts of the system. HTS algorithm imitates the behavior of system and surrounding exhibit during the attainment of thermal equilibrium. A system remains in a stable state if it attains thermal equilibrium with the surrounding. The attainment of thermal equilibrium between system and surrounding takes place through the heat transfer between them in the form of the conduction, convection, and radiation. Likewise, the HTS algorithm is composed of three phases called ‘conduction phase,’ ‘convection phase,’ and ‘radiation phase.’ Further, equal importance is given to each phase of the HTS algorithm during the course of optimization. However, any one phase is executed randomly during each generation of the HTS algorithm in the process of optimization.

In the HTS algorithm, populations play a role of molecules of the system while temperature level of the molecules is treated as design variables. At first step, initialization of population takes place randomly, which is subsequently updated in each generation through any one phase of the algorithm mention previously. Each phase shares equal importance, and execution of any one phase takes place randomly with the help of a random number. Further, the greedy selection is

incorporated in the HTS algorithm, so it can accept the updated value of objective function if it is improved. Also, to give more chance to the best solutions, the concept of elitism is also incorporated into the HTS algorithm. Finally, identical solutions (if exists) are replaced to avoid the local trapping of the HTS algorithm. The solution updating process of each phase of the HTS algorithm is explained below.

The conduction phase of the HTS algorithm simulated the conduction heat transfer between the molecules of the substance. In conduction heat transfer, higher-energy-level molecules transmit heat to adjacent lower-energy-level molecules. In the course of optimization with the HTS algorithm, higher- and lower-energy-level molecules are analogous to a population having higher and lesser objective function value. If ' $n$ ' indicates the population size (i.e., number of molecules), ' $m$ ' indicates the design variables (i.e., the temperature level of molecules), and ' $g$ ' indicates the number of generation (i.e., iteration), then in the conduction phase solutions are updated based on the following formula:

$$X'_{j,i} = \begin{cases} X_{k,i} + (-R^2 X_{k,i}), & \text{if } f(X_j) > f(X_k) \\ X_{j,i} + (-R^2 X_{j,i}), & \text{if } f(X_j) < f(X_k) \end{cases}; \quad \text{if } g \leq g_{\max}/\text{CDF} \quad (2.25)$$

$$X'_{j,i} = \begin{cases} X_{k,i} + (-r_i X_{k,i}), & \text{if } f(X_j) > f(X_k) \\ X_{j,i} + (-r_i X_{j,i}), & \text{if } f(X_j) < f(X_k) \end{cases}; \quad \text{if } g > g_{\max}/\text{CDF} \quad (2.26)$$

where  $X'_{j,i}$  is the updated solution;  $j = 1, 2, \dots, n$ ;  $k$  is a randomly selected solution;  $j \neq k$ ;  $k \in (1, 2, \dots, n)$ ;  $i$  is a randomly selected design variable;  $i \in (1, 2, \dots, m)$ ;  $g_{\max}$  is the maximum number of generation specified; CDF is the conduction factor;  $R$  is the probability variable;  $R \in [0, 0.3333]$ ; and  $r_i \in [0, 1]$  is a uniformly distributed random number.

The convection phase of the HTS algorithm simulates convection heat transfer between system and surrounding. In the convective heat transfer, the mean temperature of the system interacts with the surrounding temperature to set a thermal equilibrium. In the course of optimization with the HTS algorithm, the best solution is assumed as a surrounding while the rest of the solution composes the system. So, the design variable of the best solution interacts with the corresponding mean design variable of the population. In this phase, solutions are updated according to the following equations. In the convection phase, solutions are updated based on the following formulas:

$$X'_{j,i} = X_{j,i} + R \times (X_s - X_{ms} \times \text{TCF}) \quad (2.27)$$

$$\text{TCF} = \begin{cases} \text{abs}(R - r_i), & \text{if } g \leq g_{\max}/\text{COF} \\ \text{round}(1 + r_i), & \text{if } g > g_{\max}/\text{COF} \end{cases} \quad (2.28)$$

where  $X'_{j,i}$  is the updated solution;  $j = 1, 2, \dots, n$ ;  $i = 1, 2, \dots, m$ . COF is the convection factor;  $R$  is the probability variable;  $R \in [0.6666, 1]$ ;  $r_i \in [0, 1]$  is a uniformly distributed random number;  $X_s$  be the temperature of the surrounding and  $X_{ms}$  be the mean temperature of the system; and TCF is a temperature change factor.

The radiation phase of the HTS algorithm simulates the radiation heat transfer within the system as well as between system and surrounding. Here, the system (i.e., solution) interacts with the surrounding (i.e., the best solution) or within the system (i.e., other solution) to establish a thermal balance. In other words, this situation represents the update of any solution with the help of the best solution or any other randomly selected solution. In this phase, solutions are updated below:

$$X'_{j,i} = \begin{cases} X_{j,i} + R \times (X_{k,i} - X_{j,i}), & \text{if } f(X_j) > f(X_k) \\ X_{j,i} + R \times (X_{j,i} - X_{k,i}), & \text{if } f(X_j) < f(X_k) \end{cases}; \text{ if } g \leq g_{\max}/\text{RDF} \quad (2.29)$$

$$X'_{j,i} = \begin{cases} X_{j,i} + r_i \times (X_{k,i} - X_{j,i}), & \text{if } f(X_j) > f(X_k) \\ X_{j,i} + r_i \times (X_{j,i} - X_{k,i}), & \text{if } f(X_j) < f(X_k) \end{cases}; \text{ if } g > g_{\max}/\text{RDF} \quad (2.30)$$

where  $X'_{j,i}$  is the updated solution;  $j = 1, 2, \dots, n$ ;  $i = 1, 2, \dots, m$ ;  $j \neq k$ ;  $k \in (1, 2, \dots, n)$  and  $k$  is a randomly selected molecules; RDF is the radiation factor;  $R$  is the probability variable;  $R \in [0.3333, 0.6666]$ ; and  $r_i \in [0, 1]$  is a uniformly distributed random number. The detailed pseudocode of the HTS algorithm is given below.

## START

Initialize algorithm parameters: population size ( $n$ ), number of function evaluation ( $F$ ), number of design variables ( $m$ ), upper and lower limits for the design variables ( $x_{\max}$ ,  $x_{\min}$ ), conduction factor, convection factor, and radiation factor.

Evaluate the initial population and obtain the fitness value (i.e., objective function value)

For  $i=1$  to  $F$

    Randomly generate the probability ‘R’

    If  $R \leq 0.3333$

        Update the solution based on conduction phase using Equations (2.25) and (2.26).

    Else If  $0.3333 < R \leq 0.6666$

        Update the solution based on radiation phase using Equations (2.27) and (2.28).

    Else

        Update the solution based on convection phase using Equations (2.29) and (2.30).

    End

    Apply greedy selection process to preserve the modified solutions.

End

## STOP

## 2.10 Passing Vehicle Search (PVS) Algorithm

The PVS algorithm, proposed by Savsani and Savsani (2016), is a novel metaheuristic algorithm. The PVS algorithm mimics the vehicle passing mechanism on a two-lane highway. The most important criteria are to have a safe overtaking opportunity (passing) on a two-lane vehicle passing mechanism. This mechanism depends on many complex, interdependent parameters such as the availability of gaps in the opposing traffic stream, speed, and acceleration of individual vehicles, traffic, and a driver's skill, as well as road and weather conditions. The PVS algorithm considers three types of vehicles (namely back vehicle (BV), front vehicle (FV), and oncoming vehicle (OV)) on two-lane highways, which are responsible for the passing mechanism. BV intends to pass FV. However, it is only possible if FV speed is slower as compared to BV. If FV speed is higher as compared to BV, then no passing is possible. Moreover, passing depends on the position and speed of OV, and also on the distance between them and their velocities. Therefore, Savsani and Savsani (2016) considered various conditions as follows:

Assume three different vehicles (BV, FV, and OV) on a two-lane highway having different velocities ( $V_1$ ,  $V_2$ , and  $V_3$ ) with  $x$  being the distance between BV and FV, and  $y$  being the distance between FV and OV at any particular time instance. This results in two primary conditions based on the velocity of FV and BV, i.e., FV is slower than BV ( $V_1 > V_3$ ) and vice versa. If FV is faster than BV, then no passing is possible, and BV can move with its desired velocity. Passing is possible only if FV is slower than BV. In this situation also, overtaking is only possible, if the distance from the FV at which overtaking occurs is less than the distance traveled by OV. Therefore, different conditions arise for the selected vehicles. The mathematical formulation of these conditions is given below:

**Primary condition—I (FV is slower than BV)**

$$X'_{r_1} = X_{r_1} + V_{co} \times \text{rand} \times (X_{r_1} - X_{r_3}) \quad (2.31)$$

where  $X_{r_1}$  is the current solution, i.e., BV.  $X'_{r_1}$  is the updated value of the current solution.  $X_{r_3}$  is the randomly selected solution, i.e., FV.  $V_{co}$  is the relative velocity by considering FV and BV and is given by

$$V_{co} = \frac{V_1}{V_1 - V_3} \quad (2.32)$$

where the vehicle velocity ( $V$ ) is calculated based on the following equation:

$$V_k = \frac{R_k}{1 - D_k} \quad k = 1, 2, 3 \quad \text{and} \quad R \in [0, 1] \quad (2.33)$$

$$D_k = \frac{r_k}{n} \quad k = 1, 2, 3 \quad (2.34)$$

where  $D$  is the distance travel and  $n$  is the population size.

**Secondary condition—1 (FV is slower than BV, but distance travel by OV is less than Overtaking distance)**

$$X'_{r_1} = X_{r_1} + \text{rand} \times (X_{r_1} - X_{r_2}) \quad (2.35)$$

where rand is the random number between 0 and 1, and  $X_{r_2}$  is the randomly selected solution, i.e., OV.

**Primary condition—2 (FV is Faster than BV)**

$$X'_{r_1} = X_{r_1} + \text{rand} \times (X_{r_3} - X_{r_1}) \quad (2.36)$$

where  $X_{r_1}$  is the current solution, i.e., BV.  $X'_{r_1}$  is the updated value of the current solution.  $X_{r_3}$  is the randomly selected solution, i.e., FV.  $X_{r_2}$  is the randomly selected solution, i.e., OV. The detailed pseudocode of the PVS algorithm is given below.

START

    Initialize algorithm parameters: population size ( $n$ ), number of function evaluation ( $F$ ), number of design variables ( $m$ ), upper and lower limits for the design variables ( $x_{max}$ ,  $x_{min}$ ).

    Evaluate the initial population and obtain the fitness value (i.e., objective function value)

    For  $i=1$  to  $F$

        Select three vehicles (BV, OV, and FV) i.e.,  $r_1$ ,  $r_2$ , and  $r_3$  such that  $r_1 = r_i$  (BV i.e., current solution)

        Select two random vehicles  $r_2$  (OV) and  $r_3$  (FV);  $r_1 \neq r_2 \neq r_3$ /

        Calculate the distances ( $D$ ) and velocities ( $V$ ) of the vehicles using Equations (2.32) to (2.34).

        Update the position of the vehicle, i.e., (update solution) based on the primary and secondary condition using Equations (2.31), (2.35) and (2.36).

        Apply greedy selection process to preserve the modified solutions.

    End

STOP

## 2.11 Sine Cosine Algorithm (SCA)

The SCA algorithm, proposed by Mirjalili (2016), is an effective metaheuristic. The SCA theory mimics a mathematical model based on sine and cosine functions. The cyclic configuration of sine and cosine function guides exploration and exploitation of the search space. The SCA algorithm starts with a set of randomly generated random population. In the next stage, the population is updated through a set of rules in each generation by sine and cosine functions. Subsequently, the SCA algorithm gradually transits from exploration to exploitation with the use of several random and adaptive variables. The process is repeated until the termination criterion is satisfied.

The SCA is a population-based algorithm that starts with a random set of solutions positioned randomly in the search space. The search agents are guided toward an optimal solution in the search space. The SCA maintains a population of  $n$  search agents, and each agent is represented by  $d$ -dimensions decision variable vector. Also, the algorithm keeps track of the best solution's position achieved by all search agents in the population. The mathematical model used in the SCA algorithm is based on the following update function:

$$X_{i,j}^{\text{new}} = \begin{cases} X_{i,j} + r_1 \text{Sin}(r_2) |r_3 P_j - X_{i,j}| & \text{if } r_4 < 0.5 \\ X_{i,j} + r_1 \text{Cos}(r_2) |r_3 P_j - X_{i,j}| & \text{if } r_4 \geq 0.5 \end{cases} \quad (2.37)$$

where  $X_{i,j}$  is the position of current solution;  $r_1$ ,  $r_2$ ,  $r_3$ , and  $r_4$  are the random numbers; and  $P$  is the position of the best solution.

As the above equation shows, there are four main parameters in SCA:  $r_1$ ,  $r_2$ ,  $r_3$ , and  $r_4$ . The parameter  $r_1$  dictates the next position regions (or movement direction) which could be either in the space between the solution and destination or outside it. The parameter  $r_2$  defines how far the movement should be toward or outward the destination. The parameter  $r_3$  gives random weights for a destination in order to stochastically emphasize ( $r_3 > 1$ ) or deemphasize ( $r_3 < 1$ ) the effect of desalination in defining the distance. Finally, the parameter  $r_4$  equally switches between the sine and cosine components of the above equation. In order to balance the exploration and exploitation in SCA algorithm,  $r_1$  is given by the below equation:

$$r_1 = a - \frac{a \times g}{g_{\max}} \quad (2.38)$$

where  $g$  is the current iteration,  $g_{\max}$  is the maximum iteration, and  $a$  is the constant. The detailed pseudocode of the SCA algorithm is given below.

START

Initialize algorithm parameters: population size ( $n$ ), number of function evaluation ( $F$ ), number of design variables ( $m$ ), upper and lower limits for the design variables ( $x_{max}$ ,  $x_{min}$ ).

Evaluate the initial population and obtain the fitness value (i.e., objective function value)

For  $i=1$  to  $F$

    Identify the best solution of the populations

    Generate the random number  $r_1, r_2, r_3$ , and  $r_4$

    Update the solution by using Equation (2.37) based on the value of  $r_1, r_2, r_3$ , and  $r_4$

    Apply greedy selection process to preserve the modified solutions

    Update  $r_1$  using Equation (2.38)

End

STOP

## 2.12 Parameter Tuning of Algorithms

The performance of the metaheuristic algorithms for obtaining the optimum value of any problem is always depended on the tuning of the control parameters of the algorithms. All the metaheuristic algorithms are probabilistic algorithms and require common controlling parameters like population size and the number of function evaluation. Apart from the common control parameters, the different algorithm requires its own algorithm-specific control parameters. So, a series of experiments are conducted with all the metaheuristic algorithms considered in this work with a different combination of control parameters. Based on the experimental results, the following control parameters are set for the different algorithms used for the optimization of various thermal systems in this work.

- **Genetic algorithm (GA)**

Population size = 50

Number of function evaluation = 10,000

Mutation rate = 0.05

Crossover rate = 0.8

- **Particle swarm optimization (PSO) algorithm**

Population size = 50

Number of function evaluation = 10,000

Inertia weight ( $w$ ) = 0.9

Cognitive parameter ( $c_1$ ) = 2

Social parameter ( $c_2$ ) = 2

- **Differential evolution (DE) algorithm**

Population size = 50

Number of function evaluation = 10,000

Combination factor ( $K$ ) = 1

Scaling factor ( $F$ ) = 0.5

Crossover constant ( $CR$ ) = 0.8

- **Artificial bee colony (ABC) algorithm**

Population size = 50

Number of function evaluation = 10,000

Limit = 50

- **Cuckoo search optimization (CSO)**

Population size = 50

Number of function evaluation = 10,000

Fraction of worse nests ( $p_a$ ) = 0.5

Lévy exponent ( $\lambda$ ) = 1.5

- **Teaching–learning-based optimization (TLBO) algorithm**

Population size = 50

Number of function evaluation = 10,000

- **Symbiotic organism search (SOS) algorithm**

Population size = 50

Number of function evaluation = 10,000

- **Water wave optimization (WWO) algorithm**

Population size = 50

Number of function evaluation = 10,000

Maximum height of wave ( $h_{\max}$ ) = 10

Wavelength reduction coefficient ( $\alpha$ ) = 1.0026

Maximum breaking coefficient ( $\beta_{\max}$ ) = 0.25

Minimum breaking coefficient ( $\beta_{\min}$ ) = 0.001

$\varepsilon$  = 0.0000001;

- **Heat transfer search (HTS) algorithm**

Population size = 50

Number of function evaluation = 10,000

Conduction factor = 2

Convection factor = 10

Radiation factor = 2

- **Passing vehicle search (PVS) algorithm**

Population size = 50

Number of function evaluation = 10,000

- **Sine cosine algorithm (SCA)**

Population size = 50

Number of function evaluation = 10,000

Constant parameter ( $a$ ) = 1

The above-mentioned control parameters are set for each of the metaheuristic algorithms during the optimization of various thermal systems in the subsequent chapters.

## References

- Cheng M.Y., Prayogo D. (2014) ‘Symbiotic Organisms Search: A new metaheuristic optimization algorithm’, *Computers & Structures*, vol. 139, 98–112.
- Holland J. (1975) *Adaptation in Natural and Artificial Systems*. University of Michigan Press, Ann Arbor.
- Karaboga, D. (2005) An idea based on honey bee swarm for numerical optimization, Technical Report TR06, Computer Engineering Department, Erciyes University, Turkey, 2005.
- Karaboga, D., Basturk, B. (2007a) A powerful and efficient algorithm for numerical function optimization: artificial bee colony algorithm, *Journal of Global Optimization* 39, 45–47.
- Karaboga, D., Basturk, B. (2007b) Artificial bee colony (ABC) optimization algorithm for solving constrained optimization problems, *Lecture Notes in Artificial Intelligence* 4529, Springer-Verlag, Berlin.
- Kennedy, J., Eberhart, R. (1995) Particle swarm optimization, In: *Proceedings of IEEE International Conference on Neural Networks*, Perth, Australia, pp. 1942–1948.
- Kennedy, J., Eberhart, R. (1997) A discrete binary version of the particle swarm algorithm, In: *Proceedings of IEEE International Conference on Systems, Man, and Cybernetics*, Piscataway, NJ, pp. 4104–4109.
- Mirjalili S. (2016) ‘SCA: a sine-cosine algorithm for solving optimization problems. *Knowledge-Based Systems*’, vol. 96, pp. 120–133.
- Patel V.K. and Savsani V.J. (2015) ‘Heat transfer search (HTS): a novel optimization algorithm’, *Information Sciences*, vol. 324, pp. 217–246.
- Payne, R. B., Sorenson, M. D., & Klitz, K. (2005). *The cuckoos* (Vol. 15). Oxford University Press.
- Rao SS. (2009) *Engineering optimization: theory and practice*. John Wiley & Sons.
- Rao R.V., Savsani V.J. and Vakharia D.P. (2011) ‘Teaching–learning-based optimization: a novel method for constrained mechanical design optimization problems’, *Computer-Aided Design*, vol. 43(3), pp. 303–315.
- Savsani P. and Savsani V. (2016) ‘Passing vehicle search (PVS): A novel metaheuristic algorithm’, *Applied Mathematical Modelling*, vol. 40(5–6), pp. 3951–3978.
- Storn R., Price K. (1997) ‘Differential evolution – a simple and efficient heuristic for global optimization over continuous spaces’, *Journal of Global Optimization*, vol. 11, 341–359.
- Wolpert, D.H., Macready, W.G. (1997) ‘No free lunch theorems for optimization’, *IEEE Transactions on Evolutionary Computation*, vol. 1(1), 67–82.
- Yang, X. S., & Deb, S. (2009). Cuckoo search via Levey flights. In *Proceedings of the World Congress on nature and biologically inspired computing* (Vol. 4, pp. 210–214), NABIC: Coimbatore.
- Yang, X. S., & Deb, S. (2010). Engineering optimization by cuckoo search. *International Journal of Mathematical Modelling & Numerical Optimization*, 1(4), 330–343.
- Yang, X. S. (2010). *Nature-inspired metaheuristic algorithms*. Luniver Press.
- Zheng Y.J. (2015) ‘Water wave optimization: a new nature-inspired metaheuristic. *Computers & Operations Research*’, vol. 55, pp. 1–11.

# Chapter 3

## Thermal Design and Optimization of Heat Exchangers



**Abstract** Heat exchangers are energy conservation equipment used to transfer heat between hot and cold fluid. In this chapter, thermal modeling of different types of heat exchangers like shell and tube heat exchanger, plate-fin heat exchanger, fin and tube heat exchanger, plate heat exchanger, and rotary regenerator is presented. The objective function for each of the heat exchanger is derived from the thermal model. Optimization of a derived objective is performed by implementing 11 different metaheuristic algorithms for each heat exchanger, and comparative results are tabulated and discussed.

Heat exchangers are one of the important equipment which serves the purpose of heat recovery through heat transfer between two or more streams of fluid available at a different temperature. Thermal design and optimization of heat exchangers play an important role in the effective heat recovery from any heat exchanger, which requires an integrated knowledge of thermodynamics, heat transfer, fluid dynamics, and cost evaluation (Hewitt 1998; Shah and bell 2000; Rohsenow and Hartnett 1973). Generally, objectives involved in the optimization of heat exchangers are the minimum cost, maximum effectiveness, minimum pressure drop, etc. The conventional approach for the optimization of heat exchangers is lengthy and doesn't ensure the optimum solution. On the other hand, the application of metaheuristic algorithms makes the design-optimization process of heat exchanger easy and accurate. In the subsequent section, thermal modeling and optimization of various heat exchangers are presented and discussed.

### 3.1 Shell and Tube Heat Exchanger (STHE)

Shell and tube heat exchanger (STHE) is a widely used heat exchanger. This heat exchanger is generally made of a bundle of round tubes mounted in a cylindrical shell. One fluid flows inside the tubes, and the other flows across and along with the tubes. The major parts of this heat exchanger are tubes, shell, front-end head,

rear-end head, baffles, and tube sheets. The most common types of shell and tube heat exchangers are fixed tube design, U-tube design, and floating head design. In all three types, the front head is stationary while the rear-end head can be either fixed or moving. In fixed tube design, the tube sheet is joined to the shell. This results in uncomplicated construction, and tube bores can be washed mechanically and chemically. U-tube designs have two passes of fluid in the heat exchanger tubes, which increases the effectiveness of the heat exchanger. In floating head type, the tube sheet at the rear header end is not welded to the shell but allowed to move or float. The tube sheet at the front header is of bigger diameter than shell secured in the same way to that used in the fixed tube sheet design. A floating head exchanger is suitable for precise duties related to high temperature and pressure but is more costly than equivalent fixed tube sheet exchanger. Figure 3.1 shows the schematic diagram of STHE with major components.

The wide applicability of STHE is due to its robustness and ability to operate under a wide range of fluid pressures, fluid flow rate, and fluid temperatures. The other advantages of STHEs are less pressure drop compared to the compact heat exchanger; pressure measurement and leak test can be easily done mounted gauges; and high effectiveness as compared to double-tube heat exchanger. At the same time, some drawbacks are also associated with the STHE like thermal expansion of the tubes can be problematic if clearance is inadequate or fluid is at a higher temperature; cleaning and maintenance are difficult; and fouling inside the tubes is a major concern. STHEs are generally used in power generation, refrigeration, refineries and petrochemical industries, heating and air-conditioning industries, and pharmaceutical industries.

The heat duty of any STHEs is decided based on fluid flow rate and temperatures of hot and cold fluid. After that, the size of the heat exchanger is determined. Determination of the size of heat exchanger requires appropriate selection of design

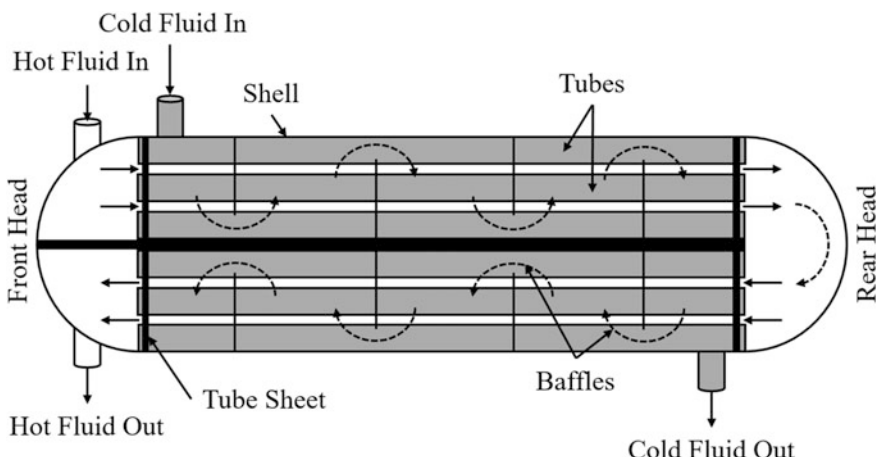


**Fig. 3.1** Schematic diagram of shell and tube heat exchanger

variables like shell diameter, tube diameter, number of tubes, tube pitch, etc., which can meet the required heat duty and also economically viable. The total cost of any STHEs includes initial cost and operating cost. Initial cost is associated with the heat transfer area while operating cost is associated with the pumping power and maintenance. Further, the heat exchanger geometry aimed for minimum initial cost results in higher operating cost and vice versa (Kakac and Liu 2002; Shah and Sekulic 2003a, b). Hence, the optimization of design variables is essential for the minimum total cost design of STHEs.

Thermal design of STHEs is based on either Kern's methodology (1950) or Bell–Delaware methodology (1963, 1981). Kern's method for design of STHEs is a simplified one while Bell–Delaware method is more accurate. Previously, researchers carried out the optimization of STHEs by adapting Kern's or Bell–Delaware method and using different optimization algorithms. Soltan et al. (2004) optimized the baffle spacing of STHE for minimizing the capital and operating cost of STHE. Selbas et al. (2006) carried out the optimization of STHE for minimization of total cost of the heat exchanger. The authors used genetic algorithm (GA) as an optimization tool and considered shell diameter, tube diameter, tube layout, tube passes, baffle spacing, and baffle cut as design variables. Eryener (2006) performed thermo-economical analysis to determine the optimum baffle spacing of STHEs. Ozcelik (2007) used GA to optimize nonlinear sizing problem of STHE. The author considered minimization of total cost of the heat exchanger in his investigation. Wildi-Tremblay and Gosselin (2007) adopted the standard Bell–Delaware approach combined with maintenance consideration of STHE for obtaining the cost-effective geometry of STHE. The authors considered eleven design variables and used GA as an optimization tool in their investigation. Babu and Munawar (2007) perform the economic optimization of STHEs by adopting differential evolution (DE) algorithm. The authors also present comparative performance of GA and DE in the optimization of STHEs. Caputo et al. (2008) obtained the optimal geometry of STHE for minimum total annual cost consideration by optimizing shell diameter, tube diameter, and baffle spacing. The authors used GA as an optimization tool. Agarwal and Gupta (2008) obtained the STHE geometry for minimum total cost and minimum cooling water requirement consideration by applying GA and Bell–Delaware approach. Costa and Queiroz (2008) presented a mathematical formulation of STHE in order to reduce excess area and pressure drop of the heat exchanger, which in turn reduces the cost of the heat exchanger.

Guo et al. (2009) carried out thermodynamic optimization of STHEs by using GA. The authors considered optimization of five design variables for minimum entropy generation of STHEs. Fesanghary et al. (2009) used the harmony search algorithm for the economic optimization of STHE. The authors also performed the sensitivity analysis to identify the important design variables of STHE. Ponce-Ortega et al. (2009) adopted Bell–Delaware approach combined with GA for the optimization of STHE. The authors optimized geometric parameters of STHEs like tube diameter, tube layout, tube-passes, tube pitch, number of sealing strips, and baffle spacing for the minimum total cost of STHE. Ravagnani et al.

(2009) used the particle swarm optimization (PSO) algorithm to minimize the area and pumping cost of STHEs. The authors used Bell–Delaware method for the shell-side calculations and analyzed three case studies of STHEs. Sanaye and Hajabdollahi (2010a, b) presented STHE geometry for maximum effectiveness and minimum total cost criteria by considering seven design variables and GA. Rao and Patel (2010) applied PSO algorithm to the obtained optimal geometric parameter of STHE, which in turn reduces the total cost of the heat exchanger. The authors analyzed four case studies of STHE in their investigation.

Rao and Patel (2011a, b, c) presented a comparative performance of swarm optimization algorithms, namely PSO and civilized swarm optimization (CSO) algorithms, for economic optimization of STHE. Hajabdollahi et al. (2011a, b) presented a comparative performance of GA and PSO algorithm in the thermo-economic optimization of the shell and tube condenser. Azad et al. (2011) employed constructal theory-based approach combined with GA to obtain the cost-effective design of STHEs. Caputo et al. (2011) presented the optimal configuration of STHE for minimum life cycle cost of the heat exchanger by adapting GA. Şahin et al. (2011) used artificial bee colony (ABC) algorithm combined with Kern’s methodology for the economic optimization of STHEs. Hajabdollahi et al. (2012) implemented GA to obtain the maximum exergetic efficiency and minimum total cost design of STHEs. The authors used e-NTU method combined with Bell–Delaware procedure in their investigation. Hadidi et al. (2013) obtained the optimized value of tube diameter, tube length, and baffle spacing by applying imperialist competitive algorithm (ICA) for minimum cost design of STHEs. Hadidi and Nazari (2013) analyzed three case studies of STHE for economic optimization. Rao and Patel (2013) performed the thermo-economic optimization of STHE by using a modified version of teaching–learning-based optimization (TLBO) algorithm. The authors considered heat transfer rate and total cost of the heat exchanger as objective functions.

Amin and Bazargan (2014) carried out thermodynamic optimization of STHE with eleven design variables. The authors considered maximum heat transfer rate and minimum total cost of the heat exchange as objective functions. The authors employed biogeography-based optimization (BBO) algorithm as an optimization tool. Sadeghzadeh et al. (2015) demonstrated the performance of GA and PSO algorithm in the techno-economical optimization of STHE. Caputo et al. (2015) analyzed four case studies of STHE for its weight reduction by using GA. The authors also compared the optimal geometry of the heat exchanger obtained with GA and commercial software. Khosravi et al. (2015) presented the performance comparison of three different evolutionary algorithms employed for economic optimization of STHE. Mohanty (2016a, b) used gravitational search algorithm (GSA) and firefly algorithm for economic optimization of STHE. Wong et al. (2016) carried out the optimization of capital cost and operating cost of STHE using GA. Wen et al. (2016a, b, c) carried out the optimization of helical baffle STHE with three design variables and demonstrated the comparison between optimized and conventional STHE design in their investigation. Caputo et al. (2016) obtained optimum length-to-diameter ratio of STHE based on their mathematical model.

Hajabdollahi et al. (2016) attempted a STHE problem with nine design variables and employed GA to perform its economic optimization. The authors also investigated the effect of design variable on optimum value of objective function.

Abed et al. (2016) used the electromagnetism-like algorithm (EM) to reduce the cost of STHEs. The authors analyzed different case studies of STHE to demonstrate the effectiveness of EM algorithm. Hajabdollahi and Hajabdollahi (2016) used GA to optimize STHE with nanoparticles from the thermo-economic viewpoint and investigated the effect of nanoparticles on the optimized geometry of STHE. Mirzaei et al. (2017) applied GA coupling with the constructal theory to obtain STHEs design aiming for maximum effectiveness and minimum total cost. Segundo et al. (2017) applied Tsallis differential evolution algorithm to identify the optimum value of shell diameter, tube diameter, and baffle spacing to obtain the cost-effective design of STHEs. Raja et al. (2017a, b, c) performed the many-objective optimization of STHEs by adapting the heat transfer search (HTS) algorithm. The authors considered maximization of effectiveness and minimization of total cost, pressure drop, and the number of entropy generation units of heat exchanger simultaneously.

### 3.1.1 Thermal Model

Heat transfer, pressure drop, and economic estimation of STHEs are carried out in this section. Bell–Delaware method is adopted in this work for the shell-side design while Kern’s methodology is used for the tube side design of STHE. Further, the thermal–hydraulic model presented here is based on the previous works of Shah and Sekulic (2003a, b), Wildi-Tremblay and Gosselin (2007), and Rao and Patel (2011a, b, c). Figure 3.2 shows the geometry of STHE for a better understanding of the thermal–hydraulic model. Moreover, during the discussion of the thermal–hydraulic model, the subscripts associated with different equations are as follows: t stands for tube side; s stands for shell side; h stands for hot fluid; c stands for cold fluid; i stands for the internal side; and o stands for outer side.

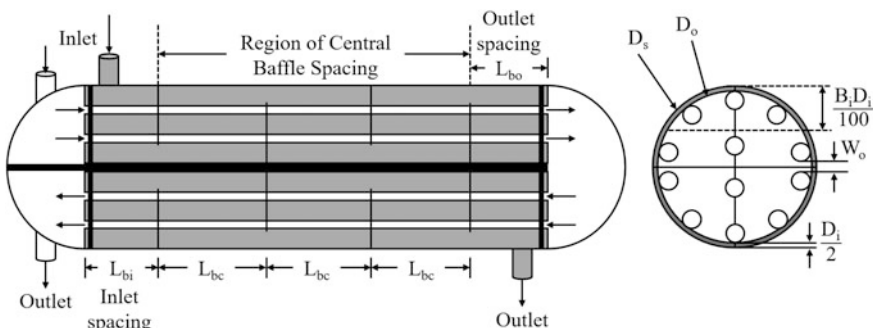


**Fig. 3.2** Shell and tube heat exchanger geometry

### (a) Tube-side heat transfer and pressure drop

The velocity of the fluid passing through the tubes ( $v_t$ ) is required for the calculation of tube-side heat transfer coefficient. Further, the flow velocity of the tube-side fluid depends on the number of tubes ( $N_t$ ) and tube passes ( $N_p$ ) and is calculated from the below equation:

$$v_t = \frac{m_t}{A_t \rho_t} * \left( \frac{N_p}{N_t} \right) \quad (3.1)$$

where  $A_t$  is the cross-section area of the tube and is given by

$$A_t = \frac{\pi}{4} d_{i,t}^2 \quad (3.2)$$

Tube-side heat transfer coefficient ( $h_t$ ) is calculated from the following equation:

$$h_t = 0.023 \frac{k_t}{d_i} Re_t^{0.8} Pr_r^{1/3} \left( \frac{\mu_t}{\mu_w} \right)^{0.14} \quad (3.3)$$

where  $k$  is the thermal conductivity,  $Pr$  is the Prandtl number,  $\mu$  is the viscosity,  $d_i$  is the tube internal diameter, and  $Re_t$  is the tube-side Reynolds number and are computed using the below equation.

$$Re_t = \left( \frac{\rho v d_i}{\mu} \right)_t \quad (3.4)$$

Tube-side pressure drop can be easily obtained by combining the pressure drop in straight tubes and pressure drop in the elbow, fitting, etc. The following equation is used to calculate the total pressure drop in the tube side:

$$\Delta P_t = \frac{\rho_t v_t^2}{2} \left( \frac{L}{d_i} f_t + 4 \right) N_p \quad (3.5)$$

where  $\rho$  is the density of the fluid,  $L$  is the length of the tubes, and  $f_t$  is the tube-side friction factor and are computed using the following equation.

$$f_t = (1.82 \log 10^{Re_t} - 1.64)^{-2} \quad (3.6)$$

### (b) Shell-side heat transfer and pressure drop

Bell–Delaware method is used for the calculation of the shell-side heat transfer and pressure drop. According to the Bell–Delaware method, shell-side heat transfer

coefficient is based on the ideal heat transfer coefficient and different correction factors. The ideal heat transfer coefficient ( $h_{id}$ ) for shell side is calculated by the following equation:

$$h_{id} = j \frac{C_{ps} Pr_s^{-\frac{2}{3}}}{A_{o,cr}} \quad (3.7)$$

where  $j$  is the Colburn factor,  $C_p$  is the specific heat of the fluid, and  $A_{o,cr}$  is the flow area near the shell centerline for one cross-flow section. Based on the ideal heat transfer coefficient, the actual heat transfer coefficient for the shell side is calculated by

$$h_s = h_{id} J_c J_s J_l J_b J_r \quad (3.8)$$

where  $J_c$ ,  $J_s$ ,  $J_l$ ,  $J_b$ , and  $J_r$  are correction factors.  $J_c$  takes into account the effect of baffle cut and spacing and is given by

$$J_c = 0.55 + 0.72 F_c \quad (3.9)$$

where  $F_c$  represents the fraction of the total number of tubes in the cross-flow section.

Second correction factor  $J_s$  takes into account the effect of variation in baffle spacing and is calculated by

$$J_s = \frac{N_b - 1 + (L_i)^{1-e} + (L_o)^{1-e}}{N_b - 1 + L_i + L_o} \quad (3.10)$$

where  $N_b$  is the number of baffles and  $e$  is the coefficient and depends on the type of flow ( $e = 0.33$  for laminar flow and  $e = 0.6$  for turbulent flow). Factors  $L_i$  and  $L_o$  correlated the central baffle distance with inlet and outlet and are obtained using the following equations:

$$L_i = \frac{L_{b,i}}{L_{b,c}} \quad (3.11)$$

$$L_o = \frac{L_{b,o}}{L_{b,c}} \quad (3.12)$$

where  $L_{b,i}$ ,  $L_{b,o}$ , and  $L_{b,c}$  are inlet, outlet, and central baffle spacing, respectively.

The third correction factor ( $J_l$ ) takes into account the effect of shell-to-baffle and tube-to-baffle leakage and is given by

$$J_l = 0.44(1 - r_s) + [1 - 0.44(1 - r_s)] \exp\left(\frac{-2.2}{r_{lm}}\right) \quad (3.13)$$

where the factors  $r_s$  and  $r_{lm}$  depend on the shell-to-baffle leakage flow area ( $A_{o,sb}$ ) and tube-to-baffle leakage flow area ( $A_{o,tb}$ ) and are calculated by

$$r_s = \frac{A_{o,sb}}{A_{o,sb} + A_{o,tb}} \quad (3.14)$$

$$r_{lm} = \frac{A_{o,sb} + A_{o,tb}}{A_{o,cr}} \quad (3.15)$$

Fourth correction factor  $J_b$  takes into account the effect of the bundle and pass partition bypass stream and is given by

$$J_b = \exp \left[ -Cr_b \left( 1 - (2N_{ss}^+)^{0.33} \right) \right] \text{ (for } N_{ss}^+ \leq 0.5 \text{)} \quad (3.16)$$

$$J_b = 1 \text{ (for } N_{ss}^+ \geq 0.5 \text{)} \quad (3.17)$$

where  $C = 1.35$  for  $Re_s \leq 100$  and  $C = 1.25$  for  $Re_s \geq 100$ ; the factors  $N_{ss}^+$  and  $r_b$  depend on the flow bypass surface area ( $A_{o,bp}$ ) and number of sealing strip ( $N_{ss}$ ) and are given by

$$r_b = \frac{A_{o,bp}}{A_{o,cr}} \quad (3.18)$$

$$N_{ss}^+ = \frac{N_{ss}}{N_{r,cc}} \quad (3.19)$$

Fifth correction factor  $J_r$  takes into account any adverse temperature gradient. In the present study, we consider its value as 1.

The Colburn factor required to calculate shell-side heat transfer coefficient is obtained by the following equation:

$$j = a_1 \left( \frac{1.33}{P_T/d_o} \right)^a (Re_s)^{a_2} \quad (3.20)$$

where  $P_T$  is the tube pitch and  $d_o$  is the outer tube diameter. The coefficient  $a$  is obtained from the following equation:

$$a = \left( \frac{a_3}{1 + 0.14(Re_s)^{a_4}} \right) \quad (3.21)$$

where the coefficients  $a_1$ ,  $a_2$ ,  $a_3$ , and  $a_4$  are obtained from Table 3.1.  $Re_s$  is the Reynolds number of shell-side fluid and is obtained using the following equation:

**Table 3.1** Coefficient for Colburn factor and friction factor

Angle	Reynolds Number	$a_1$	$a_2$	$a_3$	$a_4$	$b_1$	$b_2$	$b_3$	$b_4$
90	<10	0.97	-0.667	-	-	35	-1	-	-
	$10^1\text{--}10^2$	0.9	-0.631	-	-	32.1	-0.963	-	-
	$10^2\text{--}10^3$	0.408	-0.46	-	-	6.09	-0.602	-	-
	$10^3\text{--}10^4$	0.107	-0.266	-	-	0.0815	0.022	-	-
	$10^4\text{--}10^5$	0.37	-0.395	1.187	0.37	0.391	-0.418	6.3	0.378
45	<10	1.55	-0.667	-	-	32	-1	-	-
	$10^1\text{--}10^2$	0.498	-0.656	-	-	26.2	-0.913	-	-
	$10^2\text{--}10^3$	0.73	-0.5	-	-	3.5	-0.476	-	-
	$10^3\text{--}10^4$	0.37	-0.396	-	-	0.333	-0.136	-	-
	$10^4\text{--}10^5$	0.37	-0.396	1.93	0.5	0.303	-0.126	6.59	0.52
30	<10	1.4	-0.667	-	-	48	-1	-	-
	$10^1\text{--}10^2$	1.36	-0.657	-	-	45.1	-0.973	-	-
	$10^2\text{--}10^3$	0.593	-0.477	-	-	4.57	-0.476	-	-
	$10^3\text{--}10^4$	0.321	-0.388	-	-	0.486	-0.152	-	-
	$10^4\text{--}10^5$	0.321	-0.388	1.45	0.519	0.372	-0.123	7	0.5

$$Re_s = \frac{m_s d_o}{\mu_s A_{o,cr}} \quad (3.22)$$

where  $m_s$  is the mass flow rate of shell-side fluid and  $A_{o,cr}$  is the flow area at the shell centerline for one cross-flow section.

The heat transfer surface area ( $A$ ) of the shell and tube heat exchanger is obtained by

$$A = \frac{Q}{UF\Delta T_{LM}} \quad (3.23)$$

where  $Q$  is the heat duty of heat exchanger,  $F$  is the temperature correction factor,  $U$  is the overall heat transfer coefficient, and  $\Delta T_{LM}$  is the logarithmic mean temperature difference of the heat exchanger and are obtained using the following equations:

$$Q = m_h C_{p,h} (T_{h,i} - T_{h,o}) = m_c C_{p,c} (T_{c,o} - T_{c,i}) \quad (3.24)$$

$$U = \frac{1}{\left(\frac{1}{h_s} + R_{fs} + \left(\frac{d_o \ln\left(\frac{d_o}{d_i}\right)}{2k_w}\right) + \frac{d_o}{d_i} \left(R_{ft} + \frac{1}{h_i}\right)\right)} \quad (3.25)$$

$$\Delta T_{LM} = \frac{(T_{h,i} - T_{c,o}) - (T_{h,o} - T_{c,i})}{\ln \left( \frac{(T_{h,i} - T_{c,o})}{(T_{h,o} - T_{c,i})} \right)} \quad (3.26)$$

where  $T$  is the temperature of the fluid and  $R_f$  is the fouling factor.

Based on the heat transfer surface area, the required length of the heat exchanger is obtained by

$$L = \frac{A}{\pi d_o N_t} \quad (3.27)$$

For the estimation of pressure drop, the effective number of tube rows is required. The number of effective tube rows crosses in one window section ( $N_{r,cw}$ ) and the number of effective tube rows baffle section ( $N_{r,cc}$ ) are calculated using the following equations:

$$N_{r,cw} = \frac{0.8}{P_p} \left[ D_s \left( \frac{B_c}{100} \right) - \frac{D_s - D_{ctl}}{2} \right] \quad (3.28)$$

$$N_{r,cc} = \frac{D_s}{P_p} \left[ 1 - 2 \left( \frac{B_c}{100} \right) \right] \quad (3.29)$$

where  $B_c$  is the percentage baffle cut,  $D_s$  is the shell diameter,  $D_{ctl}$  is the tube bundle outer diameter, and  $P_p$  is the parallel tube pitch.

The ideal pressure drop in the central section ( $\Delta P_{b,id}$ ) can be estimated by using the following equation:

$$P_{b,id} = \frac{4f_s G_s^2 N_{r,cc}}{2\rho_s} \left( \frac{\mu_{sw}}{\mu_s} \right)^{0.25} \quad (3.30)$$

where  $G$  is the mass velocity of shell-side fluid, and  $f$  is the friction factor of shell-side fluid and is calculated by using the following equation:

$$f_s = b_1 \left( \frac{1.33}{\frac{P_T}{d_o}} \right)^b (Re_s)^{b_2} \quad (3.31)$$

where coefficient  $b$  is obtained from the following equation:

$$b = \left( \frac{b_3}{1 + 0.14(Re_s)^{b_4}} \right) \quad (3.32)$$

where the coefficients  $b_1$ ,  $b_2$ ,  $b_3$ , and  $b_4$  are obtained from Table 3.1.

The pressure drop associated with an ideal one window section ( $\Delta P_{w,id}$ ) can be estimated by

$$\Delta P_{w,id} = \frac{(2 + 0.6N_{r,cw})m_s^2 N_{r,cc}}{2\rho_s A_{o,cr} A_{o,w}} \quad (3.33)$$

where  $A_{o,w}$  is the net flow area in one window section.

Based on the ideal pressure drop in the central section and window section, the total shell-side pressure drop is obtained by the following equation:

$$\Delta P_s = [(N_b - 1)P_{b,id}\gamma_b + N_b P_{w,id}] \gamma_0 + 2P_{b,id} \left(1 + \frac{N_{r,cw}}{N_{r,cc}}\right) \gamma_b \gamma_s \quad (3.34)$$

where  $N_b$  is the number of baffles.  $\gamma_b$ ,  $\gamma_0$  and  $\gamma_s$  are the correction factors for the shell-side pressure drop calculations and are obtained using the following equations:

$$\gamma_b = \exp\left(-3.7r_b\left[1 - (2N_{ss}^+)^{0.33}\right]\right) \text{ (for } N_{ss}^+ \leq 0.5\text{)} \quad (3.35)$$

$$\gamma_b = 1 \text{ (for } N_{ss}^+ \geq 0.5\text{)} \quad (3.36)$$

$$\gamma_0 = \exp(-1.33(1 + r_s)r_{lm}^s) \quad (3.37)$$

$$\gamma_s = \left(\frac{L_{b,c}}{L_{b,o}}\right)^{1.8} + \left(\frac{L_{b,c}}{L_{b,i}}\right)^{1.8} \quad (3.38)$$

Inside and outside fouling of the tubes is a common problem in the STHEs. Due to fouling, the overall heat transfer coefficient, and pressure drop is increased. Fouling is a transient process: the fouling resistance is initially zero and gradually increases with the time. The design of heat exchanger should be such that its performance will not vary widely with the time due to fouling. However, when the fouling resistance increases and affects the performance of heat exchange, the equipment needs to undergo a cleaning, which involves a shutdown and therefore capital losses. Thus, to minimize the number of maintenance cleanings of heat exchangers, the system should be over-dimension, which is done by defining a surface coefficient ( $I_s$ ) as

$$I_s = \left(\frac{A - A_c}{A_c}\right) \quad (3.39)$$

where  $A_c$  and  $A$  are the total surface area with and without fouling resistance, respectively. The high value of  $I_s$  indicates that the performance of heat exchanger turns down rapidly with fouling; hence, more maintenance cleanings are required.

On the other hand, a small value of  $I_s$  results in expensive heat exchange. In practice, the value of  $I_s$  should range from 15 to 25%.

### (c) Cost estimation

The total cost ( $C_{\text{tot}}$ ) of a heat exchanger includes the capital cost ( $C_{\text{cp}}$ ) and the operating cost ( $C_{\text{oc}}$ ) of the device. The capital cost of a heat exchanger is estimated from the following correlation:

$$C_{\text{cp}} = \delta_T \delta_P \delta_M PC \quad (3.40)$$

where  $PC$  is the purchase cost of the equipment in \$;  $\delta_T$ ,  $\delta_P$ , and  $\delta_M$  are the correction factor for operating temperature, pressure, and material used for the heat exchanger, respectively.

Table 3.2 shows the above-mentioned correction factor.

The purchase cost of the equipment depends on the heat transfer surface area and material used for the construction of the equipment. For example, the following correlation can be used for calculating the purchase cost of the heat exchanger fabricated from carbon steel (Smith 2005)

$$C = 3.28 * 10^4 * \left( \frac{A}{80} \right)^{0.68} \quad (3.41)$$

The operating cost depends on the pumping power required for driving the shell-side and tube-side fluids through the exchanger. The operating cost can be determined by the following equation:

**Table 3.2** Capital cost factors

Design temperature (°C)	Correction factor $\delta_T$
500–300	2.1
300–100	1.6
100	1
Design pressure (Pa)	Correction factor $\delta_P$
1E+07–5E+06	1.9
5E+06–7E+5	1.5
7E+ 5–5E+4	1
5E+4–1E+4	1.3
1E+3	2
Material of construction	Correction factor $\delta_M$
SS shell and tubes	2.9
CS shell and aluminum tubes	1.3
CS shell and monel tubes	2.1
CS shell and tubes	1
CS shell and SS tubes	1.7

$$C_{oc} = \frac{(E_s + E_t) \times op \times ec}{1000} \quad (3.42)$$

where  $E_t$  and  $E_s$  are the pumping powers in Watt for the tube side and shell side, respectively. Then, the total cost of the heat exchanger is calculated by using the following equation:

$$C_{tot} = C_{cp} \frac{i(1+i)^{ny}}{(1+i)^{ny}-1} + C_{oc} \quad (3.43)$$

where  $i$  is the % interest rate per year and  $ny$  is the lifetime of the heat exchanger.

The above-mentioned cost estimation is used to calculate the objective function of the case study described in the next section.

### 3.1.2 Case Study, Objective Function Description, and Constraints

Crude oil–heavy gas oil heat exchanger requires to be designed and optimized for total cost minimization. Hot heavy gas oil at a temperature of 319 °C enters into the heat exchanger and needs to be cooled down to 269 °C by crude oil which enters into the heat exchanger at 209 °C. The flow rates of gas oil and crude oil are 29.36 and 102.12 kg/s, respectively. The heat load of the heat exchanger between two fluids is 5 MW, which means that the leaving temperature of the crude oil is 226 °C. Maximum allowable pressure drops on both the sides (i.e., shell side and tube side) of the heat exchanger are 10 kPa. Surface coefficient ( $I_s$ ) of the heat exchanger should not be greater than 25%. Fluid inlet and outlet temperatures, flow rates, number of pass divider lane, number of seal strip pairs, and width of the pass divider lane are considered as design specifications. Tube outer diameter ( $d_o$ ), shell diameter ( $D_s$ ), shell-to-baffle diametrical clearance ( $\delta_{sb}$ ), tube-to-baffle diametrical clearance ( $\delta_{tb}$ ), tube bundle outer diameter ( $D_{oil}$ ), baffle spacing at center ( $L_{bc}$ ), baffle spacing at inlet and outlet ( $L_{bi}$  and  $L_{bo}$ ), baffle cut ( $B_c$ ), tube pitch ( $P_T$ ), and number of tube passes ( $N_p$ ) are considered as design variables which need to be optimized for minimum total cost of the heat exchanger. The lower bound and upper bound of the design variables are listed in Table 3.3, while Fig. 3.2 indicates the heat exchanger geometry along with all the design variables. The design specifications, presented in Table 3.4, are supplied as an input to the heat exchanger case study. Further, the following values are considered to compute the operating cost of heat exchanger: lifetime of the heat exchanger ( $ny$ ) = 20 year; annual interest rate ( $i$ ) = 5%; energy cost ( $ec$ ) = 0.1 \$/kWh; annual operating period ( $op$ ) = 5000 h/year; and pumping efficiency ( $\eta$ ) = 0.85. The correction factors for the operating temperature, pressure, and material are taken as 1.6, 1.2, and 1, respectively.

**Table 3.3** Ranges of design variables for STHE optimization

Design variable	Lower bound	Upper bound
Tube outer diameter ( $d_o$ ) (mm)	15.87	63.5
Shell diameter ( $D_s$ ) (mm)	300	1000
Shell-to-baffle diametrical clearance ( $\delta_{sb}$ )	$0.01D_s$	$0.1D_s$
Tube-to-baffle diametrical clearance ( $\delta_{tb}$ )	$0.01d_o$	$0.1d_o$
Tube bundle outer diameter ( $D_{out}$ )	0.8	$0.95(D_s - \delta)$
Baffle spacing at center ( $L_{bc}$ )	$(D_s - \delta_{sb})$	$0.55D_s$
Baffle spacing at inlet and outlet ( $L_{bi} = L_{bo}$ )	$0.2D_s$	$1.6L_{bc}$
Baffle cut ( $B_c$ )	$L_{bc}$	45%
Tube pitch ( $P_T$ )	1.25 $d_o$ or 1.5 $d_o$	
Tube layout pattern	30°, 45°, and 90°	
Number of tube passes ( $N_P$ )	1, 2 or 4	

**Table 3.4** Design specification and process input for STHE case study

	Tube side	Shell side
Fluid	Cooling water	Naphtha
Flow rate, $m$ (kg/s)	30	2.7
Inlet temperature, $T_i$ (°C)	33	114
Outlet temperature, $T_o$ (°C)	37.2	40
Density, $\rho$ (kg/m³)	1000	656
Heat capacity, $C_p$ (KJ/kg K)	4.187	2.646
Fouling resistance, $R_f$ (m² K/W)	0.0004	0.0002
Operating pressure, $P$ (Pa)	$4 \times 10^5$	$8 \times 10^5$
Allowable pressure drop, $\Delta P$ (Pa)	$7 \times 10^4$	$7 \times 10^4$

As mentioned above, minimization of the total cost ( $C_{tot}$ ) of the heat exchanger is taken as an objective function in the present study. Further, the heat exchanger geometry which results in minimum total cost also satisfies the pressure drop, flow velocity, heat exchanger length-to-shell diameter ratio, and surface coefficient constraints. So, considering all the aspects, the objective function for STHE is formulated as the follows:

$$\left\{ \begin{array}{l} \text{Minimize } f(X) = C_{tot}(X) + \sum_{j=1}^n G_1(g_j(X))^2 \\ X = [x_1, x_2, x_3, \dots, x_D], \quad x_{i,\text{minimum}} \leq x_i, \leq x_{i,\text{maximum}}, \quad i = 1, 2, 3, \dots, D \\ g_j(X) \leq 0, \quad j = 1, 2, 3, \dots, n \end{array} \right. \quad (3.44)$$

where  $X$  is the vector of design variables, which should be bounded between its minimum and maximum values.  $G_1$  is the penalty parameter, and entire term takes into account the effect of constraints violation. This term comes into picture when the constraint violation takes place.  $g_j(X)$  indicates the constraints. The following constraints are considered for the STHE.

$$I_s \leq 25\% \quad \text{Surface coefficient constraint} \quad (3.45)$$

$$1 < v_t < 3 \quad \text{Tube side flow velocity constraint} \quad (3.46)$$

$$L/D_s < 15 \quad \text{Length to shell diameter constraint} \quad (3.47)$$

$$\Delta P \leq 10 \text{ kPa} \quad \text{Pressure drop constraint} \quad (3.48)$$

The next section describes the results and discussion of the case study.

### 3.1.3 Results and Discussion

The considered problem of STHE is investigated using 11 different metaheuristic approaches to obtain a minimum total annual cost. As all these methods are stochastic in their working, each algorithm is implemented 100 times on the considered problem to estimate the statistical variations of the algorithms. Each algorithm is implemented with the population size of 50, and the termination criteria are set as 100,000 function evaluations. The results obtained using each algorithm are presented in the form of the best solution, the worst solution, average solution, standard deviation, and success rate obtained in 100 runs in Table 3.5. Here, the

**Table 3.5** Comparative results of different algorithms for STHE optimization

Algorithms	Best	Worst	Average	SD	Success rate (%)
GA	5690.6	5699.5	5694.3	2.22	56
PSO	5695.6	5744.1	5700.8	9.60	00
DE	5688.8	5695.2	5691.7	1.94	84
ABC	5688.5	5718.5	5696.7	5.34	24
CSA	5690.5	5696.8	5694.0	2.00	44
TLBO	5690.7	5701.8	5695.2	2.16	28
SOS	5691.2	5700.2	5695.7	1.74	20
WWO	5690.0	5699.3	5696.3	1.94	12
HTS	5690.4	5697.9	5694.4	2.39	56
PVS	5690.5	5695.7	5692.8	1.42	88
SCA	5691.9	5700.6	5696.5	2.61	24

solutions which are infeasible (i.e., affected by penalty) are eliminated while obtaining the worst solution, average solution, standard deviation, and success rate. Further, the success rate of the algorithm is obtained by considering 0.1% variation from the global optimum value.

It can be observed from the comparative results that DE and ABC have produced a minimum total annual cost design of STHE as compared to other algorithms. However, the average performance of DE is better followed by PVS in comparison with other algorithms. The performance of PSO is inferior in producing the best and average total annual cost. Further, the success rate of PVS algorithm in obtaining the optimum value is the highest followed by the DE algorithm. PSO algorithm is unable to obtain the optimum value and hence produced 0 success rate. It can be observed from the results that it is difficult to judge the performance of individual algorithm as all the algorithms have produced a different performance to obtain the best, worst, and average results, and success rate. So, the Friedman rank test is implemented to judge the most suitable algorithm for STHE design considering the ability to obtain the best, worst, and average solutions, and success rate. The results of the Friedman rank test are presented in Table 3.6, and its graphical representation is given in Fig. 3.3. The results are presented in the form of Friedman value, normalized value with '1' as the best performing algorithm and its rank. It is observed from the results that DE has obtained the first rank followed by PVS and CSA.

The optimized design of STHE obtained using the DE is presented in Table 3.7. It can be noted from the results that the higher tube-side pressure drop is observed as compared to shell-side pressure drop in optimum STHE design. Also, the expenditure of the initial cost is approximately 97%, while remaining expenditure is related to operating cost in optimized STHE design. All the constraints are satisfied within the specified limits in the optimized design. However, the optimized design results in a lower limit of tube-side flow velocity and a higher limit of the surface coefficient.

**Table 3.6** Friedman rank test results for STHE optimization

Algorithms	Friedman value	Normalized value	Rank
GA	27.5	0.327	5
PSO	55	0.164	11
DE	9	1	1
ABC	38.5	0.234	9
CSA	21	0.429	3
TLBO	35	0.257	8
SOS	34	0.265	7
WWO	30	0.3	6
HTS	24.5	0.367	4
PVS	12	0.75	2
SCA	43.5	0.207	10

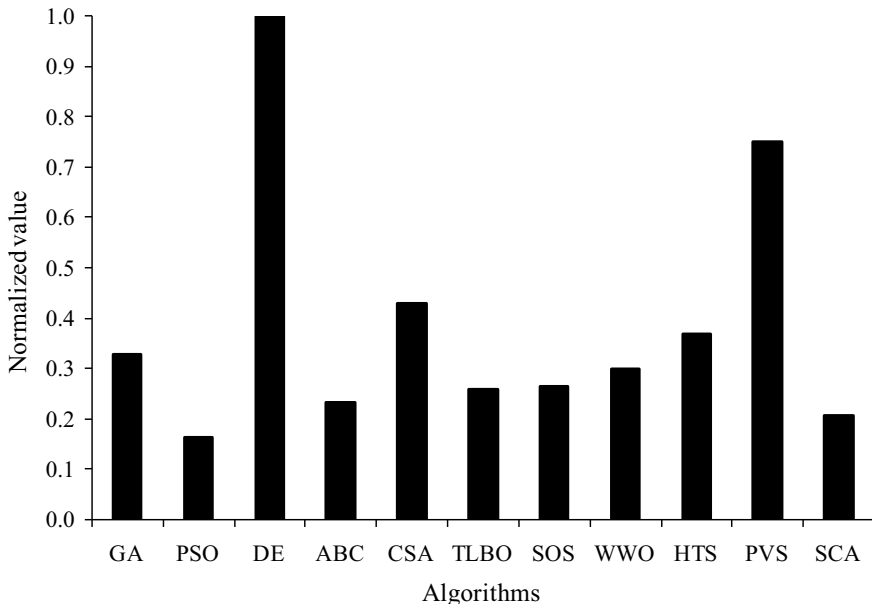


**Fig. 3.3** Graphical presentation of Friedman rank test for STHE optimization

### 3.2 Plate-Fin Heat Exchanger (PFHE)

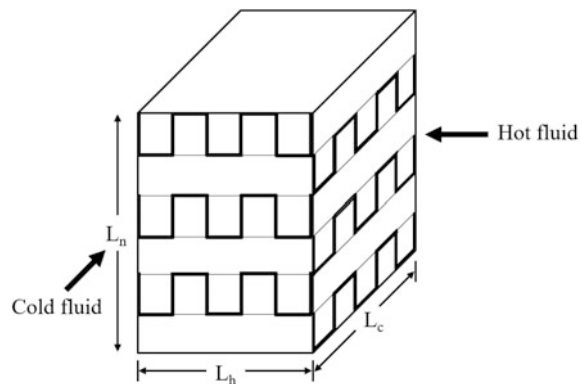
Plate-fin heat exchanger (PFHE) belongs to the category of compact heat exchanger due to its large heat transfer surface area per unit volume (Kays and London 1984). Plate-fin heat exchangers are widely used in gas–gas applications. As they are used for gas–gas applications, fins provided on both the sides of heat exchangers to increase their surface area in turn increase the heat transfer rate. In PFHEs, plates are separate from each other at some distance in which fins are sandwiched. When hot fluid and cold fluid pass through this heat exchanger, heat transfer takes place through plates and fins.

Plate-fin heat exchangers may be counter-flow type or cross-flow type. Figure 3.4 shows the schematic diagram of cross-flow PFHE. Construction of plate-fin type heat exchanger consists of a number of alternate layers of corrugated metal fins and plates. These are arranged in such a way that it forms a honeycomb structure. Due to this type of structure, it has high resistance to vibration and shock. Bars are provided at edges of plates, which are used to confine each fluid to the space provided between adjacent plates. The whole structure is joined by the brazing process. The different types of fins used in PFHE are plane fin, perforated fin, serrated fin, and herringbone fin.

The plate-fin heat exchanger has large heat transfer surface area per unit volume (because fins are employed on both), high thermal conductivity due to a small thickness of the plate, and high effectiveness (because fins interrupt boundary layer

**Table 3.7** The optimized shell and tube heat exchanger design geometry

Operating parameters	Optimized value
<i>Design variables</i>	
Tube outer diameter, $d_o$ (mm)	20.77
Shell diameter, $D_s$ (mm)	446.69
Shell-to-baffle diametrical clearance, $d_{sb}$ (mm)	11.08
Tube-to-baffle diametrical clearance, $d_{tb}$ (mm)	11.19
Tube bundle outer diameter, $D_{oil}$ (m)	0.849
Baffle spacing at center, $L_{bc}$ (mm)	290.33
Baffle spacing at inlet $L_{bi}$ (mm)	108.85
Baffle spacing at the outlet, $L_{bo}$ (mm)	103.59
Baffle cut, $B_c$ (%)	27.96
Tube pitch, $P_T$ (mm)	31.13
Tube layout pattern ( $^\circ$ )	60
Number of tubes, $N_t$	117
Tube length, $L$ (m)	6.6
Number of baffles, $N_b$	12
<i>Constraints</i>	
Tube-side flow velocity, $v$ (m/s)	1
Tube length/Shell diameter, $(L/D_s)$	14.78
Surface coefficient, $(L_s)$	0.25
Pressure drop on the shell side, $\Delta P_s$ (Pa)	$8.91 \times 10^2$
Pressure drop on tube side, $\Delta P_t$ (Pa)	$5.66 \times 10^3$
<i>Objective function</i>	
Operating cost, $C_{oc}$ (\$/year)	173.75
Initial cost including interest, $C_{op}$ (\$/year)	5515.1
Total cost, $C_{tot}$ (\$/year)	5688.8

**Fig. 3.4** Schematic diagram of cross-flow plate-fin heat exchanger

growth). The above-mentioned characteristics of PFHE result in the reduction of space requirement, weight, and cost (Flamant et al. 2011). However, this greater thermal performance of the PFHE is at the expense of higher pressure drop. Therefore, the optimum design of PFHE always required the trade-off between the thermal and hydraulic performance of the heat exchanger within the given set of constraints. Generally, the objectives involved in the design optimization of PFHE are thermodynamics (i.e., maximum effectiveness, minimum entropy generation rate, minimum pressure drop, etc.), and economics (i.e., minimum cost, minimum weight, etc.).

Earlier, several investigators used various optimization techniques with different methodologies and objective functions to optimize PFHE. In addition to using traditional mathematical methods (Reneaume et al. 2000; Reneaume and Niclout 2003), simulated annealing (Reneaume and Niclout 2001), and artificial neural network (Jia and Sundén 2003), many researchers have successfully employed evolutionary and swarm intelligence-based computation in design optimization of PFHE.

Mishra et al. (2004) and Mishra and Das (2009) used GA for optimal design of plate-fin heat exchangers. The authors considered minimization of the total annual cost and total thermo-economic cost. Peng and Ling (2008) used neural networks cooperated with genetic algorithm for the optimal design of PFHE. The authors considered minimization of weight and minimization of total annual cost as objectives. Xie et al. (2008a, b) applied GA for optimization of plate-fin heat exchangers with minimization of total annual cost as an objective function and pressure drop as a constraint. Peng et al. (2010) used PSO to optimize the structure dimensions of PFHE. The authors considered the total weight and total annual cost minimization of the heat exchanger as an objective function for given constrained conditions. Sanaye and Hajabdollahi (2010a, b) performed a simultaneous optimization of total cost and effectiveness using a design which featured NSGA-II and PFHE. Rao and Patel (2010) carried out thermodynamic optimization of cross-flow plate-fin heat exchanger aiming for minimum entropy generation units of PFHE. Zhang et al. (2010) developed a three-dimensional distributed parameter model for designing the plate-fin heat exchanger. The authors used this model for minimum entropy generation of PFHE. Najafi et al. (2005) carried out multi-objective optimization of PFHE considering the total heat transfer rate and total annual cost of the heat exchanger simultaneously using multi-objective GA. Yousefi et al. (2011) explored the GA hybrid with PSO for optimization of the heat transfer area and pressure drop of the plate-fin heat exchanger. Ghosh et al. (2011) developed a methodology to determine the optimal stacking pattern of multi-stream plate-fin heat exchangers using a genetic algorithm. The authors found out the stacking pattern, which gave the maximum heat load for a given number of fluid streams. Rao and Patel (2011a, b, c) applied teaching–learning-based optimization for the thermodynamic optimization of a plate-fin heat exchanger. Ahmadi et al. (2011) carried out thermo-economic optimization of PFHE using NSGA-II. The authors obtained the Pareto solutions for cost and entropy generation unit of PFHE.

Yousefi et al. (2012a, b) applied the imperialist competitive algorithm (ICA) for optimization of the cross-flow plate-fin heat exchanger. The authors analyzed seven design variables for minimum weight and cost design of PFHE. Yousefi et al. (2012a, b) developed a learning automata-based particle swarm optimization (LAPSO) algorithm for the optimization of PFHE. The efficiency and accuracy of the LAPSO method are demonstrated through the examples of PFHE that included three objectives, namely minimum total annual cost, minimum weight, and a minimum number of entropy generation units. Rao and Patel (2013) performed a multi-objective optimization of PFHE with effectiveness and total cost of the heat exchanger as objective functions. The authors used a modified version of teaching–learning-based optimization (TLBO) algorithm as an optimization tool. Zaho and Li (2013) developed an effective layer pattern optimization model for multi-stream plate-fin heat exchanger using genetic algorithm. Yousefi et al. (2013) proposed a variant of harmony search algorithm for design optimization of plate-fin heat exchangers. The authors demonstrated the efficiency and accuracy of the algorithm by comparing the optimization results with GA and PSO. Zhou et al. (2014) presented an optimization model for PFHE based on entropy generation minimization method. They considered specific entropy generation rate as an objective function and total heat transfer area of PFHE as a constraint. Patel and Savsani (2014) obtained a Pareto front between conflicting thermodynamic and economic objectives of PFHE by implementing multi-objective improved TLBO (MO-ITLBO) algorithm.

Zarea et al. (2014) investigated bees algorithm for the plate-fin heat exchanger optimization. The authors considered maximization of the effectiveness and minimization of entropy generation unit as objective functions in their study. Babaelahi et al. (2014) obtained the Pareto front between thermal and pressure entropy generation units of PFHE with the help of the multi-objective evolutionary algorithm. Hajabdollahi (2015) investigated the effect of nonsimilar fins in the thermo-economic optimization of plate-fin heat exchanger. They considered total annual cost and effectiveness of heat exchanger as objective functions and utilized NSGA-II for optimization. Wang and Li (2015) introduced and applied an improved multi-objective cuckoo search (IMOCS) algorithm for optimization of PFHE. The authors considered conflicting thermo-economic objectives for optimization. Yin and Ooka (2015) performed the structural parameters optimization of a water-to-water plate-fin heat exchanger used in the air-conditioning system. The authors employed GA to obtain single-objective and multi-objective optimization results. Hadidi (2015) employed biogeography-based optimization (BBO) algorithm for optimization of the heat transfer area and total pressure drop of the PFHE. Wang et al. (2015) presented few layer pattern criterion models to determine optimal stacking pattern of the multi-stream plate-fin heat exchanger (MPFHE). The authors developed these models by employing genetic algorithm and observed that the performance of MPFHE in relation to heat transfer and fluid flow was effectively improved by the optimization design of layer pattern. Yousefi et al. (2015)

presented a learning automata-based particle swarm optimization employed to multi-stage thermo-economical optimization of compact heat exchangers.

Wen et al. (2016a, b, c) performed thermodynamic optimization of PFHE. The authors considered two conflicting objectives, namely Colburn factor and friction factor for optimization and used genetic algorithm (GA) as an optimization tool. Du et al. (2016) focused on a double-flow plate-fin heat exchanger for improving its thermal and hydraulic behavior using GA. Turgut (2016) investigated hybrid chaotic quantum behaved particle swarm optimization (HCQPSO) algorithm for minimizing the heat transfer area and total pressure drop of PFHE. Ayala et al. (2016) presented Pareto optimal solution for multi-objective optimization of PFHE by combining free search algorithm with the differential evolutionary algorithm. The authors compared the obtained Pareto front with available Pareto front from NSGA-II. Wen et al. (2016a, b, c) optimized the Colburn factor and friction factor of plate-fin heat exchanges by combining a Kriging response surface and multi-objective genetic algorithm. Segundo et al. (2017) introduced adaptive differential evolution with optional external archive (JADE) and a novel JADE variant, called Tsallis JADE (TJADE) algorithm, for thermodynamic optimization of PFHE. Raja et al. (2017a, b, c) performed the many-objective optimization of the plate-fin heat exchanger by employing heat transfer search algorithm. The authors compared the many-objective optimization results of PFHE with multi-objective optimization results. Cho et al. (2017) optimized layer patterning on a plate-fin heat exchanger for minimum thermal stress using GA. Liu et al. (2017) combined CFD simulation and GA to optimize the design of PFHE. The authors considered the optimization of two conflicting objectives, namely Colburn factor and friction factor of PFHE. Raja et al. (2018a, b) performed thermodynamic as well as thermo-economic optimization of a PFHE by considering the heat transfer search algorithm.

### 3.2.1 Thermal Model

In the present work, a cross-flow plate-fin heat exchanger with offset strip fin is considered for the optimization. The geometry of PFHE is shown in Fig. 3.4, while the detail of offset strip fin is shown in Fig. 3.5. In this work, the  $\epsilon$ -NTU approach is used to predict the performance of PFHE. The PFHE is running under a steady state, and the area distribution and heat transfer coefficients are assumed to be uniform and constant. Further, the thermal–hydraulic model presented here is based on the previous works of Sanaye and Hajabdollahi (2010a, b), Rao and Patel (2013), Patel and Savsani (2014), and Raja et al. (2017a, b, c). Moreover, the subscripts  $h$  and  $c$  stand for hot side and cold side, respectively, in the different equations of the thermal–hydraulic model.

For the cross-flow heat exchanger with both fluids unmixed, effectiveness ( $\epsilon$ ) is given by Incropera and DeWitt (1998) as follows:

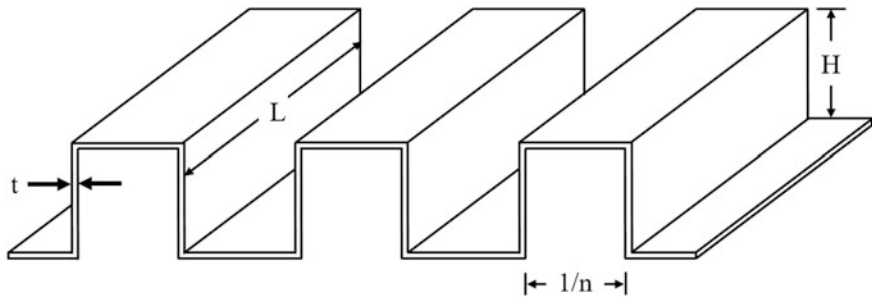


**Fig. 3.5** Detailed geometry of offset strip fin

$$\varepsilon = 1 - \exp \left[ \left( \frac{1}{C_r} \right) NTU^{0.23} [\exp(-C_r NTU^{0.78}) - 1] \right] \quad (3.49)$$

where the heat capacity ratio ( $C_r$ ) is given as

$$C_r = C_{\min} C_{\max} \quad (3.50)$$

where  $C_{\min}$  and  $C_{\max}$  are the minimum and maximum heat capacity fluids, respectively. The heat of the fluid is given by

$$C = mC_p \quad (3.51)$$

where  $C_p$  is the specific heat of the fluid.

The number of transfer units (NTU) is given by the following equation:

$$\frac{1}{NTU} = \frac{C_{\min}}{UA} = C_{\min} \left[ \frac{1}{(hA)_h} + \frac{1}{(hA)_c} \right] \quad (3.52)$$

where  $h$  is the convective heat transfer coefficient,  $U$  is the overall heat transfer coefficient, and  $A$  is the heat transfer surface area.

Heat transfer areas of the hot and cold sides of the heat exchanger are obtained by

$$A_h = L_h L_c N_h [1 + 2n_h (H_h - T_h)] \quad (3.53)$$

$$A_c = L_h L_c N_h [1 + 2n_c (H_c - T_c)] \quad (3.54)$$

where  $L_c$  and  $L_h$  indicate cold-side and hot-side flow length,  $N_h$  and  $N_c$  indicate the number of hot-side and cold-side layer,  $H_h$  and  $H_c$  indicate fin height on the hot side and cold side,  $t_h$  and  $t_c$  indicate fin thickness on the hot side and cold side, and  $n_h$  and  $n_c$  indicate fin frequency on the hot side and cold side, respectively.

Based on the hot side and cold side, the total heat transfer area of the heat exchanger is formulated as

$$A = A_h + A_c = L_h L_c [N_h (1 + 2n_h (H_h - T_h)) + (N_h (1 + 2n_c (H_c - T_c))) \quad (3.55)$$

The free flow area ( $A_{ff}$ ) for the hot side and cold side of the plate-fin heat exchanger geometry is given by

$$A_{ff,h} = (H_h - t_h)(1 - n_h t_h) L_c N_h \quad (3.56)$$

$$A_{ff,c} = (H_c - t_c)(1 - n_c t_c) L_h N_c \quad (3.57)$$

The heat transfer coefficient of the plate-fin heat exchanger is given by

$$h = j G C_p (pr)^{-0.667} \quad (3.58)$$

where  $j$  is the Colburn factor,  $Pr$  is the Prandtl number, and  $G$  is the mass flux velocity and are obtained using the following equations:

$$Pr = \frac{\mu C_p}{k} \quad (3.59)$$

$$G = \frac{m}{A_{ff}} \quad (3.60)$$

where  $\mu$  and  $k$  are the viscosity and thermal conductivity of the fluids, respectively.

The Colburn factor required to calculate the heat transfer coefficient is obtained by the correlation given by Manglik and Bergles (1995),

$$j = \left( 0.6522 (Re)^{-0.5403} (\alpha)^{-0.1541} (\delta)^{0.1499} (\gamma)^{-0.0678} \left[ 1 + 5.269 \times 10^{-5} (Re)^{1.34} (\alpha)^{0.504} (\delta)^{0.456} (\gamma)^{-1.055} \right] \right)^{0.1} \quad (3.61)$$

where  $Re$  is the Reynolds number;  $\alpha$ ,  $\delta$ , and  $\gamma$  are dimensionless parameters and are given by

$$Re = \frac{G d_h}{\mu} \quad (3.62)$$

$$\alpha = \frac{f_s}{H - T} \quad (3.63)$$

$$\delta = \frac{t}{l_f} \quad (3.64)$$

$$\gamma = \frac{t}{f_s} \quad (3.65)$$

$$f_s = \left( \frac{1}{n} - t \right) \quad (3.66)$$

where  $f_s$  is the fin spacing,  $l_f$  is the lance length of the fin, and  $d_h$  is the hydraulic diameter and are calculated by the below equation.

$$d_h = \frac{4f_s l_f (H - T)}{2(f_s l_f + (H - T)l_f + (H - T)t) + t f_s} \quad (3.67)$$

The pressure drop of both the fluid streams of the plate-fin heat exchanger is obtained using the correlation given by Shah and Sekulic (2003a, b) as

$$\Delta P_h = \frac{2f_h L_h G_h^2}{\delta_h d_{h,h}} \quad (3.68)$$

$$\Delta P_c = \frac{2f_c L_c G_c^2}{\rho_c d_{h,c}} \quad (3.69)$$

where  $f$  is the friction factor and is obtained by the following equation:

$$f = (9.6243(Re)^{-0.7422}(\alpha)^{-0.1856}(\delta)^{0.3053}(\gamma)^{-0.2659})^{0.1} \left[ 1 + 7.669 \times 10^{-8}(Re)^{4.429}(\alpha)^{0.920}(\delta)^{3.767}(\gamma)^{0.236} \right]^{0.1} \quad (3.70)$$

The above thermal–hydraulic model of PFHE is used for the cost estimation of the heat exchanger.

#### (a) Cost estimation

The total cost ( $C_{tot}$ ) of a heat exchanger includes the capital cost ( $C_{cp}$ ) and the operating cost ( $C_{oc}$ ) of the device. The capital cost of a heat exchanger is estimated from the following correlation:

$$C_{cp} = A_{cf} C_A A^{n_1} \quad (3.71)$$

where  $C_A$  is the cost per unit surface area,  $n_1$  is the exponent of nonlinear increase with area increase, and  $A_{cf}$  is the annual coefficient factor and is calculated by

$$A_{cf} = \frac{\text{roi}}{1 - (1 + \text{roi})^{-Z_1}} \quad (3.72)$$

where  $\text{roi}$  and  $Z_1$  represent interest rate and depreciation time, respectively.

The operating cost is governed by pumping power required for driving the hot and cold fluids through the exchanger and is calculated by

$$C_{\text{op}} = \left[ \zeta \tau \frac{\Delta PV}{\eta \rho} \right]_h + \left[ \zeta \tau \frac{\Delta PV}{\eta \rho} \right]_c \quad (3.73)$$

where  $V$  is the volumetric flow rate of the fluid,  $\zeta$  is the electricity price,  $\tau$  is the hours of operations, and  $\eta$  is the compressor efficiency.

So, the total annual cost of the PFHE is given by

$$C_{\text{tot}} = C_{\text{cp}} + C_{\text{op}} \quad (3.74)$$

The above-mentioned cost estimation is used to calculate the objective function of the case study described in the next section.

### 3.2.2 Case Study, Objective Function Description, and Constraints

A gas-to-air single-pass cross-flow plate-fin heat exchanger is needed in order to design and optimize the minimum total annual cost. The heat duty of the heat exchanger is 1069.8 kW. The hot flow, cold flow, and no flow length of the heat exchanger are 1, 1, and 1.5 m, respectively. The offset strip fin is employed on both the sides of heat exchanger. Specifications of offset strip fin on both the sides of the heat exchanger are identical. The PFHE is constructed from the aluminum with a density of 2700 kg/m<sup>3</sup>. The maximum allowable pressure drop on the hot side is 9.5 kPa and on the cold side is 8 kPa. The mass flow rate and temperature of the fluids are considered as design specifications. Hot-side flow length ( $L_h$ ), cold-side flow length ( $L_c$ ), fin height ( $H$ ), fin thickness ( $t$ ), fin frequency ( $n$ ), lance length of fin ( $l_f$ ), and the number of hot-side layers ( $N_h$ ) are considered as design variables which are needed to optimize the minimum total cost of the heat exchanger. Table 3.8 presents the operating conditions of PFHE, which is supplied as an input to the heat exchanger case study. The lower bound and upper bound of the design variables are listed in Table 3.9, while Figs. 3.4 and 3.5 indicates the heat exchanger geometry along with the design variables. Further, all the parameters required for cost evaluations are presented in Table 3.10.

As mentioned above, minimization of the total cost ( $C_{\text{tot}}$ ) of the PFHE is taken as an objective function in the present study. Further, the heat exchanger geometry which results in minimum total cost also satisfies the pressure drop and other constraints. So, considering all the aspects, the objective function for PFHE is formulated as below:

**Table 3.8** Process input and physical properties for the PFHE case study

Parameters	Hot side	Cold side
Mass flow rate, $m$ (kg/s)	1.66	2
Inlet temperature, $T$ (°C)	900	200
Density, $\rho$ (kg/m <sup>3</sup> )	0.6296	0.9638
Specific heat, $C_p$ (J/kg K)	1122	1073
Viscosity, $\mu$ (N s/m <sup>2</sup> )	4.01E-05	3.36E-05
Prandtl number, $Pr$	0.731	0.694

**Table 3.9** Lower and upper bounds of design variables for PFHE optimization

Design variables	Lower bound	Upper bound
Cold flow length, $L_c$ (m)	0.1	1
Hot flow length, $L_h$ (m)	0.1	1
Fin height, $H$ (mm)	2	10
Fin thickness, $t$ (mm)	0.1	0.2
Fin frequency, $n$ ( $m^{-1}$ )	100	1000
Fin offset length, $l_f$ (mm)	1	10

**Table 3.10** Economic parameters of PFHE

Cost per unit area, $C_A$ (\$/m <sup>2</sup> )	90
Electricity price, $\zeta$ (\$/MWh)	20
Hours of operation, $\tau$ (h)	5000
Nonlinear exponent, $n_1$	0.6
Depreciation time, $z_1$ (year)	10
Compressor efficiency, $\eta$	0.6
The rate of interest, roi	0.1

$$\left\{ \begin{array}{l} \text{Minimize } f(X) = C_{\text{tot}}(X) + \sum_{j=1}^n G_1(g_j(X))^2 \\ X = [x_1, x_2, x_3, \dots, x_D], \quad x_{i,\text{minimum}} \leq x_i \leq x_{i,\text{maximum}}, \quad i = 1, 2, 3, \dots, D \\ g_j(X) \leq 0, \quad j = 1, 2, 3, \dots, n \end{array} \right. \quad (3.75)$$

where  $X$  is the vector of design variables which should be bounded between its minimum and maximum values.  $G_1$  is the penalty parameter, and entire term takes into account the effect of constraints violation. This term comes into the picture when the constraint violation takes place.  $g_j(X)$  indicates the constraints. The following constraints are considered for the PFHE.

$$0.134 < \alpha < 0.997 \quad (3.76)$$

$$0.012 < \delta < 0.048 \quad (3.77)$$

$$120 < Re < 10^4 \quad (3.78)$$

$$0.041 < \gamma < 0.121 \quad (3.79)$$

$$\Delta P_h \leq 9.5 \text{ kPa} \quad (3.80)$$

$$\Delta P_c \leq 8 \text{ kPa} \quad (3.81)$$

$$T_w \leq 500 \text{ kg} \quad (3.82)$$

The next section describes the results and discussion of the case study.

### 3.2.3 Results and Discussion

The considered problem of PFHE is investigated using 11 different metaheuristic approaches to obtain a minimum total annual cost. Each algorithm is implemented 100 times on the considered problem to estimate the statistical variations of the algorithms. Each algorithm is implemented with the population size of 50, and the termination criteria are set as 100,000 function evaluations. The results obtained using each algorithm are presented in the form of the best solution, the worst solution, average solution, standard deviation, and success rate obtained in 100 runs in Table 3.11. Here, the solutions which are infeasible (i.e., affected by penalty) are eliminated while obtaining the worst solution, average solution, standard deviation, and success rate. Further, the success rate of the algorithm is obtained by considering 0.1% variation from the global optimum value.

**Table 3.11** Comparative results of different algorithms for PFHE optimization

Algorithms	Best	Worst	Average	SD	Success rate (%)
GA	937.9	994.9	964.1	15.0	00
PSO	931.0	994.9	971.6	22.1	00
DE	927.5	929.9	927.7	0.5	93
ABC	927.7	997.8	969.6	21.6	04
CSA	927.5	929.6	927.8	0.5	88
TLBO	927.5	935.5	928.9	2.1	56
SOS	927.5	934.3	929.0	1.7	52
WWO	933.8	1162.1	998.1	53.3	00
HTS	927.5	929.6	927.7	0.6	84
PVS	927.5	928.0	927.7	0.1	92
SCA	928.7	941.0	932.5	2.7	00

It can be observed from the comparative results that DE, PVS, CSA, TLBO, SOS, and HTS performed equally good and produced minimum total annual cost design of PFHE as compared to other algorithms. However, the average performance of DE, PVS, and HTS is better as compared to other competitive algorithms. Further, the success rate of DE algorithm in obtaining the optimum value is the highest followed by the PVS algorithm. The GA, PSO, WWO, and SCA algorithms are unable to obtain the optimum value and hence produced zero success rate. It can be observed from the results that it is difficult to judge the performance of the algorithm as all the algorithms have produced a different performance to obtain the best, worst, and average results, and success rate. So, the Friedman rank test is implemented to judge the best suitable algorithm for PFHE design considering the capability to obtain the best, worst, and average solutions, and success rate. The results of the Friedman rank test are presented in Table 3.12, and its graphical representation is given in Fig. 3.6. The results are presented in the form of Friedman value, normalized value with '1' as the best performing algorithm and its rank. It is observed from the results that DE has obtained the first rank followed by PVS and CSA.

The optimized design of PFHE obtained using the DE is presented in Table 3.13. It can be noted from the results that the higher cold-side flow length is observed as compared to hot-side flow length in optimum PFHE design. However, the pressure drop on both the sides of the heat exchanger is identical because of the mass flow rate and free flow area. Also, the expenditure of capital cost is approximately 73.19%, while remaining expenditure is related to the operating cost in optimized PFHE design. Further, all the constraints are satisfied within the specified limits in the optimized design.

**Table 3.12** Friedman rank test results for PFHE optimization

Algorithm	Friedman value	Normalized value	Rank
GA	45	0.23333	9
PSO	47	0.2234	10
DE	10.5	1	1
ABC	42	0.25	8
CSA	12	0.875	3
TLBO	25	0.42	5
SOS	27	0.38889	6
WWO	52.5	0.2	11
HTS	19	0.55263	4
PVS	11.5	0.91304	2
SCA	38.5	0.27273	7

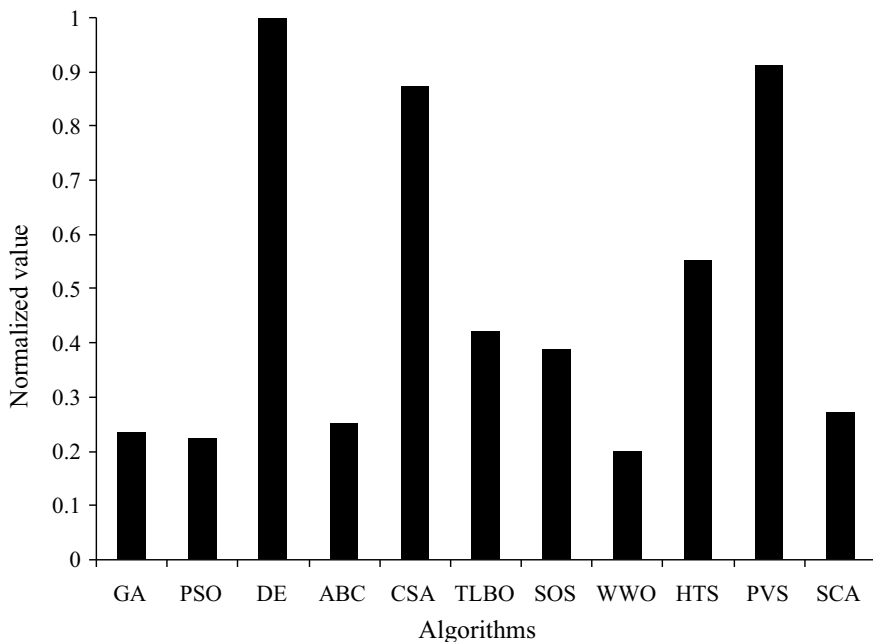


**Fig. 3.6** Graphical presentation of Friedman rank test for PFHE optimization

**Table 3.13** Optimized plate-fin heat exchanger design geometry

Heat exchanger parameter	Optimized value
<i>Design variables</i>	
Hot-side flow length, $L_h$ (m)	0.8363
Cold-side flow length, $L_c$ (m)	1
Fin height, $H$ (mm)	9.986
Fin thickness, $t$ (mm)	0.1927
Fin frequency, $n$ ( $m^{-1}$ )	204.3
Fin offset length $l_f$ (mm)	5.189
Number of hot-side layer, ( $N_h$ )	71
No flow length, $L_n$ (m)	1.5
Effectiveness (%)	82
<i>Constraints</i>	
Hot-side pressure drop, $\Delta P_h$ (kPa)	99.67
Cold-side pressure drop, $\Delta P_c$ (kPa)	99.67
Total weight, $T_w$ (kg)	349.39
$\gamma$	0.041
$\alpha$	0.4801
$\delta$	0.0371
$Re_h$	381.87

(continued)

**Table 3.13** (continued)

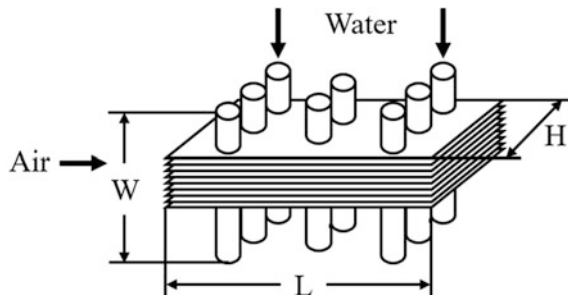
Heat exchanger parameter	Optimized value
$Rec$	647.41
<i>Objective function</i>	
Capital cost, $C_{cp}$ (\$)	678.98
Operating cost, $C_{op}$ (\$)	248.61
Total cost, $C_{tot}$ (\$)	927.59

### 3.3 Fin and Tube Heat Exchanger (FTHE)

Fin and tube heat exchangers (FTHE) belong to the compact heat exchangers and generally used for gas to liquid heat transfer. In a gas-to-liquid heat exchange, the heat transfer coefficient on the liquid side is generally higher than that on the gas side. Hence, to balance the thermal conductance on both sides, fins are used on the gas side to increase the surface area. Figure 3.7 shows the schematic diagram of FTHE. A finned tube heat exchanger has tubes with fins attached to the outside surface. However, in some applications fins are mounted on the inside surface of tubes also. Usually, liquid flows through the tubes and air, or some other gas flows outside the tubes. Fins are radial for cross-flow fin and tube arrangement. For counter-flow or parallel flow FTHE, the fins should be longitudinal instead of radial. Depending on the type of fin, FTHEs are: FTHE having normal fins on individual tubes, FTHE having flat fins, the fins can be plain, wavy, or interrupted, and the tubes can be circular, oval, or rectangular shapes, and longitudinal fins on individual tubes.

The major advantages of FTHE are wide application and temperature spectrum, handle low heat transfer coefficient fluids, and high tube-side velocity prevents fouling inside the tubes. At the same time, some drawbacks are also associated with FTHE like it cannot handle slurry fluids, deposition of the particle at fin corner reduces the heat transfer rate, cleaning is difficult, and high-pressure drop. Finned tube heat exchangers are often used in power plants as a preheating and exhaust gas heat exchanger. In industrial dryers, finned tube heat exchangers are used for heating of air. Apart from these, FTHEs are also used in power and chemical engineering applications such as compressors, intercoolers, air coolers, and fan coils because of their high compactness and relatively good heat transfer efficiency.

**Fig. 3.7** Schematic diagram of fin and tube heat exchanger



The design of a FTHE is a complex task based on trial and error process in which geometrical and operational parameters are selected to satisfy specified requirements such as heat duty, pressure drop, outlet temperature. Earlier, several investigators used various optimization algorithms with different methodologies and objective functions to optimize FTHEs. Wang et al. (1997) performed extensive experiments to identify the heat transfer and pressure drop performance of wavy fin and tube heat exchangers. Romero-Méndez et al. (2000) examined the influence of fin spacing on the over-tube side of a single-row fin-tube heat exchanger through flow visualization and numerical computation. Pacheco-Vega et al. (2001, 2003) performed sets of experiments and obtained the data to predict the heat transfer performance of FTHE. Based on the numerical data, the authors obtained the correlation for heat transfer performance through regression analysis, which was further optimized using SA and GA. Xie et al. (2005) used a mathematical-based traditional optimization technique to carry out the optimum design of fin and tube heat exchanger. The authors considered minimization of total annual cost of FTHE as an objective function.

Yang et al. (2006) carried out the optimization of design parameters for a fin-tube heat exchanger of a household refrigerator under frosting conditions to improve its thermal performance. They considered the average heat transfer rate, frost mass, and operating time as objective functions and used response surface and Taguchi methods as an optimization tool. Xie et al. (2008a, b) used GA for minimization of a total annual cost and a total weight of FTHE. The authors considered seven design variables for the optimization objectives and performed the optimization through GA routine and a thermal design routine. Wu et al. (2008) applied genetic algorithm to optimize the refrigerant circuit of fin and tube heat exchangers for maximum heat transfer or minimize tube length. Saechan and Wongwises (2008) presented a mathematical model to determine the optimal configuration of fin-tube condensers used in air-conditioning system. The authors utilized this model to analyze and optimize the entropy generation of FTHE. Tang et al. (2009) applied GA for optimization of air-side heat transfer performance of FTHE. The authors investigated various fin patterns and developed heat transfer and friction factor correlations, which were further optimized by implementing GA. Lemouedda et al. (2010) combined a CFD analysis, genetic algorithms, and the response surface methodology to obtain an optimum angle of attack of delta-winglet vortex generators in a plate-fin and tube heat exchanger.

Hajabdollahi et al. (2011a, b) investigated the thermo-economic optimization of the plane fin and tube heat exchanger. They considered the total annual cost and effectiveness of heat exchanger as objective functions and utilized NSGA-II for optimization. Singh et al. (2011) performed CFD simulation and optimization of air to refrigerant fin and tube heat exchanger. Hsieh et al. (2012) applied the Taguchi method for parametric study and optimization of louver finned-tube heat exchangers. Based on their work, the authors concluded that fin collar outside diameter, transverse tube pitch, and fin pitch are the main factors that influenced significantly the thermal-hydraulic performance of the FTHE. Jang et al. (2013) performed optimization of the span angle and location of vortex generators in a plate-fin and tube

heat exchanger by considering a simplified conjugate-gradient method. Raja et al. (2017a, b, c) presented a thermal model of the fin and tube heat exchanger. The authors performed the optimization of the thermal model for minimum weight and minimum total cost geometry by adapting heat transfer search algorithm.

### 3.3.1 Thermal Model

In the present work, an intercooler is investigated for the optimization. This intercooler is a fin and tube heat exchanger having rectangular fin and the cylindrical tube. The water flows through the tube while air flows on the fin side. The geometry of FTHE is shown in Fig. 3.7 while the detail of fin arrangement is shown in Fig. 3.8. The FTHE is running under a steady state, and the area distribution and heat transfer coefficients are assumed to be uniform and constant. Further, the thermal-hydraulic model presented here is based on the previous works of Xie et al. (2008a, b) and Raja et al. (2017a, b, c). Moreover, the subscripts  $w$  and  $a$  stand for water side and air side in the different equations of the thermal-hydraulic model.

#### (a) Heat transfer

For the staggered tube arrangement, the minimum free flow area on air side ( $A_{\min}$ ) is calculated by

$$A_{\min} = \left[ \left( \frac{W}{p_t} - 1 \right) c + (p_t - d_o)(1 - t_f N_f) \right] H \quad (3.83)$$

where  $p_t$  is the transverse tube pitch,  $d_o$  is the outer tube diameter,  $t_f$  is the fin thickness,  $N_f$  is the number of fins,  $H$  is the height of heat exchanger, and  $W$  is the width of the heat exchanger. The coefficient  $c$  is calculated by the following equation:

$$c = 2a \quad \text{if } 2a < 2b \quad (3.84)$$

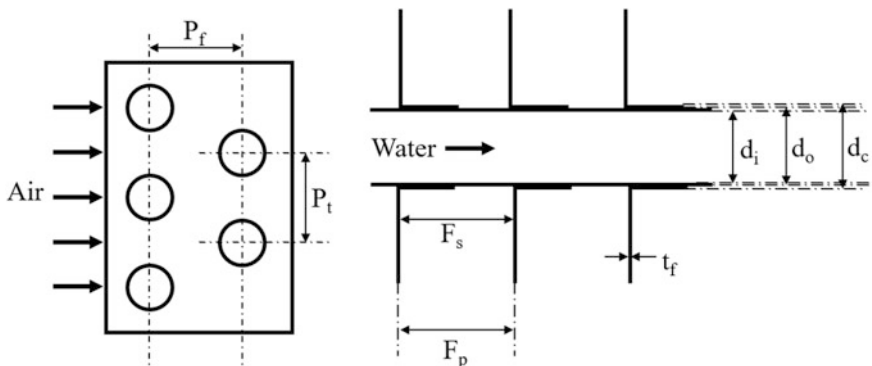


**Fig. 3.8** Details of fin geometry and its arrangement

$$c = 2b \quad \text{if } 2b < 2a \quad (3.85)$$

where values of  $2a$  and  $2b$  are calculated by the following equations:

$$2a = (p_t - d_0)(1 - t_f N_f) \quad (3.86)$$

$$2b = (0.5p_t^2 + p_t^2)^{0.5} - d_0 - (p_t - d_0)t_f N_f \quad (3.87)$$

The total heat transfer surface area ( $A$ ) of the heat exchanger is calculated by

$$A = A_p + A_f \quad (3.88)$$

where  $A_p$  and  $A_f$  are primary surface area and secondary (i.e., fin) surface area of the heat exchanger and are calculated by

$$A_p = 3.14d_o W N_t (1 - t_f N_f) \quad (3.89)$$

$$A_f = 2N_f (LH - 0.785d_o^2 N_t) + 2t_f N_f WH \quad (3.90)$$

where  $L$  is the length of the tube,  $N_t$  and  $N_f$  are number of tubes and fins, respectively, and are calculated by

$$N_t = \left( \frac{H}{p_t} - 1 \right) N \quad (3.91)$$

$$N_f = \frac{W}{F_p} + 1 \quad (3.92)$$

where  $N$  is the number of tube rows and  $F_p$  is the fin pitch.

Reynolds number on air side is calculated by considering fin collar outside diameter ( $d_c$ ) and is given by

$$Re_{dc} = \frac{G_a d_c}{\mu_a} \quad (3.93)$$

where  $\mu_a$  is the air viscosity and  $G_a$  is the mass velocity of air based on minimum free flow area.

For the air side, when the number of tube rows is greater than one, the Colburn factor ( $j_a$ ) is obtained from the following co-relation suggested by Wang (2000):

$$j_a = 0.086 Re_{dc}^{j1} N^{j2} \left( \frac{F_p}{d_c} \right)^{j3} \left( \frac{F_p}{d_h} \right)^{j4} \left( \frac{F_p}{p_t} \right)^{-0.93} \quad (3.94)$$

where  $j1-j4$  are different coefficients. Detailed mathematical formulations for calculation of  $j1-j4$  are given below based on the previous work of Wang (2000):

$$j1 = -0.361 - \frac{0.042N}{\ln(Re_{dc})} + 0.158 \ln\left(N\left(\frac{F_p}{d_c}\right)^{0.41}\right) \quad (3.95)$$

$$j2 = -1.224 - \frac{0.076\left(\frac{p_i}{d_h}\right)^{1.42}}{\ln(Re_{dc})} \quad (3.96)$$

$$j3 = -0.083 + \frac{0.058N}{\ln(Re_{dc})} \quad (3.97)$$

$$j4 = -5.735 + 1.21\ln\left(\frac{Re_{dc}}{N}\right) \quad (3.98)$$

where  $Re_{dc}$  is the Reynolds number based on cooler diameter and  $d_h$  is the hydraulic diameter.

Then the heat transfer coefficient on air side ( $h_a$ ) can be determined by

$$h_a = j_a \frac{4\rho_a v_a C_{p,a}}{Pr_a^{0.67}} \quad (3.99)$$

where  $v$  is the air velocity,  $C_p$  is the specific heat of air,  $Pr$  is the Prandtl number, and  $\rho$  is the air density.

For water side, Nusselt number  $Nu_w$  is obtained by using the co-relation given by Gnielinsk (1976):

$$Nu_w = \frac{\frac{f_w}{8}(Re_w - 1000)Pr_w}{1 + 12.7\left(\frac{f_w}{8}\right)^{1/2}\left(Pr_w^{2/3} - 1\right)} \quad (3.100)$$

where  $Re_w$  and  $Pr_w$  represent Reynolds number and Prandtl number on water side, respectively.  $f_w$  is a friction factor and is calculated by

$$f_w = (1.82 \log_{10} Re_w - 1.64)^{-2} \quad (3.101)$$

Then the heat transfer coefficient on the water side ( $h_w$ ) can be obtained by

$$h_w = \frac{Nu_w k_w}{d_i} \quad (3.102)$$

where  $d_i$  is the tube internal diameter and  $k_w$  is the thermal conductivity of water.

Considering overall heat transfer coefficient ( $U$ ), the heat transfer surface area ( $A$ ) is computed as follows:

$$A_h = \frac{Q}{UF\Delta T_{LM}} \quad (3.103)$$

where  $Q$  is the heat transfer rate, and  $F$  is the fouling factor.  $U$  is the overall heat transfer coefficient depends on both the air-side and water-side heat transfer coefficients.  $\Delta T_{LM}$  is the logarithmic mean temperature difference.

### (a) Pressure drop

For the air side, friction factor ( $f_a$ ) is obtained from the following co-relation given by Wang (2000):

$$f_a = 0.0267 Re_{dc}^{f1} \left( \frac{p_t}{p_1} \right)^{f2} \left( \frac{F_p}{d_c} \right)^{f3} \quad (3.104)$$

where  $f1-f3$  are different coefficients. Detailed mathematical formulations for calculation of  $f1-f3$  are given by Wang (2000) as follows.

$$f1 = -0.0764 + 0.739 \left( \frac{p_t}{p_1} \right) - 0.177 \left( \frac{F_p}{d_c} \right) - \frac{0.00758}{N} \quad (3.105)$$

$$f2 = -15.689 + \frac{64.021}{\ln(Re_{dc})} \quad (3.106)$$

$$f3 = -1.696 - \frac{15.695}{\ln(Re_{dc})} \quad (3.107)$$

Then the pressure drop on air side can be obtained by

$$\Delta P_a = \frac{G_a^2}{2\rho_i} \left[ \frac{A}{A_{min}} \frac{\rho_{a,m}}{\rho_{a,i}} f_a + (1 + \sigma^2) \left( \frac{\rho_{a,i}}{\rho_{a,o}} - 1 \right) \right] \quad (3.108)$$

where  $\sigma$  is the contraction ratio of cross-sectional area.

Finally, the pressure drop on the water side can be determined by

$$\Delta P_w = \frac{f_w \rho_w v_w^2 L}{2d_i} \quad (3.109)$$

where  $v$  is the velocity of water flow.

### (b) Cost estimation

The total annual cost ( $C_{tot}$ ) of a FTHE can be seen as the combination of two major costs: the initial cost ( $C_{in}$ ) and the operating cost ( $C_{op}$ ). The initial cost of a heat exchanger is estimated from the following correlation:

$$C_{\text{in}} = C_A A^n \quad (3.110)$$

where  $C_A$  is the cost per unit surface area and  $n$  is the exponent of nonlinear increase with area increase.

The operating cost is governed by the pumping power required for driving the hot and cold fluids through the exchanger and is calculated by

$$C_{\text{op}} = \left( k_{\text{el}} \tau \frac{\Delta PV_t}{\eta} \right)_a + \left( k_{\text{el}} \tau \frac{\Delta PV_t}{\eta} \right)_w \quad (3.111)$$

where  $V$  is the volumetric flow rate of the fluid,  $k_{\text{el}}$  is the electricity price,  $\tau$  is the hours of operations, and  $\eta$  is the pump/compressor efficiency.

So, the total annual cost of the heat exchanger is given by

$$C_{\text{tot}} = C_{\text{in}} + C_{\text{op}} \quad (3.112)$$

Based on the above thermal model, the objective function for the present work is defined in the next section.

### 3.3.2 Case Study, Objective Function Description, and Constraints

A 3.155MW duty air-to-water fin and tube intercooler (shown in Figs. 3.7 and 3.8) needs to be designed and optimized. For considered intercooler, hot air flows normal to a finned tube bundle, while cold water flows inside the smooth tubes exchanger. The plain fins are selected on the outside of the tube bundle. However, other fin surfaces may also be considered with the corresponding design. Hot air with a flow rate of 58.2 kg/s is supplied at a temperature of 104 °C to fin side of FTHE, and it is required to be cooled up to 51 °C temperature. The cooling of air is carried out with the help of water that is supplied to the tube side of FTHE at a temperature of 20 °C with a flow rate of 39.2 kg/s. The other design specifications are presented in Table 3.14 and supplied as an input. All the parameters required for cost evaluations are presented in Table 3.15. Seven design variables, such as tube diameter ( $d_o$ ), transverse tube pitch ( $p_t$ ), longitudinal tube pitch ( $p_l$ ), number of tube rows ( $N$ ), fin pitch ( $F_p$ ), the height of heat exchanger ( $H$ ), and width of the heat exchanger ( $W$ ), are considered for optimization. The upper and lower bounds for the design variables imposed in the considered approaches are listed in Table 3.16.

As mentioned above, the minimization of total cost of the FTHE is taken as an objective function in the present study. Further, the heat exchanger geometry which results in minimum total cost also satisfies the pressure drop and other constraints. So, considering all the aspects, the objective function for FTHE is formulated as below:

**Table 3.14** Process input and physical properties for the FTHE case study

	Tube side	Fin side
Fluid	Water	Air
Inlet pressure, $P$ (kPa)	174.5	174.5
Allowable pressure drop, $\Delta P$ (Pa)	5200	5200
Heat duty, $Q$ (kW)	3115	3115
Material of construction	Stainless steel	Aluminum
Density, $\rho$ (kg/m <sup>3</sup> )	7820	2790
Thermal Conductivity, $k$ (W/m K)	15	170

**Table 3.15** Economic parameters of FTHE

Cost per unit area, $C_A$ (\$/m <sup>2</sup> )	100
The exponent for the area, $n$	0.6
Hour of operation, $\tau$ (h/year)	6500
Electricity price, $kel$ (\$/MWh)	30
Pump efficiency, $\eta$	0.5

**Table 3.16** Ranges of design variables for FTHE optimization

Design variables	Lower bound	Upper bound
Outer tube diameter, $d_o$ (mm)	6.9	13
Transverse pitch, $p_t$ (mm)	20.4	30.8
Longitudinal pitch, $p_l$ (mm)	12.7	32
Number of tube rows, $N$	1	6
Fin pitch, ( $F_p$ ) mm	1	8.7
The height of heat exchanger, $H$ (m)	4.5	80
The width of the heat exchanger, $W$ (m)	3	5

$$\left\{ \begin{array}{l} \text{Minimize } f(X) = C_{\text{tot}}(X) + \sum_{j=1}^n G_1(g_j(X))^2 \\ X = [x_1, x_2, x_3, \dots, x_D], \quad x_{i,\text{minimum}} \leq x_i \leq x_{i,\text{maximum}}, \quad i = 1, 2, 3, \dots, D \\ g_j(X) \leq 0, \quad j = 1, 2, 3, \dots, n \end{array} \right. \quad (3.113)$$

where  $X$  is the vector of design variables which should be bounded between its minimum and maximum values.  $G_1$  is the penalty parameter, and entire term takes into account the effect of constraints violation. This term comes into picture when constraint violation takes place.  $g_j(X)$  indicates the constraints. Following constraints are considered for the FTHE.

$$\Delta P_a \leq 30 \text{ Pa} \quad (3.114)$$

$$\Delta P_w \leq 4500 \text{ Pa} \quad 1 < \frac{A}{A_h} < 1.2 \quad (3.115)$$

$$\frac{W}{d_o} \geq 60 \quad (3.116)$$

$$TW < 480 \text{ kg} \quad (3.117)$$

The next section describes the results and discussion of the case study.

### 3.3.3 Results and Discussion

The considered problem of FTHE is investigated using 11 different metaheuristic approaches to obtain the minimum total annual cost. Each algorithm is implemented 100 times on the considered problem to estimate the statistical variations of the algorithms. Each algorithm is implemented with the population size of 50, and the termination criteria are set as 100,000 function evaluations. The results obtained using each algorithm are presented in the forms of the best solution, the worst solution, average solution, standard deviation, and success rate obtained in 100 runs in Table 3.17. Here, the solutions which are infeasible (i.e., affected by penalty) are eliminated while obtaining the worst solution, average solution, standard deviation, and success rate. Further, the success rate of the algorithm is obtained by considering 0.1% variation from the global optimum value.

It can be observed from the comparative results that all the algorithms performed equally good and produced minimum total annual cost design of FTHE. The average performance of SOS is better as compared to other competitive algorithms. However, the success rate of SCA algorithm is better while the ABC algorithm

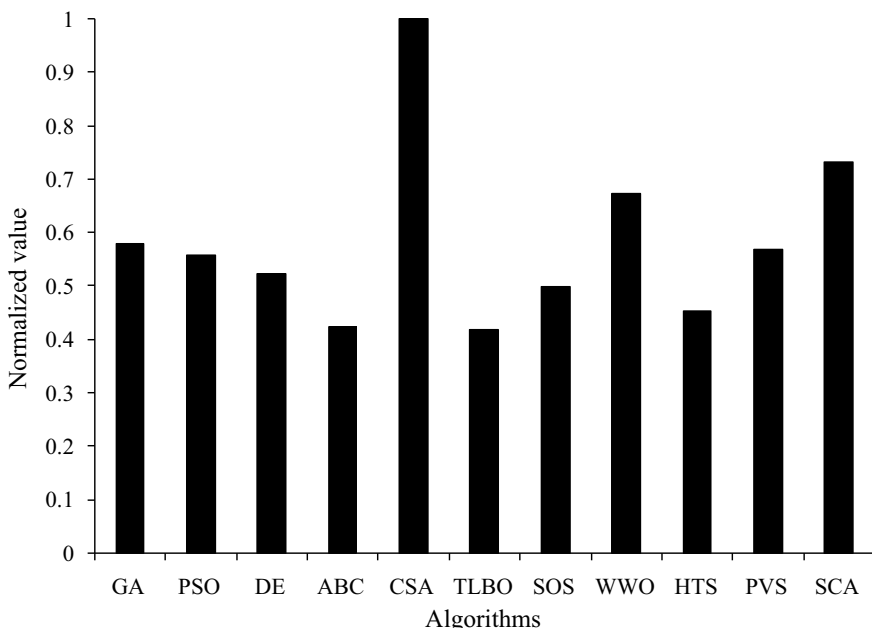
**Table 3.17** Comparative results of different algorithms for FTHE optimization

Algorithms	Best	Worst	Average	SD	Success rate (%)
GA	3457.35	3865.48	3545.67	99.81	16
PSO	3457.33	4091.99	3610.2	276.33	76
DE	3457.33	4091.99	3635.04	290.83	72
ABC	3457.35	4091.99	3625.57	226.69	15
CSA	3457.33	4091.99	3482.98	126.88	92
TLBO	3457.33	4091.99	3660.42	302.15	67
SOS	3457.33	4091.99	3635.04	290.83	71
WWO	3457.46	3509.92	3470.78	15.10	28
HTS	3457.33	4091.99	3641.72	288.49	68
PVS	3457.34	4091.99	3609.66	276.63	76
SCA	3457.86	3484.13	3465.10	6.29	28

**Table 3.18** Friedman rank test results for FTHE optimization

Algorithm	Friedman value	Normalized value	Rank
GA	28.5	0.578947	4
PSO	29.5	0.559322	5
DE	31.5	0.52381	7
ABC	39	0.423077	11
CSA	16.5	1	1
TLBO	39.5	0.417722	10
SOS	33	0.5	8
WWO	24.5	0.673469	3
HTS	36.5	0.452055	9
PVS	29	0.568966	6
SCA	22.5	0.733333	2

produces least success rate in obtaining the global optimum value. It can be observed from the results that it is difficult to judge the performance of the algorithm as all the algorithms have produced a different performance to obtain the best, worst, and average results, and success rate. So, the Friedman rank test is implemented to judge the best suitable algorithm for FTHE design considering the capability to obtain the best, worst, and average results, and success rate. The results of the Friedman rank test are presented in Table 3.18, and its graphical representation is given in Fig. 3.9. The results are presented in the form of the Friedman value, normalized value with

**Fig. 3.9** Graphical presentation of Friedman rank test for FTHE optimization

**Table 3.19** Optimized fin and tube heat exchanger design geometry

Operating parameters	Optimized value
<i>Design variables</i>	
Outside diameter of the tube, $d_o$ (mm)	13
The transverse pitch of tube, $p_t$ (mm)	20.4
Longitudinal pitch of tube, $p_l$ (mm)	15.243
Number of tube rows, $N$	2
Fin pitch, $F_p$ (mm)	1.8214
The height of heat exchanger, $H$ (m)	4.5
The width of the heat exchanger, $W$ (m)	3
<i>Constraints</i>	
Pressure drop on the air side, $\Delta P_a$ (Pa)	20.48
Pressure drop on the water side, $\Delta P_w$ (Pa)	3620.89
Initial to final heat transfer area, $A/A_h$	1
Shape width to tube diameter, $W/d_o$	170.77
Total weight, $T_w$ (kg)	477.11
<i>Objective function</i>	
Capital cost, $C_{cp}$ (\$/year)	3116.44
Operating cost, $C_{op}$ (\$/year)	340.89
Total annual cost, $C_{tot}$ (\$/year)	3457.33

'1' as the best performing algorithm and its rank. It is observed from the results that CSA has obtained the first rank followed by SCA and WWO.

The optimized design of FTHE obtained using the CSA is presented in Table 3.19. It can be noted from the results that the higher transverse tube pitch is observed as compared to longitudinal tube pitch in optimum FTHE design. Further, the height of the heat exchanger is more as compared to its width. Moreover, the pressure drop on the air side is negligible as compared to the pressure drop on the tube side. Also, the expenditure of capital cost is approximately 90.1%, while remaining expenditure is related to the operating cost in the optimized FTHE design. Further, all the constraints are satisfied within the specified limits in the optimized design.

### 3.4 Regenerative Heat Exchanger (Rotary Regenerator)

A regenerator is a sizeable porous disc characterized by its compact size and high heat-transfer area density. The heat transfer area or flow passages of regenerator are generally made with the fine mesh of the metal having high heat capacity (Kays and London 1985; Shah and Sekulic 2003a, b). This fine mesh in the form of matrix is fitted on the rotor which rotates at very low speeds with a constant fraction of the

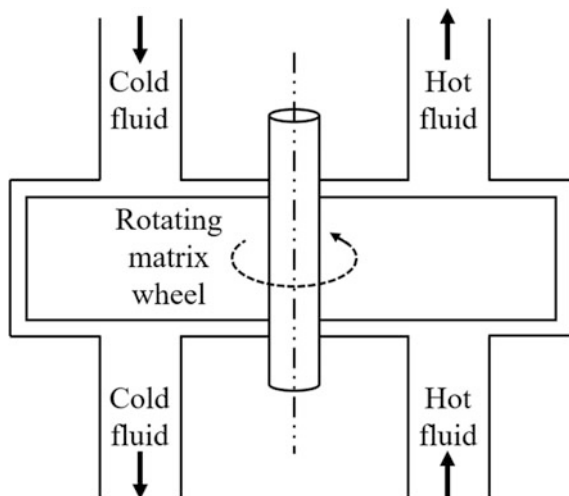
matrix-facing partially for the hot and cold fluid. Due to the rotation of the matrix, this type of regenerator is known as the rotary regenerator. Figure 3.10 shows the schematic rotary regenerator. In rotary regenerator, thermal energy is stored in the hot side of the matrix. During the cold gas flow through the same passages later, the matrix wall delivers the thermal energy to the cold fluid. Thus, the matrix is alternately heated and cooled, and in this manner, heat is transmitted indirectly from hot fluid to cold fluid.

If the matrix is stationary, then regenerator is referred to as periodic flow or fixed matrix regenerative heat exchanger. In this type of regenerator, the hot and cold fluids are ducted through the use of valves to the different matrices of the regenerator in alternate operating periods. In case of the fixed matrix, regenerative heat exchanger, the hot fluid at higher temperature enters one side of the heat exchanger where the matrix membrane absorbs the heat. This heat is then released to the cold fluid which enters from the same or the other side of the regenerator.

It includes much more compact surface compared to recuperative (i.e., shell and tube heat exchanger, plate-fin heat exchanger, etc.), which provides reduced exchange volume for given exchanger effectiveness and pressure drop, thereby making a regenerator economical compared to an equivalent recuperative heat exchanger. Regenerators are exclusively used for exhaust heat recovery in high-temperature applications like the boiler, furnace, turbine, etc. In addition to this, regenerators are widely used for low-temperature applications like liquefaction of air, oxygen, nitrogen, etc.

As mentioned above, regenerators are characterized by high thermal effectiveness owing to high heat-transfer area density. However, this superior thermal performance of the regenerators is at the expense of higher pressure drop (Kays and London 1985; Skiepko and Shah 2004). Therefore, the optimum design of

**Fig. 3.10** Schematic of the rotary regenerator



regenerators always requires the optimal trade-off between the effectiveness and pressure drop within the given set of constraints. Generally, the objectives involved in the design optimization of rotary regenerator are the maximum effectiveness, minimum entropy generation rate, minimum pressure drop, and minimum cost.

Earlier, investigators used various optimization techniques with different methodologies and the objective functions to optimize rotary regenerator. Colgate (1995) performed the optimization of regenerator used in Sterling cycle refrigerator for minimum entropy generation. The author considered entropy generation due to transverse and parallel heat conduction and due to friction with the wall in his optimization investigation. Büyükalaca and Yilmaz (2002) analyzed the influence of rotational speed on the effectiveness of rotary regenerator. Sadrnneli (2003) carried out the simulation of the rotary regenerator to identify the effect of operating parameters on the effectiveness of rotary regenerator. Wu et al. (2006) developed a mathematical model of the regenerator for the thermal analysis of the fluid and wheel matrix. Sanaye et al. (2008) determined the optimum operating condition of rotary regenerator for achieving the maximum regenerator effectiveness using GA. The authors also compared the numerical optimization results with the experimental results.

Sanaye and Hajabdollahi (2009) experimented genetic algorithm (GA) for the multi-objective optimization of the regenerator and obtained approximated Pareto front between the conflicting objectives, namely effectiveness and pressure drop. Rao and Patel (2011a, b, c) investigated the artificial bee colony (ABC) algorithm for the multi-objective optimization of the rotary regenerator. The authors considered maximization of regenerator effectiveness and minimization of total pressure drop as objective functions. Mioralli and Ganzarolli (2013) analyzed the influence of matrix porosity on rotary regenerator performance. The authors also conducted a simulation and optimization study of rotary regenerator with a computational model. Raja et al. (2016) obtained a set of Pareto optimal solution between the conflicting objectives of regenerator used for exhaust heat recovery. Authors considered the effectiveness and total pressure drop of regenerator as the objective function and used TS-TLBO algorithm as an optimization tool. Hajabdollahi (2017) carried out the performance comparison of the rotary regenerator and plate-fin heat exchanger through multi-objective optimization. The author considered optimization of effectiveness, heat exchanger volume, and total pressure drop in his investigation and used TLBO algorithm as an optimization tool.

### **3.4.1 Thermal Model**

In the present work, a radial-flow rotary regenerator with a randomly stacked woven-screen matrix is investigated for the optimization. Figure 3.11 shows the flow arrangement and detail geometry of the regenerator and matrix. The considered regenerator is used for exhaust heat recovery in gas furnace application. Further, the thermal-hydraulic model presented here is based on the previous works

of Kays and London (1985), Sanaye and Hajabdollahi (2009), Rao and Patel (2011a, b, c), and Raja et al. (2016). Moreover, during the discussion of the thermal-hydraulic model, the subscripts associated with different equations are given as follows:  $h$  stands for hot fluid,  $c$  stands for cold fluid,  $i$  stands for inlet, and  $o$  stands for the outlet.

For the radial-flow rotary regenerator, the heat transfer surface area and the total volume of the exchanger are correlated as

$$\alpha = \frac{A}{V} = \frac{\pi}{dx_t} \quad (3.118)$$

where  $A$  and  $V$  are the total heat transfer area of one side of the exchanger and total exchanger volume, respectively, and  $d$  and  $x_t$  are the matrix rod diameter and transverse pitch of the rod, respectively.

The total heat transfer surface area ( $A$ ) of the regenerator is represented in terms of hot-side and cold-side areas as

$$A = A_c + A_h = \alpha V \quad (3.119)$$

where  $A_c$  and  $A_h$  are the cold-side and hot-side heat transfer areas, respectively.

The hot-side frontal area ( $A_{fr,h}$ ) and cold-side frontal area ( $A_{fr,c}$ ) of the regenerator are correlated with each other by dimensionless term defined as split ( $s$ ) and are represented by

$$s = \frac{A_{fr,h}}{A_{fr,c}} = \frac{A_h}{A_c} \quad (3.120)$$

The free flow cross-section area of the regenerator is given by

$$A_{ff} = pA_{fr} \quad (3.121)$$

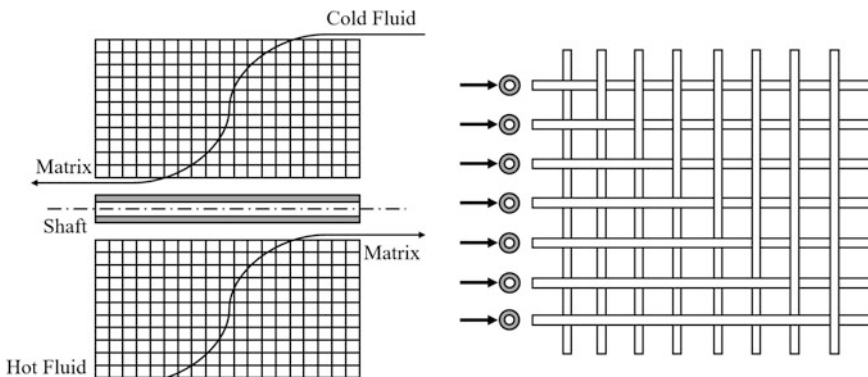


**Fig. 3.11** Radial-flow rotary regenerator and randomly stacked woven-screen matrix

where  $p$  is the porosity of matrix material and defined as the ratio of void volume to the total volume of the matrix surface and represented as follows:

$$p = \alpha r_h = 1 - \frac{\pi}{4x_t} \quad (3.122)$$

where  $r_h$  is the hydraulic radius of the matrix rod.

The hot-side and cold-side heat transfer coefficient ( $h$ ) for regenerative exchanger is calculated from the following correlation:

$$h = St G C_p \quad (3.123)$$

where  $G$  is the mass velocity,  $C_p$  is the specific heat of fluid, and  $St$  is Stanton number and defined as follows:

$$St = \frac{j}{Pr^{2/3}} \quad (3.124)$$

where  $Pr$  is the Prandtl number. The following equation calculates Colburn factor ( $j$ ) for a randomly stacked woven-screen matrix

$$j = a_1 Re^{-a_2} + a_3 \quad (3.125)$$

where  $a_1$ ,  $a_2$ , and  $a_3$  are constant coefficients and are given in Table 3.20.  $Re$  is the Reynolds number and is calculated by

$$Re = \frac{4r_h G}{\mu} \quad (3.126)$$

where  $\mu$  is the fluid viscosity.  $G$  is the mass velocity and is given by

$$G = \frac{m}{A_{ff}} \quad (3.127)$$

where  $m$  is the mass flow rate of the fluid.

The effectiveness of the regenerator is defined as the ratio of the actual heat transfer rate to the maximum possible heat transfer rate and represented as

**Table 3.20** Coefficient for calculation of Colburn factor

Porosity	0.602	0.725	0.766	0.832
$a_1$	0.5209	0.7568	0.9237	1.904
$a_2$	0.4072	0.4358	0.4479	0.5413
$a_3$	0.00035	0.00161	0.00193	0.00591

$$\varepsilon = \frac{Q}{Q_{\max}} = \frac{C_h(T_{h,i} - T_{h,o})}{C_{\min}(T_{h,i} - T_{c,i})} = \frac{C_c(T_{c,o} - T_{c,i})}{C_{\min}(T_{h,i} - T_{c,j})} \quad (3.128)$$

where  $Q$  is the heat transfer rate,  $C$  is the heat capacity of the fluid, and  $T$  is the temperature of the fluid.

The thermal effectiveness of rotary regenerator using  $\varepsilon$ -NTU method is also represented as a function of three nondimensional numbers: NTU,  $C^*$ , and  $C_r^*$  are estimated as follows:

$$\varepsilon = f(\text{NTU}, C^*, C_r^*) = \varepsilon_o \varphi_r \varphi_c \quad (3.129)$$

where  $\varphi_c$  and  $\varphi_r$  are the correction factors,  $\varphi_c$  is the correction factor for the cleanliness and considered as unity in the present work,  $\varepsilon_o$  denotes the effectiveness of a cross-flow heat exchanger and is calculated as

$$\varepsilon = \frac{1 - \exp[-\text{NTU}(1 - C^*)]}{1 - C^* \exp[-\text{NTU}(1 - C^*)]} \quad (3.130)$$

where  $C^*$  represents the heat capacity rate ratio and NTU represents the number of the transfer unit of the exchanger and are calculated as

$$C^* = \frac{C_{\min}}{C_{\max}} \quad (3.131)$$

$$\text{NTU} = \frac{UA}{C_{\min}} = \left( \frac{1}{C_{\min}} \right) \left( \frac{1}{(1/h_h A_h) + (1/h_c A_c)} \right) \quad (3.132)$$

The correction factor for rotational speed ( $\varphi_r$ ) is given by

$$\varphi_r = 1 - \frac{1}{9C_r^{*1.93}} \quad (3.133)$$

where  $C_r^*$  is the heat capacity rate ratio of the regenerator matrix and is defined as

$$C_r^* = \frac{C_r}{C_{\min}} = \frac{M_m C_m (N_m / 60)}{C_{\min}} \quad (3.134)$$

where  $M_m$  is mass of matrix material,  $C_m$  is the specific heat of the matrix, and  $N_m$  is the rotational speed of the matrix.

The hot-side and cold-side pressure drop for rotary regenerator is calculated from the following correlation:

$$\Delta P = \frac{G^2}{2} v_{\text{in}} \left[ (K_c + 1 - p^2) + 2 \left( \frac{v_{\text{out}}}{v_{\text{in}}} - 1 \right) + \left( f \frac{A}{A_{\text{ff}}} \frac{v_{\text{ave}}}{v_{\text{in}}} \right) - \frac{v_{\text{out}}}{v_{\text{in}}} (1 - p^2 - K_e) \right] \quad (3.135)$$

where  $K_c$  and  $K_e$  are coefficients of pressure drop at the entrance and exit cross-sections, respectively;  $v$  is the specific volume of the fluid; and  $f$  is the friction factor.

The following equation calculates the friction factor for a randomly stacked woven-screen matrix

$$f = 10^{g(\log(Re))} \quad (3.136)$$

where the value of  $g$  is obtained from the following function:

$$g(z) = b_1 z^3 + b_2 z^2 + b_3 z + b_4 \quad (3.137)$$

where  $b_1$ ,  $b_2$ ,  $b_3$ , and  $b_4$  are coefficients and are given in Table 3.21.

Based on the above thermal model, the objective function for the present work is defined in the next section.

### 3.4.2 Case Study, Objective Function Description, and Constraints

A radial-flow rotary regenerator with a randomly stacked woven-screen matrix needs to be designed and optimized for the maximum effectiveness and minimum pressure drop. The considered regenerator is used to preheat the compressed air. The fresh air is having the mass flow rate of 12 kg/s and coming out from the compressor at a temperature of 400 K. This air is preheated in the regenerator with the help of hot gases coming out from the furnace having 100 ton/h melting load. In the furnace, the fuel-air ratio is about 0.08 for combustion. The property values of air and hot gases are considered to be temperature dependent. Six design variables, such as the frontal area of regenerator ( $A_{\text{fr}}$ ), matrix thickness ( $t$ ), matrix rod diameter ( $d$ ), split ( $s$ ), porosity ( $p$ ), and the rotational speed of the regenerator ( $N_m$ ), are considered for the optimization problem. The upper and lower bounds of design

**Table 3.21** Coefficient for calculation of friction factor

Porosity	0.602	0.725	0.766	0.832
$b_1$	-0.0337	-0.0283	-0.0327	-0.0462
$b_2$	0.3851	0.3477	0.398	0.552
$b_3$	-1.614	-1.524	-1.709	-2.258
$b_4$	1.988	1.739	1.994	2.688

**Table 3.22** Ranges of design variables for rotary regenerator optimization

Design variables	Lower bound	Upper bound
Frontal area ( $\text{m}^2$ )	3	4
Matrix rod diameter (mm)	3	10
Split	0.33	3
Matrix thickness (m)	0.1	0.5
Matrix rotational speed (rpm)	1	1000
Porosity	0.602, 0.725, 0.766, 0.832	

variables are presented in Table 3.22. Out of six design variables, porosity ( $p$ ) is discrete while remaining five is continuous. Four different porosity values (0.602, 0.725, 0.766, 0.832) are considered for optimization.

As mentioned above, the maximization of regenerator effectiveness ( $\varepsilon$ ) is taken as the objective function in the present study. Further, the regenerator geometry which results in the maximum effectiveness also satisfies the pressure drop and heat duty constraints. So, considering all the aspects, the objective function for rotary regenerator is formulated as follows:

$$\left\{ \begin{array}{l} \text{Minimize } f(X) = \in (X) + \sum_{j=1}^n G_1(g_j(X))^2 \\ X = [x_1, x_2, x_3, \dots, x_D], \quad x_{i,\text{minimum}} \leq x_i \leq x_{i,\text{maximum}}, \quad i = 1, 2, 3, \dots, D \\ g_j(X) \leq 0, \quad j = 1, 2, 3, \dots, n \end{array} \right. \quad (3.138)$$

where  $X$  is the vector of design variables which should be bounded between its minimum and maximum values.  $G_1$  is the penalty parameter, and the entire term takes into account the effect of constraints violation. This term comes into the picture when the constraint violation takes place.  $g_j(X)$  indicates the constraints. The following constraints are considered for the rotary regenerator.

$$\Delta P \leq 25 \text{ kPa} \quad \text{pressure drop constraints} \quad (3.139)$$

$$Q \geq 7855 \text{ kW} \quad \text{heat duty constraints} \quad (3.140)$$

The next section describes the results and discussion of the case study.

### 3.4.3 Results and Discussion

The considered problem of the rotary regenerator is investigated using 11 different metaheuristic approaches to obtain the maximum effectiveness of regenerator. Each algorithm is implemented 100 times on the considered problem to estimate the statistical variations of the algorithms. Each algorithm is implemented with the

population size of 50, and the termination criteria are set as 100,000 function evaluations. The results obtained using each algorithm are presented in the forms of the best solution, worst solution, average solution standard deviation, and success rate obtained in 100 runs in Table 3.23. Here, the solutions which are infeasible (i.e., affected by penalty) are eliminated while obtaining the worst solution, average solution, standard deviation, and success rate. Further, the success rate of the algorithm is obtained by considering 0.1% variation from the global optimum value.

It can be observed from the comparative results that all the algorithms performed equally good and produced almost identical maximum effectiveness of regenerator. However, the average performance of the HTS algorithm is marginally better as compared to other competitive algorithms. The performance of the ABC algorithm is inferior in producing the best and average total annual cost as compared to another algorithm. Further, all the algorithms (except GA, PSO, ABC, and PVS), produced 100% success rate in obtaining the optimum value. It can be observed from the results that it is difficult to judge the performance of the algorithm as all the algorithms have produced a different performance to obtain the best, worst, and average results, and success rate. So, the Friedman rank test is implemented to judge the best suitable algorithm for rotary regenerator design considering the capability to obtain the best, worst, and average solutions, and success rate. The results of the Friedman rank test are presented in Table 3.24, and its graphical representation is given in Fig. 3.12. The results are presented in the form of Friedman value, normalized value with '1' as the best performing algorithm and its rank. It is observed from the results that HTS has obtained the first rank followed by TLBO and DE.

The optimized design of rotary regenerator obtained using the HTS is presented in Table 3.25. It can be noted from the results that the regenerator geometry with the maximum frontal area, minimum matrix rod diameter, and porosity results in the maximum regenerator effectiveness. The split produced the conflicting effect on

**Table 3.23** Comparative results of different algorithms for rotary regenerator optimization

Algorithms	Best	Worst	Average	SD	Success rate (%)
GA	0.929298	0.91	0.926204	7.2E-03	84
PSO	0.929339	0.91	0.927003	6.4E-03	88
DE	0.92934	0.92929	0.929325	2.1E-05	100
ABC	0.929339	0.91	0.925135	7.7E-03	72
CSA	0.929339	0.92929	0.929316	1.7E-05	100
TLBO	0.929339	0.929338	0.929338	4.1E-08	100
SOS	0.929339	0.929289	0.929327	1.8E-05	100
WWO	0.929339	0.929289	0.929302	1.8E-05	100
HTS	0.929339	0.929339	0.929339	2.3E-16	100
PVS	0.929339	0.91	0.926235	7.2E-03	84
SCA	0.929339	0.92929	0.929306	1.7E-05	100

**Table 3.24** Friedman rank test results for rotary regenerator optimization

Algorithms	Friedman value	Normalized value	Rank
GA	49	0.265306	11
PSO	39.5	0.329114	8
DE	20	0.65	3
ABC	48.5	0.268041	10
CSA	23	0.565217	4
TLBO	16	0.8125	2
SOS	25.5	0.509804	6
WWO	26.5	0.490566	7
HTS	13	1	1
PVS	44	0.295455	9
SCA	25	0.52	5

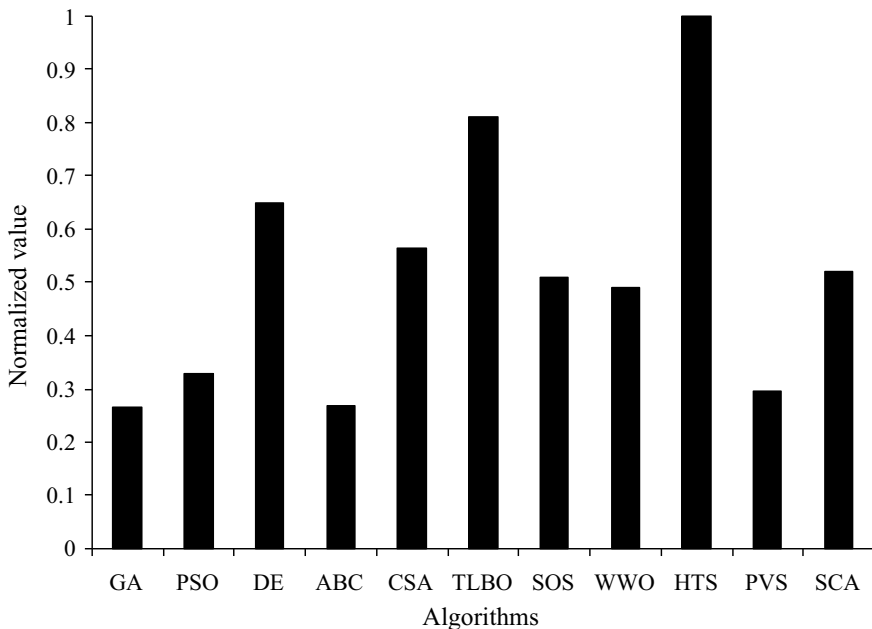


**Fig. 3.12** Graphical presentation of Friedman rank test for rotary regenerator optimization

achieving the maximum regenerator effectiveness within allowable pressure drop. Further, the total pressure drop occurs at the limiting value in the optimized regenerator design. Moreover, constraints are satisfied within the specified limits in the optimized design.

**Table 3.25** Optimized design geometry of rotary regenerator

Regenerator parameters	Optimized value
<i>Design variables</i>	
Frontal area, $A_{fr}$ ( $m^2$ )	4
Matrix rod diameter, $d_m$ (mm)	3
Matrix rotational speed, $N_r$ (rpm)	958.1
Split (s)	1.517
Matrix thickness, $t$ (m)	0.4105
Porosity	0.602
<i>Constraints</i>	
Total pressure drop, $\Delta P_t$ (kPa)	24.99
Heat transfer rate, $Q$ (kW)	7855.4
<i>Objective function</i>	
Effectiveness	0.92934

### 3.5 Plate Heat Exchanger (PHE)

Plate heat exchangers (PHE) are categorized as the compact heat exchangers. In PHEs, the heat transfer between two fluids takes place through a series of metal plates. In plate heat exchangers, a series of large rectangular thin metal plates clamped together to form narrow parallel plate channels (passages). Hot and cold fluids flow through the alternate channel in PHE and carry out the heat transfer. Figure 3.13 shows the schematic of PHE with the fluid flow path. The main parts of PHEs consist of the following:

1. Frame: It includes pressure sustaining parts, tightening bolts, carrying and guide bars, fixed and movable cover plates. The fluids will enter through one of the cover plate.
2. Thin metal plates: It clamped between two cover plates with the help of tightening bolts.

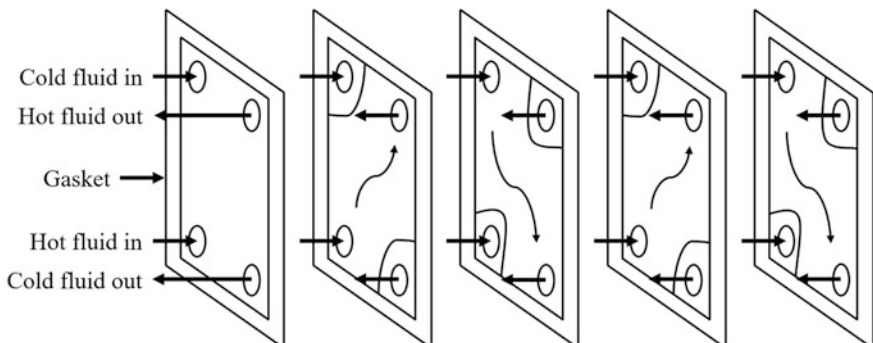


**Fig. 3.13** Schematic of plate heat exchanger with a fluid flow path

3. Gaskets: It serves the purpose of sealing the fluid as well as directing the fluid along the channels. The circular portion of the gasket will send one of the fluids to the next channel while the remaining portion allows the second fluid to flow across the channel.

In PHEs, a narrow channel is formed between every two consecutive plates with the help of gasket. So, the fluid will flow in these channels along the plane of the plates. Gaskets are placed and designed in such a way that it allows the same fluid to flow in alternate channels. Also, both the fluids are separated by thin metal plates which provide turbulence to the fluid flow. As shown in Fig. 3.13, both the fluids entered and exited from the first plate (i.e., cover plate) and directed to next plates. Here, gasket allowed hot fluid to flow through the first channel (formed between the cover plate and first thin metal plate), while cold fluid moved to the second channel (formed between first and second metal plate). In this way, the same fluid flows in alternate channels and hence the heat transfer takes place between them through thin metal plates.

There are four main types of PHEs, namely gasket plate heat exchanger, brazed plate heat exchanger, welded plate heat exchanger, and semi-welded plate heat exchanger. Irrespective of its types, PHEs are one of the most efficient classes of heat exchangers due to its smart and innovative design. Due to their stunning advantages, such as compactness, high thermal effectiveness, ease of maintenance, less fouling and flexibility, PHE is preferred to conventional shell and tube heat exchangers in many cases (Najafi and Najafi 2010). At the same time, few disadvantages are also associated with PHEs like metal plates are expensive, so the initial cost is high, leakage detection is difficult, higher pressure drop, and limited temperature range due to bonding material between plates. Plate heat exchangers are the best option in some industries like food, dairy, and chemical applications including heating glycerin, condensing ethanol and cooling sulfuric acid, salt solution, hexane, and kerosene.

As mentioned above, high surface area density and thermal effectiveness of PHEs reduced their size and weight compared to other types of heat exchangers. On the other end, high hydraulic losses (i.e., pressure drop) occurred in PHEs. Thus, the trade-off between thermal and hydraulic behavior within the given set of constraints is always required to reach an optimum design of PHEs. As a result, metaheuristic algorithms are more suitable to obtain the optimized design of PHEs as compared to conventional optimization methods. Generally, objectives involved in the design optimization of PHE are the maximum effectiveness, minimum pressure drop, minimum cost, minimum weight, etc.

Earlier, researchers carried out different types of numerical works to optimize PHEs design with different methodologies. Wang and Sunden (2003) used a derivative-based optimization method for the economic optimization of plate heat exchanger. Gut and Pinto (2003, 2004) presented a mathematical model of the gasket plate heat exchanger (2003) and performed shape optimization (2004) of that model. Further, the authors presented a screening method for the selection of optimal configurations of plate heat exchangers. Zhu and Zhang (2004) performed

the heat transfer area optimization of the plate heat exchanger used for the geothermal heating application. Durmus et al. (2009) carried out an experimental investigation of plate heat exchanger having different surface geometry. They proposed heat transfer, friction factor, and exergy loss correlations for plate heat exchanger based on the experimental results.

Najafi and Najafi (2010) performed a multi-objective optimization of PHE with the pressure drop and heat transfer coefficient of a heat exchanger as objective functions. The authors used NSGA-II as an optimization tool. Arsenyeva et al. (2011) proposed a mathematical model based on the area optimization of the multi-pass plate-and-frame heat exchanger. Hajabdollahi et al. (2013) obtained the optimized geometric parameters of the gasket plate heat exchanger for the maximum effectiveness and minimum total cost by adapting NSGA-II. Lee and Lee (2015) carried out a thermodynamic optimization of PHE. The authors considered two conflicting objectives, namely Colburn factor and friction factor, for optimization and used GA as an optimization tool. Further, the authors also developed the correlation for Colburn factor and friction factor. Hajabdollahi et al. (2016) presented the comparative study of gasket plate and shell and tube heat exchangers from the economic point of view by using a genetic algorithm (GA). Raja et al. (2018a, b) performed the thermal–hydraulic optimization of a plate heat exchanger by adapting the heat transfer search algorithm. The authors also validated the optimization results by conducting the experimentation of the scale model of plate heat exchanger.

### 3.5.1 Thermal Model

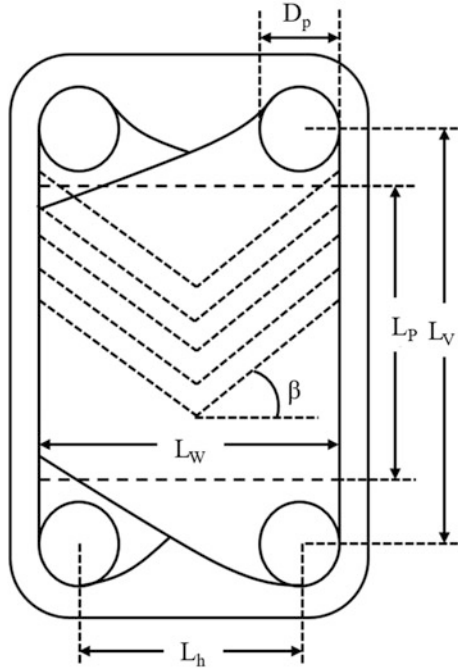
In the present work, a chevron plate heat exchanger is investigated for the optimization. The geometry of PHE is shown in Fig. 3.13, while the detail of chevron plates is shown in Fig. 3.14. In this work, the  $\varepsilon$ -NTU approach is utilized to predict the performance of PHE (Shah and Sekulic 2003a, b). The PHE is assumed to run under a steady state, with negligible heat loss and uniform velocities. Further, the heat transfer coefficients are assumed to be uniform and constant. The thermal–hydraulic model presented here is based on the previous works of Shah and Sekulic (2003a, b), Najafi and Najafi (2010), Hajabdollahi et al. (2013), and Raja et al. (2017a, b, c).

#### (a) Heat transfer

The effectiveness of counter-flow heat exchanger is obtained using the following correlation:

$$\varepsilon = \frac{1 - e^{-\text{NTU}(1-C^*)}}{1 - C^* e^{-\text{NTU}(1-C^*)}} \quad (3.141)$$

**Fig. 3.14** Schematic of chevron plate



where  $C^*$  represents the heat capacity rate ratio and NTU represents the number of the transfer unit of the exchanger and are calculated as

$$C^* = \frac{(mC_p)_{\min}}{(mC_p)_{\max}} \quad (3.142)$$

$$\text{NTU} = \frac{UA_e}{(mC_p)_{\min}} \quad (3.143)$$

where  $m$  is the mass flow rate of the fluid,  $C_p$  is the specific heat of fluid,  $A_e$  is the effective heat transfer area, and  $U$  is the overall heat transfer coefficient of the exchanger and is given by

$$U = \frac{1}{\left(\frac{1}{h_h}\right) + R_{f,h} + \left(\frac{1}{h_c}\right) + R_{f,c} + \left(\frac{t}{k}\right)_w} \quad (3.144)$$

where subscripts  $h$  and  $c$  stand for hot side and cold side, respectively, while  $w$  stands for wall condition.  $R_f$  is the fouling resistance,  $k$  is the thermal conductivity of plate material,  $t$  is the plate thickness, and  $h$  is the heat transfer coefficient and is obtained using the following equation:

$$h = n(Re)^{n_1} (Pr)^{\frac{1}{3}} \left( \frac{\mu_b}{\mu_w} \right)^{0.17} \left( \frac{k}{d_h} \right) \quad (3.145)$$

where the values of coefficient  $n$  and  $n_1$  depend on the flow characteristic and chevron angle. The value of  $n$  and  $n_1$  is given in Table 3.26 for different chevron angles. Also,  $\mu$  is the fluid viscosity,  $Pr$  is the Prandtl number,  $Re$  is the Reynolds number, and  $d_h$  is the hydraulic diameter.

In plate heat exchanger, the length of the compact plate is given by

$$L_p = L_v - D_p \quad (3.146)$$

where  $D_p$  is the port diameter and  $L_v$  is the vertical distance between ports and is obtained using the following equation:

$$L_v = L_h + D_p \quad (3.147)$$

where  $L_h$  is the horizontal distance between ports.

The mean flow channel gap ( $b$ ) of the PHEs can be determined as follows:

$$b = p - t \quad (3.148)$$

where  $t$  is the plate thickness and  $p$  is the plate pitch and is obtained using the following equation:

$$P = \frac{L_c}{N} \quad (3.149)$$

where  $L_c$  is the vertical distance between ports and  $N$  is the number of plates.

**Table 3.26** Value of coefficients  $n$  and  $n_1$  for different chevron angles

Chevron angle	Reynolds number	$n$	$n_1$
$\geq 65$	<20	0.562	0.326
	20–500	0.331	0.503
	>500	0.087	0.718
60	<20	0.562	0.326
	20–400	0.306	0.529
	>400	0.108	0.703
50	<20	0.63	0.333
	20–300	0.291	0.591
	>300	0.13	0.732
45	<10	0.718	0.349
	10–100	0.4	0.598
	>100	0.3	0.663
$\leq 30$	$\leq 10$	0.718	0.349
	>10	0.348	0.663

The enlargement factor of PHE is obtained using the following equation:

$$\varphi = \frac{A_1}{L_p L_w} \quad (3.150)$$

where  $A_1$  is the heat transfer area and  $A_{1p}$  is the projected area of the plate and is obtained using the following equation:

$$A_{1p} = L_p L_w \quad (3.151)$$

where  $L_w$  is the plate width.

The effective heat transfer area ( $A_e$ ) of the PHEs can be expressed as follows:

$$A_e = A_1 N_e \quad (3.152)$$

where  $N_e$  is the effective number of plates in PHE.

The number of channels per pass ( $N_{cp}$ ) of the plate heat exchanger is obtained using the following equation:

$$N_{cp} = \frac{N - 1}{2N_p} \quad (3.153)$$

where  $N_p$  is the number of passes.

The Reynolds number of the fluid flow is obtained using the following equation:

$$Re = \frac{Gd_h}{\mu} \quad (3.154)$$

where  $G$  and  $d_h$  are the mass velocity in the channel and hydraulic diameter, respectively, and are obtained using the following equations:

$$G = \frac{m}{N_{cp} b L_w} \quad (3.155)$$

$$d_h = \frac{4bL_w}{2(b + L_w\Phi)} \approx \frac{2b}{\Phi} \quad (3.156)$$

### (b) Pressure drop

The pressure drop through the channels can be given as

$$\Delta P_{\text{channel}} = \frac{4fL_v N_p G^2}{2d_h \rho} \quad (3.157)$$

where  $\rho$  is the density of the fluid, and  $f$  is the friction factor and is obtained using the following equation:

$$f = \frac{n_2}{Re^{n_3}} \quad (3.158)$$

where the values of coefficient  $n_2$  and  $n_3$  depend on the flow characteristic and chevron angle. The values of  $n_2$  and  $n_3$  are given in Table 3.27 for different chevron angles.

The pressure drop in inlet and outlet ports may be given as

$$\Delta P_{\text{port}} = 1.4N_p \frac{G_p^2}{2\rho} \quad (3.159)$$

where  $G_p$  is the mass velocity in the port and is obtained using the following correlation:

$$G_p = \frac{4m}{\pi D_p^2} \quad (3.160)$$

The total pressure drop is the summation of the channel pressure drop and the port pressure drop and is given by

$$\Delta P_{\text{total}} = \Delta P_{\text{channel}} + \Delta P_{\text{port}} \quad (3.161)$$

Based on the above thermal model, the objective function for the present work is defined in the next section.

**Table 3.27** Value of coefficients  $n_2$  and  $n_3$  for different chevron angles

Chevron angle	Reynolds number	$n_2$	$n_3$
$\geq 65$	<50	24	1
	50–500	2.8	0.451
	>500	0.639	0.213
60	<40	24	1
	40–400	3.24	0.457
	>400	0.76	0.215
50	<20	34	1
	20–300	11.25	0.631
	>300	0.772	0.161
45	<15	47	1
	15–300	18.29	0.652
	>300	1.441	0.206
$\leq 30$	<10	50	1
	10–100	19.4	0.589
	>100	2.99	0.183

### 3.5.2 Case Study, Objective Function Description, and Constraints

It is intended to design and optimize chevron plate heat exchanger for minimum pressure drop. The PHE is constructed from SS304 and used for water-to-water heat exchange. The hot water at 338 K is entering into PHE with the mass flow rate of 140 kg/s. The cold water having the mass flow rate of 140 kg/s is supplied to PHE at a temperature of 295 K. The desired outlet temperature of the hot fluid is 318 K. Temperature-dependent thermo-physical properties values of both the fluids are considered during the optimization procedure. Six design variables such as the horizontal distance of ports ( $L_h$ ), vertical distance of ports ( $L_v$ ), length of compact plates ( $L_c$ ), port diameter ( $D_p$ ), plate thickness ( $t$ ), enlargement factor ( $\varphi$ ), and number of plates ( $N$ ) are considered for the optimization problem. The upper and lower bounds of design variables are presented in Table 3.28.

As mentioned above, the minimization of the total pressure drop of the heat exchanger ( $\Delta P_{\text{total}}$ ) is taken as an objective function in the present study. Further, the heat exchanger geometry which results in minimum pressure drop also satisfies the heat transfer coefficient and heat duty constraints. So, considering all the aspects, the objective function for plate heat exchanger is formulated as follows:

$$\left\{ \begin{array}{l} \text{Minimize } f(X) = \Delta P_{\text{total}}(X) + \sum_{j=1}^n G_1(g_j(X))^2 \\ X = [x_1, x_2, x_3, \dots, x_D], \quad x_{i,\text{minimum}} \leq x_i \leq x_{i,\text{maximum}}, \quad i = 1, 2, 3, \dots, D \\ g_j(X) \leq 0, \quad j = 1, 2, 3, \dots, n \end{array} \right. \quad (3.162)$$

where  $X$  is the vector of design variables which should be bounded between its minimum and maximum values.  $G_1$  is the penalty parameter, and entire term takes into account the effect of constraints violation. This term comes into picture when constraint violation takes place.  $g_j(X)$  indicates the constraints. The following constraints are considered for the plate heat exchanger design.

$$U \geq 4240 \text{ W/m}^2\text{K} \quad \text{Overall heat transfer coefficient constraint} \quad (3.163)$$

**Table 3.28** Ranges of design variables for PHE optimization

Design variables	Lower bound	Upper bound
Port diameter, $D_p$ (mm)	100	400
The vertical length of plats, $L_v$ (mm)	1100	2000
The horizontal length of plats, $L_h$ (mm)	300	700
The total length of compact plates, $L_c$ (mm)	300	600
Enlargement factor, $\varphi$	1.15	1.25
Plate thickness, $t$ (mm)	0.3	0.9
Number of plates, $N$	100	1900

$$Q \geq 11.58 \text{ MW} \quad \text{Heat duty constraint} \quad (3.164)$$

The next section describes the results and discussion of the case study.

### 3.5.3 Results and Discussion

The considered problem of plate heat exchanger is investigated using 11 different metaheuristic approaches to obtain the minimum pressure drop of the heat exchanger. Each algorithm is implemented 100 times on the considered problem to estimate the statistical variations of the algorithms. Each algorithm is implemented with the population size of 50, and the termination criteria are set as 100,000 function evaluations. The results obtained using each algorithm are presented in the forms of the best solution, worst solution, average solution, standard deviation, and success rate obtained in 100 runs in Table 3.29. Here, the infeasible solutions (i.e., affected by penalty) are eliminated while obtaining the worst solution, average solution, standard deviation, and success rate. Furthermore, the success rate of the algorithm is obtained by considering 0.1% variation from the global optimum value.

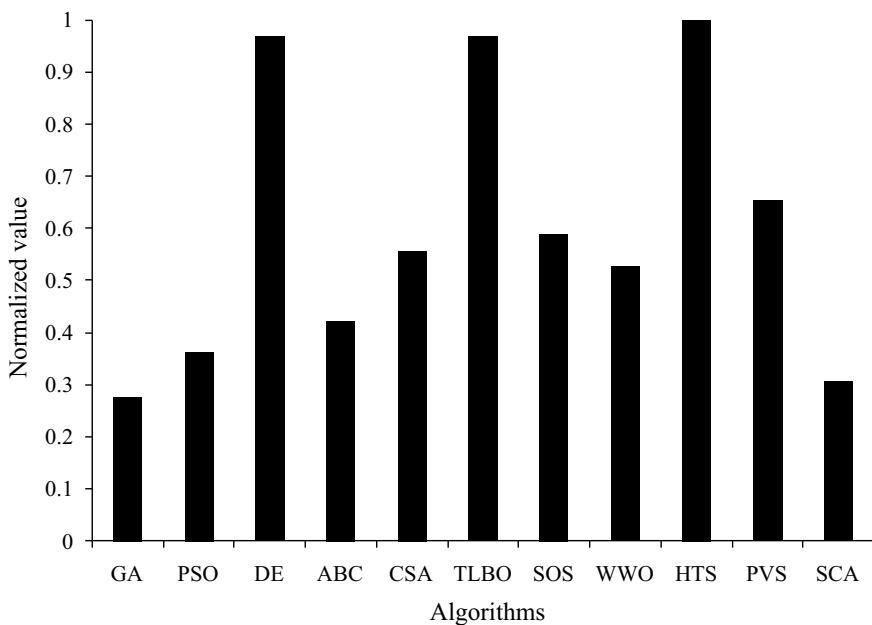
It can be observed from the comparative results that all the algorithms perform equally well (except GA and SCA) in obtaining the minimum pressure drop geometry of the plate heat exchanger. However, the average performance of HTS is better followed by DE and TLBO in comparison with other algorithms. The performance of GA and SCA is inferior in producing the best and average pressure drop. Further, the success rate of majority of algorithms (except GA, PSO, ABC, and SCA) is 100% in obtaining the minimum pressure drop design of PHE. It can be observed from the results that it is difficult to judge the performance of the algorithm as all the algorithms have produced a different performance to obtain the best, worst, and average solutions, and success rate. So, the Friedman rank test is

**Table 3.29** Comparative results of different algorithms for PHE optimization

Algorithms	Best	Worst	Average	SD	Success rate (%)
GA	21,494.3	21,913.42	21,750.85	1.01E+02	21
PSO	21,492.55	21,567.82	21,501.59	2.49E+01	88
DE	21,492.55	21,492.86	21,492.59	1E-01	100
ABC	21,492.55	21,521.67	21,497.29	6.2	96
CSA	21,492.55	21,496.47	21,493.18	1.46	100
TLBO	21,492.55	21,492.91	21,492.79	1.18E-09	100
SOS	21,492.55	21,496.47	21,493.33	1.59	100
WWO	21,492.55	21,501.02	21,493.88	2.89	100
HTS	21,492.55	21,492.55	21,492.55	0	100
PVS	21,492.55	21,492.94	21,492.81	7.18E-04	100
SCA	21,503.26	21,546.08	21,517.97	15.29	56

**Table 3.30** Friedman rank test results for PHE optimization

Algorithms	Friedman value	Normalized value	Rank
GA	54	0.277778	10
PSO	41.5	0.361446	8
DE	15.5	0.967742	2
ABC	35.5	0.422535	7
CSA	27	0.555556	5
TLBO	15.5	0.967742	2
SOS	25.5	0.588235	4
WWO	28.5	0.526316	6
HTS	15	1	1
PVS	23	0.652174	3
SCA	49	0.306122	9

**Fig. 3.15** Graphical presentation of Friedman rank test for PHE optimization

implemented to judge the best suitable algorithm for plate heat exchanger design considering the capability to obtain the best, worst, and average solutions, and success rate. The results of the Friedman rank test are presented in Table 3.30, and its graphical representation is given in Fig. 3.15. The results are presented in the form of Friedman value, normalized value with ‘1’ as the best performing algorithm and its rank. It is observed from the results that HTS has obtained the first rank. The DE and TLBO algorithm performed equally well and shared the second rank.

**Table 3.31** Optimized design geometry of plate heat exchanger

Operating parameters	Optimized value
<i>Design variable</i>	
Port diameter, $D_p$ (mm)	400
The vertical length of plats, $L_v$ (mm)	2000
The horizontal length of plats, $L_h$ (mm)	700
The total length of compact plates, $L_c$ (mm)	600
Enlargement factor, $\varphi$	1.23
Plate thickness, $t$ (mm)	0.30
Number of plates, $N$	1900
<i>Constraints</i>	
Overall heat transfer coefficient, $U$ (W/m <sup>2</sup> K)	4242.8
Heat duty, $Q$ (MW)	11.586
<i>Objective function</i>	
Total pressure drop, $\Delta P_s$ (Pa)	21,492.55

The optimized design of the plate heat exchanger obtained using the HTS is presented in Table 3.31. It can be noted from the results that the plate heat exchanger geometry with the maximum port diameter, vertical length of plats, horizontal length of plats, total length of compact plates, number of plates, and minimum plate thickness results in minimum total pressure drop. The enlargement factor produced the conflicting effect on achieving the minimum total pressure drop. Furthermore, the constraints are satisfied within the specified limits in the optimized design of the plate heat exchanger.

## References

- Abed, A. M., Abed, I. A., Majdi, H. S., Al-Shamani, A. N., & Sopian, K. (2016). A new optimization approach for shell and tube heat exchangers by using electromagnetism-like algorithm (EM), *Heat and Mass Transfer*, 52(12), 2621–2634.
- Agarwal A, and Gupta SK. (2008) ‘Jumping gene adaptations of NSGA-II and their use in the multi-objective optimal design of shell and tube heat exchangers’, *Chemical Engineering Research and Design*, vol. 86, 123–139.
- Ahmadi P, Hajabdollahi H and Dincer I. (2011) ‘Cost and entropy generation minimization of a cross-flow plate fin heat exchanger using multi-objective genetic algorithm’, *Journal of Heat Transfer-The American Society of Mechanical Engineering*, vol. 133, 21801-21809.
- Amini M and Bazargan M. (2014) ‘Two objective optimization in shell-and-tube heat exchangers using genetic algorithm’, *Applied Thermal Engineering*, vol. 69, 278–285.
- Arsenyeva OP, Tovazhniansky LL, and Kapustenko PO. (2011) ‘Optimal design of plate and frame heat exchangers for efficient heat recovery in process industries’, *Energy*, vol. 36, 4588–4598.
- Ayala HVH, Keller P, Morais MF, Mariani VC, Coelho LS and Rao RV. (2016) ‘Design of heat exchangers using a novel multi objective free search differential evolution paradigm’, *Applied Thermal Engineering*, vol. 94, 170–177.

- Azad AV and Amidpour M. (2011) 'Economic optimization of shell and tube heat exchanger based on constructal theory', *Energy*, vol. 36, 1087–1096.
- Babaieh M, Sadri S and Sayyaadi H. (2014) 'Multi-objective optimization of a cross-flow plate heat exchanger using entropy generation minimization', *Chemical Engineering Technology*, vol. 37, 87–94.
- Babu BV and Munawar SA. (2007) 'Differential evolution strategies for optimal design of shell-and-tube heat exchangers', *Chemical Engineering Science*, vol. 62, 3720–3739.
- Bejan A. (1997) 'The concept of irreversibility in heat exchanger design: counter flow heat exchangers for gas-to-gas applications', *Journal of Heat Transfer-The American Society Mechanical Engineering*, vol. 99, 374–380.
- Bell KJ. *Delaware method for shell side design*, In Kakac S., A.E., Bergles, F. and Mayinger, F. (eds.) (1981) *Heat Exchangers: Thermal-Hydraulic Fundamentals and Design*, Hemisphere/McGraw-Hill, Washington, DC.
- Bell KJ. (1963) Final report of the cooperative research program on shell and tube heat exchangers, *University of Delaware Engineering Experimental Station Bulletin No. 5*, Newark, Delaware.
- Büyükkalaca O and Yilmaz T. (2002) 'Influence of rotational speed on effectiveness of rotary type heat exchanger', *Heat and Mass Transfer*, vol. 38, 441–447.
- Caputo AC, Pelagagge PM and Salini P. (2008) 'Heat exchanger design based on economic optimization', *Applied Thermal Engineering*, vol. 28, 1151–1159.
- Caputo AC, Pelagagge PM and Salini P. (2015) 'Heat exchanger optimized design compared with installed industrial solutions', *Applied Thermal Engineering*, vol. 87, 371–380.
- Caputo AC, Pelagagge PM and Salini P. (2011) 'Joint economic optimization of heat exchanger design and maintenance policy', *Applied Thermal Engineering*, vol. 31, 1381–1392.
- Caputo AC, Pelagagge PM and Salini P. (2016) 'Manufacturing cost model for heat exchangers optimization', *Applied Thermal Engineering*, vol. 94, 513–533.
- Cho DH, Seo SK, Lee CJ and Lim Y. (2017) 'Optimization of Layer Patterning on a Plate Fin Heat Exchanger Considering Abnormal Operating Conditions', *Applied Thermal Engineering*.
- Colgate SA. (1995) Regenerator Optimization for Stirling Cycle Refrigeration, In *Cryocoolers* (pp. 247–258). Springer, US.
- Costa ALH and Queiroz EM. (2008) 'Design optimization of shell and tube heat exchanger', *Applied Thermal Engineering*, vol. 28, 1798–1805.
- De Vasconcelos Segundo EH, Amoroso AL, Mariani VC and dos Santos Coelho L. (2017) 'Thermodynamic optimization design for plate-fin heat exchangers by Tsallis JADE', *International Journal of Thermal Sciences*, vol. 113, 136–44.
- Du J, Ni YM and Fang YS. (2016) 'Correlations and optimization of a heat exchanger with offset fins by genetic algorithm combining orthogonal design', *Applied Thermal Engineering*, vol. 107, 1091–1103.
- Durmus A, Benil B, Kurtbas I and Gul H. (2009) 'Investigation of heat transfer and pressure drop in plate heat exchangers having different surface profiles', *International Journal of Heat Mass Transfer*, vol. 52, 1451–1457.
- Eryener D. (2006) 'Thermo-economic optimization of baffle spacing for shell and tube heat exchangers', *Energy Conversion and Management*, vol. 47, 1478–1489.
- Fesanghary M, Damangir E and Soleimani I. (2009) 'Design optimization of shell and tube heat exchangers using global sensitivity analysis and harmony search algorithm', *Applied Thermal Engineering*, vol. 29, 1026–1031.
- Foli K, Okabe T, Olhofer M, Jin Y, and Sebdhoff B. (2006) 'Optimization of micro heat exchanger: CFD, analytical approach and multi-objective evolutionary algorithms' *International Journal of Heat and Mass Transfer*, vol. 49, 1090–1099.
- Gandomi AH, Alavi AH and Krill herd. (2012) 'A new bio-inspired optimization algorithm', *Communications in Nonlinear Science and Numerical Simulation*, vol. 17(12), 4831–45.
- Ghodsipour N and Sadrameli M. (2003) 'Experimental and sensitivity analysis of a rotary air pre-heater for the flue gas heat recovery', *Applied Thermal Engineering*, vol. 23, 571–580.
- Ghosh S, Ghosh I, Pratihar DK, Maiti B and Das PK. (2011) 'Optimum stacking pattern for multi-stream plate-fin heat exchanger through a genetic algorithm', *International Journal Thermal Science*, vol. 50, 214–224.

- Gnielinski V. (1976), 'New equations for heat and mass transfer in turbulent pipe and channel flows', *International Chemical Engineering*, vol. 16, 359–368.
- Guo J, Cheng L and Xu M. (2009) 'Optimization design of shell-and-tube heat exchanger by entropy generation minimization and genetic algorithm', *Applied Thermal Engineering*, vol. 29, 2954–2960.
- Gut JAW and Pinto JM. (2003) 'Modeling of plate heat exchangers with generalized configurations', *International Journal of Heat and Mass Transfer*, vol. 46, 2571–2585.
- Gut JAW and Pinto JM. (2004) 'Optimal configuration design for plate heat exchangers', *International Journal of Heat and Mass Transfer*, vol. 47, 4833–4848.
- Hadidi A and Nazari A. (2013) 'Design and economic optimization of shell-and-tube heat exchangers using biogeography-based (BBO) algorithm', *Applied Thermal Engineering*, vol. 51, 1263–1272.
- Hadidi A. (2015) 'A robust approach for optimal design of plate fin heat exchangers using biogeography-based optimization (BBO) algorithm', *Applied Energy*, vol. 150, 196–210.
- Hadidi A, Hadidi M and Nazari A. (2013) 'A new design approach for shell-and-tube heat exchangers using imperialist competitive algorithm (ICA) from economic point of view', *Energy Conversion and Management*, vol. 67, 66–74.
- Hajabdollahi F, Hajabdollahi Z and Hajabdollahi H. (2013) 'Optimum design of gasket plate heat exchanger using multimodal genetic algorithm', *Heat Transfer Research*, vol. 43, 1–19.
- Hajabdollahi H, Ahmadi P and Dincer I. (2011) 'Multi-objective optimization of plain fin-and-tube heat exchanger using evolutionary algorithm', *Journal of Thermophysics and Heat Transfer*, vol. 25(3), 424–31.
- Hajabdollahi H, Ahmadi P, and Dincer I. (2011) 'Thermo-economic optimization of a shell and tube condenser using both genetic algorithm and particle swarm', *International Journal of Refrigeration*, vol. 34(4), 1066–1076.
- Hajabdollahi H and Hajabdollahi Z. (2016) 'Assessment of nanoparticles in thermo-economic improvement of shell and tube heat exchanger', *Applied Thermal Engineering*, vol. 106, 827–837.
- Hajabdollahi H. (2012) 'Exergetic optimization of shell-and-tube heat exchanger using NSGA-II', *Heat Transfer Engineering*, vol. 33, 618–628.
- Hajabdollahi H. (2015) 'Investigating the effect of non-similar fins in thermo-economic optimization of plate fin heat exchanger', *Applied Thermal Engineering*, vol. 82, 152–161.
- Hajabdollahi H, Naderi M and Adimi S. (2016) 'A comparative study on the shell and tube and gasket-plate heat exchangers: The economic viewpoint', *Applied Thermal Engineering*, vol. 92, 271–282.
- Hajabdollahi H. (2017) 'Comparison of stationary and rotary matrix heat exchangers using teaching-learning-based optimization algorithm', *Proceedings of the Institution of Mechanical Engineers, Part E: Journal of Process Mechanical Engineering*.
- Hewitt GF. (1998) *Heat Exchanger Design Handbook*, Begell House, New York.
- Hsieh CT and Jang JY. (2012) 'Parametric study and optimization of louver finned-tube heat exchangers by Taguchi method', *Applied Thermal Engineering*, vol. 42, 101–10.
- Hwang CL and Yoon K. (2012) 'Multiple attribute decision making: methods and applications a state-of-the-art survey', *Springer Science & Business Media*, vol. 186.
- Incropera FP and DeWitt DP. (1998) *Fundamentals of Heat and Mass Transfer*, John Wiley, New York, USA.
- Jang JY, Hsu LF and Leu JS. (2013) 'Optimization of the span angle and location of vortex generators in a plate-fin and tube heat exchanger', *International Journal of Heat and Mass Transfer*, vol. 67, 432–44.
- Jia, R., & Sundén, B. (2003, January). Optimal design of compact heat exchangers by an artificial neural network method. In ASME 2003 Heat Transfer Summer Conference (pp. 655–664). American Society of Mechanical Engineers.
- Kakac S and Liu H. (2002) *Heat exchangers: Selection, rating and thermal design*, CRC Press, New York.
- Kays WM and London AL. (1984) *Compact Heat Exchangers*, McGraw Hill, New York.
- Kays WM, London AL. (1985) *Compact Heat Exchangers*, 3rd ed., McGraw Hill, New York, USA.

- Khosravi R, Khosravi A, Nahavandi S and Hajabdollahi H. (2015) 'Effectiveness of evolutionary algorithms for optimization of heat exchangers', *Energy Conversion and Management*, vol. 89, 281–288.
- Lee J and Lee KS. (2015) 'Friction and Colburn factor correlations and shape optimization of chevron-type plate heat exchangers', *Applied Thermal Engineering*, vol. 89, 62–69.
- Lemouedda A, Breuer M, Franz E, Botsch T and Delgado A. (2010) 'Optimization of the angle of attack of delta-winglet vortex generators in a plate-fin-and-tube heat exchanger', *International journal of heat and mass transfer*, vol. 53(23), 5386–99.
- Li Q, Flamant G, Yuan X, Neveu P and Luo L. (2011) Compact heat exchangers: a review and future applications for a new generation of high temperature solar receivers', *Renewable and Sustainable Energy Reviews*, vol. 15, 4855–4875.
- Liu C, Bu W and Xu D. (2017) 'Multi-objective shape optimization of a plate-fin heat exchanger using CFD and multi-objective genetic algorithm', *International Journal of Heat and Mass Transfer*, vol. 111, 65–82.
- Manglik RM and Bergles AE. (1995) 'Heat transfer and pressure drop correlations for the rectangular offset strip fin compact heat exchanger', *Experimental Thermal and Fluid Science*, vol. 10 (2), 171–180.
- Mioralli PC and Ganzarolli MM. (2013) 'Thermal analysis of a rotary regenerator with fixed pressure drop or fixed pumping power', *Applied Thermal Engineering*, vol. 52(1), 187–197.
- Mirjalili S, Mirjalili SM and Lewis A. (2014) 'Grey wolf optimizer'. *Advances in Engineering Software*, vol. 69, 46–61.
- Mirzaei M, Hajabdollahi H and Fadakar H. (2017) 'Multi-objective optimization of shell- and tube heat exchanger by constructal theory', *Applied Thermal Engineering*, vol. 125, 9–19.
- Mishra M, Das PK and Sarangi S. (2004) 'Optimum design of cross flow plate-fin heat exchangers through genetic algorithm', *International Journal of Heat Exchangers*, vol. 5(2), 379–402.
- Mishra M, Das PK. (2009) 'Thermo-economic design-optimization of cross flow plate-fin heat exchanger using genetic algorithm', *International Journal of Exergy*, vol. 6(6), 237–252.
- Mohanty DK. (2016b) 'Application of firefly algorithm for design optimization of a shell and tube heat exchanger from economic point of view', *International Journal of Thermal Science*, vol. 102, 228–238.
- Mohanty DK. (2016a) 'Gravitational search algorithm for economic optimization design of a shell and tube heat exchanger', *Applied Thermal Engineering*, vol. 107, 184–193.
- Najafi H and Najafi B. (2010) 'Multi-objective optimization of a plate and frame heat exchanger via genetic algorithm', *Heat Mass Transfer*, vol. 46, 639–647.
- Najafi H, Najafi B and Hoseinpouri P. (2005) 'Energy and cost optimization of a plate and fin heat exchanger using genetic algorithm'. *Applied Thermal Engineering*, vol. 31, 1839–1847.
- Ozcelik Y. (2007) 'Exergetic optimization of shell and tube heat exchanger using a genetic based algorithm', *Applied Thermal Engineering*, vol. 27, 1849–1856.
- Pacheco-Vega A, Sen M, Yang KT and McClain RL. (2001), 'Correlations of fin-tube heat exchanger performance data using genetic algorithm, simulated annealing and interval methods', In: *Proceedings of ASME heat transfer division*, vol. 369, USA, pp. 143–151.
- Pacheco-Vega A, Sen M and Yang KT. (2003) 'Simultaneous determination of in-and-over- tube heat transfer correlations in heat exchangers by global regression', *International Journal Heat and Mass Transfer*, vol. 46(6), 1029–1040.
- Patel VK and Rao RV. (2011) 'Design optimization of shell-and-tube heat exchanger using particle swarm optimization technique', *Applied Thermal Engineering*, vol. 30, 1417–1425.
- Patel VK and Savsani VJ. (2014) 'Optimization of a plate-fin heat exchanger design through an improved multi-objective teaching-learning based optimization (MO-ITLBO) algorithm', *Chemical Engineering Research and Design*, vol. 92, 2371–2382.
- Peng H, Ling X and Wu E. (2010) 'An improved Particle Swarm Algorithm for Optimal Design of Plate-Fin Heat Exchangers', *Industrial and Engineering Chemistry Research*, vol. 49, 6144–6149.
- Peng H, Ling X. (2008) 'Optimal design approach for the plate-fin heat exchangers using neural networks cooperated with genetic algorithms', *Applied Thermal Engineering*, vol. 28, 642–650.

- Ponce-Ortega JM, Serna-Gonzalez M and Jimenez-Gutierrez A. (2009) 'Use of genetic algorithms for the optimal design of shell and tube heat exchangers', *Applied Thermal Engineering*, vol. 29, 203–209.
- Raja BD, Jhala RL and Patel VK. (2017a) 'Many-objective optimization of shell and tube heat exchanger', *Thermal Science and Engineering Progress*, vol. 2, 87–101.
- Raja BD, Jhala RL and Patel V. (2017b) 'Many-objective optimization of cross-flow plate-fin heat exchanger', *International Journal of Thermal Sciences*, vol. 118, 320–39.
- Raja BD, Jhala RL and Patel V. (2016) 'Multi-objective optimization of a rotary regenerator using tutorial training and self-learning inspired teaching-learning based optimization algorithm (TS-TLBO)'. *Applied Thermal Engineering*, vol. 93, 456–67.
- Raja BD, Patel VK and Jhala RL. (2017c) 'Thermal design and optimization of fin-and-tube heat exchanger using heat transfer search algorithm', *Thermal Science and Engineering Progress*, vol. 4, 45–57.
- Raja BD, Jhala RL. and Patel VK. (2018) 'Multi-objective thermo-economic and thermodynamics optimization of a plate-fin heat exchanger', *Heat Transfer—Asian Research*, vol. 47, 253–270.
- Raja BD, Jhala, RL and Patel VK. (2018) 'Thermal-hydraulic optimization of plate heat exchanger: A multi-objective approach', *International Journal of Thermal Sciences*, 124, 522–535.
- Rao RV and Patel VK. (2011a) 'Design optimization of shell and tube heat exchangers using swarm optimization algorithms', *Proceedings of the Institution of Mechanical Engineers, Part A: Journal of Power and Energy*, vol. 225, 619–634.
- Rao, RV. and Patel, VK. (2011b) 'Thermodynamic optimization of plate-fin heat exchanger using teaching-learning-based optimization (TLBO) algorithm' *Optimization*, vol. 10, 11–12.
- Rao RV and Patel VK. (2011c) 'Design optimization of rotary regenerator using artificial bee colony algorithm', *Proceedings of the Institution of Mechanical Engineers Part A: Journal of Power and Energy*, vol. 225(8), 1088–1098.
- Rao RV and Patel VK. (2013) 'Multi-objective optimization of heat exchangers using a modified teaching-learning-based optimization algorithm', *Applied Mathematical Modelling*, vol. 37, 1147–1162.
- Rao RV and Patel VK. (2010) 'Thermodynamic optimization of cross-flow plate-fin heat exchangers using a particle swarm optimization technique', *International Journal of Thermal Science*, vol. 49, 1712–1721.
- Ravagnani MASS, Silva AP, Biscaya Jr EC and Caballero JA. (2009) 'Optimal Design of Shell-and-Tube Heat Exchangers Using Particle Swarm Optimization', *Industrial & Engineering Chemistry Research*, vol. 48, 2927–2935.
- Reneaume, J. M., & Niclout, N. (2001). Plate fin heat exchanger design using simulated annealing. In Computer Aided Chemical Engineering (Vol. 9, pp. 481–486). Elsevier.
- Reneaume, J. M., & Niclout, N. (2003). MINLP optimization of plate fin heat exchangers, *Chemical and Biochemical Engineering Quarterly*, 17(1), 65–76.
- Reneaume, J. M., Pingaud, H., & Niclout, N. (2000). Optimization of plate fin heat exchangers: a continuous formulation, *Chemical Engineering Research and Design*, 78(6), 849–859.
- Rohsenow WM and Hartnett JP. (1973) *Handbook of Heat Transfer*, McGraw-Hill, New York.
- Romero-Méndez R, Sen M, Yang KT and McClain R. (2000) 'Effect of fin spacing on convection in a plate fin and tube heat exchanger', *International Journal of Heat and Mass Transfer*, vol.43(1), 39–51.
- Sadeghzadeha H, Ehyaeib MA and Rosen MA. (2015) 'Techno-economic optimization of a shell and tube heat exchanger by genetic and particle swarm algorithms', *Energy Conversion and Management*, vol. 93, 84–91.
- Saechan P and Wongwises S. (2008) 'Optimal configuration of cross flow plate finned tube condenser based on the second law of thermodynamics', *International Journal of Thermal Science*, vol. 47, 1473–1481.
- Şahin AŞ, Kılıç B and Kılıç U. (2011) 'Design and economic optimization of shell and tube heat exchangers using Artificial Bee Colony (ABC) algorithm', *Energy Conversion and Management*, vol. 52, 3356–3362.
- Sanaye S and Hajabdollahi H. (2009) 'Multi-objective optimization of rotary regenerator using genetic algorithm', *International Journal of Thermal Sciences*, vol. 30(14–15), 1937–1945.

- Sanaye S and Hajabdollahi H. (2010) 'Multi-objective optimization of shell and tube heat exchangers', *Applied Thermal Engineering*, vol. 30, 1937–1945.
- Sanaye S and Hajabdollahi H. (2010) 'Thermal-economic multi-objective optimization of plate fin heat exchanger using genetic algorithm', *Applied Energy*, vol. 87, 1893–1902.
- Sanaye S, Jafari S and Ghaebi H. (2008) 'Optimum operational conditions of a rotary regenerator using genetic algorithm', *Energy and Buildings*, vol. 40(9), 1637–1642.
- Segundo EH, Amoroso AL, Mariani VC and dos Santos Coelho L. (2017) 'Economic optimization design for shell-and-tube heat exchangers by a tsallis differential evolution', *Applied Thermal Engineering*, vol. 111, 143–51.
- Selbas R, Kizilkan O and Reppich M. (2006) 'A new design approach for shell- and-tube heat exchangers using genetic algorithms from economic point of view', *Chemical Engineering and Processing*, vol. 45, 268–275.
- Shah RK and Bell KJ. (2000) *Handbook of Thermal Engineering*, CRC Press, Florida.
- Shah RK, and Sekulic P. (2003a) *Fundamental of Heat Exchanger Design*, John Wiley & Sons, New York.
- Shah RK, Sekulic P. (2003b) *Fundamental of Heat Exchanger Design*, Wiley, New York.
- Singh V, Abdelaziz O, Aute V and Radermacher R. (2011) 'Simulation of air-to-refrigerant fin-and-tube heat exchanger with CFD-based air propagation', *International Journal of Refrigeration*, vol. 34(8), 1883–97.
- Skiepko T and Shah RK. (2004) 'A comparison of rotary regenerator theory and experimental results for an air pre-heater for a thermal power plant', *Experimental Thermal and Fluid Science*, vol. 28, 257–264.
- Smith R. (2005) *Chemical Process Design and Integration*, Wiley, New York.
- Soltan BK, Saffar-Aval M and Damangir E. (2004) 'Minimizing capital and operating costs of shell and tube condensers using optimum baffle spacing', *Applied Thermal Engineering*, vol. 24, 2801–2810.
- Taborek, J. (1998) 'Shell-and-tube heat exchangers: single-phase flow' in *Handbook of Heat Exchanger Design* (Ed. G. F. Hewitt), pp. 3.3.3.1–3.3.11.5 (Begell House, New York).
- Tang LH, Zeng M and Wang QW. (2009) 'Experimental and numerical investigation on air-side performance of fin-and-tube heat exchangers with various fin patterns', *Experimental Thermal and Fluid Science*, vol. 33, 818–827.
- Turgut OE. (2016) 'Hybrid Chaotic Quantum behaved Particle Swarm Optimization algorithm for thermal design of plate fin heat exchangers', *Applied Mathematical Modelling*, vol. 40, 50–69.
- Wang CC, Fu WL and Chang CT. (1997) 'Heat transfer and friction characteristics of typical wavy fin-and-tube heat exchangers', *Experimental Thermal and Fluid Science*, vol. 14(2), 174–86.
- Wang CC. (2000) 'Recent progress on the air-side performance of fin-and-tube heat exchangers', *International Journal of Heat Exchangers*, vol. 2, 57–84.
- Wang L and Sundem B. (2003) 'Optimal design of plate heat exchangers with and without pressure drop specifications', *Applied Thermal Engineering*, vol. 23, 295–311.
- Wang Z and Li Y. (2015) 'Irreversibility analysis for optimization design of plate fin heat exchangers using a multi-objective cuckoo search algorithm', *Energy Conversation and Management*, vol. 101, 126–135.
- Wang Z, Li Y and Zhao M. (2015) 'Experimental investigation on the thermal performance of multi-stream plate-fin heat exchanger based on genetic algorithm layer pattern design', *International Journal of Heat Mass Transfer*, vol. 82, 510–520.
- Wen J, Yang H, Jian G, Tong X, Li K and Wang S. (2016) 'Energy and cost optimization of shell and tube heat exchanger with helical baffles using Kriging meta-model based on MOGA', *International Journal of Heat and Mass Transfer*, vol. 98, 29–39.
- Wen J, Ynag H, Tong X, Li K, Wang S and Li Y. (2016) 'Configuration parameters design and optimization for plate fin heat exchangers with serrated fin by multi-objective genetic algorithm', *Energy Conversation and Management*, vol. 117, 482–489.
- Wen J, Yang H, Tong X, Li K, Wang S and Li Y. (2016) 'Optimization investigation on configuration parameters of serrated fin in plate-fin heat exchanger using genetic algorithm', *International Journal of Thermal Science*, vol. 101, 116–125.

- Wildi-Tremblay P and Gosselin L. (2007) 'Minimizing shell and tube heat exchanger cost with genetic algorithms and considering maintenance', *International Journal Energy Research*, vol. 31, 867–885.
- Wong JYQ, Sharma S and Rangaiah GP. (2016) 'Design of shell-and-tube heat exchangers for multiple objectives using elitist non-dominated sorting genetic algorithm with termination criteria', *Applied Thermal Engineering*, vol. 93, 888–899.
- Wu Z, Ding G, Wang K and Fukaya M. (2008) 'Application of a genetic algorithm to optimize the refrigerant circuit of fin-and-tube heat exchangers for maximum heat transfer or shortest tube', *International Journal of Thermal Sciences*, vol. 47(8), 985–97.
- Wu Z, Roderick VN and Finn B. (2006) 'Model-based analysis and simulation of regenerative heat wheel', *Energy and Buildings*, vol. 38, 502–514.
- Xie GN, Chen QY, Tang LH, Zeng M and Wang QW. (2005) 'Thermal design and comparison of two fin-and-tube heat exchangers', In: *Proceedings of 2nd Chinese Heat Transfer Technology*, China, pp. 8–11.
- Xie GN, Sunden B and Wang QW. (2008) 'Optimization of compact heat exchangers by a genetic algorithm', *Applied Thermal Engineering*, vol. 28, 895–906.
- Xie GN, Wang WQ and Sunden B. (2008a) 'Application of a genetic algorithm for thermal design of fin-and-tube heat exchangers', *Heat Transfer Engineering*, vol. 29(7), 597–607.
- Yang DK, Lee KS and Song S. (2006b) 'Fin spacing optimization of a fin-tube heat exchanger under frosting conditions', *International Journal of Heat and Mass Transfer*, vol. 49(15), 2619–25.
- Yin H and Ooka R. (2015) 'Shape optimization of water-to-water plate-fin heat exchanger using computational fluid dynamics and genetic algorithm', *Applied Thermal Engineering*, vol. 80, 310–318.
- Yousefi M, Darus AN and Hooshyar D. (2015) 'Multi-stage thermal-economical optimization of compact heat exchangers: a new evolutionary-based design approach for real-world problems', *Applied Thermal Engineering*, vol. 83, 71–80.
- Yousefi M, Darus AN and Mohammadi H. (2012) 'An imperialist competitive algorithm for optimal design of plate-fin heat exchangers', *International Journal Heat and Mass Transfer*, vol. 55, 3178–3185.
- Yousefi M, Enayatifar R, and Darus AN. (2011) 'Optimal design of plate-fin heat exchangers by a hybrid evolutionary algorithm', *International Communication in Heat and Mass Transfer*, vol. 39, 258–263.
- Yousefi M, Enayatifar R, Darus AN and Abdullah AH. (2012) 'A robust learning based evolutionary approach for thermal-economic optimization of compact heat exchangers', *International Communication of Heat Mass Transfer*, vol. 39, 1605–1615.
- Yousefi M, Enayatifar R, Darus AN and Abdullah AH. (2013) 'Optimization of plate-fin heat exchangers by an improved harmony search algorithm', *Applied Thermal Engineering*, vol. 50, 877–885.
- Zarea H, Kashkooli FM, Mehryan AM, Saffarian MR and Beherghani EN. (2014) 'Optimal design of plate-fin heat exchangers by a Bees Algorithm', *Applied Thermal Engineering*, vol. 69, 267–277.
- Zhang L, Yang C and Zhou J. (2010) 'A distributed parameter model and its application in optimizing the plate-fin heat exchanger based on the minimum entropy generation', *International Journal of Thermal Science*, vol. 49, 1427–1436.
- Zhang W, Chen L and Sun F. (2009) 'Power and efficiency optimization for combined Brayton and inverse Brayton cycles', *Applied Thermal Engineering*, vol. 29, 2885–2894.
- Zhao M and Li Y. (2013) 'An effective layer pattern optimization model for multi-stream plate-fin heat exchanger using genetic algorithm', *International Journal of Heat and Mass Transfer*, vol. 60, 480–489.
- Zhou Y, Zhu L, Yu J and Li Y. (2014) 'Optimization of plate-fin heat exchangers by minimizing specific entropy generation rate', *International Journal of Heat and Mass Transfer*, vol. 78, 942–946.
- Zhua J and Zhang W. (2004) 'Optimization design of plate heat exchangers (PHE) for geothermal district heating systems', *Geothermics*, vol. 33, 337–347.

# Chapter 4

## Thermal Design and Optimization of Heat Engines and Heat Pumps



**Abstract** Heat engines are the devices which convert the thermal energy into mechanical work, while heat pumps transfer heat energy from low temperature to high temperature. In this chapter, thermal modeling of different types of heat engines and heat pumps like Carnot heat engine, Rankine heat engine, Ericsson heat engine, Stirling heat pump, Brayton heat pump, etc. is presented. The objective function of each of the heat engine and the heat pump is derived from the thermal model. Optimization of a derived objective is performed by implementing 11 different metaheuristic algorithms for each heat engine, and heat pump and comparative results are tabulated and discussed.

The heat engine is a device that converts the thermal energy into mechanical work. Heat engine does this by using the temperature difference between a hot source and a cold sink. Heat is transferred from the source, through the working substance of the engine, to the sink, and in this process, some of the heat energy changes into work by using the qualities of working substance inside the engine. Heat engines are classified based on their working cycle. Figure 4.1 shows the working principle of the heat engine. The performance parameter of any heat engine is its thermal efficiency, which is defined as work produced by the heat engine ( $W_{\text{out}}$ ) to the heat supplied ( $Q_H$ ) to obtain the same work.

Likewise, the heat pump is a device that transfers the heat energy from low temperature to high temperature. The transfer of the heat energy from low temperature to high temperature takes place by additional external work to the working substance of the heat pump. Heat pumps are also classified based on their working cycle. The performance parameter of any heat pump system is known as the coefficient of performance (COP), which is defined as the amount of heat rejected to the high-temperature reservoir ( $Q_H$ ) to the work required ( $W_{\text{in}}$ ) in order to reject that heat. Thermal design and optimization of the heat engine and heat pump are essential for its efficient operation. Generally, objectives involved in the optimization of the heat engine and heat pump are the maximum thermal efficiency, minimum pressure drop, maximum power output, maximum coefficient of

**Fig. 4.1** Working principle of the heat engine

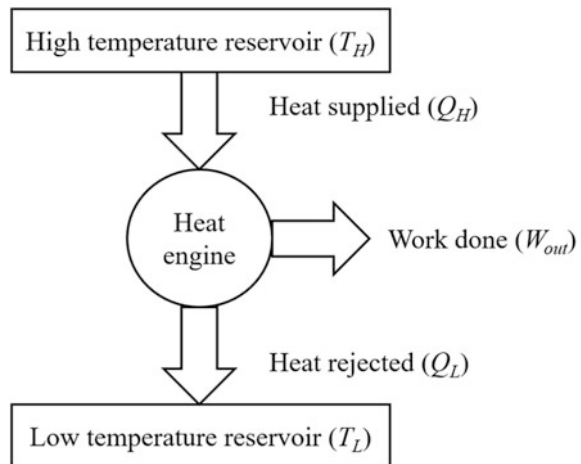
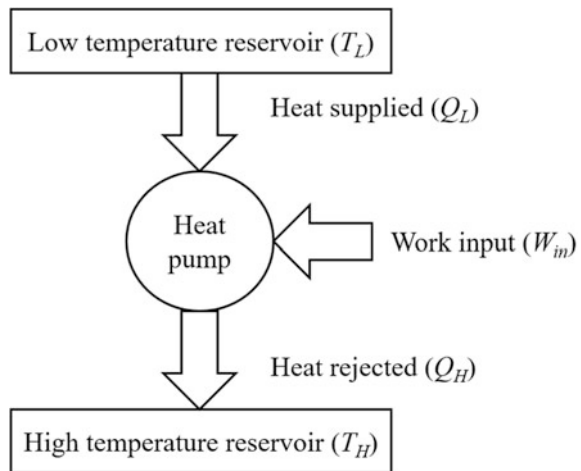


**Fig. 4.2** Working principle of the heat pump



performance, etc. In the subsequent section, thermal modeling and optimization of various heat engines and heat pumps are presented and discussed (Fig. 4.2).

## 4.1 Carnot Heat Engine

A Carnot heat engine is operated on the reversible Carnot cycle. A thermodynamic cycle occurs when the system passes through a series of different states and finally returned to its original state. Figure 4.1 shows the schematic arrangement that explains the work produces by the Carnot heat engine. It can be observed from the figure that the heat engine operates between high-temperature and low-temperature

reservoir. The working fluid of the heat engine receives heat  $Q_H$  from the high-temperature reservoir and rejects heat  $Q_L$  to the low-temperature reservoir. The amount of heat  $Q_H$  is higher as compared to  $Q_L$ . So, the difference between heat  $Q_H$  and  $Q_L$  results in work ( $W$ ) produced by the heat engine. As mentioned previously, the Carnot heat engine works on the reversible Carnot cycle. The thermodynamic representation (pressure-volume and temperature-entropy) of the working of the Carnot heat engine is shown in Fig. 4.3 and explained.

Process 1–2 (isothermal expansion): In this process, the working fluid of the heat engine is allowed to expand, and it does work on the surroundings. The temperature of the working fluid does not change during the process, and thus the expansion is isothermal. The isothermal expansion is propelled by absorption of heat energy  $Q_H$  from the high-temperature reservoir. Process 2–3 (adiabatic expansion): In this process, the working fluid continues to expand, doing work on the surroundings, and losing an equivalent amount of internal energy. In this process, the temperature of the working fluid is reduced while its entropy remains constant. Process 3–4 (isothermal compression): In this process, the working fluid of the heat engine undergoes the isothermal compression process by rejecting heat to the low-temperature reservoir. In this process, the temperature of the working fluid remains constant while its pressure is increased. Process 4–1 (adiabatic compression): In this process, the working fluid of the heat engine undergoes the adiabatic compression, which increases its internal energy. In this process, the temperature and pressure of the working fluid increase while its entropy remains constant. The main advantage of the Carnot heat engine is its higher efficiency. However, it is difficult to operate the heat engine on the Carnot cycle due to a combination of the isothermal and adiabatic processes.

Earlier, researchers had carried out different types of numerical works related to Carnot heat engine. Chen (1994) presented a thermal model of Carnot heat engine considering the effect of thermal resistance, heat leakage, and irreversibility

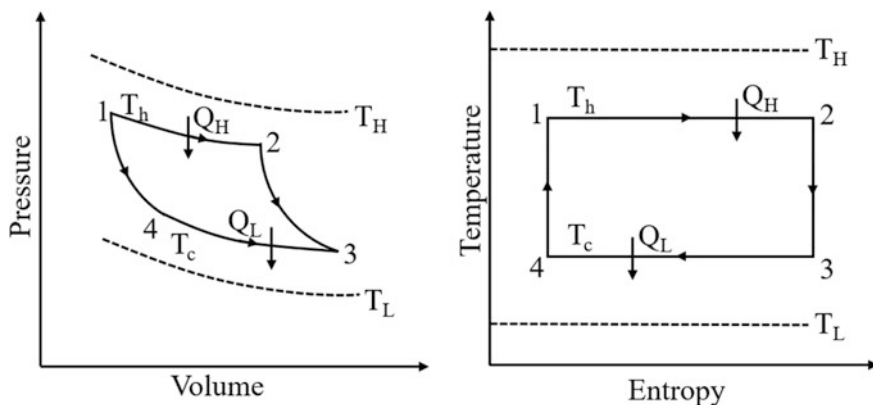


**Fig. 4.3** Thermodynamic presentation of Carnot heat engine

resulting from the working fluid. The author adopted a power output and efficiency of the Carnot heat engine as an objective function and obtains the condition for maximum efficiency and maximum power output of the presented model. Sahin et al. (1995) analyzed endoreversible Carnot heat engine based on the maximum power-density criteria and compared the obtained results with the available results of maximum power analysis. The authors concluded that the design parameters at the maximum power density lead to smaller and more efficient endoreversible Carnot heat engines than those working at the maximum power output. Bojić (1997) analyzed endoreversible Carnot engine for the cogeneration of power and heat by using the finite-time thermodynamics. The author obtained a different optimum condition for achieving maximum annual worth in the production of heat and power. Göktun and Özkanak (1997) investigated the optimal performance of a corrugated, collector-driven, irreversible Carnot heat engine through energetic optimization. The authors developed a relation between the operating parameter and the efficiency of the Carnot heat engine. Cheng and Chen (1997) carried out the ecological optimization of irreversible Carnot heat engine based on the finite-time thermodynamics, finite thermal capacitance rates of the heat reservoirs, and finite total conductance of the heat exchangers. The author optimized the ecological function with respect to the cycle temperature ratio and the heat conductance ratio. Wu (1988) performed the power optimization of a finite-time Carnot heat engine. The author derived a mathematical expression to obtain the power output of a Carnot heat engine and compared the power of the existing engine with that derived from a mathematical expression.

Kodal et al. (2000) performed the finite-time thermodynamic optimization of an irreversible Carnot heat engine considering the maximum power density criterion. The authors observed that the design parameters at maximum power density lead to smaller and more efficient heat engines. Furthermore, the authors concluded that the irreversibilities have a greater influence on the performances at maximum power density conditions compared to the maximum power conditions. Salas et al. (2002) performed the optimization of Carnot-like heat engines with the nonlinear inverse, Dulong–Petit, and Stefan–Boltzmann heat transfer laws for the maximization of engine efficiency and power output. Chen et al. (2004) performed the ecological optimization of an irreversible Carnot heat engine considering the power and entropy production rate of the engine. The authors presented an application example to demonstrate the effect of various losses and irreversibility on the optimal performance of the heat engine. Qin et al. (2005) carried out the frequency-dependent performance analysis of an endoreversible Carnot heat engine model. The authors derived the relationship between average power output, efficiency, available temperature drop, and the cycle frequency of an endoreversible Carnot heat engine. Üst et al. (2005) performed the thermo-ecological optimization of a generalized irreversible Carnot heat engine considering losses due to heat transfer across finite temperature differences, heat leak, and internal irreversibilities. The authors considered the ecological coefficient of performance of the heat engine as an objective function and obtained its optimum value analytically. Chen et al. (2006) derived the analytical formulae for power, efficiency, and entropy generation

rate of the heat engine using the finite-time thermodynamics. Moreover, the authors carried out the analysis and optimization of the developed model in order to investigate the effect of the cycle process on the performance of the cycles.

Chen et al. (2007a, b) carried out the exergy-based ecological optimization of a generalized irreversible Carnot engine considering the losses due to heat resistance, heat leakage, and internal irreversibility. Lurie and Kribus (2010) developed a model of saturation phase-change internal Carnot engine (SPICE) considering thermodynamic, mechanical, and heat transfer aspects and derived the efficiency and maximum power of the engine. Zhan et al. (2011) investigated the optimal ecological performance of a generalized irreversible Carnot heat engine. The authors considered the losses of heat resistance, heat leak, and internal irreversibility in the optimization model. Chen et al. (2013) developed an optimization problem of multi-stage irreversible Carnot heat engines and obtained complete numerical solutions of the optimization problem using dynamic programming. The authors also analyzed the effects of internal irreversibility and heat transfer laws on the optimization results of the engine. The entransy dissipation value of the systems is defined, and the relationships between the power output, exergy output, entropy generation, and entransy dissipation values of a heat engine are obtained. Açıkkalp (2014) performed the entransy analysis of irreversible Carnot-like heat engine. Park and Kim (2014) performed the thermodynamic analysis of a sequential Carnot cycle with a finite heat source and an infinite heat sink. The authors developed a mathematical model of the cycle and obtained the optimized value of efficiency and the specific work of the cycle. Zhang et al. (2016) performed the power optimization of chemically driven heat engine based on the first- and second-order reaction kinetic theory and obtained the effects of the finite-time thermodynamic on the power optimization. Han et al. (2017) investigated the exergy loss and the entransy loss of the generalized irreversible Carnot engine. The authors proposed the potential entransy loss and entransy degeneration for the heat engine system.

#### 4.1.1 Thermal Model

In the present work, a heat engine working on the Carnot cycle is considered for the optimization. The thermodynamic presentation of the Carnot heat engine is shown in Fig. 4.3. The thermal model presented here is based on the previous work of Sayyaadi et al. (2015), Chang (2007), Sogut and Durmazay (2006), and Cheng and Chen (1997). Moreover, the subscripts H and L stand for high-temperature and low-temperature reservoir sides while h and c stand for high-temperature and low-temperature working fluid sides, respectively, in the different equations of the thermal model.

The heat transfer between the low-temperature reservoir and the working fluid is given by

$$Q_L = \alpha_{L,c}(T_c - T_L) \quad (4.1)$$

where  $\alpha_{L,c}$  is the capacitance rate of the cold fluid.

The heat transfer between the high-temperature reservoir and the working fluid is given by

$$Q_H = \alpha_{H,r}(T_H^4 - T_h^4) + \alpha_{H,c}(T_H - T_h) \quad (4.2)$$

where  $\alpha_{H,c}$  is the capacitance rate of the hot fluid and  $\alpha_{H,r}$  is the radiation parameter.

As per the first law of thermodynamics, the power output of the heat engine is given by

$$W = Q_H - Q_L = Q_H\eta \quad (4.3)$$

where  $\eta$  is the thermal efficiency of the Carnot heat engine.

For the Carnot heat engine, the second law of thermodynamics with finite temperature difference can be given by

$$\frac{Q_H}{T_h} = \frac{Q_L}{T_c} \quad (4.4)$$

Based on the above equations, the relation between  $T_h$  and  $T_c$  is given by

$$T_c = \frac{T_L}{1 - \frac{\alpha_{H,r}}{\alpha_{L,c}} \left( \frac{T_H^4 - T_h^4}{T_h} \right) - \frac{\alpha_{H,c}}{\alpha_{L,c}} \left( \frac{T_H - T_h}{T_h} \right)} \quad (4.5)$$

Also, the output power of the heat engine in terms of  $T_h$  and  $T_c$  is described by

$$W = [\alpha_{H,r}(T_H^4 - T_h^4) + \alpha_{H,c}(T_H - T_h)] \left( 1 - \frac{T_c}{T_h} \right) \quad (4.6)$$

The entropy generation rate for the considered heat engine is presented by

$$S_g = \frac{Q_L}{T_L} - \frac{Q_H}{T_H} \quad (4.7)$$

Based on the entropy generation rate, ecological function (Angulo-Brown 1991a, b) of the considered system is given by

$$E = W - T_0 S_g \quad (4.8)$$

where  $T_0$  is the environment temperature. In the present work, the lower temperature of the system ( $T_L$ ) and environment temperature are considered to be equal.

The thermal efficiency of the Carnot heat engine is given by

$$\eta = 1 - \frac{\tau}{\chi - \beta(1 - \chi^4) - \psi(1 - \chi)} \quad (4.9)$$

where  $\tau$  is the engine temperature ratio,  $\beta$  is the heat source to heat sink allocation temperature,  $\chi$  is the heat source temperature ratio,  $\psi$  is the heat transfer ratio of the allocation parameters and are given by

$$\tau = \frac{T_L}{T_H} \quad (4.10)$$

$$\beta = \frac{\alpha_{H,r} T_H^3}{\alpha_{L,c}} \quad (4.11)$$

$$\chi = \frac{T_h}{T_H} \quad (4.12)$$

$$\psi = \frac{\alpha_{H,c}}{\alpha_{L,c}} \quad (4.13)$$

The nondimensional form of power output is given by

$$W = [\beta(1 - \chi^4) - \psi(1 - \chi)]\eta \quad (4.14)$$

Likewise, the nondimensional form of the ecological function is given by

$$E = [\beta(1 - \chi^4) - \psi(1 - \chi)] * \left[ \eta - \frac{\tau\{\beta(1 - \chi^4) + \psi(1 - \chi) - \chi + 1\}}{\{\chi - \beta(1 - \chi^4) - \psi(1 - \chi)\}} \right] \quad (4.15)$$

Based on the above thermal model, the objective function for the present work is defined in the next section.

#### **4.1.2 Case Study, Objective Function Description, and Constraints**

The Carnot heat engine working between the heat source temperature ( $T_H$ ) 1000 K and heat sink temperature ( $T_L$ ) 300 K needs to be designed and optimized for the maximum thermal efficiency. The considered heat engine used ideal gas as a working fluid. Four design variables such as engine temperature ratio ( $\tau$ ), heat source to heat sink allocation temperature ( $\beta$ ), heat source temperature ratio ( $\chi$ ), and heat transfer ratio of the allocation parameters ( $\psi$ ) are considered for the optimization problem. The upper and lower bounds of design variables are presented in Table 4.1.

**Table 4.1** Ranges of design variables for Carnot heat engine optimization

Design variable	Lower bound	Upper bound
Engine temperature ratio, $\tau$	0.2	0.2
Heat source to heat sink allocation temperature, $\beta$	0.1	1
Heat source temperature ratio, $\gamma$	0.7	0.8
Heat transfer ratio of the allocation parameters, $\psi$	0.1	1

As mentioned above, the maximization of thermal efficiency of the Carnot heat engine is taken as an objective function in the present study. Further, the operating parameters which result in maximum thermal efficiency also satisfy the dimensionless output power and ecological constraints. So, considering all the aspects, the objective function of the Carnot heat engine is formulated as below:

$$\left\{ \begin{array}{l} \text{Minimize } f(X) = \eta(X) + \sum_{j=1}^n G_1(g_j(X))^2 \\ X = [x_1, x_2, x_3, \dots, x_D], \quad x_{i,\text{minimum}} \leq x_i \leq x_{i,\text{maximum}}, \quad i = 1, 2, 3, \dots, D \\ g_j(X) \leq 0, \quad j = 1, 2, 3, \dots, n \end{array} \right. \quad (4.16)$$

where  $X$  is the vector of design variables which should be bounded between its minimum and maximum values.  $G_1$  is the penalty parameter, and entire term takes into account the effect of constraints violation. This term comes into the picture when constraint violation takes place.  $g_j(X)$  indicates the constraints. The following constraints are considered for the Carnot heat engine.

$$\text{Nondimensional power output, } W \geq 0.175 \quad (4.17)$$

$$\text{Nondimensional Ecological function, } E \geq 65 \quad (4.18)$$

The next section describes the results and discussion of the case study.

#### 4.1.3 Results and Discussion

The considered problem of Carnot heat engine is investigated using 11 different metaheuristic approaches to obtain the maximum thermal efficiency of the heat engine. Each algorithm is implemented 100 times on the considered problem to estimate the statistical variations of the algorithms. Each algorithm is implemented with the population size of 50, and the termination criteria are set as 100,000 function evaluations. The results obtained using each algorithm are presented in the form of the best solution, worst solution, average solution standard deviation, and

**Table 4.2** Comparative results of different algorithms for Carnot heat engine optimization

Algorithms	Best	Worst	Average	SD	Success rate (%)
GA	0.54321	0.54301	0.543163	1.02E-04	16
PSO	0.54322	0.54321	0.54322	4.08E-07	96
DE	0.54321	0.54302	0.543151	1.14E-04	12
ABC	0.54321	0.54321	0.543218	5.35E-07	28
CSA	0.54322	0.54301	0.543185	8.57E-05	24
TLBO	0.54321	0.54301	0.543149	1.20E-04	12
SOS	0.54321	0.54321	0.543218	3.41E-16	92
WWO	0.54321	0.54301	0.543188	7.86E-05	28
HTS	0.54322	0.54301	0.543199	6.64E-05	40
PVS	0.54322	0.54302	0.543207	5.16E-05	60
SCA	0.54322	0.543	0.543151	6.82E-05	88

success rate obtained in 100 runs in Table 4.2. Here, the infeasible solutions (i.e., affected by penalty) are eliminated while obtaining the worst solution, average solution, standard deviation, and success rate. Further, the success rate of the algorithm is obtained by considering 0.1% variation from the global optimum value.

It can be observed from the comparative results that all the algorithms performed equally good and produced almost identical maximum thermal efficiency of the Carnot heat engine. Furthermore, the average performance of all the considered algorithm is less or more identical. However, the success rate of PSO algorithm is better, while TLBO algorithm produced the least success rate in obtaining the global optimum value. It can be observed from the results that it is difficult to judge the performance of the algorithm as all the algorithms produced a different performance to obtain the best, worst, and average results, and success rate. So, the Friedman rank test is implemented to judge the best suitable algorithm for the Carnot heat engine design considering the capability to obtain the best, worst, and average results, and success rate. The results of the Friedman rank test are presented Table 4.3, and its graphical representation is given in Fig. 4.4. The results are presented in the form of Friedman value, normalized value with ‘1’ as the best performing algorithm and its rank. It is observed from the results that PSO has obtained the first rank followed by SOS and PVS algorithms.

The optimized operating condition of Carnot heat engine obtained using the PSO algorithm is presented in Table 4.4. It can be noted from the results that the Carnot heat engine with the maximum heat source temperature ratio, minimum engine temperature ratio, and minimum heat transfer ratio of the allocation parameters results in the maximum thermal efficiency. The heat source to heat sink allocation temperature produced a conflicting effect on achieving the maximum thermal efficiency of the Carnot heat engine. Also, the constraints are at the limiting value in the optimized operating condition of the Carnot heat engine.

**Table 4.3** Friedman rank test results for Carnot heat engine optimization

Algorithms	Friedman value	Normalized value	Rank
GA	42.5	0.2	9
PSO	8.5	1	1
DE	45	0.188889	10
ABC	24	0.354167	4
CSA	34	0.25	7
TLBO	46.5	0.182796	11
SOS	15	0.566667	2
WWO	36	0.236111	8
HTS	26	0.326923	5
PVS	19.5	0.435897	3
SCA	33	0.257576	6

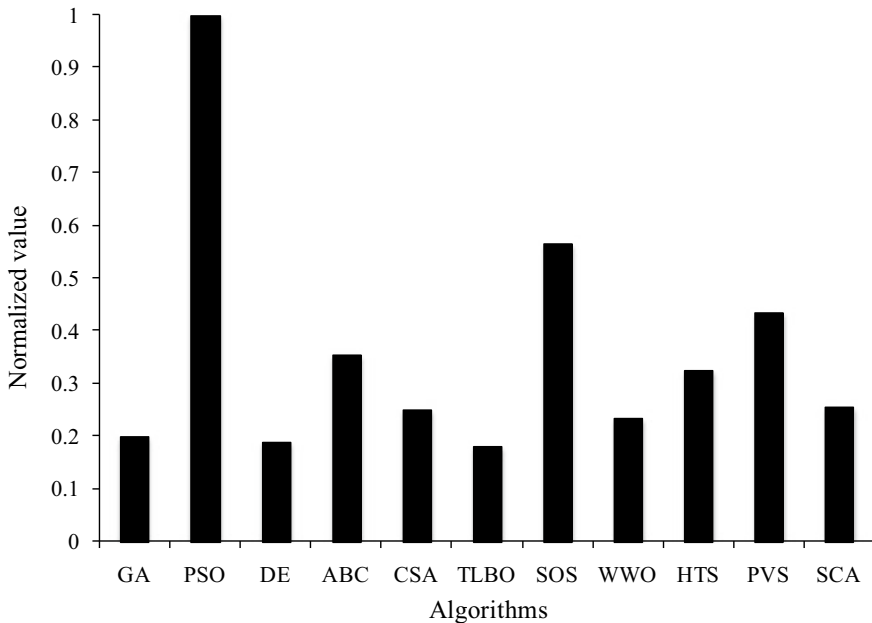


**Fig. 4.4** Graphical presentation of Friedman rank test for Carnot heat engine optimization

## 4.2 Rankine Heat Engine

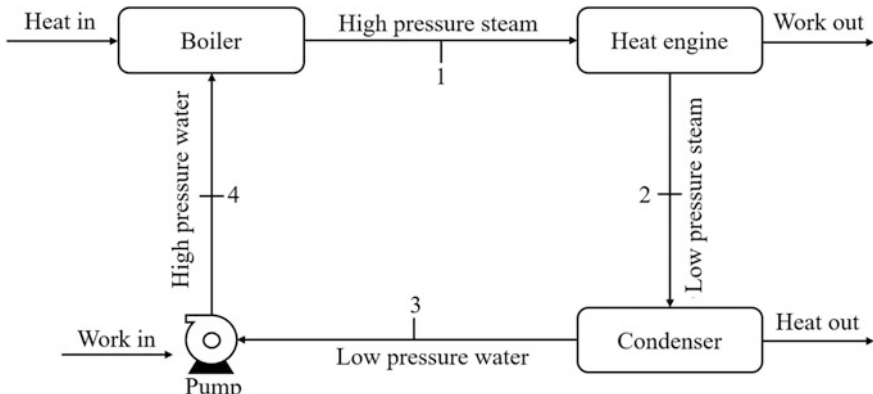
A Rankine heat engine operates on the Rankine cycle. In the Rankine cycle, the working fluid takes the heat from the heat source and produces the mechanical work by phase-changing phenomenon. It is operated on the closed cycle. Generally, water is used as a working fluid in the Rankine cycle. It consists of various

**Table 4.4** The optimized operating condition of Carnot heat engine

Operating parameters	Optimized value
<b>Design variable</b>	
Engine temperature ratio, $\tau$	0.2
Heat source to heat sink allocation temperature, $\beta$	0.5795
Heat source temperature ratio, $\chi$	0.8
Heat transfer ratio of the allocation parameters, $\psi$	0.1
<b>Constraints</b>	
Nondimensional power output, $W$	0.175
Nondimensional Ecological function, $E$	65
<b>Objective function</b>	
Thermal efficiency	0.54322

components like the pump, steam generator, engine, condenser, etc. The operation of the Rankine heat engine consists of four processes (i.e., two isentropic processes and two constant pressure processes). The schematic arrangement of Rankine heat engine is shown in Fig. 4.5.

The thermodynamic presentation of the Rankine heat engine is shown in Fig. 4.6. The pump sucked the water and pressurized it from the lower pressure to higher pressure, and supplied it to the steam generator (process 3–4). The pumping process is isentropic. In the steam generator, the water is converted into steam through heat supplied (process 4–1). The steam generation process is the constant pressure process during which water is converted into steam. From the steam generator, high-pressure and high-temperature steam is supplied to the steam engine. Expansion of steam takes place in the steam engine (process 1–2). The expansion process is isentropic. During the expansion process, engine produces the work and pressure of the steam reduces from high pressure to low pressure. At the

**Fig. 4.5** Schematic arrangement of Rankine heat engine

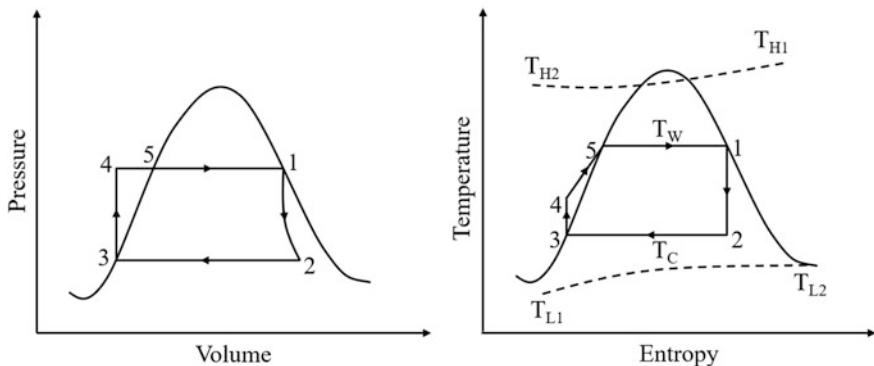


**Fig. 4.6** Thermodynamic presentation of Rankine heat engine

end of expansion, low-pressure, two-phase flow (i.e., the mixture of water and steam) exists. After expansion, the mixture of water and steam is supplied to the condenser where this two-phase mixture is converted into water by rejecting heat to the cooling media (process 2–3) and completes the cycle.

Earlier, researchers had carried out different types of numerical works related to Rankine heat engine. Lee and Kim (1992) perform the finite-time optimization of a Rankine heat engine to study the power and efficiency of a low-grade energy Rankine heat engine, which is widely used for power generation. The authors developed an analytical formula for estimating the finite-time Rankine power cycle efficiency at maximum power from heat reservoirs with finite heat capacity rate to obtain a bound on the power conversion systems. Ibrahim and Klein (1995) presented an analysis of the multi-stage Rankine cycle by adapting the finite-time thermodynamics. The authors considered the optimization of the power output of the Rankine cycle. Khaliq (2004) performed power optimization of the Rankine cycle heat engine by using the finite-time thermodynamic theory. The author observed that power output of the Rankine heat engine increases significantly with the increase in the heat capacity rate of the heating fluid. However, the thermal efficiency at maximum power remains constant. Ringler et al. (2009) performed an analysis to identify the potential of the Rankine cycle as an additional power generation process in IC engine.

Wu et al. (2016) proposed a novel oxy-fuel combustion method named internal combustion Rankine cycle (ICRC) used in reciprocating engines. The proposed concept has the potential for high thermal efficiency and low emission for Rankine cycle engine. Ahmadi et al. (2016a, b, c) performed the multi-objective optimization of Rankine heat engine. Maximization of efficiency and power output of the engine is considered as an objective function. The authors used NSGA-II as an optimization tool and considered five operating parameters of the heat engine as design variables. Furthermore, the authors adapted decision-making techniques to figure out the final optimal solution from the Pareto front. Punov et al. (2017)

presented an optimization study of the Rankine cycle as a function of diesel engine operating mode. The authors estimated numerically an output power and efficiency of the Rankine cycle by means of simulation code.

### 4.2.1 Thermal Model

In this part of the work, the heat engine working on the Rankine cycle is considered for the optimization. The thermodynamic presentation of Rankine heat engine is shown in Fig. 4.6. Moreover, the subscripts H and L stand for the heat source and heat sink side, respectively, in the different equations of the thermal model. The thermal model presented here is based on the previous work of Ahmadi et al. (2016a, b, c). To develop the thermal model of Rankine heat engine, the entropic mean temperature is employed in the present work, which turns the ideal Rankine cycle to the Carnot cycle as shown in Fig. 4.7. The area under zone 4–5–1 in the Rankine cycle (Fig. 4.6) depicts the heat supplied ( $Q_H$ ) to the cycle. This area can be changed to be an equivalent area below the horizontal line of the entropic mean temperature (area below line 4–1 in Fig. 4.7).

Entropic mean temperature is defined as

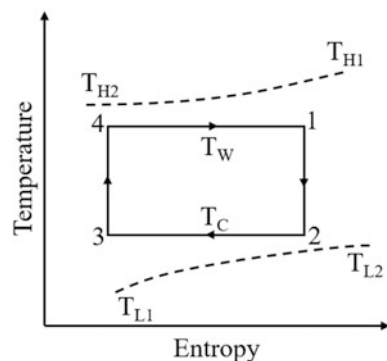
$$T_{\dot{W}} = \frac{\Delta Q}{\Delta S} \quad (4.19)$$

Entropic mean temperature ( $T_{\dot{W}}$ ) of the modified Rankine cycle (Fig. 4.7) is given by

$$T_{\dot{W}} = \frac{H_1 - H_4}{S_1 - S_4} \quad (4.20)$$

where  $H$  is the enthalpy and  $S$  is the entropy of the working fluid.

**Fig. 4.7** Thermodynamic presentation of modified Rankine heat engine



The heat supplied rate to the Rankine heat engine is given by

$$Q_H = \frac{Q_H}{t_H} = U_H A_H LMTD_H = m_H C_{PH}(T_{H1} - T_{H2}) \quad (4.21)$$

where  $A_H$  is the surface area of the heat exchanger operating between the heat source and the heat engine.  $m_H$  is the mass flow rate of the heat source fluid.  $C_{PH}$  is the specific heat of the heat source fluid.  $T_{H1}$  and  $T_{H2}$  are the inlet and outlet temperatures of the heat source fluid to the heat engine.  $t_H$  is the time duration for the heat supply.  $U_H$  is the hot-side overall heat transfer coefficient.  $LMTD_H$  is the hot side of logarithmic mean temperature difference and is given by

$$LMTD_H = \frac{[(T_{H1} - T_W) - (T_{H2} - T_W)]}{\ln[(T_{H1} - T_W) - (T_{H2} - T_W)]}. \quad (4.22)$$

where  $T_W$  is the temperature of the working fluid during phase change. The heat rejection rate of the Rankine heat engine is expressed by

$$Q_L = \frac{Q_L}{t_C} = U_L A_L LMTD_L = m_L C_{PL}(T_{L2} - T_{L1}) \quad (4.23)$$

where  $A_L$  is the surface area of the heat exchanger operating between the heat sink and heat engine.  $m_L$  is the mass flow rate of the heat sink fluid.  $C_{PL}$  is the specific heat of heat sink fluid.  $T_{L1}$  and  $T_{L2}$  are the inlet and outlet temperatures of the heat sink fluid to the heat engine.  $t_C$  is the time duration for heat rejection.  $U_L$  is the heat sink side overall heat transfer coefficient.  $LMTD_L$  is the cold-side logarithmic mean temperature difference and is given by

$$LMTD_L = [(T_C - T_{L1}) - (T_C - T_{L2})] / \ln[(T_C - T_{L1}) - (T_C - T_{L2})] \quad (4.24)$$

where  $T_C$  is the temperature of the working fluid during phase change.

If  $t_{12}$  and  $t_{34}$  are the time duration for isentropic process 1–2 and 3–4, respectively, then the time required for the entire cycle ( $t_{cy}$ ) is given by

$$t_{cy} = t_H + t_C + t_{12} + t_{34} \quad (4.25)$$

Since the isentropic process is fast process, if we ignore the time required during isentropic processes 1–2 and 3–4, respectively, then the time required for the entire cycle is given by

$$t_{cy} = t_H + t_C \quad (4.26)$$

Based on the previous equation of the heat transfer rate for the heat source and heat sink, the time required for the entire cycle is given by

$$t_{\text{cy}} = \frac{Q_H}{m_H C_{\text{PH}}(T_{H1} - T_{H2})} + \frac{Q_L}{m_L C_{\text{PL}}(T_{L2} - T_{L1})} \quad (4.27)$$

$$t_{\text{cy}} = \frac{Q_H}{HE(T_{H1} - T_W)} + \frac{Q_L}{LE(T_C - T_{L1})}. \quad (4.28)$$

where the parameters  $HE$  and  $LE$  are given by the following equations.

$$HE = m_H C_{\text{PH}} \left( 1 - e^{-\frac{(T_{H1} - T_W) - (T_{H2} - T_W)}{\text{LMTD}_H}} \right) \quad (4.29)$$

$$LE = m_L C_{\text{PL}} \left( 1 - e^{-\frac{(T_C - T_{L1}) - (T_C - T_{L2})}{\text{LMTD}_L}} \right) \quad (4.30)$$

The net output of the heat engine is described by

$$W = Q_H - Q_L \quad (4.31)$$

Assuming the Rankine cycle is endoreversible, it worked between the temperatures  $T_C$  and  $T_W$  (as shown in Fig. 4.6) and resulted in zero net entropy change.

$$Q_H = \frac{WT_W}{T_W - T_C} \quad (4.32)$$

$$Q_L = \frac{WT_C}{T_W - T_C} \quad (4.33)$$

Based on the above equations, the time required for the entire cycle ( $t_{\text{cy}}$ ) is defined by

$$t_{\text{cy}} = \left[ \frac{WT_W}{HE(T_{H1} - T_W)(T_W - T_C)} + \frac{WT_C}{LE(T_C - T_{L1})(T_W - T_C)} \right]^{-1} \quad (4.34)$$

The average power produced by the considered heat engine is given by

$$P = \frac{W}{t_{\text{cy}}} = \left[ \frac{T_W}{HE(T_W - T_C)(T_{H1} - T_W)} + \frac{T_C}{LE(T_W - T_C)(T_C - T_{L1})} \right] \quad (4.35)$$

Total conductance ( $C_e$ ) of a heat engine is given by the following equations:

$$C_e = U_H A_H + U_L A_L \quad (4.36)$$

$$C_e = \frac{U_H A_H}{a} \quad (4.37)$$

$$C_e = \frac{U_L A_L}{(1 - a)} \quad (4.38)$$

where  $a$  is the heat conductance allocation ratio.

Likewise, the total capacitance ( $mC_p$ ) of the heat engine is given by the following equations:

$$mC_p = m_{\dot{H}} C_{PH} + m_L C_{PL} \quad (4.39)$$

$$mC_p = \frac{m_{\dot{H}} C_{PH}}{b} \quad (4.40)$$

$$mC_p = \frac{m_L C_{PL}}{(1 - b)} \quad (4.41)$$

where  $b$  is the heat capacitance ratio.

The thermal efficiency of the heat engine can be gained through the following equation.

$$\eta = \left(1 - \frac{T_C}{T_W}\right) \left(1 - \sqrt{\frac{T_{L1}}{T_{H1}}}\right) \quad (4.42)$$

Based on the above thermal model, the objective function for the present work is defined in the next section.

#### **4.2.2 Case Study, Objective Function Description, and Constraints**

The Rankine heat engine needs to be designed and optimized for the maximum thermal efficiency. The considered heat engine used water as the working fluid. Six design variables such as inlet temperature of the heat source ( $T_{H1}$ ), inlet temperature of the heat sink ( $T_{L1}$ ), heat source temperature difference ( $T_{H1} - T_w$ ), heat sink temperature difference ( $T_C - T_{L1}$ ), heat conductance ( $UA$ ), and heat capacitance ( $mC_p$ ) are considered for the optimization problem. The upper and lower bounds of design variables are presented in Table 4.5.

As mentioned above, the maximization of thermal efficiency of the Rankine heat engine is taken as an objective function in the present study. Further, the operating parameters which result in the maximum thermal efficiency also satisfy the output power constraints. So, considering all the aspects, the objective function of the Rankine heat engine is formulated as below:

**Table 4.5** Ranges of design variables for Rankine heat engine optimization

Design variable	Lower bound	Upper bound
The inlet temperature of a heat source, $T_{H1}$ (K)	358	783
The inlet temperature of the heat sink, $T_{L1}$ (K)	298	333
Heat source temperature difference, $(T_{H1} - T_w)$ (K)	15.1	150
Heat sink temperature difference, $(T_c - T_{L1})$ (K)	40.9	48.4
Heat conductance, $UA$ (W/K)	1	1
Heat capacitance, $mC_p$ (W/K)	0.2	0.2

$$\left\{ \begin{array}{l} \text{Minimize } f(X) = \eta(X) + \sum_{j=1}^n G_1(g_j(X))^2 \\ X = [x_1, x_2, x_3, \dots, x_D], x_{i,\text{minimum}} \leq x_i \leq x_{i,\text{maximum}}, \quad i = 1, 2, 3, \dots, D \\ g_j(X) \leq 0, \quad j = 1, 2, 3, \dots, n \end{array} \right. \quad (4.43)$$

where  $X$  is the vector of design variables which should be bounded between its minimum and maximum values.  $G_1$  is the penalty parameter, and entire term takes into account the effect of constraints violation. This term comes into the picture when constraint violation takes place.  $g_j(X)$  indicates the constraints. The following constraint is considered for the Rankine heat engine optimization.

$$P \geq 0.182 \text{ kW} \quad (4.44)$$

The next section describes the results and discussion of the case study.

#### 4.2.3 Results and Discussion

The considered problem of Rankine heat engine is investigated using 11 different metaheuristic approaches to obtain maximum thermal efficiency. As all these methods are stochastic in their working, each algorithm is implemented 100 times on the considered problem to estimate the statistical variations of the algorithms. Each algorithm is implemented with the population size of 50, and the termination criteria are set as 100,000 function evaluations. The results obtained using each algorithm are presented in the form of the best solution, worst solution, average solution, standard deviation, and success rate obtained in 100 runs in Table 4.6. Here, the infeasible solutions (i.e., affected by penalty) are eliminated while obtaining the worst solution, average solution, standard deviation, and success rate. Also, the success rate of the algorithm is obtained by considering 0.1% variation from the global optimum value.

It can be observed from the comparative results that all the algorithm performed equally good and produced almost identical maximum thermal efficiency of the Rankine heat engine. However, the average performance of HTS is better followed

**Table 4.6** Comparative results of different algorithms for Rankine heat engine optimization

Algorithms	Best	Worst	Average	SD	Success rate (%)
GA	0.5878	0.5438	0.58032	1.61E-02	44
PSO	0.5878	0.5569	0.58174	1.12E-02	32
DE	0.5878	0.5439	0.58254	1.29E-02	56
ABC	0.5878	0.5592	0.58214	1.11E-02	40
CSA	0.5878	0.5439	0.5799	1.60E-02	40
TLBO	0.5878	0.5573	0.58288	1.12E-02	52
SOS	0.5877	0.5462	0.58022	1.52E-02	40
WWO	0.5878	0.5478	0.57969	1.56E-02	36
HTS	0.5878	0.5679	0.58525	6.77E-03	64
PVS	0.5877	0.5637	0.58348	9.24E-03	48
SCA	0.5878	0.54317	0.57945	1.78E-02	44

by PVS in comparison with other algorithms. The average performance of CSA is inferior compared to other algorithms. Also, the success rate of HTS algorithm in obtaining the optimum value is the highest followed by the DE algorithm. The success rate of the PSO algorithm is the lowest compared to other algorithms. It can be observed from the results that it is difficult to judge the performance of the algorithm as all the algorithms have produced a different performance to obtain the best, worst, and average results, and success rate. So, the Friedman rank test is implemented to judge the best suitable algorithm for the Rankine heat engine optimization considering the capability to obtain the best, worst, and average solutions, and success rate. The results of the Friedman rank test are presented in Table 4.7, and its graphical representation is given in Fig. 4.8. The results are presented in the form of Friedman value, normalized value with '1' as the best performing algorithm and its rank. It is observed from the results that HTS has obtained the first rank followed by TLBO and PVS algorithm.

**Table 4.7** Friedman rank test results for Rankine heat engine optimization

Algorithms	Friedman value	Normalized value	Rank
GA	37.5	0.24	7
PSO	31	0.29032	6
DE	25.5	0.35294	5
ABC	24	0.375	4
CSA	39.5	0.22785	9
TLBO	20	0.45	2
SOS	40.5	0.22222	10
WWO	39	0.23077	8
HTS	9	1	1
PVS	20.5	0.43902	3
SCA	43.5	0.2069	11

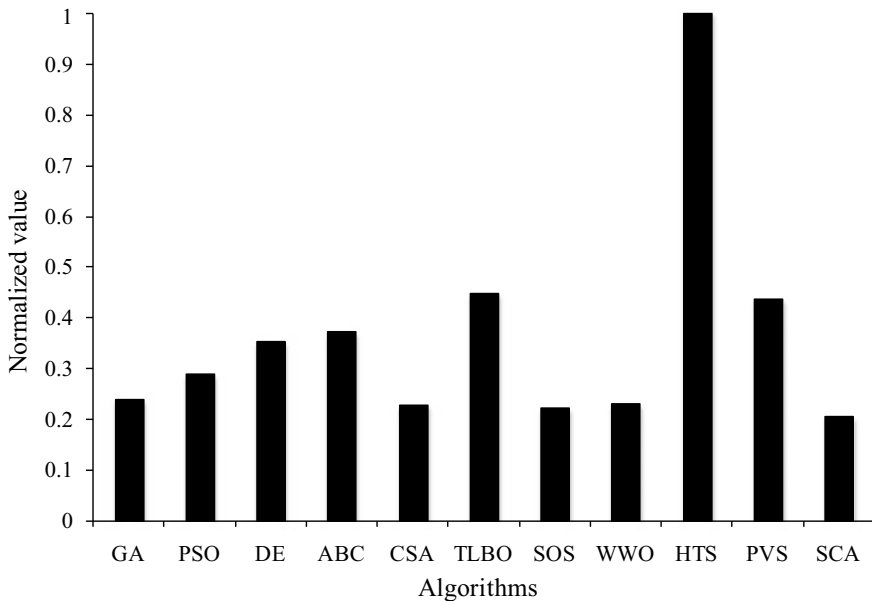


**Fig. 4.8** Graphical presentation of Friedman rank test for Rankine heat engine optimization

The optimized operating parameters of Rankine heat engine obtained using the HTS algorithm is presented in Table 4.8. It can be noted from the results that the Rankine heat engine with maximum heat source temperature, heat conductance, and minimum heat sink temperature, heat sink temperature difference, and heat capacitance results in maximum thermal efficiency. The heat source temperature difference produced a conflicting effect on achieving the maximum thermal efficiency of the Rankine heat engine. Further, power output constraint is at limiting value in the optimized operating condition of Rankine heat engine.

**Table 4.8** The optimized operating condition of Rankine heat engine

Operating parameters	Optimized value
<b><i>Objective function</i></b>	
The inlet temperature of a heat source, $T_{H1}$	782.96
The inlet temperature of the heat sink, $T_{L1}$	298.02
Heat source temperature difference ( $T_{H1} - T_w$ )	135.57
Heat sink temperature difference, ( $T_c - T_{L1}$ )	40.95
Heat conductance, $UA$	6.79
Heat capacitance, $mC_p$	1.39
<b><i>Constraint</i></b>	
Power output, $P$	0.182
<b><i>Objective function</i></b>	
Thermal efficiency	0.5878

### 4.3 Stirling Heat Engine

The Stirling heat engine is operated on the Stirling cycle. The Stirling engine is a closed-cycle regenerative heat engine operated by cyclic compression and expansion of air or other gases at different temperature levels, so that the net conversion of heat energy to mechanical work takes place (Walker 1980; Holman 1980; Stirling 1816; Senft 1993). Unlike internal combustion engines, the heat is applied externally to the Stirling engine. Regenerator is one of the important parts of the Stirling engine which provides the thermal storage. It is the inclusion of the regenerator that differentiates the Stirling engine from other closed-cycle hot air engines. As the Stirling engine relies on an external heat source, any alternative or renewable heat source is used with the Stirling engine (Blank et al. 1994; Kongtragool and Wongwises 2003, 2007). This compatibility of Stirling engine with alternative and renewable energy sources catches the attention of the researchers for its performance improvement. It is observed from the literature survey that in most instances, the engine is operated between temperature ranges 338–923 K and its efficiency is higher than 30%. The schematic of the Stirling heat engine is shown in Fig. 4.9.

The idealized Stirling engine consists of four thermodynamic processes acting on the working fluid. Figure 4.10 shows the thermodynamic cycle of the Stirling engine on pressure-volume (P-V) and temperature-entropy (T-S) coordinates. The process 1–2 is isothermal compression where the compression space and associated heat sink are maintained at a constant low-temperature  $T_1$  and  $T_C$ , respectively, so the gas undergoes near isothermal compression, rejecting heat to the cold sink. Then the gas passes through regenerator where it recovers much of the heat

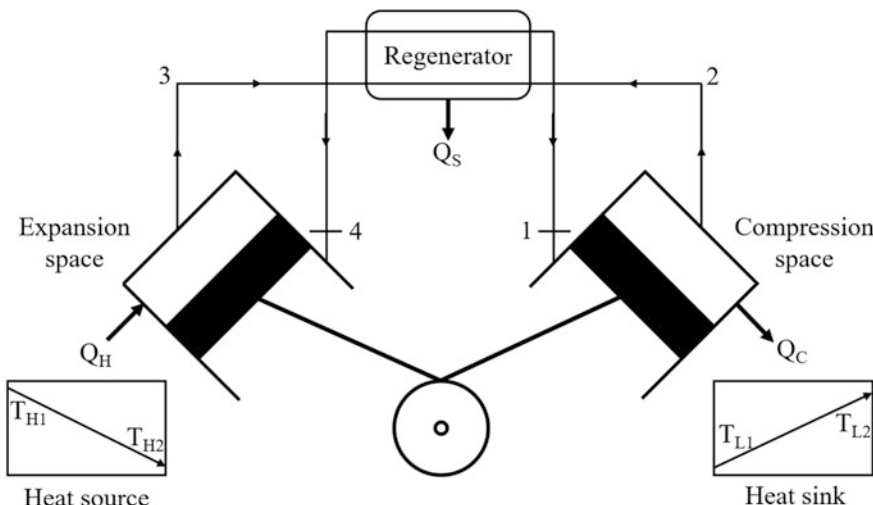
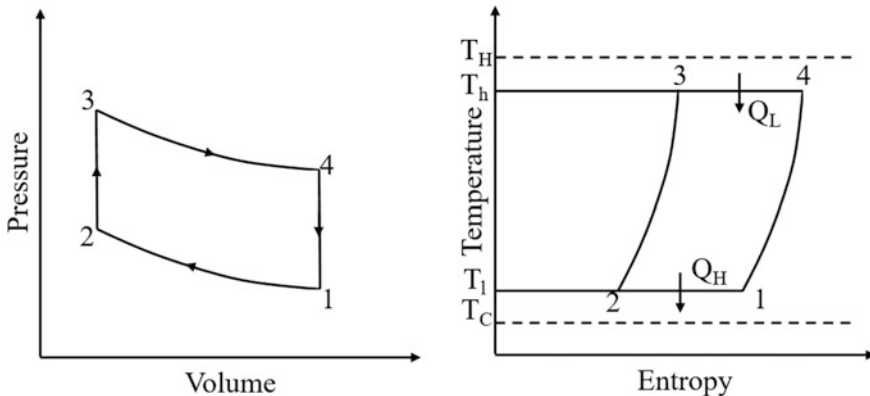


Fig. 4.9 Schematic arrangement of Stirling heat engine



**Fig. 4.10** Thermodynamic cycle of Stirling engine on P-V and T-S coordinates

transferred during the earlier cycle and heated up to high-temperature  $T_h$  undergoing constant volume process 2–3. After that, the gas undergoes isothermal expansion process 3–4 where it absorbed heat from the hot source maintained at temperature  $T_h$ . Finally, the gas is passed through the regenerator (process 4–1), where it cools up to temperature  $T_l$ , transferring heat to the regenerator for use in the next cycle.

Earlier, researchers carried out extensive work related to the development of the thermal model of Stirling heat engines. Optimizing the value of absorber and working fluid temperature was done for the maximization of output power and thermal efficiency of solar power Stirling engine using NSGA-II (Ahmadi et al. 2013a). Campos et al. (2012) performed optimization of Stirling engine under different operating and design conditions and reported the behavior of cycle efficiency under these conditions. Simultaneous optimization of thermal efficiency, power output, and entropy generation rate of a solar dish Stirling engine was performed by adapting the finite-time thermodynamics and NSGA-II (Ahmadi et al. 2013b, c, d). Thermo-economic optimization of a solar dish Stirling based on dimensionless thermo-economic objective function was demonstrated by using NSGA-II (Ahmadi et al. 2013b, c, d). Optimization of output power, thermal efficiency, and total pressure losses were reported using NSGA-II and finite speed thermodynamic (Ahmadi et al. 2013b, c, d). Stirling engine based on the nonideal adiabatic analysis (Toghyani et al. 2014a, b) and third-order thermodynamic analysis (Toghyani et al. 2014a, b) was reported using NSGA-II. Duan et al. (2014) performed multi-objective optimization between power output and efficiency of the Stirling engine with cycle irreversibility consideration.

Hooshang et al. (2015) obtained an optimized value of output power and efficiency of Stirling engines based on neural network concepts. Li et al. (2016) analyzed and optimized mechanical power, thermal efficiency, and entropy generation rate of Stirling engine using finite physical dimensions thermodynamics and genetic algorithm. Babaelahi and Sayyaadi (2015) developed a thermal model of

Stirling engine for thermal simulation of its prototype. Hosseinzade et al. (2015) also proposed a thermal model of the Stirling engine and obtained its simulation and optimization results. Araoz et al. (2015) presented a thermodynamic model for the performance analysis of the Stirling engine. Recently, researchers reported the work related to optimization of Stirling heat engine using metaheuristic algorithms. Ahmadi et al. (2016a, b) employed finite-speed thermodynamic analysis to obtain the optimum power output and pressure loss of the Stirling heat engine. Maximization of dimensionless output power, thermal efficiency, and entransy rate of the solar dish Stirling system was done using thermodynamic analysis and NSGA-II algorithm (Ahmadi et al. 2016a, b, c).

Ferreira et al. (2016) performed the thermo-economic optimization of Stirling engine used for the micro-cogeneration purpose. The authors optimized geometric and operational parameters of the engine for thermo-economic consideration. Multi-objective optimization of Patel and Savsani (2016) investigated a variant of the teaching–learning-based optimization algorithm for maximizing thermal efficiency, power output, and minimizing total pressure drop of the Stirling engine simultaneously. Zare and Tavakolpour-Saleh (2016) adopted genetic algorithm and presented the optimized design of frequency based on free piston Stirling engine. Punnathanam and Kotecha (2016) optimized thermal efficiency, output power, and entropy generation rate of Stirling engine by adapting NSGA-II. Arora et al. (2016) investigated NSGA-II for thermo-economic optimization of solar parabolic dish Stirling heat engine. The author considered power output, efficiency, and economic function of the engine for optimization. Luo et al. (2016) performed a multi-objective optimization of a GPU-3 Stirling engine and reported an output power of more than 3 kW with 5% rise in thermal efficiency. Patel et al. (2017) performed many-objective optimization problems of Stirling heat engine using multi-objective heat transfer search algorithm. The authors considered simultaneous optimization of thermal efficiency, power output, ecological function, and exergy efficiency of Stirling heat engine.

### **4.3.1 Thermal Model**

In this part of the work, the heat engine working on the Stirling cycle is considered for the optimization. The thermodynamic presentation of the Stirling heat engine is shown in Fig. 4.10. Moreover, the subscripts H and C stand for the heat source and heat sink, respectively, while subscripts h and l stand for hot side and cold side, respectively. The subscripts g, r, and c stand for the gas side, regenerator, and Carnot cycle, respectively, in the different equations of the thermal model. The thermal model presented here is based on the previous work of Patel and Savsani (2016).

In the present work, thermal modeling of Stirling heat engine is carried out considering the irreversibility associated with the cycle. The output power of the engine ( $P_{out}$ ) is calculated as

$$P_{\text{out}} = \eta Q_{\text{H}} \quad (4.45)$$

where  $\eta$  is the efficiency of the engine, and  $Q_{\text{H}}$  is the heat transfer rate to working fluid and is obtained as follows:

$$Q_{\text{H}} = (q_{\text{h}} + \Delta q_{\text{r}}) \frac{N}{60} \quad (4.46)$$

where  $N$  is the rotational speed of the engine,  $q_{\text{h}}$  is the heat released between the heat source and working fluid, and  $\Delta q_{\text{r}}$  is the heat loss during the two regenerative processes in the cycle and are obtained using the following equations (Petrescu et al. 2002):

$$q_{\text{h}} = m_{\text{g}} R (T_{\text{H}} - \Delta T_{\text{H}}) \left( 1 - \frac{\Delta p_{\text{v}}((\lambda + 1)(\tau + 1))}{4p_{\text{m}}} - \frac{b\Delta p_{\text{r}}}{2p_{\text{m}}} - \frac{f\Delta p_{\text{f}}}{p_{\text{m}}} \right) \ln \lambda \quad (4.47)$$

$$\Delta q_{\text{r}} = m_{\text{g}} C_{\text{vg}} X R (T_{\text{H}} - \Delta T_{\text{H}} - T_{\text{C}} - \Delta T_{\text{C}}) \quad (4.48)$$

where  $m_{\text{g}}$  is the mass of the gas in the engine;  $R$  is the gas constant;  $\Delta p_{\text{v}}$  and  $\Delta p_{\text{f}}$  are the pressure drop take place due to piston speed and mechanical friction, respectively;  $b$  is the distance between wires in the regenerator;  $f$  is the coefficient of friction;  $C_{\text{vg}}$  is the specific heat of the gas at constant volume;  $\Delta T_{\text{H}}$  is the temperature difference between the heat source and working fluid; and  $\Delta T_{\text{C}}$  is the temperature difference between the heat sink and working fluid, respectively, and are calculated by

$$\Delta T_{\text{H}} = T_{\text{H}} - T_{\text{h}} \quad (4.49)$$

$$\Delta T_{\text{c}} = T_{\text{l}} - T_{\text{c}} \quad (4.50)$$

The efficiency of the Stirling engine in terms of the Carnot efficiency is given by the following equation (Ahmadi et al. 2013a, b, c, d):

$$\eta = \eta_{\text{c}} \eta_{\text{II}} \quad (4.51)$$

where  $\eta_{\text{c}}$  is the Carnot efficiency and  $\eta_{\text{II}}$  is the second law efficiency which takes into account irreversibility associated with the cycle and are obtained using the following equation (Ahmadi et al. 2013a, b, c, d):

$$\eta_{\text{c}} = 1 - \frac{T_{\text{C}} - \Delta T_{\text{C}}}{T_{\text{H}} - \Delta T_{\text{H}}} \quad (4.52)$$

$$\eta_{\text{II}} = \eta_{\text{II}\Delta p} \eta_{\text{II}(x)} \quad (4.53)$$

where  $\eta_{II(\Delta P)}$  and  $\eta_{II(X)}$  indicate the irreversibility associated with the pressure drop and regenerative heat transfer process, respectively.  $\eta_{II(\Delta P)}$  is calculated using the following equation (Ahmadi et al. 2013a, b, c, d):

$$\eta_{II(\Delta P)} = 1 - \left( \frac{3\mu \frac{\Delta p_{\text{total}}}{P_1}}{\eta \left( \frac{T_H - \Delta T_H}{T_C + \Delta T_C} \right) \ln \lambda} \right) \quad (4.54)$$

where  $p_1$  is the inlet pressure of cycle. Parameter  $\eta'$  correlates Carnot efficiency and the second law efficiency associated with the regeneration process while parameter  $\mu'$  associates with the volumetric ratio during regeneration processes. These parameters are calculated using the following equations (Ahmadi et al. 2013a, b, c, d):

$$\eta = \eta_c \eta_{II(1-\varepsilon_r)} \quad (4.55)$$

$$\mu = 1 - \left( \frac{1}{3\lambda} \right) \quad (4.56)$$

$$P_1 = \frac{4P_m}{(1+\lambda)(1+\tau)} \quad (4.57)$$

where  $P_m$  is the mean effective pressure,  $\lambda$  is the volumetric ratio during regeneration processes, and  $\tau$  is the temperature ratio and is defined as

$$\tau = \frac{T_h}{T_l} \quad (4.58)$$

Irreversibility associated with the regenerative heat transfer process, respectively, is calculated using the following equation:

$$\eta_{II(X)} = \frac{1}{1 + \left( \frac{X}{(\gamma-1)\ln\lambda} \right) \eta_c} \quad (4.59)$$

where  $X$  is the regenerative losses coefficient and is obtained using the following experimental correlation (Ahmadi et al. 2013a, b, c, d; Petrescu et al. 2002):

$$X = X'X_1 + (1 - X')X_2 \quad (4.60)$$

where parameters  $X_1$  and  $X_2$  are obtained by the following correlation:

$$X_1 = \frac{1 + 2M + \exp(-B)}{2(1 + M)} \quad (4.61)$$

$$X_2 = \frac{M + \exp(-B)}{1 + M} \quad (4.62)$$

where parameters  $M$  and  $B$  are obtained by the following correlation (Ahmadi et al. 2013a, b, c, d; Petrescu et al. 2002):

$$M = \frac{m_g C_{vg}}{m_r C_r} \quad (4.63)$$

$$B = (1 + M) \left( \frac{h A_r}{m_g C_{vg}} \right) \left( \frac{30}{N} \right) \quad (4.64)$$

where  $m_g$  and  $m_r$  are the mass of gas and regenerator, respectively, while  $h$  and  $A_r$  represent the convective heat transfer coefficient and regenerator area and are calculated as

$$h = \frac{0.395 \left( \frac{4P_m}{RT_c} \right) \left( \frac{sN}{30} \right)^{0.424} C_{pg} \nu^{0.576}}{(1 + \tau) \left[ 1 - \frac{\pi}{4(\frac{b}{d} + 1)} \right] D_r^{0.576} P r^{0.667}} \quad (4.65)$$

$$m_r = \frac{\pi^2 D_r^2 L d \rho_r}{16(b + d)} \quad (4.66)$$

$$A_r = \frac{\pi^2 D_r^2 L}{4(b + d)} \quad (4.67)$$

where  $d$  is the diameter of the regenerator wire,  $b$  is the distance between wires in the regenerator,  $s$  is the stroke length, and  $L$  is the length of the regenerator.

Frictional pressure drop takes place in the regenerator of the engine and is calculated by using the following equation (Ahmadi et al. 2013a, b, c, d).

$$\Delta p_r = \frac{15}{\gamma} \left( \frac{P_m}{2R(\tau + 1)(T_c + \Delta T_c)} \right) \left( \frac{s^2 N^2}{900} \right) \left( \frac{D_c^2}{n_r D_r^2} \right) N_r \quad (4.68)$$

Pressure drop takes place due to mechanical friction in different parts of the engine and is expressed by (Ahmadi et al. 2013a, b, c, d).

$$\Delta P_f = \left( \frac{(0.94 + 0.0015 s N) 10^5}{3\mu'} \right) \left( 1 - \frac{1}{\lambda} \right) \quad (4.69)$$

Pressure drop that takes place due to piston speed is calculated using the following equation (Ahmadi et al. 2013a, b, c, d).

$$\Delta p_v = \left( \frac{sN}{60} \right) \left( \frac{4p_m}{(1 + \lambda)(1 + \tau)} \right) \left( \frac{\lambda \ln \lambda}{\lambda - 1} \right) \left( \frac{1}{\sqrt{T_c + \Delta T_c}} \right) \left( 1 + \sqrt{\left( \frac{T_h - \Delta T_h}{T_c + \Delta T_c} \right) \sqrt{\frac{\gamma}{R}}} \right) \quad (4.70)$$

So, the total pressure drop takes place in the Stirling engine and is given by

$$\Delta p_{\text{total}} = \Delta p_r + \Delta p_f + \Delta p_v \quad (4.71)$$

The ecological function of Stirling heat engine is expressed as (Angulo-Brown 1991a, b):

$$EF = P_{\text{out}} - T_0 S_{\text{gen}} \quad (4.72)$$

where  $S_{\text{gen}}$  is the entropy generation rate of Stirling heat engine. Finally, the exergy efficiency of Stirling heat engine is obtained by

$$\eta_{\text{ex}} = \frac{\left( \left( 1 - \frac{T_0}{T_H} \right) Q_H \right) - \left( \left( 1 - \frac{T_0}{T_C} \right) Q_L \right)}{(Q_H - Q_C)} \quad (4.73)$$

where  $T_0$  is the environment temperature.

Based on the above thermal model, the objective function for the present work is defined in the next section.

#### **4.3.2 Case Study, Objective Function Description, and Constraints**

The Stirling heat engine with 0.001135 kg of gas needs to be designed and optimized for the maximum power output. The density of regenerator material used in the engine is considered as 8030 kg/m<sup>3</sup>. Eight regenerators per cylinder ( $N_r$ ) are used in the considered Stirling engine. The diameter of the regenerator ( $d$ ) wire is 0.04 mm, and the distance between wires in regenerator ( $b$ ) is 0.0688 mm. The volumetric ratio ( $\lambda$ ) during the regeneration process is 1.2. Specific heat of regenerator material ( $C_r$ ) is 502.48 J/kg K. Specific heat of the gas at constant pressure ( $C_{pg}$ ) and constant volume ( $C_{vg}$ ) are 5193 and 3115.6 J/kg K, respectively. The kinematic viscosity of gas ( $\nu$ ) is 0.3249 mm<sup>2</sup>/s, and Prandtl number of gas ( $P_r$ ) is 0.71. Coefficient related to the friction ( $f$ ) contribution is 0.556. Eleven design variables such as the engine's rotation speed ( $N$ ), mean effective pressure ( $p_m$ ), stroke length ( $s$ ), number of gauzes of the matrix ( $n_r$ ), piston diameter ( $D_c$ ), regenerator diameter ( $D_r$ ), regenerator length ( $L$ ), temperature of the heat source ( $T_H$ ), temperature of the heat sink ( $T_C$ ), temperature difference between the heat source and working fluid ( $\Delta T_H$ ), and temperature difference between the heat sink and working fluid ( $\Delta T_C$ ) are considered for the optimization problem. The upper and lower bounds of design variables are presented in Table 4.9.

As mentioned above, the maximization of the power output of the Stirling heat engine is taken as an objective function in the present study. Further, the operating parameters which result in maximum power output also satisfy the thermal efficiency ( $\eta$ ), ecological function (ECF), and exergetic efficiency ( $\eta_{\text{ex}}$ ) constraints. So,

**Table 4.9** Ranges of design variables for Stirling heat engine optimization

Design variable	Lower bound	Upper bound
Engine's rotation speed, $N$ (rpm)	1200	30,000
Mean effective pressure, $P_m$ (MPa)	0.69	6.89
Stroke length, $s$ (m)	0.06	1
Number of gauzes of the matrix, $n_r$	250	4000
Piston diameter, $D_c$ (m)	0.05	0.14
Regenerator diameter, $D_r$ (m)	0.02	0.6
Regenerator length, $L$ (m)	0.006	0.73
temperature of the heat source, $T_H$ (K)	200	1300
Temperature of the heat sink, $T_C$ (K)	288	360
Temperature difference between the heat source and working fluid, $\Delta T_H$ (K)	64.2	237.6
Temperature difference between the heat sink and working fluid, $\Delta T_C$ (K)	5	25

considering all the aspects, the objective function of the Stirling heat engine is formulated as below:

$$\left\{ \begin{array}{l} \text{Minimize } f(X) = P_{\text{out}}(X) + \sum_{j=1}^n G_1(g_j(X))^2 \\ X = [x_1, x_2, x_3, \dots, x_D], x_{i,\text{minimum}} \leq x_i \leq x_{i,\text{maximum}}, i = 1, 2, 3, \dots, D \\ g_j(X) \leq 0, \quad j = 1, 2, 3, \dots, n \end{array} \right. \quad (4.74)$$

where  $X$  is the vector of design variables which should be bounded between its minimum and maximum values.  $G_1$  is the penalty parameter, and entire term takes into account the effect of constraints violation. This term comes into the picture when constraint violation takes place.  $g_j(X)$  indicates the constraints. The following constraints are considered for the Stirling heat engine.

$$\text{Thermal efficiency } (\eta) > 17\% \quad (4.75)$$

$$\text{Ecological function (ECF)} > 65 \quad (4.76)$$

$$\text{Exergetic efficiency } (\eta_{\text{ex}}) > 82\% \quad (4.77)$$

The next section describes the results and discussion of the case study.

### 4.3.3 Results and Discussion

The considered problem of Stirling heat engine is investigated using 11 different metaheuristic approaches to obtain the maximum power output. As all these

methods are stochastic in their working, each algorithm is implemented 100 times on the considered problem to estimate the statistical variations of the algorithms. Each algorithm is implemented with the population size of 50, and the termination criteria are set as 100,000 function evaluations. The results obtained using each algorithm are presented in the form of the best solution, worst solution, average solution, standard deviation, and success rate obtained in 100 runs in Table 4.10. Here, the infeasible solutions (i.e., affected by penalty) are eliminated while obtaining the worst solution, average solution, standard deviation, and success rate. Further, the success rate of the algorithm is obtained by considering 0.1% variation from the global optimum value.

It can be observed from the comparative results that all the algorithms performed equally good and produced almost identical maximum power output of the Stirling heat engine. The average performance of all the algorithms (except GA and SCA) is almost equal. The average performance of GA is inferior compared to other algorithms. Also, the success rate of HTS algorithm in obtaining the optimum value is the highest followed by the TLBO algorithm. The success rate of the SCA algorithm is the lowest compared to other algorithms. It can be observed from the results that it is difficult to judge the performance of each algorithm as all the algorithms have produced a different performance to obtain the best, worst, and average results, and success rate. So, the Friedman rank test is implemented to judge the best suitable algorithm for Stirling heat engine optimization considering the capability to obtain the best, worst, and average solutions, and success rate. The results of the Friedman rank test are presented in Table 4.11, and its graphical representation is given in Fig. 4.11. The results are presented in the form of Friedman value, normalized value with '1' as the best performing algorithm and its rank. It is observed from the results that HTS has obtained the first rank followed by TLBO and ABC algorithms.

**Table 4.10** Comparative results of different algorithms for Stirling heat engine optimization

Algorithms	Best	Worst	Average	SD	Success rate (%)
GA	16.3681	14.6701	15.8167	6.60E-01	40
PSO	16.3681	15.8875	16.3208	1.02E-01	52
DE	16.3681	16.3681	16.3681	1.15E-06	48
ABC	16.3681	16.2999	16.3632	1.82E-02	52
CSA	16.3681	16.3681	16.3681	7.28E-15	84
TLBO	16.3681	15.4985	16.3240	1.78E-01	91
SOS	16.3681	16.1343	16.3322	8.43E-02	83
WWO	16.3677	16.1239	16.3384	6.01E-02	60
HTS	16.3681	16.1343	16.3494	6.47E-02	92
PVS	16.3681	16.3680	16.3681	3.16E-05	41
SCA	16.3681	16.0573	16.2447	1.01E-01	28

**Table 4.11** Friedman rank test results for Stirling heat engine optimization

Algorithms	Friedman value	Normalized value	Rank
GA	26	0.75	6
PSO	45	0.433333	10
DE	30	0.65	8
ABC	22.5	0.866667	3
CSA	23.5	0.829787	4
TLBO	21.5	0.906977	2
SOS	25.5	0.764706	5
WWO	47	0.414894	11
HTS	19.5	1	1
PVS	42	0.464286	9
SCA	27.5	0.709091	7

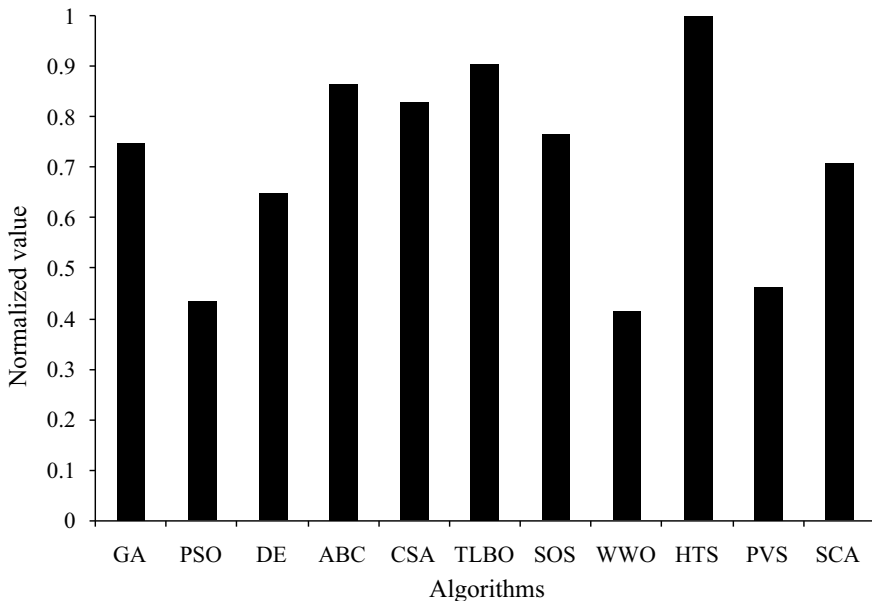


**Fig. 4.11** Graphical presentation of Friedman rank test for Stirling heat engine optimization

The optimized operating parameters of the Stirling heat engine obtained using the HTS algorithm are presented in Table 4.12. It can be noted from the results that the Stirling heat engine with the maximum mean effective pressure, number of gauzes of the matrix, regenerator diameter, regenerator length, heat sink and working fluid temperature difference, and heat source temperature results in the maximum power output. Likewise, the minimum stroke length, piston diameter, heat source and working fluid temperature difference, and heat sink temperature

**Table 4.12** The optimized operating condition of Stirling heat engine

Operating parameters	Optimized value
<b><i>Operating variable</i></b>	
Engine's rotation speed, $N$ (rpm)	3356.29
Mean effective pressure, $P_m$ (MPa)	6.89
Stroke length, $s$ (m)	0.06
Number of gauzes of the matrix, $n_r$	4000
Piston diameter, $D_c$ (m)	0.05
Regenerator diameter, $D_r$ (m)	0.6
Regenerator length, $L$ (m)	0.73
Temperature of the heat source, $T_H$ (K)	1300
Temperature of the heat sink, $T_C$ (K)	288
Temperature difference between the heat source and working fluid, $\Delta T_H$ (K)	64.2
Temperature difference between the heat sink and working fluid, $\Delta T_C$ (K)	5
<b><i>Constraint</i></b>	
Thermal efficiency, $\eta$	17%
Ecological function, ECF (kW)	74.34
Exergetic efficiency ( $\eta_{ex}$ )	82.96%
<b><i>Objective function</i></b>	
Power output, $P_{out}$ (kW)	16.3681

results in maximum power output of Stirling heat engine. The engine's rotational speed produced a conflicting effect on achieving the maximum power output of the Stirling heat engine. Also, the thermal efficiency constraint is at the limiting value in the optimized operating condition of Stirling heat engine.

## 4.4 Brayton Heat Engine

The Brayton heat engine operates on the Brayton cycle. In the Brayton cycle, the working fluid takes the heat from the heat source and produces the mechanical work without phase changing phenomenon. It is operated on a closed cycle. Generally, the air or other gases are used as the working fluid in the Brayton cycle. It consists of three main components: compressor, combustion chamber, and engine. The schematic arrangement of the Brayton heat engine is shown in Fig. 4.12. The operation of Brayton heat engine consists of four processes (i.e., two isentropic and two are constant pressure process). The thermodynamic presentation of the Brayton heat engine is shown in Fig. 4.13 and explained.

The working fluid (i.e., air or other gases) is sucked by the compressor and then compressed it to high pressure (process 1–2<sub>S</sub>). The ideal compression process is isentropic. The high pressure is passed through the regenerative heat exchanger

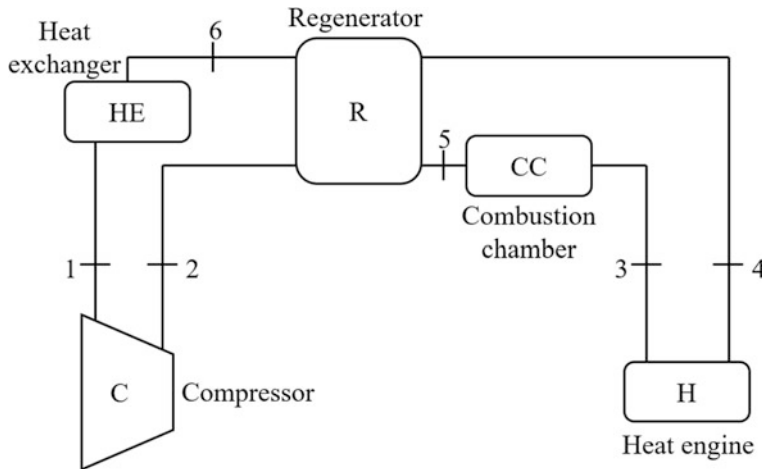


**Fig. 4.12** Schematic arrangement of Brayton heat engine

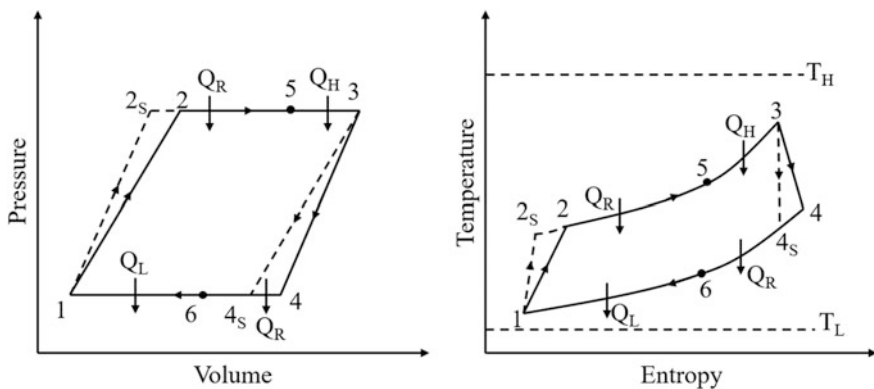


**Fig. 4.13** Thermodynamic cycle of Brayton heat engine

where it is heated by the exhaust gas coming out after expansion from the engine (process  $2_s-5$ ). After that, the gas is supplied to the combustion chamber where the heat is supplied to the working fluid at constant pressure (process  $5-3$ ). This high-temperature gas is then expanded isentropically (process  $3-4_s$ ) and produced mechanical work. After the expansion, the working fluid undergoes the heat rejection in regenerative heat exchanger (process  $4_s-6$ ) and heat sink (process  $6-1$ ) to complete the cycle. In the thermodynamic presentation, the processes  $1-2_s$  and  $3-4_s$  are isentropic processes while processes  $1-2$  and  $3-4$  are the actual processes with some isentropic efficiency.

Earlier, researchers carried out various works related to the analysis and optimization of the Brayton heat engine. Wu (1991) analyzed and optimized power output of the simple endoreversible Brayton gas heat engine. This approach carried out the more realistic prediction of the heat engine efficiency and power output than the ideal Brayton cycle. Sahin et al. (1995) analyzed the reversible Joule-Brayton engine at maximum power density. The authors identified that design parameters at the maximum power density led to smaller and more efficient Joule-Brayton engine. Sahin et al. (1996a, b) carried out the performance analysis of an irreversible Joule-Brayton heat engine based on the power density criterion. The authors concluded that irreversibility in the heat engine reduces the power and thermal efficiency by a certain amount; however, the maximum power density conditions still gave a better performance than at the maximum power output conditions. Sahin et al. (1998) carried out the performance analysis of the irreversible regenerative reheating Joule-Brayton engine based on the maximum power density criterion. The authors investigated the overall effects of reheating, regeneration, and internal irreversibility on the heat engine.

Cheng and Chen (1999) worked on the ecological optimization of irreversible Brayton heat engine. The authors used the finite-time thermodynamics to determine the maximum ecological function and its corresponding thermal efficiency and power output of the irreversible Brayton heat engine. Huang et al. (2000) carried out the exergy analysis based on the ecological optimization criterion for the irreversible Brayton engine. The authors observed that the ecological exergy analysis results in the better performance than that obtained with the maximum power (or work) output conditions. Ordóñez (2000) used liquid nitrogen fuel for Brayton heat engine and concluded that in the closed Brayton cycle, liquid nitrogen power system is found to be a promising alternative than other mobile power systems. Kaushik and Tyagi (2002) presented the parametric study of an irreversible regenerative Brayton cycle with nonisentropic compression and expansion processes for finite heat capacitance rates of external reservoirs. The authors obtained expressions for the maximum power output and the corresponding thermal efficiency of the Brayton heat engine. Lin and Chen (2003) carried out the performance optimization of the harmonic quantum Brayton heat engine. The authors investigated the general performance characteristics of the engine and obtained expressions for several essential performance parameters.

Zhang et al. (2005) analyzed the irreversible Brayton heat engine and its general optimum performance characteristics. The authors observed that when the efficiency of the heat engine is less, at that time the power output without regeneration may be larger than that of regenerative Brayton heat engine. Ust et al. (2005) carried out performance optimization of an irreversible regenerative Brayton heat engine based on the ecological coefficient of performance (ECOP) criterion. The authors concluded that for the regenerative Brayton engine, the design based on the maximum ECOP conditions is more advantageous from the point of view of entropy generation rate, thermal efficiency, and investment cost. Ust et al. (2006a, b) presented the performance optimization of irreversible Brayton heat engine based on ECOP and obtained the optimal performance and design parameters at the

maximum ECOP conditions. Sogut et al. (2006) presented the thermo-ecological performance analysis of an irreversible intercooled and regenerated closed Brayton heat engine exchanging heat with variable-temperature thermal reservoirs. The authors also carried out the comparative performance analysis considering the ecological coefficient of performance and power output. Yilmaz (2007) analyzed the performance optimization of the Joule–Brayton heat engine based on the efficient power criterion. Zhang et al. (2007) worked on the optimum performance characteristics of the irreversible solar-driven Brayton heat engine at the maximum overall efficiency. Kumar et al. (2015) performed the optimization of Brayton heat engine with the variable specific heat of the working fluid. The authors used the finite-time thermodynamics for the optimization of a heat engine.

#### 4.4.1 Thermal Model

In this part of the work, the heat engine working on the Brayton cycle is considered for the optimization. The thermodynamic presentation of Brayton heat engine is shown in Fig. 4.13. Moreover, the subscripts H and L stand for the heat source (i.e., high temperature) and heat sink (i.e., low temperature) side, respectively, while subscript W stands for working fluid in the different equations of the thermal model. The thermal model presented here is based on the previous work of Ust et al. (2006a, b).

The heat supplied to the working fluid ( $Q_H$ ) from heat sources and heat rejected by working fluid ( $Q_L$ ) to the heat sink is given by

$$Q_H = C_{\dot{W}} \varepsilon_H (T_H - T_5) = c_{\dot{W}} (T_3 - T_5) \quad (4.78)$$

$$Q_L = C_{\dot{W}} \varepsilon_L (T_6 - T_L) = c_{\dot{W}} (T_6 - T_1) \quad (4.79)$$

where  $C_{\dot{W}}$  is the heat capacity of working fluid.  $\varepsilon_H$  and  $\varepsilon_L$  are the heat exchanger effectiveness on heat source side and heat sink side, respectively, and are given by the following equations:

$$\varepsilon_H = 1 - e^{-N_H} \quad (4.80)$$

$$\varepsilon_L = 1 - e^{-N_L} \quad (4.81)$$

where  $N_H$  and  $N_L$  are the number of transfer units of the heat exchanger and are given by

$$N_H = (U_H A_H) / c_{\dot{W}} \quad (4.82)$$

$$N_L = (U_L A_L) / c_{\dot{W}} \quad (4.83)$$

where  $U$  is the overall heat transfer coefficient of the heat exchanger and  $A$  is the heat exchanger are defined, respectively, as follows.

The rate of heat leakage ( $Q_{LK}$ ) from the heat source to heat sink is given by

$$Q_{LK} = C_i(T_H - T_L) = \xi C_W(T_H - T_L) \quad (4.84)$$

where  $C_i$  is the internal conductance of the heat engine and  $\xi$  is the ratio of heat engine internal conductance to the heat capacity of working fluid.

So, the total heat rate from the heat source ( $Q_{HT}$ ) is given by

$$Q_{HT} = Q_H + Q_{LK} = C_W \varepsilon_H (T_H - T_5) + \xi C_W (T_H - T_L) \quad (4.85)$$

Likewise, the total heat rate transferred to the heat sink ( $Q_{LT}$ ) is given by

$$Q_{LT} = Q_L + Q_{LK} = C_W \varepsilon_L (T_6 - T_L) + \xi C_W (T_H - T_L) \quad (4.86)$$

The temperature ratio of the compressor and expansion ratio of the heat engine are given by

$$\phi = T_{2S}/T_1 = T_3/T_{4S} \quad (4.87)$$

The actual temperature of the working fluid after compressor ( $T_2$ ) and expansion ( $T_4$ ) is given by

$$T_2 = T_1[a_1(\phi - 1) + 1] \quad (4.88)$$

$$T_4 = T_1(a_5 + a_6\phi) + a_7 \quad (4.89)$$

where the following equations give  $a_1$ ,  $a_5$ ,  $a_6$ , and  $a_7$ .

$$a_1 = \frac{1}{\eta_c} \quad (4.90)$$

$$a_2 = \varepsilon_L T_L \quad (4.91)$$

$$a_3 = \varepsilon_R(1 - \varepsilon_L) \quad (4.92)$$

$$a_4 = (1 - \varepsilon_L)(1 - \varepsilon_R) \quad (4.93)$$

$$a_5 = \frac{[1 + a_3(a_1 - 1)]}{a_4} \quad (4.94)$$

$$a_6 = -\frac{a_1 a_3}{a_4} \quad (4.95)$$

$$a_7 = -\frac{a_2}{a_4} \quad (4.96)$$

The temperature of the working fluid after the combustion chamber ( $T_3$ ) is given by

$$T_3 = T_1(a_{11} + a_{12}\phi) + a_{13} \quad (4.97)$$

where the following equations give  $a_{11}$ ,  $a_{12}$ , and  $a_{13}$ .

$$a_8 = \varepsilon_H T_H \quad (4.98)$$

$$a_9 = \varepsilon_R(1 - \varepsilon_H) \quad (4.99)$$

$$a_{10} = (1 - \varepsilon_H)(1 - \varepsilon_R) \quad (4.100)$$

$$a_{11} = a_5 a_9 + a_{10}(1 - a_1) \quad (4.101)$$

$$a_{12} = a_6 a_9 + a_1 a_{10} \quad (4.102)$$

$$a_{13} = a_8 + a_7 a_9 \quad (4.103)$$

The temperature of the working fluid after isentropic expansion ( $T_{4s}$ ) is given by

$$T_{4s} = T_1(a_{15} + a_{16}\phi) + a_{17} \quad (4.104)$$

where the following equations give  $a_{15}$ ,  $a_{16}$ , and  $a_{17}$ .

$$a_{14} = \frac{1}{\eta_T} \quad (4.105)$$

$$a_{15} = a_5 a_{14} + a_{11}(1 - a_{14}) \quad (4.106)$$

$$a_{16} = a_6 a_{14} + a_{12}(1 - a_{14}) \quad (4.107)$$

$$a_{17} = a_7 a_{14} + a_{13}(1 - a_{14}) \quad (4.108)$$

Based on the above variables, the temperature of the working fluid before compression ( $T_1$ ) is given by

$$T_1 = \frac{a_{13} - a_{17}\phi}{a_{16}\phi^2 + a_{18}\phi - a_{11}} \quad (4.109)$$

where the following equations give  $a_{18}$ .

$$a_{18} = a_{15} - a_{12} \quad (4.110)$$

The power output ( $\dot{W}$ ) of the heat engine is given by

$$\dot{W} = C_{\dot{W}} \left\{ \frac{(a_{13} - a_{17}\phi)(a_{21} - a_{22}\phi)}{a_{16}\phi^2 + a_{18}\phi - a_{11}} + a_{23} \right\} \quad (4.111)$$

where  $a_{21}$ ,  $a_{22}$ , and  $a_{23}$  are given by the following equations.

$$a_{21} = a_{19}(a_1 - 1) - a_5 a_{20} \quad (4.112)$$

$$a_{19} = \varepsilon_L \varepsilon_R + \varepsilon_H(1 - \varepsilon_R) \quad (4.113)$$

$$a_{20} = \varepsilon_H \varepsilon_R + \varepsilon_L(1 - \varepsilon_R) \quad (4.114)$$

$$a_{22} = a_1 a_{19} + a_6 a_{20} \quad (4.115)$$

$$a_{23} = a_2 + a_8 - a_7 a_{20} \quad (4.116)$$

The entropy generation ( $S_{\dot{g}}$ ) rate of the heat engine is given by

$$S_{\dot{g}} = C_W \left\{ \frac{(a_{13} - a_{17}\phi)(a_{29} - a_{30}\phi)}{a_{16}\phi^2 + a_{18}\phi - a_{11}} + a_{28} \right\} \quad (4.117)$$

where  $a_{28}$ ,  $a_{29}$ , and  $a_{30}$  are given by the following equations:

$$a_{28} = a_{24} + a_{27} + a_7 + a_{26} \quad (4.118)$$

$$a_{24} = \frac{\xi(\tau - 1)^2}{\tau} \quad (4.119)$$

$$a_{26} = \frac{\varepsilon_H \varepsilon_R}{T_H} \quad (4.120)$$

$$a_{27} = -(\varepsilon_L + \varepsilon_H) \quad (4.121)$$

$$a_{29} = a_5 a_{26} + a_{25}(1 - a_1) \quad (4.122)$$

$$a_{25} = \frac{\varepsilon_L \varepsilon_R}{T_L} + \frac{\varepsilon_H(1 - \varepsilon_R)}{T_L} \quad (4.123)$$

$$a_{30} = a_1 a_{25} + a_6 a_{26} \quad (4.124)$$

where  $\xi$  is the ratio of the heat engine internal conductance to the heat capacity of working fluid and  $\tau$  is the ratio of the heat source to heat sink temperature.

The following equation gives the ecological function ( $\dot{E}$ ) for the heat engine:

$$\dot{E} = \dot{W} - T_0 S_{\dot{g}} \quad (4.125)$$

where  $T_0$  is the ambient temperature. The simplified equation of ecological function ( $\dot{E}$ ) is given by

$$\dot{E} = C_{\dot{W}} \left\{ \frac{(x_1 - y_1) + (x_2 - y_2)\phi + (x_3 - y_3)}{a_{16}\phi^2 + a_{18}\phi - a_{11}} \right\} \quad (4.126)$$

where  $x_1$  to  $x_3$  and  $y_1$  to  $y_3$  are given by the following equations.

$$x_1 = a_{17}a_{22} + a_{16}a_{23} \quad (4.127)$$

$$x_2 = a_{18}a_{23} - a_{13}a_{22} - a_{17}a_{21} \quad (4.128)$$

$$x_3 = a_{13}a_{21} - a_{11}a_{23} \quad (4.129)$$

$$y_1 = T_0(a_{16}a_{28} - a_{17}a_{30}) \quad (4.130)$$

$$y_2 = T_0(a_{13}a_{30} - a_{17}a_{29} + a_{18}a_{28}) \quad (4.131)$$

$$y_3 = T_0(a_{13}a_{29} - a_{11}a_{28}) \quad (4.132)$$

The ecological coefficient of performance (ECOP) of the heat engine is given by

$$\text{ECOP} = \frac{\dot{W}}{T_0 S_{\dot{g}}} \quad (4.133)$$

Based on the above thermal model, the objective function for the present work is defined in the next section.

#### **4.4.2 Case Study, Objective Function Description, and Constraints**

The Brayton heat engine working between the heat source temperature ( $T_H$ ) 1500 K and heat sink temperature ( $T_L$ ) 300 K needs to be designed and optimized for the maximum ecological coefficient of performance (ECOP). The considered heat engine used the ideal gas as the working fluid. The effectiveness of heat source side heat exchanger ( $\varepsilon_H$ ) and heat sink side heat exchanger ( $\varepsilon_L$ ) is 0.9. The isentropic efficiency of the compressor ( $\eta_c$ ) is 0.85, while the isentropic efficiency of the turbine ( $\eta_t$ ) is 0.9. The ratio of heat engine internal conductance to the heat capacity of working fluid ( $\xi$ ) is 0.02. Three design variables such as the isentropic temperature ratio ( $\phi$ ), ratio of the heat source to heat sink temperature ( $\tau$ ), and

**Table 4.13** Ranges of design variables for Brayton heat engine optimization

Design variable	Lower bound	Upper bound
Isentropic temperature ratio, $\phi$	1	1
Ratio of the heat source to heat sink temperature, $\tau$	0.1	5
Regenerator effectiveness, $\varepsilon_R$	0.5	0.5

regenerator effectiveness ( $\varepsilon_R$ ) are considered for the optimization problem. The upper and lower bounds of design variables are presented in Table 4.13.

As mentioned above, the maximization of the ecological coefficient of performance (ECOP) of the Brayton heat engine is taken as an objective function in the present study. Also, the operating parameters which result in the maximum ECOP also satisfy the dimensionless power output ( $W' = W/C_W T_L$ ) and dimensionless entropy generation rate ( $S'_g = S_g - C_W$ ) constraints. So, considering all the aspects, the objective function of Brayton heat engine is formulated as follows:

$$\left\{ \begin{array}{l} \text{Minimize } f(X) = \text{ECOP}(X) + \sum_{j=1}^n G_1(g_j(X))^2 \\ X = [x_1, x_2, x_3, \dots, x_D], x_{i,\text{minimum}} \leq x_i \leq x_{i,\text{maximum}}, \quad i = 1, 2, 3, \dots, D \\ g_j(X) \leq 0, \quad j = 1, 2, 3, \dots, n \end{array} \right. \quad (4.134)$$

where  $X$  is the vector of design variables which should be bounded between its minimum and maximum values.  $G_1$  is the penalty parameter, and entire term takes into account the effect of constraints violation. This term comes into the picture when constraint violation takes place.  $g_j(X)$  indicates the constraints. The following constraints are considered for the Brayton heat engine.

$$\text{Dimensionless power output } (W') > 0.7 \quad (4.135)$$

$$\text{Dimensionless entropy generation} - (S'_g) > 0.5 \quad (4.136)$$

The next section describes the results and discussion of the case study.

#### 4.4.3 Results and Discussion

The considered problem of Brayton heat engine is investigated using 11 different metaheuristic approaches to obtain maximum thermal efficiency. As all these methods are stochastic in their working, each algorithm is implemented 100 times on the considered problem to estimate the statistical variations of the algorithms. Each algorithm is implemented with the population size of 50, and the termination criteria are set as 100,000 function evaluations. The results obtained using each algorithm are presented in the form of the best solution, worst solution, average

solution, standard deviation, and success rate. The success rate is obtained in 100 runs in Table 4.14. Here, the infeasible solutions (i.e., affected by penalty) are eliminated while obtaining the worst solution, average solution, standard deviation, and success rate. Also, the success rate of the algorithm is obtained by considering 0.1% variation from the global optimum value.

It can be observed from the comparative results that all the algorithms performed equally good and produced almost identical maximum ECOP of the Brayton heat engine. However, the average performance of HTS is better followed by DE in comparison with other algorithms. The average performance of PVS is inferior compared to other algorithms. Also, the success rate of HTS algorithm in obtaining the optimum value is the highest followed by the DE and SOS algorithms. The success rate of the PSO algorithm is the lowest compared to other algorithms. It can be observed from the results that it is difficult to judge the performance of the algorithm as all the algorithms have produced a different performance to obtain the best, worst, and average results, and success rate. Thus, the Friedman rank test is implemented to judge the best suitable algorithm for the Brayton heat engine optimization considering the capability to obtain the best, worst, and average solutions, and success rate. The results of the Friedman rank test are presented in Table 4.15, and its graphical representation is presented in Fig. 4.14. The results are presented in the form of Friedman value, normalized value with ‘1’ as the best performing algorithm and its rank. It is observed from the results that HTS has obtained the first rank followed by DE and TLBO algorithms.

The optimized operating parameters of the Brayton heat engine obtained using the HTS algorithm are presented in Table 4.16. It can be noted from the results that the Brayton heat engine with the maximum heat source to the heat sink temperature ratio and regenerator effectiveness results in maximum ECOP. The isentropic

**Table 4.14** Comparative results of different algorithms for Brayton heat engine optimization

Algorithms	Best	Worst	Average	SD	Success rate (%)
GA	1.475	1.1204	1.3089	1.62E-01	44
PSO	1.475	1.1246	1.3390	1.42E-01	36
DE	1.475	1.1293	1.4011	1.09E-01	52
ABC	1.475	1.1324	1.3842	1.33E-01	48
CSA	1.475	1.1345	1.3700	1.10E-01	40
TLBO	1.475	1.234	1.3662	1.08E-01	44
SOS	1.475	1.1123	1.3661	1.41E-01	52
WWO	1.475	1.1009	1.3112	1.58E-01	40
HTS	1.475	1.21	1.4371	7.50E-02	56
PVS	1.475	1.1013	1.2880	1.74E-01	44
SCA	1.475	1.1003	1.3238	1.51E-01	40

**Table 4.15** Friedman rank test results for the Brayton heat engine optimization

Algorithms	Friedman value	Normalized value	Rank
GA	39	0.282051	8
PSO	37	0.297297	7
DE	18.5	0.594595	2
ABC	22	0.5	4
CSA	26	0.423077	5
TLBO	20	0.55	3
SOS	28.5	0.385965	6
WWO	43	0.255814	10
HTS	11	1	1
PVS	43	0.255814	10
SCA	42	0.261905	9

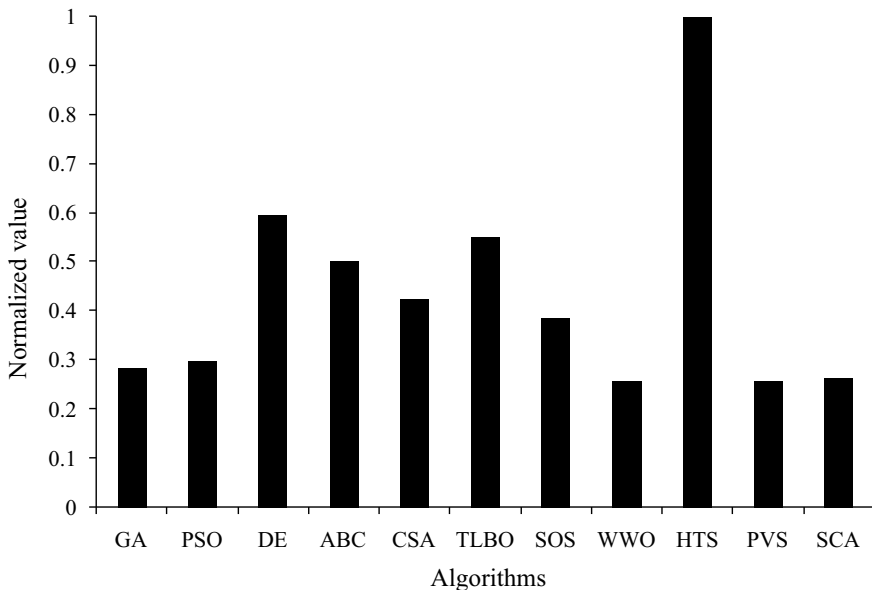


**Fig. 4.14** Graphical presentation of Friedman rank test for Brayton heat engine optimization

temperature ratio produced the conflicting effect on achieving the maximum ECOP of the Brayton heat engine. Furthermore, the dimensionless entropy generation rate constraint is at the limiting value in the optimized operating condition of the Brayton heat engine.

**Table 4.16** The optimized operating condition of the Brayton heat engine

Operating parameters	Optimized value
<b><i>Operating variable</i></b>	
Isentropic temperature ratio, $\phi$	1.325
The ratio of the heat source to heat sink temperature, $\tau$	5
Regenerator effectiveness, $\varepsilon_R$	0.9
<b><i>Constraint</i></b>	
Dimensionless power output, $W'$	0.74
Dimensionless entropy generation rate, $S'_g$	0.49
<b><i>Objective function</i></b>	
Ecological coefficient of performance (ECOP)	1.475

## 4.5 Ericsson Heat Engine

Ericsson heat engine works on the Ericsson cycle. The Ericsson engine composed of three main parts: compressor, expander, and regenerator/recuperator. Figure 4.15 shows the schematic arrangement of the Ericsson heat engine. The regenerator or recuperator is placed between the compressor and the expander. The engine can be run opened or closed cycle. Expansion occurs simultaneously with compression on the opposite sides of the piston.

The Ericsson cycle consists of the four processes. Thermodynamic presentation of Ericsson cycle is shown in Fig. 4.16 on the pressure-volume and temperature-entropy coordinates. The ideal Ericsson cycle consists of two isothermal processes and two constant pressure processes. The compression of the working fluid takes place isothermally (process 1<sub>S</sub>-2) in Ericsson cycle with an irreversible heat rejection at constant temperature ( $T_C$ ) to the heat sink of finite heat capacity whose temperature varies from  $T_{L1}$  to  $T_{L2}$ . After compression, working fluid is passed through the regenerator where heat addition to the working fluid takes place at constant pressure with the help of exhaust gas coming out from expander (process 2-3<sub>S</sub> in ideal and 2-3 in real cycles). The heat addition process is followed by the isothermal expansion process (process 3-4). The expansion process takes place through expander with irreversible heat addition at constant temperature  $T_H$  from the source of finite heat capacity whose temperature varies from  $T_{H1}$  to  $T_{H2}$ . Finally, the heat rejection during the regeneration is modeled as constant pressure process 4-1<sub>S</sub> in ideal and 4-1 in real cycles. The heat transfer processes in Ericson cycle take place externally and must occur in finite time. This, in turn, requires that these heat transfer processes occur through finite temperature difference and externally irreversible. Similarly, the entropy change during process 4-1 is more than process 2-3; thus, there is some net entropy generation within the cycles, and hence these cycles are also internally irreversible. Also, regenerator is nonideal so there is some heat loss through the regenerator.

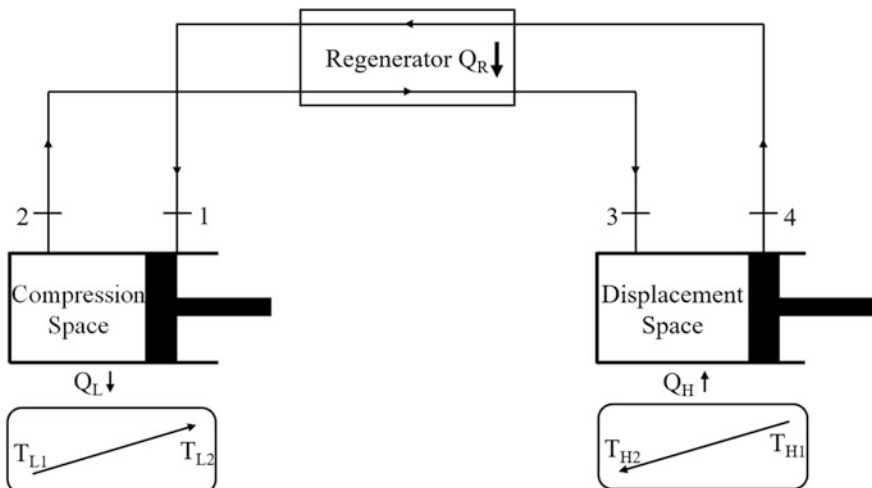


**Fig. 4.15** Schematic arrangement of Ericsson heat engine

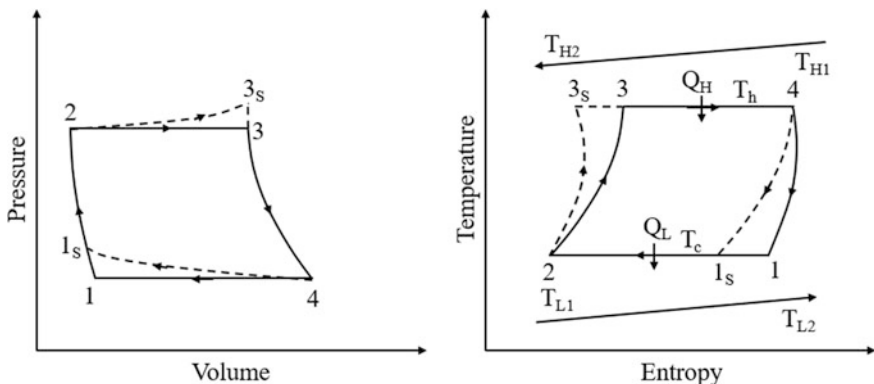


**Fig. 4.16** Thermodynamic cycle of Ericsson engine

Earlier, few works had been reported by the researchers related to the analysis and optimization of Ericsson heat engine. Bădescu (1992) evaluated the performances of the solar converter in combination with the Ericsson heat engine by taking into consideration both the convective losses and the longwave radiation flux incident on the converter. Blank and Wu (1996) analyzed endoreversible Ericsson engine with perfect regeneration. The authors obtained maximum power and efficiency at maximum power based on the higher and lower temperature bounds. Blank and Wu (1998) studied finite-time optimized solar-radiant Ericsson heat engine and obtained mathematical expressions for the optimum power and the efficiency of Ericsson heat engine. Erbay and Yavuz (1999) analyzed the

irreversible Ericsson heat engine with realistic regenerator, turbine and compressor efficiency, and pressure drop in the regenerator. The authors optimized the irreversible Ericsson heat engine using the maximum-power-density technique to obtain more efficient and small-sized engine.

Chenab and Schouten (1999) investigated the influence of irreversibility due to finite-rate heat transfer, regenerative losses, and heat leak losses on the performance of the Ericsson heat engine. The author considered power output of an Ericsson heat engine as an objective function for optimization. The influence of major irreversibilities on the maximum power output and the corresponding efficiency is also analyzed in detail. Kaushik and Kumar (2001) investigated Ericsson heat engine based on the finite-time thermodynamics. The author obtained the power output and thermal efficiency of engine considering finite heat capacitance rates of the heat source and heat sink, finite-time heat transfer, and regenerative heat losses. Tyagi et al. (2002a, b) performed the ecological optimization of the irreversible Ericsson heat engine with imperfect regenerator and entropy generations within the cycle. The authors also analyzed the effect of operating temperatures, effectiveness of the hot-cold-side heat exchangers, and heat capacitance rates on the performance of the Ericsson cycle.

#### 4.5.1 Thermal Model

In this part of the work, the heat engine working on the Ericsson cycle is considered for the optimization. The thermodynamic presentation of Ericsson heat engine is shown in Fig. 4.16. Moreover, the subscripts H and L stand for heat source (i.e., high temperature) and heat sink (i.e., low temperature) side, respectively, while subscripts h and c stand for hot side and cold side, respectively, in the different equations of the thermal model. The thermal model of the Ericsson heat engine presented here is based on the previous work of Tyagi et al. (2002a, b).

The following equation gives the amount of heat absorbed ( $Q_h$ ) from the heat source at temperature  $T_H$ .

$$Q_h = T_H \Delta S_3 - 4 = C_H (T_{H1} - T_{H2}) t_H \quad (4.137)$$

where  $\Delta S_3 - 4$  is entropy changes during the isothermal process,  $C_H$  heat capacitance rates of the source, and  $t_h$  is the time of heat addition.

The following equation gives the amount of heat released ( $Q_c$ ) to the heat sink at temperature  $T_C$ .

$$Q_c = T_C \Delta S_1 - 2 = C_L (T_{L2} - T_{L1}) t_L \quad (4.138)$$

where  $\Delta S_1 - 2$  is entropy changes during the isothermal process,  $C_L$  heat capacitance rates of the sink, and  $t_L$  is times of heat addition to the sink.

From heat transfer theory, the heat addition ( $Q_h$ ) is given by

$$Q_h = U_H A_H (\text{LMTD})_H t_h \quad (4.139)$$

where  $U_H$  is the heat transfer coefficient,  $A_H$  is heat transfer area,  $(\text{LMTD})_H$  is log mean temperature differences of the source and is given by

$$(\text{LMTD})_H = ((T_{H1} - T_h) - (T_{H2} - T_h)) / \ln((T_{H1} - T_h) - (T_{H2} - T_h)) \quad (4.140)$$

Likewise, heat rejection ( $Q_c$ ) is given by

$$Q_c = U_L A_L (\text{LMTD})_L t_L \quad (4.141)$$

where  $U_L$  is heat transfer coefficient,  $A_L$  is heat transfer area,  $(\text{LMTD})_L$  is log mean temperature differences of the sink and is given by

$$(\text{LMTD})_L = ((T_c - T_{L1}) - (T_c - T_{L2})) / \ln((T_c - T_{L1}) - (T_c - T_{L2})) \quad (4.142)$$

The below equations also give the heat addition ( $Q_h$ ) and heat rejection ( $Q_c$ )

$$Q_h = C_H \varepsilon_H (T_{H1} - T_h) t_h \quad (4.143)$$

$$Q_c = C_L \varepsilon_L (T_c - T_{L1}) t_L \quad (4.144)$$

where  $C_H$  and  $C_L$  are the specific heat values at the hot side and cold side, respectively.  $\varepsilon_H$  and  $\varepsilon_L$  are the effectiveness values of the hot-side and cold-side heat exchangers, respectively, and are given by the following equations:

$$\varepsilon_H = 1 - \exp\left(-\frac{U_H A_H}{C_H}\right) = 1 - e^{-NH} \quad (4.145)$$

$$\varepsilon_L = 1 - \exp\left(-\frac{U_L A_L}{C_L}\right) = 1 - e^{-NL} \quad (4.146)$$

where  $NH$  and  $NL$  are the number of transfer units at hot side and cold side, respectively.

Regenerative heat loss per cycle ( $Q_R$ ) during the regeneration process is given by

$$Q_R = n c_f (1 - \varepsilon_R) (T_h - T_c) \quad (4.147)$$

where  $n$  is the number of moles,  $c_f$  is the molar specific heat of fluid, and  $\varepsilon_R$  is the effectiveness of the regenerator, and it is given by

$$\varepsilon_R = \frac{N_R}{1 + N_R} \quad (4.148)$$

where  $N_R$  is the number of the transfer unit of the regenerator, and it is given by

$$N_R = \frac{(UA)_R}{C_f} \quad (4.149)$$

where  $(UA)_R$  is the overall heat transfer of regenerator.

The time of regenerative processes ( $t_R$ ) is given by

$$t_R = t_3 + t_4 = 2 \propto (T_h - T_c) \quad (4.150)$$

where  $\alpha$  is the proportionality constant and is independent of the temperature difference but depends on the property of the regenerative material.

Considering the above mention losses, the net amount of heat absorbed from the source ( $Q_H$ ) and the net amount of heat released from the sink ( $Q_L$ ) is given by

$$Q_H = Q_h + \Delta Q_R \quad (4.151)$$

$$Q_L = Q_c + \Delta Q_R \quad (4.152)$$

From the first law of thermodynamics work done by cycle ( $W$ ) and power output ( $P$ ) and efficiency ( $\eta$ ) is given by

$$W = Q_H - Q_L = Q_h - Q_c \quad (4.153)$$

$$P = \frac{W}{t_{\text{cycle}}} = (Q_h - Q_c)/(t_h + t_L + t_R) \quad (4.154)$$

$$\eta = \frac{W}{Q_h} = (Q_h - Q_c)/(Q_h + \Delta Q_R) \quad (4.155)$$

where  $t_{\text{cycle}}$  is the total cycle time.

The Irreversibility parameter ( $R_{\Delta s}$ ) associated with the system is given by

$$\frac{\frac{Q_h}{T_h}}{\frac{Q_c}{T_c}} = \frac{(s_4 - s_3)}{s_1 - s_2} = R_{\Delta s} < 1 \quad (4.156)$$

where  $s_1, s_2, s_3$ , and  $s_4$  are the entropy values at a different state corresponding to Fig. 4.16.

Based on simplification, it is represented by the following equations.

$$\frac{Q_h}{T_h} = \frac{R_{\Delta s} Q_c}{T_c} \quad (4.157)$$

From the second law and irreversibility parameter, we can define the power output ( $P$ ) and thermal efficiency ( $\eta$ ) of the system as below:

$$P = (R_{\Delta s} T_h - T_c) \left[ \frac{R_{\Delta s} T_h}{\varepsilon_H C_H (T_{H1} - T_h)} + \frac{T_c}{\varepsilon_L C_L (T_c - T_{L1})} + \frac{2\alpha(T_h - T_c)}{S_1 - S_2} \right]^{-1} \quad (4.158)$$

$$\eta = (R_{\Delta s} T_h - T_c) / (R_{\Delta s} T_h + a(T_h - T_c)) \quad (4.159)$$

The following equation gives the ecological function ( $E$ ) of the system:

$$E = P - T_0 S_{\text{gen}} \quad (4.160)$$

$$E = P - T_0 \left( \frac{Q_L}{T_c} - \frac{Q_H}{T_h} \right) \quad (4.161)$$

where  $T_0$  is the ambient temperature and  $S_{\text{gen}}$  is the entropy generation rate.

Based on the above thermal model, the objective function for the present work is defined in the next section.

#### 4.5.2 Case Study, Objective Function Description, and Constraints

The Ericsson heat engine working between the heat source temperature ( $T_{H1}$ ) 900 K and heat sink temperature ( $T_{L1}$ ) 300 K needs to be designed and optimized for maximum thermal efficiency ( $\eta$ ). The considered heat engine used the ideal gas as a working fluid. The effectiveness of cold-side heat exchanger ( $\varepsilon_L$ ) and regenerator ( $\varepsilon_R$ ) is 0.9. The volume ratio of the fluid ( $v_1/v_2$ ) is 2. The internal irreversibility parameter ( $R_{\Delta s}$ ) of the heat engine is 0.85. Three design variables such as cycle temperature ratio ( $x = T_h/T_c$ ), heat capacitance rate ratio ( $C_L/C_H$ ), and hot-side heat exchanger effectiveness ( $\varepsilon_H$ ) are considered for the optimization problem. The upper and lower bounds of design variables are presented in Table 4.17.

As mentioned above, maximization of thermal efficiency ( $\eta$ ) of the Ericsson heat engine is taken as an objective function in the present study. Further, the operating parameters which result in the maximum thermal efficiency also satisfy the dimensionless power output ( $P/C_L T_{L1}$ ), and dimensionless ecological function ( $E/C_L T_{L1}$ ) constraints. So, considering all the aspects, the objective function of the Ericsson heat engine is formulated as below:

$$\begin{cases} \text{Minimize } f(X) = \eta(X) + \sum_{j=1}^n G_j(g_j(X))^2 \\ X = [x_1, x_2, x_3, \dots, x_D], x_{i,\text{minimum}} \leq x_i \leq x_{i,\text{maximum}}, \quad i = 1, 2, 3, \dots, D \\ g_j(X) \leq 0, \quad j = 1, 2, 3, \dots, n \end{cases} \quad (4.162)$$

**Table 4.17** Ranges of design variables for Ericsson heat engine optimization

Design variable	Lower bound	Upper bound
Cycle temperature ratio, $x = T_h/T_c$	0.5	10
Capacitance rate ratio, $C_L/C_H$	0.5	10
Hot-side heat exchanger effectiveness, $\varepsilon_H$	0.5	0.9

where  $X$  is the vector of design variables which should be bounded between its minimum and maximum values.  $G_1$  is the penalty parameter, and entire term takes into account the effect of constraints violation. This term comes into the picture when constraint violation takes place.  $g_j(X)$  indicates the constraints. The following constraints are considered for the Ericsson heat engine.

$$\text{Dimensionless power output } (P/C_L T_{L1}) \geq 0.07 \quad (4.163)$$

$$\text{Dimensionless ecological function } (E/C_L T_{L1}) > -0.1 \quad (4.164)$$

The next section describes the results and discussion of the case study.

#### 4.5.3 Results and Discussion

The considered problem of Ericsson heat engine is investigated using 11 different metaheuristic approaches to obtain the maximum thermal efficiency. As all these methods are stochastic in their working, each algorithm is implemented 100 times on the considered problem to estimate the statistical variations of the algorithms. Each algorithm is implemented with the population size of 50, and the termination criteria are set as 100,000 function evaluations. The results obtained using each algorithm are presented in the form of the best solution, the worst solution, average solution, standard deviation, and success rate obtained in 100 runs in Table 4.18.

**Table 4.18** Comparative results of different algorithms for Ericsson heat engine optimization

Algorithms	Best	Worst	Average	SD	Success rate (%)
GA	0.3235	0.1695	0.2851	5.96E-02	62
PSO	0.3235	0.1695	0.2763	7.04E-02	68
DE	0.3235	0.1865	0.2991	4.64E-02	76
ABC	0.3235	0.1725	0.2939	4.86E-02	64
CSA	0.3235	0.1695	0.2708	6.76E-02	58
TLBO	0.3235	0.0825	0.2635	9.60E-02	68
SOS	0.3235	0.1865	0.2656	6.77E-02	56
WWO	0.3235	0.0721	0.2227	1.12E-01	52
HTS	0.3235	0.1585	0.296	5.21E-02	72
PVS	0.3235	0.1425	0.2627	7.64E-02	60
SCA	0.3235	0.0786	0.2303	1.02E-01	48

Here, the infeasible solutions (i.e., affected by penalty) are eliminated while obtaining the worst solution, average solution, standard deviation, and success rate. Further, the success rate of the algorithm is obtained by considering 0.1% variation from the global optimum value.

It can be observed from the comparative results that all the algorithms performed equally good and produced almost identical maximum thermal efficiency of Ericsson heat engine. However, variations are observed in the average performance of all the considered algorithms. The average performance of DE is better followed by the HTS and ABC in comparison with other algorithms. The average performance of SCA is inferior compared to other algorithms. Further, the success rate of the DE algorithm in obtaining the optimum value is the highest followed by the HTS algorithm. The success rate of the SCA algorithm is the lowest compared to other algorithms. It can be observed from the results that it is difficult to judge the performance of each algorithm as all the algorithms have produced a different performance to obtain the best, worst, and average results, and success rate. So, the Friedman rank test is implemented to judge the best suitable algorithm for Ericsson heat engine optimization considering the capability to obtain the best, worst, and average solutions, and success rate. The results of the Friedman rank test are presented in Table 4.19, and its graphical representation is given in Fig. 4.17. The results are presented in the form of Friedman value, normalized value with '1' as the best performing algorithm and its rank. It is observed from the results that DE has obtained the first rank followed by ABC and HTS algorithms.

The optimized operating parameters of Ericsson heat engine obtained using the DE algorithm are presented in Table 4.20. It can be noted from the results that the Ericsson heat engine with the maximum heat exchanger effectiveness results in the maximum thermal efficiency of the heat engine. The cycle temperature ratio and heat capacitance rate ratio produced a conflicting effect on achieving the maximum thermal efficiency of Ericsson heat engine. Also, the dimensionless entropy generation rate constraint is at the limiting value in the optimized operating condition of Ericsson heat engine.

**Table 4.19** Friedman rank test results for Ericsson heat engine optimization

Algorithms	Friedman value	Normalized value	Rank
GA	25	0.42	4
PSO	26	0.403846	5
DE	10.5	1	1
ABC	19	0.552632	2
CSA	30	0.35	7
TLBO	36	0.291667	8
SOS	29.5	0.355932	6
WWO	49	0.214286	11
HTS	20	0.525	3
PVS	38	0.276316	9
SCA	47	0.223404	10

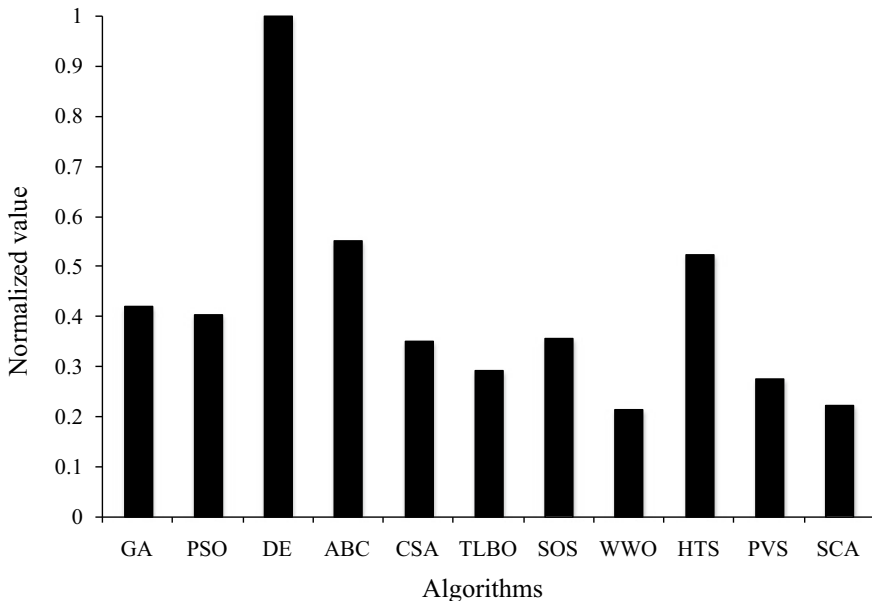


**Fig. 4.17** Graphical presentation of Friedman rank test for Ericsson heat engine optimization

**Table 4.20** The optimized operating condition of Ericsson heat engine optimization

Operating parameters	Optimized value
<b><i>Operating variable</i></b>	
Cycle temperature ratio, $x = T_h/T_c$	1.5
Heat capacitance rate ratio, $C_L/C_H$	1.15
Hot-side heat exchanger effectiveness, $\varepsilon_H$	0.9
<b><i>Constraints</i></b>	
Dimensionless power output, $P/C_LT_{L1}$	0.07
Dimensionless ecological function, $E/C_LT_{L1}$	0.05
<b><i>Objective function</i></b>	
Thermal efficiency, $\eta$	0.3235

## 4.6 Diesel Heat Engine

The Diesel heat engine operates on the Diesel cycle. Diesel heat engine uses diesel as a fuel. In this engine, high-pressure pump and fuel injector are used to inject fuel in the combustion chamber. The working of the Diesel cycle is completed in four strokes. The ideal operations of the Diesel engine are shown schematically in Fig. 4.18 and described.

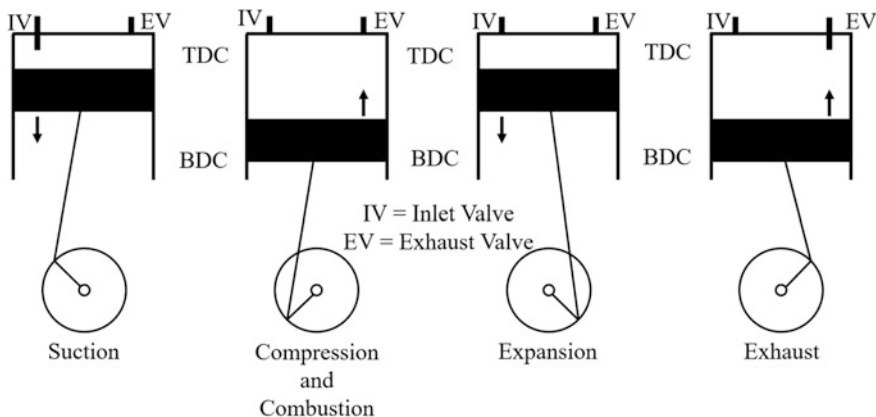
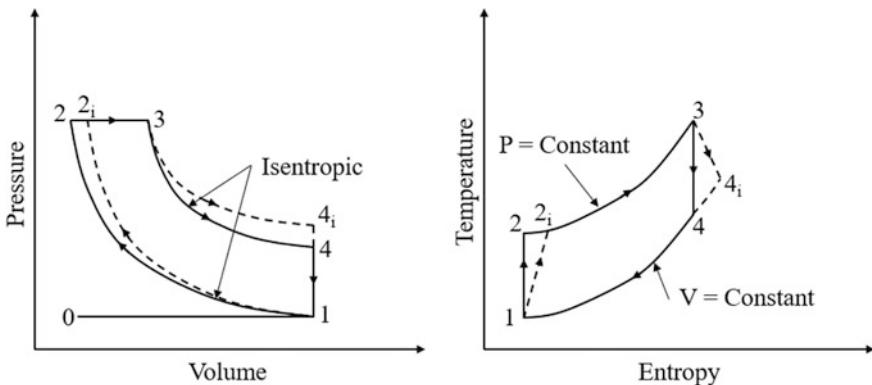


Fig. 4.18 Schematic arrangement of Diesel engine operation

The first stroke of the Diesel engine is termed as ‘Suction stroke.’ During this stroke, the piston moves from the top dead center (TDC) to bottom dead center (BDC); thus, vacuum is created inside the combustion chamber. Then, the inlet valve is opened, and fresh air will enter into the combustion chamber. The second stroke of the Diesel engine is ‘compression stroke.’ During this stroke, both inlet and outlet valves are closed. The piston moves from the BDC to TDC; therefore, air is compressed in this stroke. The third stroke of the Diesel engine is ‘expansion stroke.’ At the end of compression stroke, fuel is injected into the combustion chamber with the help of fuel injector. Fuel is injected in such a way that combustion maintains the constant pressure inside the combustion chamber. Thus, the heat is assumed to be added at constant pressure. When fuel is completely injected, then the combustion products expand in this combustion chamber. During this stroke, both valves are closed. The fourth stroke of the Diesel engine is ‘exhaust stroke.’ In this stroke, piston moved from BDC to TDC which pushed out the combustion products. During this stroke, the inlet valve is closed, and the outlet valve is opened. When combustion products are entirely out, then the inlet valve is open, and fresh air comes in the chamber and cycle is repeated.

The thermodynamic presentation of the Diesel engine is shown in Fig. 4.19. It can be observed from the thermodynamic presentation that four different processes constitute the Diesel engine cycle. Process 1–2 is the isentropic compression process (process 1–2<sub>i</sub> is the compression process with certain isentropic efficiency) where the air is isentropically compressed in the combustion chamber from state 1 to state 2. Process 2–3 is the constant pressure heating process. In this process, heat is added at constant pressure in the chamber. Process 3–4 is the isentropic expansion process (process 3–4<sub>i</sub> is the expansion process with certain isentropic efficiency). In this process, combustion products expand isentropically from state 3 to state 4. Process 4–1 is the constant volume cooling process. During this process, heat is rejected at constant volume from state 3 to state 4.



**Fig. 4.19** Thermodynamic cycle of Diesel engine

Earlier, few works had been reported by the researchers related to the analysis and optimization of Diesel heat engine. Wickman et al. (2001) optimized the combustion chamber geometry of a heavy duty diesel engine and a high-speed direct-injection small-bore diesel engine within the framework of genetic algorithm. Zhao et al. (2006) established an irreversible cycle model of the Diesel heat engine. The authors carried out the optimization of power output and efficiency of the Diesel engine and analyzed the influence of some of the main performance parameters on the performance of the cycle. Leung et al. (2006) studied and optimized the performance of biodiesel in a single-cylinder diesel engine by varying the engine settings, including the injection timing, injection pressure, and fuel pump plunger diameter. Zhao and Chen (2007) presented a more reasonable estimate for the optimal performance of the irreversible Diesel heat engine with variable heat capacities of the working fluid. The authors carried out the parametric analysis to identify the effect of a different operating variable on the performance of Diesel heat engine. Abusoglu and Kanoglu (2008) carried out the first and second law analysis of diesel engine powered cogeneration system. The authors evaluated exergo-economic analysis to estimate the production costs of the diesel cogeneration system.

Zheng and Lin (2010) analyzed the cyclic model of the irreversible Diesel heat engine. The authors optimized the power output and efficiency of the Diesel heat engine considering the finite-time thermodynamics and optimal control theory approaches Xingcai et al. (2010) analyzed the influence of ethanol additives on the performance and combustion characteristics of the diesel engine. The analysis shows certain advantages like reduction in engine smoke and CO emission. Wahono et al. (2012) focused on the minimization of nitrogen oxides emission, as well as improving brake specific fuel consumption and power in a diesel engine. The authors formulated it as a multi-objective optimization problem and solved it by implementing particle swarm optimization algorithm. Pohit and Misra (2013) determined the optimum blend of biodiesel that would result in the better engine

performance along with the minimum emission characteristics. Jafari et al. (2016) carried out the optimization of operating conditions of a diesel engine by the response surface method. The author considered the first and second law efficiency of the Diesel engine and used a multi-objective variant of the genetic algorithm as an optimization tool. Ahmad and Sunthiram (2018) performed the optimization study of the diesel engine using the biodiesel fuel. The authors considered the maximization of brake power and brake torque as well as the minimum of brake specific fuel consumption of diesel engine as the objective function and adopted Bees Algorithm as an optimization tool.

#### 4.6.1 Thermal Model

In this part of the work, the heat engine working on the Diesel cycle is considered for the optimization. The thermodynamic presentation of Diesel heat engine is shown in Fig. 4.19. The thermal model of the Diesel heat engine presented here is based on the previous work of Zheng and Lin (2010).

The heat added to the cyclic working fluid during the constant pressure process ( $Q_{2i-3}$ ) is given by the following equation:

$$Q_{2i-3} = kc_v(T_3 - T_{2i}) \quad (4.165)$$

where  $k$  is the ratio of the specific heat at constant pressure  $c_p$  and specific heat at constant volume  $c_v$ .

The heat rejected to the ambient during the constant volume process ( $Q_{4i-1}$ ) is expressed by the following equation.

$$Q_{4i-1} = c_v(T_{4i} - T_1) \quad (4.166)$$

The heat loss through the cylinder wall ( $Q_L$ ) may be given by

$$Q_L = \int_0^{t_p} \gamma(T - T_0) dt \quad (4.167)$$

where  $\gamma$  is loss coefficient.

The cycle period ( $\tau$ ) can be obtained from the following equation:

$$\tau = t_p + t_v = k_1(T_3 - T_{2i}) + k_2(T_{4i} - T_1) \quad (4.168)$$

where  $t_p$  is the time required for the constant pressure process,  $t_v$  is the time required for the constant volume process, and  $k_1, k_2$  are two positive constants which are given by

$$\frac{d_T}{d_t} = k_1^{-1} \text{ for process 2i-3} \quad (4.169)$$

$$\frac{d_T}{d_t} = -k_2^{-1} \text{ for process 4i-1} \quad (4.170)$$

The following equation gives the heat loss through the cylinder wall ( $Q_L$ ) during combustion:

$$Q_L = \gamma k_1 (T_3 - T_{2i}) \left[ \frac{T_3 + T_{2i}}{2} - T_0 \right] \quad (4.171)$$

where  $\gamma$  is the loss coefficient,  $k_1$  is a positive constant which is described above. The expansion isentropic efficiency ( $\eta_1$ ) can be given by

$$\eta_1 = \frac{T_3 - T_{4i}}{T_3 - T_4} \quad (4.172)$$

The compression isentropic efficiency ( $\eta_2$ ) can be given by

$$\eta_2 = \frac{T_2 - T_1}{T_{2i} - T_1} \quad (4.173)$$

The relation between different temperature, pressure, and volume of the Diesel cycle is given by

$$\frac{T_2}{T_1} = r_p^{\frac{k-1}{k}} \quad (4.174)$$

$$\frac{T_3}{T_4} = (V_1/V_3)^{k-1} \quad (4.175)$$

$$(P_1 V_1)/T_1 = (P_2 V_3)/T_3 \quad (4.176)$$

where  $r_p$  is pressure ratio and is given by

$$r_p = p_2/p_1 \quad (4.177)$$

Temperature after irreversible compression and expansion can be obtained with the help of the following equations:

$$T_{2i} = (1+a)T_1 \quad (4.178)$$

$$T_{4i} = bT_3 \quad (4.179)$$

where  $a$  and  $b$  are constants which are given by the following equations:

$$a = \frac{\left[ r_p^{k-1/k} - 1 \right]}{\eta_2} \quad (4.180)$$

$$b = 1 - \eta_1 + \eta_1 \left[ \frac{T_3}{r_p T_1} \right]^{k-1} \quad (4.181)$$

The power output ( $P$ ) of the irreversible diesel heat engine cycle can be given by

$$P = \frac{Q_{2i-3} - Q_{4i-1}}{\tau} = \frac{C_V}{k_1} \frac{k - A}{1 + (k_2/k_1)A} \quad (4.182)$$

where the following equation gives the parameter  $A$ .

$$A = \frac{(bT_3 - T_1)}{[T_3 - T_1(1 + a)]} \quad (4.183)$$

The efficiency of irreversible diesel heat engine cycle ( $\eta$ ) can be given by

$$\eta = \frac{Q_{2i-3} - Q_{4i-1}}{Q_{2i-3} - Q_L} \quad (4.184)$$

$$\eta = \frac{k - A}{k + \left[ \frac{\gamma k_1 T_0}{2C_V} \right] \left\{ \frac{[T_3 + T_1(1 + a)]}{T_0 - 2} \right\}} \quad (4.185)$$

where  $Q_L$  is the heat loss due to combustion,  $\gamma$  is loss coefficient, and  $k$  is specific heat ratio.

If the irreversibility in the two adiabatic processes is negligible, the dimensionless power output ( $P$ ) is given by

$$P = \frac{c_v}{k_1} \frac{k - A_1}{1 + (k_2/k_1)A_1} \quad (4.186)$$

where  $A_1$  is constant and is given by the following equation.

$$A_1 = \frac{\left( \frac{T_3^k}{r_p^{k-1} T_1^{k-1}} - T_1 \right)}{\left( T_3 - T_1 r_p^{(k-1)/k} \right)} \quad (4.187)$$

The following equation gives the temperature at states 1 and 3 in power and efficiency equation.

$$T_{2i} = T_1 r_p^{(k-1)/k} \quad (4.188)$$

$$T_{4i} = \left( T_3^k / r_p T_1 \right)^{k-1} \quad (4.189)$$

Based on the above thermal model, the objective function for the present work is defined in the next section.

#### 4.6.2 Case Study, Objective Function Description, and Constraints

The Diesel heat engine working between the minimum temperature ( $T_1$ ) 300 K and maximum temperature ( $T_3$ ) 1500 K needs to be designed and optimized for the maximum thermal efficiency ( $\eta$ ). The ambient temperature is 300 K. Ratio of specific heat ( $k$ ) is taken as 1.4 while isentropic efficiency ( $\eta$ ) is considered as 0.97. Three design variables such as cycle pressure ratio ( $r_p$ ), temperature after irreversible compression ( $T_{2i}$ ), and temperature after irreversible expansion ( $T_{4i}$ ) are considered for the optimization problem. The upper and lower bounds of design variables are presented in Table 4.21.

As mentioned above, the maximization of thermal efficiency ( $\eta$ ) of the Diesel heat engine is taken as an objective function in the present study. Also, the operating parameters which result in the maximum thermal efficiency also satisfy the dimensionless power output ( $P^* = P k_1 / c_v$ ) constraints. So, considering all the aspects, the objective function of the Diesel heat engine is formulated as follows:

$$\begin{cases} \text{Minimize } f(X) = \eta(X) + \sum_{j=1}^n G_1(g_j(X))^2 \\ X = [x_1, x_2, x_3, \dots, x_D], x_{i,\text{minimum}} \leq x_i \leq x_{i,\text{maximum}}, i = 1, 2, 3, \dots, D \\ g_j(X) \leq 0, \quad j = 1, 2, 3, \dots, n \end{cases} \quad (4.190)$$

where  $X$  is the vector of design variables which should be bounded between its minimum and maximum values.  $G_1$  is the penalty parameter, and entire term takes into account the effect of constraints violation. This term comes into picture when constraint violation takes place.  $g_j(X)$  indicates the constraints. The following constraint is considered for the Diesel heat engine

**Table 4.21** Ranges of design variables for Diesel heat engine optimization

Design variable	Lower bound	Upper bound
Cycle pressure ratio, $r_p$	1	160
Temperature after irreversible compression, $T_{2i}$	350	1750
Temperature after irreversible expansion, $T_{4i}$	300	1700

$$\text{Dimensionless power } (P^* = Pk_1/c_v) \geq 50 \quad (4.191)$$

The next section describes the results and discussion of the case study.

### 4.6.3 Results and Discussion

The considered problem of the Diesel heat engine is investigated using 11 different metaheuristic approaches to obtain the maximum thermal efficiency. As all these methods are stochastic in their working, each algorithm is implemented 100 times on the considered problem to estimate the statistical variations of the algorithms. Each algorithm is implemented with the population size of 50, and the termination criteria are set as 100,000 function evaluations. In Table 4.22, the results obtained using each algorithm are presented in the form of the best solution, worst solution, average solution, standard deviation, and success rate over 100 runs. Here, the infeasible solutions (i.e., affected by penalty) are eliminated while obtaining the worst solution, average solution, standard deviation, and success rate. Furthermore, the success rate of the algorithm is obtained by considering 0.1% variation from the global optimum value.

It can be observed from the comparative results that all the algorithms performed equally good and produced almost identical maximum thermal efficiency of Diesel heat engine. However, the average performance of ABC is better followed by TLBO and DE in comparison with other algorithms. The average performance of WWO is inferior compared to other algorithms. Also, the success rate of the ABC algorithm in obtaining the optimum value is the highest followed by the TLBO and GA algorithms. The success rate of WWO algorithm is the lowest as compared to other algorithms. It can be observed from the results that it is difficult to judge the

**Table 4.22** Comparative results of different algorithms for Diesel heat engine optimization

Algorithms	Best	Worst	Average	SD	Success rate (%)
GA	0.2393	0.1114	0.1984	6.09E-02	68
PSO	0.2393	0.0853	0.2009	5.96E-02	62
DE	0.2393	0.0883	0.2097	4.86E-02	64
ABC	0.2393	0.1123	0.2157	4.44E-02	76
CSA	0.2393	0.1023	0.1907	6.14E-02	58
TLBO	0.2393	0.0743	0.2118	5.21E-02	72
SOS	0.2393	0.1023	0.1814	6.77E-02	56
WWO	0.2393	0.056	0.1606	8.11E-02	48
HTS	0.2393	0.0573	0.1931	7.16E-02	68
PVS	0.2393	0.0583	0.1785	7.64E-02	60
SCA	0.2393	0.07	0.1625	8.21E-02	52

performance of each algorithm as all the algorithms have produced a different performance to obtain the best, worst, and average results, and success rate. Thus, the Friedman rank test is implemented to judge the best suitable algorithm for Diesel heat engine optimization considering the capability to obtain the best, worst, and average solutions, and success rate. The results of the Friedman rank test are presented in Table 4.23, and its graphical representation is given in Fig. 4.20. The results are presented in the form of Friedman value, normalized value with ‘1’ as

**Table 4.23** Friedman rank test results for Diesel heat engine optimization

Algorithms	Friedman value	Normalized value	Rank
GA	21.5	0.465116	4
PSO	26	0.384615	5
DE	21	0.47619	3
ABC	10	1	1
CSA	30.5	0.327869	6
TLBO	20	0.5	2
SOS	33.5	0.298507	7
WWO	49	0.204082	11
HTS	33.5	0.298507	8
PVS	40	0.25	9
SCA	45	0.222222	10

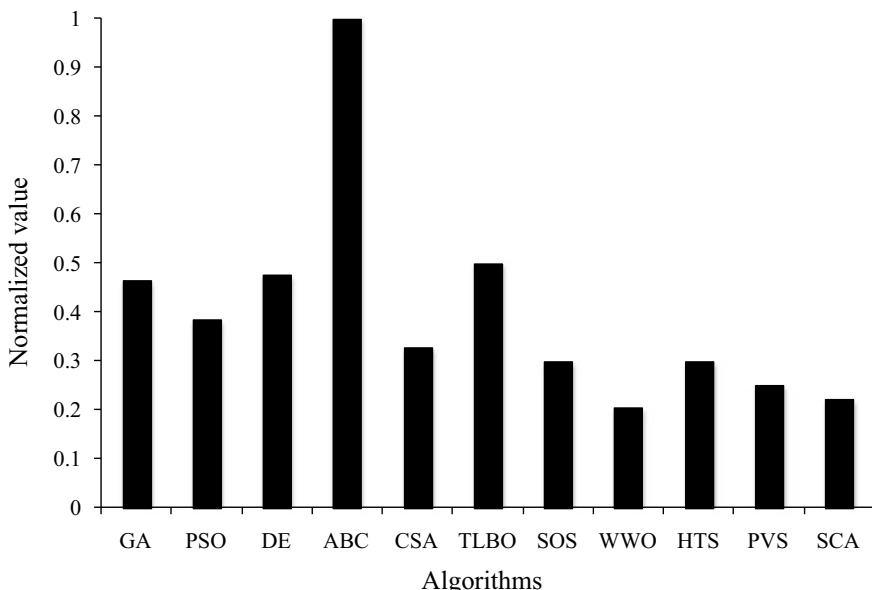


**Fig. 4.20** Graphical presentation of Friedman rank test for Diesel heat engine optimization

**Table 4.24** The optimized operating condition of Diesel heat engine

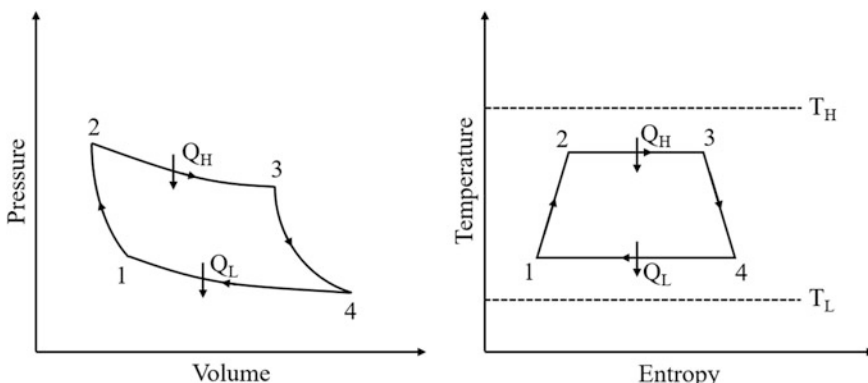
Operating parameters	Optimized value
<b><i>Operating variable</i></b>	
Cycle pressure ratio, $r_p$	49.2
Temperature after irreversible compression, $T_{2i}$	1090
Temperature after irreversible expansion, $T_{4i}$	590
<b><i>Constraint</i></b>	
Dimensionless power output, $P^* = Pk_1/c_v$	50
<b><i>Objective function</i></b>	
Thermal efficiency, $\eta$	0.2393

the best performing algorithm and its rank. It is observed from the results that ABC has obtained the first rank followed by TLBO and DE algorithms.

The optimized operating parameters of the Diesel heat engine obtained using the ABC algorithm are presented in Table 4.24. It can be noted from the results that all three-design variable produced a conflicting effect on achieving the maximum thermal efficiency of the Diesel engine. Furthermore, the dimensionless power output is at the limiting value in the optimized operating condition of the Diesel heat engine.

## 4.7 Radiative-Type Heat Engine

The radiative-type heat engine operates with the radiative heat transfer conditions. In this part of the work, the Carnot heat engine with radiative heat transfer condition is analyzed as the radiative heat engine. For making the analysis more realistic, irreversibility associated with all process of the Carnot cycle is considered in the

**Fig. 4.21** Thermodynamic cycle of the radiative heat engine operating on Carnot cycle

present work. The thermodynamic presentation of the radiative type Carnot heat engine is shown in Fig. 4.21. The working fluid flows through the closed system in a steady state condition. The cycle consists of two isothermals (2–3, 4–1) and two adiabatic (1–2, 3–4). All the processes are irreversible.

Earlier, work had been reported by the researchers related to the analysis and optimization of the radiative-type heat engine. Göktun et al. (1993) obtained the condition for maximum power output for the endoreversible heat engine model operating under radiative heat-transfer conditions. Özkanak et al. (1994) developed a relation between the design parameters of an internally and externally irreversible radiative heat engine to find the maximum power and efficiency at the maximum power output. The authors found that the ratio of the reservoir temperatures must be less than half of the cycle-irreversibility parameter for the optimum thermal efficiency and maximum power output. Furthermore, increasing the cycle-irreversibility parameter and the heat-transfer area of the cold side improves thermal efficiency and maximum power output of the heat engine. Chen et al. (1996) studied the effect of irreversibility on the performance of radiative-type heat engine. The authors also carried out the power output optimization and derived maximum specific power output and the corresponding efficiency of the radiative-type heat engine. Badescu (2004) studied the optimal heating paths with Newton's and radiative heat transfer laws by taking the minimum entropy generation, and minimum lost available work as the objectives. The author expressed the obtained analytical expressions of the optimal paths in dimensionless forms. Maheshwari et al. (2005a, b, c) analyzed the radiative heat engine under the maximum efficient power (MEP) conditions and concluded that MEP conditions had an advantage of smaller size and were more efficient than those designed at the maximum power (MP) and maximum power density (MPD) conditions. The authors derived the optimal design parameters analytically and evaluated the effect of irreversibilities on general and optimal performances of the engine.

Song et al. (2006, 2007a, b) determined the optimal configuration of an endoreversible heat engine for the maximum efficiency objective and maximum power output objective with linear phenomenological heat transfer law (2006) and those for maximum power output with fixed duration and radiative heat transfer law (2007). Song et al. (2007a, b) obtained the optimal configuration of the endoreversible heat engine for the maximum power output with fixed cycle duration and radiative heat-transfer law in the heat-transfer processes between the working fluid and heat reservoirs. Maheshwari et al. (2009) carried out the maximum efficient power analysis for an internally and externally irreversible radiative heat engine model. The authors also investigated the optimal performance and design parameters of heat engine under MEP conditions. Chen et al. (2010) studied the endoreversible radiative heat engine configuration for the maximum efficiency consideration. The authors determined the optimal configuration of a class of endoreversible heat engines with the fixed duration, input energy, and radiative heat transfer law in the heat transfer processes between the working fluid and the heat reservoirs. Ahmadi and Ahmadi (2016) performed the optimization of the irreversible radiative-type heat engine by employing the evolutionary algorithm. The

author considered dimensionless power, thermal efficiency, and the dimensionless ecological function of the heat engine as objective functions and four operating parameters of the heat engine as decision variables. Raman and Maheshwari (2017) carried out performance analysis of the generalized radiative heat engine based on new maximum efficient power density (EPD) approach. Furthermore, the results obtained using EPD criteria are compared with those obtained using the maximum efficient power, maximum power density, and maximum power criteria.

#### 4.7.1 Thermal Model

In the present work, the heat engine working on the Carnot cycle with the radiative heat transfer conditions is considered for the optimization. The thermodynamic presentation of the Carnot heat engine with radiative heat transfer condition is shown in Fig. 4.21. The thermal model presented here is based on the previous work of Maheshwari et al. (2007). Moreover, the subscripts H and L stand for high-temperature and low-temperature reservoir sides in the different equations of the thermal model.

The following equation gives the rate of heat flow ( $Q_H$ ) from the heat engine to the source:

$$Q_H = U_H A_H (T_H^4 - T_x^4) \quad (4.192)$$

where  $U_H$  is overall heat transfer coefficient of source,  $A_H$  is the heat transfer area of the heat exchanger between the heat source and heat engine, respectively, and  $T_x$  is the warm working fluid temperature.

The following equation gives the rate of heat flow ( $Q_L$ ) from the heat engine to the source:

$$Q_L = U_L A_L (T_y^4 - T_L^4) \quad (4.193)$$

where  $U_L$  is the overall heat transfer coefficient,  $A_L$  is the heat transfer area of the heat exchanger between the heat sink and heat engine, respectively, and  $T_y$  is the cold working fluid temperature.

The following equation gives the total heat transfer conductance.

$$U_L A_L + U_H A_H = UA = \text{Constant} \quad (4.194)$$

The following equation gives the thermal conductance allocation ratio ( $x$ ) for the heat source size.

$$x = \frac{U_H A_H}{UA} \quad (4.195)$$

$$1 - x = \frac{U_L A_L}{UA} \quad (4.196)$$

Employing the first law of thermodynamics, the output power ( $W$ ) of the heat engine can be given by the following equation.

$$W = Q_H - Q_L \quad (4.197)$$

The following equation gives the second law of thermodynamics for an irreversible cycle.

$$\frac{dQ}{T} = \left( \frac{Q_H}{T_x} - \frac{Q_L}{T_y} \right) < 0 \quad (4.198)$$

Rewriting the inequality of irreversibility equation results in

$$\frac{Q_L}{T_y} - R \frac{Q_H}{T_x} = 0 \quad (4.199)$$

The following equation gives the internal irreversibility parameter ( $R$ ).

$$R = \frac{S_4 - S_1}{S_3 - S_2} \quad (4.200)$$

Substituting heat equation into irreversibility parameter equation, we get the following equation:

$$\frac{(1-x)\left(\left(\frac{T_y}{T_H}\right)^4 - \tau^4\right)}{x(1-\psi^4 y)} = \frac{R}{\psi} \quad (4.201)$$

$$\left(\frac{T_Y}{T_H}\right)^4 = \frac{\psi\tau^4 - \psi x\tau^4 - Rx}{\psi - \psi\chi + R\chi\psi^4} \quad (4.202)$$

where  $\tau$  and  $\psi$  are the extreme heat temperature ratio and cycle temperature ratio, respectively, and are given by

$$\tau = T_L/T_H \quad (4.203)$$

$$\psi = \frac{T_x}{T_y} \quad (4.204)$$

The following equation gives the dimensionless power ( $P^*$ ).

$$P^* = \frac{\dot{W}}{UAT_H^4} = \chi \left( 1 - \frac{R}{\psi} \right) \left( 1 - \psi \left( \frac{T_Y}{T_H} \right)^4 \right) \quad (4.205)$$

The following equation gives the thermal efficiency of the heat engine.

$$\eta = 1 - \frac{Q_L}{Q_H} \quad (4.206)$$

$$\eta = 1 - \frac{R}{\psi} \quad (4.207)$$

The following equation can calculate the entropy generation rate in the cycle.

$$S_g = \left( \frac{Q_L}{T_L} - \frac{Q_H}{T_H} \right) \quad (4.208)$$

Dimensionless entropy generation ( $S_g^*$ ) equation can be obtained by combining thermal heat conduction equation, second law equation, and entropy generation equation and is represented as

$$S_g^* = \frac{S_g}{UAT_H^3} = x \left( 1 - \psi \left( \frac{T_Y}{T_H} \right)^4 \right) \left( \frac{R}{\psi\tau} - 1 \right) \quad (4.209)$$

The following equation gives the ecological performance function ( $E_C$ ).

$$E_C = P - (T_L S_g) \quad (4.210)$$

The following equation can also represent the dimensionless ecological function ( $E^*$ ).

$$E^* = X \left( 1 - \frac{R}{\psi} \right) \left( 1 - \psi \left( \frac{T_Y}{T_H} \right)^4 \right) - \left[ \tau x \left( 1 - \psi \left( \frac{T_Y}{T_H} \right)^4 \right) \left( \frac{R}{\psi\tau} - 1 \right) \right] \quad (4.211)$$

Based on the above thermal model, the objective function for the present work is defined in the next section.

**Table 4.25** Ranges of design variables for Carnot type radiative heat engine optimization

Design variable	Lower bound	Upper bound
Working fluid temperatures ratio, $\psi = T_x/T_y$	1.4	2.5
Cold working fluid temperature, $T_y$	350	400
Internal irreversibility parameter, $R$	1.1	1.4
Extreme heat temperature ratio, $\tau = T_L/T_H$	0.2	0.4

#### 4.7.2 Case Study, Objective Function Description, and Constraints

The Carnot heat engine with the radiative heat transfer conditions working between the heat source temperature ( $T_H$ ) 1200 K and heat sink temperature ( $T_L$ ) 300 K is needed to be designed and optimized for the maximum thermal efficiency ( $\eta$ ). The considered heat engine used ideal gas as the working fluid. Thermal conductance allocation ratio ( $x$ ) of the engine is 0.3. Four design variables such as working fluid temperatures ratio ( $\psi = T_x/T_y$ ), cold working fluid temperature ( $T_y$ ), internal irreversibility parameter ( $R$ ), and extreme heat temperature ratio ( $\tau = T_L/T_H$ ) are considered for the optimization problem. The upper and lower bounds of design variables are presented in Table 4.25.

As mentioned above, the maximization of thermal efficiency ( $\eta$ ) of the Carnot type radiative heat engine is taken as an objective function in the present study. Also, the operating parameters which result in maximum thermal efficiency also satisfy the dimensionless power output ( $P^*$ ), and dimensionless ecological function ( $E^*$ ) constraints. Thus, considering all the aspects, the objective function of Carnot type radiative heat engine is formulated as follows:

$$\left\{ \begin{array}{l} \text{Minimize } f(X) = \eta(X) + \sum_{j=1}^n G_1(g_j(X))^2 \\ X = [x_1, x_2, x_3, \dots, x_D], x_{i,\text{minimum}} \leq x_i \leq x_{i,\text{maximum}}, \quad i = 1, 2, 3, \dots, D \\ g_j(X) \leq 0, \quad j = 1, 2, 3, \dots, n \end{array} \right. \quad (4.212)$$

where  $X$  is the vector of design variables which should be bounded between its minimum and maximum values.  $G_1$  is the penalty parameter, and entire term takes into account the effect of constraints violation. This term comes into the picture when constraint violation takes place.  $g_j(X)$  indicates the constraints. The following constraints are considered for the radiative heat engine.

$$\text{Dimensionless power, } P^* \geq 0.124 \quad (4.213)$$

$$\text{Dimensionless ecological function, } E^* \geq 0.05 \quad (4.214)$$

The next section describes the results and discussion of the case study.

**Table 4.26** Comparative results of different algorithms for the radiative heat engine

Algorithms	Best	Worst	Average	SD	Success rate (%)
GA	0.5287	0.4008	0.498	5.58E-02	78
PSO	0.5287	0.3747	0.49413	6.10E-02	74
DE	0.5287	0.4524	0.51954	2.53E-02	90
ABC	0.5287	0.4017	0.50938	4.10E-02	82
CSA	0.5287	0.3917	0.49762	5.34E-02	75
TLBO	0.5287	0.3637	0.5052	5.11E-02	80
SOS	0.5287	0.3917	0.51469	4.00E-02	88
WWO	0.5287	0.3454	0.48536	7.38E-02	72
HTS	0.5287	0.3467	0.50674	5.44E-02	84
PVS	0.5287	0.3777	0.49246	6.58E-02	76
SCA	0.5287	0.3594	0.48807	7.38E-02	73

#### 4.7.3 Results and Discussion

The considered problem of Carnot heat engine with radiative heat transfer conditions is investigated using 11 different metaheuristic approaches to obtain the maximum thermal efficiency. As all these methods are stochastic in their working, each algorithm is implemented 100 times on the considered problem to estimate the statistical variations of the algorithms. Each algorithm is implemented with the population size of 50, and the termination criteria are set as 100,000 function evaluations. In Table 4.26, the results obtained using each algorithm are presented in the form of the best solution, worst solution, average solution, standard deviation, and success rate over 100 runs. Here, the infeasible solutions (i.e., affected by penalty) are eliminated while obtaining the worst solution, average solution, standard deviation, and success rate. Furthermore, the success rate of the algorithm is obtained by considering 0.1% variation from the global optimum value.

It can be observed from the comparative results that all the algorithms performed equally good and produced almost identical maximum thermal efficiency of the radiative heat engine. However, the average performance of DE is better followed by SOS and ABC in comparison with other algorithms. The average performance of WWO is inferior compared to other algorithms. Furthermore, the success rate of DE algorithm in obtaining the optimum value is the highest followed by the SOS and HTS algorithms. The success rate of WWO algorithm is lowest as compared to other algorithms. It can be observed from the results that it is difficult to judge the performance of each algorithm as all the algorithms have produced a different performance to obtain the best, worst, and average results, and success rate. Thus, the Friedman rank test is implemented to judge the best suitable algorithm for radiative heat engine optimization considering the capability to obtain the best, worst, and average solutions, and success rate. The results of the Friedman rank test are presented in Table 4.27, and its graphical representation is given in Fig. 4.22.

**Table 4.27** Friedman rank test results for radiative heat engine optimization

Algorithms	Friedman value	Normalized value	Rank
GA	28	0.354286	5
PSO	38	0.263158	9
DE	10	1	1
ABC	18	0.555556	3
CSA	30.5	0.327869	7
TLBO	28	0.357143	4
SOS	16.5	0.606061	2
WWO	50	0.2	11
HTS	29	0.344828	6
PVS	37	0.27027	8
SCA	45	0.222222	10

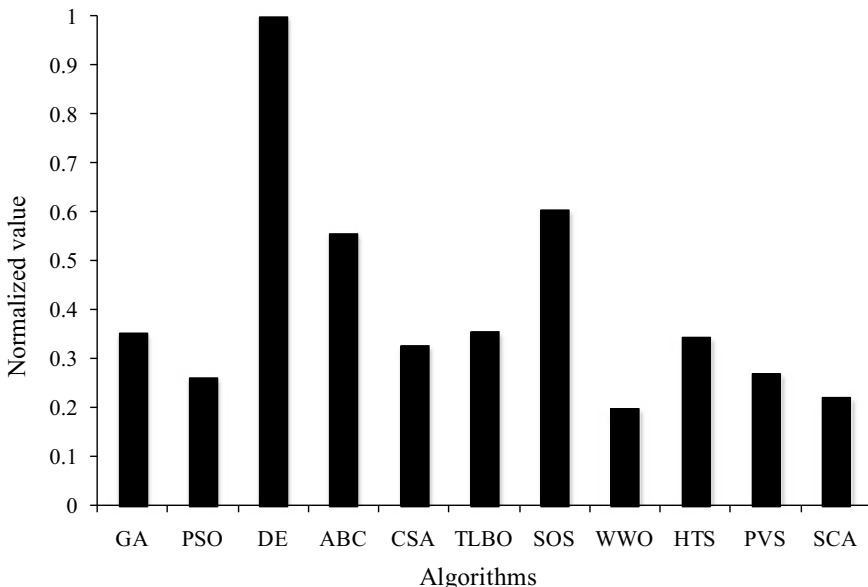


**Fig. 4.22** Graphical presentation of Friedman rank test for radiative heat engine optimization

The results are presented in the form of Friedman value, normalized value with ‘1’ as the best performing algorithm and its rank. It is observed from the results that DE has obtained the first rank followed by SOS and ABC algorithms.

The optimized operating parameters of radiative heat engine obtained using the ABC algorithm is presented in Table 4.28. It can be noted from the results that the radiative heat engine with maximum working fluid temperatures ratio ( $\psi$ ), minimum cold working fluid temperature ( $T_y$ ), and internal irreversibility parameter ( $R$ ) results in the maximum thermal efficiency of the radiative heat engine. The

**Table 4.28** The optimized operating condition of the Radiative heat engine

Operating parameters	Optimized value
<b><i>Operating variable</i></b>	
Working fluid temperatures ratio, $\psi$	2.5
Cold working fluid temperature, $T_y$	350
Internal irreversibility parameter, $R$	1.1
Extreme heat temperature ratio, $\tau$	0.315
<b><i>Constraints</i></b>	
Dimensionless power ( $P^*$ )	0.1243
Dimensionless ecological function ( $E^*$ )	0.062
<b><i>Objective function</i></b>	
Thermal efficiency, $\eta$	0.5287

extreme heat temperature ratio ( $\tau$ ) produced a conflicting effect on achieving the maximum thermal efficiency of the radiative heat engine. Furthermore, the dimensionless ecological function is above the limiting value while dimensionless power output constraint is at the limiting value in the optimized operating condition of the radiative heat engine.

## 4.8 Stirling Heat Pump

The Stirling heat pump operates on the Stirling cycle. In compliance with the second law of thermodynamics, heat cannot spontaneously flow from cold system to the hot system without external work being performed on the system. Heat can flow from colder to a hotter body, but only when forced by an external work. Stirling heat pump uses mechanical power to heat the space. Heating is accomplished by alternately compressing and expanding a fixed quantity of working fluid at a different temperature. Mechanical components of Stirling pumps are the compressor, regenerator, and expander. Compression of the working gas is isothermal in nature. This mechanism requires rejection of heat to heat sink. Regenerative heat exchanger consists of the matrix material, which is used to transfer the energy of working gas. The solid matrix of regenerator alternately stores heat extracted from the hot fluid and then delivers it to the cold fluid. Finally, the working gas expands isothermally in expander by extracting heat from the heat source. The schematic arrangement of the Stirling heat pump is shown in Fig. 4.23.

Thermodynamic cycle of Stirling heat pump is demonstrated in Fig. 4.24. It can be observed from Fig. 4.24 that thermodynamic cycle of the Stirling heat pump consists of two isothermal and two constant volume processes. The irreversible Stirling heat pump follows the cycle 1–2–3–4 while the reversible Stirling heat pump follows the 1<sub>S</sub>–2–3<sub>S</sub>–4. During process 1–2, the low-pressure working gas expands isothermally at the cold end by absorbing heat from the cold space. Here pressure is decreased from  $P_1$  to  $P_2$  and volume is increased from  $V_1$  to  $V_2$ . During

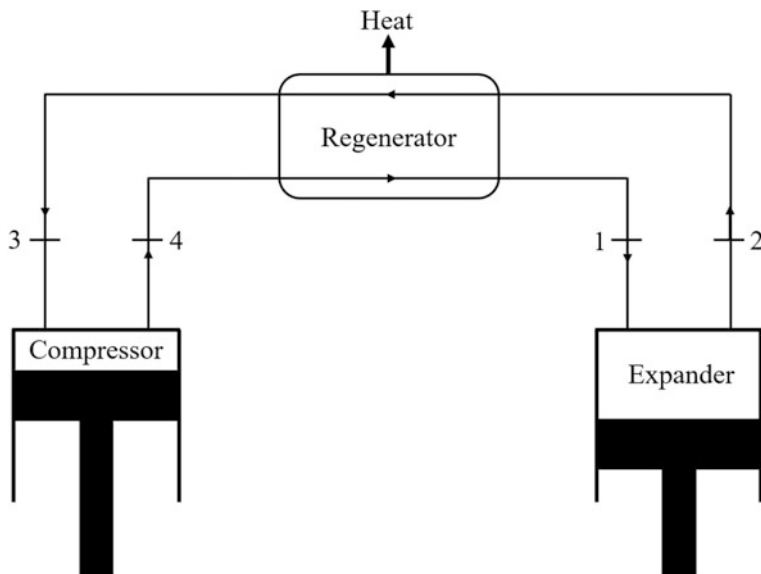


**Fig. 4.23** Schematic arrangement of the Stirling heat pump

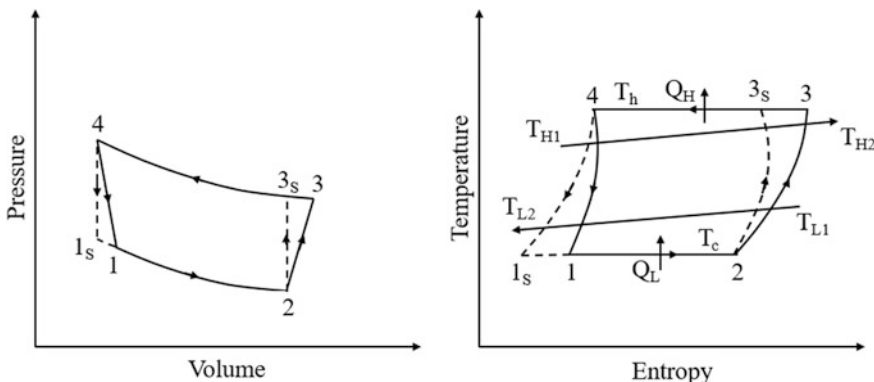


**Fig. 4.24** Thermodynamic cycle of Stirling heat pump

process 2–3, both compressor and expander move together to displace the working gas through the regenerator to the hot end of the system. Heat is delivered to the gas as it passes through the regenerator, thus raising the temperature of the gas to that of the hot space. As the temperature rises, the gas pressure increases from  $P_2$  to  $P_3$ . During process 3–4, the working gas compressed isothermally ( $T_3 = T_4$ ) at hot end temperature; hence, it will reject heat at hot space. In this process, pressure increases from  $P_3$  to  $P_4$  and volume reduced from  $V_3$  to  $V_4$ . During process 4–1,

both piston and expander move together to transfer all the working gas through the regenerator to the cold end of the system. Heat is absorbed from the gas as it passes through the regenerator, thus lowering the temperature of the gas to that of the cold space. As the temperature reduces, the gas pressure drops from  $P_4$  to  $P_1$ .

Earlier, work had been reported by the researchers related to the analysis and optimization of the Stirling heat pump. Wu et al. (1998a, b) carried out the performance optimization of the quantum Stirling heat pump by adapting the finite-time thermodynamics and nonequilibrium quantum statistical theory. The authors also derived the optimization criteria for the forward and reversed quantum Stirling cycles at several limiting cases. Kaushik and Kumar (2000) presented the finite-time thermodynamic evaluation of irreversible Stirling heat pump cycles, using real gas as the working substance along with the infinite heat capacities of the heat source and heat sink reservoirs. Kaushik et al. (2001) studied the effects of operating inlet temperatures and capacitance rates of source-sink reservoirs, regenerator effectiveness, and the internal irreversibility parameter on the heat transfers, COP, and power input of the Stirling heat pump. The authors considered both the external and internal irreversibilities in their study. Tyagi et al. (2002a, b) performed the ecological optimization of the Stirling heat pump. The ecological function is optimized with respect to working fluid temperatures, and the expressions for various parameters at the optimal operating condition were obtained. The effects of different operating parameters on the performance of the heat pump were also studied and reported by the authors.

Tyagi et al. (2004) presented thermo-economic optimization of the irreversible Stirling heat pump cycle. The thermo-economic function is defined as the heating load divided by the total cost of the system and optimized with respect to the working fluid temperatures. The authors also carried out the parametric study to identify the effects of different operating parameters on the performance of the cycle. Ahmadi et al. (2014a, b) carried out the thermodynamic optimization of the Stirling heat pump. Simultaneous optimization is carried out by considering the maximization of heating load, coefficient of performance, and minimization of power input to the system. Ahmadi et al. (2015a, b) performed the thermo-economic optimization of the Stirling heat pump by using the nondominated sorting genetic algorithm. The authors considered maximization of the coefficient of performance, heating load and thermo-economic criterion as an objective function in their study and optimized six operating variables of the heat pump. Furthermore, the optimum solution was selected by the various decision-making methods from the Pareto front. Xu (2016) carried out a thermodynamic analysis of Stirling heat pump based on thermo-economic optimization criteria.

### 4.8.1 Thermal Model

In this part of the work, the heat pump working on the Stirling cycle is considered for the optimization. The thermodynamic presentation of the Stirling heat pump is shown in Fig. 4.24. Moreover, the subscripts H and L stand for high-temperature side and low-temperature side, respectively. The subscript R stands for regenerator in the different equations of the thermal model. The thermal model presented here is based on the previous work of Ahmadi et al. (2015a, b).

In the present work, thermal modeling of Stirling heat pump is carried out considering the irreversibility associated with the cycle. Heat gained ( $Q_c$ ) from the source is given by the following equation:

$$Q_c = T_c \Delta S = C_L(T_{L1} - T_{L2})t_L = U_L A_L (\text{LMTD})_L t_L \quad (4.215)$$

where  $\Delta S$  is the entropy changes of the fluid,  $T_c$  is the working fluid temperature,  $C_L$  is the heat capacitance of the source,  $t_L$  is the times of heat addition,  $U_L$  is the heat transfer coefficient of cold side,  $A_L$  is the heat transfer area of cold side, and  $(\text{LMTD})_L$  is the log mean temperature of source and is given by the following equation:

$$(\text{LMTD})_L = \frac{(T_{L1} - T_c) - (T_{L2} - T_c)}{\ln \left( \frac{(T_{L1} - T_c)}{(T_{L2} - T_c)} \right)} \quad (4.216)$$

Heat delivered ( $Q_h$ ) at temperature  $T_h$  to the sink is given by the following equation:

$$Q_h = T_h \Delta S = C_H(T_{H2} - T_{H1})t_H = U_H A_H (\text{LMTD})_H t_H \quad (4.217)$$

where  $T_h$  is the working fluid temperature,  $C_H$  is the heat capacitance of the sink,  $t_H$  is the times of heat rejection,  $U_H$  is the heat transfer coefficient of hot side,  $A_H$  is heat transfer area of hot side, and  $(\text{LMTD})_H$  is the log mean temperature of the sink which is given by the following equation.

$$(\text{LMTD})_H = \frac{(T_h - T_{H1}) - (T_h - T_{H2})}{\ln \left( \frac{(T_h - T_{H1})}{(T_h - T_{H2})} \right)} \quad (4.218)$$

The following equation gives the entropy change of the fluid:

$$\Delta S = nR \ln \lambda \quad (4.219)$$

where  $n$  is the number of mole of the working fluid,  $R$  is the gas constant of the working fluid, and  $\lambda$  is the volume ratio of the working fluid.

The following equation gives the regeneration heat loss ( $Q_R$ ).

$$\Delta Q_R = nC_v(1 - \varepsilon_R)(T_h - T_c) \quad (4.220)$$

where  $n$  is the number of moles of the working fluid,  $C_v$  specific heat at constant volume, and  $\varepsilon_R$  is regenerator effectiveness.

The following equation gives the time of the regenerative process ( $t_R$ ):

$$t_R = t_3 + t_4 = 2\alpha(T_h - T_c) \quad (4.221)$$

where  $\alpha$  is the proportionality constant. The following equation gives the total cycle time.

$$t_{cycle} = (t_H + t_L + t_R) \quad (4.222)$$

The following equation gives the value of net heat that gained from the source.

$$Q_H = Q_h - \Delta Q_R \quad (4.223)$$

Likewise, the value of the net heat that delivered from the sink is given by the following equation.

$$Q_L = Q_c - \Delta Q_R \quad (4.224)$$

The following equation gives the power input ( $P$ ) to the heat pump.

$$P = \frac{(Q_H - Q_L)}{t_{cycle}} \quad (4.225)$$

The following equation can calculate the heating load ( $R_H$ ).

$$R_H = \frac{Q_H}{t_{cycle}} \quad (4.226)$$

The following equation gives the coefficient of performance of heat pump (COP<sub>H</sub>).

$$\text{COP}_H = \frac{R_H}{P} \quad (4.227)$$

The power required to drive the heat pump is simplified based on the time of the regenerative process and is given by the following equation.

$$P = \frac{\chi - 1}{\left(\frac{\chi}{\varepsilon_R C(\chi T_c - T_{H1})}\right) + \left(\frac{1}{\varepsilon_L C(\chi T_{L1} - T_c)}\right) + b_1(\chi - 1)} \quad (4.228)$$

Likewise, the heating load of the heat pump is simplified based on the time of the regenerative process and is given by the following equation.

$$R_H = \frac{\chi - F_1(\chi - 1)}{\left( \frac{\chi}{\varepsilon_H C (\chi T_c - T_{HI})} \right) + \left( \frac{1}{\varepsilon_L C (\chi T_{LI} - T_c)} \right) + b_1(\chi - 1)} \quad (4.229)$$

The following equation gives the simplification of the coefficient of performance.

$$\text{COP}_H = \frac{\chi - F_1(\chi - 1)}{\chi - 1} \quad (4.230)$$

where the parameters  $\chi$ ,  $b_1$ , and  $F_1$  are given by the following equations.

$$\chi = \frac{T_h}{T_c} \quad (4.231)$$

$$b_1 = \frac{2\alpha}{\eta R \ln \lambda} \quad (4.232)$$

$$F_1 = \frac{C_v(1 - \varepsilon_R)}{R \ln \lambda} \quad (4.233)$$

The thermo-economic criterion for Stirling heat pump is defined as the total price of the unit heating load which includes both capital and energy costs and is given by the following equation:

$$F = \frac{R_H}{C_i + C_e} \quad (4.234)$$

where  $C_i$  and  $C_e$  are the capital and energy costs in the unit of time, respectively, and it is given by the following equation:

$$C_i = k_1(A_H + A_L + A_R) \quad (4.235)$$

$$C_e = k_2 P \quad (4.236)$$

where  $k_1$  is the capital recovery factor and  $k_2$  is the unit cost of energy. Substituting all the value in thermo-economic function results in

$$F = \frac{R_H}{K_1(A_H + A_L + A_R) + k_2 P} \quad (4.237)$$

where  $A_H$ ,  $A_L$ , and  $A_R$  are the heat transfer areas for the hot side, cold side, and regenerator and are given by the following equations.

$$A_H = \left( \frac{C}{U_H} \right) \ln \left( \frac{1}{1 - \varepsilon_H} \right) \quad (4.238)$$

$$A_L = \left( \frac{C}{U_L} \right) \ln \left( \frac{1}{1 - \varepsilon_L} \right) \quad (4.239)$$

$$A_R = \left( \frac{C}{U_R} \right) \ln \left( \frac{\varepsilon_R}{1 - \varepsilon_R} \right) \quad (4.240)$$

Based on the above thermal model, the objective function for the present work is defined in the next section.

#### 4.8.2 Case Study, Objective Function Description, and Constraints

The Stirling heat pump needs to be designed and optimized for minimum power input. This heat pump is used to maintain the temperature of hot side ( $T_h$ ) at 330 K by extracting heat from cold side ( $T_c$ ) maintain at 290 K. The volumetric ratio ( $\lambda$ ) during regeneration process is 1.2. Specific heat of regenerator material ( $C_r$ ) is 502.48 J/kg K. Specific heat of the gas at constant volume ( $C_v$ ) is 15 J/mol K. Gas constant for the working fluid is 4.3 J/mol K. The effectiveness of the regenerator is 0.9. Six design variables such as hot-side heat exchanger effectiveness ( $\varepsilon_H$ ), cold-side heat exchanger effectiveness ( $\varepsilon_L$ ), cold-side temperature ( $T_c$ ), temperature ratio ( $x = T_h/T_c$ ), heat capacitance in the heat source ( $C_L$ ), and heat capacitance in the heat sink ( $C_H$ ) are considered for the optimization problem. The upper and lower bounds of design variables are presented in Table 4.29.

As mentioned above, the minimization of power input of the Stirling heat pump is taken as an objective function in the present study. Also, the operating parameters which result in minimum power input also satisfy the coefficient of performance, heating load, and ecological function (ECF) constraints. So, considering all the aspects, the objective function of the Stirling heat pump is formulated as follows:

**Table 4.29** Ranges of design variables for Stirling heat pump optimization

Design variable	Lower bound	Upper bound
Hot-side heat exchanger effectiveness, $\varepsilon_H$	0.005	0.8
Cold-side heat exchanger effectiveness, $\varepsilon_L$	0.005	0.8
Cold-side temperature, $T_c$	255	270
Temperature ratio, $x = T_h/T_c$	1.3	2.4
Heat capacitance in the heat source, $C_L$	6	1000
Heat capacitance in the heat sink, $C_H$	6	1000

$$\left\{ \begin{array}{l} \text{Minimize } f(X) = P(X) + \sum_{j=1}^n G_1(g_j(X))^2 \\ X = [x_1, x_2, x_3, \dots, x_D], \quad x_{i,\text{minimum}} \leq x_i \leq x_{i,\text{maximum}}, \quad i = 1, 2, 3, \dots, D \\ g_j(X) \leq 0, \quad j = 1, 2, 3, \dots, n \end{array} \right. \quad (4.241)$$

where  $X$  is the vector of design variables which should be bounded between its minimum and maximum values.  $G_1$  is the penalty parameter, and entire term takes into account the effect of constraints violation. This term comes into the picture when constraint violation takes place.  $g_j(X)$  indicates the constraints. The following constraints are considered for the Stirling heat pump.

$$\text{The coefficient of performance (COP)} \geq 1 \quad (4.242)$$

$$\text{Heating load } (R_H) \geq 4500 \text{ W} \quad (4.243)$$

$$\text{Ecological function (ECF)} \geq 300 \quad (4.244)$$

The next section describes the results and discussion of the case study.

#### 4.8.3 Results and Discussion

The considered problem of Stirling heat pump is investigated using 11 different metaheuristic approaches to obtain the minimum power input. As all these methods are stochastic in their working, each algorithm is implemented 100 times on the considered problem to estimate the statistical variations of the algorithms. Each algorithm is implemented with the population size of 50, and the termination criteria are set as 100,000 function evaluations. In Table 4.30, the results obtained

**Table 4.30** Comparative results of different algorithms for Stirling heat pump optimization

Algorithms	Best	Worst	Average	SD	Success rate (%)
GA	3894.23	3928.27	3910.11	1.57E+01	24
PSO	3891.62	3891.72	3891.63	2.30E-02	92
DE	3891.62	3891.62	3891.62	0.00E+00	100
ABC	3891.62	3912.5	3897.31	6.26E+00	52
CSA	3891.62	3892.12	3891.73	1.54E-03	100
TLBO	3891.62	3891.62	3891.62	0.00E+00	100
SOS	3891.62	3891.62	3891.62	0.00E+00	100
WWO	3891.64	3923.45	3897.78	7.21E+00	48
HTS	3891.62	3891.62	3891.62	0.00E+00	100
PVS	3891.62	3891.62	3891.62	0.00E+00	100
SCA	3892.29	3922.6	3903.63	8.97E+00	20

using each algorithm are presented in the form of the best solution, worst solution, average solution, standard deviation, and success rate over 100 runs. Here, the infeasible solutions (i.e., affected by penalty) are eliminated while obtaining the worst solution, average solution, standard deviation, and success rate. Furthermore, the success rate of the algorithm is obtained by considering 0.1% variation from the global optimum value.

It can be observed from the comparative results that all the algorithms performed equally good (except GA and SCA) and produced identical minimum power requirement of Stirling heat pump. The average performance of DE, TLBO, SOS, HTS, and PVS are also identical and dominated the performance of other algorithms. The average performance of GA is inferior compared to other algorithms. Furthermore, the success rate of DE, CSA, TLBO, SOS, HTS, and PVS algorithms in obtaining the optimum value is 100%. The success rate of the SCA algorithm is the lowest compared to other algorithms. It can be observed from the results that it is difficult to judge the performance of each algorithm as all the algorithms have produced a different performance to obtain the best, worst, and average results, and success rate. So, the Friedman rank test is implemented to judge the best suitable algorithm for Stirling heat pump optimization considering the capability to obtain the best, worst, and average solutions, and success rate. The results of the Friedman rank test are presented in Table 4.31, and its graphical representation is given in Fig. 4.25. The results are presented in the form of Friedman value, normalized value with '1' as the best performing algorithm and its rank. It is observed from the results that DE, TLBO, SOS, HTS, and PVS algorithms performed equally well and obtained the first rank followed by CSA and PSO algorithms.

The optimized operating parameters of the Stirling heat pump obtained using the DE algorithm are presented in Table 4.32. It can be noted from the results that the Stirling heat pump with maximum hot-side heat exchanger effectiveness ( $\varepsilon_H$ ) and cold-side heat exchanger effectiveness ( $\varepsilon_L$ ) results in the minimum power input.

**Table 4.31** Friedman rank test results for Stirling heat pump optimization

Algorithms	Friedman value	Normalized value	Rank
GA	54	0.314815	7
PSO	29	0.586207	3
DE	17	1	1
ABC	40	0.425	4
CSA	26	0.653846	2
TLBO	17	1	1
SOS	17	1	1
WWO	46	0.369565	5
HTS	17	1	1
PVS	17	1	1
SCA	50	0.34	6

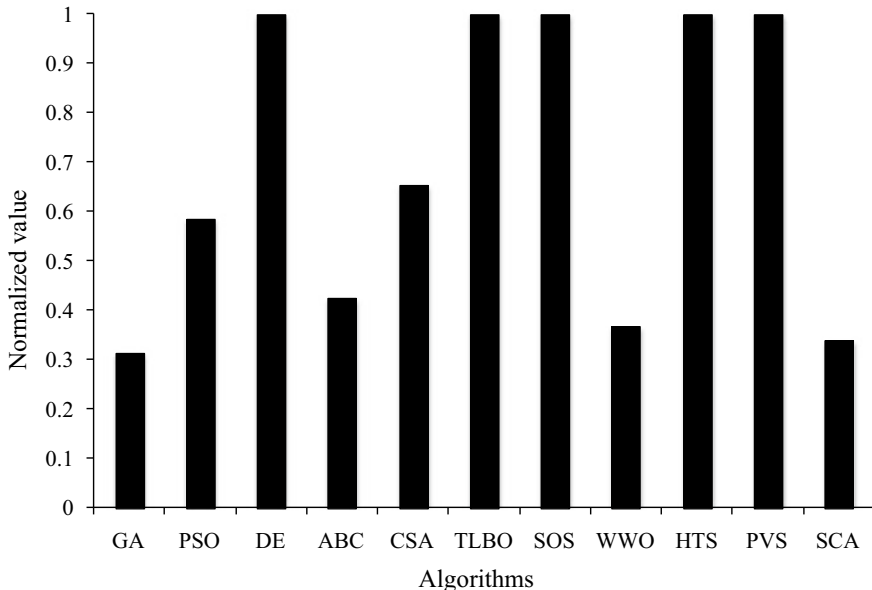


**Fig. 4.25** Graphical presentation of Friedman rank test for Stirling heat pump optimization

**Table 4.32** The optimized operating condition of the Stirling heat pump

Operating parameters	Optimized value
<b><i>Operating variable</i></b>	
Hot-side heat exchanger effectiveness, $\epsilon_H$	0.8
Cold-side heat exchanger effectiveness, $\epsilon_L$	0.8
Cold-side temperature, $T_c$	235.35
Temperature ratio, $x = T_h/T_c$	1.37
Heat capacitance in the heat source, $C_L$	1000
Heat capacitance in the heat sink, $C_H$	1000
<b><i>Constraint</i></b>	
The coefficient of performance, (COP)	1.156
Heating load ( $R_H$ ), W	4500 W
Ecological function (ECF), W	317.04
<b><i>Objective function</i></b>	
Power input, $P$ (W)	3891.65

Similarly, the Stirling heat pump with the minimum heat capacitance in the heat source ( $C_L$ ) and heat sink ( $C_H$ ) results in minimum power input. The temperature ratio of the hot side and cold side produced a conflicting effect on achieving the minimum power input of the Stirling heat pump. Moreover, COP and ecological function constraints are above the required value while heating load constraints

dimensionless is at the limiting value in the optimized operating condition of Stirling heat pump.

## 4.9 Heat Pump Working on Reverse Brayton Cycle

The Brayton cycle is the power-generating cycle. If the Brayton cycle is driven in reverse direction, then it is known as the reverse Brayton cycle. The purpose of reverse Brayton cycle is to move the heat from colder to a hotter body, rather than producing work. Reverse Brayton cycle heat pumps, also referred as reverse Bell Coleman cycle heat pumps, are similar in design to reverse Rankine cycle, but are operated without the liquid/ vapor phase change and thus solely in single-phase configuration and gaseous media. Reverse Brayton cycle heat pumps, therefore, do not have an evaporator and a condenser, but rather two gas-to-gas or liquid-to-gas heat exchangers. One heat exchanger is used to remove the heat from an external heat source; this heat exchanger is operated at low temperature and pressure. The second heat exchanger is used to provide the heat to an external heat sink; this heat exchanger is operated at high temperature and pressure.

The thermodynamic cycle of heat pump operated on a reverse Brayton cycle is shown in Fig. 4.26. The cycle presented by point 1–2–3–4 is the heat pump cycle with irreversibility while 1<sub>S</sub>–2–3<sub>S</sub>–4 represent the same cycle without irreversibility. It can be observed from the figure that heat pump is operated with two isentropic and two constant pressure process. During process 1–2, heat is absorbed by the heat pump from lower temperature heat sink at constant pressure hence the temperature of working fluid is increased from  $T_1$  to  $T_2$ . During process 2–3, the working fluid compressed from lower pressure to higher pressure and hence its temperature is increased. During process 3–4, the working fluid rejects the heat in the space which requires heating at constant pressure and hence the temperature of

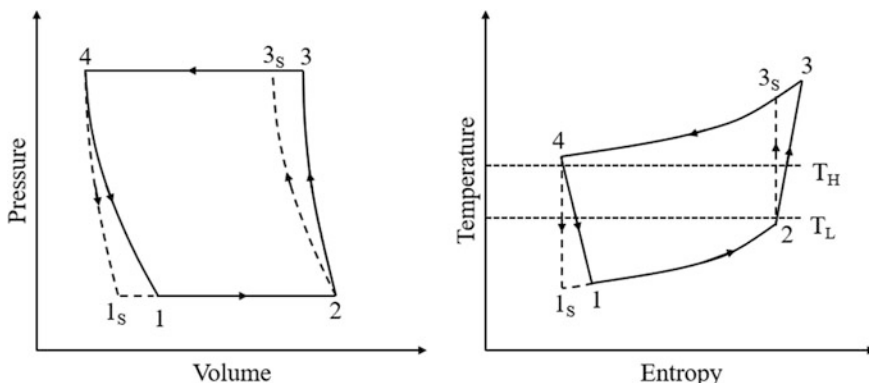


**Fig. 4.26** Thermodynamic presentation of heat pump working on reverse Brayton cycle

working fluid reduces from  $T_3$  to  $T_4$ . Finally, during process 4–1, the working fluid expands from higher temperature to lower temperature; hence, its pressure is reduced. In that way, the cycle is repeated and extracts heat from the lower temperature and rejects heat to higher temperature.

Earlier, work had been reported by the researchers related to the analysis and optimization of the heat pump working on reverse Brayton cycle. Wu et al. (1998a, b) studied the finite-time thermodynamic performance of steady flow Brayton heat pump for both finite and infinite thermal capacitance rates of heat reservoirs. The authors analyzed the effect of finite thermal capacitance rates of the working fluid and heat reservoirs on cycle performance and obtained the fundamental optimal relations of the cycle. Chen et al. (1999) analyzed the performance of the regenerated Brayton heat pump based on the finite-time thermodynamics. The authors obtained the analytical relations between heating load and pressure ratio, and between the coefficient of performance and pressure ratio of the regenerated Brayton heat pump cycles coupled to constant- and variable-temperature heat reservoirs. Angelino and Invernizzi (1995) analyzed the reversed Brayton cycle heat pump working with real gas. The authors observed that heat pump cycles based on the reversed regenerative Brayton cycle could achieve a reasonable efficiency provided the expansion take place in the vicinity of the critical point.

Ni et al. (1999) analyzed the finite-time thermodynamic performance of isentropic closed regenerated Brayton heat pump coupled with constant and variable temperature heat reservoirs. The authors also derived the relations between heating load and pressure ratio and between the coefficient of performance and pressure ratio for the two cases of heat reservoirs. Chen et al. (2001) analyzed and optimized the performance of an irreversible regenerated closed Brayton cycle with variable-temperature heat reservoirs using the power density objective. The authors compared the obtained results with the available results obtained using the maximum power criterion. Chen et al. (2007a, b) carried out the power optimization of a regenerated closed variable-temperature heat reservoir Brayton cycle. The authors also derived the analytical relations between power output and pressure ratio in the optimization condition. White (2009) carried out the thermodynamic analysis of the reverse Joule-Brayton cycle heat pump for domestic heating. The author investigated the effects of irreversibility on the performance of the heat pump.

Bi et al. (2010) performed the performance analysis and optimization of the irreversible heat pumps working on reversed Brayton cycle with constant-temperature heat reservoirs. The authors considered exergetic efficiency as an objective function and developed analytical formulas for the heating load, coefficient of performance and exergetic efficiency of the heat pump system. Ahmadi et al. (2016a, b, c) performed the thermodynamic analysis and optimization of an irreversible heat pump working on the reversed Brayton cycle by adapting NSGA-II. The authors defined two different scenarios for the optimization of Brayton heat pump. In the first scenario, maximization of the coefficient of performance, ecological coefficient of performance, and exergetic efficiency of heat pump considered simultaneously. In the second scenario, maximization of the coefficient of performance, ecological coefficient of performance, and ecological

function of the heat pump considered simultaneously. Also, the decision-making techniques were also implemented to select the best solution.

#### 4.9.1 Thermal Model

In this part of the work, the heat pump working on reverse Brayton cycle is considered for the optimization. The thermodynamic presentation of such the heat pump is shown in Fig. 4.24. Moreover, the subscripts H and L stand for high-temperature side and low-temperature side, respectively. The thermal model presented here is based on the previous work of Ahmadi et al. (2016a, b).

The heat transfer from the heat source ( $Q_L$ ) is given by

$$Q_L = \frac{U_L(T_2 - T_1)}{\ln \frac{T_1 - T_L}{T_L - T_2}} = C_{wf}E_L(T_L - T_1) \quad (4.245)$$

where  $U_L$  is the heat conductance of heat source,  $C_{wf}$  is the specific heat of fluid,  $N_L$  is the number of the transfer unit of heat source,  $E_L$  is the effectiveness of the heat source, and it is given by the following equation.

$$E_L = 1 - \exp(-N_L) \quad (4.246)$$

$$N_L = \frac{U_L}{C_{wf}} \quad (4.247)$$

The rate of heat transfer from the heat sink ( $Q_H$ ) is given by

$$Q_H = \frac{U_H(T_2 - T_1)}{\ln \frac{T_3 - T_H}{T_4 - T_H}} = C_{wf}E_H(T_3 - T_H) \quad (4.248)$$

where  $U_H$  is the heat conductance of sink,  $C_{wf}$  is the specific heat of fluid,  $N_H$  is the number of the transfer unit of sink,  $E_H$  is the effectiveness of sink, and it is given by the following equation.

$$E_H = 1 - \exp(-N_H) \quad (4.249)$$

$$N_H = \frac{U_H}{C_{wf}} \quad (4.250)$$

The following equation gives the compressor efficiency.

$$\eta_c = \frac{T_{3s} - T_2}{T_3 - T_2} \quad (4.251)$$

The following equation gives the expander efficiency.

$$\eta_t = \frac{T_4 - T_1}{T_4 - T_{1s}} \quad (4.252)$$

By combining all the efficiency and heat transfer rate, we can find out the temperature of the heat exchanger:

$$T_1 = \frac{E_H T_H \eta_c (\eta_t \pi^{-m} - \eta_t + 1) + E_L T_L (1 - E_H) (\pi^m + \eta_c - 1) (\eta_t \pi^{-m} - \eta_t + 1)}{\eta_c - (1 - E_H) (1 - E_L) (\pi^m + \eta_c - 1) (\eta_t \pi^{-m} - \eta_t + 1)} \quad (4.253)$$

$$T_2 = \frac{\eta_c [E_L T_L + E_H T_H (1 - E_L) (\eta_t \pi^{-m} - \eta_t + 1)]}{\eta_c - (1 - E_H) (1 - E_L) (\pi^m + \eta_c - 1) (\eta_t \pi^{-m} - \eta_t + 1)} \quad (4.254)$$

where  $\pi$  is the pressure ratio of the compressor and  $m$  is the parameter given by the following equation.

$$m = \frac{k - 1}{k} \quad (4.255)$$

The rate of heat transfer ( $Q_H$ ) released to the heat sink is given by

$$Q_H = \frac{C_{wf} E_H \{(\pi^m + \eta_c - 1) E_L T_L - [\eta_c - (1 - E_L) (\pi^m + \eta_c - 1) (\eta_t \pi^{-m} - \eta_t + 1)] T_H\}}{\eta_c - (1 - E_H) (1 - E_L) (\pi^m + \eta_c - 1) (\eta_t \pi^{-m} - \eta_t + 1)} \quad (4.256)$$

The following equation gives the coefficient of performance of heat pump:

$$\text{COP} = 1 - \frac{E_H \{(\pi^m + \eta_c - 1) E_L - [\eta_c - (1 - E_L) (\pi^m + \eta_c - 1) (\eta_t \pi^{-m} - \eta_t + 1)] \tau\}}{(E_L \{[\eta_c - (1 - E_H) (\pi^m + \eta_c - 1) (\eta_t \pi^{-m} - \eta_t + 1)] - E_H (\eta_t \pi^{-m} - \eta_t + 1) \eta_c \tau\})} \quad (4.257)$$

where  $\tau$  is the temperature ratio of the compressor.

Entropy generation ( $S_{gen}$ ) can be calculated from the following equation.

$$S_{gen} = \frac{Q_H}{T_H} - \frac{Q_L}{T_L} \quad (4.258)$$

The following equation gives the ecological coefficient of performance.

$$\text{ECOP} = \frac{Q_H}{T_0 S_{\text{gen}}} \quad (4.259)$$

The following equation gives the rate of exergy input and output.

$$\epsilon_{\text{IN}} = -W_{\text{CV}} = Q_H - Q_L \quad (4.260)$$

$$\epsilon_{\text{OUT}} = \sum_j \left( \frac{T_0}{T_j} - 1 \right) Q_j = \int_L^H \left( 1 - \frac{T_0}{T} \right) dQ \quad (4.261)$$

For the purposes of computing the heat exergy, heat rejection and heat reception are presumed to take place at  $T_H$  and  $T_L$ , respectively. Hence, the exergy output is given by the following equation.

$$\epsilon_{\text{OUT}} = \left( 1 - \frac{T_0}{T_H} \right) Q_H - \left( 1 - \frac{T_0}{T_L} \right) Q_L \quad (4.262)$$

From the above equation, we can say that

$$\epsilon_{\text{OUT}} = \epsilon_{\text{IN}} - \epsilon_d \quad (4.263)$$

where  $\epsilon_d$  is the exergy destruction of the system.

The following equation gives the exergetic efficiency ( $\eta_{\text{ex}}$ ).

$$\eta_{\text{ex}} = \frac{\epsilon_{\text{OUT}}}{\epsilon_{\text{IN}}} \quad (4.264)$$

From simplification of the efficiency equation, we can derive the following relation.

$$\sigma_{\text{ex}} = \frac{\left( 1 - \frac{T_0}{T_H} \right) Q_H - \left( 1 - \frac{T_0}{T_L} \right) Q_L}{Q_H - Q_L} \quad (4.265)$$

The following equation gives the ecological function.

$$\text{ECF} = \epsilon_{\text{IN}} - T_0 S_{\text{gen}} \quad (4.266)$$

Based on the above thermal model, the objective function for the present work is defined in the next section.

**Table 4.33** Ranges of design variables for the optimization of heat pump working on reverse Brayton cycle

Design variable	Lower bound	Upper bound
Hot-side heat exchanger effectiveness, $E_H$	0.7	0.9
Cold-side heat exchanger effectiveness, $E_L$	0.2	0.9
Temperature ratio, $\tau$	1.1	1500
Compressor pressure ratio, $\pi$	0	7

#### 4.9.2 Case Study, Objective Function Description, and Constraints

The heat pump working on the reversed Brayton cycle needs to be designed and optimized for the maximum coefficient of performance (COP). This heat pump is worked with heat sink temperature ( $T_L$ ) 298.15 K. The ambient temperature ( $T_0$ ) is 300 K. The compressor and expander efficiency are 80%, respectively. Thermal capacitance rate is 0.8 kW/K. Four design variables such as hot-side heat exchanger effectiveness ( $E_H$ ), cold-side heat exchanger effectiveness ( $E_L$ ), temperature ratio ( $\tau$ ), and compressor pressure ratio ( $\pi$ ) are considered for the optimization problem. The upper and lower bounds of design variables are presented in Table 4.33.

As mentioned above, the maximization of the coefficient of performance of the heat pump is taken as an objective function in the present study. Also, the operating parameters which result in the maximum COP also satisfy the exergetic efficiency ( $\eta_{ex}$ ), ecological function (ECF), and ecological coefficient of performance (ECOP) constraints. So, considering all the aspects, the objective function of heat pump working on the reverse Brayton cycle is formulated as follows:

$$\left\{ \begin{array}{l} \text{Minimize } f(X) = \text{COP}(X) + \sum_{j=1}^n G_1(g_j(X))^2 \\ X = [x_1, x_2, x_3, \dots, x_D], x_{i,\text{minimum}} \leq x_i \leq x_{i,\text{maximum}}, i = 1, 2, 3, \dots, D \\ g_j(X) \leq 0, \quad j = 1, 2, 3, \dots, n \end{array} \right. \quad (4.267)$$

where  $X$  is the vector of design variables which should be bounded between its minimum and maximum values.  $G_1$  is the penalty parameter, and entire term takes into account the effect of constraints violation. This term comes into the picture when the constraint violation takes place.  $g_j(X)$  indicates the constraints. The following constraints are considered for the heat working on reverse Brayton cycle.

$$\text{Exergetic efficiency } (\eta_{ex}) \geq 0.3 \quad (4.268)$$

$$\text{Ecological function } (\text{ECF}) \geq 30 \quad (4.269)$$

**Table 4.34** Comparative results of different algorithms for the optimization of heat pump working on reverse Brayton cycle

Algorithms	Best	Worst	Average	SD	Success rate (%)
GA	1.124	1.1231	1.1237	3.27E-04	28
PSO	1.124	1.1231	1.1237	3.57E-04	40
DE	1.124	1.1231	1.1235	5.10E-04	16
ABC	1.124	1.124	1.124	8.49E-06	68
CSA	1.124	1.124	1.124	2.28E-16	84
TLBO	1.124	1.124	1.124	1.32E-05	28
SOS	1.124	1.1231	1.1238	3.84E-04	36
WWO	1.124	1.124	1.124	1.43E-05	24
HTS	1.124	1.124	1.124	1.27E-05	56
PVS	1.124	1.124	1.124	1.28E-05	80
SCA	1.124	1.1235	1.1238	1.36E-04	88

$$\text{Ecological COP(ECOP)} \geq 1.6 \quad (4.270)$$

The next section describes the results and discussion of the case study.

### 4.9.3 Results and Discussion

The considered problem of the heat pump working on the reverse Brayton cycle is investigated using 11 different metaheuristic approaches to obtain the maximum coefficient of performance (COP). As all these methods are stochastic in their working, each algorithm is implemented 100 times on the considered problem to estimate the statistical variations of the algorithms. Each algorithm is implemented with the population size of 50, and the termination criteria are set as 100,000 function evaluations. In Table 4.34, the results obtained using each algorithm are presented in the form of the best solution, worst solution, average solution, standard deviation, and success rate over 100 runs. Here, the solutions which are infeasible (i.e., affected by penalty) are eliminated while obtaining the worst solution, average solution, standard deviation, and success rate. Furthermore, the success rate of the algorithm is obtained by considering 0.1% variation from the global optimum value.

It can be observed from the comparative results that all the algorithms performed equally well and produced an identical maximum coefficient of performance (COP) of the heat pump. Moreover, the average performance of all the considered algorithms is less or more similar in obtaining the COP value of the heat pump. Also, the success rate of the SCA algorithm is the highest in obtaining the optimum value followed by CSA and PVS algorithms. The success rate of DE algorithm is the lowest as compared to other algorithms. It can be observed from the results that it is

**Table 4.35** Friedman rank test results for the optimization of heat pump working on reverse Brayton cycle

Algorithms	Friedman value	Normalized value	Rank
GA	39	0.282051	8
PSO	38.5	0.285714	7
DE	47.5	0.231579	9
ABC	20.5	0.536585	4
CSA	11	1	1
TLBO	16	0.6875	2
SOS	38.5	0.285714	7
WWO	27.5	0.4	6
HTS	39	0.282051	8
PVS	17.5	0.628571	3
SCA	25	0.44	5

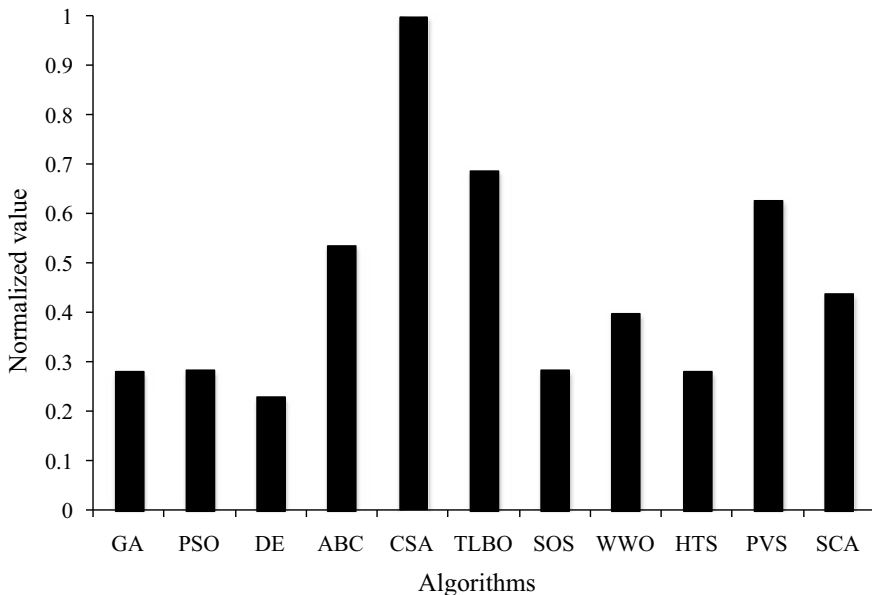


**Fig. 4.27** Graphical presentation of Friedman rank test for the optimization of heat pump working on reverse Brayton cycle

difficult to judge the performance of the algorithm as all the algorithms have produced a different performance to obtain the best, worst, and average results, and success rate. So, the Friedman rank test is implemented to judge the best suitable algorithm for the heat pump working on the reverse Brayton cycle considering the capability to obtain the best, worst, and average solutions, and success rate. The results of the Friedman rank test are presented in Table 4.35, and its graphical representation is given in Fig. 4.27. The results are presented in the form of

**Table 4.36** The optimized operating condition of heat pump working on the Brayton cycle

Operating parameters	Optimized value
<b><i>Operating variable</i></b>	
Hot-side heat exchanger effectiveness, $E_H$	0.9
Cold-side heat exchanger effectiveness, $E_L$	0.9
Temperature ratio, $\tau$	1.372
Compressor pressure ratio, $\pi$	7
<b><i>Constraints</i></b>	
Exergetic efficiency ( $\eta_{ex}$ )	0.3
Ecological function (ECF)	31.27
Ecological COP (ECOP)	1.61
<b><i>Objective function</i></b>	
The coefficient of performance (COP)	1.124

Friedman value, normalized value with ‘1’ as the best performing algorithm and its rank. It can be observed from the results that CSA has obtained the first rank followed by TLBO and PVS algorithms.

The optimized operating parameters of heat pump working on the reversed Brayton cycle obtained using the CSA algorithm is presented in Table 4.36. It can be noted from the results that the heat pump with the maximum hot-side heat exchanger effectiveness ( $E_H$ ), cold-side heat exchanger effectiveness ( $E_L$ ), and compressor pressure ratio ( $\pi$ ) results in the maximum coefficient of performance (COP). The temperature ratio ( $\tau$ ) of the cycle produced a conflicting effect on achieving the maximum COP of the heat pump. Furthermore, the ecological function constraints are above the required value while the exergetic efficiency and ecological COP constraints are at the limiting value in the optimized operating condition of heat pump working on the reverse Brayton cycle.

## 4.10 Absorption Heat Pump

Absorption heat pump is driven by the thermal heat source like natural gas, propane, geothermal heated water, etc. The absorption heat pump is commonly useful in the situation where both heating and cooling are required. Absorption heat pump works based on the principle of absorption and evaporation of refrigerant. Absorption heat pump uses a pair of absorber and refrigerator like ammonia-water pair or lithium bromide–water pair. The schematic arrangement of the absorption heat pump is shown in Fig. 4.28, while its thermodynamic cycle is given in Fig. 4.29. Absorption heat pump works based on two cycles described below.

Absorption medium cycle: At high pressure, the heat is added by the heat source to the generator of the heat pump. So, the refrigerant is evaporated out from the

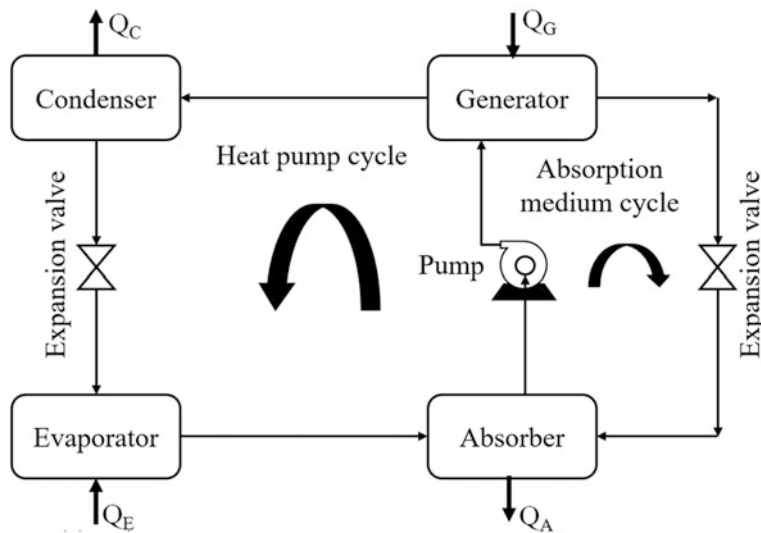
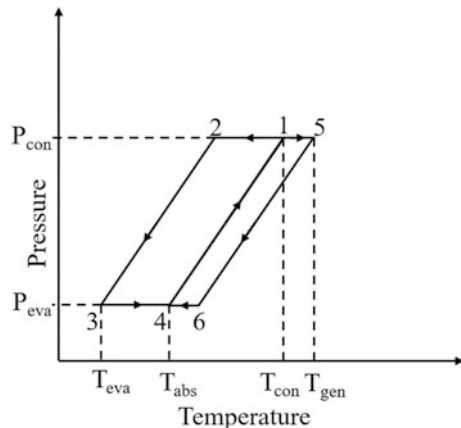


**Fig. 4.28** Schematic of the absorption heat pump

**Fig. 4.29** Thermodynamic cycle of absorption heat pump



absorption medium at where the pressure is high. This absorption medium is passing through the expansion valve. The pressure is reduced due to the expansion process in the expansion valve. After expansion, absorption medium flows toward absorber. This absorption medium absorbed gaseous refrigerant and released useful heat at an intermediate temperature. This mixture then flows back to generator using a pump. This pump increased the pressure of the mixture.

Refrigeration cycle: when the heat source adds its thermal energy to the generator, the refrigerant is evaporated from the absorption medium at high pressure.

This refrigerant is passed through the condenser. The condenser refrigerant released the heat to its environment and converted into the liquid from the gas phase. The liquid refrigerant is passed through an expansion valve to get lower pressure. This low-pressure liquid refrigerant flows toward evaporator, at where the heat is added to the refrigerant, and the refrigerant is getting to be evaporated. This gaseous refrigerant flows toward the absorber to absorb in the absorption medium. Here due to the absorption, useful heat is released.

Earlier, work had been reported by the researchers related to the analysis and optimization of the absorption heat pump. Chen and Andresen (1995) carried out the coefficient of the performance optimization of the absorption heat pump. The authors determined the optimal regions of the coefficient of the performance and specific heating load of the heat pump. Chen (1999) analyzed the absorption heat pump operating between four temperature levels and affected by the irreversibility of finite-rate heat transfer and the internal irreversibilities of the working material. The author optimized the coefficient of performance of the heat pump for a given specific heating load. The author also generated the characteristic curves of the dimensionless specific heating load versus the coefficient of performance for the absorption heat pump. Kodal et al. (2003) carried out the thermo-economic optimization of the irreversible absorption heat pump by using the finite-time thermodynamic. The authors derived the optimal design parameter for the thermo-economic objective function. Furthermore, the effect of the internal irreversibility and economical parameter on the optimal performances of the heat pump was investigated. Chen et al. (2005) established and analyzed a generalized irreversible four heat-reservoir absorption heat pump cycle. The authors derived the optimal relations between the coefficient of performance (COP) and heating-load, maximum COP and corresponding heating-load, maximum heating load and corresponding COP, as well as the optimal temperatures of the working substance and optimal heat-transfer surface areas of the four heat-exchangers are derived by using the finite-time thermodynamics. Moreover, the effect of the cycle parameters on the characteristics of the cycle was studied by numerical examples.

Huang et al. (2008) analyzed the optimal performance of the absorption heat pump operating between four temperature levels. The authors considered the minimization of the total heat transfer area of the heat exchangers as an objective function which was described in terms of the rate of the entropy changes of four heat reservoirs. The authors also investigated the effects of thermal reservoir temperature and the internal irreversibility on the ecological function of the system. Li et al. (2011) presented a new heating method to realize renewable energy recovery by the absorption heat pumps. Ahmadi et al. (2014a, b) carried out the multi-objective optimization of the four-temperature-level absorption refrigeration/heat pump cycle. The authors considered the maximization of the coefficient of performance, ecological function, and thermo-economic criteria as an objective function and adopted a multi-objective evolutionary algorithm as an optimization tool.

Ahmadi et al. (2015a, b) performed the thermo-economic analysis and optimization of irreversible three-heat-source absorption heat pump by adapting

NSGA-II. The authors considered the maximization of the coefficient of performance, ecological coefficient of performance, and minimization of a specific heating load of the heat pump as an objective function. Decision-making techniques were implemented to identify the best possible solution. The authors also performed sensitivity analysis and error analysis of the obtained results. Esfahani et al. (2015) evaluated conventional and advanced exergy and exergoeconomic analyses for a multi-effect evaporation absorption heat pump desalination system. Sahraie et al. (2015) presented a comprehensive thermodynamic modeling and thermo-economic optimization of an irreversible absorption heat pump. The authors considered the maximization of the coefficient of performance, thermo-economic benchmark, and specific heating load as an objective function and adopted NSGA-II as an optimization tool. The authors also applied decision-making techniques to identify the best possible solution.

#### 4.10.1 Thermal Model

In this part of the work, the absorption heat pump is considered for the optimization. The thermodynamic presentation of the absorption heat pump is shown in Fig. 4.29. The thermal model presented here is based on the previous work of Ahmadi et al. (2015a, b).

The following equation gives the first law of thermodynamics for the absorption heat pump:

$$\dot{Q}_G + \dot{Q}_E - \dot{Q}_C - \dot{Q}_A = 0 \quad (4.271)$$

where  $\dot{Q}_G$  is the heat addition in the generator,  $\dot{Q}_E$  is the heat addition in the evaporator,  $\dot{Q}_C$  is the heat rejection in the condenser, and  $\dot{Q}_A$  is the heat rejection in the absorber.

The total amount of heat rejected ( $Q_o$ ) by absorption heat pump is included and the heat rejected in the absorber and heat rejected in the condenser are given by

$$Q_o = \dot{Q}_C + \dot{Q}_A \quad (4.272)$$

The second law of thermodynamics can be represented by absorption heat pump as follows:

$$\oint \frac{\delta Q}{T} = \frac{\dot{Q}_G}{T_1} + \frac{\dot{Q}_E}{T_2} + \frac{\dot{Q}_o}{T_3} < 0 \quad (4.273)$$

where  $T_1$  and  $T_2$  are the temperature of the working fluid in the generator and evaporator, respectively.  $T_3$  is the average temperature of working fluid considering absorber and condenser.

The following equation gives the irreversibility factor ( $I$ ) of the heat pump.

$$\frac{\dot{Q}_G}{T_1} + \frac{\dot{Q}_E}{T_2} + \frac{\dot{Q}_o}{IT_3} = 0 \quad (4.274)$$

The following equation gives the heat transfer in the condenser:

$$\dot{Q}_C = U_C A_C (T_G - T_1) \quad (4.275)$$

where  $U_C$  is the heat transfer coefficient of condenser,  $A_C$  is the heat transfer area of the condenser, and  $T_G$  is the generator temperature.

The following equation gives the heat transfer in the evaporator:

$$\dot{Q}_E = U_E A_E (T_E - T_2) \quad (4.276)$$

where  $U_E$  is the heat transfer coefficient of evaporator,  $A_E$  is the heat transfer area of the evaporator, and  $T_E$  is the evaporator temperature.

The following equation gives the overall heat transfer rate:

$$\dot{Q}_O = U_O (A_A + A_C) (T_3 - T_O) \quad (4.277)$$

where  $U_O$  is the overall all heat transfer coefficient and  $A_A$  is the heat transfer area of the absorber.  $T_O$  is the temperature of absorber and condenser.

The following equation gives the heat loss due to leakage:

$$\dot{Q}_L = K_L (T_O - T_E) \quad (4.278)$$

where  $K_L$  is heat leak coefficient.

The following equation gives the specific heating load ( $q$ ) of the absorption heat pump:

$$\begin{aligned} q &= \frac{\dot{Q}_O - \dot{Q}_L}{A} \\ &= \left[ \frac{1}{U_O(T_3 - T_O)} + \frac{T_1(IT_3 - T_2)}{U_G(T_G - T_1)(T_1 - T_2)IT_3} + \frac{T_2(IT_3 - T_1)}{U_E(T_E - T_2)(T_2 - T_1)IT_3} \right]^{-1} \\ &\quad - \xi(T_O - T_E) \end{aligned} \quad (4.279)$$

where  $\xi$  is the heat leakage coefficient which is given by

$$\xi = \frac{K_L}{A} \quad (4.280)$$

where  $A$  is the total heat transfer area and is given by

$$A = A_G + A_E + A_0 \quad (4.281)$$

The following equation gives the coefficient of performance of the absorption heat pump.

$$\text{COP} = \frac{Q_O - Q_L}{Q_G} \quad (4.282)$$

By considering all the above-derived value, COP can be represented by the following equation.

$$\begin{aligned} \text{COP} &= \frac{IT_3(T_2 - T_1)}{T_1(T_2 - IT_3)} \\ &\times \left\{ 1 - \xi(T_O - T_E) * \left[ \frac{1}{U_O(T_3 - T_O)} + \frac{T_1(IT_3 - T_2)}{U_G(T_G - T_1)(T_1 - T_2)IT_3} \right. \right. \\ &\left. \left. + \frac{T_2(IT_3 - T_1)}{U_E(T_E - T_2)(T_2 - T_1)IT_3} \right] \right\} \end{aligned} \quad (4.283)$$

The following equation gives the specific entropy generation rate ( $S$ ) for the heat mentioned above pump with heat leak loss:

$$\begin{aligned} S &= \frac{\sigma}{A} \\ &= \left( \frac{1}{T_E} - \frac{1}{T_O} \right) \\ &\times \left\{ \left[ \xi(T_O - T_E) - \left[ 1 + \frac{\varepsilon_r T_1 (IT_3 - T_2)}{IT_3 (T_2 - T_1)} \right] \right] \right. \\ &\left. * \left[ \frac{1}{U_O(T_3 - T_O)} + \frac{T_1 (IT_3 - T_2)}{U_G(T_G - T_1)(T_1 - T_2)IT_3} + \frac{T_2 (IT_3 - T_1)}{U_E(T_E - T_2)(T_2 - T_1)IT_3} \right] \right\} \end{aligned} \quad (4.284)$$

where  $\varepsilon_r$  is the coefficient of performance for reversible three heat source refrigerator and  $\xi$  is the heat leakage coefficient and are given by

$$\xi = \frac{K_I}{A} \quad (4.285)$$

$$\varepsilon_r = \left( 1 - \frac{T_E}{T_G} \right) \left( \frac{T_O}{(T_O - T_E)} \right) \quad (4.286)$$

The following equation gives the ecological coefficient of performance:

$$\text{ECOP} = \frac{q}{T_0 S} \quad (4.287)$$

where  $T_0$  is the ambient temperature.

Based on the above thermal model, the objective function for the present work is defined in the next section.

#### 4.10.2 Case Study, Objective Function Description, and Constraints

The absorption heat pump needs to be designed and optimized to produce the maximum coefficient of performance (COP). The generator temperature ( $T_G$ ) of the heat pump is 393 K. The evaporator temperature is 288 K. The average temperature considering absorber and condenser ( $T_o$ ) is 303 K. The ambient temperature ( $T_{\text{env}}$ ) is 290 K. The overall heat transfer coefficient of generator ( $U_G$ ), evaporator ( $U_E$ ) and combined absorber and condenser ( $U_O$ ) is 500 W/m<sup>2</sup>K. The internal irreversibility parameter ( $I$ ) is 1.025 and the heat leakage coefficient is 1.082 kW/m<sup>2</sup>K. Three design variables such as working fluid temperature through the generator ( $T_1$ ), working fluid temperature through the evaporator ( $T_2$ ), and fluid temperature through condenser and absorber ( $T_3$ ) are considered for the optimization problem. The upper and lower bounds of design variables are presented in Table 4.37.

As mentioned above, the maximization of the coefficient of performance of the absorption heat pump is taken as an objective function in the present study. Furthermore, the operating parameters which result in maximum COP also satisfy the specific heating load ( $q$ ) and ecological coefficient of performance (ECOP) constraints. So, considering all the aspects, the objective function of absorption heat pump is formulated as follows.

$$\left\{ \begin{array}{l} \text{Minimize } f(X) = \text{COP}(X) + \sum_{j=1}^n G_1(g_j(X))^2 \\ X = [x_1, x_2, x_3, \dots, x_D], \quad x_{i,\text{minimum}} \leq x_i \leq x_{i,\text{maximum}}, \quad i = 1, 2, 3, \dots, D \\ g_j(X) \leq 0, \quad j = 1, 2, 3, \dots, n \end{array} \right. \quad (4.288)$$

where  $X$  is the vector of design variables which should be bounded between its minimum and maximum values.  $G_1$  is the penalty parameter, and entire term takes

**Table 4.37** Ranges of design variables for absorption heat pump optimization

Design variable	Lower bound	Upper bound
Working fluid temperature through the generator, $T_1$ (K)	380	398
Working fluid temperature through the evaporator, $T_2$ (K)	270	282
Fluid temperature through condenser and absorber, $T_3$ (K)	320	370

into account the effect of constraints violation. This term comes into the picture when the constraint violation takes place.  $g_j(X)$  indicates the constraints. The following constraints are considered for the absorption heat pump.

$$\text{Specific heat load}(q) \geq 1600 \text{ W/m}^2 \quad (4.289)$$

$$\text{Ecological COP} \geq 17.15 \quad (4.290)$$

The next section describes the results and discussion of the case study.

#### 4.10.3 Results and Discussion

The considered problem of absorption heat pump is investigated using 11 different metaheuristic approaches to obtain the maximum coefficient of performance (COP). As all these methods are stochastic in their working, each algorithm is implemented 100 times on the considered problem to estimate the statistical variations of the algorithms. Each algorithm is implemented with the population size of 50, and the termination criteria are set as 100,000 function evaluations. The results obtained using each algorithm are presented in the form of the best solution, worst solution, average solution, standard deviation, and success rate over 100 runs in Table 4.38. Here, the infeasible solutions (i.e., affected by penalty) are eliminated while obtaining the worst solution, average solution, standard deviation, and success rate. Furthermore, the success rate of the algorithm is obtained by considering 0.1% variation from the global optimum value.

It can be observed from the comparative results that all the algorithms performed equally well and produced an identical maximum coefficient of performance (COP) of the absorption heat pump. Moreover, the average performance of HTS and

**Table 4.38** Comparative results of different algorithms for absorption heat pump optimization

Algorithms	Best	Worst	Average	SD	Success rate (%)
GA	1.94	1.6463	1.8824	1.02E-01	72
PSO	1.94	1.6808	1.8892	9.79E-02	76
DE	1.94	1.6774	1.9135	6.66E-02	81
ABC	1.94	1.6755	1.9179	6.22E-02	82
CSA	1.94	1.6579	1.8969	9.42E-02	79
TLBO	1.94	1.8068	1.9201	4.68E-02	84
SOS	1.94	1.6804	1.8969	8.39E-02	75
WWO	1.94	1.6736	1.8639	1.16E-01	74
HTS	1.94	1.6960	1.9206	5.78E-02	83
PVS	1.94	1.6815	1.9162	5.99E-02	80
SCA	1.94	1.6800	1.9071	6.61E-02	77

**Table 4.39** Friedman rank test results for absorption heat pump optimization

Algorithms	Friedman value	Normalized value	Rank
GA	48.5	0.206186	11
PSO	36.5	0.273973	8
DE	28.5	0.350877	5
ABC	24.5	0.408163	4
CSA	38.5	0.25974	9
TLBO	10.5	0.952381	2
SOS	34.5	0.289855	7
WWO	47.5	0.210526	10
HTS	10	1	1
PVS	20.5	0.487805	3
SCA	30.5	0.327869	6

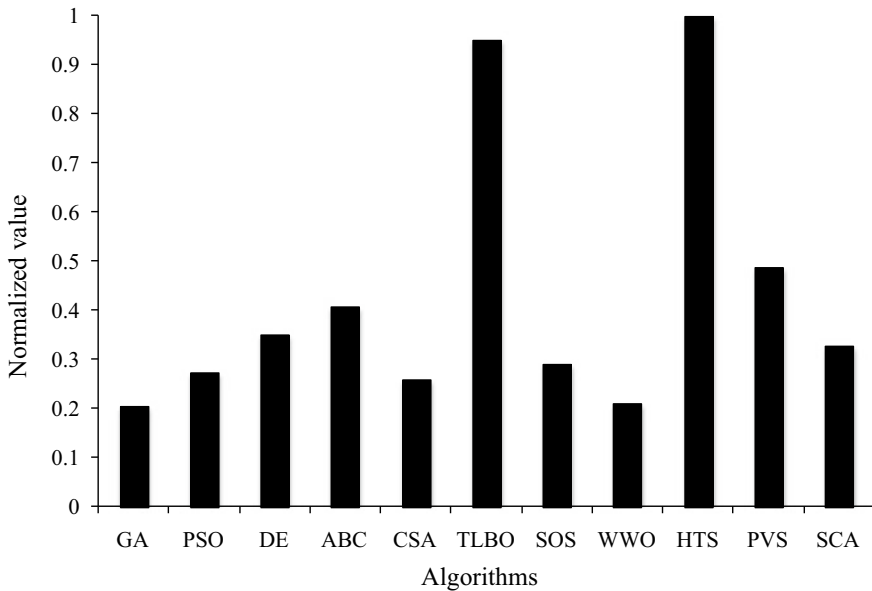


**Fig. 4.30** Graphical presentation of Friedman rank test for absorption heat pump optimization

TLBO algorithms is less or more similar in obtaining the COP value of heat pump. Furthermore, the success rate of TLBO algorithm is the highest in obtaining the optimum value of COP followed by HTS and ABC algorithm. The success rate of GA is the lowest as compared to other algorithms. It can be observed from the results that it is difficult to judge the performance of each algorithm as all the algorithms have produced a different performance to obtain the best, worst, and average results, and success rate. So, the Friedman rank test is implemented to

**Table 4.40** The optimized operating condition of heat pump working on the Brayton cycle

Operating parameters	Optimized value
<b>Operating variable</b>	
Working fluid temperature through the generator, $T_1$ (K)	389.91
Working fluid temperature through the evaporator, $T_2$ (K)	282
Fluid temperature through condenser and absorber, $T_3$ (K)	320
<b>Constraints</b>	
Specific heat load, $q$ (W/m <sup>2</sup> )	1601.4
Ecological COP	17.17
<b>Objective function</b>	
The coefficient of performance (COP)	1.94

judge the best suitable algorithm for the absorption heat pump considering the capability to obtain the best, worst, and average solutions, and success rate. The results of the Friedman rank test are presented in Table 4.39, and its graphical representation is given in Fig. 4.30. The results are presented in the form of Friedman value, normalized value with '1' as the best performing algorithm and its rank. It can be observed from the results that HTS has obtained the first rank followed by TLBO and PVS algorithms.

The optimized operating parameters of the absorption heat pump obtained using the HTS algorithm are presented in Table 4.40. It can be noted from the results that the heat pump with maximum working fluid temperature through the evaporator ( $T_2$ ) and minimum working fluid temperature through condenser and absorber ( $T_3$ ) results in the maximum coefficient of performance (COP). The working fluid temperature through the generator ( $T_1$ ) produced a conflicting effect on achieving the maximum COP of the heat pump. Furthermore, the specific heating load ( $q$ ) constraints are above the required value while ecological COP constraints are at the limiting value in the optimized operating condition of the absorption heat pump.

## References

- Abusoglu A, Kanoglu M. (2008) 'First and second law analysis of diesel engine powered cogeneration systems', *Energy Conversion and Management* in Turkey, vol. 49, 2026–2031.
- Açikkalp E. (2014) 'Entransy analysis of irreversible Carnot-like heat engine and refrigeration cycles and the relationships among various thermodynamic parameters', *Energy Conversion and Management*, vol. 80, pp. 535–542.
- Ahmad S.A. and Sunthiram D. (2018) 'Optimization of diesel engine performance by the Bees Algorithm', *In IOP Conference Series: Materials Science and Engineering*, Vol. 319, No. 1, p. 012064.
- Ahmadi M.H., Ahmadi MA, Mellit A, Pourfayaz F, Feidt M. (2016a) 'Thermodynamic analysis and multi objective optimization of performance of solar dish Stirling engine by the centrality of entransy and entropy generation', *International Journal of Electric Power*, Vol. 78, 88–95.

- Ahmadi M.H., Ahmadi MA, Pourfayaz F, Bidi M, Hosseinzade H, Feidt M. (2016b) ‘Optimization of powered Stirling heat engine with finite speed thermodynamics’, *Energy Conversation and Management*, vol. 108, 96–105.
- Ahmadi M.H., Hosseinzade H, Sayyaadi H, Mohammadi AH, Kimiaghalam F. (2013a). Application of the multi-objective optimization method for designing a powered Stirling heat engine: Design with maximized power, thermal efficiency and minimized pressure loss. *Renewable Energy*, vol. 60, 313–322.
- Ahmadi M.H., Mohammadi AH, Dehghani S, Barranco-Jiménez MA (2013b), ‘Multi-objective thermodynamic-based optimization of output power of solar dish-stirling engine by implementing an evolutionary algorithm’, *Energy Conversation and Management*, vol. 75, 438–445.
- Ahmadi M.H., Sayyaadi H, Dehghani S, Hosseinzade H. (2013c) ‘Designing a solar powered Stirling heat engine based on multiple criteria: Maximized thermal efficiency and power’, *Energy Conversation and Management* vol. 75, 282–291.
- Ahmadi M.H., Sayyaadi H, Mohammadi AH, Barranco-Jimenez MA. (2013d) ‘Thermo-economic multi objective optimization of solar dish-stirling engine by implementing evolutionary algorithm’, *Energy Conversation and Management*, vol. 73, 370–380.
- Ahmadi M.H. and Ahmadi M.A. (2016) ‘Thermodynamic analysis and optimisation of an irreversible radiative-type heat engine by using non-dominated sorting genetic algorithm’. *International Journal of Ambient Energy*, vol. 37(4), pp. 403–408.
- Ahmadi M.H., Ahmadi M.A., Bayat R., Ashouri M. and Feidt M. (2015a) ‘Thermo-economic optimization of Stirling heat pump by using non-dominated sorting genetic algorithm’, *Energy Conversion and Management*, vol. 91, pp. 315–322.
- Ahmadi M.H., Ahmadi M.A., Mehrpooya M. and Sameti M. (2015b) ‘Thermo-ecological analysis and optimization performance of an irreversible three-heat-source absorption heat pump’, *Energy Conversion and Management*, vol. 90, pp. 175–183.
- Ahmadi M.H., Ahmadi M.A., Mehrpooya M., Hosseinzade H. and Feidt M. (2014a) ‘Thermodynamic and thermo-economic analysis and optimization of performance of irreversible four-temperature-level absorption refrigeration’, *Energy Conversion and Management*, vol. 88, pp. 1051–1059.
- Ahmadi M.H., Ahmadi M.A., Mohammadi A.H., Mehrpooya M. and Feidt M. (2014b). ‘Thermodynamic optimization of Stirling heat pump based on multiple criteria’, *Energy Conversion and Management*, vol. 80, pp. 319–328.
- Ahmadi M.H., Ahmadi M.A., Pourfayaz F. and Bidi M. (2016c) ‘Thermodynamic analysis and optimization for an irreversible heat pump working on reversed Brayton cycle’, *Energy Conversion and Management*, vol. 110, pp. 260–267.
- Angelino G. and Invernizzi C. (1995) ‘Prospects for real-gas reversed Brayton cycle heat pumps’, *International Journal of Refrigeration*, vol. 18(4), pp. 272–280.
- Angulo-Brown F. (1991a) ‘An ecological optimization criterion for finite time heat engines’, *Journal of Applied Physics*, vol. 69(11), 7465–7469.
- Angulo-Brown F. (1991b) ‘An ecological optimization criterion for finite-time heat engines’, *Journal of Applied Physics*, vol. 69(11), 7465–7469.
- Araoz JA, Cardozoa E, Salomona M, Alejo L, Fransson TH (2015) ‘Development and validation of a thermodynamic model for the performance analysis of a gamma Stirling engine prototype’, *Applied Thermal Engineering*, vol. 83, 16–30.
- Arora R, Kaushik SC, Kumar R, Arora R. (2016) ‘Multi-objective thermo-economic optimization of solar parabolic dish Stirling heat engine with regenerative losses using NSGA-II and decision making’, *International Journal of Electric Power*, vol. 74, 25–35.
- Babaelahi M, Sayyaadi H. (2015) ‘A new thermal model based on polytropic numerical simulation of Stirling engines’, *Applied Energy*, vol. 141, 143–159.
- Bădescu V. (1992) ‘Optimum operation of a solar converter in combination with a Stirling or Ericsson heat engine’, *Energy*, vol. 17(6), 601–607.
- Bădescu V. (2004) ‘Optimal paths for minimizing lost available work during usual finite-time heat transfer process’, *Journal of Non-equilibrium Thermodynamics*, vol. 29; 53–73.

- Bi Y., Chen L. and Sun F. (2010) 'Exergetic efficiency optimization for an irreversible heat pump working on reversed Brayton cycle', *Pramana*, vol. 74(3), pp. 351–363.
- Blank DA, Davis GW, Wu C. (1994) 'Power optimization of an endoreversible Stirling cycle with regeneration', *Energy*, vol. 19, 125–133.
- Blank D. A. and Wu C. (1996) 'Power limit of an endoreversible Ericsson cycle with regeneration', *Energy Conversion and Management*, vol. 37(1), pp. 59–66.
- Blank D. A. and Wu C. (1998) 'Finite-time power limit for solar-radiant Ericsson engines in space applications', *Applied Thermal Engineering*, vol. 18(12), pp. 1347–1357.
- Bojić M. (1997) 'Cogeneration of power and heat by using endoreversible Carnot engine', *Energy Conversion and Management*, vol. 38(18), pp. 1877–1880.
- C.Y. Cheng, C.K. Chen (1997) 'The ecological optimization of an irreversible Carnot heat engine', *Journal of Physics D: Applied Physics*, vol. 30, 1602–1609.
- CA. Ordóñez (2000) 'Liquid nitrogen fueled, closed Brayton cycle cryogenic heat engine', *Energy Conversion and Management*, vol. 41, 331–341.
- Campos MC, Vargas JVC, Ordóñez JC. (2012) 'Thermodynamic optimization of a Stirling engine', *Energy*, vol. 44(1), 902–910.
- Chen J. and Andresen B. (1995) 'Optimal analysis of primary performance parameters for an endoreversible absorption heat pump', *Heat Recovery Systems and CHP*, vol. 15(8), pp. 723–731.
- Chen J. (1994) 'The maximum power output and maximum efficiency of an irreversible Carnot heat engine', *Journal of Physics D: Applied Physics*, vol. 27(6), p. 1144.
- Chen Jincan, (1999) The general performance characteristics of an irreversible absorption heat pump operating between four temperature levels. *Journal of Physics D: Applied Physics*, 32 (12):1428–1433.
- Chen J., Wu C. and Kiang R.L. (1996) 'Maximum specific power output of an irreversibleradiant heat engine', *Energy Conversion and Management*, vol. 37(1), pp. 17–22.
- Chen L., Ni N., Wu C. and Sun F. (1999) 'Performance analysis of a closed regenerated Brayton heat pump with internal irreversibilities' *International Journal of Energy Research*, vol. 23 (12), pp. 1039–1050.
- Chen L., Qin X., Sun F. and Wu C. (2005) 'Irreversible absorption heat-pump and its optimal performance', *Applied Energy*, vol. 81(1), pp. 55–71.
- Chen L., Song H. and Sun F. (2010) 'Endoreversible radiative heat engine configuration for maximum efficiency', *Applied Mathematical Modelling*, vol. 34(7), pp. 1710–1720.
- Chen L., Sun F. and Wu C. (1997) 'Influence of heat transfer law on the performance of a Carnot engine', *Applied Thermal Engineering*, vol. 17(3), pp. 277–282.
- Chen L., Sun F. and Wu C. (2007) 'Power optimization of a regenerated closed variable temperature heat reservoir Brayton cycle', *International Journal of Sustainable Energy*, vol. 26 (1), pp. 1–17.
- Chen L., Xia S. and Sun F. (2013) 'Maximum power output of multistage irreversible heat engines under a generalized heat transfer law by using dynamic programming', *Scientia Iranica*, vol. 20(2), pp. 301–312.
- Chen L., Zhang W. and Sun F. (2007) 'Power, efficiency, entropy-generation rate and ecological optimization for a class of generalized irreversible universal heat-engine cycles', *Applied Energy*, vol. 84(5), pp. 512–525.
- Chen L., Zhou J., Sun F. and Wu C. (2004) 'Ecological optimization for generalized irreversible Carnot engines. *Applied Energy*, 77(3), pp. 327–338.
- Chen L., Zhu X., Sun F. and Wu C. (2006) 'Exergy-based ecological optimization of linear phenomenological heat-transfer law irreversible Carnot-engines', *Applied Energy*, vol. 83(6), pp. 573–582.
- Chen L.G., Zheng J.L., Sun F.R. and Wu, C. (2001) 'Power density analysis and optimization of a regenerated closed variable-temperature heat reservoir Brayton cycle', *Journal of Physics D: Applied Physics*, vol. 34(11), p. 1727.
- Chenab J, Schouten JA (1999) 'The comprehensive influence of several major irreversibilities on the performance of an Ericsson heat engine', *Applied Thermal Engineering*, vol. 19(5), 555–564.

- Cheng CH, Yu YJ. (2010) 'Numerical model for predicting thermodynamic cycle and thermal efficiency of a beta-type Stirling engine with rhombic-drive mechanism', *Renewable Energy*, vol. 35(11), 590–601.
- Cheng CY, Chen CK. (1999) 'Ecological optimization of an irreversible Brayton heat engine', *Journal of Physics D: Applied Physics*, vol. 32, 350–357.
- Chin Wu (1991) 'Power optimization of an endoreversible brayton gas heat engine', *Energy Conversion and Management*, vol. 31, No. 6, pp. 561–565.
- Duan C, Wang X, Shu S, Jing C, Chang H. (2014) 'Thermodynamic design of Stirling engine using multi-objective particle swarm optimization algorithm', *Energy Conversion and Management*, vol. 84, 88–96.
- Erbay LB, Yavuz H. (1999) 'Analysis of an irreversible Ericsson engine with a realistic regenerator', *Applied Energy*, vol. 62, 155–167.
- Esfahani I.J., Lee S. and Yoo C. (2015) 'Evaluation and optimization of a multi-effect evaporation–absorption heat pump desalination based conventional and advanced exergy and exergoeconomic analyses', *Desalination*, vol. 359, pp. 92–107.
- Ferreira AC, Nunes ML, Teixeira JCF, Martins LASB, Teixeira SFCC (2016) 'Thermody and economic optimization of a solar-powered Stirling engine for micro-cogeneration purposes', *Energy*, vol. 111, 1–17.
- Göktun S. and Özkaraynak S. (1997) 'Optimum performance of a corrugated, collector-driven, irreversible Carnot heat engine and absorption refrigerator', *Energy*, vol. 22(5), pp. 481–485.
- Göktun S., Özkaraynak S. and Yavuz H. (1993) 'Design parameters of a radiative heat engine', *Energy*, vol. 18 (6), pp. 651–655.
- H. Sayyaadi, M.H. Ahmadi, S. Dehghani, (2015) 'Optimal Design of a Solar-Driven Heat Engine Based on Thermal and Ecological Criteria', *Journal of Energy Engineering*, vol. 141(3), 1–7.
- H. Song, L. Chen, F. Sun (2007a) 'Endoreversible heat engines for maximum power output with fixed duration and radiative heat-transfer law', *Applied Energy*, vol. 84(4), 374–388.
- H. Song, L. Chen, J. Li, F. Sun, C. Wu (2006) 'Optimal configuration of a class of endoreversible heat engines with linear phenomenological heat transfer law', *Journal of Applied Physics*, vol. 100(12), 124907.
- Han Y., Wang D., Zhang C. and Zhu Y. (2017) 'The entransy degeneration and entransy lossequations for the generalized irreversible Carnot engine system', *International Journal of Heat and Mass Transfer*, vol. 106, pp. 895–907.
- Holman JP. (1980) *Thermodynamics*, McGraw-Hill, New York.
- Hooshang M, Moghadam RA, Nia SA, Masouleh MT (2015) 'Optimization of Stirling engine design parameters using neural networks', *Renewable Energy*, vol. 74, 855–866.
- Hosseinzade H, Sayyaadi H, Babaelahi M. (2015) 'A new closed-form analytical thermal model for simulating Stirling engines based on polytropic-finite speed thermodynamics', *Energy Conversion and Management*, vol. 90, 395–408.
- Huang Y., Sun D. and Kang Y. (2008) 'Performance optimization for an irreversible four temperature-level absorption heat pump', *International Journal of Thermal Sciences*, vol. 47 (4), pp. 479–485.
- Ibrahim O.M. and Klein S.A. (1995) 'High-power multi-stage Rankine cycles', *Journal of Energy Resources Technology*, vol. 117(3), pp. 192–196.
- Jafari M, Parhizkar MJ, Amani E, Naderan H. (2016) 'Inclusion of entropy generation minimization in multi-objective CFD optimization of diesel engines', *Energy*, vol. 114, 526–541.
- Kaushik SC, Kumar S. (2000) 'Finite time thermodynamic evaluation of irreversible Ericsson and Stirling heat pump cycles', In: *Proceedings of 4th Minsk International Seminar on Heat Pipes, Heat Pumps Refrigerators*, Minsk, Belarus, p. 113–26.
- Kaushik SC, Tyagi SK, Bose SK, Singhal MK. (2001) 'Performance evaluation of irreversible Stirling and Ericsson heat pump cycle', *International Journal of Thermal Science*, vol. 41, 193–200.
- Kaushik S. C. and Kumar S. (2001) 'Finite time thermodynamic evaluation of irreversible Ericsson and Stirling heat engines', *Energy Conversion and Management*, vol. 42(3), pp. 295–312.

- Khaliq A. (2004) 'Finite-time heat-transfer analysis and generalized power-optimization of an endoreversible Rankine heat-engine', *Applied Energy*, vol. 79(1), pp. 27–40.
- Kodal A., Sahin B. and Yilmaz T. (2000) 'A comparative performance analysis of irreversible Carnot heat engines under maximum power density and maximum power conditions', *Energy Conversion and Management*, 41(3), pp. 235–248.
- Kodal A., Sahin B., Ekmekci I. and Yilmaz T. (2003) 'Thermoeconomic optimization for irreversible absorption refrigerators and heat pumps', *Energy Conversion and Management*, vol. 44(1), pp. 109–123.
- Kongtragool B., Wongwises S. (2003) 'A review of solar-powered Stirling engines and low temperature differential Stirling engines', *Renewable and Sustainable Energy Reviews*, vol. 7, 131–154.
- Kongtragool B., Wongwises S. (2007) 'Performance of a twin power piston low temperature differential Stirling engine powered by a solar simulator', *Solar Energy*, vol. 81, 884–895.
- Kumar R., Kaushik SC., Kumar R. (2015) 'Performance analysis of brayton heat engine at maximum efficient power using temperature dependent specific heat of working fluid', *Journal of Thermal Engineering*, Vol. 1, No. 2, pp. 345–354.
- Lee W.Y. and Kim S.S. (1992) 'Finite time optimization of a Rankine heat engine', *Energy Conversion and Management*, vol. 33(1), 59–67.
- Leung D.Y., Luo Y. and Chan T.L. (2006) 'Optimization of exhaust emissions of a diesel engine fuelled with biodiesel', *Energy & Fuels*, vol. 20(3), pp. 1015–1023.
- Li R., Grosu L., Queiros-Conde D. (2016) 'Multi-objective optimization of Stirling engine using Finite Physical Dimensions Thermodynamics (FPDT) method', *Energy Conversion and Management*, vol. 124, 517–527.
- Li Y., Fu L., Zhang S. and Zhao X. (2011) 'A new type of district heating system based on distributed absorption heat pumps', *Energy*, vol. 36(7), pp. 4570–4576.
- Lin B., Chen J. (2003) 'Optimization on the performance of a harmonic quantum Brayton heat engine', *Journal of Applied Physics*, vol. 94, 6185.
- Luo Z., Sultan U., Ni M., Peng H., Shi B., Xiao G. (2016) 'Multi-objective optimization for GPU3 Stirling engine by combining multi-objective algorithms', *Renewable Energy*, vol. 94, 114–125.
- Lurie E. and Kribus A. (2010) 'Analysis of a microscale ‘saturation phase-change internal carnot engine’, *Energy Conversion and Management*, vol. 51(6), pp. 1202–1209.
- Maheshwari G., A. I. Khandwawala and S. C. Kaushik (2005a) 'A Comparative Performance Analysis of an Endoreversible Heat Engine with Thermal Reservoir of Finite Heat Capacitance Under Maximum Power Density and Maximum Power Conditions' *International Journal of Ambient Energy*, vol. 26, 147–154.
- Maheshwari G., A. I. Khandwawala, and S. C. Kaushik (2005b) 'Maximum Power Density Analysis for an Irreversible Radiative Heat Engine', *International Journal of Ambient Energy*, vol. 26, 71–80.
- Maheshwari G., Chaudhary S. and Somani S.K. (2009) 'Performance analysis of a generalized radiative heat engine based on new maximum efficient power approach' *International Journal of Low-Carbon Technologies*, vol. 4(1), pp. 9–15.
- Maheshwari G., Chaudhary S. and Somani S. K. (2007) Optimum criteria on the performance of a generalised irreversible Carnot heat engine based on a thermoeconomic approach, *International Journal of Ambient Energy* 28(4):197–204.
- Maheshwari G., Khandwawala A.I. and Kaushik S.C. (2005c) 'Maximum power density analyses for an irreversible radiative heat engine', *International Journal of Ambient Energy*, vol. 26(2), pp. 71–80.
- Mohammad H. Ahmadi, Mohammad Ali Ahmadi, Mehdi Mehrpooya, Seyed Mohsen Pourkiaei and Maryam Khalili (2016) 'Thermodynamic analysis and evolutionary algorithm based on multi-objective optimisation of the Rankine cycle heat engine', *International Journal of Ambient Energy*, vol. 37(4), 363–371.
- Ni N., Chen L., Wu C. and Sun F. (1999) 'Performance analysis for endoreversible closed regenerated Brayton heat pump cycles', *Energy Conversion and Management*, vol. 40(4), pp. 393–406.

- Özkaynak S., Gokun S. and Yavuz H. (1994) 'Finite-time thermodynamic analysis of a radiative heat engine with internal irreversibility', *Journal of Physics D: Applied Physics*, vol. 27(6), p. 1139.
- Park H. and Kim M.S. (2014) 'Thermodynamic performance analysis of sequential Carnot cycles using heat sources with finite heat capacity', *Energy*, vol. 68, pp. 592–598.
- Patel VK, Savsani VJ, Mudgal A. (2017) 'Many objective thermodynamic optimization of Stirling heat engine', *Energy*, vol. 125, 629–642.
- Patel VK, Savsani VJ (2016) 'Multi-objective optimization of a Stirling heat engine using TS-TLBO (tutorial training and self-learning inspired teaching-learning based optimization) algorithm', *Energy*, vol. 95, 528–541.
- Petrescu S, Harman C, Costea M, Popescu G, Petre C, Florea T. (2002) 'Analysis and optimization of solar/dish Stirling engines', In: *Proceedings of the 31st American Solar Energy Society Annual Conference*, 15–20, USA.
- Pohit G. and Misra D. (2013) 'Optimization of performance and emission characteristics of diesel engine with biodiesel using grey-taguchi method', *Journal of Engineering*,
- Punnathanam V, Kotecha P. (2016) 'Effective multi-objective optimization of Stirling engine systems', *Applied Thermal Engineering*, vol. 108, 261–276.
- Punov P., Milkov N., Danel Q., Perilhon C., Podevin P. and Evtimov T. (2017), 'Optimization of automotive Rankine cycle waste heat recovery under various engine operating condition', In *AIP Conference Proceedings*, Vol. 1814, No. 1, p. 020074, AIP Publishing.
- Qin X., Chen L., Sun F. and Wu C. (2005) 'Frequency-dependent performance of an endoreversible Carnot engine with a linear phenomenological heat-transfer law', *Applied Energy*, vol. 81(4), pp. 365–375.
- Raman R, Maheshwari G. (2017) 'Performance analysis of a generalised radiative heat engine based on new maximum efficient power density approach', *International Journal of Ambient Energy*, vol. 38(8), 819–825.
- Ringler J., Seifert M., Guyotot V. and Hübner W. (2009) 'Rankine cycle for waste heat recovery of IC engines', *SAE International Journal of Engines*, vol. 2(2009-01-0174), pp. 67–76.
- S. C. Kaushik, S. K. Tyagi (2002) 'Finite time thermodynamic analysis of an irreversible regenerative closed cycle brayton heat engine', *International Journal of Solar Energy*, Vol. 22 (34), pp. 141–151, India.
- Sahin B, Kodal A, Kaya SS. (1998) 'A comparative performance analysis of irreversible regenerative reheating Joule–Brayton engines under maximum power density and maximum power conditions', *Journal of Physics D: Applied Physics*, vol. 31, 2125–2131.
- Sahin B, Kodal A, Yavuz H. (1995) 'Efficiency of a Joule–Brayton engine at maximum power density', *Journal of Physics D: Applied Physics*, vol. 28, 1309–1313, UK.
- Sahin B, Kodal A, Yilmaz T, Yavuz H. (1996a), 'Maximum power density analysis of an irreversible Joule–Brayton engine', *Journal of Physics D: Applied Physics*, vol. 29, 1162–1167, UK.
- Şahin B., Kodal A. and Yavuz H. (1996b) 'Maximum power density for an endoreversible Carnot heat engine', *Energy*, vol. 21(12), pp. 1219–1225.
- Sahraie H., Mirani M.R., Ahmadi M.H. and Ashouri M. (2015) 'Thermo-economic and thermodynamic analysis and optimization of a two-stage irreversible heat pump', *Energy Conversion and Management*, vol. 99, pp. 81–91.
- Salas N.S., Velasco S. and Hernández A.C. (2002) 'Unified working regime of irreversible Carnot-like heat engines with nonlinear heat transfer laws', *Energy Conversion and Management*, vol. 43(17), pp. 2341–2348.
- Senft JR. (1993) *Ringbom Stirling Engines*, Oxford University Press, New York.
- Sogut OS, Ust Y, Sahin B. (2006) 'The effects of intercooling and regeneration on the thermo ecological performance analysis of an irreversible-closed Brayton heat engine with variable-temperature thermal reservoirs', *Journal of Physics D: Applied Physics*, vol. 39, 4713–4721.
- Sogut O. S., and Durmazay A. (2006) 'Ecological performance optimization of a solar-driven heat engine', *Energy Institute*, vol. 79(4), 246–250.

- Song H., Chen L. and Sun F. (2007a) 'Endoreversible heat-engines for maximum power-output with fixed duration and radiative heat-transfer law', *Applied Energy*, 84(4), pp. 374–388.
- T Yilmaz (2007) 'Performance optimization of a Joule–Brayton engine based on the efficient power criterion Article in Proceedings of the Institution of Mechanical Engineers Part A', *Journal of Power and Energy*, vol. 221(5), 603–607.
- T.B. Chang (2007) 'Exergetic Efficiency Optimization for an Irreversible Carnot Heat Engine', *Journal of Mechanics*, vol. 23(2), 181–186.
- Toghyani S, Kasaeian A, Ahmadi MH. (2014a) 'Multi-objective optimization of Stirling engine using non-ideal adiabatic method', *Energy Conversion and Management*; vol. 80, 54–62.
- Toghyani S, Kasaeian A, Hashemabadi SH, Salimi M. (2014b) 'Multi-objective optimization of GPU3 Stirling engine using third order analysis', *Energy Conversion and Management*, vol. 87, 521–529.
- Tyagi SK, Kuashik SC, Salhotra R. (2002a) 'Ecological optimization of irreversible Stirling and Ericsson heat pump cycles', *Journal of Physics D: Applied Physics*, vol. 35, 2058–65.
- Tyagi S. K., Kaushik S. C. and Salhotra R. (2002b) 'Ecological optimization and performance study of irreversible Stirling and Ericsson heat engines', *Journal of Physics D: Applied Physics*, 35(20), pp. 2668–2675.
- Tyagi S.K., Chen J. and Kaushik S.C. (2004) 'Thermoeconomic optimization and parametric study of an irreversible Stirling heat pump cycle', *International Journal of Thermal Sciences*, 43(1), pp. 105–112.
- Ust Y., Sahin B, Kodal A. (2006) 'Performance analysis of an irreversible Brayton heat engine based on ecological coefficient of performance criterion', *International Journal of Thermal Sciences*, vol. 45, 94–101.
- Üst Y., Sahin B. and Kodal A. (2005) 'Ecological coefficient of performance (ECOP) optimization for generalized irreversible Carnot heat engines', *Journal of the Energy Institute*, vol. 78(3), pp. 145–151.
- Ust Y., Sahin B., Kodal A., Akcay I. H. (2006) 'Ecological coefficient of performance analysis and optimization of an irreversible regenerative-Brayton heat engine', *Applied Energy*, vol. 83(6), 558–572.
- Wahono B., Ogai H., Ogawa M., Kusaka J. and Suzuki Y. (2012) 'December. Diesel engine optimization control methods for reduction of exhaust emission and fuel consumption', In *System Integration (SII), 2012 IEEE/SICE International Symposium*, pp. 722–727.
- Walker G. (1980) *Stirling engines*, Clarendon Press, Oxford.
- White A.J., (2009) 'Thermodynamic analysis of the reverse Joule–Brayton cycle heat pump for domestic heating', *Applied Energy*, vol. 86(11), pp. 2443–2450.
- Wickman D.D., Senecal P.K. and Reitz R.D. (2001) 'Diesel engine combustion chamber geometry optimization using genetic algorithms and multi-dimensional spray and combustion modeling' (No. 2001-01-0547).
- Wu C. (1988) 'Power optimization of a finite-time Carnot heat engine', *Energy*, vol. 13(9), pp. 681–687.
- Wu C., Chen L. and Sun F. (1998) 'Optimization of steady flow heat pumps', *Energy Conversion and Management*, vol. 39(5–6), pp. 445–453.
- Wu F., Chen L., Sun F., Wu C. and Zhu Y. (1998) 'Performance and optimization criteria for forward and reverse quantum Stirling cycles', *Energy Conversion and Management*, vol. 39 (8), pp. 733–739.
- Wu Z., Fu L., Gao Y., Yu X., Deng J. and Li L. (2016) 'Thermal efficiency boundary analysis of an internal combustion Rankine cycle engine', *Energy*, vol. 94, pp. 38–49.
- Xingcai L, Zhen H, Wugao Z, Degang L. (2010) 'The influence of ethanol additives on the performance and combustion characteristics of diesel engines', *Combustion Science and Technology*, Volume-176, Issue-8, 1309–1329.
- Xu L. (2016) 'Thermodynamic Analysis of Stirling Heat Pump based on Thermo-economic Optimization Criteria', In *MATEC Web of Conferences* (Vol. 61).
- YC huang, CI Hung, Chen CK, (2000) 'An ecological exergy analysis for an irreversible Brayton engine with an external heat source', *Journal of Power and Energy*, vol. 214, 413.

- Zare SH, Tavakolpour-Saleh AR (2016) ‘Frequency-based design of a free piston Stirling engine using genetic algorithm’, *Energy*, vol. 109, 466–480.
- Zhan Y.B., Ma P.C. and Zhu X.Q. (2011) ‘Ecological optimization for a generalized irreversible Carnot engine with a universal heat transfer law’, *Procedia Environmental Sciences*, vol. 11, pp. 945–952.
- Zhang Y, Lin B, Chen J. (2007) ‘Optimum performance characteristics of an irreversible solar driven Brayton heat engine at the maximum overall efficiency’, *Renewable Energy*, vol. 32, 856–867.
- Zhang Y, Qu C, Lin B, Chen J. (2006) ‘The Regenerative Criteria of an Irreversible Brayton Heat Engine and its General Optimum Performance Characteristics’, *Journal of Energy Resources Technology*, vol. 128(3), 216–222.
- Zhang L., Chen L. and Sun F. (2016) ‘Power optimization of chemically driven heat engine based on first and second order reaction kinetic theory and probability theory’, *Physica A: Statistical Mechanics and its Applications*, vol. 445, pp. 221–230.
- Zhao Y, Chen J. (2007) ‘Optimum performance analysis of an irreversible Diesel heat engine affected by variable heat capacities of working fluid’, *Energy Conversion and Management*, vol. 48, 2595–2603.
- Zhao Y, Lin B, Zhang Y, Chen J. (2006) ‘Performance analysis and parametric optimum design of an irreversible Diesel heat engine’, *Energy Conversion and Management*, vol. 47, 3383–3392.
- Zheng S, Lin G. (2010) ‘Optimization of power and efficiency for an irreversible Diesel heat

# Chapter 5

## Thermal Design and Optimization of Refrigeration Systems

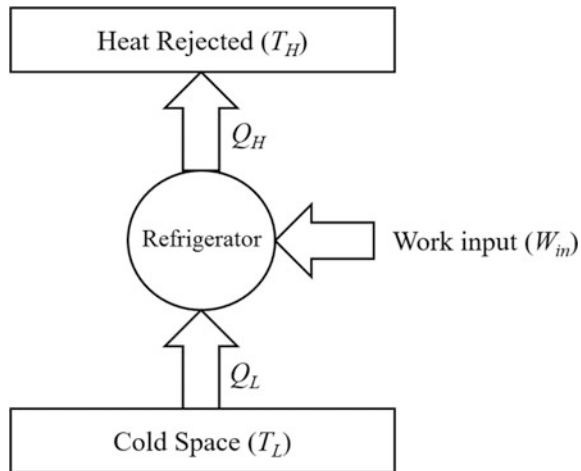


**Abstract** Refrigeration systems are used to lower temperatures by extracting heat. As heat is transmitted from lower temperatures to a higher temperature, work input is required to run the refrigeration system. In this chapter, the thermal modeling of different types of refrigerating systems including the Carnot refrigerator, the vapor absorption refrigerator, the thermo-electric refrigerator, the Stirling cryogenic refrigerator, and the Ericsson cryogenic refrigerator is presented. The objective function for each of the refrigerating systems is derived from the thermal model. The optimization of a derived objective is performed by implementing 11 different metaheuristic algorithms for each refrigerating system. Afterward, comparative results are tabulated and discussed.

Refrigeration is defined as the process of removing heat from a body or enclosed space so that its temperature is first lowered and then maintained at a level below the temperature of its surroundings. In such a case, the body or enclosed space is said to be a refrigerated system. The equipment used to maintain the required temperature is called refrigerating equipment. The working substance used to produce refrigeration is called a refrigerant. The refrigerating system operates on a thermodynamic cycle and transfers a certain amount of heat from bodies at a lower temperature to bodies at a higher temperature by consuming a certain amount of external work. Domestic refrigerators and room air conditioners are prime examples. In a refrigerator, the required output is the heat extracted from the low-temperature body. The basic working principle of the refrigerating system is shown in Fig. 5.1. Refrigerating systems are used for the storage and the transportation of food products including dairy products, fruits, vegetables, meat, and fish, the preservation of medicines and serums, the manufacturing of ice, for photographic films, for rubber products, and for textiles. They are also used for cooling liquids in chemical plants, for the comfortable air conditioning of auditoriums, hospitals, residence, offices, factories, hotels, computer rooms, etc. for the liquefaction of gases like N<sub>2</sub>, O<sub>2</sub>, H<sub>2</sub>, etc. and for cooling water and beverages.

It can be observed from the figure that the refrigerator operates on a range between low temperatures and as high as atmospheric temperatures. The performance

**Fig. 5.1** Working principle of a refrigerating system



parameter of any refrigerating system is known as the coefficient of performance (COP), which is defined as the amount of heat absorbed from the low-temperature body ( $Q_L$ ) to the work required ( $W_{in}$ ) to extract that heat.

## 5.1 Carnot Refrigerator

The Carnot refrigerator operates on the reversible Carnot cycle. The Carnot refrigerator consists of four main devices: the compressor, the expander, and two heat exchangers. The schematic arrangement of the Carnot refrigerator is shown in Fig. 5.2. It can be observed from the figure that one end of the compressor is connected with a high-temperature heat exchanger while another end is connected with a low-temperature heat exchanger. Similarly, one end of the expander is connected with the high-temperature heat exchanger while the other is also connected with the low-temperature heat exchanger.

A Thermodynamics cycle occurs when the system passes through the series of different states and finally returns to its original state. The thermodynamic representation ( $P-V$  and  $T-S$ ) of the Carnot refrigerator is shown in Fig. 5.3. It can be observed from the figure that the thermodynamic cycle of Carnot refrigerator consists of two isothermal and two isentropic processes, which are all reversible. Above, process 1–2 is the isentropic compression process. During process 1–2, the refrigerant (i.e., working fluid of the refrigerator) is compressed isentropically. The compressor is perfectly insulated so that there is no heat lost or absorbed. The refrigerant is compressed till the temperature rises from  $T_E$  to  $T_C$ . Process 2–3 is the isothermal compression. During process 2–3, the refrigerant is compressed isothermally at temperature  $T_C$ . Here, heat rejection from the refrigerant takes place. Process 3–4 is the isentropic expansion. During process 3–4, the expansion of the

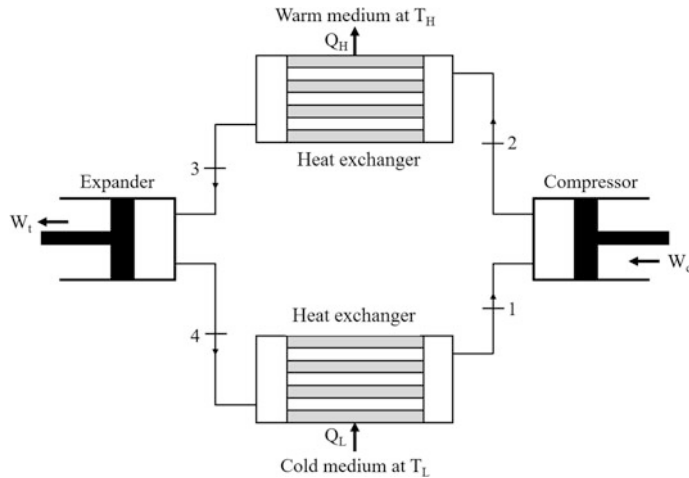


**Fig. 5.2** Schematic arrangement of the Carnot refrigerator

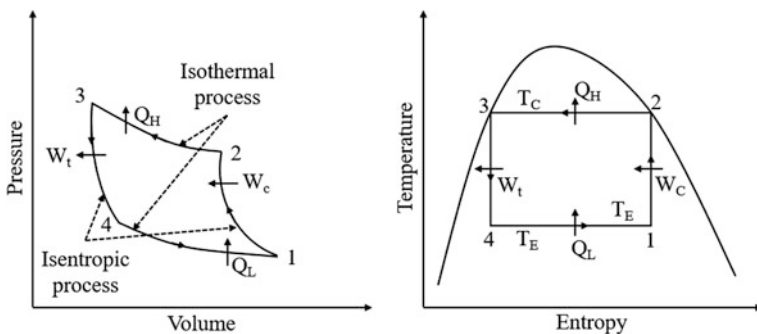


**Fig. 5.3** Thermodynamic cycle of Carnot refrigerator

refrigerant takes place isentropically. The expander is perfectly insulated so that there is no heat lost or absorbed. The refrigerant expands till the temperature reduces from  $T_C$  to  $T_E$ . Finally, process 4–1, which is the isothermal expansion, occurs. During process 4–1, the refrigerant expands isothermally at temperature  $T_E$ . In this process, heat from the space is required to be maintained at lower temperature is absorbed by the refrigerant. Then and cycle repeats.

Earlier, researchers have carried out works related to the analysis and optimization of the Carnot refrigerator. For example, Yan and Chen (1996) studied the optimal performances related to the exergy of a Carnot refrigerator under the influence of thermal resistance by using finite-time thermodynamic theory. The authors had also derived the optimal relations between the rate of exergy output and the coefficient of performance. In addition, the rate of exergy output and the rate of

refrigeration are derived. Velasco et al. (1997) analyzed an endoreversible Carnot refrigerator that operates under conditions of maximum per-unit-time COP and reported the results of time-dependent COP and associate heat conductance. Sahin and Kodal (1999) carried out the finite-time thermo-economic optimization for an endoreversible refrigerator. The authors considered the maximization of the cooling load per unit total cost of the refrigerator as an objective function for the optimization. In addition, the optimum performance parameters which maximized the objective functions were also investigated. Yan and Lin (2000) investigated the ecological optimization performance and derived the optimal cooling rate, the coefficient of performance, and the entropy production rate for the refrigerators. Chen et al. (2001a, b) carried out the exergoeconomic optimization of an endoreversible Carnot refrigerator. In the work, the authors derived a relation between the economic parameter and associated thermodynamic parameter for the Carnot refrigerator.

Chen et al. (2004) presented the ecological optimization of a generalized Carnot refrigerator by considering heat loss, heat leakage, and other irreversibility. Chen et al. (2005) present a generalized irreversible Carnot refrigerator model by taking into account several internal irreversibilities of the refrigerator, such as heat leakage, friction, turbulence, and other undesirable factors. The authors derived a relation between optimal cooling load and the coefficient of performance (COP) based on a generalized heat transfer law. The effect of heat leakage, internal irreversibility, and heat transfer law on the optimal performance of the generalized irreversible Carnot refrigerator was also investigated. Zhu et al. (2006) carried out the exergy-based ecological optimization of a generalized irreversible Carnot refrigerator. In the work, numerical examples were also given to demonstrate the effects of heat transfer law, heat leakage, and internal irreversibility on the optimal performance of the generalized irreversible refrigerator. In another work, Ust and Sahin (2007) carried out a performance analysis and optimization based on a new thermo-ecological optimization for the Carnot refrigerator. The maximum of the ecological performance criterion and the corresponding optimal conditions had been derived analytically. They had also investigated the optimum performance parameters which would maximize both the objective function and the effects of the irreversibility parameters on the general and optimal performances. Li et al. (2008) derived the fundamental optimal relation between the cooling load and the coefficient of performance of a generalized irreversible Carnot refrigerator based on a new generalized heat transfer law, including a generalized convective heat transfer law and generalized radiative heat transfer law. In addition, the effects of heat transfer laws and various loss terms on the performance of the generalized irreversible Carnot refrigerator were also analyzed.

In another work, Chen et al. (2012) analyzed the optimal exergy-based ecological performance of a generalized irreversible Carnot refrigerator. They took into account the losses of heat resistance, heat leakage, and internal irreversibility by taking an ecological optimization criterion as the objective. In 2012, de Tomás et al. proposed a unified optimization criterion for Carnot refrigerators. This criterion

consisted of multiplying the maximized product of the heat absorbed by the working system with the efficiency per unit time of the refrigerator. Ahmadi et al. (2015a, b) performed the thermodynamic analysis and optimization of an irreversible Carnot refrigerator by adapting the multi-objective evolutionary algorithm (MOEA) joined with the NSGA-II approach. The authors defined two different scenarios for the optimization of the Carnot refrigerator. In the first scenario, the maximization of the cooling load, the ecological coefficient of performance, and the exergy input to the system were all considered simultaneously. In the second scenario, the maximization of the ecological coefficient of performance, the exergy input to the system, and the exergetic performance criteria of the Carnot refrigerator were considered simultaneously. In addition, decision-making methods including LINAMP, TOPSIS, and FUZZY were employed to ascertain final solutions. Finally, Su et al. (2017) developed the thermodynamic model of an irreversible Carnot refrigerator with heat recovery (CRHR) that worked between two high-temperature reservoirs and one low-temperature heat reservoir. The authors optimized the developed thermal models for the allocation of the heat transfer area and the theoretical value for the optimal allocation of the heat transfer areas for the CRHR.

### 5.1.1 Thermal Model

In the present work, a refrigerator working on the Carnot cycle is considered for optimization. The thermodynamic presentation of the Carnot heat engine is shown in Fig. 5.3, and the heat transfer model of the Carnot refrigerator is shown in Fig. 5.4. The thermal model presented here is based on the previous works of Ahmadi et al. (2015a, b). Note that subscripts H and L stand for high-temperature and low-temperature reservoirs, respectively.

The amount of heat transfer taking place at higher temperature of the cycle ( $Q_H$ ) is given by the following equations:

$$Q_H = T_c \Delta S \quad (5.1)$$

$$Q_H = C_H(T_{HO} - T_{HI}) = U_H A_H (\text{LMTD})_C \quad (5.2)$$

where  $\Delta S$  is entropy change of system,  $C_H$  is the specific heat of the fluid at high temperatures,  $U_H$  is the overall heat transfer coefficient of the condenser,  $A_H$  is the heat transfer area of the condenser, and  $(\text{LMTD})_C$  log is the mean temperature difference of the condenser, given by the following equation:

$$(\text{LMTD})_c = \frac{(T_C - T_{HI}) - (T_C - T_{HO})}{\ln \frac{(T_C - T_{HI})}{(T_C - T_{HO})}} \quad (5.3)$$

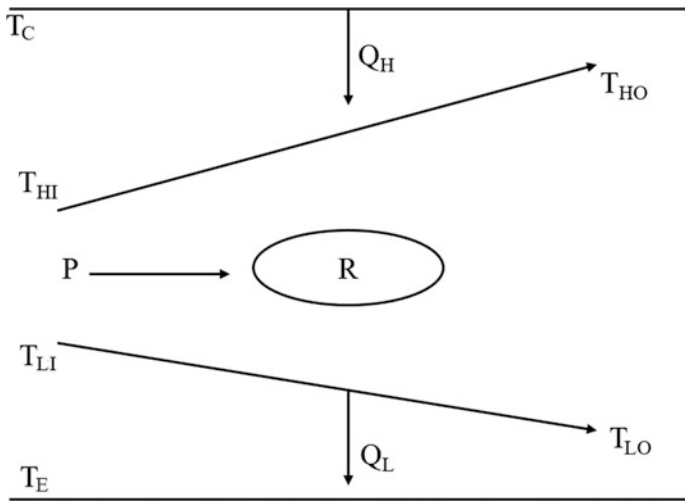


**Fig. 5.4** Heat transfer model of Carnot refrigerator

where  $T_C$ ,  $T_{HI}$ , and  $T_{HO}$  represent the mean temperature of the condenser, the input temperature of the heat source, and output temperature of the heat source respectively. They are related by the following equation:

$$T_{HO} = C_H(1 - \varepsilon_H)T_{HI} + \varepsilon_H T_C \quad (5.4)$$

where  $\varepsilon_H$  is the effectiveness of the condenser, which is given by the following equation:

$$\varepsilon_H = 1 - e^{-N_H} \quad (5.5)$$

in which  $N_H$  is the number of the transfer units of the condenser. This is given by the following equation.

$$N_H = \frac{U_H A_H}{C_H} \quad (5.6)$$

The following equation also gives the heat transfer ( $Q_H$ ) at high temperature:

$$Q_H = \alpha(T_C - T_{HI}) \quad (5.7)$$

where parameter  $\alpha$  is described by the following.

$$\alpha = C_H \varepsilon_H \quad (5.8)$$

The amount of heat transfer taking place at the low temperatures of the cycle ( $Q_L$ ) is given by the following equations:

$$Q_L = T_E \Delta S \quad (5.9)$$

$$Q_L = C_L(T_{LI} - T_{LO}) = U_L A_L (\text{LMTD})_E \quad (5.10)$$

where  $\Delta S$  is entropy change of the system,  $C_L$  is the specific heat of the fluid in the evaporator,  $U_L$  is the overall heat transfer coefficient of the evaporator,  $A_L$  is the heat transfer area, and  $(\text{LMTD})_E$  is the log mean temperature difference of evaporator, which is given by the following equation:

$$(\text{LMTD})_E = \frac{(T_{LI} - T_E) - (T_{LO} - T_E)}{\ln \frac{(T_{LI} - T_E)}{(T_{LO} - T_E)}} \quad (5.11)$$

where  $T_E$ ,  $T_{LI}$ , and  $T_{LO}$  represent the mean temperature of the evaporator, the input temperature of the heat sink, and the output temperature of the heat sink respectively. They are illustrated by the following equation:

$$T_{LO} = (1 - \varepsilon_L)T_{HI} + \varepsilon_L T_E \quad (5.12)$$

where  $\varepsilon_L$  is the effectiveness of the evaporator and is given by the following equation:

$$\varepsilon_L = 1 - e^{-N_L} \quad (5.13)$$

where  $N_L$  is the number of the transfer units of the evaporator. It's given by the following equation.

$$N_L = \frac{U_L A_L}{C_L} \quad (5.14)$$

In addition, the following equation also gives the amount of heat transfer at low temperature s( $Q_L$ ):

$$Q_L = \beta(T_{LI} - T_E) \quad (5.15)$$

where parameter  $\beta$  is given by

$$\beta = C_L \varepsilon_L \quad (5.16)$$

As such, the network required for the Carnot refrigeration system can be given by the following equation.

$$P = Q_H - Q_L \quad (5.17)$$

Considering the internal irreversibility parameter ( $I$ ), the second law of thermodynamics for the system is given by the following equation.

$$I \frac{Q_L}{T_E} = \frac{Q_H}{T_C} \quad (5.18)$$

Based on the irreversibility definition, heat transfer ( $Q_L$ ) in the evaporator is given by the following equation:

$$Q_L = \frac{yz(T_{LI} - xT_{HI})}{(I + y)(1 + y)} \quad (5.19)$$

where the parameters  $x$ ,  $y$ , and  $z$  are the fluid temperature ratio, heat conductance rate ratio, and the sum of heat conductance rate, respectively. They are given by

$$x = \frac{T_E}{T_C} \quad (5.20)$$

$$y = \frac{\alpha}{\beta} \quad (5.21)$$

$$z = \alpha + \beta \quad (5.22)$$

The following equation gives the entropy generation ( $S_{gen}$ ) of the system:

$$S_{gen} = \left( \frac{Q_H}{T_{Hm}} - \frac{Q_L}{T_{Lm}} \right) \quad (5.23)$$

where  $T_{Hm}$  and  $T_{Lm}$  are the average temperatures and are given by the following equations.

$$T_{Hm} = \frac{T_{HI} + T_{HO}}{2} = \frac{(2 - \varepsilon_H)T_{HI} + \varepsilon_H T_C}{2} \quad (5.24)$$

$$T_{Lm} = \frac{T_{LI} + T_{LO}}{2} = \frac{(2 - \varepsilon_L)T_{LI} + \varepsilon_L T_E}{2} \quad (5.25)$$

The following equation gives the exergy input ( $E_x$ ) to the system.

$$E_x = Q_L \left( \frac{T_0}{T_{Lm}} - 1 \right) - Q_H \left( \frac{T_0}{T_{Hm}} - 1 \right) \quad (5.26)$$

The below equation gives the ecological coefficient of performance (ECOP).

$$\text{ECOP} = \frac{Q_L}{T_0 S_{gen}} \quad (5.27)$$

This last equation gives the exergetic performance criterion (EPC) of the system.

$$EPC = \frac{E_x}{T_{0S_{gen}}} \quad (5.28)$$

Based on the above thermal model, the objective function for the present work is defined in the next section.

### 5.1.2 Case Study, Objective Function Description, and Constraints

For this case, a Carnot refrigerator is designed and optimized for the maximum cooling load. The input temperature of the heat source ( $T_{H1}$ ) is taken as 300 K, the input temperature of the heat sink ( $T_{L1}$ ) is 265 K, the mean temperature of the condenser ( $T_C$ ) is 336 K, and the atmospheric temperature ( $T_0$ ) is 298 K. In addition, the internal irreversibility parameter ( $I$ ) of the system is 1.05. For this problem, five design variables are considered: the ratio of fluid temperature ( $x$ ), the heat conduction rate parameter ( $y$ ), the total heat conduction rate ( $z$ ), the effectiveness of the condenser ( $\varepsilon_H$ ), and the effectiveness of evaporator ( $\varepsilon_L$ ). The upper and lower bounds of the design variables are presented in Table 5.1.

As mentioned above, the maximization of the cooling load of the Carnot refrigerator is taken as an objective function in the present study. Note that for this study, the operating parameters which resulted in a maximum cooling load also satisfied the exergy input to the system ( $E_x$ ), as well as the ecological coefficient of the performance (ECOP) constraints. So, considering these aspects, the objective function of a Carnot refrigerator is formulated as below:

$$\begin{cases} \text{Minimize } f(X) = Q_L(X) + \sum_{j=1}^n G_1(g_j(X))^2 \\ X = [x_1, x_2, x_3, \dots, x_D], \quad x_{i,\text{minimum}} \leq x_i \leq x_{i,\text{maximum}}, \quad i = 1, 2, 3, \dots, D \\ g_j(X) \leq 0, \quad j = 1, 2, 3, \dots, n \end{cases} \quad (5.29)$$

**Table 5.1** Ranges of design variables for Carnot refrigerator optimization

Design variable	Lower bound	Upper bound
The ratio of fluid temperature ( $x$ )	0.6	1000
Heat conduction rate parameter ( $y$ )	0.5	1
Total heat conduction rate ( $z$ )	0.08	1.8
The effectiveness of condenser ( $\varepsilon_H$ )	0.7	0.9
The effectiveness of evaporator ( $\varepsilon_L$ )	0.7	0.9

where  $X$  is the vector of the design variables bounded between its minimum and maximum values and  $G_1$  is the penalty parameter. The above term takes into account the effect of the constraints violation and is used when the constraint's violation takes place. Above,  $g_j(X)$  indicates such constraints. The following constraints are considered for the Carnot refrigerator.

$$\text{Exergy input to the system}(E_x) \geq 6.75 \text{ kW} \quad (5.30)$$

$$\text{The ecological coefficient of performance (ECOP)} \geq 15 \quad (5.31)$$

The next section describes the results and discussion of the case study.

### 5.1.3 Results and Discussion

The considered problem of Carnot refrigerator is investigated using 11 different metaheuristic approaches to obtain the maximum thermal efficiency of the heat engine. Each algorithm is implemented 100 times on the considered problem to estimate the statistical variations of the algorithms. In addition, each algorithm was implemented with a population size of 50, and the termination criteria are set as 100,000 function evaluations. The results obtained using each algorithm are presented in Table 5.2 in the form of the best solution, the worst solution, average solution standard deviation, and success rate. These results are based on the 100 runs. In addition, the infeasible solutions (i.e., affected by penalty) are eliminated. Afterward, the worst solution, average solution, standard deviation, and success rate (which are obtained by considering a maximum of 0.1% variation from the global optimum value) were obtained.

**Table 5.2** Comparative results of different algorithms for Carnot refrigerator optimization

Algorithms	Best	Worst	Average	SD	Success rate (%)
GA	25.65	25.6120	25.6473	1.01E-02	56
PSO	25.65	25.5699	25.6040	2.15E-02	64
DE	25.65	25.65	25.65	3.69E-15	56
ABC	25.65	25.6077	25.6239	1.98E-02	96
CSA	25.65	25.65	25.65	1.09E-14	92
TLBO	25.65	25.65	25.65	1.09E-14	84
SOS	25.65	25.65	25.65	1.09E-14	92
WWO	25.65	25.6120	25.6469	1.05E-02	52
HTS	25.65	25.6077	25.6246	2.13E-02	80
PVS	25.65	25.65	25.65	1.09E-14	92
SCA	25.65	25.6004	25.6209	1.29E-02	88

It can be observed from the comparative results that these algorithms performed equally well in terms of producing an almost identical maximum cooling load for the Carnot refrigerator. That being said, the DE, CSA, TLBO, SOS, and PVS algorithms obtained identical average performances. Additionally, the success rate of the ABC algorithm is the highest, while that of the WWO algorithm is the lowest. As the results vary significantly, the Friedman rank test is implemented to judge the best suitable algorithm for Carnot refrigerator. The test considers each algorithm's ability to obtain the best, worst, and average results, and success rate. The results of the Friedman rank test are presented in Table 5.3, and its graphical representation is given in Fig. 5.5. The results are presented in the form of Friedman value, a normalized value with '1' being the best performing algorithm

**Table 5.3** Friedman rank test results for Carnot refrigerator optimization

Algorithms	Friedman value	Normalized value	Rank
GA	33	0.515152	4
PSO	46	0.369565	9
DE	21.5	0.790698	2
ABC	37	0.459459	5
CSA	17	1	1
TLBO	22	0.772727	3
SOS	38	0.447368	6
WWO	42.5	0.4	8
HTS	39	0.435897	7
PVS	17	1	1
SCA	38	0.447368	6

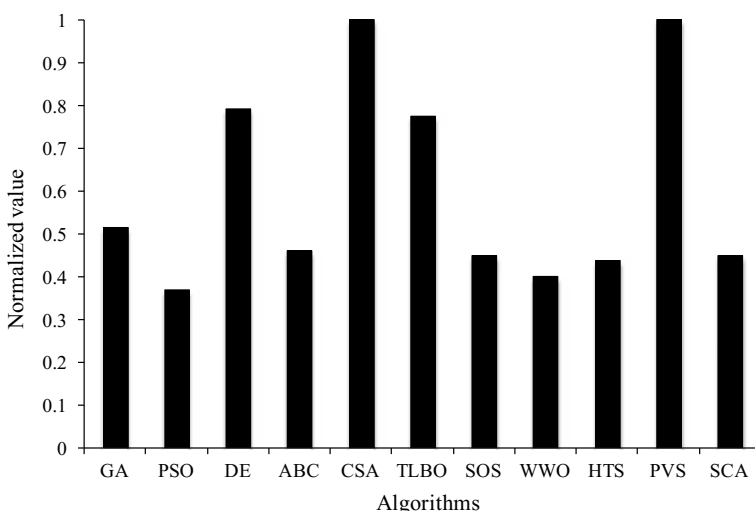


**Fig. 5.5** Graphical presentation of Friedman rank test for Carnot refrigerator optimization

**Table 5.4** The optimized operating condition of Carnot refrigerator

Operating parameters	Optimized value
<i>Design variable</i>	
The ratio of fluid temperature ( $x$ )	0.6885
Heat conduction rate parameter ( $y$ )	1
Total heat conduction rate ( $z$ )	1.8
The effectiveness of condenser ( $\varepsilon_H$ )	0.9
The effectiveness of evaporator ( $\varepsilon_L$ )	0.9
<i>Constraints</i>	
Exergy input to the system ( $E_s$ ), kW	6.75
Ecological COP (ECOP)	15
<i>Objective function</i>	
Cooling load ( $Q_L$ ), W	25.65

and its rank. It can be observed from the results that CSA and PVS have obtained the first rank followed by DE and TLBO algorithms.

The optimized operating condition of Carnot refrigerator obtained using the CSA algorithm is presented in Table 5.4. It can be noted from the results that the Carnot refrigerator with the maximum heat conduction rate, total heat conduction rate, effectiveness of the condenser, and evaporator results in a maximum cooling load. On the other hand, the fluid temperature ratio produced a conflicting effect on achieving the maximum cooling load. Note that for this section, both the constraints are at the limiting value in the optimized operating condition of Carnot refrigerator.

## 5.2 Single-Effect Vapor Absorption Refrigerator

Vapor absorption refrigeration systems (VARS) belong to a class of refrigeration cycles which require thermal energy for their working instead on mechanical energy. Hence, they are also known as heat-operated or thermal energy-driven systems. Furthermore, the vapor absorption system requires a pair of refrigerants and absorbents for its working. Since vapor absorption refrigeration system run on low-grade thermal energy, they are preferred when low-grade energy such as waste heat or solar energy is available. Since conventional absorption systems use natural refrigerants like water or lithium bromide (LiBr), they are environmentally friendly. Vapor absorption refrigeration systems using the water–lithium bromide pair are extensively used in large capacity air-conditioning systems. For these systems, water is used as a refrigerant, and a solution of lithium bromide in water is used as the absorbent. Since water is used as the refrigerant, these systems cannot provide refrigeration at sub-zero temperatures. As such, they are only used in applications requiring refrigeration at temperatures above 0 °C.

The schematic arrangement of the LiBr–H<sub>2</sub>O absorption refrigerating system is shown in Fig. 5.6. It can be observed from the figure that the main components of

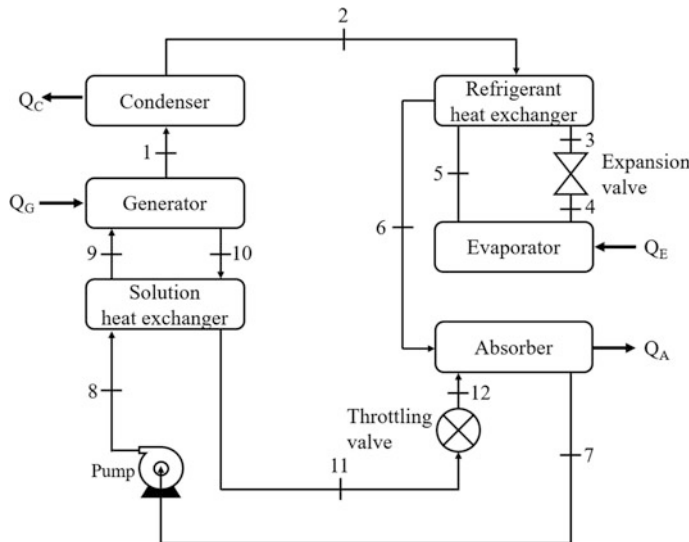


**Fig. 5.6** Schematic arrangement of LiBr—water vapor absorption refrigeration system

the VARS are the generator, condenser, expansion valve, evaporator, absorber, and pump. The function of the generator is to supply heat to the absorbent–refrigerant mixture in a way that it separates the refrigerant from the absorbent. The function of the condenser is to convert the vapor refrigerant into liquid. The expansion valve reduces the pressure of the refrigerant from condenser pressure to evaporator pressure, hence reducing the temperature of the refrigerant. The function of the evaporator is to extract heat from the space that needs to be cooled. In the process, an absorber absorbs the refrigerant and prepares the homogeneous refrigerant–absorbent mixture. This mixture is supplied to the generator with the help of a pump from the absorber. The working principle of the —LiBr–H<sub>2</sub>O absorption system is explained below.

First, the low-pressure LiBr vapor leaves the evaporator and enters the absorber, where it is absorbed by cold water, hence forming a strong solution of LiBr. Since the absorption of LiBr into water is exothermic in nature, the temperature of the solution increases. Note that the cooling arrangement occurs in the absorber in which the coolant removes any heat generated. The strong solution is then pumped to the generator through a heat exchanger which increases the temperature of the solution. The strong solution of LiBr is further heated in the generator with the help of steam and the heating coil/solar energy source. The heating process separates the water from LiBr and generates water vapor. The hot, high-pressure water vapor is then condensed in the condenser using water as a coolant. The weak, but high-pressurized solution then flows to the absorber, passing through a pressure reducing valve. After condensation, the refrigerant (i.e., water) expands in the expansion valve. After undergoing the expansion process, it then enters into the

evaporator where it absorbs heat and produces the refrigeration effect. The low-pressure water vapor from the evaporator then reenters the absorber, where it is again absorbed to form a strong solution and the cycle repeats itself.

The major advantages of vapor absorption refrigeration systems are that they only have a few moving parts (i.e., only pump), so it is less noisy, the waste heat or solar energy can be used as a source of heat energy, the performance of the system is not affected by load variation, and the system can be easily controlled. That being said, there are a few disadvantages associated with vapor absorption system, which include the system has a low coefficient of performance, the system requires more space, and it is susceptible to leakage.

In past years, researchers have carried out various works related to the analysis and optimization of the single-effect vapor absorption refrigeration system. For example, Misra et al. (2002) presented the thermo-economic optimization methodology which was based on the theory of exergetic costs. It was applied to the case of single-effect LiBr–H<sub>2</sub>O vapor absorption refrigeration system for air-conditioning applications. In their study, the authors considered the minimization of the overall economic cost of the product as an objective function. Misra et al. (2003) investigated the economic optimization of a single-effect water/LiBr vapor absorption refrigeration system for air-conditioning application. They aimed at minimizing its overall operation and amortization cost. The authors compared the optimum results with the base case and they show the percentage variations in the system's operation cost. Another work is Bhardwaj et al. (2003) who present a finite-time thermodynamic optimization of a vapor absorption refrigeration system that's affected by both external and internal irreversibilities. The authors obtained the optimum value of both the coefficient of performance and the working fluid temperatures of the absorption system at the maximum cooling capacity. Bhardwaj et al. (2005) presented a finite-time thermodynamic analysis of the vapor absorption of refrigeration systems considering both external as well as internal irreversibility. The authors observed that the internal irreversibility parameters are a dominant factor for the performance reduction of the system. Furthermore, the internal irreversibility parameter of the generator-absorber assembly is more sensitive to performance reduction rather than the internal irreversibility parameter of the evaporator-condenser assembly.

In another work, Misra et al. (2006) carried out the thermo-economic optimization of an aqua-ammonia vapor-absorption refrigeration system. The author considered the minimization of the overall product cost as an objective function and calculated the economic costs of all the internal flows and products of the system by formulating thermo-economic cost balances. Kizilkan et al. (2007) performed a thermo-economic optimization of a LiBr absorption refrigeration system. In the work, various components of the system such as the condenser, evaporator, generator, and the absorber heat exchangers were optimized. The authors also determined the optimum heat exchanger areas with their corresponding optimum operating temperatures. In 2007, Kilic and Kaynakli used the first and second laws of thermodynamics to analyze the performance of a single-stage water–lithium bromide absorption refrigeration system. The authors developed a mathematical

model based on the exergy method to evaluate the system's performance, the exergy loss of each component, and the total exergy loss of the entire system's components. Furthermore, the parameters connected with the performance of the cycle circulation ratio, the coefficient of performance, the exergetic efficiency, and the efficiency ratio were also calculated at various operating conditions.

Kaushik and Arora (2009) performed the energy and exergy analysis of single-effect water–lithium bromide absorption system. The analysis involves the determination of the effects of the generator, the absorber, and the evaporator temperatures on the energetic and exergetic performance of these systems. The authors also prove that the coefficient of performance of the single-effect system lies in between 0.6 and 0.75. In another work, Karamangil et al. (2010) carried out the simulation study of the performance evaluation of single-stage absorption refrigeration system that uses conventional working fluids and alternatives. In addition, Rubio-Maya et al. (2012) performed the optimization of a LiBr–H<sub>2</sub>O absorption refrigeration system that considers the minimization of the annual operating cost of the system as an objective function. The authors established the optimization problem as a nonlinear programming model and solved the model using the CONOPT solver. In 2017, Pandya et al. performed the thermodynamic optimization of a single-effect LiBr–H<sub>2</sub>O vapor absorption cooling system of 1 TR capacity based on the first and second laws. The authors developed a mathematical model of the system and solved it using an engineering equation solver. Finally, Pandya et al. (2018) performed the performance optimization of single-stage NH<sub>3</sub>–H<sub>2</sub>O-type absorption cooling system integrated with a different solar collector.

### 5.2.1 Thermal Model

In the present work, a single-effect LiBr–H<sub>2</sub>O vapor absorption refrigerator is considered for optimization. The thermal model presented here is based on the previous work of Kili and Kaynakli (2007). Note that the subscripts 1–12 used in the different equations of the thermal model are explained in Fig. 5.6.

The energy balance equations for the generator ( $Q_G$ ), the absorber ( $Q_A$ ), the condenser ( $Q_C$ ), and the evaporator ( $Q_E$ ) of the absorption system are given by

$$\dot{Q}_G = \dot{m}_1 h_1 + \dot{m}_{10} h_{10} - \dot{m}_9 h_9 \quad (5.32)$$

$$\dot{Q}_A = \dot{m}_6 h_6 + \dot{m}_{12} h_{12} - \dot{m}_7 h_7 \quad (5.33)$$

$$\dot{Q}_C = \dot{m}_1 h_1 - \dot{m}_2 h_2 \quad (5.34)$$

$$\dot{Q}_E = \dot{m}_5 h_5 - \dot{m}_4 h_4 \quad (5.35)$$

where  $m$  is the mass flow rate and  $h$  is the enthalpy of the working substance at the different states mentioned in Fig. 5.6.

Likewise, the energy balance equations for the solution heat exchanger ( $\dot{Q}_{\text{SHE}}$ ), refrigerant heat exchanger ( $\dot{Q}_{\text{RHE}}$ ), and pump ( $\dot{W}_P$ ) are given by the following equations:

$$\dot{Q}_{\text{SHE}} = \dot{m}_{10}(h_{10} - h_{11}) = \dot{m}_8(h_9 - h_8) \quad (5.36)$$

$$\dot{Q}_{\text{RHE}} = \dot{m}_2(h_2 - h_3) = \dot{m}_5(h_6 - h_5) \quad (5.37)$$

$$\dot{W}_P = \dot{m}_7(h_8 - h_7) = \dot{m}_7\vartheta_7(P_C - P_E)/\eta_P \quad (5.38)$$

where  $\eta_P$  is the pump's efficiency,  $P_C$  is the condenser, and  $P_E$  is evaporator pressure, respectively.

The exergy balance equation of the vapor absorption system is given by

$$\sum \dot{m}_i e_i - \sum \dot{m}_o e_o + \dot{Q} \left( 1 - \frac{T_0}{T} \right) - \dot{W} - \dot{E}_D = 0 \quad (5.39)$$

where  $\dot{W}$  is the mechanical work transferred to or from the system,  $\dot{E}_D$  is the exergy destroyed due to the internal irreversibility, and  $e$  is the specific exergy and is given by the following equation.

$$e = (h - h_o) - T_o(s - s_o) \quad (5.40)$$

The irreversibility rate ( $\dot{I}$ ) associated with any process is given by

$$\dot{I} = T_o \dot{S}_{\text{gen}} = T_o \left( \sum \dot{m}_o s_o - \sum \dot{m}_i s_i - \dot{Q}/T \right) \quad (5.41)$$

where  $\dot{S}_{\text{gen}}$  is the entropy generation rate of the system and  $T_o$  is the ambient temperature.

The exergy loss rate associated with the different components of the vapor absorption system [i.e., generator ( $\Delta\dot{E}_G$ ), absorber ( $\Delta\dot{E}_A$ ), condenser ( $\Delta\dot{E}_C$ ), evaporator ( $\Delta\dot{E}_E$ ), pump ( $\Delta\dot{E}_P$ ), solution heat exchanger ( $\Delta\dot{E}_{\text{SHE}}$ ), refrigerant heat exchanger ( $\Delta\dot{E}_{\text{RHE}}$ ), solution expansion valve ( $\Delta\dot{E}_{\text{SEV}}$ ), and refrigerant expansion valve ( $\Delta\dot{E}_{\text{REV}}$ )] are given by the following equations:

$$\Delta\dot{E}_G = \dot{m}_9 e_9 - \dot{m}_{10} e_{10} - \dot{m}_1 e_1 + \dot{Q}_G \left( 1 - \frac{T_0}{T_G} \right) \quad (5.42)$$

$$\Delta\dot{E}_A = \dot{m}_6 e_6 + \dot{m}_{12} e_{12} - \dot{m}_7 e_7 - \dot{Q}_A \left( 1 - \frac{T_0}{T_A} \right) \quad (5.43)$$

$$\Delta\dot{E}_C = \dot{m}_1 e_1 - \dot{m}_2 e_2 - \dot{Q}_C \left( 1 - \frac{T_0}{T_C} \right) \quad (5.44)$$

$$\Delta\dot{E}_E = \dot{m}_4 e_4 - \dot{m}_5 e_5 + \dot{Q}_E \left( 1 - \frac{T_0}{T_E} \right) \quad (5.45)$$

$$\Delta\dot{E}_P = \dot{m}_7 (e_7 - e_8) + \dot{W}_P \quad (5.46)$$

$$\Delta\dot{E}_{SHE} = \dot{m}_8 (e_8 - e_9) + \dot{m}_{10} (e_{10} - e_{11}) \quad (5.47)$$

$$\Delta\dot{E}_{RHE} = \dot{m}_2 (e_2 - e_3) + \dot{m}_5 (e_5 - e_6) \quad (5.48)$$

$$\Delta\dot{E}_{SEV} = \dot{m}_{11} (e_{11} - e_{12}) \quad (5.49)$$

$$\Delta\dot{E}_{REV} = \dot{m}_3 (e_3 - e_4) \quad (5.50)$$

where  $T_G$ ,  $T_A$ ,  $T_E$ , and  $T_C$  are the temperature of the generator, absorber, evaporator, and condenser, respectively.

The following equation gives the total exergy loss rate ( $\dot{E}_t$ ) of the absorption refrigerator system.

$$\Delta\dot{E}_t = \Delta\dot{E}_G + \Delta\dot{E}_A + \Delta\dot{E}_C + \Delta\dot{E}_E + \Delta\dot{E}_P + \Delta\dot{E}_{SHE} + \Delta\dot{E}_{RHE} + \Delta\dot{E}_{SEV} + \Delta\dot{E}_{REV} \quad (5.51)$$

The following equation gives the nondimensional exergy loss ( $\psi_j$ ) of each component:

$$\psi_j = \frac{\Delta\dot{E}_j}{\Delta\dot{E}_t} \quad (5.52)$$

where  $\Delta\dot{E}_j$  is the exergy loss rate of the  $j$ th component of the vapor absorption system.

The equation below gives the coefficient of performance (COP) of the refrigeration system.

$$COP = \frac{\dot{Q}_E}{\dot{Q}_G + \dot{W}_P} \quad (5.53)$$

where  $Q_G$  and  $Q_E$  are the heat transfer rates associated with the generator and evaporator respectively.

The following equation gives the circulation ratio (CR) of the vapor absorption refrigeration system.

$$CR = \frac{\dot{m}_7}{\dot{m}_1} \quad (5.54)$$

Exergetic efficiency ( $\xi$ ) of the vapor absorption refrigeration system is given by

$$\xi = \frac{\dot{Q}_E \left(1 - \frac{T_0}{T_E}\right)}{\dot{Q}_G \left(1 - \frac{T_0}{T_G}\right) + \dot{W}_P} \quad (5.55)$$

Finally, the following equation gives the efficiency ratio ( $\tau$ ) of the vapor absorption refrigeration system:

$$\tau = \frac{\text{COP}}{\text{COP}_c} \quad (5.56)$$

where  $\text{COP}_c$  is the Carnot coefficient of performance and is described below.

$$\text{COP}_c = \left(\frac{T_G - T_A}{T_G}\right) \left(\frac{T_E}{T_C - T_E}\right) \quad (5.57)$$

Based on the above thermal model, the objective function for the present work is defined in the next section.

### 5.2.2 Case Study, Objective Function Description, and Constraints

A single-effect LiBr–H<sub>2</sub>O vapor absorption refrigeration system is designed and optimized for maximum exergetic efficiency ( $\xi$ ). For this case, the heat load of the evaporator ( $\dot{Q}_E$ ) is 3.5 kW, and the ambient temperature is 25 °C. The effectiveness of the solution heat exchanger ( $\epsilon_{\text{SHE}}$ ) and refrigerant heat exchanger ( $\epsilon_{\text{RHE}}$ ) is 0.7. The efficiency of the pump is taken as 0.95. For this problem, four design variables are considered for optimization. These variables are the generator's temperature ( $T_G$ ), the absorber's temperature ( $T_A$ ), the condenser's temperature ( $T_C$ ), and the evaporator temperature ( $T_E$ ). The upper and lower bounds of the design variables are presented in Table 5.5.

As mentioned above, the maximization of exergetic efficiency ( $\xi$ ) of the LiBr–H<sub>2</sub>O vapor absorption refrigeration system is taken as an objective function in the present study. Fortunately, the operating parameters resulting in maximum exergetic efficiency also satisfy the coefficient of performance (COP) as well as the

**Table 5.5** Ranges of design variables for vapor absorption refrigerator optimization

Design variable	Lower bound	Upper bound
Generator temperature ( $T_G$ ), K	75	100
Absorber temperature ( $T_A$ ), K	30	50
Condenser temperature ( $T_C$ ), K	30	50
Evaporator temperature ( $T_E$ ), K	8	15

condenser-absorber temperature difference constraints. So, considering the mentioned aspects, the objective function of the LiBr–H<sub>2</sub>O vapor absorption refrigeration system is formulated as below:

$$\begin{cases} \text{Minimize } f(X) = \xi(X) + \sum_{j=1}^n G_1(g_j(X))^2 \\ X = [x_1, x_2, x_3, \dots, x_D], \quad x_{i,\text{minimum}} \leq x_i \leq x_{i,\text{maximum}}, \quad i = 1, 2, 3, \dots, D \\ g_j(X) \leq 0, \quad j = 1, 2, 3, \dots, n \end{cases} \quad (5.58)$$

where  $X$  is the vector of design variables, bounded between its minimum and maximum values. In addition,  $G_1$  is the penalty parameter. For the study, the entire term takes into account the effects of the constraints violation. This term comes into picture when the constraint violation takes place ( $g_j(X)$  indicates the constraints). The following constraints are considered for the absorption refrigerating system.

$$\text{Condenser-absorber temperature difference}(T_C - T_A) > 0 \quad (5.59)$$

$$\text{The coefficient of performance (COP)} \geq 0.85 \quad (5.60)$$

The next section describes the results and discussion of the case study.

### 5.2.3 Results and Discussion

The considered problem of the LiBr–H<sub>2</sub>O vapor absorption refrigeration system is investigated using 11 different metaheuristic approaches to obtain the maximum exergetic efficiency of the refrigerator. Each algorithm is implemented 100 times on the considered problem to estimate the statistical variations of the algorithms. Each algorithm is implemented with the population size of 50, and the termination criteria are set as 100,000 function evaluations. The results obtained using each algorithm are presented in Table 5.6 in the form of the best solution, the worst solution, average solution standard deviation, and success rate (based on the 100 runs). In this section, the infeasible solutions (i.e., affected by penalty) are eliminated. Afterward, the worst solution, the average solution, the standard deviation, and the success rate are obtained. Note that the success rate of the algorithm is obtained by considering a 0.1% variation from the global optimum value.

It can be observed from the comparative results that these algorithms performed well, producing almost identical maximum exergetic efficiency for the refrigerator. In addition, the average performance of the considered algorithms is also similar. That being said, the PSO algorithm has the highest success rate, while the SOS algorithm produces the lowest. Since it is difficult to judge the best performing algorithm, the Friedman rank test is implemented to judge the best suitable

**Table 5.6** Comparative results of different algorithms for vapor absorption refrigerator optimization

Algorithms	Best	Worst	Average	SD	Success rate (%)
GA	0.3583	0.3468	0.3547	5.51E-03	44
PSO	0.3583	0.3468	0.3578	2.46E-03	84
DE	0.3583	0.3465	0.3552	5.28E-03	62
ABC	0.3583	0.3468	0.3560	4.65E-03	80
CSA	0.3583	0.3468	0.3557	4.94E-03	68
TLBO	0.3583	0.3462	0.3567	4.12E-03	76
SOS	0.3583	0.3450	0.3501	6.57E-03	24
WWO	0.3583	0.3450	0.3524	6.13E-03	28
HTS	0.3583	0.3468	0.3565	4.32E-03	64
PVS	0.3583	0.3459	0.3562	4.65E-03	56
SCA	0.3583	0.3453	0.3534	5.73E-03	36

**Table 5.7** Friedman rank test results for vapor absorption refrigerator optimization

Algorithms	Friedman value	Normalized value	Rank
GA	35	0.242857	8
PSO	8.5	1	1
DE	28.5	0.298246	6
ABC	17.5	0.485714	3
CSA	27	0.314815	5
TLBO	16.5	0.515152	2
SOS	51.5	0.165049	11
WWO	48.5	0.175258	10
HTS	22	0.386364	4
PVS	31	0.274194	7
SCA	44	0.193182	9

algorithm for the vapor absorption refrigerator. The test considered each algorithm's capability to obtain the best, worst, and average results, as well as the success rate. The results of the Friedman rank test are presented in Table 5.7, and its graphical representation is given in Fig. 5.7. The results are presented in the form of a Friedman value, a normalized value with '1' being the best performing algorithm and its rank. It can be observed from the results that PSO has obtained the first rank followed by TLBO and ABC algorithm.

The optimized operating condition of LiBr–H<sub>2</sub>O vapor absorption refrigeration system obtained using the PSO algorithm is presented in Table 5.8. It can be noted from the results that the absorption refrigerator with the lowest condenser temperature, absorber temperature, generator temperature, and evaporator temperature results in the highest exergetic efficiency of the system. Note that all the constraints are at the limiting value for optimized operating condition of this absorption refrigerating system.

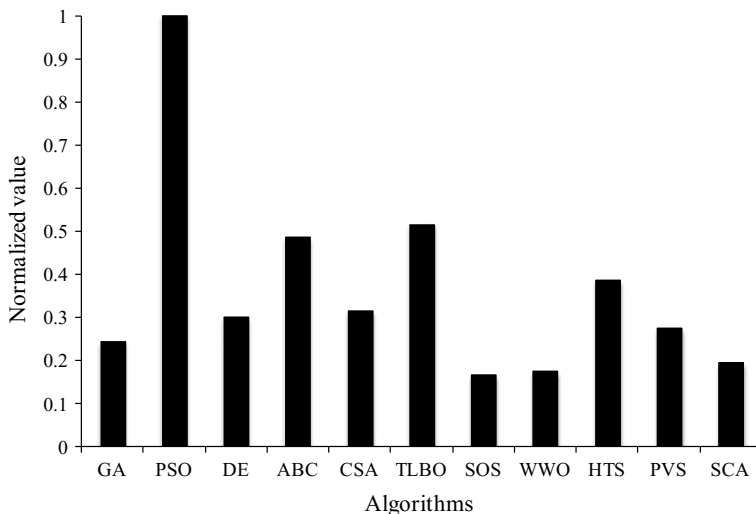


**Fig. 5.7** Graphical presentation of Friedman rank test for vapor absorption refrigerator optimization

**Table 5.8** The optimized operating condition of LiBr–water vapor absorption refrigerator

Operating parameters	Optimized value
<i>Design variable</i>	
Generator temperature ( $T_G$ ), K	75
Absorber temperature ( $T_A$ ), K	30
Condenser temperature ( $T_C$ ), K	30.5
Evaporator temperature ( $T_E$ ), K	8
<i>Constraints</i>	
Condenser-absorber temperature difference	0.5
Coefficient of performance (COP)	0.85
<i>Objective function</i>	
Exergetic efficiency ( $\xi$ )	0.3583

### 5.3 Multi-temperature Vapor Absorption Refrigerator

In the multi-temperature vapor absorption refrigerator, a series of generators and condenser are operating at progressively increasing/reducing temperature. The pressure of the generator and condenser may or may not be same. The components of multi-temperature vapor absorption refrigerator are similar to simple vapor absorption system along with the multiple generator and condenser. The pair of refrigerant–absorbent in multi-temperature absorption refrigerator is also similar to simple vapor absorption refrigerating system (i.e.,  $\text{NH}_3\text{--H}_2\text{O}$ ,  $\text{LiBr}\text{--H}_2\text{O}$ , etc.)

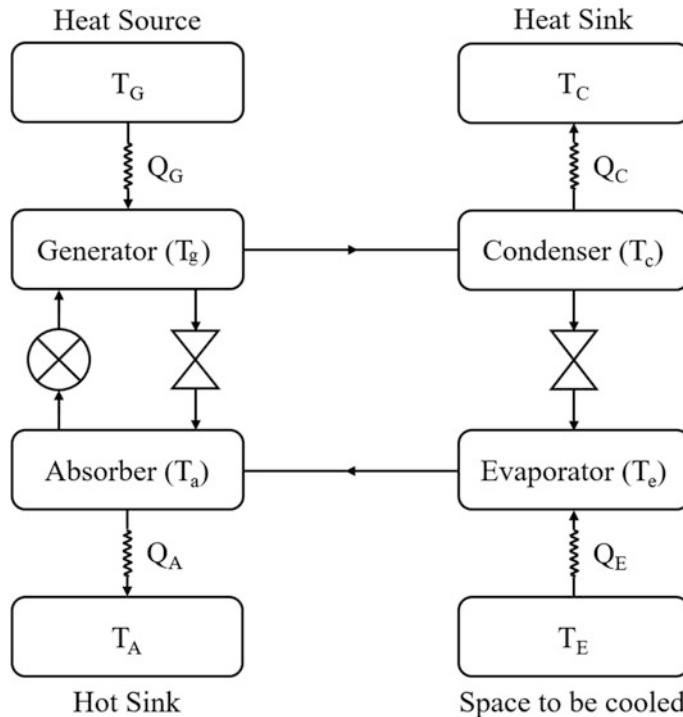


**Fig. 5.8** Schematic of four-temperature-level absorption refrigerator

The schematic arrangement of the multi-temperature absorption refrigerator is shown in Fig. 5.8. It can be observed from the figure that considered multi-temperature absorption refrigerator composed of two generators and two condensers. The high-temperature generator maintains at temperature  $T_G$  while the low-temperature generator maintains at temperature  $T_g$ . Likewise, low-temperature condenser maintains at temperature  $T_c$  while high-temperature condenser maintains at temperature  $T_c$ . Remaining components of the system are similar to the simple vapor absorption system. The high-temperature generator comes into picture when heat supplied by the waste heat in a low-temperature generator is not sufficient to fulfill the desired load. Similarly, the low-temperature condenser comes into the picture when the heat absorbs by the high-temperature condenser is not sufficient to run the system.

Earlier, work had been reported by the researchers related to the analysis and optimization of double-effect vapor absorption refrigerating system. Xu and Dai (1997) carried out the thermodynamic analysis to study the effect of design parameters including heat-recovery ratio, solution circulation ratio, and the distribution ratio of the solution on the performance of a double-effect absorption chiller of the parallel-flow-type using water–lithium bromide as the working fluid. Arun et al. (2000) evaluated the equilibrium temperatures at the low-pressure generator

for double-effect series flow LiBr–H<sub>2</sub>O vapor absorption and estimated the system performance at these temperatures. The authors presented correlations for equilibrium low-pressure generator temperature, internal heat transfer at the low-pressure generator, circulation ratio, the coefficient of performance, optimum high-pressure generator temperature, and optimum circulation ratio for the maximum coefficient of performance in terms of operating temperatures. Arun et al. (2001) analyzed the double-effect parallel flow absorption refrigeration cycle with the water–lithium bromide as working fluid based on the concept of equilibrium temperature at the low-pressure generator. Furthermore, the authors compared the coefficient of performance and its sensitivity to the operating conditions with those for series flow cycle. Misra et al. (2005) carried out the thermo-economic optimization of the double-effect LiBr–H<sub>2</sub>O vapor absorption refrigeration system considering the minimization of overall product cost as an objective function. Furthermore, the authors formulate the thermo-economic cost balances to calculate the economic costs of all the internal flows and products of the system.

Manohar et al. (2006) presented the steady-state modeling of the double-effect absorption chiller using steam as the heat input by adopting an artificial neural network technique. This model predicts the chiller performance based on the chilled water inlet and outlet temperatures, cooling water inlet and outlet temperatures, and steam pressure. Chen et al. (2006a, b) analyzed the Irreversible four-temperature-level absorption refrigerator and derived the optimal relationships between the coefficient of performance (COP) and the cooling load; the maximum COP and the corresponding cooling load; and the maximum cooling load and the corresponding COP of the cycle by using finite-time thermodynamics. Gomri and Hakimi (2008) presented the exergy analysis of double-effect lithium bromide–water absorption refrigeration system. The authors estimated the coefficient of performance, exergetic efficiency, and the number of exergy of each component of the system. The authors also identified that the highest exergy loss occurs in the absorber and the high-pressure generator. Kaushik and Arora (2009) performed the energy and exergy analysis of double-effect water–lithium bromide absorption systems. The authors developed the computational parametric investigation of this system. The authors also investigated the effect of parameters such as temperature difference between heat source and generator and evaporator and cold space on the performance of the system. Gomri (2009) carried out a comparative study between single-effect and double-effect absorption refrigeration systems with an identical cold output. The authors also investigated the influence of the various operating parameters on the performance coefficient and exergetic efficiency of both the systems.

Marcos et al. (2011) proposed a novel method to optimize the COP in the water and air-cooled double-effect LiBr–H<sub>2</sub>O absorption chiller. The suggested method determines the effect of condensation temperatures and the solution concentration variation on COP. Farshi et al. (2013) reported the exergoeconomic analyses for three classes of double-effect LiBr–H<sub>2</sub>O absorption refrigeration systems in order to investigate the influence of various operating parameters on investment costs of the overall systems. The authors also presented the advantages and disadvantages of

different configurations of double-effect LiBr–H<sub>2</sub>O absorption refrigeration systems from their analysis. Ahmadi et al. (2014) performed the thermodynamic and thermo-economic analysis and optimization of irreversible four-temperature-level absorption refrigeration. The authors considered the maximization of the coefficient of performance, ecological function, and thermo-economic criterion as an objective function and adapted multi-objective evolutionary approach as an optimization tool. Kaynakli et al. (2015) performed the energy and exergy analysis of a double-effect series flow LiBr–H<sub>2</sub>O absorption refrigeration system with various heat sources such as hot water, hot air, and steam via high-pressure generator. Lubis et al. (2016) presented the mathematical model of solar-assisted double-effect absorption chiller and validated through an experimental investigation. Nouadje et al. (2016) carried out the finite-time thermodynamics optimization analysis of parallel flow double-effect absorption refrigerator based on the coefficient of performance and the ecological coefficient of performance criteria. The authors also identified the maximum coefficient of performance and the corresponding optimal conditions for the considered system.

### 5.3.1 Thermal Model

In the present work, four-temperature-level absorption refrigerator as shown in Fig. 5.6 is considered for the optimization. The thermal model presented here is based on the previous work of Ahmadi et al. (2014).

According to the first law of thermodynamics, the energy balance of the generator–absorber assembly is given by

$$\dot{Q}_G - \dot{Q}_A - \dot{W} = 0 \quad (5.61)$$

where  $\dot{Q}_G$  is the heat input from the generator heat source and maintained at temperature  $T_G$ .  $\dot{Q}_A$  is the heat output to the absorber heat sink.

The following equation gives the heat input from the generator heat source ( $\dot{Q}_G$ ).

$$\dot{Q}_G = \alpha A_G (T_G - T_g) \quad (5.62)$$

The heat output to the absorber heat sink ( $\dot{Q}_A$ ) is given by the following equation:

$$\dot{Q}_G = \beta A_A (T_a - T_A) \quad (5.63)$$

where  $\alpha$  and  $\beta$  are the heat transfer coefficients in generator and absorber, respectively.

The second law of the thermodynamics for the generator–absorber assembly is given by

$$\frac{\dot{Q}_G}{T_G} - \frac{\dot{Q}_A}{T_a} \leq 0 \quad (5.64)$$

Introducing the irreversibility parameter ( $I_H$ ) for generator–absorber assembly simplified the above equation as below:

$$\frac{\dot{Q}_A}{T_a} = I_H \frac{\dot{Q}_G}{T_g} \quad (5.65)$$

Based on the heat input to the generator, temperature  $T_g$  of the generator is given by the following equation:

$$T_g = \frac{I_H \alpha T_G \chi_H + a_H \beta T_A}{\chi_H (a_H \beta + I_H \alpha)} \quad (5.66)$$

where  $\chi_H$  and  $a_H$  are the working fluid temperature ratio and heat transfer area ratio, respectively, and are given by

$$\chi_H = \frac{T_a}{T_g} \quad (5.67)$$

$$a_H = \frac{A_A}{A_G} \quad (5.68)$$

Based on the heat output from the absorber, temperature  $T_a$  of the absorber is given by the following equation.

$$T_a = \frac{I_H \alpha T_G \chi_H + a_H \beta T_A}{(a_H \beta + I_H \alpha)} \quad (5.69)$$

The following formula also gives the rate of heat input to the generator:

$$\dot{Q}_G = \frac{\alpha A_{T,H}}{1 + a_H} \left( \frac{a_H \beta (T_G \chi_H - T_A)}{X_H (a_H \beta + I_H \alpha)} \right) \quad (5.70)$$

where  $A_{T,H}$  is the total heat transfer area of the generator–absorber assembly and is given by the following equation.

$$A_{T,H} = A_G + A_A \quad (5.71)$$

Applying the first law on evaporator–condenser assembly results in

$$\dot{Q}_C - \dot{Q}_E - \dot{W} = 0 \quad (5.72)$$

where  $\dot{Q}_E$  is the heat input to the evaporator and  $\dot{Q}_C$  is the heat rejection from the condenser and are given by the following equations:

$$\dot{Q}_C = \mu A_C (T_c - T_e) \quad (5.73)$$

$$\dot{Q}_E = \theta A_E (T_e - T_c) \quad (5.74)$$

where  $\mu$  and  $\theta$  are the heat transfer coefficients in condenser and evaporator, respectively.

The second law of thermodynamics for condenser-evaporator assembly results in

$$\frac{\dot{Q}_C}{T_c} - \frac{\dot{Q}_E}{T_e} \leq 0 \quad (5.75)$$

Introducing the irreversibility parameter ( $I_R$ ) for condenser-evaporator assembly simplified the above equation as follows:

$$\frac{\dot{Q}_C}{T_c} = I_R \frac{\dot{Q}_E}{T_e} \quad (5.76)$$

The following equations give the temperature of the evaporator ( $T_e$ ) and temperature of the condenser ( $T_c$ ):

$$T_e = \frac{\mu T_c \chi_R \alpha_R + \theta I_R T_E}{(\alpha_R \mu + I_R \theta)} \quad (5.77)$$

$$T_c = \frac{\mu T_E \chi_R a_R + \theta I_R T_E}{\chi_R (\alpha_R \mu + I_R \theta)} \quad (5.78)$$

where  $\chi_r$  and  $a_R$  is the working fluid temperature ratio and heat transfer area ratio, respectively, and are given by

$$\chi_R = \frac{T_e}{T_c} \quad (5.79)$$

$$a_R = \frac{A_c}{A_e} \quad (5.80)$$

The following equations give the heat absorbed in the evaporator ( $\dot{Q}_E$ ) and heat rejected in the condenser ( $\dot{Q}_C$ ):

$$\dot{Q}_E = \frac{\theta A_{T,R}}{1 + a_R} \left( \frac{a_R \mu (T_E - T_c \chi_R)}{(a_R \mu + I_R \theta)} \right) \quad (5.81)$$

$$\dot{Q}_C = \frac{\theta A_{T,R}}{1 + \alpha_R} \left( \frac{I_R a_R \mu (T_E - T_C \chi_R)}{X_R (\alpha_R \mu + I_R \theta)} \right) \quad (5.82)$$

where  $A_{T,R}$  is the total heat transfer of the condenser-evaporator assembly and is given by

$$A_{T,R} = A_C + A_E \quad (5.83)$$

The following equation gives the ecological function ( $E$ ) of the absorption cooling system.

$$E = \dot{Q}_E + \dot{Q}_G - \dot{Q}_A - T_O \left( \frac{\dot{Q}_A}{T_A} + \frac{\dot{Q}_G}{T_G} + \frac{\dot{Q}_C}{T_C} - \frac{\dot{Q}_E}{T_E} \right) \quad (5.84)$$

where  $T_O$  is the ambient temperature.

The following equation gives the coefficient of performance (COP) of the absorption system.

$$\text{COP} = \frac{\dot{Q}_E}{\dot{Q}_G} \quad (5.85)$$

The specific cooling load ( $r$ ) is given by the following equation:

$$r = \frac{\dot{Q}_E}{A} \quad (5.86)$$

where  $A$  is the total heat transfer area of the absorption system and is given by the following equation:

$$A = A_{T,H} + A_{T,R} \quad (5.87)$$

The following equation gives the thermo-economic criterion ( $f$ ) for absorption refrigerators with four reversible heat sources.

$$f = \frac{\dot{Q}_E}{C_i + C_e} \quad (5.88)$$

where  $C_i, C_e$  are capital and energy and are given by the following equation:

$$C_i = k_1 A \quad (5.89)$$

$$C_e = k_2 \dot{Q}_G \quad (5.90)$$

where  $k_1$  and  $k_2$  are the capital recovery factor and unit cost of energy, respectively.

Substituting all the values in thermo-economic function results in

$$f = \frac{\dot{Q}_E}{k_1 A + k_2 \dot{Q}_G} = \frac{1}{\frac{k_1}{r} + \frac{k_2}{\text{COP}}} \quad (5.91)$$

The simplified form of the thermo-economic function is given by

$$F = k_2 f = \frac{1}{\frac{k}{r} + \frac{1}{\text{COP}}} \quad (5.92)$$

where parameter  $k$  is given by

$$k = \frac{k_1}{k_2} \quad (5.93)$$

Based on the above thermal model, the objective function for the present work is defined in the next section.

### 5.3.2 Case Study, Objective Function Description, and Constraints

Four-temperature-level vapor absorption refrigeration system needs to be designed and optimized for the maximum coefficient of performance (COP). The temperature of the evaporator, generator, absorber, and condenser are 288, 393, 315, and 313 K, respectively. The ambient temperature is 290 K. The heat transfer area of the evaporator and generator is 150 and 45 m<sup>2</sup>, respectively. The irreversibility parameter associated with the generator-absorber assembly ( $I_H$ ) and condenser-evaporator assembly ( $I_R$ ) is 1.05. The heat transfer coefficient in the generator, absorber, condenser, and evaporator is 2.3, 0.4, 3.265, and 0.195 W/m<sup>2</sup> K, respectively. Four design variables such as the ratio of heat transfer surface area of absorber-generator ( $a_H$ ), the ratio of heat transfer surface area of condenser-evaporator ( $a_R$ ), hot working fluid temperature ratio ( $\chi_H$ ), and refrigerant working fluid temperature ratio ( $\chi_R$ ) are considered for the optimization problem. The upper and lower bounds of design variables are presented in Table 5.9.

As mentioned above, the maximization of the coefficient of performance of the four-temperature-level absorption refrigeration system is taken as an objective function in the present study. Furthermore, the operating parameters which result in maximum COP should also satisfy the ecological function ( $E$ ) and thermo-economic criteria ( $f$ ) constraints. So, considering all the aspects, the objective function of the four-temperature-level absorption refrigeration system is formulated as follows:

**Table 5.9** Ranges of design variables for four-temperature-level vapor absorption refrigerator optimization

Design variable	Lower bound	Upper bound
The ratio of heat transfer area of absorber-generator ( $a_H$ )	2	2000
The ratio of heat transfer area of condenser-evaporator ( $a_R$ )	0.1	0.3
Hot working fluid temperature ratio ( $\chi_H$ )	0.85	1000
Refrigerant working fluid temperature ratio ( $\chi_R$ )	0.55	1000

$$\left\{ \begin{array}{l} \text{Minimize } f(X) = \text{COP}(X) + \sum_{j=1}^n G_1(g_j(X))^2 \\ X = [x_1, x_2, x_3, \dots, x_D], \quad x_{i,\text{minimum}} \leq x_i, \leq x_{i,\text{maximum}}, \quad i = 1, 2, 3, \dots, D \\ g_j(X) \leq 0, \quad j = 1, 2, 3, \dots, n \end{array} \right. \quad (5.94)$$

where  $X$  is the vector of design variables which should be bounded between its minimum and maximum values.  $G_1$  is the penalty parameter, and entire term takes into account the effect of constraints violation. This term comes into the picture when the constraint violation takes place.  $g_j(X)$  indicates the constraints. The following constraints are considered for the absorption refrigerating system.

$$\text{Ecological function } (E) > 900 \quad (5.95)$$

$$\text{Thermo-economic criteria}(f) \geq 2.75 \quad (5.96)$$

The next section describes the results and discussion of the case study.

### 5.3.3 Results and Discussion

The considered problem of four-temperature-level vapor absorption refrigeration system is investigated using 11 different metaheuristic approaches to obtain the maximum exergetic efficiency of the refrigerator. Each algorithm is implemented 100 times on the considered problem to estimate the statistical variations of the algorithms. Each algorithm is implemented with the population size of 50, and the termination criteria are set as 100,000 function evaluations. The results obtained in 100 runs using each algorithm are presented in the form of the best solution, the worst solution, average solution standard deviation, and success rate in Table 5.10. Here, the infeasible solutions (i.e., affected by penalty) are eliminated while

obtaining the worst solution, average solution, standard deviation, and success rate. Further, the success rate of the algorithm is obtained by considering 0.1% variation from the global optimum value.

It can be observed from the comparative results that all the algorithms performed equally good and produced almost identical maximum coefficient of performance of the refrigerator. Furthermore, the average performance of all the considered algorithms is also less or more similar. However, the success rate of SCA algorithm is better while DE algorithm produces least success rate in obtaining the global optimum value. It can be observed from the results that it is difficult to judge the performance of the algorithm as all the algorithms have produced a different performance to obtain the best, worst, and average results, and success rate. So, the Friedman rank test is implemented to judge the best suitable algorithm for vapor absorption refrigerator considering the capability to obtain the best, worst, and average results, and success rate. The results of the Friedman rank test are presented in Table 5.11, and its graphical representation is given in Fig. 5.7. The results are presented in the form of Friedman value, normalized value with ‘1’ as the best performing algorithm and its rank. It can be observed from the results that SOS has obtained the first rank followed by PSO and TLBO algorithms (Fig. 5.9).

The optimized design of four-temperature-level absorption refrigeration system obtained using the SOS algorithm is presented in Table 5.12. It can be noted from the results that the absorption refrigerator with the minimum ratio of heat transfer area of absorber-generator, hot working fluid temperature ratio, and maximum ratio of heat transfer area of condenser-evaporator results in the maximum coefficient of performance of the system. The refrigerant working fluid temperature ratio produced a conflicting effect on achieving the maximum coefficient of performance of four-temperature-level absorption refrigerator. Furthermore, both the constraints are at limiting value in the optimized operating condition of absorption refrigerating system.

**Table 5.10** Comparative results of different algorithms for four-temperature-level vapor absorption refrigerator optimization

Algorithms	Best	Worst	Average	SD	Success rate (%)
GA	4.3576	4.1290	4.3337	7.20E-02	32
PSO	4.3576	4.3413	4.3544	4.89E-03	46
DE	4.3576	4.2930	4.3382	3.12E-02	28
ABC	4.3576	4.3100	4.3377	2.40E-02	56
CSA	4.3576	4.2930	4.3438	2.75E-02	44
TLBO	4.3576	4.3138	4.3383	2.22E-02	58
SOS	4.3576	4.3162	4.3432	2.02E-02	62
WWO	4.3576	4.1756	4.3079	8.29E-02	64
HTS	4.3576	4.2100	4.3160	6.75E-02	68
PVS	4.3576	4.3070	4.3374	2.53E-02	60
SCA	4.3576	4.2930	4.3386	2.90E-02	72

**Table 5.11** Friedman rank test results for four-temperature-level vapor absorption refrigerator optimization

Algorithms	Friedman value	Normalized value	Rank
GA	46.5	0.258065	11
PSO	21	0.571429	2
DE	38.5	0.311688	9
ABC	28.5	0.421053	6
CSA	26	0.461538	5
TLBO	23.5	0.510638	3
SOS	12	1	1
WWO	41.5	0.289157	10
HTS	36.5	0.328767	8
PVS	25	0.48	4
SCA	30	0.4	7

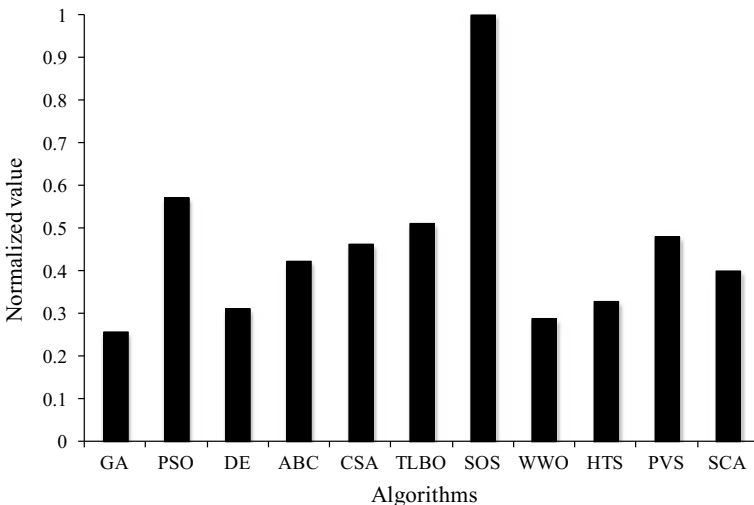


**Fig. 5.9** Graphical presentation of Friedman rank test for four- temperature-level vapor absorption refrigerator optimization

## 5.4 Cascade Refrigerator

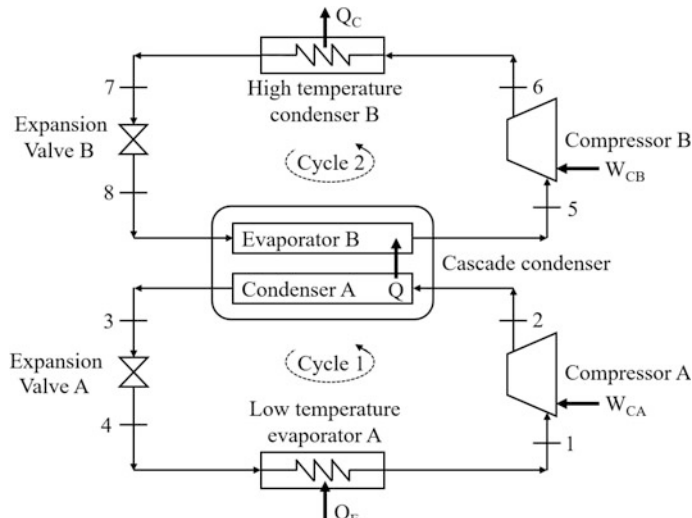
Cascade refrigeration system (CRS) is the combination of two or more vapor compression refrigeration (VCR) cycles with different refrigerants in each cycle whose boiling point and melting point temperatures are in the range of their corresponding evaporator and compressor temperature limits. In cascade refrigeration system, the individual vapor compression refrigeration circuits are clubbed at the condenser-evaporator part to take competitive advantage of the nature of heat transfer in them. In VCR circuit, the heat is removed from the condenser which

**Table 5.12** Optimized design geometry of four-temperature-level absorption refrigerator

Operating parameters	Optimized value
<i>Design variable</i>	
The ratio of heat transfer area of absorber-generator ( $a_H$ )	2
The ratio of heat transfer area of condenser-evaporator ( $a_R$ )	0.3
Hot working fluid temperature ratio ( $\chi_H$ )	0.85
Refrigerant working fluid temperature ratio ( $\chi_R$ )	0.58798
<i>Constraints</i>	
Ecological function ( $E$ ), W	900
Thermo-economic criteria ( $f$ )	2.77
<i>Objective function</i>	
Coefficient of performance	4.3576

requires the external air/ water cooling arrangement. CRS uses the heat released from the condenser of one VCR circuit to vaporize the refrigerant in the other VCR circuit; thus, the heat transfer is wisely utilized along with the lower refrigeration temperature attainable. If a single VCR circuit is to be used for low-temperature application, the work input with any compressor would be high because lesser evaporator temperature results in high suction volume at the compressor inlet.

The schematic arrangement of the two-stage cascade refrigerator is shown in Fig. 5.10. It consists of two vapor compression refrigeration system with different refrigerants in each cycle. Here the condenser A of lower stage system (cycle 1) is coupled to the evaporator B of the next higher stage system (cycle 2). Condenser A

**Fig. 5.10** Schematic arrangement of two-stage Cascade refrigerator

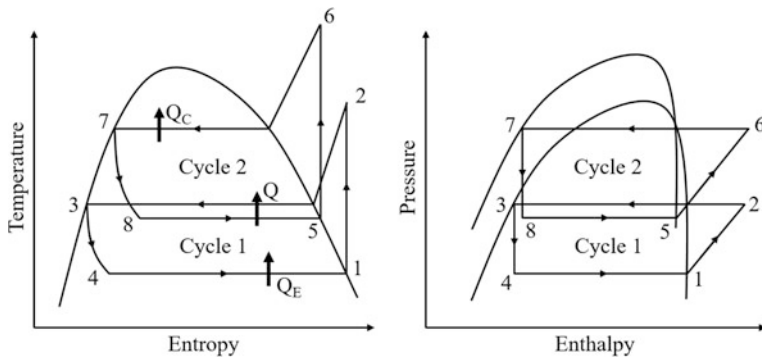


**Fig. 5.11** Thermodynamic cycle of Cascade refrigerator

and evaporator B together called as cascade condenser or simply a heat exchanger. In cycle 1 and cycle 2, all four necessary components of a single VCR cycle, i.e., compressor, condenser, expansion valve, and evaporator, are further designated with letters A and B, respectively, to differentiate them. The thermodynamic cycle of the cascade refrigerator is shown in Fig. 5.11 and explained below.

During process 1–2, isentropic compression of low-temperature refrigerant takes place in the compressor of cycle 1. The pressure and temperature of the refrigerant increased at the end of compression. The process 2–3 is a constant pressure process and takes place in cascade condenser. During process 2–3, the low-temperature vapor refrigerant of cycle 1 will get converted to liquid refrigerant by rejecting heat to evaporator B of cycle 2 at cascade condenser pressure. Ideally, the pressure and temperature of these components (combination of which is called cascade condenser) are the same. Process 3–4 is the isenthalpic expansion process. During process 3–4, the expansion of the liquid refrigerant of cycle 1 takes place in an isenthalpic manner while passing through the expansion valve. Hence, the pressure of refrigerant gets reduced from the condenser pressure to evaporator pressure in cycle 1. Process 4–1 is the constant pressure process. During this process, the low-pressure and low-temperature liquid refrigerant of cycle 1 enters into evaporator A where it extracts the heat from the space to be cool and gets converted to vapor refrigerant at evaporator pressure. And then, it again enters the compressor A and hence cycle 1 repeats. Cycle 2 performs in the same manner as that of cycle 1 with different state points (5–6–7–8–5). In this cycle, the high-temperature refrigerant extracts the heat from condenser A while passing through evaporator B. In this manner, it changes its liquid phase to the vapor phase. Also, while passing through high-temperature condenser B of cycle 2, it rejects the heat to the surrounding.

Some of the advantages associated with the cascade refrigerator are: very-high or very-low condenser and evaporator pressures, respectively, can be avoided as each cycle uses a different refrigerant; it is possible to select a pair of refrigerants that suits the best for the desired temperature range; high volumetric efficiency obtained

in each cycle; the cascade systems are used in the liquefaction of petroleum vapors; liquefaction of industrial gases that works at low temperature and low pressure; and it is also used for the dry-ice manufacturing.

Earlier, work had been reported by the researchers related to the analysis and optimization of the cascade refrigeration system. Bhattacharyya et al. (2005) presented the optimization of the cascaded system for simultaneous refrigeration and heating with CO<sub>2</sub>-based high-temperature cycle and C<sub>3</sub>H<sub>8</sub>-based low-temperature cycle. The authors presented the performance trend of the system with variation in the design parameters and operating. Further, the authors also developed the expressions for selecting suitable design parameters of the system. Bhattacharyya et al. (2007) performed a thermodynamic analysis of the endoreversible two-stage cascade cycle to obtain the optimum intermediate temperature for the maximum exergy and refrigeration effect of the CO<sub>2</sub>-C<sub>3</sub>H<sub>8</sub> cascade system. Getu and Bansal (2008) worked on the thermodynamic analysis of the cascade refrigeration system, operating at -50 °C evaporative temperature and 40 °C condensing temperatures. They found out that COP of the system was the highest for ethanol followed by R717 and the lowest for R404A for the same operating condition. Also, the highest mass flow rate of R404A was required as compared to R717 in the high-temperature circuit of the cascade system. The authors also performed the regression analysis in order to develop mathematical expressions for the maximum COP. Bhattacharyya et al. (2008) performed an analytical study on the performance of a cascade refrigeration-heat pump system based on a model incorporating both internal and external irreversibilities. The authors also suggested the optimum allocation of heat exchanger inventories in cascade refrigeration cycles for the maximization of performance and minimization of system cost.

Bhattacharyya et al. (2009) carried out thermodynamic analysis and optimization of a novel N<sub>2</sub>O-CO<sub>2</sub> cascade system for simultaneous refrigeration and heating with nitrous oxide (N<sub>2</sub>O) as the high-temperature fluid and CO<sub>2</sub> as the low-temperature fluid. The authors optimized intermediate temperature and pressure of the system to obtain the maximum COP by varying different design and operating parameters. Kilicarsalm and Hosoz (2010) performed the energy and irreversibility analysis of the cascade refrigeration system by employing various refrigerants for 1 kW refrigeration load at -40 °C refrigerated space temperature. The authors concluded that the refrigerant pair of R717-R23 has the highest COP and the lowest irreversibility while R507-R23 has the lowest COP and the highest irreversibility. Zhang and Xu (2011) presented a general methodology for the optimal synthesis of the cascade refrigeration system to maximize energy efficiency. The authors also developed an exergy-embedded MINLP model for the optimal synthesis of a general cascade refrigeration system. Rezayan and Behbahaninia (2011) carried out thermo-economic optimization and exergy analysis of CO<sub>2</sub>/NH<sub>3</sub> cascade refrigeration systems by considering the total annual cost of the system as an objective function. The authors considered condensing temperature of NH<sub>3</sub>, condensing temperature of CO<sub>2</sub>, the evaporative temperature of CO<sub>2</sub>, and temperature difference in cascade condenser as optimization variables. Colarodo et al. (2012) simulated a cascade system for simultaneous refrigeration and heating with

different working fluids. Colorado and Velazquez (2013) performed the analysis of first and second laws of cascade system with the aim of finding the best working fluid performance and appropriate operation parameters.

Aminyavari et al. (2014) carried out the multi-objective optimization of a CO<sub>2</sub>/NH<sub>3</sub> cascade refrigeration system from exergetic, economic, and environmental points of view. The authors considered minimization of the total cost and maximization of the exergetic efficiency of the system as the objective function and obtained the Pareto solution for those objectives. The decision-making methods were utilized to choose the final optimum design point from the Pareto solutions. Dokandari et al. (2014) performed the thermodynamic analysis and optimization of a novel ejector-expansion CO<sub>2</sub>/NH<sub>3</sub> cascade refrigeration cycle. The authors observed that the maximum COP and second law efficiency of the novel system are higher as compared to the conventional system. Dubey et al. (2014) performed thermodynamic analysis of propylene–carbon dioxide transcritical cascade system. The authors concluded that the transcritical cycle with CO<sub>2</sub>–propylene gives better system performance than subcritical cascade cycle. Ust and Karakurt (2014) carried out theoretical performance analysis based on the exergetic performance coefficient (EPC) criterion for cascade refrigeration with different refrigerant couples. Eini et al. (2016) performed multi-objective optimization of a cascade refrigeration system considering exergetic, economic, inherent safety level as objective functions. The authors adopted NSGA-II as an optimization tool and obtained Pareto solution between the objectives. Furthermore, the decision-making techniques were utilized to select the final optimum point. Nasruddin et al. (2016) optimized the cascade refrigeration system using C<sub>3</sub>H<sub>8</sub> refrigerant in high-temperature circuits and a mixture of C<sub>2</sub>H<sub>6</sub>/CO<sub>2</sub> in low-temperature circuits. Asgari et al. (2017) carried out parametric assessment and multi-objective optimization of an internal auto-cascade refrigeration cycle based on advanced exergy and exergoeconomic concepts. The multi-objective optimization indicated improvements in the objective functions relative to the base design point.

#### 5.4.1 Thermal Model

In the present work, a two-stage cascade refrigerator is considered for the optimization. The thermodynamic presentation of two-stage cascade refrigerator is shown in Fig. 5.9. The thermal model of the two-stage cascade refrigerator presented here is based on the previous works of Nasruddin et al. (2016) and Rezayan and Behbahaninia (2011). The state points 1–8 appear in the thermal model, see Fig. 5.9.

The cooling load to be taken by an evaporator to maintain the required cold space temperature for the plant is given by

$$\dot{Q}_L = \dot{m}_L(h_1 - h_4) \quad (5.97)$$

where  $\dot{m}_L$  is the mass flow rate of the refrigerant passing through the low-temperature evaporator.

Work input in the form of electricity to run evaporator fan ( $\dot{W}_{\text{fan,epv}}$ ) is given by

$$\dot{W}_{\text{fan,epv}} = \dot{Q}_{\text{Air,epv}} \Delta P_{\text{epv}} \quad (5.98)$$

where  $\dot{Q}_{\text{Air,epv}}$  is the volumetric flow rate of air and  $\Delta P_{\text{epv}}$  is the air pressure drop. Exergy destruction in the evaporator is calculated as follows:

$$\dot{E}x_{\text{Dest,epv}} = \left(1 - \frac{T_o}{T_{\text{cold}}}\right) \dot{Q}_L + \dot{m}_L(\varepsilon x_4 - \varepsilon x_1) + \dot{W}_{\text{fan,epv}} \quad (5.99)$$

where  $T_{\text{cold}}$  is the cold space temperature, and  $\varepsilon x$  is the rate of exergy.

Work input in the form of electricity to run a low-temperature cycle (LTC) compressor fan is given by

$$\dot{W}_{\text{LTC,com}} = \frac{\dot{m}_L(h_{2s} - h_1)}{\eta_{\text{isen}} \eta_m \eta_{\text{elec}}} = \frac{\dot{m}_L(h_2 - h_1)}{\eta_m \eta_{\text{elec}}} \quad (5.100)$$

where  $\eta_m \eta_{\text{elec}}$  is combined electrical and mechanical efficiency of the system.

Exergy destruction in LTC compressor is calculated as follows.

$$\dot{E}x_{\text{Dest,LTC,com}} = \dot{m}_L(\varepsilon x_1 - \varepsilon x_2) + \dot{W}_{\text{LTC,com}} \quad (5.101)$$

The LTC, as well as high-temperature cycle (HTC) expansion valves, has been assumed to be isenthalpic.

$$h_3 = h_4 \quad (5.102)$$

$$h_7 = h_8 \quad (5.103)$$

The exergy destruction in LTC and HTC expansion valves, respectively, are given by

$$\dot{E}x_{\text{Dest,LTC,Exp}} = \dot{m}_L(\varepsilon x_3 - \varepsilon x_4) \quad (5.104)$$

$$\dot{E}x_{\text{Dest,HTC,exp}} = \dot{m}_H(\varepsilon x_7 - \varepsilon x_8) \quad (5.105)$$

The heat exchange in cascade condenser by the refrigerants of two circuits is assumed to take place without losses and is calculated as follows.

$$\dot{Q}_M = \dot{m}_H(h_5 - h_8) = \dot{m}_L(h_2 - h_3) \quad (5.106)$$

The exergy destruction associated with cascade condenser is given by

$$\dot{Ex}_{Dest,cas,cond} = \dot{m}_L(ex_2 - ex_3) + \dot{m}_H(ex_8 - ex_5) \quad (5.107)$$

The heat duty of condenser is given by

$$\dot{Q}_H = \dot{m}_H(h_7 - h_6) \quad (5.108)$$

Work input to condenser fan in the form of electricity is given by

$$\dot{W}_{fan,cond} = \dot{Q}_{Air,cond} \Delta P_{cond} \quad (5.109)$$

Exergy destruction in the condenser is calculated as follows.

$$\dot{Ex}_{Dest,cond} = \left(1 - \frac{T_0}{T_c}\right) \dot{Q}_H + \dot{m}_H(ex_6 - ex_7) + \dot{W}_{fan,cond} \quad (5.110)$$

Work input in the form of electricity to run HTC compressor fan is given by

$$\dot{W}_{HTC,comp} = \frac{\dot{m}_H(h_{6s} - h_s)}{\eta_{isen} \eta_m \eta_{elec}} = \frac{\dot{m}_H(h_6 - h_5)}{\eta_m \eta_{elec}} \quad (5.111)$$

Exergy destruction in LTC compressor is calculated as follows.

$$\dot{Ex}_{Dest,HTC,com} = \dot{m}_H(ex_5 - ex_6) + \dot{W}_{HTC,com} \quad (5.112)$$

The isentropic efficiencies of the compressors are found using the following expressions:

For HTC compressor:

$$\eta_{isen} = 0.83955 - 0.01026R_p - 0.00097R_p^2 \quad (5.113)$$

For LTC compressor:

$$\eta_{isen} = 0.89810 - 0.09238R_p + 0.00476R_p^2 \quad (5.114)$$

The total exergy input to the system in the form of power consumed by compressors and fans is equal to

$$\dot{Ex}_{in} = \dot{W}_{HTC,com} + \dot{W}_{LTC,com} + \dot{W}_{fan,cond} + \dot{W}_{fan,epv} \quad (5.115)$$

Similarly, the total exergy output of system/ product exergy is the summation of exergy output of individual components:

$$\dot{Ex}_{out} = \left( \frac{T_o}{T_{cold}} - 1 \right) \dot{Q}_L \quad (5.116)$$

The total exergy destruction of the cascade system and the second law efficiency can be calculated by

$$\begin{aligned} \dot{Ex}_{Dest,tot} &= \dot{Ex}_{in} - \dot{Ex}_{out} \\ &= \dot{Ex}_{Dest,epv} + \dot{Ex}_{Dest,LTC,com} + \dot{Ex}_{Dest,LTC,Exp} + \dot{Ex}_{Dest,HTC,exp} \\ &\quad + \dot{Ex}_{Dest,cas,cond} + \dot{Ex}_{Dest,cond} + \dot{Ex}_{Dest,HTC,com} \end{aligned} \quad (5.117)$$

$$\begin{aligned} \dot{Ex}_{Dest,tot} &= \dot{Ex}_{in} - \dot{Ex}_{out} \\ &= \dot{Ex}_{Dest,epv} + \dot{Ex}_{Dest,LTC,com} + \dot{Ex}_{Dest,LTC,Exp} + \dot{Ex}_{Dest,HTC,exp} \\ &\quad + \dot{Ex}_{Dest,cas,cond} + \dot{Ex}_{Dest,cond} + \dot{Ex}_{Dest,HTC,com} \end{aligned} \quad (5.118)$$

$$\eta = 1 - \frac{\dot{Ex}_{Dest,tot}}{\dot{Ex}_{in}} \quad (5.119)$$

The total cost of the system over a definite time interval can be given as follows:

$$C_{total} = \sum c_i \dot{Ex}_{in} + \sum_m z_m = \sum c_o \dot{Ex}_{out} \quad (5.120)$$

where  $c_i$  represents the cost of input exergy which is essentially the electricity cost.  $z_m$  is the capital cost of each equipment.  $c_o$  is the cost of product exergy.

The capital cost/equipment cost of each component is given by

$$C_{HTC,com} = 9624.2 W_H^{0.46} \quad (5.121)$$

$$C_{LTC,com} = 10167.5 W_L^{0.46} \quad (5.122)$$

$$C_{cond} = 1397 A_{o,cond}^{0.89} + 629.05 W_{fan,cond}^{0.76} \quad (5.123)$$

$$C_{epv} = 1397 A_{o,epv}^{0.89} + 629.05 W_{fan,epv}^{0.76} \quad (5.124)$$

$$C_{cas,cond} = 2382.9 A_{o,cas,cond}^{0.68} \quad (5.125)$$

Generally, engineering economic analysis is carried out to assess the total annual cost of the system in order to recover the investment over a period of years. For the same, the capital recovery factor (CRF) is calculated as follows:

$$\text{CRF} = \frac{i(1+i)^n}{(1+i)^n - 1} \quad (5.126)$$

where  $i$  is the annual interest rate, and  $n$  is the number of years of operation. Finally, using all the above costs, the annual cost of the system can be approximated as the follows:

$$\begin{aligned} C_{\text{total}} = & [C_{\text{HTC,com}} + C_{\text{LTC,com}} + C_{\text{cond}} + C_{\text{evp}} + C_{\text{cas,cond}}] \cdot \text{CRF} \\ & + C_{\text{el}} \cdot H [\dot{W}_{\text{HTC,com}} + \dot{W}_{\text{LTC,com}} + \dot{W}_{\text{fan,cond}} + \dot{W}_{\text{fan,evp}}] \end{aligned} \quad (5.127)$$

Based on the above thermal model, the objective function for the present work is defined in the next section.

#### 5.4.2 Case Study, Objective Function Description, and Constraints

A two-stage cascade refrigeration system needs to be designed and optimized for minimum exergy destruction ( $\dot{\text{Ex}}_{\text{Dest,tot}}$ ). The temperature of the evaporator required to maintain the cascade system is 228 K. The amount of refrigeration effect required is 50 kW. The high-temperature cycle operates with NH<sub>3</sub> refrigerant while low-temperature cycle operates with CO<sub>2</sub> refrigerant. Air velocity on condenser and evaporator side is 10.3 and 13.5 m/s, respectively. The specification of high-temperature cycle condenser and low-temperature cycle evaporator are presented in Table 5.13. The specification of cascade condenser is presented in Table 5.14. Three design variables such as high-temperature cycle condenser temperature ( $T_C$ ), low-temperature cycle condenser temperature ( $T_{mc}$ ), and cascade condenser temperature difference ( $\Delta T$ ) are considered for the optimization problem.

**Table 5.13** Specification of condenser and evaporator of cascade refrigerator

Specification	Condenser	Evaporator
Lateral pitch (mm)	57	57
Longitudinal pitch (mm)	49.7	49.7
Length of the pass (mm)	1000	350
The outer diameter of the tube (mm)	12.7	15.9
Tube thickness (mm)	0.889	0.889
Number of tube rows	6	6
Number of fins per 1000 mm	300	200
Fin thickness (mm)	0.25	0.25
The thermal conductivity of tube (W/m K)	52	389

**Table 5.14** Specification of cascade condenser

Specification	Value
The outer diameter of the tube (mm)	25
Tube thickness (mm)	1.65
Number of tubes	16
Number of passes	2
Shell diameter (mm)	200
Baffle spacing (mm)	350
Square pitch (mm)	25.4
The thermal conductivity of tube (W/m K)	52

**Table 5.15** Ranges of design variables and economic parameters for cascade refrigerator optimization

Design variable	Lower bound	Upper bound
High-temperature cycle condenser temperature ( $T_C$ )	303	343
Low-temperature cycle condenser temperature ( $T_{mc}$ )	260	275
Cascade condenser temperature difference ( $\Delta T$ )	275	285
<i>Economic Parameters</i>		
Operating period ( $n$ )	15 years	
Period of operation per year ( $H$ )	6570 h	
Annual interest rate	8%	
Electricity cost	0.07 \$/kWh	

The upper and lower bounds of design variables along with economic parameters are presented in Table 5.15.

As mentioned above, minimization of exergy destruction of the cascade refrigerator is taken as an objective function in the present study. Furthermore, the operating parameters which result in the minimum exergy destruction should also satisfy the total cost ( $C_{total}$ ) constraint. So, considering all the aspects, the objective function of the two-stage cascade refrigeration system is formulated as the follows:

$$\begin{cases} \text{Minimize } f(X) = \dot{E}x_{\text{Dest,tot}}(X) + \sum_{j=1}^n G_1(g_j(X))^2 \\ X = [x_1, x_2, x_3, \dots, x_D], \quad x_{i,\text{minimum}} \leq x_i, \leq x_{i,\text{maximum}}, \quad i = 1, 2, 3, \dots, D \\ g_j(X) \leq 0, \quad j = 1, 2, 3, \dots, n \end{cases} \quad (5.128)$$

where  $X$  is the vector of design variables which should be bounded between its minimum and maximum values.  $G_1$  is the penalty parameter, and entire term takes into account the effect of constraints violation. This term comes into the picture

when constraint violation takes place.  $g_j(X)$  indicates the constraints. The following constraint is considered for the two-stage cascade refrigeration system.

$$\text{Total cost}(C_{\text{total}}) \leq 160,000\$ \quad (5.129)$$

The next section describes the results and discussion of the case study.

### 5.4.3 Results and Discussion

The considered problem of two-stage cascade refrigerator is investigated using 11 different metaheuristic approaches to obtain the minimum exergy destruction of the system. Each algorithm is implemented 100 times on the considered problem to estimate the statistical variations of the algorithms. Each algorithm is implemented with the population size of 50, and the termination criteria are set as 100,000 function evaluations. The results obtained using each algorithm are presented in the form of the best solution, worst solution, average solution standard deviation, and success rate over 100 runs in Table 5.16. Here, the infeasible solutions (i.e., affected by penalty) are eliminated while obtaining the worst solution, average solution, standard deviation, and success rate. Furthermore, the success rate of the algorithm is obtained by considering 0.1% variation from the global optimum value.

It can be observed from the comparative results that all the algorithms performed equally good and produced almost identical minimum exergy destruction of the cascade refrigeration system. Furthermore, the average performance of GA and SOS are almost similar and better compared to other algorithms. However, the success rate of the genetic algorithm is better while SCA produces the least success rate in obtaining the global optimum value. It can be observed from the results that it is difficult to judge the performance of the algorithm as all the algorithms have produced a different performance to obtain the best, worst, and average results, and success rate. So, the Friedman rank test is implemented to judge the best suitable algorithm for two-stage cascade refrigerator considering the capability to obtain the best, worst, and average results, and success rate. The results of the Friedman rank test are presented in Table 5.17, and its graphical representation is given in Fig. 5.10. The results are presented in the form of Friedman value, normalized value with '1' as the best performing algorithm and its rank. It can be observed from the results that GA obtained the first rank followed by DE and SOS algorithms.

The optimized design of two-stage cascade refrigerator obtained using the GA is presented in Table 5.18. It can be noted from the results that the two-stage cascade refrigerator with the minimum high-temperature cycle condenser temperature, low-temperature cycle condenser temperature, and cascade condenser temperature difference results in the minimum exergy destruction rate of the system. Furthermore, the total cost constraint is at the limiting value in the optimized operating condition of the cascade refrigerating system (Fig. 5.12).

**Table 5.16** Comparative results of different algorithms for cascade refrigerator optimization

Algorithms	Best	Worst	Average	SD	Success rate (%)
GA	31.9824	32.9873	32.1457	2.57E-01	60
PSO	31.9824	33.1341	32.2771	4.01E-01	42
DE	31.9824	32.9724	32.1798	2.97E-01	56
ABC	31.9824	32.8758	32.2577	3.39E-01	48
CSA	31.9824	32.9384	32.2870	3.35E-01	44
TLBO	31.9824	32.9800	32.1837	2.78E-01	44
SOS	31.9824	32.9898	32.1304	2.57E-01	48
WWO	31.9824	32.9898	32.2226	3.46E-01	45
HTS	31.9824	33.1341	32.4122	4.69E-01	43
PVS	31.9824	32.9989	32.3146	3.77E-01	40
SCA	31.9824	32.9841	32.3273	3.61E-01	32

**Table 5.17** Friedman rank test results for Cascade refrigerator optimization

Algorithms	Friedman value	Normalized value	Rank
GA	17	1	1
PSO	42.5	0.4	9
DE	18	0.944444	2
ABC	22.5	0.755556	4
CSA	27.5	0.618182	6
TLBO	23.5	0.723404	5
SOS	19	0.894737	3
WWO	30.5	0.557377	7
HTS	46.5	0.365591	11
PVS	43	0.395349	10
SCA	40	0.425	8

**Table 5.18** The optimized operating condition of two-stage cascade refrigerator

Operating parameters	Optimized value
<i>Design variable</i>	
High temperature cycle condenser temperature ( $T_C$ ), K	309.12
Low temperature cycle condenser temperature ( $T_{mc}$ ), K	260
Cascade condenser temperature difference ( $\Delta T$ ), K	2
<i>Constraints</i>	
Total cost ( $C_{total}$ ), \$	159512.9
<i>Objective function</i>	
Exergy destruction ( $\dot{E}x_{Dest,tot}$ ), kW	31.9824

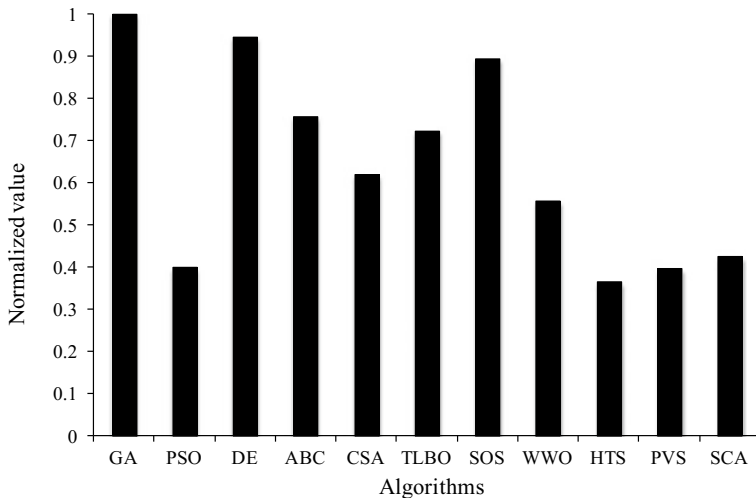


Fig. 5.12 Graphical presentation of Friedman rank test for cascade refrigerator optimization

## 5.5 Ejector Refrigerator

Ejector refrigeration system is one of the oldest methods for producing refrigeration with the help of steam and water. Nowadays, such a cycle is used to harness solar heat or other low-grade heat sources and employ various refrigerants instead of water or steam. The schematic arrangement of the ejector refrigerator is shown in Fig. 5.13, and its corresponding thermodynamic presentation is given in Fig. 5.14.

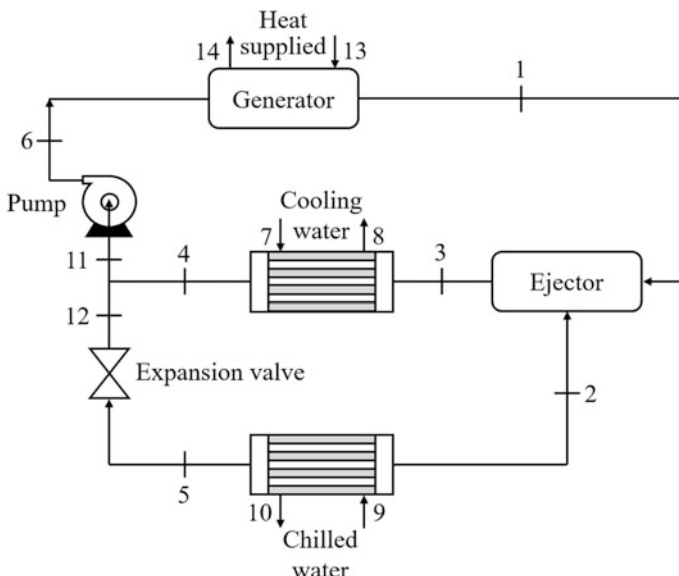
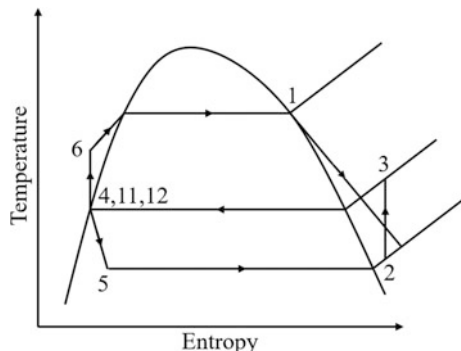


Fig. 5.13 Schematic arrangement of the ejector refrigerator

**Fig. 5.14** Thermodynamic cycle of the ejector refrigerator



It can be observed from Fig. 5.13 that the system consists of a generator, a condenser, an evaporator, an ejector, a pump, and an expansion valve. The waste heat/solar heat or other available heat supplied to the generator will generate the high-pressure vapor refrigerant in the generator. This vapor is known as primary fluid. The refrigerant exits the generator as a saturated vapor at high pressure before entering the primary nozzle of the ejector. The primary fluid is accelerated while passing through the primary nozzle. The supersonic jet stream of the primary fluid is produced within the mixing chamber. A very low-pressure region at the mixing chamber is obtained as a consequence. This low-pressure region can draw secondary fluid from the evaporator (where the refrigeration effect is produced) into the mixing chamber. The primary fluid and the secondary fluid then mix within the mixing chamber. Due to the high momentum of the primary fluid, the mixed stream is still in the form of the supersonic flow. At the end of the throat section, due to the large difference in pressure between the mixed stream and back pressure (condenser pressure), the series of oblique shocks are thought to be induced. The shock causes a major compression effect to occur and flow is suddenly changed from supersonic to subsonic. Furthermore, the compression of the flow is achieved as it is brought to stagnation through a subsonic diffuser. The ejector is discharged at the pressure (back pressure) equal to the saturation pressure in the condenser. The subsonic flow is discharged to the condenser where it is condensed to liquid. The condensed liquid is then divided into two streams: one part flows to the pump and the other passes to the expansion valve. The former is pressurized before being vaporized in the generator, and the latter is throttled before being vaporized in the evaporator to provide cooling.

The ejector is an essential component of the ejector refrigerator. A schematic diagram of the ejector is shown in Fig. 5.15. A typical ejector consists of a motive nozzle, a suction chamber, a mixing section, and a diffuser. The working principle of the ejector is based on converting internal energy and pressure related flow work contained in the motive fluid stream into kinetic energy. The motive nozzle is typically of a converging-diverging design. This allows the high-speed jet exiting the nozzle to become supersonic.

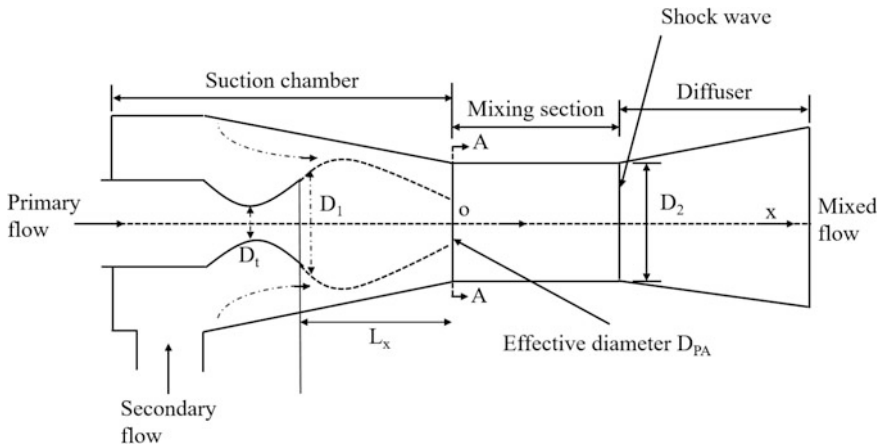


**Fig. 5.15** Schematic diagram of an ejector

Earlier, work had been reported by the researchers related to the analysis and optimization of ejector refrigerating system. Cizungu et al. (2005) carried out the modeling and optimization of two-phase ejectors for cooling systems considering NH<sub>3</sub> and NH<sub>3</sub>-H<sub>2</sub>O as a working fluids and compared the optimization results with available experimental results. Sarkar (2008) presented optimum parameter correlations, using constant area mixing model for ejector-expansion transcritical CO<sub>2</sub> heat pump cycle. The author also studied the energetic and exergetic performance of the heat pump cycle for simultaneous cooling and heating applications. Yapıcı et al. (2008) carried out the experimental performance optimization of the ejector refrigeration system by using six configurations of ejector and R-123 as working fluid. Furthermore, the authors studied the effect of the ejector area ratio on the performance parameter of the system. Dai et al. (2009) performed the exergetic optimization of a novel combined power and ejector refrigeration cycle considering the maximization of exergetic efficiency as the objective function and applied genetic algorithm as an optimization tool. The authors also conducted the parametric analysis to evaluate the effects of the key thermodynamic parameters on the performance of the combined cycle. Guo and Shen (2009) investigated the performance of a solar-driven ejector refrigeration system using R134a as a working fluid.

Yari (2009) presented two-stage ejector-expansion transcritical CO<sub>2</sub> refrigeration cycle which uses an internal heat exchanger and intercooler to enhance the performance of the cycle. The author carried out the theoretical analysis on the performance characteristics for the proposed cycle based on the first and second laws of thermodynamics and observed better second law efficiency of the proposed cycle as compared to the conventional two-stage transcritical CO<sub>2</sub> cycle. Yen et al. (2013) analysed the performance of the variable throat ejector solar refrigeration system using CFD simulations. They concluded that the ejector with a greater throat area and larger solar collector allows a wider operating range of generator temperatures,

but may be overdesigned and expensive. Conversely, decreasing the throat area limits the operating range of generator temperatures. Thus, the ejector with a fixed throat area may be unsuitable to use solar energy as a heat source. Sadeghi et al. (2015) carried out the multi-objective optimization of the ejector refrigeration cycle powered by an internal combustion engine using the genetic algorithm. The authors considered the maximization of exergy efficiency and minimization of product cost as an objective function and obtained the optimum value of design variables such as generator, condenser, and evaporator temperatures.

Sadeghi et al. (2017) carried out the thermodynamic analysis and optimization of a novel combined power and ejector refrigeration cycle-desalination system using a zeotropic mixture as working fluid. A parametric study is performed to specify the decision variables influencing the system performance. Furthermore, the optimization is conducted in two cases. In the first case, a single-objective optimization is carried out to maximize the overall exergy efficiency. In the second case, a multi-objective optimization is accomplished considering the net output power and refrigeration capacity as the objective functions. Rashidi et al. (2017) performed the thermodynamic analysis of the ejector refrigeration cycle to identify the effect of generator pressure and temperature difference on the cycle parameters such as COP, heat transfer in generator and condenser. The authors used the artificial neural network to find out the effects of generator pressure and temperature difference as a function for cycles parameters and adapted GA and PSO algorithms for finding the maximum cycle parameters. Allouche et al. (2017) developed a dynamic model to investigate the performance of an integrated solar-driven ejector based air-conditioning system combined with a phase-change material cold storage. Jeon et al. (2017) investigated the effects of ejector geometries on the performance of a two-phase ejector refrigeration cycle. They reported that for the optimized value of mixing section diameter, the maximum COP of the system is improved compared to the basic cycle.

### 5.5.1 Thermal Model

In the present work, the ejector refrigerator is considered for the optimization. The thermodynamic presentation of two-stage cascade refrigerator is shown in Fig. 5.14. The thermal model of the ejector refrigerator presented here is based on the previous work of Sadeghi et al. (2015). The state points 1–12 appear in the thermal model, see Fig. 5.14.

Primary mass flow rate at the throat section for choking condition is given by

$$m_p = P_p A_t \sqrt{\left(\frac{2}{1+\gamma}\right)^{\frac{\gamma+1}{\gamma-1}} \left(\frac{\gamma m_p}{R_g T_p}\right)} \quad (5.130)$$

where  $n_p$  is the isentropic efficiency of the compressible flow in the nozzle,  $P_p$  is the inlet pressure of the primary flow, and  $T_p$  is the inlet temperature of the primary flow.

For a particular geometry of the primary nozzle, Mach number at the exit can be obtained as follows:

$$\left(\frac{D_s}{D_t}\right)^2 = \left[\frac{2 + (\gamma - 1)M_1^2}{2 + (\gamma + 1)}\right]^{\frac{(\gamma+1)}{2(\gamma-1)}} \left(\frac{1}{M_1}\right) \quad (5.131)$$

where  $D_1$  is the diameter of the exit section,  $D_t$  is the diameter of the throat section, and  $M_1$  is the Mach number and correlated by the following equations:

$$\frac{T_p}{T_1} = 1 + \frac{1}{2}(\gamma - 1)M_1^2 \quad (5.132)$$

$$V_1 = M_1 \sqrt{R_g * T_1 * \gamma} \quad (5.133)$$

where  $T_1$  is the temperature at exit and  $V_1$  is the exit velocity.

Based on the assumption that the outlet pressure of the primary nozzle is equal to the inlet pressure of the secondary nozzle, primary flow Mach number and its properties at effective area are given by

$$\frac{p_p}{p_s} = \left[1 + \frac{1}{2}(\gamma - 1)M_{pA}^2\right]^{\frac{\gamma}{\gamma-1}} \quad (5.134)$$

$$\frac{T_p}{T_{pA}} = 1 + \frac{1}{2}(\gamma - 1)M_{pA}^2 \quad (5.135)$$

$$V_{pA} = M_{pA} \sqrt{\gamma R_g T_{pA}} \quad (5.136)$$

$$\left(\frac{D'_{pA}}{D_1}\right)^2 = \left[\frac{2 + (\gamma - 1)M_{pA}^2}{2 + (\gamma + 1)M_1^2}\right]^{\frac{(\gamma+1)}{2(\gamma-1)}} \left(\frac{M_1}{M_{pA}}\right) \quad (5.137)$$

where  $T_{pA}$  is the temperature of the primary mass flow at section A-A (as shown in Fig. 5.15),  $V_{pA}$  is the velocity of the primary mass flow at section A-A, and  $M_{pA}$  is the Mach number of the primary mass flow at section A-A.

For isentropic expansion process, the effective diameter of the primary flow at the constant area  $D_{pA}$  can be estimated as follows.

$$D_{pA} = \left(\frac{D'_{pA}}{\sqrt{n_p n_s}}\right) \quad (5.138)$$

where  $n_p$  is the isentropic coefficient of primary flow, and  $n_s$  is the isentropic coefficient of secondary flow.

The velocity profile in the radial direction ( $V_r$ ) is estimated by an exponential function as follows:

$$V_r = V_{pA} \left( 1 - \frac{r}{R_2} \right)^{\frac{1}{n}} \quad (5.139)$$

where  $V_{pA}$  is the primary flow velocity at section A-A.

The value of exponent ' $n$ ' can be obtained using the following equation.

$$n = \frac{\ln\left(1 - \frac{r}{R_2}\right)}{\ln\left(\frac{V_r}{V_{pA}}\right)} \quad (5.140)$$

The mean velocity ( $\tilde{V}_{sA}$ ) and mass flow rate ( $m_s$ ) of the entrained flow at section A-A is obtained by the following two equations, respectively:

$$\tilde{V}_{sA} = \frac{\int_{R_{pA}}^{R_2} 2\pi r V_r dr}{\pi(R_2^2 - R_{pA}^2)} \quad (5.141)$$

$$m_s = \int_{R_{pA}}^{R_2} \rho_r V_r dA \quad (5.142)$$

The entrained flow pressure and temperature are uniformly distributed in the  $r$  direction so based on that, we can have following equations.

$$\begin{aligned} \tilde{V}_{sA} &= \frac{2V_{pA}}{(R_2^2 - R_{pA}^2)} \int_{R_{pA}}^{R_2} \left( \frac{R_2}{R_{pA}} r \left( 1 - \frac{r}{R_2} \right)^{\frac{1}{n}} \right) dr \\ &= \frac{2V_{pA}}{(R_2^2 - R_{pA}^2)} \left[ \frac{nR_2^2}{n+1} \left( 1 - \frac{R_{pA}}{R_2} \right)^{\frac{n+1}{n}} - \frac{nR_2^2}{2n+1} \left( 1 - \frac{R_{pA}}{R_2} \right)^{\frac{2n+1}{n}} \right] \end{aligned} \quad (5.143)$$

$$\begin{aligned} m_s &= \frac{2\pi V_{pA} P_{sA}}{RT_{sA}} \int_{R_{pA}}^{R_2} \left( \frac{R_2}{R_{pA}} r \left( 1 - \frac{r}{R_2} \right)^{\frac{1}{n}} \right) dr \\ &= \frac{2\pi V_{pA} P_{sA}}{RT_{sA}} \left[ \frac{nR_2^2}{n+1} \left( 1 - \frac{R_{pA}}{R_2} \right)^{\frac{n+1}{n}} - \frac{nR_2^2}{2n+1} \left( 1 - \frac{R_{pA}}{R_2} \right)^{\frac{2n+1}{n}} \right] \end{aligned} \quad (5.144)$$

The energy conservation for the flows from the ejector inlets to the effective area section can be written as follows:

$$m_p c_p T_p + \dot{m}_s c_p T_s = m_p \left( c_p T_{pA} + \frac{1}{2} V_{pA}^2 \right) + \dot{m}_s \left( c_p T_{sA} + \frac{1}{2} V_{sA}^2 \right) + \dot{E}_{\text{loss}} \quad (5.145)$$

where  $\dot{E}_{\text{loss}}$  is the energy loss and can be calculated as follows

$$\dot{E}_{\text{loss}} = \frac{1}{2} (1 - n_p) m_p V_1^2 + \frac{1}{2} (1 - n_p) m_s V_{sA}^2 + \frac{1}{2} (1 - \sqrt{n_p n_s}) m_p V_{sA}^2 \quad (5.146)$$

The velocity and temperature of the mixed flow can be estimated as follows:

$$V_m = \frac{(m_p V_{pA} + m_s V_{sA})}{(m_p + m_s)} \quad (5.147)$$

$$T_m = \frac{\dot{m}_p \left( c_p T_{pA} + \frac{V_{pA}^2}{2} \right) + \dot{m}_s \left( c_p T_{sA} + \frac{V_{sA}^2}{2} \right) - (\dot{m}_p + \dot{m}_s) \left( \frac{V_m^2}{2} \right)}{(\dot{m}_p + \dot{m}_s) C_p} \quad (5.148)$$

The Mach number and enthalpy of the mixed flow can be calculated as follows:

$$M_m = \frac{V_m}{\sqrt{\gamma R_g T_m}} \quad (5.149)$$

$$h_m = C_p T_m \quad (5.150)$$

The mixed flow pressure and Mach number, after the shock, can be calculated as

$$\frac{P_2}{P_m} = 1 + \frac{2\gamma}{\gamma+1} (M_m^2 - 1) \quad (5.151)$$

$$M_2 = \sqrt{\frac{1 + \left(\frac{\gamma-1}{2}\right) M_m^2}{\gamma M_m^2 - \frac{\gamma-1}{2}}} \quad (5.152)$$

where  $P_2$  is the exit pressure,  $P_m$  is the mixed flow pressure, and  $M_m$  is the mach number of mixed flow.

The following equations can calculate the mixed flow pressure and temperature at the diffuser exit:

$$\frac{P_{c2}}{P_2} = \left( 1 + \left( \frac{\gamma-1}{2} \right) M_2^2 \right)^{\frac{\gamma}{\gamma-1}} \quad (5.153)$$

$$n_d = \frac{T_2 - T_{cs}}{T_2 - T_{cond}} \quad (5.154)$$

where  $P_2$  is the exit pressure,  $M_2$  is the exit Mach number, and  $n_d$  is the diffuser efficiency.

The energy balance for a system component can be expressed as follows

$$Q_{dot} - W_{dot} = \sum_i m_i h_i - \sum_e m_e h_e \quad (5.155)$$

where  $Q_{dot}$  is the heat transfer rate,  $W_{dot}$  is the work transfer rate, and  $h$  is the enthalpy.

The exergy flow rate of a stream at a given state is given as

$$E_i = m_i(h_i - h_o) - T_o(s - s_o) \quad (5.156)$$

The exergy rate balance for a control volume at steady state can be written as

$$\dot{E}_i = \dot{E}_P + \dot{E}_D + \dot{E}_L \quad (5.157)$$

where  $\dot{E}_i$  is the exergy flow rate of the fuel,  $\dot{E}_P$  is the exergy flow rate of the product,  $\dot{E}_D$  is the exergy flow rate of the destruction, and  $\dot{E}_L$  is the exergy flow rate of the losses

The exergy efficiency of the system is given by

$$\varepsilon = \frac{E_{10} - E_9}{E_{13} - E_{14} + W_{dotm}} \quad (5.158)$$

where  $E_9$  and  $E_{10}$  are exergy flow rates of the outlet product while  $E_{13}$  and  $E_{14}$  are the exergy flow rates of input product.  $W_{dotm}$  is the motor work.

The coefficient of performance of the considered system can be given by

$$COP = \frac{Q_e}{Q_g + W_{dotm}} \quad (5.159)$$

where  $Q_e$  is the heat absorbed in the evaporator and  $Q_g$  is the heat supplied to the generator.

Based on the above thermal model, the objective function for the present work is defined in the next section.

### 5.5.2 Case Study, Objective Function Description, and Constraints

The ejector refrigerator working with R141b refrigerant needs to be designed and optimized for the maximum coefficient of performance (COP). The heat is supplied to the generator at 1 bar. An ejector with effective diameter 15.9 mm is used in the refrigerator. The throat diameter is 9.35 mm. The isentropic efficiency of primary and secondary flow is 0.85 and 0.95, respectively. The diffuser efficiency is 0.9. The ambient temperature and pressure are 298 K and 1 bar pressure. Three design variables, such as the temperature of the evaporator ( $T_{eva}$ ), the temperature of the generator ( $T_{gen}$ ), and temperature of the condenser ( $T_{con}$ ), are considered for the optimization problem. The upper and lower bounds of design variables are presented in Table 5.19.

As mentioned above, the maximization of the coefficient of the performance of the ejector refrigeration system is taken as an objective function in the present study. Furthermore, the operating parameters which result in maximum COP should also satisfy the exergetic efficiency constraint. So, considering all the aspects, the objective function of the ejector refrigeration system is formulated as follows:

$$\begin{cases} \text{Minimize } f(X) = \text{COP}(X) + \sum_{j=1}^n G_1(g_j(X))^2 \\ X = [x_1, x_2, x_3, \dots, x_D], \quad x_{i,\text{minimum}} \leq x_i, \leq x_{i,\text{maximum}}, \quad i = 1, 2, 3, \dots, D \\ g_j(X) \leq 0, \quad j = 1, 2, 3, \dots, n \end{cases} \quad (5.160)$$

where  $X$  is the vector of design variables which should be bounded between its minimum and maximum values.  $G_1$  is the penalty parameter, and entire term takes into account the effect of constraints violation. This term comes into the picture when the constraint violation takes place.  $g_j(X)$  indicates the constraints. The following constraint is considered for the ejector refrigeration system.

$$\text{Exergetic efficiency}(\eta_{\text{ex}}) > 4\% \quad (5.161)$$

The next section describes the results and discussion of the case study.

**Table 5.19** Ranges of design variables for the ejector refrigerator optimization

Design variable	Lower bound	Upper bound
Temperature of the evaporator ( $T_{eva}$ )	271	285
Temperature of the generator ( $T_{gen}$ )	348	368
Temperature of the condenser ( $T_{con}$ )	306	313

### 5.5.3 Results and Discussion

The considered problem of the ejector refrigeration system is investigated using 11 different metaheuristic approaches to obtain the maximum exergetic efficiency of the refrigerator. Each algorithm is implemented 100 times on the considered problem to estimate the statistical variations of the algorithms. Each algorithm is implemented with the population size of 50, and the termination criteria are set as 100,000 function evaluations. The results obtained using each algorithm are presented in the form of the best solution, worst solution, average solution standard deviation, and success rate over 100 runs in Table 5.20. Here, the infeasible solutions (i.e., affected by penalty) are eliminated while obtaining the worst solution, average solution, standard deviation, and success rate. Furthermore, the success rate of the algorithm is obtained by considering 0.1% variation from the global optimum value.

It can be observed from the comparative results that all the algorithms performed equally good and produced almost identical maximum coefficient of performance of the ejector refrigerator. Furthermore, the average performance of TLBO algorithm in producing the maximum value of the objective function is better as compared to other competitive algorithms. Moreover, the success rate of TLBO algorithm is better while the SCA algorithm produces the least success rate in obtaining the global optimum value. It can be observed from the results that it is difficult to judge the performance of the algorithm as all the algorithms have produced a different performance to obtain the best, worst, and average results, and success rate. So, the Friedman rank test is implemented to judge the best suitable algorithm for the ejector refrigerator considering the capability to obtain the best, worst, and average results, and success rate. The results of the Friedman rank test are presented in Table 5.21, and its graphical representation is given in Fig. 5.16. The results are presented in the form of Friedman value, normalized value with ‘1’ as the best

**Table 5.20** Comparative results of different algorithms for the ejector refrigerator optimization

Algorithms	Best	Worst	Average	SD	Success rate (%)
GA	0.5182	0.4811	0.5058	1.29E-02	43
PSO	0.5182	0.4803	0.5036	1.43E-02	42
DE	0.5182	0.4814	0.5089	1.12E-02	56
ABC	0.5182	0.4782	0.5051	1.48E-02	48
CSA	0.5182	0.4824	0.5075	1.21E-02	44
TLBO	0.5182	0.4819	0.5110	1.10E-02	60
SOS	0.5182	0.4822	0.5067	1.38E-02	48
WWO	0.5182	0.4788	0.5045	1.52E-02	45
HTS	0.5182	0.4793	0.5097	1.22E-02	44
PVS	0.5182	0.4824	0.5087	1.16E-02	40
SCA	0.5182	0.4793	0.5091	1.30E-02	32

**Table 5.21** Friedman rank test results for the ejector refrigerator optimization

Algorithms	Friedman value	Normalized value	Rank
GA	34	0.382353	7
PSO	42	0.309524	10
DE	19	0.684211	2
ABC	39.5	0.329114	9
CSA	23.5	0.553191	3
TLBO	13	1	1
SOS	27.5	0.472727	5
WWO	42	0.309524	10
HTS	28.5	0.45614	6
PVS	26	0.5	4
SCA	35	0.371429	8

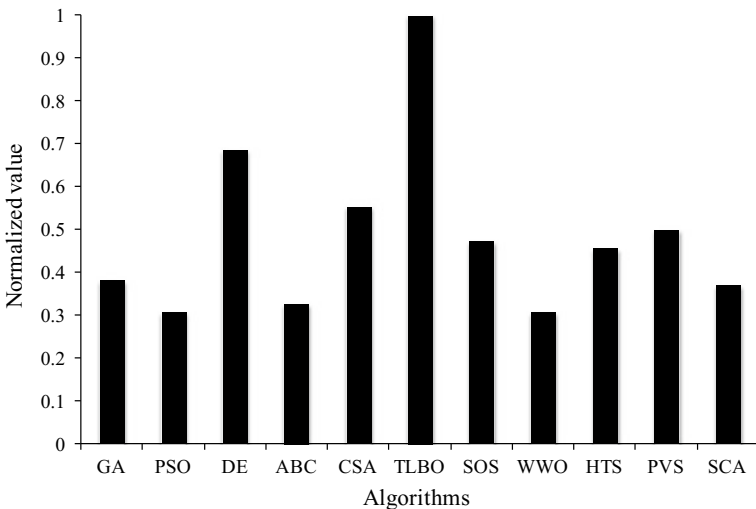


**Fig. 5.16** Graphical presentation of Friedman rank test for the ejector refrigerator optimization

performing algorithm and its rank. It can be observed from the results that the TLBO algorithm obtained the first rank followed by DE and CSA algorithms.

The optimized design of the ejector refrigerator obtained using the TLBO algorithm is presented in Table 5.22. It can be noted from the results that the ejector refrigerator with the minimum generator and condenser temperature results in the maximum coefficient of performance. The evaporator temperature produced a conflicting effect on achieving the maximum coefficient of performance of the ejector refrigerator. Furthermore, the exergetic efficiency is at the limiting value in the optimized operating condition of the ejector refrigerator.

**Table 5.22** Optimized design geometry of the ejector refrigerator

Operating parameters	Optimized value
<i>Design variable</i>	
Temperature of evaporator ( $T_{eva}$ )	278.5
Temperature of generator ( $T_{gen}$ )	348
Temperature of condenser ( $T_{con}$ )	306
<i>Constraints</i>	
Exergetic efficiency ( $\eta_{ex}$ )	4.013
<i>Objective function</i>	
The coefficient of performance (COP)	0.5182

## 5.6 Thermo-Electric Refrigerator

Thermo-electric refrigeration is a method to remove thermal energy from a medium, device, or component by applying a voltage of constant polarity to a junction between dissimilar electrical conductors or semiconductors. Thermo-electric refrigeration uses the Peltier effect to create a heat flux between the junctions of two different types of materials. It can be used either for heating or cooling application. The thermo-electric refrigerators can produce steady, environment-friendly operating condition for various applications such as aerospace, medical, and electronic cooling. However, the cooling capacity and coefficient of performance of thermo-electric refrigerators are low compared to other commercial systems. So, the effort had been placed continuously to improve the performance of thermo-electric refrigerator.

A single-stage thermo-electric refrigerator produced 70 K temperature difference when its hot end is maintained at room temperature. Therefore, two-stage thermo-electric refrigerators should be employed when a large temperature difference is required. Generally, two-stage thermo-electric refrigerators are arranged in the cascade: the cold stage is attached to the heat source, and the hot stage exhausts total heat to the environment. Furthermore, the two-stage thermo-electric refrigerators are arranged in two different design configurations—electrically serial and electrically separate. Figure 5.17 shows both the arrangement. The thermo-electric modules are composed of *p*-type and *n*-type of the semiconductor. If the current is passed through them, the cooling is produced at one junction and heat is produced at other junction. If the hot end is maintained at ambient temperature, then the temperature of the cold end will be lower than the ambient temperature.

Earlier, work had been reported by the researchers related to the analysis and optimization of the thermo-electric refrigerator. Xuan (2002) presented the performance analyses of three types of two-stage thermo-electric coolers, which are supplied with serial, parallel, and separate electric currents and obtained the optimum coefficient performance for each configuration. Chen et al. (2002) optimized the internal structure parameter of the thermo-electrical refrigerator for the maximum COP and rate of refrigeration. The authors also compared the optimum performance of single- and two-stage thermo-electrical refrigerator. Xuan et al. (2002a)

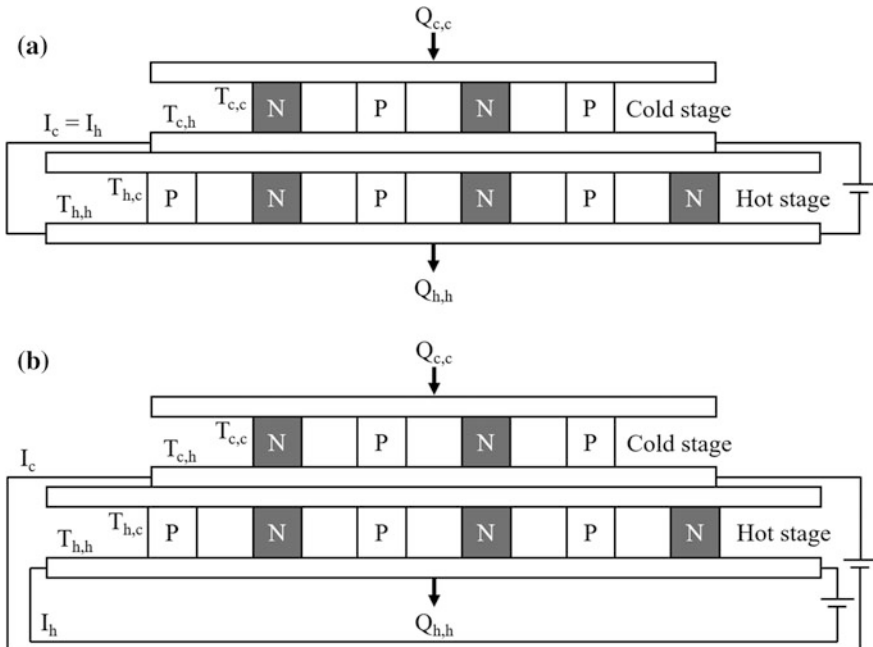


**Fig. 5.17** Schematic arrangement of the two-stage thermo-electric refrigerator **a** electrically serial **b** electrically separate

investigated two different design configuration of the thermo-electric cooler and obtained the optimum ratio of the number of thermo-electric modules between the stages and optimum ratio of the electric current between stages for the maximum cooling capacity and COP. Xuan et al. (2002b) carried out the performance analysis of a two-stage thermo-electric cooler considering maximum cooling capacity, maximum COP and the maximum temperature difference of the two-stage thermo-electric cooler. Lai et al. (2004) established a model of two-stage combined semiconductor thermo-electric device that is used as the heat pump. The internal structure parameter of the thermo-electric device is optimized to obtain the maximum COP of the cycle. Chen et al. (2005) proposed a model of two-stage semiconductor thermo-electric refrigerators with the external heat transfer. The performance of the refrigerator is analyzed using the combination of the finite-time thermodynamics and nonequilibrium thermodynamics. Analytical formulas for cooling load versus working electrical current and the coefficient of performance (COP) versus working electrical current were also derived by the authors.

Cheng and Lin (2005) determined the optimum value of the structure parameter of the thermo-electric device for obtaining the maximum cooling capacity by adopting genetic algorithm as an optimization tool. Cheng and Shih (2006) adapted GA for obtaining the maximum cooling capacity and COP of a two-stage thermo-electric refrigerator. The authors determined the optimum value of input

current and number of thermo-electric modules for two different design configurations. Chen et al. (2006a, b) performed the parametric optimization of the thermo-electric device for obtaining maximum COP and rate of refrigeration of the system. Pan et al. (2007) carried out the parametric optimization and performance analysis of a multi-couple thermo-electric refrigerator. The authors determined the optimum operating state of the COP for the thermo-electric refrigeration device. Abramzon (2007) performed numerical optimization of the thermo-electric cooler for obtaining the maximum cooling rate of the thermo-electric cooler using multi-start adaptive random search method. Yu et al. (2007) analyzed the influence of different parameters on the cooling performance of the thermo-electric module to identify the optimum configuration of two-stage thermo-electric modules.

Meng et al. (2009) proposed a new configuration of two-stage thermo-electric refrigerator driven by the two-stage thermo-electric generator. The thermodynamic model of the combined device is built by using nonequilibrium thermodynamic theory. Furthermore, the allocations of the thermo-electric element pairs among the two thermo-electric generators and the two thermo-electric refrigerators were optimized for the maximum cooling load and COP. Zhou and Yu (2012) presented a generalized theoretical model for the optimization of the thermo-electric cooling system, in which the thermal conductance from the hot and cold sides of the system is taken into account. Rao and Patel (2013) adapted teaching-learning-based optimization for the multi-objective optimization of a two-stage thermo-electric cooler considering the maximization of cooling capacity and coefficient of performance of the thermo-electric cooler as an objective function. The authors investigated two different arrangements of the thermo-electric cooler, namely electrically separated and electrically serial for the optimization. The authors considered the maximization. Ding et al. (2015) established a combined thermionic–thermo-electric refrigerator model with external finite rate heat transfer. The authors derived the general expressions for cooling load and coefficient of the performance versus applied voltage. Hadidi (2017) performed optimization of electrically serial two-stage thermo-electric refrigeration systems using a chemical reaction optimization algorithm. The authors considered the cooling capacity and coefficient of performance of the thermo-electric refrigeration system as objective functions and compared the obtained results with the available results in the literature.

### 5.6.1 *Thermal Model*

In the present work, a two-stage electrically separate thermo-electric refrigerator is considered for the optimization. The schematic arrangement of the considered refrigerator is shown in Fig. 5.15. The thermal model presented here is based on the previous work of Cheng and Shih (2006) and Rao and Patel (2013). Moreover, the subscripts  $c$  and  $h$  stand for cold stage/cold side and hot stage/hot side, respectively, in the different equations of the thermal model. Further, the subscripts  $n$  and  $p$  stand for  $n$ -type and  $p$ -type semiconductors, respectively.

The cooling capacity of the cold side of the cold stage ( $Q_{c,c}$ ) and heat rejected at the hot side of the hot stage are given by

$$Q_{c,c} = \frac{N_t}{r+1} \left[ \alpha_c I_c T_{c,c} - \frac{1}{2} I_c^2 R_c - K_c (T_{c,h} - T_{c,c}) \right] \quad (5.162)$$

$$Q_{h,h} = \frac{N_t r}{r+1} \left[ \alpha_h I_h T_{h,h} + \frac{1}{2} I_h^2 R_h - K_h (T_{h,h} - T_{h,c}) \right] \quad (5.163)$$

where  $N_t$  is the total number of thermo-electric modules of two stages and  $r$  is the ratio of the number of thermo-electric modules between the hot stage ( $N_h$ ) to the cold stage ( $N_c$ ).  $T_{c,c}$ ,  $T_{c,h}$ ,  $T_{h,h}$ , and  $T_{h,c}$  are the temperature of the cold side of the cold stage, hot side of the cold stage, hot side of the hot stage, and cold side of the hot stage, respectively.  $I_c$  and  $I_h$  are the input current to the cold stage and the hot stage, respectively.  $\alpha$ ,  $R$ , and  $K$  are the Seebeck coefficient, electrical resistance, and thermal conductance and are given by the following equations.

$$\alpha_i = (\alpha_{i,p} - \alpha_{i,n})_{T_{i,ave}} \quad (5.164)$$

$$R_i = \frac{[\rho_{i,p} + \rho_{i,n}]_{T_{i,ave}}}{G} \quad (5.165)$$

$$K_i = (k_{i,p} + k_{i,n})_{T_{i,ave}} G \quad (5.166)$$

where subscript  $i$  stands for the cold side and the hot side of the thermo-electric refrigerator. Subscript ave indicates the average value, and subscripts  $p$  and  $n$  indicate the properties of  $p$ -type and  $n$ -type of thermo-electric modules.  $G$  is the structure parameter of the thermo-electric modules and indicates the ratio of cross-section area to the length of thermo-electric modules.  $\rho$  and  $k$  are the electric resistivity and thermal conductivity of the thermo-electric material, respectively.

The material properties are considered to be temperature dependent and are calculated by the following correlations.

$$\alpha_{i,p} = -\alpha_{i,n} = (22224 + 9300.6T_{i,avg} - 0.9905T_{i,avg}^2) 10^{-9} \quad (5.167)$$

$$\rho_{i,p} = \rho_{i,n} = (5112 + 163.4T_{i,avg} + 0.627T_{i,avg}^2) 10^{-10} \quad (5.168)$$

$$k_{i,p} = k_{i,n} = (62605 - 277.7T_{i,avg} + 0.413T_{i,avg}^2) 10^{-4} \quad (5.169)$$

The total thermal resistance ( $RS_t$ ) existing between the interface of the thermo-electric refrigerator is given by

$$RS_t = RS_{sprd} + RS_{cont} \quad (5.170)$$

where  $RS_{sprd}$  and  $RS_{cont}$  are the spreading resistance and contact resistance between the interfaces of the two thermo-electric refrigerators, respectively.

The spreading resistances between the interfaces of the two thermo-electric refrigerators are calculated from the following equation:

$$RS_{sprd} = \frac{\psi_{max}}{k_{h,s} rad_{c,s} \sqrt{\pi}} \quad (5.171)$$

where  $k_{h,s}$  is the thermal conductivity of the substrate of the hot stage and  $rad_{c,s}$  is the equilibrium radius of the substrates of the cold stage and is calculated by the following equation:

$$rad_{c,s} = \sqrt{\frac{2aN_t/r + 1}{\pi}} \quad (5.172)$$

where factor  $2a$  represents the linear relationship between the cross-sectional area of the substrate and the thermo-electric modules.

The dimensionless parameter  $\psi_{max}$  of the equation is given by

$$\psi_{max} = \frac{\varepsilon\tau}{\sqrt{\pi}} + \frac{1}{\sqrt{\pi}}(1 - \varepsilon)\varphi \quad (5.173)$$

where  $\varepsilon$  and  $\tau$  are the dimensionless parameters and are calculated by

$$\varepsilon = \frac{rad_{c,s}}{rad_{h,s}} = \sqrt{\frac{1}{r}} \quad (5.174)$$

$$\tau = \frac{S_{h,s}}{rad_{h,s}} \quad (5.175)$$

where  $rad_{h,s}$  is the equilibrium radius of the substrate of the hot stage and  $S_{h,s}$  is the substrate thickness of the hot stage and is given by

$$rad_{h,s} = \sqrt{\frac{2aN_t r / r + 1}{\pi}} \quad (5.176)$$

The dimensionless parameter  $\varphi$  of is given by

$$\varphi = \frac{\tanh(\tau \times \lambda) + \frac{\lambda}{Bi}}{1 + \tanh(\tau \times \lambda) \frac{\lambda}{Bi}} \quad (5.177)$$

where  $Bi$  is the Biot number, and its value is infinity, i.e., ( $Bi = \infty$ ) for the isothermal cold side of the hot stage.

The dimensionless parameter  $\lambda$  is given by

$$\lambda = \pi + \frac{1}{\varepsilon\sqrt{\pi}} \quad (5.178)$$

The contact thermal resistance ( $RS_{\text{cont}}$ ) at the interface of the thermo-electric refrigerator is calculated by

$$RS_{\text{cont}} = \frac{RS_j}{2aN_t/r + 1} \quad (5.179)$$

where  $RS_j$  is the joint resistance at the interface of the thermo-electric refrigerator.

The heat rejected at the hot side of the cold stage ( $Q_{c,h}$ ) and cooling capacity at the cold side of the hot stage ( $Q_{h,c}$ ) are obtained by considering the heat balance at the interface of the thermo-electric refrigerator and are given by

$$Q_{c,h} = \frac{N_t}{r+1} \left[ \alpha_c I_c T_{c,h} + \frac{1}{2} I_c^2 R_c - K_c (T_{c,h} - T_{c,c}) \right] \quad (5.180)$$

$$Q_{h,c} = \frac{N_t r}{r+1} \left[ \alpha_h I_h T_{h,c} - \frac{1}{2} I_h^2 R_h - K_h (T_{h,h} - T_{h,c}) \right] \quad (5.181)$$

The COP of the two-stage thermo-electric refrigerator is given by

$$\text{COP} = \frac{Q_{c,c}}{Q_{h,h} - Q_{c,c}} \quad (5.182)$$

Based on the above thermal model, the objective function for the present work is defined in the next section.

### 5.6.2 Case Study, Objective Function Description, and Constraints

A two-stage electrically separate thermo-electric refrigerator needs to be designed and optimized for maximum cooling capacity. The considered thermo-electric refrigerator is used to produce the temperature of 210 K at the cold stage when its hot stage is maintained at a temperature of 300 K. The total number of thermo-electric modules of the two stages is 50, and the ratio of cross-sectional area to the length of thermo-electric modules is 0.0018 m. Thermal resistance is present at the interface of the thermo-electric refrigerator. Alumina having thermal conductivity of 30 W/m K is acting as a substrate to take into account the spreading resistance. The thickness of the substrate is 1 mm. To take into account the contact resistance between the two stages, the joint resistance is taken as  $2 \text{ cm}^2 \text{ K/W}$ . Three

**Table 5.23** Ranges of design variables for thermo-electric refrigerator optimization

Design variable	Lower bound	Upper bound
Hot-stage input electric current ( $I_h$ ), A	4	11
Cold-stage input electric current ( $I_c$ ), A	4	11
The ratio of the number of thermo-electric modules between the hot stage to the cold stage ( $r$ )	2	7.33

design variables such as hot-stage input electric current ( $I_h$ ), cold-stage input electric current ( $I_c$ ), and the ratio of the number of thermo-electric modules between the hot stage and the cold stage ( $r$ ) are considered for the optimization problem. The upper and lower bounds of design variables are presented in Table 5.23.

As mentioned above, the maximization of the cooling capacity of the thermo-electric refrigerator is taken as an objective function in the present study. Furthermore, the operating parameters which result in maximum cooling capacity should also satisfy the coefficient of performance constraint. So, considering all the aspects, the objective function of the thermo-electric refrigerator is formulated as follows:

$$\begin{cases} \text{Minimize } f(X) = Q_{c,c}(X) + \sum_{j=1}^n G_1(g_j(X))^2 \\ X = [x_1, x_2, x_3, \dots, x_D], \quad x_{i,\text{minimum}} \leq x_i \leq x_{i,\text{maximum}}, \quad i = 1, 2, 3, \dots, D \\ g_j(X) \leq 0, \quad j = 1, 2, 3, \dots, n \end{cases} \quad (5.183)$$

where  $X$  is the vector of design variables which should be bounded between its minimum and maximum values.  $G_1$  is the penalty parameter, and entire term takes into account the effect of constraints violation. This term comes into the picture when the constraint violation takes place.  $g_j(X)$  indicates the constraints. The following constraint is considered for the thermo-electric refrigerator.

$$\text{The coefficient of performance (COP)} \geq 0.05 \quad (5.184)$$

The next section describes the results and discussion of the case study.

### 5.6.3 Results and Discussion

The considered problem of the thermo-electric refrigerator is investigated using 11 different metaheuristic approaches to obtain the maximum cooling capacity of the refrigerator. Each algorithm is implemented 100 times on the considered problem to estimate the statistical variations of the algorithms. Each algorithm is implemented

with the population size of 50, and the termination criteria are set as 100,000 function evaluations. In Table 5.24, the results obtained over 100 runs using each algorithm are presented in the form of the best solution, worst solution, average solution standard deviation, and success rate. Here, the infeasible solutions (i.e., affected by penalty) are eliminated while obtaining the worst solution, average solution, standard deviation, and success rate. Furthermore, the success rate of the algorithm is obtained by considering 0.1% variation from the global optimum value.

It can be observed from the comparative results that all the algorithms performed equally good and produced the identical maximum cooling capacity of the thermo-electric refrigerator. Further, the average performance of CSA and TLBO algorithms are almost identical and better than other algorithms. However, the success rate of the CSA algorithm is better while the WWO algorithm produces the least success rate in obtaining the global optimum value. It can be observed from the results that it is difficult to judge the performance of the algorithm as all the algorithms have produced a different performance to obtain the best, worst, and average results, and success rate. So, the Friedman rank test is implemented to judge the best suitable algorithm for thermo-electric refrigerator considering the capability to obtain the best, worst, and average results, and success rate. The results of the Friedman rank test are presented in Table 5.25, and its graphical representation is given in Fig. 5.18. The results are presented in the form of Friedman value, normalized value with ‘1’ as the best performing algorithm and its rank. It can be observed from the results that CSA obtained the first rank followed by TLBO and DE algorithms.

**Table 5.24** Comparative results of different algorithms for thermo-electric refrigerator optimization

Algorithms	Best	Worst	Average	SD	Success rate (%)
GA	2.142	1.4333	1.8217	2.69E-01	10
PSO	2.142	1.0389	1.7601	3.04E-01	9
DE	2.142	1.6997	2.0030	1.17E-01	16
ABC	2.142	0.9430	1.7072	3.20E-01	13
CSA	2.142	1.9767	2.0764	6.03E-02	24
TLBO	2.142	1.9767	2.0624	7.65E-02	22
SOS	2.142	1.3195	1.9277	2.47E-01	11
WWO	2.142	1.2569	1.7764	3.34E-01	8
HTS	2.142	1.6325	1.9789	1.78E-01	21
PVS	2.142	1.4562	1.8827	1.79E-01	14
SCA	2.142	1.1090	1.6922	2.84E-01	12

**Table 5.25** Friedman rank test results for thermo-electric refrigerator optimization

Algorithms	Friedman value	Normalized value	Rank
GA	35	0.285714	7
PSO	44	0.227273	10
DE	19	0.526316	3
ABC	43	0.232558	9
CSA	10	1	1
TLBO	14	0.714286	2
SOS	32	0.3125	6
WWO	44	0.227273	10
HTS	21	0.47619	4
PVS	27	0.37037	5
SCA	41	0.243902	8

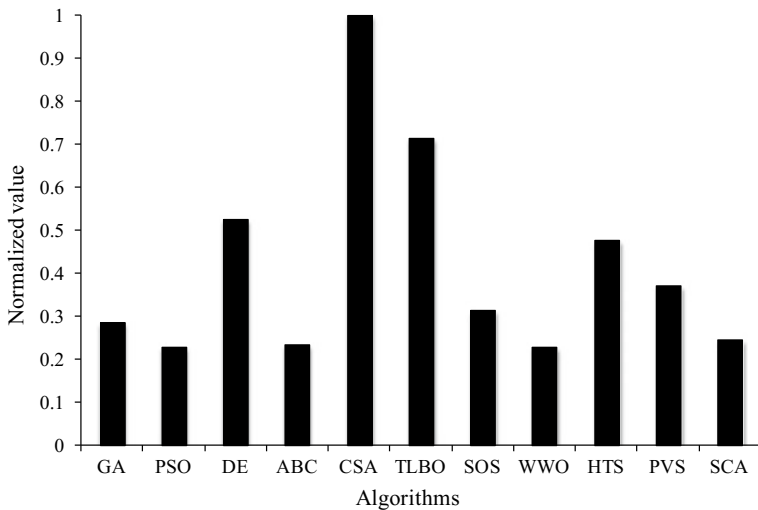


**Fig. 5.18** Graphical presentation of Friedman rank test for thermo-electric refrigerator optimization

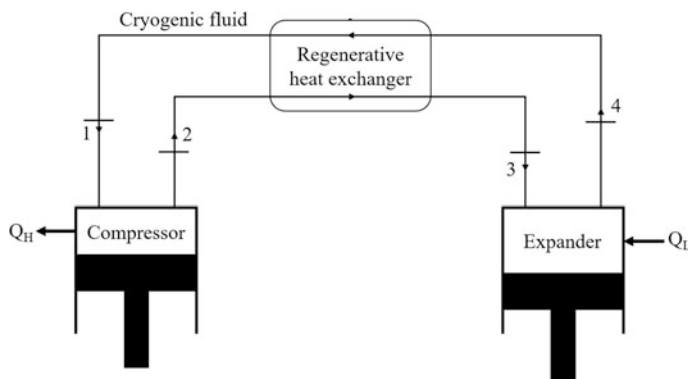
The optimized operating condition of thermo-electric refrigerator obtained using the CSA algorithm is presented in Table 5.26. It can be noted from the results that the thermo-electric refrigerator with the maximum cold-stage input current results in the maximum cooling capacity of the refrigerator. The hot-stage input current and ratio of the number of thermo-electric modules between the hot stage and the cold stage produced a conflicting effect on achieving the maximum cooling capacity of the thermo-electric refrigerator. Furthermore, the coefficient of performance constraint is at the limiting value in the optimized operating condition of the thermo-electric refrigerator.

**Table 5.26** The optimized operating condition of the thermo-electric refrigerator

Operating parameters	Optimized value
<i>Design variable</i>	
Hot-stage input electric current ( $I_h$ ), A	7.9886
Cold-stage input electric current ( $I_c$ ), A	10.6165
The ratio of the number of thermo-electric modules between the hot stage and the cold stage ( $r$ )	4.55
<i>Constraints</i>	
Coefficient of performance	0.05
<i>Objective function</i>	
Cooling capacity ( $Q_{c,c}$ ), W	2.142

## 5.7 Stirling Cryogenic Refrigerator

The Stirling cryogenic refrigerator is an important model for the low-temperature production in the cryogenic range. Stirling cryogenic refrigerator is operating with Stirling cycle. It is a closed regenerative cycle as the regenerative heat exchanger is used in the system. The schematic arrangement of the Stirling cryogenic refrigerator is shown in Fig. 5.19. It can be observed from the figure that the main components of the Stirling refrigerator are the compressor, expander with displacer, and regenerative heat exchanger. Different cryogens like helium, argon, nitrogen, etc. can be used as a working fluid in the Stirling cryogenic refrigerator. The function of the compressor is to carry out isothermal compression of cryogen. The regenerative heat exchanger absorbs the heat from cryogen during forwarding cycle and rejects the heat to the cryogen in return cycle. The expander along with the displacer performed the expansion of the cryogen and returned it to the compressor via regenerator. The ideal Stirling cycle consists of two isothermal and two constant

**Fig. 5.19** Schematic arrangement of Stirling cryogenic refrigerator

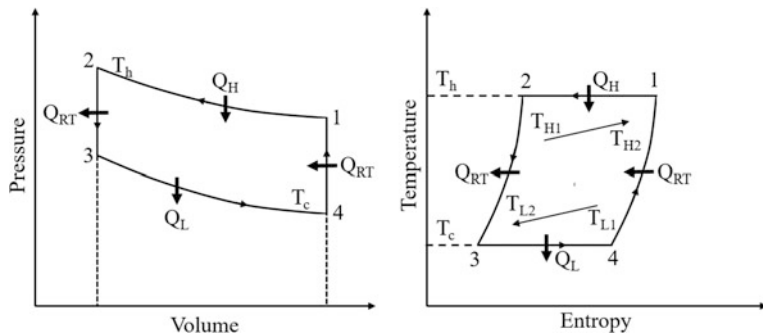


**Fig. 5.20** Thermodynamic presentation of Stirling cryorefrigerator

volume processes. The thermodynamic presentation of the ideal Stirling refrigeration cycle is shown in Fig. 5.20 and explained below.

During process 1–2, the working substance (i.e., the cryogen) compressed isothermally at the temperature ( $T_h$ ) in the compressor during which it rejects the heat ( $Q_h$ ) to the surrounding. The isothermal compression will take place only up to the state point 2. After which the compressor will continue to compress the working fluid, but at the same time the expander will start to expand the working fluid and hence to keep the volume constant. This is achieved by maintaining the proper phase angle between compressor and displacer motion. Also, during this process working fluid will pass through the regenerative heat exchanger where it rejects some heat ( $Q_{RT}$ ). At the end of process 2–3, the compressor will be at its top dead center. Hence, it will stop further compression. However, as the expander is in half of its way, it will continue expanding the working fluid. This process will be isothermal at the temperature ( $T_c$ ), and some heat ( $Q_L$ ) will be absorbed from the region to be refrigerated. At the end of process 3–4, expander and compressor will be at their extreme positions. So further both will move in such a way that working fluid will sustain constant volume and is transferred from the expander to compressor via the regenerative heat exchanger. In the heat exchanger, the matrix which is having stored heat during the process 2–3 will reject to the working substance. After this process, the process 1–2 starts and hence cycle repeats.

Earlier, work had been reported by the researchers related to the analysis and optimization of Stirling cryogenic refrigerator. Chen and Yan (1996) investigated the influence of finite-rate heat transfer and regenerative losses on the performance of Stirling refrigerator using an ideal or Van der Waals gas as the working substance. The author derived the optimal relation between the cooling rate and the coefficient of performance and obtained the maximum cooling rate and the corresponding coefficient of the performance for different cases. Colgate (1995) carried out the regenerator optimization of Stirling cycle refrigeration. The author investigated the heat transfer behavior and entropy production rate of the cycle. Chen (1998) developed an irreversible cycle model for predicting the performance of the Stirling refrigerator using an ideal or Van der Waals gas as the working substance.

The author optimized the power input of the Stirling refrigerator under a given cooling rate. Furthermore, the power input versus cooling rate and the coefficient of performance versus cooling rate behavior is presented. Huang et al. (2002) carried out the performance optimization of an irreversible quantum Stirling cooler considering heat leaks and other irreversible losses. The authors derived the relation between the optimal cooling load and the COP by adapting finite-time thermodynamics and nonequilibrium statistical mechanics in their work. Tyagi et al. (2002a, b) presented the parametric study of irreversible Stirling cryogenic refrigeration cycles including external and internal irreversibilities along with the finite heat capacities of external reservoirs. Tyagi et al. (2004) carried out thermo-economic optimization of an irreversible Stirling cryogenic refrigerator cycle. The authors calculated various performance parameters at the optimal operating conditions with respect to the working fluid temperatures.

Lin and Chen (2006) performed an analysis of an irreversible quantum Stirling cryogenic refrigeration cycle using an ideal Fermi or Bose gas as a working substance. The authors studied the influence of quantum degeneracy and the finite-rate heat transfer between the working substance and the heat reservoirs on the optimal performance of the system. The authors also derived the expressions for COP, cooling rate and power input using numerical solutions at optimum condition. Jafarian et al. (2009) presented the second-law-based optimum design of a high capacity double inlet Stirling type pulse tube refrigerator. The authors applied second law to determine work loss in the regenerator for optimizing the cryocooler performance. Jafari et al. (2013) carried out multi-objective optimization of the Stirling-type pulse tube by using genetic algorithm and 1-D finite volume method. The authors considered the maximization of COP and cold end temperature as their objective functions and derived closed-form relations for Pareto optimal solutions of pulse tube refrigerator. Ahmadi et al. (2014) performed the multi-objective optimization of an irreversible Stirling cryogenic refrigerator for minimization of input power and the maximization of cooling load and coefficient of performance of the system. Zhou et al. (2015) investigated regenerator materials for Stirling-type pulse tube refrigerator for liquid hydrogen temperature range. The authors carried out the performance comparison of different sphere shape regenerator materials to identify the most suitable one in liquid hydrogen temperature range. Açıkkalp et al. (2016) assessed the nano-scale Stirling refrigerator using working fluid as Maxwell–Boltzmann gases by thermo-ecological and sustainability criteria. Li and Grosu (2017) carried out the parameter effect analysis for the Stirling cryocooler by using an isothermal model with various losses such as regenerator imperfection thermal loss, piston finite speed loss, gas spring hysteresis loss, displacer shuttle heat loss, clearance heat pump loss, heat conduction loss, and flow viscosity loss. The authors investigated the effects of various working parameters and concluded that friction and conduction losses contribute majorly to mechanical and heat loss, respectively.

Ahmadi et al. (2017a) carried out the thermodynamic analysis and optimization of a nanoscale irreversible Stirling refrigeration cycle using ideal Maxwell–Boltzmann gas as a working fluid. Furthermore, the authors performed the multi-objective optimization of the proposed system considering two different

scenarios. In the first scenario, the maximization of the ecological coefficient of performance, the coefficient of performance and dimensionless ecological function of the system considered simultaneously. In the second scenario, the maximization of exergy efficiency, the coefficient of performance and dimensionless ecological function of the system considered simultaneously. Furthermore, NSGA-II was implemented for the optimization of both the scenarios. Hachem et al. (2017) carried out the experimental and numerical study of Beta-type Stirling refrigerator. The authors estimated the net cooling capacity, input power and COP of the refrigerator at different conditions and also obtained the optimum geometric variable such as dead volume, swept volume, regenerator length, regenerator diameter, and regenerator porosity for the considered refrigerator. Ahmadi et al. (2017b) performed the optimization of a nano scale Stirling cryogenic refrigerator. The authors carried out the multi-objective optimization by considering the energetic sustainability index and ecological coefficient of performance simultaneously. Batooei and Keshavarz (2018) carried out the multi-objective optimization of Gamma type Stirling refrigerator considering cooling capacity, the coefficient of performance, and pressure drop of the system as an objective and helium and air as a working fluid. Authors used experimental data for multi-objective optimization and adopted the design of experiments for the optimization. The experimental and simulation results showed that the cooling capacity increases continuously with the rotational speed where the COP has a maximum value.

### 5.7.1 Thermal Model

In this part of the work, the cryorefrigerator working on the Stirling cycle is considered for the optimization. The thermodynamic presentation of Stirling cryorefrigerator is shown in Fig. 5.20. The thermal model presented here is based on the previous work of Ahmadi et al. (2014).

The following equation gives the absorbed heat ( $Q_c$ ) of the cycle at temperature  $T_c$ .

$$Q_c = T_c \Delta S = C_L(T_{L2} - T_{L1})t_L = U_L A_L (\text{LMTD})_L t_L \quad (5.185)$$

Rejected heat ( $Q_h$ ) of the cycle at temperature  $T_h$  is given by the following equation:

$$Q_h = T_h \Delta S = C_H(T_{H2} - T_{H1})t_H = U_H A_H (\text{LMTD})_H t_H \quad (5.186)$$

where  $\Delta S$  is entropy difference,  $C_L$  and  $C_H$  is the heat capacitance of source and sink, respectively,  $U_L A_L$  and  $U_H A_H$  are the products of the overall heat transfer coefficient and area of source and sink, respectively,  $(\text{LMTD})_L$  and  $(\text{LMTD})_H$  are the log mean temperatures of source and sink which are given by the following equations.

$$(LMTD)_L = \frac{(T_{L1} - T_c) - (T_{L2} - T_c)}{\ln\left(\frac{(T_{L1} - T_c)}{(T_{L2} - T_c)}\right)} \quad (5.187)$$

$$(LMTD)_H = \frac{(T_h - T_{H1}) - (T_h - T_{H2})}{\ln\left(\frac{(T_h - T_{H1})}{(T_h - T_{H2})}\right)} \quad (5.188)$$

Entropy difference of the system is given by

$$\Delta S = nR\ln(\lambda) \quad (5.189)$$

where  $n$  is number of mole and  $\lambda$  is the volume ratio.

The following equation gives the regenerator heat loss ( $Q_R$ ) between two isothermal processes:

$$\Delta Q_R = nC_v(1 - \varepsilon_R)(T_h - T_c) \quad (5.190)$$

where  $n$  is the number of mole of the working fluid,  $C_v$  is working fluid's specific heat capacity through the processes of the regenerative in the unit of mole, and  $\varepsilon_R$  is the regenerator effectiveness.

The following equation gives the regenerative time ( $t_R$ )

$$t_R = t_3 + t_4 = 2\alpha(T_h - T_c) \quad (5.191)$$

where  $\alpha$  is the proportionality constant.

The following equation gives the total cycle time ( $t_{cycle}$ )

$$t_{cycle} = (t_H + t_L + t_R) \quad (5.192)$$

Considering irreversibility, the heat released to the source ( $Q_L$ ) is given by the following equation.

$$Q_L = Q_c - \Delta Q_R \quad (5.193)$$

Considering irreversibility, the heat released to the sink ( $Q_H$ ) is given by the following equation.

$$Q_H = Q_h - \Delta Q_R \quad (5.194)$$

The following equation gives the power input ( $P$ ) of the Stirling cryorefrigerator.

$$P = \frac{(Q_H - Q_L)}{t_{cycle}} \quad (5.195)$$

The following equation gives the coefficient of performance (COP<sub>L</sub>) of the Stirling cryorefrigerator:

$$\text{COP}_L = \frac{R_L}{P} \quad (5.196)$$

where  $R_L$  is the cooling load which is given by

$$R_L = \frac{Q_L}{t_{\text{cycle}}} \quad (5.197)$$

The following equation gives the second law of thermodynamics for the irreversible cycle.

$$\frac{Q_c}{T_c} - \frac{Q_h}{T_h} < 0 \quad (5.198)$$

By applying irreversibility constant ( $\phi$ ), the relation becomes

$$\frac{Q_c}{T_c} = \phi \frac{Q_c}{T_c} \quad (5.199)$$

The following equation gives the power required to run the Stirling cryorefrigerator:

$$P = \frac{x - \phi}{\left( \frac{x}{\varepsilon_H C_H (x T_c - T_{H1})} \right) + \left( \frac{\phi}{\varepsilon_L C_L (T_{L1} - T_c)} \right) + b_1 (x - 1)} \quad (5.200)$$

The following equation gives the cooling load ( $R_L$ ) produced by the Stirling cryorefrigerator.

$$R_L = \frac{\phi - F_1 (x - 1)}{\left( \frac{x}{\varepsilon_H C_H (x T_c - T_{H1})} \right) + \left( \frac{\phi}{\varepsilon_L C_L (T_{L1} - T_c)} \right) + b_1 (x - 1)} \quad (5.201)$$

where parameters  $b_1$  and  $F_1$  are given by

$$b_1 = \frac{2\alpha}{n R \ln(\lambda)} \quad (5.202)$$

$$F_1 = \frac{C_v (1 - \varepsilon_R)}{R \ln(\lambda)} \quad (5.203)$$

Based on the above equations, the coefficient of performance of the system is given by the following equation:

$$\text{COP}_L = \frac{\phi - F_1(x - 1)}{x - \phi} \quad (5.204)$$

where  $x$  is temperature ratio and is given by

$$x = \frac{T_h}{T_c} \quad (5.205)$$

Entropy generation of the system is given by

$$S_{\text{gen}} = \left( \frac{Q_H}{T_{HM}} - \frac{Q_L}{T_{LM}} \right) * \frac{1}{t_{\text{cycle}}} \quad (5.206)$$

where  $T_{HM}$  and  $T_{LM}$  are the average temperature.

The exergetic efficiency of the system is given by

$$\eta_{\text{ex}} = \frac{\left( \left( 1 - \frac{T_0}{T_H} \right) * Q_H \right) - \left( \left( 1 - \frac{T_0}{T_L} \right) * Q_L \right)}{(Q_H - Q_L)} \quad (5.207)$$

where  $T_0$  is the ambient temperature.

Based on the above thermal model, the objective function for the present work is defined in the next section.

### 5.7.2 Case Study, Objective Function Description, and Constraints

The Stirling cryorefrigerator working between the heat source temperature 300 K and heat sink temperature 250 K needs to be designed and optimized for the maximum coefficient of performance. The volumetric ratio ( $\lambda$ ) during the regeneration process is 2. Molar specific heat capacity ( $C_v$ ) of the working fluid is 15 J/mol K. The gas constant ( $R$ ) for the working fluid is 4.3 J/mol K. The proportionality constant to estimate the regenerator temperature is  $10^{-5}$  s/K. Irreversibility factor of the system ( $\phi$ ) is 0.8. The effectiveness of regenerative heat exchanger ( $\varepsilon_R$ ) is 0.8. Six design variables such as temperature of cold side ( $T_c$ ), temperature ratio ( $x$ ), heat source's capacitance rate ( $C_L$ ), heat sink capacitance rate ( $C_H$ ), effectiveness of the cold-side heat exchange ( $\varepsilon_L$ ), and effectiveness of the hot-side heat exchanger ( $\varepsilon_H$ ) are considered for the optimization problem. The upper and lower bounds of design variables are presented in Table 5.27.

As mentioned above, the maximization of the coefficient of performance of the Stirling cryorefrigerator is taken as an objective function in the present study. Furthermore, the operating parameters which result in a maximum coefficient of performance should also satisfy the cooling load ( $R_L$ ), exergetic efficiency ( $\eta_{\text{ex}}$ ), and

**Table 5.27** Ranges of design variables for Stirling cryorefrigerator optimization

Design variable	Lower bound	Upper bound
Temperature of the cold side ( $T_c$ ), K	10	240
Temperature ratio ( $x$ )	1.3	1.4
Heat source's capacitance rate ( $C_L$ )	600	1000
Heat sink capacitance rate ( $C_H$ )	600	1000
Effectiveness of the cold-side heat exchange ( $\varepsilon_L$ )	0.5	0.8
Effectiveness of the hot-side heat exchanger ( $\varepsilon_H$ )	0.5	0.8

entropy generation ( $S_{\text{gen}}$ ) constraints. So, considering all the aspects, the objective function of Stirling cryorefrigerator is formulated as follows:

$$\begin{cases} \text{Minimize } f(X) = \text{COP}(X) + \sum_{j=1}^n G_1(g_j(X))^2 \\ X = [x_1, x_2, x_3, \dots, x_D], \quad x_{i,\text{minimum}} \leq x_i, \leq x_{i,\text{maximum}}, \quad i = 1, 2, 3, \dots, D \\ g_j(X) \leq 0, \quad j = 1, 2, 3, \dots, n \end{cases} \quad (5.208)$$

where  $X$  is the vector of design variables which should be bounded between its minimum and maximum values.  $G_1$  is the penalty parameter, and entire term takes into account the effect of constraints violation. This term comes into the picture when the constraint violation takes place.  $g_j(X)$  indicates the constraints. The following constraints are considered for the Stirling cryorefrigerator.

$$\text{Cooling load}(R_L) \geq 5000 \text{W} \quad (5.209)$$

$$\text{Exergetic efficiency}(\eta_{\text{ex}}) \geq 0.86 \quad (5.210)$$

$$\text{Entropy generation}(S_{\text{gen}}) \leq 3.65 \quad (5.211)$$

The next section describes the results and discussion of the case study.

### 5.7.3 Results and Discussion

The considered problem of the Stirling cryorefrigerator is investigated using 11 different metaheuristic approaches to obtain the maximum power output. As all these methods are stochastic in their working, each algorithm is implemented 100 times on the considered problem to estimate the statistical variations of the algorithms. Each algorithm is implemented with the population size of 50, and the termination criteria are set as 100,000 function evaluations. In Table 5.28, the

**Table 5.28** Comparative results of different algorithms for Stirling cryorefrigerator optimization

Algorithms	Best	Worst	Average	SD	Success rate (%)
GA	1.0895	1.0795	1.0844	5.70E-03	14
PSO	1.0892	1.0856	1.0880	2.11E-03	10
DE	1.0895	1.0795	1.0839	4.95E-03	24
ABC	1.0895	1.0795	1.0843	4.31E-03	36
CSA	1.0895	1.0795	1.0867	4.87E-03	28
TLBO	1.0895	1.0845	1.0879	2.36E-03	18
SOS	1.0895	1.0795	1.0867	4.82E-03	8
WWO	1.0895	1.0876	1.0887	9.30E-04	12
HTS	1.0895	1.0795	1.0885	2.72E-03	40
PVS	1.0895	1.0795	1.0879	2.99E-03	38
SCA	1.0895	1.0809	1.0867	3.49E-03	16

results obtained in 100 runs using each algorithm are presented in the form of the best solution, worst solution, average solution, standard deviation, and success rate. Here, the infeasible solutions (i.e., affected by penalty) are eliminated while obtaining the worst solution, average solution, standard deviation, and success rate. Furthermore, the success rate of the algorithm is obtained by considering 0.1% variation from the global optimum value.

It can be observed from the comparative results that all the algorithms performed equally good and produced almost identical coefficient of performance of Stirling cryorefrigerator. Furthermore, the average performance of all the algorithms is less or more identical. However, the success rate of HTS algorithm in obtaining the optimum value is the highest followed by the PVS algorithm. The success rate of the SOS algorithm is the lowest compared to other algorithms. It can be observed from the results that it is difficult to judge the performance of the algorithm as all the algorithms have produced a different performance to obtain the best, worst, and average results, and success rate. So, the Friedman rank test is implemented to judge the best suitable algorithm for the Stirling cryorefrigerator optimization considering the capability to obtain the best, worst, and average solutions, and success rate. The results of the Friedman rank test are presented in Table 5.29, and its graphical representation is given in Fig. 5.21. The results are presented in the form of Friedman value, normalized value with ‘1’ as the best performing algorithm and its rank. It can be observed from the results that WWO has obtained the first rank followed by HTS and TLBO algorithms.

The optimized design of Stirling cryorefrigerator obtained using the WWO algorithm is presented in Table 5.30. It can be noted from the results that the Stirling cryorefrigerator with the maximum heat source’s capacitance rate ( $C_L$ ), heat sink capacitance rate ( $C_H$ ), effectiveness of the cold-side heat exchange ( $\epsilon_L$ ), and effectiveness of the hot-side heat exchanger ( $\epsilon_H$ ) results in the maximum coefficient of performance of cryorefrigerator. The temperature of the cold side ( $T_c$ ) and temperature ratio ( $x$ ) produced a conflicting effect on achieving the maximum coefficient of

**Table 5.29** Friedman rank test results for Stirling cryorefrigerator optimization

Algorithms	Friedman value	Normalized value	Rank
GA	43.5	0.37931	10
PSO	28	0.589286	5
DE	43	0.383721	9
ABC	37	0.445946	8
CSA	33	0.5	7
TLBO	21.5	0.767442	3
SOS	37	0.445946	8
WWO	16.5	1	1
HTS	19	0.868421	2
PVS	23	0.717391	4
SCA	28.5	0.578947	6

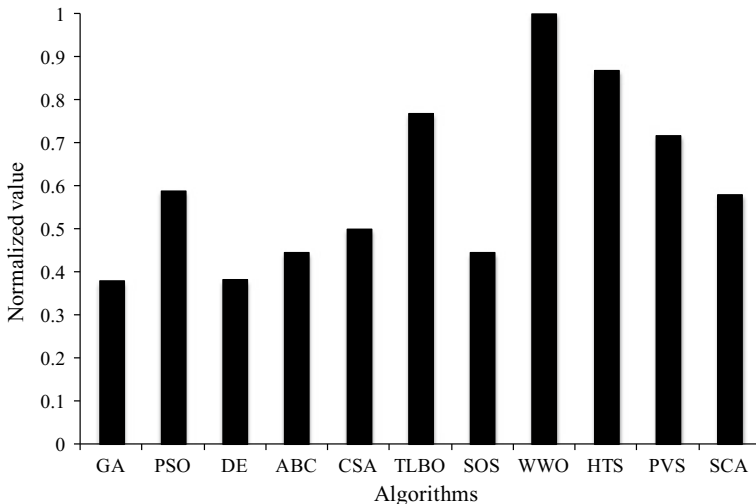


**Fig. 5.21** Graphical presentation of Friedman rank test for Stirling cryorefrigerator optimization

performance of cryorefrigerator. Furthermore, cooling load constraint is above the limiting value while exergetic efficiency and entropy generation rate is at the limiting value in the optimized operating condition of Stirling cryorefrigerator.

## 5.8 Ericsson Cryogenic Refrigerator

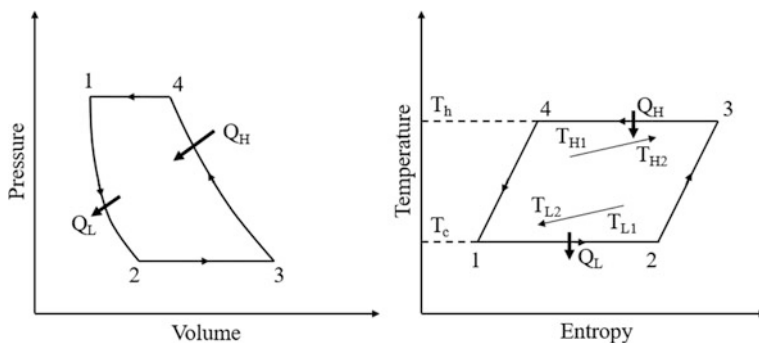
The Ericsson cryogenic refrigerator is used to produce low-temperature production in the cryogenic range. Ericsson cryogenic refrigerator is operating with Ericsson cycle. The main components of the Ericsson refrigerator are the compressor,

**Table 5.30** Optimized design geometry of Stirling cryogenic refrigerator

Operating parameters	Optimized value
<i>Design variable</i>	
The temperature of the cold side ( $T_c$ ), K	233.4
Temperature ratio ( $x$ )	1.396
Heat source's capacitance rate ( $C_L$ )	1000
Heat sink capacitance rate ( $C_H$ )	1000
The effectiveness of the cold-side heat exchange ( $\varepsilon_L$ )	0.8
The effectiveness of the hot-side heat exchanger ( $\varepsilon_H$ )	0.8
<i>Constraints</i>	
Cooling load ( $R_L$ ), W	5001.18
Exergetic efficiency ( $\eta_{ex}$ )	0.8621
Entropy generation ( $S_{gen}$ )	3.6087
<i>Objective function</i>	
Coefficient of performance	1.0895

expander with displacer, and regenerative heat exchanger. The ideal Ericsson cycle consists of two isothermal and two constant pressure processes. The thermodynamic presentation of the ideal Ericsson refrigeration cycle is shown in Fig. 5.22 and explained below.

The Ericsson cryogenic refrigerator cycle uses any gas or magnetic material as the working fluid that absorbs heat from the source while undergoing isothermal expansion (process 1–2) and rejects heat to the sink during isothermal compression (process 3–4). During heat absorption, the temperature of the source decreases from  $T_{L1}$  to  $T_{L2}$  and during heat rejection to the sink temperature increases from  $T_{H1}$  to  $T_{H2}$ . A regenerator is provided to exchange heat from the high-temperature high-pressure fluid from the compressor (process 4–1) to the colder fluid coming from expander (process 2–3). The process of heat transfer in the regenerator is constant pressure.

**Fig. 5.22** Thermodynamic presentation of Ericsson cryorefrigerator

Earlier, work had been reported by the researchers related to the analysis and optimization of Ericsson cryogenic refrigerator. Blank and Wu (1996) carried out analysis of an endoreversible Ericsson cycle with perfect regeneration and obtained the maximum power of the cycle and corresponding efficiency of the cycle. Tyagi et al. (2002a, b) carried out the parametric study and ecological optimization of Ericsson heat pump cycle considering internal and external irreversibility. The authors optimized the ecological function with respect to working fluid temperatures and obtained the expressions for various parameters at the optimal operating condition. Furthermore, the authors studied the effects of different operating parameters on the performance of the cycle. Tyagi et al. (2002a, b) presented a parametric study of irreversible Ericsson cryogenic refrigerator cycle including the external and internal irreversibilities along with finite heat capacities of external reservoirs. The authors identified the effect of different operating parameters on the performance parameter of the cycle and obtained the maximum cooling load of the cycle for the given power input.

Kaushik et al. (2002) carried out the performance evaluation of irreversible Ericsson heat pump cycles including the external and internal irreversibilities. The authors studied the effect of irreversibility parameters on the performance parameter of the cycle and observed that the effect of internal irreversibility parameter is more pronounced than that of other external irreversibility parameters. Tyagi et al. (2005) studied the ecological optimization and parametric study of an irreversible Ericsson cryogenic refrigerator cycle with finite heat capacities of external reservoirs. The ecological function is optimized with respect to working fluid temperatures, and the values of the cooling load, power input, loss rate of the cooling load, and COP are calculated for a set of operating parameters. Wu et al. (2006) investigated the effect of quantum properties of the working medium on the performance of an irreversible quantum Ericsson cooler. The authors derived the optimal relationship between the dimensionless cooling load and coefficient of performance for the irreversible quantum Ericsson cooler.

Xia et al. (2006) presented a general model of an irreversible Ericsson refrigeration cycle employing paramagnetic materials as the working substance. The authors derived the optimal mathematical expressions of the cooling load, the coefficient of performance, and power input to the irreversible Ericsson refrigeration cycle using paramagnetic materials as the working substance. Lin et al. (2008) established an irreversible model of an Ericsson cryogenic refrigeration cycle working with an ideal Fermi gas. The authors optimized the cooling rate of the cycle for given power input and obtained analytic expressions of optimized parameters. Hao and Xing (2013) performed the ecological optimization of an irreversible magnetic Ericsson refrigeration cycle and obtained the expression of different performance parameter as a function of operating variables. Ahmadi and Ahmadi (2015) carried out the multi-objective optimization of the Ericsson cryogenic refrigerator cycle by adapting NSGA-II as an optimization tool. The author performed the optimization of six operating variables for the minimization of input power and maximization of the coefficient of performance and ecological criteria of

the Ericsson cycle. Furthermore, the decision-making technique was implemented to identify the best possible solution.

### 5.8.1 Thermal Model

In this part of the work, the cryorefrigerator working on the Ericsson cycle is considered for the optimization. The thermodynamic presentation of Ericsson cryorefrigerator is shown in Fig. 5.22. The thermal model presented here is based on the previous work of Ahmadi and Ahmadi (2015).

Absorbed heat ( $Q_c$ ) of the cycle at temperature  $T_c$  is given by the following equation:

$$Q_c = T_c(S_2 - S_1) = nT_cR\ln\lambda = C_L(T_{L1} - T_{L2})t_L \quad (5.212)$$

Heat rejected ( $Q_h$ ) at temperature  $T_h$  of the cycle is given by the following equation:

$$Q_h = T_h(S_3 - S_4) = nT_hR\ln\lambda = C_H(T_{H2} - T_{H1})t_H \quad (5.213)$$

where  $\lambda$  is the pressure ratio for two regenerative processes,  $n$  is the number of mole of the working fluid,  $R$  is the universal gas constant, and  $C_L$  and  $C_H$  are the heat capacitance of source and sink, respectively.

Heat rejected ( $Q_h$ ) is also given by the following equation:

$$Q_h = U_H A_H (\text{LMTD})_H t_H \quad (5.214)$$

where  $U_H$  is the overall heat transfer coefficient,  $A_H$  heat transfer coefficient, and  $(\text{LMTD})_H$  is log mean temperature difference on the sink which is given by the following equation:

$$(\text{LMTD})_H = \left[ \frac{(T_h - T_{H1}) - (T_h - T_{H2})}{\frac{\ln(T_h - T_{H1})}{T_h - T_{H2}}} \right] \quad (5.215)$$

The following equation also gives the heat absorbed ( $Q_c$ ):

$$Q_c = U_L A_L (\text{LMTD})_L t_L \quad (5.216)$$

where  $U_L$  is the overall heat transfer coefficient,  $A_L$  is the heat transfer coefficient, and  $(\text{LMTD})_L$  is the log mean temperature difference on the sink which is given by the following equation.

$$(LMTD)_L = \left[ \frac{(T_{L1} - T_C) - (T_{L2} - T_C)}{\ln \left( \frac{(T_{L1} - T_C)}{(T_{L2} - T_C)} \right)} \right] \quad (5.217)$$

In a similar manner, heat absorbed ( $Q_c$ ) and heat rejected ( $Q_h$ ) are also given by the following equations:

$$Q_c = C_L \varepsilon_L (T_{L1} - T_c) t_L \quad (5.218)$$

$$Q_h = C_H \varepsilon_H (T_h - T_{H1}) t_H \quad (5.219)$$

where  $\varepsilon_L$  and  $\varepsilon_H$  are the effectiveness of the cold side and hot side of the heat exchanger, respectively, and are given by the following equations:

$$\varepsilon_L = 1 - e^{-N_L} \quad (5.220)$$

$$\varepsilon_H = 1 - e^{-N_H} \quad (5.221)$$

where  $N_L$  and  $N_H$  are the number of the transfer unit for the cold side and hot side, respectively, which are given by the following equations.

$$N_L = \frac{U_L A_L}{C_L} \quad (5.222)$$

$$N_H = \frac{U_H A_H}{C_H} \quad (5.223)$$

The following equation gives the regenerator heat loss:

$$Q_{R,loss} = n c_f (1 - \varepsilon_R) (T_h - T_c) \quad (5.224)$$

where  $c_f$  is specific heat of the working fluid and  $\varepsilon_R$  is the effectiveness of regenerator which is given by the following equation:

$$\varepsilon_R = \frac{Q_{\text{regen,actual}}}{Q_{\text{regen,ideal}}} = \frac{N_R}{N_R + 1} \quad (5.225)$$

where  $N_R$  is the number of the transfer unit of the regenerator which is given by

$$N_R = \frac{(UA)_R}{C_f} \quad (5.226)$$

The following equation gives the regenerative time ( $t_R$ ) of two isothermal processes:

$$t_R = t_3 + t_4 = 2\alpha(T_h - T_c) \quad (5.227)$$

where  $\alpha$  is the proportional constant.

The following equation gives the total cycle time ( $t_{cycle}$ ).

$$t_{cycle} = t_L + t_H + t_R \quad (5.228)$$

The following equation gives the irreversibility associated with the heat transfer at the heat sink.

$$Q_H = Q_h - Q_{R,loss} \quad (5.229)$$

The following equation gives the irreversibility associated with the heat transfer at the heat source.

$$Q_L = Q_c - Q_{R,loss} \quad (5.230)$$

The following equation gives the power input required for the Ericsson cycle.

$$P = \frac{Q_H - Q_L}{t_{cycle}} \quad (5.231)$$

The following equation gives the coefficient of performance (COP<sub>L</sub>) of the Ericsson cycle:

$$\text{COP}_L = \frac{R_L}{P} \quad (5.232)$$

where  $R_L$  is the cooling load which is given by

$$R_L = \frac{Q_L}{t_{cycle}} \quad (5.233)$$

The equations of power input and cooling load are simplified by substituting the value of heat transfer and represented by

$$P = \frac{(x - 1)}{\left[ \frac{x}{C_H \epsilon_H (xT_c - T_{H1})} + \frac{1}{C_L \epsilon_L (T_{L1} - T_c)} + b_1(x - 1) \right]} \quad (5.234)$$

$$R_L = \frac{1 - a(x - 1)}{\left[ \frac{x}{C_H \epsilon_H (xT_c - T_{H1})} + \frac{1}{C_L \epsilon_L (T_{L1} - T_c)} + b_1(x - 1) \right]} \quad (5.235)$$

where parameters  $x$ ,  $b_1$ , and  $a$  are given by

$$x = \frac{T_h}{T_c} \quad (5.236)$$

$$b_1 = \frac{2\alpha}{nR \ln \lambda} \quad (5.237)$$

$$a = \frac{c_f(1 - \varepsilon_R)}{R \ln \lambda} \quad (5.238)$$

Based on the above equations, the coefficient of performance of the Ericsson cycle is given by the following equation.

$$\text{COP}_L = \frac{1 - a(x - 1)}{x - 1} \quad (5.239)$$

The ecological function ( $E_C$ ) for a refrigeration cycle is given by the following equation:

$$E_C = R_L - LT_a \dot{S}_{\text{gen}} \quad (5.240)$$

where  $T_a$  is the ambient temperature,  $L$  is the dissipation coefficient of the cooling load, and  $\dot{S}_{\text{gen}}$  is the entropy generation of the system and are given by the following equations.

$$L = \frac{T_{L1}}{T_{H1} - T_{L1}} \quad (5.241)$$

$$\dot{S}_{\text{gen}} = \frac{1}{t_{\text{cycle}}} \left( \frac{Q_H}{T_{Hm}} - \frac{Q_L}{T_{Lm}} \right) \quad (5.242)$$

The following equation gives the  $T_{Hm}$  and  $T_{Lm}$ .

$$T_{Hm} = \frac{T_{H1} + T_{H2}}{2} = \frac{(2 - \varepsilon_H)T_{H1} + \varepsilon_H T_h}{2} \quad (5.243)$$

$$T_{Lm} = \frac{T_{L1} + T_{L2}}{2} = \frac{(2 - \varepsilon_L)T_{L1} + \varepsilon_L T_c}{2} \quad (5.244)$$

Based on the above thermal model, the objective function for the present work is defined in the next section.

### 5.8.2 Case Study, Objective Function Description, and Constraints

The Ericsson cryorefrigerator working between the heat source temperature 290 K and heat sink temperature 180 K needs to be designed and optimized for the maximum cooling load. The pressure ratio during two regeneration processes ( $\lambda$ ) is 2.5. Molar specific heat capacity ( $C_v$ ) of the working fluid is 11.82 J/mol K. The gas constant ( $R$ ) for the working fluid is 4.3 J/mol K. The proportionality constant to estimate the regenerator temperature is 0.197. The effectiveness of regenerative heat exchanger ( $\varepsilon_R$ ) is 0.8. The ambient temperature is 290 K. Six design variables such as heat sink capacitance rate ( $C_L$ ), heat source's capacitance rate ( $C_H$ ), temperature ratio ( $x$ ), effectiveness of the cold-side heat exchange ( $\varepsilon_L$ ), effectiveness of the hot-side heat exchanger ( $\varepsilon_H$ ) and temperature of the cold side ( $T_c$ ) are considered for the optimization problem. The upper and lower bounds of design variables are presented in Table 5.31.

As mentioned above, the maximization of the cooling load of the Ericsson cryorefrigerator is taken as an objective function in the present study. Furthermore, the operating parameters which result in maximum cooling load should also satisfy the power input ( $P$ ), the coefficient of performance (COP), and ecological function ( $E_F$ ) constraints. So, considering all the aspects, the objective function of the Ericsson cryorefrigerator is formulated as follows:

$$\begin{cases} \text{Minimize } f(X) = R_L(X) + \sum_{j=1}^n G_1(g_j(X))^2 \\ X = [x_1, x_2, x_3, \dots, x_D], \quad x_{i,\text{minimum}} \leq x_i \leq x_{i,\text{maximum}}, \quad i = 1, 2, 3, \dots, D \\ g_j(X) \leq 0, \quad j = 1, 2, 3, \dots, n \end{cases} \quad (5.245)$$

where  $X$  is the vector of design variables which should be bounded between its minimum and maximum values.  $G_1$  is the penalty parameter, and entire term takes into account the effect of constraints violation. This term comes into the picture

**Table 5.31** Ranges of design variables for Ericsson cryorefrigerator optimization

Design variable	Lower bound	Upper bound
Heat sink capacitance rate ( $C_H$ )	0.1	1.5
Heat source's capacitance rate ( $C_L$ )	0.1	1.5
Temperature ratio ( $x$ )	1.7	1.9
Effectiveness of the cold-side heat exchange ( $\varepsilon_L$ )	0.1	0.9
Effectiveness of the hot-side heat exchanger ( $\varepsilon_H$ )	0.1	0.9
Temperature of the cold side ( $T_c$ , K)	172	177

when the constraint violation takes place.  $g_j(X)$  indicates the constraints. The following constraints are considered for the Ericsson cryorefrigerator.

$$\text{Power input } (P) \leq 2.5\text{kW} \quad (5.246)$$

$$\text{The coefficient of performance (COP)} \geq 1 \quad (5.247)$$

$$\text{Ecological function}(E_F) \geq 1.43 \quad (5.248)$$

The next section describes the results and discussion of the case study.

### 5.8.3 Results and Discussion

The considered problem of Ericsson cryorefrigerator is investigated using 11 different metaheuristic approaches to obtain the maximum cooling load. As all these methods are stochastic in their working, each algorithm is implemented 100 times on the considered problem to estimate the statistical variations of the algorithms. Each algorithm is implemented with the population size of 50, and the termination criteria are set as 100,000 function evaluations. In Table 5.32, the results obtained in 100 runs using each algorithm are presented in the form of the best solution, the worst solution, average solution, standard deviation, and success rate. Here, the infeasible solutions (i.e., affected by penalty) are eliminated while obtaining the worst solution, average solution, standard deviation, and success rate. Furthermore, the success rate of the algorithm is obtained by considering 0.1% variation from the global optimum value.

**Table 5.32** Comparative results of different algorithms for Ericsson cryorefrigerator optimization

Algorithms	Best	Worst	Average	SD	Success rate (%)
GA	2.6277	2.6078	2.6211	1.15E-02	14
PSO	2.6278	2.6038	2.6168	1.28E-02	16
DE	2.6278	2.6038	2.6209	1.17E-02	30
ABC	2.6278	2.6038	2.6252	7.56E-03	76
CSA	2.6278	2.6038	2.6254	7.60E-03	40
TLBO	2.6278	2.6038	2.6230	1.01E-02	40
SOS	2.6278	2.6038	2.6247	7.99E-03	88
WWO	2.6278	2.6038	2.6229	1.07E-02	20
HTS	2.6278	2.6038	2.6238	9.35E-03	48
PVS	2.6278	2.6038	2.6209	1.17E-02	28
SCA	2.6277	2.6077	2.6177	1.41E-02	12

It can be observed from the comparative results that all the algorithms performed equally good and produced almost identical cooling load of Ericsson cryorefrigerator. Furthermore, the average performance of ABC and CSA algorithms is almost identical and better than other competitive algorithms. However, the success rate of the SOS algorithm in obtaining the optimum value is the highest followed by the ABC algorithm. The success rate of the SCA algorithm is the lowest compared to other algorithms. It can be observed from the results that it is difficult to judge the performance of each algorithm as all the algorithms have produced a different performance to obtain the best, worst, and average results, and success rate. So, the Friedman rank test is implemented to judge the best suitable algorithm for Ericsson cryorefrigerator optimization considering the capability to obtain the best, worst, and average solutions, and success rate. The results of the Friedman rank test are presented in Table 5.33, and its graphical representation is given in Fig. 5.23. The results are presented in the form of Friedman value, normalized value with ‘1’ as the best performing algorithm and its rank. It can be observed from the results that CSA has obtained the first rank followed by ABC, SOS, and HTS algorithms.

The optimized operating condition of Ericsson cryorefrigerator obtained using the CSA algorithm is presented in Table 5.34. It can be noted from the results that the Ericsson cryorefrigerator with the maximum heat sink capacitance rate ( $C_H$ ), heat source’s capacitance rate ( $C_L$ ), the effectiveness of the cold-side heat exchange ( $\varepsilon_L$ ), and effectiveness of the hot-side heat exchanger ( $\varepsilon_H$ ) results in the maximum cooling load. The temperature of the cold side ( $T_c$ ) and temperature ratio ( $x$ ) produced a conflicting effect on achieving the maximum cooling load of cryorefrigerator. Furthermore, all three constraints are at the limiting value in the optimized operating condition of Ericsson cryorefrigerator.

**Table 5.33** Friedman rank test results for Ericsson cryorefrigerator optimization

Algorithms	Friedman value	Normalized value	Rank
GA	35.5	0.478873	6
PSO	43	0.395349	8
DE	36	0.472222	7
ABC	20	0.85	2
CSA	17	1	1
TLBO	24	0.708333	4
SOS	20	0.85	2
WWO	36	0.472222	7
HTS	20.5	0.829268	3
PVS	33.5	0.507463	5
SCA	44.5	0.382022	9

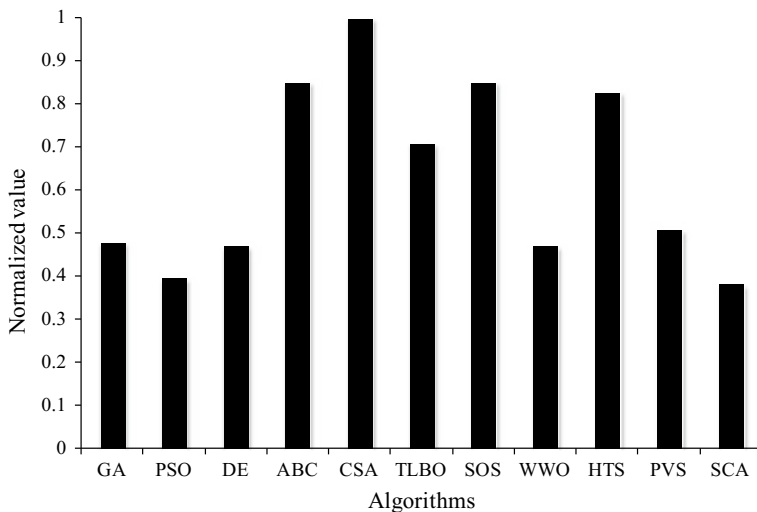


**Fig. 5.23** Graphical presentation of Friedman rank test for Ericsson cryorefrigerator optimization

**Table 5.34** The optimized operating condition of Ericsson cryorefrigerator

Operating parameters	Optimized value
<i>Design variable</i>	
Heat sink capacitance rate ( $C_H$ )	1.5
Heat source's capacitance rate ( $C_L$ )	1.5
Temperature ratio ( $x$ )	1.74
Effectiveness of the cold-side heat exchange ( $\varepsilon_L$ )	0.9
Effectiveness of the hot-side heat exchanger ( $\varepsilon_H$ )	0.9
Temperature of the cold side ( $T_c$ ), K	173.4
<i>Constraints</i>	
Power input ( $P$ ), kW	2.4979
The coefficient of performance, (COP)	1.0514
Ecological function ( $E_F$ )	1.4308
<i>Objective function</i>	
Cooling load ( $R_L$ ), W	1.0895

## References

- Abramzon B. (2007) ‘Numerical Optimization of the Thermoelectric Cooling Devices’, *Journal of Electronic Packaging*, 129(3), 339–347.
- Açıklkalp E., Savaş A.F., Caner N. and Yamık H. (2016) ‘Assessment of nano-scale Stirling refrigerator using working fluid as Maxwell–Boltzmann gases by thermo-ecological and sustainability criteria’, *Chemical Physics Letters*, vol. 658, pp. 303–308.

- Ahmadi M.H. and Ahmadi M.A. (2015) 'Thermodynamic analysis and optimization of an irreversible Ericsson cryogenic refrigerator cycle', *Energy Conversion and Management*, vol. 89, pp. 147–155.
- Ahmadi M.H., Ahmadi M.A., Mohammadi A.H., Feidt M., and Pourkiae S.M. (2015a) 'Multi-objective optimization of an irreversible Stirling cryogenic refrigerator cycle', *Energy Conversion and Management* 82 (2014) 351–360.
- Ahmadi M.H., Ahmadi M.A. and Sadatsakkak S.A. (2015b) 'Thermodynamic analysis and performance optimization of irreversible Carnot refrigerator by using multi-objective evolutionary algorithms (MOEAs)', *Renewable and Sustainable Energy Reviews*, vol. 51, 1055–1070.
- Ahmadi M.H., Ahmadi M.A., Maleki A., Pourfayaz F., Bidi M. and Açıkkalp E. (2017a) 'Exergetic sustainability evaluation and multi-objective optimization of performance of an irreversible nanoscale Stirling refrigeration cycle operating with Maxwell Boltzmann gas', *Renewable and Sustainable Energy Reviews*, vol. 78, pp. 80–92.
- Ahmadi M.H., Ahmadi M.A., Mehrpooya M., Hosseinzade H. and Feidt M. (2014) 'Thermodynamic and thermo-economic analysis and optimization of performance of irreversible four-temperature-level absorption refrigeration', *Energy Conversion and Management*, vol. 88, pp. 1051–1059.
- Ahmadi M.H., Nabakhteh M.A., Ahmadi M.A., Pourfayaz F. and Bidi M., (2017b) 'Investigation and optimization of performance of nano-scale Stirling refrigerator using working fluid as Maxwell–Boltzmann gases', *Physica A: Statistical Mechanics and its Applications*, vol. 483, pp. 337–350.
- Allouche Yosr, Varga Szabolcs, Boudjen Chiheb, Oliveira Armando C. (2017) 'Dynamic simulation of an integrated solar-driven ejector based air conditioning system with PCM cold storage', *Applied Energy*, vol. 190, 600–11.
- Aminyavari M., Najafi B., Shirazi A. and Rinaldi F. (2014) 'Exergetic, economic and environmental (3E) analyses, and multi-objective optimization of a CO<sub>2</sub>/NH<sub>3</sub> cascade refrigeration system', *Applied Thermal Engineering*, vol. 65(1), pp. 42–50.
- Arun M.B., Maiya M.P. and Murthy S.S. (2000) 'Equilibrium low pressure generator temperatures for double-effect series flow absorption refrigeration systems', *Applied Thermal Engineering*, vol. 20(3), pp. 227–242.
- Arun M.B., Maiya M.P. and Murthy S.S. (2001) 'Performance comparison of double-effect parallel-flow and series flow water–lithium bromide absorption systems', *Applied Thermal Engineering*, vol. 21(12), pp. 1273–1279.
- Asgari S., Noorpoor A.R. and Boyaghchi F.A. (2017) 'Parametric assessment and multi objective optimization of an internal auto-cascade refrigeration cycle based on advanced exergy and exergoeconomic concepts', *Energy*, vol. 125, pp. 576–590.
- Batooei A. and Keshavarz A. (2018) 'A Gamma type Stirling refrigerator optimization: An Experimental and Analytical investigation', *International Journal of Refrigeration*, vol. 91, pp. 89–100.
- Bhardwaj P.K., Kaushik S.C. and Jain S. (2003) 'Finite time optimization of an endoreversible and irreversible vapour absorption refrigeration system', *Energy conversion and management*, vol. 44(7), pp. 1131–1144.
- Bhardwaj P.K., Kaushik S.C. and Jain S. (2005) 'General performance characteristics of an irreversible vapour absorption refrigeration system using finite time thermodynamic approach', *International journal of thermal sciences*, vol. 44(2), pp. 189–196.
- Bhattacharyya S., Bose S. and Sarkar J. (2007) 'Exergy maximization of cascade refrigeration cycles and its numerical verification for a transcritical CO<sub>2</sub>–C<sub>3</sub>H<sub>8</sub> system', *International Journal of Refrigeration*, vol. 30(4), pp. 624–632.
- Bhattacharyya S., Garai A., Sarkar J. (2009) 'Thermodynamic analysis and optimization of a novel N<sub>2</sub>O–CO<sub>2</sub> cascade system for refrigeration and heating', *International Journal of Refrigeration*, vol. 32, 1077–1084.
- Bhattacharyya S., Mukhopadhyay S. and Sarkar J. (2008) 'CO<sub>2</sub>–C<sub>3</sub>H<sub>8</sub> cascade refrigeration heat pump system: Heat exchanger inventory optimization and its numerical verification', *International Journal of Refrigeration*, vol. 31(7), pp. 1207–1213.

- Bhattacharyya S., Mukhopadhyay S., Kumar A., Khurana R.K., Sarkar J. (2005) 'Optimization of a CO<sub>2</sub>-C<sub>3</sub>H<sub>8</sub> cascade system for refrigeration and heating', *International Journal of Refrigeration*, vol. 28, 1284–1292.
- Blank D.A. and Wu C. (1996) 'Power limit of an endoreversible Ericsson cycle with regeneration', *Energy Conversion and Management*, vol. 37(1), pp. 59–66.
- Chen J. and Yan Z. (1996) 'The general performance characteristics of a Stirling refrigerator with regenerative losses', *Journal of Physics D: Applied Physics*, vol. 29(4), p. 987.
- Chen J. (1998) 'Minimum power input of irreversible Stirling refrigerator for given cooling rate', *Energy Conversion and Management*, vol. 39(12), pp. 1255–1263.
- Chen J., Zhou Y., Wang H., Wang J.T. (2002) 'Comparison of the optimal performance of single- and two-stage thermoelectric refrigeration systems', *Applied Energy*, vol. 73, 285–298.
- Chen L., Li J. and Sun F. (2012) 'Ecological optimization of a generalized irreversible Carnot refrigerator in the case of Q  $\propto$  ( $\Delta T n$ ) m', *International Journal of Sustainable Energy*, vol. 31 (1), pp. 59–72.
- Chen L., Li J., Sun F., Wu C. (2005) 'Effect of heat transfer on the performance of two-stage semiconductor thermoelectric refrigerators', *Journal of Applied Physics*, vol. 98(3), 1–7.
- Chen L., Sun F. and Wu C. (2001a) 'Effect of heat transfer law on the performance of a generalized irreversible Carnot refrigerator', *Journal of Non-Equilibrium Thermodynamics*, vol. 26(3), pp. 291–304.
- Chen L., Wu C. and Sun F. (2001b) 'Effect of heat transfer law on the finite-time exergoeconomic performance of a Carnot refrigerator', *Exergy, An International Journal*, vol. 1(4), pp. 295–302.
- Chen L., Xiaoqin Z., Sun F. and Wu C. (2004) 'Ecological optimization for generalized irreversible Carnot refrigerators', *Journal of Physics D: Applied Physics*, vol. 38(1), p. 113.
- Chen L., Zheng T., Sun F. and Wu C. (2006a) 'Irreversible four-temperature-level absorption refrigerator', *Solar Energy*, vol. 80(3), pp. 347–360.
- Chen X., Lin B., Chen J. (2006b) 'The parametric optimum design of a new combined system of semiconductor thermoelectric devices', *Applied Energy*, vol. 83, 681–686.
- Cheng Y.H., Lin W.K. (2005) 'Geometric optimization of thermoelectric coolers in a confined volume using genetic algorithms' *Applied Thermal Engineering*, vol. 25, 2983–2997.
- Cheng Y.H., Shih C. (2006) 'Maximizing the cooling capacity and COP of two-stage thermoelectric coolers through genetic algorithm', *Applied Thermal Engineering*, vol. 26, 937–947.
- Cizungu K., Groll M. and Ling Z.G. (2005) 'Modelling and optimization of two-phase ejectors for cooling systems', *Applied thermal engineering*, vol. 25(13), pp. 1979–1994.
- Colgate S.A. (1995) Regenerator Optimization for Stirling Cycle Refrigeration, II. In: Ross R.G. (eds) *Cryocoolers 8*, Springer, Boston, MA, USA.
- Colorado D. and Velazquez V.M. (2013) 'Exergy analysis of a compression-absorption cascade system for refrigeration', *International Journal of Energy Research*, vol. 37(14), pp. 1851–1865.
- Colorado D., Hernandez J.A. and Rivera W. (2012) 'Comparative study of a cascade cycle for simultaneous refrigeration and heating operating with ammonia, R134a, butane, propane and CO<sub>2</sub> as working fluids', *International Journal of Sustainable Energy*, vol. 31(6), pp. 365–381.
- Dai Y., Wang J. and Gao L. (2009) 'Exergy analysis, parametric analysis and optimization for a novel combined power and ejector refrigeration cycle', *Applied Thermal Engineering*, vol. 29 (10), pp. 1983–1990.
- De Tomás C., Hernández A.C. and Roco J.M.M. (2012) 'Optimal low symmetric dissipation Carnot engines and refrigerators', *Physical Review E*, vol. 85(1), p. 010104.
- Ding Z.M., Chen L.G. and Sun F.R. (2015) 'Optimum performance analysis of a combined thermionic-thermoelectric refrigerator with external heat transfer', *Journal of the Energy Institute*, vol. 88(2), pp. 169–180.
- Dokandari D.A., Hagh A.S. and Mahmoudi S.M.S. (2014) 'Thermodynamic investigation and optimization of novel ejector-expansion CO<sub>2</sub>/NH<sub>3</sub> cascade refrigeration cycles (novel CO<sub>2</sub>/NH<sub>3</sub> cycle)', *International journal of refrigeration*, vol. 46, pp. 26–36.

- Dubey A.M., Kumar S. and Agrawal G.D. (2014) 'Thermodynamic analysis of a transcritical CO<sub>2</sub>/propylene (R744–R1270) cascade system for cooling and heating applications', *Energy Conversion and Management*, vol. 86, pp. 774–783.
- Eini S., Shahhosseini H., Delgarm N., Lee M. and Bahadori A. (2016) 'Multi-objective optimization of a cascade refrigeration system: Exergetic, economic, environmental, and inherent safety analysis', *Applied Thermal Engineering*, vol. 107, pp. 804–817.
- Farshchi L.G., Mahmoudi S.S., Rosen M.A., Yari M. and Amidpour M. (2013) 'Exergoeconomic analysis of double effect absorption refrigeration systems', *Energy Conversion and Management*, vol. 65, pp. 13–25.
- Getu H.M. and Bansal P.K. (2008) 'Thermodynamic analysis of an R744–R717 cascade refrigeration system', *International Journal of Refrigeration*, vol. 31(1), pp. 45–54.
- Gomri R. and Hakimi R. (2008) 'Second law analysis of double effect vapour absorption cooler system', *Energy conversion and management*, vol. 49(11), pp. 3343–3348.
- Gomri R. (2009) 'Second law comparison of single effect and double effect vapour absorption refrigeration systems', *Energy Conversion and Management*, vol. 50(5), pp. 1279–1287.
- Guo J. and Shen H.G. (2009) 'Modeling solar-driven ejector refrigeration system offering air conditioning for office buildings', *Energy and Buildings*, vol. 41(2), pp. 175–181.
- Hachem H., Gheith R., Aloui F. and Nasrallah S.B. (2017) 'Optimization of an air-filled Beta type Stirling refrigerator', *International Journal of Refrigeration*, vol. 76, pp. 296–312.
- Hadidi A. (2017) 'A novel approach for optimization of electrically serial two-stage thermoelectric refrigeration systems using chemical reaction optimization (CRO) algorithm', *Energy*, vol. 140, pp. 170–184.
- Hao W. and Guo-Xing W. (2013) 'Ecological optimization for an irreversible magnetic Ericsson refrigeration cycle', *Chinese Physics B*, vol. 22(8), p. 087501.
- Huang Z., Wu F., Chen L., Wu C. and Guo F. (2002) 'Performance optimization for an irreversible quantum Stirling cooler', *Journal of Thermal Science*, vol. 11(3), pp. 193–197.
- Jafari S., Mohammadi B. and Boroujerdi A.A. (2013) 'Multi-objective optimization of a stirling-type pulse tube refrigerator', *Cryogenics*, vol. 55, pp. 53–62.
- Jafarian A., Saidi M.H. and Hannani S.K. (2009) 'Second law based modeling to optimum design of high capacity pulse tube refrigerators', *International Journal of Refrigeration*, vol. 32(1), pp. 58–69.
- Jeon Yongseok, Kim Sunjae, Kim Dongwoo, Chung Hyun Joon, Kim Yongchan (2017) Performance characteristics of an R600a household refrigeration cycle with a modified two-phase ejector for various ejector geometries and operating conditions', *Applied Energy*, vol. 205, 1059–67.
- Karamangil M.I., Coskun S., Kaynakli O. and Yamankaradeniz N. (2010) 'A simulation study of performance evaluation of single-stage absorption refrigeration system using conventional working fluids and alternatives', *Renewable and Sustainable Energy Reviews*, vol. 14(7), pp. 1969–1978.
- Kaushik S.C. and Arora A. (2009) 'Energy and exergy analysis of single effect and series flow double effect water–lithium bromide absorption refrigeration systems', *International journal of Refrigeration*, vol. 32(6), pp. 1247–1258.
- Kaushik S.C., Tyagi S.K., Bose S.K. and Singhal M.K. (2002) 'Performance evaluation of irreversible Stirling and Ericsson heat pump cycles', *International Journal of Thermal Sciences*, vol. 41(2), pp. 193–200.
- Kaynakli O., Saka K. and Kaynakli F. (2015) 'Energy and exergy analysis of a double effect absorption refrigeration system based on different heat sources', *Energy Conversion and Management*, vol. 106, pp. 21–30.
- Kilic M. and Kaynakli O. (2007) 'Second law-based thermodynamic analysis of water-lithium bromide absorption refrigeration system', *Energy*, vol. 32(8), pp. 1505–1512.
- Kilicarslan A. and Hosoz M. (2010) 'Energy and irreversibility analysis of a cascade refrigeration system for various refrigerant couples', *Energy Conversion and Management*, vol. 51(12), pp. 2947–2954.

- Kızılkın Ö., Şencan A. and Kalogirou S.A. (2007) 'Thermoeconomic optimization of a LiBr absorption refrigeration system', *Chemical Engineering and Processing: Process Intensification*, vol. 46(12), pp. 1376–1384.
- Lai H., Pan Y., Chen J. (2004) 'Optimum design on the performance parameters of a two-stage combined semiconductor thermoelectric heat pump', *Semiconductor Science and Technology*, vol. 19, 17–22.
- Li J., Chen L. and Sun F. (2008) 'Cooling load and co-efficient of performance optimizations for a generalized irreversible Carnot refrigerator with heat transfer law  $q \propto (\Delta T_n)^m$ ', *Proceedings of the Institution of Mechanical Engineers, Part E: Journal of Process Mechanical Engineering*, vol. 222(1), pp. 55–62.
- Li R. and Grosu L. (2017) 'Parameter effect analysis for a stirling cryocooler', *International Journal of Refrigeration*, vol. 80, pp. 92–105.
- Lin B. and Chen J. (2006) 'Performance analysis of irreversible quantum Stirling cryogenic refrigeration cycles and their parametric optimum criteria', *Physica Scripta*, vol. 74(2), pp. 251.
- Lin B., Zhao Y. and Chen J. (2008) 'Parametric optimum analysis of an irreversible Ericsson cryogenic refrigeration cycle working with an ideal Fermi gas', *Pramana*, vol. 70(5), pp. 779–795.
- Lubis A., Jeong J., Saito K., Giannetti N., Yabase H. and Alhamid M.I. (2016) 'Solar assisted single-double-effect absorption chiller for use in Asian tropical climates', *Renewable Energy*, vol. 99, pp. 825–835.
- Manohar H.J., Saravanan R. and Renganarayanan S. (2006) 'Modelling of steam fired double effect vapour absorption chiller using neural network', *Energy Conversion and Management*, 47(15–16), pp. 2202–2210.
- Marcos J.D., Izquierdo M. and Palacios E. (2011) 'New method for COP optimization in water-and air-cooled single and double effect LiBr–water absorption machines', *International Journal of Refrigeration*, vol. 34(6), pp. 1348–1359.
- Meng F., Chen L., Sun F. (2009) 'Performance optimization for two-stage thermoelectric refrigerator system driven by two-stage thermoelectric generator', *Cryogenics*, vol. 49(2), 57–65.
- Misra R.D., Sahoo P.K. and Gupta A. (2002) 'Application of the exergetic cost theory to the LiBr/H<sub>2</sub>O vapour absorption system', *Energy*, vol. 27(11), pp. 1009–1025.
- Misra R.D., Sahoo P.K. and Gupta A. (2006) 'Thermoeconomic evaluation and optimization of an aqua-ammonia vapour-absorption refrigeration system', *International Journal of Refrigeration*, vol. 29(1), pp. 47–59.
- Misra R.D., Sahoo P.K., Sahoo S. and Gupta A. (2003) 'Thermoeconomic optimization of a single effect water/LiBr vapour absorption refrigeration system', *International Journal of Refrigeration*, vol. 26(2), pp. 158–169.
- Nasruddin N. V., Sholahudin S., Giannetti N., & Arnas N. V. (2016) 'Optimization of a cascade refrigeration system using refrigerant C<sub>3</sub>H<sub>8</sub> in high temperature circuits (HTC) and a mixture of C<sub>2</sub>H<sub>6</sub>/CO<sub>2</sub> in low temperature circuits (LTC)', *Applied Thermal Engineering*, vol. 104, 96–103.
- Nouadje B.M., Wouagfack P.N. and Tchinda R. (2016) 'Finite-time thermodynamics optimization of an irreversible parallel flow double-effect absorption refrigerator', *International Journal of Refrigeration*, vol. 67, pp. 433–444.
- Pan Y., Lin B., Chen J. (2007) 'Performance analysis and parametric optimal design of an irreversible multi-couple thermoelectric refrigerator under various operating conditions', *Applied Energy*, vol. 84, 882–892.
- Pandya B., Kumar V., Matawala V. and Patel J. (2018) 'Thermal comparison and multi objective optimization of single-stage aqua-ammonia absorption cooling system powered by different solar collectors', *Journal of Thermal Analysis and Calorimetry*, pp. 1–14.
- Pandya B., Patel J. and Mudgal A. (2017) 'Thermodynamic Evaluation of Generator Temperature in LiBr-Water Absorption System for Optimal Performance', *Energy Procedia*, vol. 109, pp. 270–278.

- R. Rezayan, A. Behbahaninia (2011) 'Thermoeconomic optimization and exergy analysis of CO<sub>2</sub>/NH<sub>3</sub> cascade refrigeration systems', *Energy*, vol. 36 888–895.
- Rao, R.V. and Patel, V. (2013) 'Multi-objective optimization of two stage thermoelectric cooler using a modified teaching–learning-based optimization algorithm. Engineering Applications of Artificial Intelligence', vol. 26(1), pp. 430–445.
- Rashidi M.M., Aghagoli A. and Raoofi R. (2017) 'Thermodynamic analysis of the ejector refrigeration cycle using the artificial neural network', *Energy*, vol. 129, pp. 201–215.
- Rubio-Maya C., Pacheco-Ibarra J.J., Belman-Flores J.M., Galván-González S.R. and Mendoza-Covarrubias C. (2012) 'NLP model of a LiBr–H<sub>2</sub>O absorption refrigeration system for the minimization of the annual operating cost', *Applied Thermal Engineering*, vol. 37, pp. 10–18.
- Sadeghi M., Mahmoudi S.M.S. and Saray R.K. (2015) 'Exergoeconomic analysis and multi objective optimization of an ejector refrigeration cycle powered by an internal combustion (HCCI) engine', *Energy Conversion and Management*, vol. 96, pp. 403–417.
- Sadeghi M., Yari M., Mahmoudi S.M.S. and Jafari M. (2017) Thermodynamic analysis and optimization of a novel combined power and ejector refrigeration cycle–Desalination system. *Applied Energy*, vol. 208, pp. 239–251.
- Sahin B. and Kodal A. (1999) 'Finite time thermoeconomic optimization for endoreversible refrigerators and heat pumps', *Energy Conversion and Management*, vol. 40(9), pp. 951–960.
- Sarkar J. (2008) 'Optimization of ejector-expansion transcritical CO<sub>2</sub> heat pump cycle', *Energy*, vol. 33(9), pp. 1399–1406.
- Su H., Gong G., Wang C. and Zhang Y. (2017) 'Thermodynamic optimization of an irreversible Carnot refrigerator with heat recovery reservoir', *Applied Thermal Engineering*, vol. 110, pp. 1624–1634.
- Tyagi S.K., Chen J., Lin G. and Kaushik S.C. (2005) 'Ecological optimization of an irreversible Ericsson cryogenic refrigerator cycle', *International Journal of Energy Research*, vol. 29(13), pp. 1191–1204.
- Tyagi S.K., Kaushik S.C. and Salohtra R. (2002) 'Ecological optimization and parametric study of irreversible Stirling and Ericsson heat pumps', *Journal of Physics D: Applied Physics*, vol. 35 (16), p. 2058.
- Tyagi S.K., Kaushik S.C. and Singhal M.K. (2002) 'Parametric study of irreversible Stirling and Ericsson cryogenic refrigeration cycles', *Energy Conversion and Management*, vol. 43(17), pp. 2297–2309.
- Tyagi S.K., Lin G., Kaushik S.C. and Chen J. (2004) 'Thermo-economic optimization of an irreversible Stirling cryogenic refrigerator cycle', *International Journal of Refrigeration*, vol. 27(8), pp. 924–931.
- Ust Y. and Karakurt, A.S. (2014) 'Analysis of a Cascade Refrigeration System (CRS) by Using Different Refrigerant Couples Based on the Exergetic Performance Coefficient (EPC) Criterion', *Arabian Journal for Science and Engineering*, vol. 39(11), pp. 8147–8156.
- Ust Y. and Sahin, B. (2007) 'Performance optimization of irreversible refrigerators based on a new thermo-ecological criterion', *International Journal of Refrigeration*, vol. 30(3), pp. 527–534.
- Velasco S., Roco J.M.M., Medina A. and Hernández A.C. (1997) 'New performance bounds for a finite-time carnot refrigerator', *Physical Review Letters*, vol. 78(17), p. 3241.
- Wu F., Chen L., Wu S. and Sun, F. (2006) 'Performance of an irreversible quantum Ericsson cooler at low temperature limit', *Journal of Physics D: Applied Physics*, vol. 39(21), p. 4731.
- Xia Z.R., Ye X.M., Lin G.X. and Brück E. (2006) 'Optimization of the performance characteristics in an irreversible magnetic Ericsson refrigeration cycle', *Physica B: Condensed Matter*, vol. 381(1–2), pp. 246–255.
- Xu G.P. and Dai Y.Q. (1997) 'Theoretical analysis and optimization of a double-effect parallel flow-type absorption chiller', *Applied thermal engineering*, 17(2), pp. 157–170.
- Xuan X.C. (2002) 'Analyses of the performance and polar characteristics of two-stage thermoelectric coolers', *Semiconductor Science and Technology*, vol. 17, 414–420.

- Xuan X.C., Ng K.C., Yap C., and Chua H.T. (2002a) ‘Optimization of two stage thermoelectric coolers with two design configurations’, *Energy Conversation and Management*, vol. 43, 2041–2052.
- Xuan X.C., Ng K.C., Yap C., and Chua H.T. (2002b) ‘The maximum temperature difference and polar characteristic of two-stage thermoelectric coolers’, *Cryogenics*, vol. 42, 273–278.
- Yan Z. and Chen L., 1996. Optimization of the rate of exergy output for an endoreversible Carnot refrigerator. *Journal of Physics D: Applied Physics*, 29(12), p. 3017.
- Yan Z. and Lin G. (2000) ‘Ecological optimization criterion for an irreversible three-heat source refrigerator’, *Applied Energy*, vol. 66(3), pp. 213–224.
- Yapıcı R., Ersoy H.K., Aktoprakoğlu A., Halkacı H.S. and Yiğit O. (2008) ‘Experimental determination of the optimum performance of ejector refrigeration system depending on ejector area ratio’, *International Journal of Refrigeration*, vol. 31(7), pp. 1183–1189.
- Yari M. (2009) ‘Performance analysis and optimization of a new two-stage ejector-expansion transcritical CO<sub>2</sub> refrigeration cycle’, *International Journal of Thermal Sciences*, vol. 48(10), pp. 1997–2005.
- Yen R.H., Huang B.J., Chen C.Y., Shiu T.Y., Cheng C.W., Chen S.S. and Shestopalov K. (2013) ‘Performance optimization for a variable throat ejector in a solar refrigeration system’, *International Journal of Refrigeration*, vol. 36(5), pp. 1512–1520.
- Yu J., Zhao H., Xie K. (2007) ‘Analysis of optimum configuration of two-stage thermoelectric modules’, *Cryogenics*, vol. 47(2), 89–93.
- Zhang J. and Xu Q. (2011) ‘Cascade refrigeration system synthesis based on exergy analysis’, *Computers & Chemical Engineering*, vol. 35(9), pp. 1901–1914.
- Zhou Q., Chen L., Pan C., Zhou Y. and Wang J. (2015) ‘Experimental Investigation on Regenerator Materials of Stirling-type Pulse-tube Refrigerator Working at 20 K’, *Physics Procedia*, vol. 67, pp. 530–535.
- Zhou Y. and Yu J. (2012) ‘Design optimization of thermoelectric cooling systems for applications in electronic devices’, *International Journal of Refrigeration*, vol. 35(4), pp. 1139–1144.
- Zhu X., Chen L., Sun F. and Wu C. (2006) ‘Exergy-based ecological optimization for a generalized irreversible Carnot refrigerator’, *Journal of the Energy Institute*, vol. 79(1), pp. 42–46.

# Chapter 6

## Thermal Design and Optimization of Power Cycles



**Abstract** Power-generating cycles are used to produce mechanical energy from thermal energy. A part of the thermal energy is converted into mechanical energy, and the remaining thermal energy can either be used for other applications or rejected into the heat sink. The mechanical energy can then be converted into electric energy. In this chapter, thermal modeling of different power-generating cycles including the Rankine cycle, the Brayton cycle, the Braysson cycle, and the Kalina cycle is presented. The objective function for each of the power-generating cycles is derived from the thermal model. Optimization of a derived objective is performed by implementing 11 different metaheuristic algorithms for each power-generating cycle, and then the comparative results are tabulated and discussed.

Power generation is defined as the process of converting thermal energy (which is generated from the chemical energy of fuel through fuel combustion) into mechanical energy. The mechanical energy is then further converted into electric energy. The entire system used to generate power is called the power-generating system. A power-generating system operates on a thermodynamic cycle. Steam and gas are the conventional working fluids for the power-generating cycles. Based on the working fluid, power-generating cycle is classified as steam power cycle or gas power cycle. The steam power cycle used water/steam as a working fluid while gas power cycle used gas as a working fluid. However, nowadays different organic fluids can also be used in power-generating cycles. The working fluid got the heat energy and converted the part of heat energy into mechanical energy. Remaining heat energy of the working fluids can be used for other applications also. In case of steam power cycle, working fluid changes its phase from liquid to vapor and again into the liquid through the power-generating process. In case of the gas power cycle, working fluid remains in the gaseous phase throughout the power generation process. Apart from the steam power cycle, nuclear power generation and hydro-power generation also used water as a working fluid.

Thermal design and optimization of power-generating cycles are essential for its efficient operation. Generally, objectives involved in the optimization of

power-generating cycles are maximum power output, maximum thermal efficiency, maximum exergetic efficiency, minimum total annual cost, minimum entropy generation, etc. In the subsequent section, thermal modeling and optimization of various power-generating cycles are presented and discussed.

## 6.1 Rankine Power Cycle

A steam power plant operates on the Rankine cycle. The Basic components of any steam power plant are pump, boiler, turbine, and condenser. Apart from these basic components, other accessories and attachments are used in the steam power plant to enhance its efficiency and to maintain safe operation. The schematic arrangement of the steam power plant as well as its different components is shown in Fig. 6.1. The functions of each of the components are mentioned below.

- Coal handling: This unit takes the coal from coal storage, converted it into pulverized form, and supplied it to boiler furnace.
- Boiler: It converts the water into high-temperature steam by utilizing the heat energy generated through fuel combustion.
- Air preheater: It is used to preheat the supplied air before entering into the boiler furnace with the help of exhaust gases from the boiler furnace.
- Economizer: It is used to heat the feed water supplied to the boiler with the help of exhaust gases from the boiler furnace.
- Steam turbine: It is used to expand high-pressure and high-temperature steam. Due to the expansion, the kinetic energy of the steam is converted into the mechanical energy.

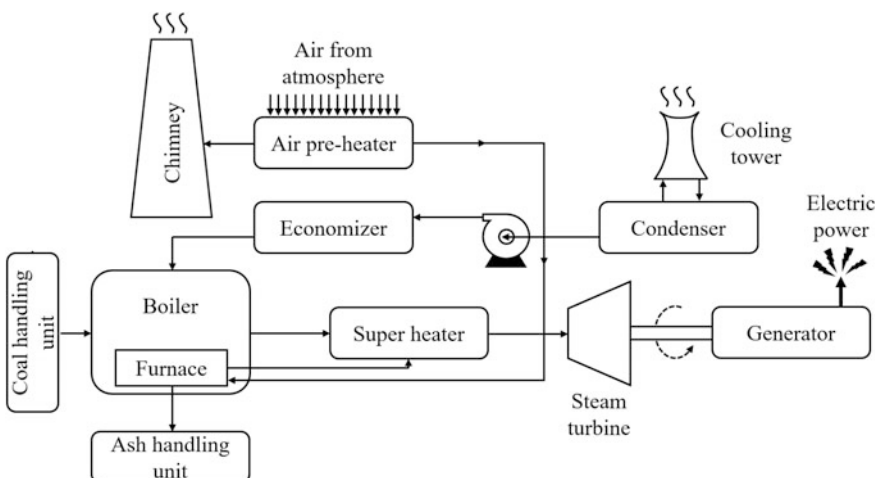


**Fig. 6.1** Schematic arrangement of steam power plant

- Generator: It is used to convert the mechanical energy generated by the turbine into the electrical energy.
- Condenser: It is used to condense low-pressure steam coming out from the turbine with the help of cooling water (steam is converted into water).
- Cooling tower: It is used to cool the water coming out of the condenser.
- Chimney: It is used to release the hot flue gases of the boiler furnace to the environment at the appropriate height.
- Feed water pump: It is used to pump the feed water coming from the condenser into the boiler.
- Ash-handling unit: This unit takes the ash from the furnace for the further process of ash dumping.

In the steam power plant, the pulverized coal is supplied to the boiler furnace where the combustion of the coal generates heat energy. With the help of this heat energy, the water present in the boiler is converted into the high-pressure, high-temperature steam. From the boiler, the high-temperature steam is passed to the superheater where it is further heated. This superheated steam supplied to the steam turbine is expanded, which converts the kinetic energy of the steam into mechanical energy. The mechanical energy generated by the turbine is further converted into electric energy with the help of a generator attached to the shaft of the turbine. After expansion, the low-pressure steam supplied to the condenser is converted into water with the help of the cooling water. The condensed water is supplied to the boiler via the economizer with the help of the feed water pump. The exhaust gases from the furnace pass through the superheater, economizer, and air preheater. The heat of the exhaust gases is utilized in the heating of steam in the superheater, the heating of the feed water in the economizer, and the heating of the air in the air preheater. After the burning of the coal in the furnace, it is transported to the ash-handling plant and finally to the ash storage.

As mentioned previously, the steam power plant works on the Rankine cycle. The thermodynamic representation (pressure-volume and temperature-entropy) of the Rankine cycle is shown in Fig. 6.2. The feed water pump supplied water from the condenser to the boiler, hence increasing its pressure (process 4–1). The pumping process is isentropic. In the boiler, the water is converted into high-temperature steam through the heat supplied (process 1–2). Here, the steam generation process refers to the process during which water is converted into steam. From the steam generator, high-pressure and high-temperature steam is supplied to the steam turbine. Expansion of steam takes place in the steam turbine (process 2–3). The expansion process is isentropic. At the end of the expansion, the existing low-pressure steam is converted into water in the condenser by rejecting heat to the cooling media (process 3–4) and completes the cycle.

Earlier, researchers carried out various works related to the analysis and optimization of the steam power plant. Dincer and Musilim (2001) presented an energy and exergy analysis of a Rankine cycle reheat steam power plant considering different system parameters such as boiler temperature, boiler pressure, mass fraction ratio, and work output. Bekdemir et al. (2003) presented the effects of a

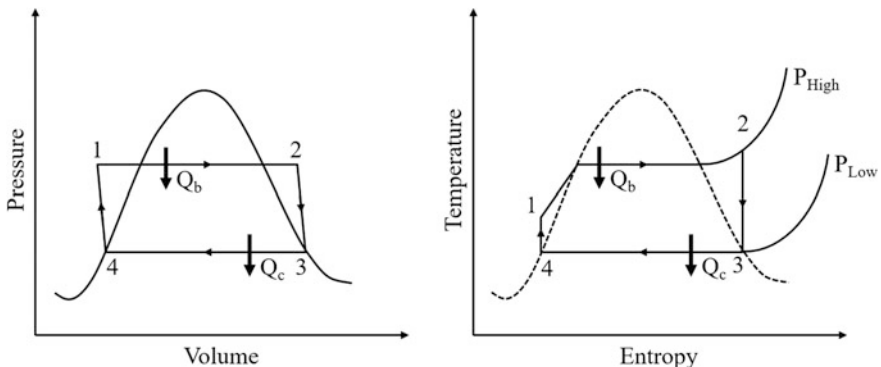


**Fig. 6.2** Thermodynamic presentation of Rankine cycle

turbine inlet condition and turbine power on heat transfer area, cooling water flow-rate, and condenser cost for surface type condenser. Ameri et al. (2009) performed the energy, exergy, and exergoeconomic analysis of the steam power plant. They estimated the exergy destruction and exergy loss of each component of this power plant. Furthermore, the authors also estimated the exergy efficiencies of the boiler, turbine, pump, heaters, and the condenser at different ambient temperatures. Aljundi (2009) presented the energy and exergy analysis of Al-Hussein power plant in Jordan. The author also analyzed the system components separately to identify and quantify the largest energy and exergy losses. Ataei and Yoo (2010) presented the simulation of a steam power plant and operational parameters of the Rankine cycle using the exergy concept combined with a pinch-based approach. Seyyedi et al. (2010) used exergoeconomic analysis, sensitivity analysis, and structural optimization method to determine the sum of the investment and exergy destruction cost flow rates for each component of the thermal power plant.

Hajabdollahi et al. (2011) carried out a multi-objective optimization of a heat recovery steam generator in a combined cycle power plant. The author considered the minimization of the total cost and maximization of the exergy efficiency of the power plant as an objective function and adopted NSGA-II as an optimization technique. The authors also presented a case study of the power plant with optimized results and its comparison with the base case. Ahmadi and Dincer (2011a, b) carried out a thermodynamic analysis and economic optimization of a combined cycle power plant with a supplementary firing. The authors obtained the optimum operating parameters of the power plant in order to minimize the total cost of the system by adopting a genetic algorithm. Hajabdollahi et al. (2012a, b) presented the thermo-economic model of the actual running steam power plant and performed its optimization. The authors considered fifteen operating variables of the steam power plant to obtain maximum thermal efficiency and the minimum total cost of the power plant. The authors adopted NSGA-II as an optimization tool and compared the optimized results with the base case result. Kaviri et al. (2013) performed the energy and exergy analysis of a heat recovery steam generators in a combined cycle

power plant for exergoenvironmental optimization. Luo et al. (2013) performed an operational planning optimization of steam power plants considering the equipment failure. Abadi et al. (2014) found the optimum integration of a steam power plant as a source and a site utility system as a sink of steam and power.

The effect of changing turbine inlet specifications to increase the overall plant efficiency is often quoted and discussed in many studies. The positive effect of changing turbine inlet temperature to increase the overall plant efficiency was demonstrated by Richert et al. (2015). Ganjehkaviri et al. (2015) demonstrated that steam turbine outlet quality was a restrictive parameter. The optimization of three cases with different steam qualities was conducted and discussed. In another study, Topel et al. (2015) studied the potential for the improvement of the performance of power plants through the increase of steam turbine flexibility at the time of start-up. Exergy and exergoeconomic analysis of commercial-sized, direct steam generation parabolics through a solar thermal power plant was demonstrated by Elsaifi (2015). Tangwe et al. (2015) developed a multiple linear regression model for the coal-based thermal power plant which included the temperature of the air heater, the main superheater steam, the high-pressure heater, the condenser well, and the mass of the coal burnt as the predictors. The authors adopted a constraint linear least square regression technique for computing the optimal input data set corresponding to the desired response. In another research work related to steam temperature, Wu et al. (2015) developed a stable fuzzy model predictive controller (SF MPC) to solve the superheated steam temperature (SST) control problem in a power plant. Dincer et al. (2017) carried out thermodynamic modeling, analysis, and optimization of steam power plants by using the genetic algorithm. The authors observed the significant improvement in the exergy efficiency of the steam power plant with optimal design parameters.

### 6.1.1 *Thermal Model*

In this part of the work, a steam power plant working on the Rankine cycle is considered for optimization. The schematic diagram of the considered steam cycle power plant is shown in Fig. 6.3. Feed water is superheated in point 32 and enters a high-pressure turbine (HPT) at 537 °C and 12.5 MPa. Then it is reheated in the boiler and enters the intermediate- (IPT) and low-pressure turbines (LPW). All the turbines, which are in a single shaft, rotate with 3000 rpm and produce 158.6 MW of power. The exhaust feed water pressure in the last expansion stage (point 7) is 8.5 kPa (condenser pressure). One open feed water heater (deaerator) and five closed feed water heaters (FWH), including three low pressures and two high-pressures ones, are used in this plant to increase the boiler inlet temperature to approximately 250 °C. High-pressure FWHs are fed by the HP and IP turbines while extraction from IP and LP turbines feeds the low-pressure FWHs. The thermal model presented here is based on the previous work of Hajabdollahi et al. (2012a, b).

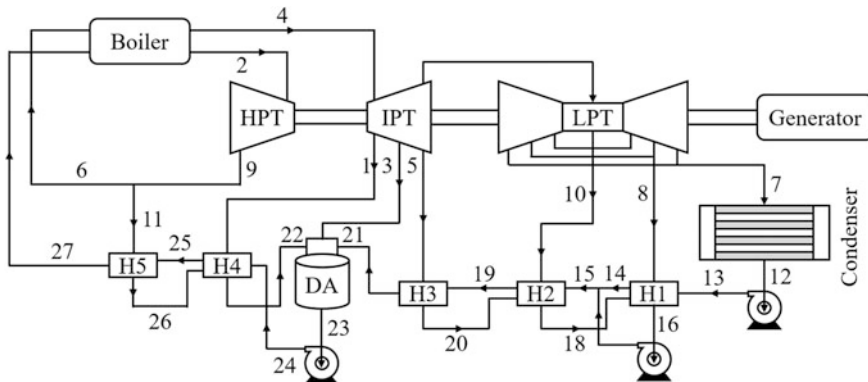


**Fig. 6.3** Schematic diagram of the steam cycle power plant considered for optimization (Hajabdollahi et al. 2012a, b; Reprinted with permission from Elsevier)

The thermal modeling of the mentioned cycle is performed in a steady state situation. Further, the subscripts 1–28 are a different state point corresponding to Fig. 6.3. The mass and energy conservation laws (for control volume) lead to the following relations:

$$\sum \dot{m}_i = \sum \dot{m}_o \quad (6.1)$$

$$\dot{Q} - \dot{W} = \sum \dot{m}_i h_i - \sum \dot{m}_o h_o \quad (6.2)$$

where the subscripts i and o are inlet and outlet streams, respectively. It is assumed that there is no heat loss in the turbines and pump. It's also assumed that there are no work interactions in the different types of heat exchangers used in this plant. Moreover, the outlet pressure in the different heat exchangers including the boiler, condenser as well as the feedwater heaters is obtained by assuming that the constant pressure drop in this equipment is as follows.

$$P_o = P_i(1 - \Delta P) \quad (6.3)$$

The actual work output ( $\dot{W}_{T,a}$ ) and associated isentropic efficiency ( $\eta_T$ ) of the steam turbine are given by the following equations:

$$\dot{W}_{T,a} = \sum \dot{m}_i h_i - \sum \dot{m}_o h_o \quad (6.4)$$

$$\eta_T = \frac{\dot{W}_{T,a}}{\dot{W}_{T,s}} = \frac{h_i - h_{o,a}}{h_i - h_{o,s}} \quad (6.5)$$

where subscripts a and s indicate the actual and isentropic situation, respectively.

The following equation gives the heat transfer rate in the boiler ( $\dot{Q}_b$ ) and its associated boiler efficiency ( $\eta_b$ ):

$$\dot{Q}_b = \dot{m}_{27}(h_2 - h_{27}) + \dot{m}_6(h_4 - h_6) \quad (6.6)$$

$$\eta_b = \frac{\dot{Q}_b}{\dot{m}_{\text{fuel}} \text{ LHV}} \quad (6.7)$$

where  $\dot{m}_{\text{fuel}}$  and LHV are the boiler fuel mass flow rate as well as the fuel lower heating value, respectively.

The following equation gives the heat transfer rate in the condenser ( $\dot{Q}_c$ ).

$$\dot{Q}_c = \dot{m}_7(h_7 - h_{12}) \quad (6.8)$$

The following equation gives the isentropic efficiency ( $\eta_T$ ) of the pump.

$$\eta_p = \frac{\dot{W}_{P,s}}{\dot{W}_{P,a}} = \frac{v_i \Delta P}{(h_e - h_i)} \quad (6.9)$$

The following equation gives the energy balance for the feedwater heater.

$$\sum \dot{m}_i h_i = \sum \dot{m}_o h_o \quad (6.10)$$

Thermodynamic properties of water could be obtained by taking two independent properties. To complete the equations, the terminal temperature difference (TTD) for the FWTs is used by the following definition:

$$\text{TTD} = T_{\text{sat,ext}} - T_{\text{o,FWH}} \quad (6.11)$$

where  $T_{\text{sat,ext}}$  and  $T_{\text{o,FWH}}$  are saturated steam temperature from turbine extraction and the temperature of the feed water leaving the FWH, respectively.

Finally, the thermal efficiency of the cycle is obtained as

$$\eta = \frac{\dot{W}_{\text{net}}}{\dot{m}_{\text{fuel}} \text{ LHV}} \quad (6.12)$$

where  $\dot{W}_{\text{net}}$  is the total net power estimated as the difference between turbines and pumps power as follows.

$$\dot{W}_{\text{net}} = (\dot{W}_{\text{HPT}} + \dot{W}_{\text{IPT}} + \dot{W}_{\text{LPT}}) - (\dot{W}_{P1} + \dot{W}_{P2} + \dot{W}_{P3}) \quad (6.13)$$

The rate of the total cost (\$/s) is suggested to be based on capital and fuel costs:

$$C_{\text{tot}} = (a \cdot \varphi C_{\text{cap}} + C_{\text{fuel}}) / (3600 N) \quad (6.14)$$

where  $\varphi$  and  $N$  are the maintenance coefficient and the operational hours in a year, respectively. Moreover,  $C_{\text{cap}}$  is the capital cost of equipment listed in Table 6.1.  $a$  is the annual cost factor defined as

$$a = \frac{ir}{1 - (1 + ir)^{-y}} \quad (6.15)$$

where  $ir$  and  $y$  are the rate of interest and lifetime, respectively. The annual boiler fuel cost (\$/year) is estimated as

$$C_{\text{fuel}} = (3600 \dot{m}_f N c_{\text{fuel}}) \quad (6.16)$$

where  $C_{\text{fuel}}$  is the unit price of fuel (\$/kg).

Based on the above thermal model, the objective function for the present work is defined in the next section.

### 6.1.2 Case Study, Objective Function Description, and Constraints

A steam cycle power plant (schematically shown in Fig. 6.3) operated on the Rankine cycle needs to be optimized for minimum total cost rate. The power station should deliver 160 MW net output power. The allowable pressure drop of 3% is considered in each side of the feedwater heaters. On the other hand, a 1% pressure drop is considered from the turbine outlet to the inlet of the heater. 5% is considered in the boiler. The terminal temperature difference (TTD) =  $+3^\circ$  for the LP feedwater heaters and TTD =  $-3^\circ$  for the HP feedwater heaters. The total cost rate is considered as an objective function. The system is optimized for depreciation time  $y = 20$  years, interest rate  $r = 0.1$ , and 0.1 \$/kg as the fuel cost. Fifteen design variables which include pressure and temperature of various state points ( $P_4, T_2, P_9, P_1, P_3, P_5, P_{10}, P_8, P_7$ ) and isentropic efficiency of various components ( $\eta_{P1}, \eta_{P2}, \eta_{P3}, \eta_{HPT}, \eta_{IPT}, \eta_{LPT}$ ) are considered for the optimization problem. The upper and lower bounds of design variables are presented in Table 6.2.

As mentioned above, the minimization of the total cost rate of the steam power plant is taken as an objective function in the present study. Furthermore, the operating parameters which result in minimum annual cost also satisfy the steam temperature at the outlet of the turbine, the dryness fraction of steam at the outlet of the turbine, and the thermal efficiency constraints. So, considering all the aspects, the objective function of the steam cycle power plant is formulated as below:

**Table 6.1** Capital cost of different equipments (Hajabdollahi et al. 2012a, b; Reprinted with permission from Elsevier)

Equipment	Capital cost (\$)
Boiler	$C_{\text{Boiler}} = \exp\left(\frac{P_6 - \bar{P}_6}{a_3}\right) * \left(1 + \left(\frac{1 - \bar{\eta}_1}{1 - \eta_1}\right)^{a_4}\right) * \left(1 + a_5 \exp\left(\frac{T_6 - \bar{T}_6}{a_6}\right)\right) \emptyset_{\text{SH/RSH}} a_1 (\dot{m}_{\text{Boiler}})^{a_2}$ <span style="float: right;">(6.17)</span>
	$\emptyset_{\text{SH/RSH}} = 1 + \frac{T_6 - T_{\text{SH}}}{T_6} + \frac{\dot{m}_{\text{RSH}}}{\dot{m}_{\text{Boiler}}} \frac{T_{\text{RSH}} - T_{\text{SH}}}{T_{\text{eSH}}}$ <span style="float: right;">(6.18)</span>
	$\bar{T}_e = 593^\circ\text{C}, \bar{P}_e = 28 \text{ bar}, \bar{\eta}_1 = 0.9,$ <span style="float: right;">(6.19)</span>
	$a_1 = 208,582 \frac{\$}{\text{kg}}^s, a_2 = 0.8, a_3 = 15 \text{ MPa}, a_4 = 7, a_5 = 5, a_6 = 10.4^\circ\text{C}$ <span style="float: right;">(6.20)</span>
Steam turbine	$C_{\text{ST}} = a_{15} P_{\text{ST}}^{0.7} \left(1 + \left(\frac{0.05}{1 - \eta_{\text{ST}}}\right)^3\right) \left(1 + 5 \exp\left(\frac{T_{\text{L}} - 866 \text{ K}^{-1}}{10.42 \text{ K}^{-1}}\right)\right)$ <span style="float: right;">(6.21)</span>
	$a_{51} = 3880.5 \$ \text{ kW}^{-0.7}$ <span style="float: right;">(6.22)</span>
Condenser	$C_{\text{cond}} = a_{61} \frac{\dot{Q}_{\text{cond}}}{k A_{\text{in}}} + a_{62} \dot{m}_{\text{CW}} + 70.5 \dot{Q}_{\text{Cond}} (-0.6936 \ln(\bar{T}_{\text{CW}} - T_b) + 2.189)$ <span style="float: right;">(6.23)</span>
	$a_{61} = 280.74 \$ \text{ m}^{-2}, a_{62} = 7462 \$ / \text{kg s}, k = 2200 \text{ W m}^{-2} \text{ K}^{-1}$ <span style="float: right;">(6.24)</span>
Deaerator	$C_{\text{DA}} = a_1 (\dot{m}_{\text{water}})^{a_2}, a_1 = 145,315 \$ \text{ kW}^{-0.7}, a_2 = 0.7$ <span style="float: right;">(6.25)</span>
Pump	$C_{\text{pump}} = a_7 P_{\text{pump}}^{0.71} \left(1 + \frac{0.2}{1 - \eta_{\text{pump}}}\right),$ <span style="float: right;">(6.26)</span>
	$a_{71} = 705 \$ \text{ kg}^{-1} \text{ s}^{-1}$ <span style="float: right;">(6.27)</span>

**Table 6.2** Ranges of design variables for Rankine power cycle optimization

Design variable	Lower bound	Upper bound
$T_2$ (°C)	500	560
$P_1$ (MPa)	1	2
$P_3$ (MPa)	0.4	1
$P_5$ (MPa)	0.3	0.4
$P_7$ (MPa)	0.005	0.05
$P_8$ (MPa)	0.05	0.1
$P_{10}$ (MPa)	0.1	0.3
$P_9$ (MPa)	2	4
$P_2$ (MPa)	8	18
$\eta_{P1}$	0.5	0.8
$\eta_{P2}$	0.5	0.8
$\eta_{P3}$	0.5	0.8
$\eta_{HPT}$	0.7	0.9
$\eta_{IPT}$	0.7	0.9
$\eta_{LPT}$	0.7	0.9

$$\begin{cases} \text{Minimize } f(X) = C_{\text{tot}}(X) + \sum_{j=1}^n G_1(g_j(X))^2 \\ X = [x_1, x_2, x_3, \dots, x_D], \quad x_{i,\text{minimum}} \leq x_i \leq x_{i,\text{maximum}} \quad i = 1, 2, 3, \dots, D \\ g_j(X) \leq 0, \quad j = 1, 2, 3, \dots, n \end{cases} \quad (6.28)$$

where  $X$  is the vector of design variables which should be bounded between its minimum and maximum values.  $G_1$  is the penalty parameter, and the entire term takes into account the effect of constraints violation. This term comes into picture when constraint violation takes place.  $g_j(X)$  indicates the constraints. The following constraints are considered for the Rankine power cycle.

$$T_7 > 40 \text{ °C} \quad (6.29)$$

$$x_7 > 0.95 \quad (6.30)$$

$$\eta \geq 40\% \quad (6.31)$$

The next section describes the results and discussion of the case study.

### 6.1.3 Results and Discussion

The considered problem of the team cycle power plant is investigated using 11 different metaheuristic approaches to obtain the minimum total cost rate. As all

these methods are stochastic in their working, each algorithm is implemented 100 times on the considered problem to estimate the statistical variations of the algorithms. Each algorithm is implemented with the population size of 50, and the termination criteria are set as 100,000 function evaluations. The results obtained using each algorithm are presented in the form of the best solution, the worst solution, the average solution, the standard deviation, and the success rate obtained in 100 runs. This is presented in Table 6.3. Here, the solutions which are infeasible (i.e., affected by penalty) are eliminated while still obtaining the worst solution, the average solution, the standard deviation, and the success rate. Furthermore, the success rate of the algorithm is obtained by considering 0.1% variation from the global optimum value.

It can be observed from the comparative results that all the algorithms performed equally good and produced almost identical minimum total cost rate of the steam cycle power plant. However, the average performance of DE and PVS is furthermore compared to other competitive algorithms. The average performance of ABC is inferior when compared to other algorithms. In the results, it is observed that the success rate of the DE algorithm in obtaining the optimum value is the highest, which is followed by the PVS algorithm. As for the lowest success rate, the HTS algorithm is the lowest when compared to other algorithms. It can be observed from the results that it is difficult to judge the performance of the algorithm as all the algorithms have performed differently to obtain the best, worst, and average results, and success rate. So, the Friedman rank test is implemented to judge the best suitable algorithm for steam cycle power plant optimization based on the capability to obtain the best, worst, and average solutions, and success rate. The results of the Friedman rank test are presented in Table 6.4, and its graphical representation is given in Fig. 6.4. The results are presented in the form of a Friedman value, where a normalized value with ‘1’ as the best performing algorithm and its rank. It is observed from the results that DE has obtained the first rank followed by PVS and CSA algorithms.

**Table 6.3** Comparative results of different algorithms for Rankine power cycle optimization

Algorithms	Best	Worst	Average	SD	Success rate (%)
GA	1.4427	1.59144	1.5077	5.96E-02	68
PSO	1.4427	1.49349	1.4573	1.72E-02	79
DE	1.4427	1.44791	1.4432	1.66E-03	94
ABC	1.4427	1.70384	1.5551	1.12E-01	60
CSA	1.4427	1.4756	1.4539	1.27E-02	84
TLBO	1.4427	1.77515	1.4823	1.10E-01	56
SOS	1.4427	1.51835	1.4576	2.27E-02	72
WWO	1.4427	1.65783	1.5052	7.11E-02	64
HTS	1.4427	1.8523	1.5247	1.83E-01	52
PVS	1.4427	1.4479	1.4433	1.63E-03	92
SCA	1.4427	1.5607	1.4881	4.63E-02	70

**Table 6.4** Friedman rank test results for Rankine power cycle optimization

Algorithms	Friedman value	Normalized value	Rank
GA	37	0.189189	7
PSO	23	0.304348	4
DE	7	1	1
ABC	46	0.152174	9
CSA	19	0.368421	3
TLBO	37	0.189189	7
SOS	27	0.259259	5
WWO	39	0.179487	8
HTS	50	0.14	10
PVS	13	0.538462	2
SCA	32	0.21875	6

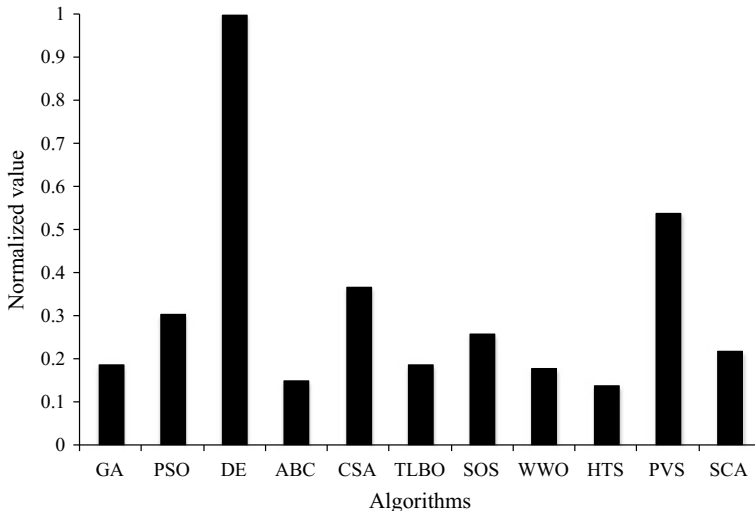


**Fig. 6.4** Graphical presentation of Friedman rank test for Rankine power cycle optimization

The optimized operating parameters of steam cycle power plant obtained using the DE algorithm are presented in Table 6.5. It can be noted from the results that the steam cycle power plant with the lowest  $P_1$ ,  $P_3$ ,  $P_5$ ,  $P_8$ , and  $P_{28}$  and the highest  $P_{10}$ ,  $\eta_{P1}$ ,  $\eta_{P2}$ ,  $\eta_{P3}$ ,  $\eta_{HPT}$ ,  $\eta_{IPT}$ , and  $\eta_{LPT}$  results in the minimum cost rate of the plant. The pressure and steam coming out of turbine ( $P_{32}$ ,  $T_{32}$ ) and the pressure of steam at the exit of the turbine ( $P_7$ ) produced a conflicting effect on achieving the minimum cost rate of the steam power plant. Further, all three constraints lower the value in the optimized operating condition of the steam power plant.

**Table 6.5** Optimized operating condition of steam cycle power plant

Operating parameters	Optimized value
<i>Operating variable</i>	
$T_2$ (°C)	547.22
$P_1$ (MPa)	1
$P_3$ (MPa)	0.5
$P_5$ (MPa)	0.3
$P_7$ (MPa)	0.007385
$P_8$ (MPa)	0.05
$P_{10}$ (MPa)	0.3
$P_9$ (MPa)	2
$P_2$ (MPa)	9.2
$\eta_{P1}$	0.8
$\eta_{P2}$	0.8
$\eta_{P3}$	0.8
$\eta_{HPT}$	0.9
$\eta_{IPT}$	0.9
$\eta_{LPT}$	0.9
<i>Constraint</i>	
$T_7$	40
$x_7$	0.95
$H$	40%
<i>Objective function</i>	
Annual cost rate (\$/s)	1.4427

## 6.2 Brayton Power Cycle

A typical gas power plant operates on the Brayton cycle. In the gas power plant, the working fluid remains in the gas phase throughout the cycle. Basic components of any gas power plants include the compressor, the combustion chamber, the heat exchanger, and the gas turbine. The schematic arrangement of the gas power plant along with various different components is shown in Fig. 6.5. The thermodynamic cycle (i.e., Brayton cycle) of the gas power plant is shown in Fig. 6.6 and is explained below.

The compressor takes the fresh atmospheric air and compresses it to a higher pressure. The compression process is isentropic in nature (process 4–1). From the compressor, the high-pressured air is passed through the regenerative heat exchanger where the air is heated with the help of exhaust gas coming from the gas turbine (process 1–5). Further heat addition to the air takes place in the combustion chamber at constant pressure (process 5–2) through fuel combustion. The high-temperature and high-pressured gas is then entered into a gas turbine where it expands isentropically (process 2–3). The expansion of gas produces mechanical energy. The gas turbine is coupled with the compressor. This indicates that the

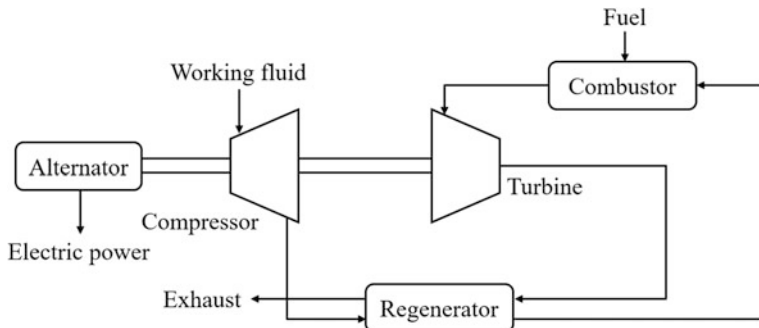


**Fig. 6.5** Schematic arrangement of the Brayton power cycle

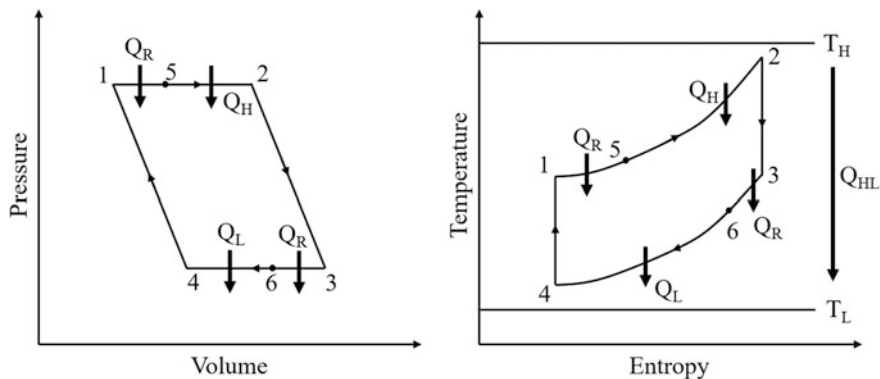


**Fig. 6.6** Thermodynamic presentation of Brayton power cycle

energy required to run the compressor is supplied directly to the compressor. The remaining mechanical energy is then converted into electric energy. After expansion, the exhaust gas is passed through a regenerator where it is used to preheat the fresh air supplied to the compressor (process 3–6). The remaining heat of the exhaust gas is then rejected to the environment (process 6–4). A gas turbine power plant is generally used when high power and speed are of key importance. For example, the gas power cycle is used in the jet propulsion unit of aircraft, in ships as a propulsion unit, and also in electric generating stations and locomotives.

Earlier, researchers carried out various works related to the analysis and optimization of the gas power plant. Radcenco et al. (1998) performed the thermodynamic performance optimization of a gas turbine power plant by adjusting the flow rate and the distribution of pressure losses along the flow path. The authors concluded that the maximized power output has additional maxima with respect to the overall pressure ratio and overall temperature ratio of the cycle. Valdés et al. (2003) performed a thermo-economic optimization of the combined cycle gas turbine

power plants using the genetic algorithm. The authors considered the minimization of the cost of production per unit of output and maximized the annual cash flow as objective functions. They then compared the results obtained with both functions to find the superior optimization strategy. Barzegar Avval et al. (2011) modeled the gas turbine power plant with the preheater and compared the simulation results of the model with one of the gas turbine power plants in Iran. The authors performed the multi-objective optimization by considering exergy efficiency, total cost rate, and the thermo-environmental objective function of the power cycle simultaneously. The authors also performed a sensitivity analysis of the obtained results.

Ahmadi and Dincer (2011a, b) developed a thermodynamic and exergoeconomic modeling of a gas turbine power plant and validated it by comparing its results with a real gas turbine power plant. The authors performed the multi-objective optimization to find the best operating parameters which resulted in the minimum total cost rate and maximum exergy efficiency of the power plant. This was done using NSGA-II. The authors also performed the sensitivity analysis to identify the effects of each design variable on the optimized value of the objective function. Cheddie (2011) investigated the Brayton cycle hybrid with a solid oxide fuel cell. The author developed a thermo-economic model to simulate the hybrid power plant and to optimize its performance using the method of Lagrange multipliers. Haseli (2013) performed the second law-based optimization of a regenerative Brayton cycle. The author identified the relationship between the regenerative heat exchanger's effectiveness and the temperature ratio on the optimum pressure ratio of the Brayton cycle.

Kumar et al. (2016) carried out a thermodynamic optimization based on finite-time thermodynamic analysis along with multiple criteria for the Brayton power cycle. The authors investigated the optimal values of various decision variables that simultaneously optimize power output, thermal efficiency and ecological functions using an evolutionary algorithm based on NSGA-II. The authors also obtained the Pareto optimal frontier between triple and dual objectives and selected the best optimal value using decision-making methods. Li et al. (2015) performed the thermo-economic optimization of a 100 kW regenerative solar-assisted Brayton power cycle. The authors developed a thermodynamic model of a such hybrid system to obtain the power output, the thermal efficiency, and the dimensionless thermo-economic performance by adapting NSGA-II. The authors also used decision-making methods to select the final optimal solution from the obtained Pareto frontier. Ghamami et al. (2016) carried out the energy and exergy analysis of the combined cycle power plant. The authors studied the variables that affect the efficiency and performance and provided a solution to improve the efficiency and performance of the gas turbine.

### **6.2.1 Thermal Model**

In this part of the work, a gas power plant working on the Brayton cycle is considered for optimization. The thermodynamic presentation of Brayton power

cycle is shown in Fig. 6.6. There, the subscripts  $H$  and  $L$  stand for heat source (i.e., high temperature) and heat sink (i.e., low temperature), respectively, in the different equations of the thermal model. The thermal model presented here is based on the previous work of Li et al. (2015).

The following equation gives the heat absorbed from the heat source ( $\dot{Q}_H$ ):

$$\dot{Q}_H = \dot{C}_{wf}\varepsilon_H(T_H - T_5) = \dot{C}_{wf}(T_2 - T_5) \quad (6.32)$$

where  $\dot{C}_{wf}$  is the heat capacity rate of the working fluid and  $\varepsilon_H$  is the effectiveness of the hot-side heat exchanger.

The following equation gives the rate of heat leakage ( $\dot{Q}_{HL}$ ) from the heat reservoir at temperature  $T_H$  to the cold reservoir at temperature  $T_L$ :

$$\dot{Q}_{HL} = \dot{C}_B(T_H - T_L) = \dot{C}_{wf}\xi(T_H - T_L) \quad (6.33)$$

where  $\dot{C}_B$  is the internal conductance of the Brayton cycle and  $\xi$  is the ratio of internal conductance of the power cycle to the heat capacity rate of the working fluid and is given by

$$\xi = \dot{C}_B/\dot{C}_{wf} \quad (6.34)$$

The heat rejected from the working fluid to heat sink ( $\dot{Q}_L$ ) is given by the following equation:

$$\dot{Q}_L = \dot{C}_{wf}\varepsilon_L(T_6 - T_L) = \dot{C}_{wf}(T_6 - T_4) \quad (6.35)$$

where  $\varepsilon_L$  is the effectiveness of the cold-side heat exchanger.

Heat exchanged in the regenerator heat exchanger ( $\dot{Q}_R$ ) is given by the following equation:

$$\dot{Q}_R = \dot{C}_{wf}\varepsilon_R(T_3 - T_1) = \dot{C}_{wf}(T_5 - T_1) = \dot{C}_{wf}(T_3 - T_6) \quad (6.36)$$

where  $\varepsilon_R$  is the effectiveness of the regenerative heat exchanger.

The effectiveness of the hot-side heat exchanger ( $\varepsilon_H$ ), the cold-side heat exchanger ( $\varepsilon_L$ ), and the regenerative heat exchanger ( $\varepsilon_R$ ) are given by

$$\varepsilon_H = 1 - e^{-N_H} \quad (6.37)$$

$$\varepsilon_L = 1 - e^{-N_L} \quad (6.38)$$

$$\varepsilon_R = \frac{N_R}{N_R + 1} \quad (6.39)$$

where  $N_H$ ,  $N_L$ , and  $N_R$  are the number of transfer units of hot-side, cold-side, and regenerative heat exchangers, respectively, and are given by

$$N_H = h_H A_H / \dot{C}_{wf} \quad (6.40)$$

$$N_L = h_L A_L / \dot{C}_{wf} \quad (6.41)$$

$$N_R = h_R A_R / \dot{C}_{wf} \quad (6.42)$$

where  $h$  and  $A$  represent the convective heat transfer coefficient and the heat exchanger area, respectively.

The temperature at the different state points of the Brayton cycle is given by

$$T_2 = \varepsilon_H T_H + (1 - \varepsilon_H) T_5 \quad (6.43)$$

$$T_4 = \varepsilon_L T_L + (1 - \varepsilon_L) T_6 \quad (6.44)$$

$$T_5 = \varepsilon_R T_3 + (1 - \varepsilon_R) T_1 \quad (6.45)$$

$$T_6 = \varepsilon_R m T_1 + (1 - \varepsilon_R) T_3 \quad (6.46)$$

For an isentropic compression and expansion process, the second law of thermodynamics requirement is given by

$$T_1 T_3 = T_2 T_4 \quad (6.47)$$

Substitution of different temperature in the above equation simplifies the equation as follows.

$$a_1 a_2^2 + a_2 T_3 + a_3 = 0 \quad (6.48)$$

The following equations give the constant.

$$a_1 = (1 - \varepsilon_H)(1 - \varepsilon_L)(1 - \varepsilon_R)\varepsilon_R \quad (6.49)$$

$$a_2 = a_4 T_1 + a_5 \quad (6.50)$$

$$a_3 = a_1 T_1^2 + a_6 T_1 + a_7 \quad (6.51)$$

$$a_4 = (1 - \varepsilon_H)(1 - \varepsilon_L)\varepsilon_R^2 + (1 - \varepsilon_H)(1 - \varepsilon_L)(1 - \varepsilon_R)^2 - 1 \quad (6.52)$$

$$a_5 = \varepsilon_L(1 - \varepsilon_H)\varepsilon_R T_H + (1 - \varepsilon_L)\varepsilon_H(1 - \varepsilon_R)T_H \quad (6.53)$$

$$a_6 = \varepsilon_H(1 - \varepsilon_L)\varepsilon_R T_H + (1 - \varepsilon_H)\varepsilon_L(1 - \varepsilon_R)T_L \quad (6.54)$$

$$a_7 = \varepsilon_H \varepsilon_L T_H T_L \quad (6.55)$$

By using the above constants, the temperature at different state points of the Brayton cycle is given by the following equations.

$$T_3 = a_8 = \left[ -a_2 - (a_2^2 - 4a_1a_3)^{1/2} \right] / 2a_1 \quad (6.56)$$

$$T_2 = \varepsilon_H T_H + (1 - \varepsilon_R)[(1 - \varepsilon_R)T_1 + \varepsilon_R a_8] \quad (6.57)$$

$$T_4 = \varepsilon_L T_L + (1 - \varepsilon_R)[(1 - \varepsilon_R)a_8 + \varepsilon_R T_1] \quad (6.58)$$

$$T_5 = (1 - \varepsilon_R)T_1 + \varepsilon_R a_8 \quad (6.59)$$

$$T_6 = (1 - \varepsilon_R)a_8 + \varepsilon_R T_1 \quad (6.60)$$

The total heat absorbed ( $\dot{Q}_{HT}$ ) from the heat reservoir is given by the following equations.

$$\dot{Q}_{HT} = \dot{Q}_H + \dot{Q}_{HL} = \dot{C}_{wf}\varepsilon_H(T_H - T_5) + \xi\dot{C}_{wf}(T_H - T_L) \quad (6.61)$$

$$\dot{Q}_{HT} = \dot{C}_{wf}\varepsilon_H(T_H - (1 - \varepsilon_R)T_1 - \varepsilon_R a_8) + \xi\dot{C}_{wf}(T_H - T_L) \quad (6.62)$$

The following equation gives the total heat released ( $\dot{Q}_{LT}$ ) to the heat reservoir.

$$\dot{Q}_{LT} = \dot{Q}_L + \dot{Q}_{HL} = \dot{C}_{wf}\varepsilon_L(T_6 - T_L) + \xi\dot{C}_{wf}(T_H - T_L) \quad (6.63)$$

$$\dot{Q}_{LT} = \dot{C}_{wf}\varepsilon_L((1 - \varepsilon_R)a_8 + \varepsilon_R T_1 - T_L) + \xi\dot{C}_{wf}(T_H - T_L) \quad (6.64)$$

As per the first law of thermodynamics, the power output ( $P$ ) of the Brayton cycle is given by the following equation.

$$P = \dot{Q}_{HT} - \dot{Q}_{LT} = \dot{C}_{wf}\varepsilon_H[T_H - (1 - \varepsilon_R)T_1 - \varepsilon_R a_8] - \dot{C}_{wf}\varepsilon_L[(1 - \varepsilon_R)a_8 + \varepsilon_R T_1 - T_L] \quad (6.65)$$

Likewise, the thermal efficiency ( $\eta_B$ ) of the Brayton power cycle is given by the following equation.

$$\begin{aligned} \eta_B &= 1 - \frac{\dot{Q}_{LT}}{\dot{Q}_{HT}} \\ &= \frac{\varepsilon_H[T_H - (1 - \varepsilon_R)T_1 - \varepsilon_R a_8] - \varepsilon_L[(1 - \varepsilon_R)a_8 + \varepsilon_R T_1 - T_L]}{\varepsilon_H[T_H - (1 - \varepsilon_R)T_1 - \varepsilon_R a_8] + \xi(T_H - T_L)} \end{aligned} \quad (6.66)$$

Based on the above thermal model, the objective function for the present work is defined in the next section.

### 6.2.2 Case Study, Objective Function Description, and Constraints

The need for a gas power plant working on the Brayton cycle to be designed and optimized for maximum thermal efficiency is high. The convective heat transfer coefficient of heat source and heat sink reservoirs ( $h_H$  and  $h_L$ ) is 2000 W/m<sup>2</sup>K. The heat capacity rate of the working fluid ( $\dot{C}_{wf}$ ) is 1050 W/K. The percentage of the internal conductance with respect to the heat capacity rate of the working fluid ( $\zeta$ ) is 0.02. Five design variables including the temperature of the hot reservoir ( $T_H$ ), the temperature of cold reservoir ( $T_L$ ), effectiveness of hot-side heat exchanger ( $\varepsilon_H$ ), the effectiveness of cold-side heat exchanger ( $\varepsilon_L$ ), and regenerator effectiveness ( $\varepsilon_R$ ) are considered for the optimization problem. The upper and lower bounds of design variables are presented in Table 6.6.

As mentioned above, the maximization of the thermal efficiency ( $\eta$ ) of the Brayton power cycle is taken as an objective function in the present study. Furthermore, the operating parameters which resulted in maximum thermal efficiency also satisfy both the power output ( $P$ ) and the air temperature at the inlet of regenerative heat exchanger ( $T_1$ ) constraints. So, considering all the aspects, the objective function of the Brayton power cycle is formulated as below:

$$\begin{cases} \text{Minimize } f(X) = \eta(X) + \sum_{j=1}^n G_1(g_j(X))^2 \\ X = [x_1, x_2, x_3, \dots, x_D], \quad x_{i,\text{minimum}} \leq x_i \leq x_{i,\text{maximum}} \quad i = 1, 2, 3, \dots, D \\ g_j(X) \leq 0, \quad j = 1, 2, 3, \dots, n \end{cases} \quad (6.67)$$

where  $X$  is the vector of design variables which should be bounded between its minimum and maximum values.  $G_1$  is the penalty parameter, and the entire term considers the effects of the constraints violation. This term comes into picture when the constraints violation takes place.  $g_j(X)$  indicates the constraints. The following constraints are considered for the Brayton power cycle.

**Table 6.6** Ranges of design variables for Brayton power cycle optimization

Design variable	Lower bound	Upper bound
The temperature of the hot reservoir ( $T_H$ ), K	100	1000
The temperature of cold reservoir ( $T_L$ ), K	300	1000
The effectiveness of hot-side heat exchanger ( $\varepsilon_H$ )	0.5	0.8
The effectiveness of cold-side heat exchanger ( $\varepsilon_L$ )	0.5	0.8
Regenerator effectiveness ( $\varepsilon_R$ )	0.5	0.9

$$\text{Power output } (P) \geq 200 \text{ kW} \quad (6.68)$$

$$\text{Air inlet temperature to the regenerative heat exchanger } (T_1), T_L < T_1 < T_H \quad (6.69)$$

The next section describes the results and discussion of the case study.

### 6.2.3 Results and Discussion

The considered problem of the gas power plant working on the Brayton cycle is investigated using 11 different metaheuristic approaches to obtain maximum thermal efficiency. As all these methods are stochastic in their working, each algorithm is implemented 100 times on the considered problem to estimate the statistical variations of the various algorithms. Each algorithm is implemented with a population size of 50, and the termination criteria are set as 100,000 function evaluations. The results obtained using each algorithm are based on the 100 runs and are presented in the form of the best solution, the worst solution, the average solution, the standard deviation, and the success rate. These are presented in Table 6.7. Here, the solutions which are considered infeasible (i.e., affected by penalty) are eliminated. This was done while still obtaining the worst solution, the average solution, the standard deviation, and the success rate. In addition, the success rate of the algorithm is derived based on the 0.1% variation obtained from the global optimum value.

It can be observed from the comparative results that excluding TLBO, SOS, WWO, and GA, the remaining algorithms produced the optimum value of thermal efficiency of the Brayton power cycle. Furthermore, from the results it can be said that the average performance of PSO, ABC, CSA, and SCA is better than the remaining algorithms. The ABC algorithm has the highest success rate in obtaining the optimum value. This is then followed by the PVS, CSA, and PVS algorithms. Since the success rate of SOS, WWO, and GA algorithms is zero, these algorithms are not able to produce the optimum value of thermal efficiency. Since all the algorithms performed differently when obtaining the best, worst, and average results, and success rate, it is difficult to judge the performance of the algorithm. As such, the Friedman rank test is implemented to judge the best suitable algorithm for the optimization of the Brayton power cycle considering the capability to obtain the best solutions, worst solutions, average solutions, and success rate. The results of the Friedman rank test are presented in Table 6.8, and its graphical representation is given in Fig. 6.7. The results are presented in the form of a Friedman value, where the normalized value of ‘1’ is the best performing algorithm. It is observed from the results that ABC has obtained the first rank followed by CSA and SCA algorithms.

The optimized operating parameters of the Brayton power cycle obtained using the ABC algorithm are presented in Table 6.9. It can be noted from the results that

**Table 6.7** Comparative results of different algorithms for Brayton power cycle optimization

Algorithms	Best	Worst	Average	SD	Success rate (%)
GA	0.44868	0.34381	0.3772	3.03E-02	0
PSO	0.44928	0.41123	0.4476	1.79E-01	88
DE	0.44928	0.33972	0.4393	3.30E-02	40
ABC	0.44928	0.4221	0.4482	1.74E-01	96
CSA	0.44928	0.42312	0.4481	1.86E-01	84
TLBO	0.39746	0.31531	0.3379	1.95E-02	0
SOS	0.34517	0.3157	0.3282	9.45E-03	0
WWO	0.34932	0.30129	0.3274	1.35E-02	0
HTS	0.44928	0.34706	0.4341	3.35E-02	72
PVS	0.44928	0.32152	0.4350	3.89E-02	84
SCA	0.44926	0.44764	0.4489	3.65E-04	68

**Table 6.8** Friedman rank test results for Brayton power cycle optimization

Algorithms	Friedman value	Normalized value	Rank
GA	39.5	0.329114	8
PSO	19	0.684211	4
DE	33	0.393939	7
ABC	13	1	1
CSA	13.5	0.962963	2
TLBO	44.5	0.292135	9
SOS	44.5	0.292135	9
WWO	47.5	0.273684	10
HTS	29	0.448276	5
PVS	30.5	0.42623	6
SCA	16	0.8125	3

the Brayton power cycle with the following conditions—the highest temperature in the hot reservoir, the hot-side heat exchanger effectiveness, cold-side heat exchanger effectiveness, regenerative heat exchanger effectiveness, and the lowest temperature of cold reservoir—results in the maximum thermal efficiency of the Brayton power cycle. Comparing the air inlet temperature to the regenerative heat exchanger produced a conflicting effect on achieving the maximum thermal efficiency of this cycle. Note that the power output constraint is at the limiting value in the optimized operating condition of the Brayton power cycle.

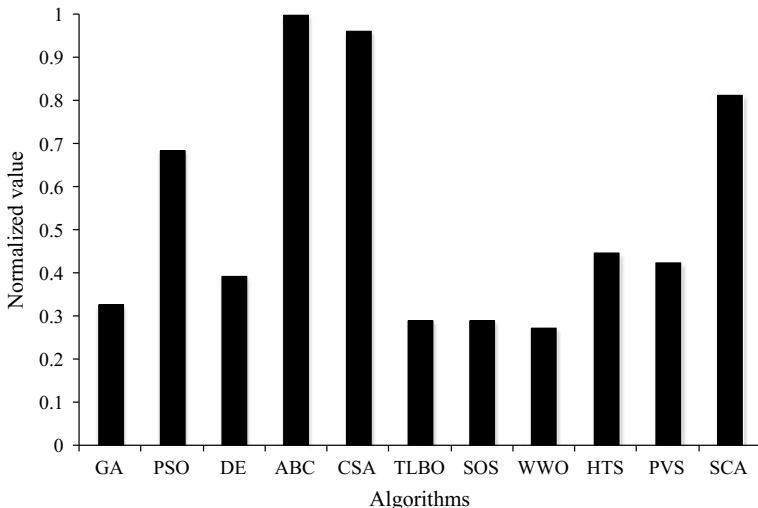


**Fig. 6.7** Graphical presentation of Friedman rank test for Brayton power cycle optimization

**Table 6.9** The optimized operating condition of the Brayton power cycle

Operating parameters	Optimized value
<i>Operating variable</i>	
The temperature of the hot reservoir ( $T_H$ ), K	1000
The temperature of cold reservoir ( $T_L$ ), K	300
The effectiveness of hot-side heat exchanger ( $\varepsilon_H$ )	0.8
The effectiveness of cold-side heat exchanger ( $\varepsilon_L$ )	0.8
Regenerator effectiveness ( $\varepsilon_R$ )	0.9
<i>Constraint</i>	
Power output ( $P$ ), kW	200
Air inlet temperature to the regenerative heat exchanger, ( $T_1$ ) K	439.2
<i>Objective function</i>	
Thermal efficiency ( $\eta$ )	0.44928

### 6.3 Braysson Power Cycle

The Braysson cycle is a gas turbine cycle that has been introduced by Frost et al. (1997). It is a hybrid cycle that combines the conventional Brayton and Ericsson gas power cycles. The Braysson cycle has a high-temperature and heat addition process of the Brayton cycle and the low-temperature heat rejection process of the Ericsson cycle. In that way, the Brayton cycle incorporates the thermodynamic advantages of a combined gas and steam turbine cycle without the irreversibilities of the boiler and the ancillaries of the steam turbine and condenser plant. Thus, the Braysson cycle is an alternative method to the conventional combined gas and

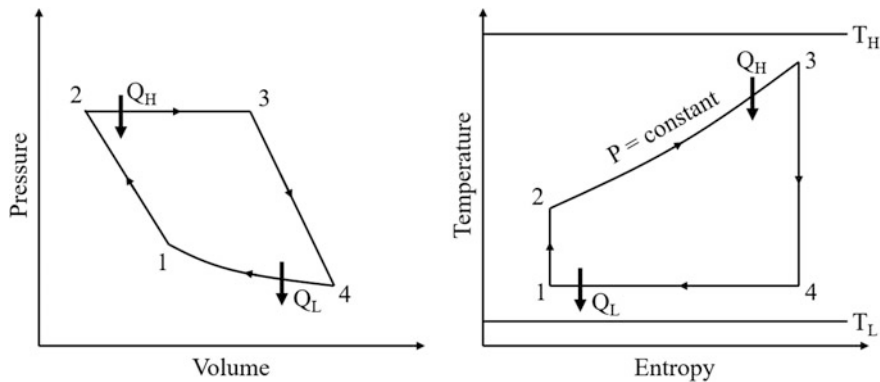


**Fig. 6.8** Thermodynamic presentation of Braysson cycle

steam turbine power plant. The Braysson cycle is composed of two isentropic processes: one a constant pressure process and the other an isothermal process. The thermodynamic presentation of the Braysson cycle is shown in Fig. 6.8 and is explained below.

Processes 1–2 and 3–4 demonstrate the isentropic processes. As for process 2–3, it represents the constant pressure process and process 4–1 denote the isothermal process. In process 1–2, the compressor compressed the air isentropically. This process follows the constant pressure heat addition (process 2–3). The expansion of high-pressure and high-temperature gas take place isentropically during process 3–4. Finally, heat rejection takes place isothermally during process 4–1. Note that there are finite temperature differences between heat source  $T_H$  and processes 2–3, as well as between process 4–1 and heat sink  $T_L$ . This is because of the heat resistance losses in the hot and cold-side heat exchangers.

Earlier, researchers carried out various works related to the analysis and optimization of the Braysson power cycle. Zheng et al. (2001) performed an exergy analysis for an irreversible Braysson cycle and derived the analytical formulae of power output and exergy efficiency. The authors also compared the result of the Braysson cycle with those of the Brayton cycle. Zheng et al. (2002a, b) carried out a performance analysis of a Braysson cycle using both entropy generation minimization as well as finite-time thermodynamics. The mentioned authors were able to derive the analytical formula of power output and the efficiency of an endoreversible Braysson cycle with heat resistance losses. Furthermore, the authors also analyzed the impact of the various design parameters on the performance of the cycle by considering numerical examples. Zheng et al. (2002a, b) performed the optimization of a Braysson cycle considering the power, power density, and efficiency of the cycle. In the work, the authors derived the relation between power output and the working fluid temperature ratio, power density and the working fluid temperature ratio, as well as between efficiency and the working fluid temperature ratio of the cycle. Zhou et al. (2004) carried out the performance analysis of an

irreversible Braysson cycle. Here, the authors considered the maximization of specific power output with respect to the cycle temperatures along with the isobaric temperature ratio.

Tyagi et al. (2004) carried out the thermo-economic optimization of a Braysson cycle. The authors considered the total cost per unit power output of the cycle as an objective function and obtained the optimum values of the state point temperatures, power output and thermal efficiency at which the objective function become minimum for a typical set of operating parameters. Üst and Yilmaz (2005) carried out the performance analysis and optimization of a Braysson cycle based on the ecological criterion and compared the results with those obtained using the maximum power criterion. Zheng et al. (2005) investigated the performance characteristics of an irreversible solar-driven Braysson heat engine for maximum efficiency consideration. Wu et al. (2010) carried out the parametric optimization of a solar-driven Braysson heat engine with the variable heat capacity of the working fluid and radiation-convection heat losses. Sadatsakkak et al. (2015) carried out the multi-objective optimization of a Braysson cycle considering the dimensionless power density and thermal efficiency of the cycle as an objective function. The authors used NSGA-II as an optimization algorithm to obtain the Pareto solution of the considered objective. Furthermore, the authors also implemented decision-making techniques to select the best solution from the Pareto front.

Ahmadi et al. (2016a, b) performed the multi-objective thermodynamic optimization of a nanoscale irreversible Braysson cycle operated with an ideal Maxwell–Boltzmann gas. The authors considered three scenarios for the optimization. In the first scenario, the objective function is considered as the maximization of the ecological coefficient of performance and energy efficiency of the system. In the second scenario, the ecological coefficient of performance and the dimensionless available work of the system are maximized simultaneously. In the third scenario, the ecological coefficient of performance, energy efficiency, and the dimensionless available work of the system are all considered simultaneously for optimization. In addition, the authors adopted NSGA-II as an optimization strategy in their study. They also implemented the decision-making method to select the best result. Açıkkalp (2017) presented a performance analysis of an irreversible molten carbonate fuel cell Braysson cycle. The author obtained the optimum value of the basic thermodynamic parameters of the cycle such as power output, efficiency, and exergy destruction rate of the cycle.

### 6.3.1 Thermal Model

In this part of the work, a gas power plant working on the Braysson cycle is considered for optimization. The thermodynamic presentation of the Braysson power cycle is shown in Fig. 6.6. Moreover, in the different equations of the thermal model, subscripts H and L stand for heat source (i.e., high temperature) and

heat sink (i.e., low temperature), respectively. The thermal model presented here is based on the previous work of Sadatsakkak et al. (2015).

The following equation gives the rate of heat absorbed ( $\dot{Q}_H$ ) from the heat source:

$$\dot{Q}_H = C_{wf}\varepsilon_H(T_H - T_2) \quad (6.70)$$

where  $\varepsilon_H$  is the effectiveness of the hot-side heat exchanger and,  $C_{wf}$  is the thermal capacitance rate of the working fluid.

The following equation gives the rate of heat transferred ( $\dot{Q}_L$ ) to the heat sink:

$$\dot{Q}_L = U_L(T_4 - T_L) \quad (6.71)$$

where  $U_L$  is the product of the heat transfer coefficient and surface area of the hot-side heat exchanger.

The following equation gives the effectiveness of the hot-side heat exchanger:

$$\varepsilon_H = 1 - e^{-N_H} \quad (6.72)$$

where  $N_H$  is the number of heat transfer unit and is given by the following equations.

$$N_H = \frac{U_H}{C_{wf}} \quad (6.73)$$

The following equation can give the power output ( $\dot{W}$ ) of Braysson cycle.

$$\dot{W} = \dot{Q}_H - \dot{Q}_L = C_{wf}\varepsilon_H(T_H - T_2) - U_L(T_4 - T_L) \quad (6.74)$$

The following equation can give the efficiency ( $\eta$ ) of the Braysson cycle.

$$\eta = 1 - \frac{\dot{Q}_L}{\dot{Q}_H} = 1 - \frac{U_L(T_4 - T_L)}{C_{wf}\varepsilon_H(T_H - T_2)} \quad (6.75)$$

The following equation also gives the rate of heat transferred ( $\dot{Q}_L$ ) to the heat sink:

$$\dot{Q}_L = T_4(S_4 - S_1) \quad (6.76)$$

where  $S_4$  and  $S_1$  are the entropy at different states corresponding to Fig. 6.8 and are given by the following equations.

$$S_4 - S_1 = \frac{U_L(T_4 - T_L)}{T_4} \quad (6.77)$$

$$S_3 - S_2 = \dot{m}C_p \ln\left(\frac{T_3}{T_2}\right) \quad (6.78)$$

Simplification of the entropy equation is given by

$$\frac{U_L(T_4 - T_L)}{T_4} = \dot{m}C_p \ln\left(\frac{T_3}{T_2}\right) = C_{wf} \ln\left(\frac{T_3}{T_2}\right) \quad (6.79)$$

where  $\dot{m}$  is the mass flow rate and  $C_p$  is the specific heat of the working fluid.

The following equation can give the dimensionless power output ( $P'$ ):

$$P' = \frac{\varepsilon_H \tau (e^x - 1)}{(e^x + \varepsilon_H - 1)} - \frac{U_L x}{(U_L - x C_{wf})} \quad (6.80)$$

where  $x$  is the dimensionless working fluid temperature ratio and is given by,

$$x = \frac{U_L(T_4 - T_L)}{C_{wf}T_4} = \ln\left(\frac{T_3}{T_2}\right) \quad (6.81)$$

The following equation can give the efficiency of the cycle ( $\eta$ ):

$$\eta = 1 - \frac{U_L x (e^x + \varepsilon_H - 1)}{\varepsilon_H \tau (U_L - x C_{wf})(e^x - 1)} \quad (6.82)$$

where  $\tau$  is the heat reservoir temperature ratio of the cycle and is given by

$$\tau = T_H/T_L \quad (6.83)$$

The power density ( $\dot{\bar{W}}$ ) of the cycle is defined as the ratio of power output to the maximum specific volume ( $v_4$ ) throughout the cycle and is given by

$$\dot{\bar{W}} = \frac{\dot{W}}{v_4} \quad (6.84)$$

The specific volume of the working fluid is correlated as follows.

$$\frac{v_4}{v_1} = \left(\frac{T_3}{T_2}\right)^{\frac{k}{k-1}} = e^{\frac{kx}{k-1}} \quad (6.85)$$

The dimensionless power density ( $P$ ) is given by

$$P = \frac{\dot{\bar{W}} v_1}{C_{wf} T_L} \quad (6.86)$$

$$P = \frac{\varepsilon_H \tau (e^x - 1)}{e^{\frac{kx}{k-1}}(e^x + \varepsilon_H - 1)} - \frac{U_L x}{e^{\frac{kx}{k-1}}(U_L - x C_{wf})} \quad (6.87)$$

The following equation gives the total heat conductance ( $U_T$ ) of the heat exchangers.

$$U_H + U_L = U_T \quad (6.88)$$

The following equation gives the heat conductance ratio ( $u$ ) of the heat exchangers.

$$u = U_H / U_T \quad (6.89)$$

Based on the above thermal model, the objective function for the present work is defined in the next section.

### 6.3.2 Case Study, Objective Function Description, and Constraints

A gas power plant using the Braysson cycle needs to be designed and optimized for maximum thermal efficiency. The thermal conductance of the working fluid ( $C_{wf}$ ) is 1 kW/K. Total heat conductance ( $U_T$ ) of the heat exchangers is 5 kW/K. The ratio of the specific heat of the fluid ( $k$ ) is 1.4. Three design variables including the heat reservoir temperature ratio of the cycle ( $\tau$ ), the heat conductance's distribution ( $u$ ), and the dimensionless working fluid temperature ratio ( $x$ ) are considered for the optimization problem. The upper and lower bounds of the design variables are presented in Table 6.10.

As mentioned above, the maximization of the thermal efficiency ( $\eta$ ) of the Braysson power cycle is taken as an objective function in the present study. Furthermore, the operating parameters which resulted in maximum thermal efficiency also satisfy the dimensionless power density ( $P$ ) constraints. So, considering all the aspects, the objective function of Braysson power cycle is formulated as below:

**Table 6.10** Ranges of design variables for Braysson power cycle

Design variable	Lower bound	Upper bound
Heat reservoir temperature ratio of the cycle, ( $\tau$ )	0.1	3
Heat conductance's distribution ( $u$ )	0.1	0.6
Dimensionless working fluid temperature ratio ( $x$ )	0.1	0.6

$$\begin{cases} \text{Minimize } f(X) = \eta(X) + \sum_{j=1}^n G_1(g_j(X))^2 \\ X = [x_1, x_2, x_3, \dots, x_D], \quad x_{i,\text{minimum}} \leq x_i \leq x_{i,\text{maximum}} \quad i = 1, 2, 3, \dots, D \\ g_j(X) \leq 0, \quad j = 1, 2, 3, \dots, n \end{cases} \quad (6.90)$$

where  $X$  is the vector of design variables. This vector is bounded between its minimum and maximum values.  $G_1$  is the penalty parameter, and the entire term takes into account the effect of the constraint's violation. This term comes into picture when the constraint violation takes place.  $g_j(X)$  indicates the constraints. The following constraint is considered for the Braysson power cycle.

$$\text{Dimensionless power density } (P) \geq 0.158 \quad (6.91)$$

The next section describes the results and discussion of the case study.

### 6.3.3 Results and Discussion

The considered problem of the gas power plant operating the Braysson cycle is investigated using 11 different metaheuristic approaches to obtain maximum thermal efficiency. As all these methods are stochastic in their working, each algorithm is implemented 100 times to estimate the statistical variations of the algorithms. Each algorithm is implemented with the population size of 50, and the termination criteria are set as 100,000 function evaluations. The overall results obtained in the 100 runs using each algorithm is presented in the form of the best, the worst, and average solution, the standard deviation, and the success rate. This can be seen in Table 6.11. The solutions which are infeasible (i.e., affected by penalty) are eliminated. This is done while still obtaining the worst solution, average solution, standard deviation, and success rate (obtained by considering a 0.1% variation from the global optimum value).

It can be observed from the comparative results that the algorithm performed on even grounds and produced nearly identical thermal efficiency of the Braysson power cycle as well as exhibiting similar averages. From the results, it is observed that the PSO, DE, ABC, SOS, and the SCA algorithms obtained the largest success rate. On the other hand, the success rate of the GA is the lowest. It can be observed from the results that it is difficult to judge the performance of the algorithms as they all produced differently when obtaining the best, worst, and average results, and the success rate. Thus, the Friedman rank test is implemented to judge the best suitable algorithm for the optimization of the Braysson power cycle, considering the

**Table 6.11** Comparative results of different algorithms for Braysson power cycle

Algorithms	Best	Worst	Average	SD	Success rate (%)
GA	0.5909	0.59088	0.59089	3.16E-06	72
PSO	0.5909	0.59088	0.59089	3.43E-06	88
DE	0.5909	0.5909	0.5909	1.14E-16	88
ABC	0.5909	0.59088	0.59089	4.09E-06	88
CSA	0.5909	0.59089	0.5909	1.14E-16	84
TLBO	0.5909	0.5909	0.5909	1.14E-16	84
SOS	0.5909	0.5909	0.5909	1.14E-16	88
WWO	0.5909	0.59089	0.59089	1.88E-06	84
HTS	0.5909	0.58859	0.5908	5.02E-04	80
PVS	0.5909	0.59088	0.59089	2.24E-06	80
SCA	0.5909	0.59084	0.59089	1.43E-05	88

**Table 6.12** Friedman rank test results for Braysson power cycle

Algorithms	Friedman value	Normalized value	Rank
GA	34.5	0.391304	7
PSO	28.5	0.473684	4
DE	13.5	1	1
ABC	30	0.45	6
CSA	29.5	0.457627	5
TLBO	19	0.710526	2
SOS	13.5	1	1
WWO	25	0.54	3
HTS	52	0.259615	10
PVS	42	0.321429	8
SCA	42.5	0.317647	9

capability to obtain the best, worst, and average solutions, and the success rate. The results of the Friedman rank test are presented in Table 6.12, and its graphical representation is given in Fig. 6.9. The results are presented in the form of a Friedman value, with a normalized value of ‘1’ being the best performing algorithm and its rank. It can be observed from the results that DE and SOS have obtained the first rank followed by TLBO and WWO algorithms.

The optimized operating parameters of the Braysson power cycle obtained using the DE algorithm are presented in Table 6.13. It can be noted from the results that the Braysson power cycle with the maximum heat reservoir temperature ratio results in the maximum thermal efficiency of the cycle. In addition, together, the Heat conductance’s distribution and the dimensionless working fluid temperature ratio produced a conflicting effect on achieving the maximum thermal efficiency of the cycle. Finally, the dimensionless power density constraint is at the limiting value in the optimized operating condition of the Braysson power cycle.

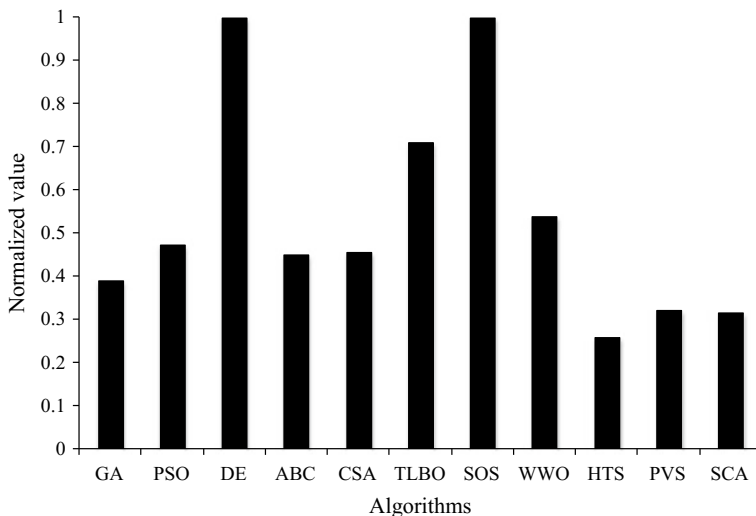


**Fig. 6.9** Graphical presentation of Friedman rank test for Braysson power cycle

**Table 6.13** The optimized operating condition of Braysson power cycle

Operating parameters	Optimized value
<i>Operating variable</i>	
Heat reservoir temperature ratio of the cycle, ( $\tau$ )	3
Heat conductance's distribution ( $u$ )	0.5108
Dimensionless working fluid temperature ratio ( $x$ )	0.2061
<i>Constraint</i>	
Dimensionless power density ( $P$ )	0.158
<i>Objective function</i>	
Thermal efficiency ( $\eta$ )	0.5909

## 6.4 Kalina Power Cycle

The Kalina power cycle has been introduced by Alexander Kalina (2003). This cycle harnesses clean energy from different sources for power generation. The cycle can utilize low-temperature heat energy from any source, but it is commonly used with solar energy as a heat source. In that way, the Kalina cycle converts solar energy into mechanical energy through the use of a turbine. An ammonia–water mixture is used as a working fluid in the power generation circuit. This mixture has a low boiling point, making it suitable for converting low-grade thermal energy to mechanical work.

The schematic arrangement of the Kalina power cycle operated with solar energy is shown in Fig. 6.10. The secondary fluid (usually oils that are stable at high

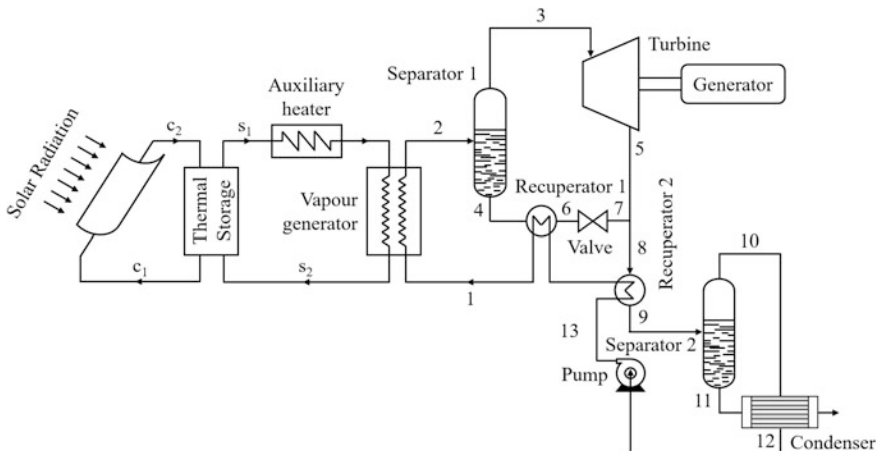


**Fig. 6.10** Schematic diagram of Kalina power cycle

temperatures) is circulated in the solar energy receiving circuit, absorbing the heat from the solar collector rising its temperature in the process. This fluid circulates in a circuit with a thermal storage tank to stabilize the operation during nonsunshine hours. It then exchanges the heat with the working fluid (ammonia–water mixture) of the power generation circuit by a recuperative heat exchanger. The auxiliary heater is installed as a backup energy source to increase the temperature of the thermal storage tank to the allowable temperature if the temperature of the thermal storage tank drops too much. After absorbing the heat, the fluid passes into separator 1, where it separates into a weak liquid solution and an ammonia-rich vapor. The evaporated part of the mixture is extracted from the separator and utilized in the turbine to generate power. The weak liquid solution, after recuperating some of the heat in heat exchanger 1, is throttled down to a lower pressure and then mixed with the ammonia-rich solution coming from the turbine to form the ammonia–water basic solution. After cooling down in heat exchanger 2, the ammonia–water basic solution is sent to separator 2, which separates the phases and using the condenser, it condenses into an ammonia–water liquid by cooling air. The ammonia–water liquid is then pumped into the vapor evaporator again after preheating through the heat exchanger.

As the two components of the working fluid have different boiling points, their mixture evaporates within a range of temperatures between their boiling points. This raises the average temperature of heat addition in the kalian power cycle and hence increases its efficiency. Furthermore, the cycle can be used as a bottoming cycle to aid waste heat recovery and increase the overall efficiency of conventional cycles. Note that the condenser requires cooling water to extract the heat from the working fluid. In addition, separators are needed in many places in the circuit to manage the two phases of the mixture.

Earlier, researchers have carried out various works related to the analysis and optimization of the Kalina power cycle. Usvika et al. (2009) carried out an energy and exergy analysis of the Kalina cycle. The author optimized the mass fraction of working fluids and turbine output pressure to obtain the maximum power output and maximum efficiency of the cycle. Bombarda et al. (2010) presented a comparison between the thermodynamic performances of the Kalina cycle and an organic Rankine cycle used for heat recovery from two diesel engines using hexamethyldisiloxane as the working fluid. Arslan (2011) developed an artificial neural network model to optimize the Kalina cycle system. The author used the back-propagation learning algorithm with three different variants in his optimization study. Singh and Kaushik (2013) provided a computer simulation of a Kalina cycle coupled with a coal-fired steam power plant. Their aim was to examine the possibility of exploiting the low-temperature heat of the exhaust gases for the conversion into electricity. The authors presented a numerical model to find out the optimum operating conditions for the Kalina cycle. Furthermore, the authors also investigated the effects of key parameters like the ammonia mass fraction in the mixture as well as the effect of the ammonia turbine inlet pressure on cycle performance.

Wang et al. (2013) developed a mathematical model to simulate the solar-driven Kalina cycle under steady-state conditions. The authors conducted a parametric analysis to examine the effects of some key thermodynamic parameters on system performance. Furthermore, the authors also optimized the solar driven Kalina cycle by considering the modified system efficiency as an objective function by means of the genetic algorithm. Sun et al. (2014) carried out energy and exergy analysis as well as parameter design optimization of the Kalina cycle solar system with an auxiliary superheater. The authors developed the thermodynamic model of the system and calculated the energy and exergy at various state points of the system. Modi and Haglind (2015) presented a detailed approach to solve and optimize a Kalina cycle for high temperature and high-pressure applications using a genetic algorithm. The authors considered a central receiver solar thermal power plant with direct steam generation as a case study. The authors optimized four different layouts for the Kalina cycle and compared some of its performance parameters including cycle efficiency and the cooling water requirement.

Ashouri et al. (2015) studied the thermodynamic and economic performance of the Kalina cycle coupled with a small-scale parabolic trough collector and a thermal storage tank along with an auxiliary heater. Another example is Saffari et al. (2016) who carried out the thermodynamic analysis for a geothermal Kalina cycle. The authors also performed the multi-objective optimization of a cycle by considering thermal efficiency and exergy efficiency of the cycle as an objective function and adopted the artificial bee colony algorithm as an optimization tool. Fallah et al. (2016) performed an advanced exergy analysis of the Kalina cycle run with the low-temperature geothermal source. The authors concluded, based on the advanced exergy analysis, that the efficiency of the system can be increased by improving the condenser's performance. Modi et al. (2016) evaluated the use of a high-temperature Kalina cycle for a central receiver concentrating solar power plant that

was with direct vapor generation and without storage. The authors also performed the thermo-economic optimization of the Kalina cycle by minimizing the levelized cost of electricity. Authors such as Boyaghchi and Sabaghian (2016) performed a multi-objective optimization of a solar-powered Kalina power cycle based on the exergy and exergoeconomic concept. They had identified the effect of the various operating parameters on the performance parameter of the cycle.

#### 6.4.1 Thermal Model

In this part of the work, a Kalina cycle is considered for optimization. The thermal model of the Kalina cycle presented here is based on the previous work of Wang et al. (2013).

The total effective flux absorbed at the absorber surface ( $S$ ) can be given by the following equation:

$$S = \left[ I_b R_b + \frac{I_d}{C} \right] \tau \rho_e \alpha \quad (6.92)$$

where  $I_b$   $R_b$  is the beam radiation flux falling on the aperture plane,  $I_d$  is the diffuse radiation,  $C$  is the acceptance angle,  $\tau$  is the transmissivity of the cover,  $\rho_e$  is the reflectivity of the concentrator surface, and  $\alpha$  is the absorptivity of the absorber surface.

The following equation gives the useful heat rate gain ( $Q_u$ ):

$$Q_u = F_R W L \left[ S - \frac{U_{lo}}{C} (T_{fi} - T_o) \right] \quad (6.93)$$

where  $W$  and  $L$  are the width and length of the collector,  $U_{lo}$  is the overall loss coefficient,  $T_{fi}$  is the inlet temperature of the solar collector, and  $F_R$  is the heat removal factor and is given by the following equation:

$$F_R = \frac{\dot{m} c_p}{b U_{lo} L} \left[ 1 - \exp \left\{ - \frac{F' b U_{lo} L}{\dot{m} c_p} \right\} \right] \quad (6.94)$$

where  $m$  is the mass flow rate,  $c_p$  is the specific heat of the fluid,  $b$  is the absorber width, and  $F'$  is the collector efficiency factor which is given by the following equation:

$$F' = U_{lo} \left[ \frac{1}{U_{lo}} + \frac{b}{N \pi D_i k} \right] \quad (6.95)$$

where  $N$  is the number of tubes,  $D_i$  is the tube diameter, and  $k$  is the heat transferring coefficient.

By applying the concept of energy balance to the thermal storage tank, we can get the following relation:

$$(\rho V C_p) \frac{dT_1}{dt} = Q_u - Q_{\text{load}} - UA(T_1 - T_0) \quad (6.96)$$

where  $U$  is the overall heat transfer coefficient,  $Q_{\text{load}}$  is the energy discharged to the Kalina cycle, and  $Q_u$  is the useful heat gain from the solar collector and are given by

$$Q_u = \dot{m}_{o,1} C_p (T_{\text{fo}} - T_1) \quad (6.97)$$

$$Q_{\text{load}} = \dot{m}_{o,2} C_p (T_1 - T_i) \quad (6.98)$$

where  $\dot{m}_{o,1}$  and  $\dot{m}_{o,2}$  are the mass flow rates of oil in the solar circuit and evaporator circuit, respectively, and  $T_{\text{fo}}$  is the outlet temperature of the solar collector. The different state points correspond to Fig. 6.10.

The following equation gives the energy balance for the evaporator:

$$\dot{m}_{o,2} (h_{s1} - h_{ga}) = \dot{m}_1 (h_2 - h_{aw}) \quad (6.99)$$

where  $\dot{m}_1$  is the mass flow rate of ammonia–water mixture and  $h$  is the enthalpy.

The following relation gives the energy balance for the economizer.

$$\dot{m}_{o,2} (h_{ga} - h_{s2}) = \dot{m}_1 (h_{aw} - h_1) \quad (6.100)$$

In separator 1, the mass balance is given by the following equation.

$$\dot{m}_3 + \dot{m}_4 = \dot{m}_2 \quad (6.101)$$

The following relation gives the ammonia mass balance:

$$\dot{m}_3 x_3 + \dot{m}_4 x_4 = \dot{m}_2 x_2 \quad (6.102)$$

where  $x$  is the mass fraction of ammonia.

The following equation gives the mass flow rate of the saturated vapor separated by separator 1.

$$\dot{m}_3 = \left( \frac{x_2 - x_4}{x_3 - x_4} \right) \dot{m}_2 \quad (6.103)$$

In recuperator 1, the energy balance is given by the following equation.

$$\dot{m}_4 (h_4 - h_6) = \dot{m}_1 (h_1 - h_{14}) \quad (6.104)$$

The following equation gives the isentropic efficiency of the turbine ( $\eta_T$ ).

$$\eta_T = \left( \frac{h_3 - h_5}{h_3 - h_{5s}} \right) \quad (6.105)$$

The following equation gives the power output of the ammonia–water mixture turbine ( $W_T$ ).

$$W_T = \dot{m}_3(h_3 - h_5) \quad (6.106)$$

The following equation gives the mass and energy balance after the turbine exit.

$$\dot{m}_5x_5 + \dot{m}_7x_7 = \dot{m}_8x_8 \quad (6.107)$$

$$\dot{m}_5h_5 + \dot{m}_7h_7 = \dot{m}_8h_8 \quad (6.108)$$

In the recuperator 2, the mass balance and energy balance are given by the following equations.

$$\dot{m}_{10} + \dot{m}_{11} = \dot{m}_9 \quad (6.109)$$

$$\dot{m}_{14}(h_{14} - h_{13}) = \dot{m}_8(h_8 - h_9) \quad (6.110)$$

The following equation gives the ammonia mass balance at separator 2.

$$\dot{m}_{10}x_{10} + \dot{m}_{11}x_{11} = \dot{m}_9x_9 \quad (6.111)$$

The equation below gives the mass flow rate of the saturated vapor separated by the separator 2.

$$\dot{m}_{10} = \left( \frac{x_9 - x_{11}}{x_{10} - x_{11}} \right) \dot{m}_9 \quad (6.112)$$

The following equation gives the condenser energy balance.

$$Q_c = \dot{m}_{10}h_{10} + \dot{m}_{11}h_{11} - \dot{m}_{12}h_{12} \quad (6.113)$$

The pump isentropic efficiencies ( $\eta_p$ ) is given by the following equation.

$$\eta_p = \left( \frac{h_{13s} - h_{12}}{h_{13} - h_{12}} \right) \quad (6.114)$$

The work input by the pump is given by the following equation.

$$W_p = \dot{m}_{12}(h_{13} - h_{12}) \quad (6.115)$$

The following equation gives the instantaneous efficiency of the cycle ( $\eta_{\text{instant}}$ ):

$$\eta_{\text{instant}} = \frac{W_{\text{net}}}{Q_u} \quad (6.116)$$

where  $W_{\text{net}}$  is the network done by the cycle.

The modified system efficiency ( $\eta_m$ ) is defined to replace instantaneous efficiency by integrating the net power output ( $W_{\text{net}}$ ) and  $Q_u$  over a period of time, which is expressed as follows.

$$\eta_m = \frac{\int_{t_1}^{t_2} W_{\text{net}}(t) dt}{\int_{t_1}^{t_2} Q_u(t) dt} \quad (6.117)$$

Based on the above thermal model, the objective function for the present work is defined in the next section.

#### **6.4.2 Case Study, Objective Function Description, and Constraints**

A power plant using the Kalina cycle needs to be designed and optimized for maximum modified system efficiency. The environment temperature and pressure are 20 °C and 101.35 kPa, respectively. The length and width of the absorber plane are 2 m and 0.06 m, respectively, while the concentration ratio of the collector is 10. In addition, the transmissivity of the cover plate is 0.89, the absorptivity of the surface is 0.94, and the reflectivity of the concentrator is 0.87. The specific heat capacity of the thermal oil is 2.8 kJ/kg K. Isentropic efficiency of the turbine is 80 and 70% for the pump. For the optimization problem, three design variables including the turbine inlet temperature, the turbine inlet pressure, and the ammonia–water concentration are considered. The upper and lower bounds of the design variables are presented in Table 6.14.

As mentioned above, the maximization of modified system efficiency ( $\eta_m$ ) of the Kalina cycle is taken as an objective function in the present study. It has been confirmed that the operating parameters resulting in the maximum modified system efficiency also satisfy the minimum quality of the turbine exhaust ( $x_5$ ) constraints. So, considering these aspects, the objective function of Kalina power cycle is formulated as below:

**Table 6.14** Ranges of design variables for Kalina cycle optimization

Design variable	Lower bound	Upper bound
Turbine inlet temperature, K	271.15	381.15
Turbine inlet pressure, bar	17	30
Ammonia–water concentration	0.5	0.9

$$\begin{cases} \text{Minimize } f(X) = \eta_m(X) + \sum_{j=1}^n G_1(g_j(X))^2 \\ X = [x_1, x_2, x_3, \dots, x_D], \quad x_{i,\text{minimum}} \leq x_i \leq x_{i,\text{maximum}} \quad i = 1, 2, 3, \dots, D \\ g_j(X) \leq 0, \quad j = 1, 2, 3, \dots, n \end{cases} \quad (6.118)$$

where  $X$  is the vector of design variables (bounded between its minimum and maximum values), and  $G_1$  is the penalty parameter. The entire term takes into account the effect of constraints violation. This term comes into picture when a constraint violation takes place.  $g_j(X)$  indicates the constraints. The following constraint is considered for the Kalina power cycle.

$$\text{Quality of turbine exhaust, } (x_5) \geq 0.8 \quad (6.119)$$

The next section describes the results and discussion of the case study.

### 6.4.3 Results and Discussion

The considered problem of power plant working on the Kalina cycle is investigated using 11 different metaheuristic approaches to obtain the highest modified system efficiency. As all these methods are stochastic in their working, each algorithm is implemented 100 times on the considered problem to estimate the statistical variations of the algorithms. Each algorithm is implemented with a population size of 50, and the termination criteria are set as 100,000 function evaluations. Like others, the results obtained are presented in the form of the best solution, the worst solution, average solution, standard deviation, and success rate. These results are based on the 100 runs and are presented in Table 6.15. Here, the solutions which are infeasible (i.e., affected by penalty) are eliminated while still obtaining the worst solution, average solution, standard deviation, and success rate which is obtained by considering a 0.1% variation from the global optimum value.

It can be observed from the comparative results that the algorithms performed well and produced almost identical modified system efficiency of the Kalina cycle. The average performance of CSA is the best, followed by the PVS and SOS. On the other hand, the performance of the SCA and WWO algorithm is inferior for producing the average solution. The CSA algorithm has the highest success rate in obtaining the optimum value. This is followed by the PVS algorithm, and GA has the lowest. It can be observed from the results that it is difficult to judge the overall performance of the algorithm as they all produce different results. So, the Friedman rank test is implemented to judge the best suitable algorithm for Kalina power cycle

**Table 6.15** Comparative results of different algorithms for Kalina power cycle optimization

Algorithms	Best	Worst	Average	SD	Success rate (%)
GA	0.854	0.45353	0.6734	0.14132	10
PSO	0.854	0.39731	0.69885	0.15034	17
DE	0.854	0.45534	0.6951	0.12702	16
ABC	0.854	0.58412	0.69666	0.08751	16
CSA	0.854	0.60981	0.77794	0.09013	28
TLBO	0.854	0.51779	0.70645	0.1261	18
SOS	0.854	0.58935	0.73473	0.08716	23
WWO	0.854	0.24875	0.64473	0.15574	11
HTS	0.854	0.53979	0.72393	0.11061	20
PVS	0.854	0.50935	0.74716	0.10576	25
SCA	0.854	0.41875	0.64253	0.15048	13

**Table 6.16** Friedman rank test results for Kalina power cycle optimization

Algorithms	Friedman value	Normalized value	Rank
GA	42	0.285714	9
PSO	37	0.324324	8
DE	35.5	0.338028	7
ABC	25.5	0.470588	5
CSA	12	1	1
TLBO	27	0.444444	6
SOS	15	0.8	2
WWO	48	0.25	11
HTS	23	0.521739	4
PVS	20	0.6	3
SCA	45	0.266667	10

optimization in considering the ability to obtain the best, worst, and average solutions, and the success rate. The results of the Friedman rank test are presented in Table 6.16, and its graphical representation is given in Fig. 6.11. The results are presented in the form of a Friedman value, where the normalized value of '1' is the best, and their overall rank. It can be observed from the results that CSA obtained the first rank followed by SOS and PVS algorithms.

The optimized operating parameters of the Kalina power cycle obtained using the CSA algorithm are presented in Table 6.17. It can be noted from the results that the Kalina power cycle with the highest turbine inlet temperature and the highest ammonia–water concentration results in the highest modified system efficiency of the cycle, while the turbine inlet pressure produced a conflicting effect. In addition, the quality of the turbine exhaust constraint is at the limiting value in the optimized operating condition.

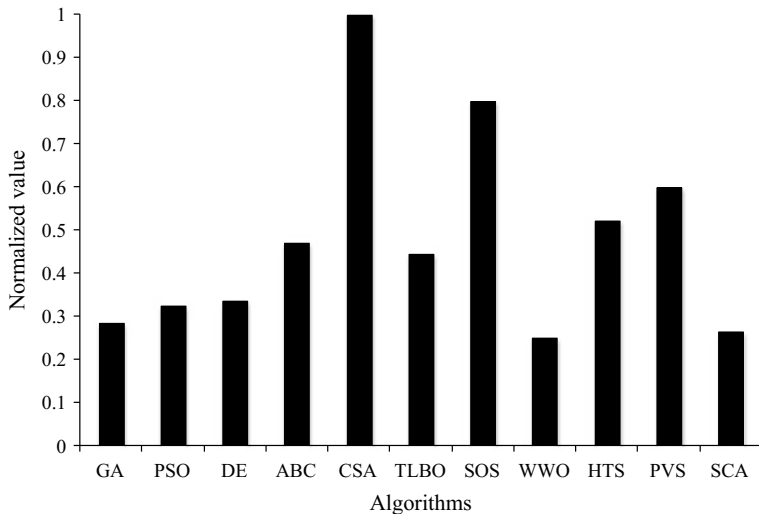


**Fig. 6.11** Graphical presentation of Friedman rank test for Kalina power cycle

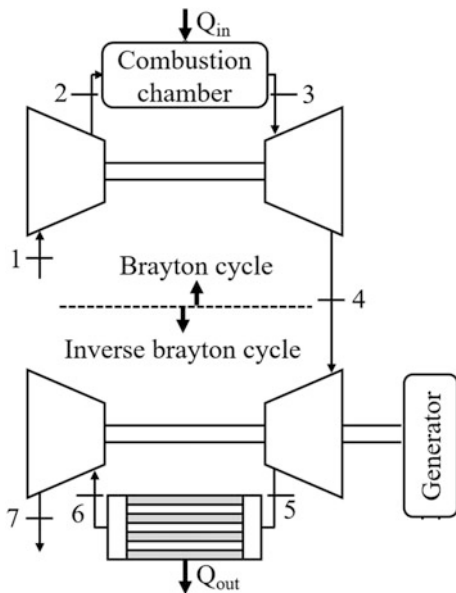
**Table 6.17** The optimized operating condition of Kalina power cycle

Operating parameters	Optimized value
<i>Operating variable</i>	
Turbine inlet temperature, K	380.96
Turbine inlet pressure, bar	25.73
Ammonia–water concentration	0.898
<i>Constraint</i>	
Quality of turbine exhaust, ( $x_5$ )	0.88
<i>Objective function</i>	
Modified system efficiency ( $\eta_m$ )	0.854

## 6.5 Combined Brayton and Inverse Brayton Power Cycle

Another method is proposed for combining the Brayton cycle and the inverse Brayton cycle. This is a hybrid arrangement for power production and cogeneration application. In this combination, the conventional Brayton cycle acts as the topping cycle and the inverse Brayton cycle acts as the bottom cycle. Figure 6.12 shows the schematic arrangement of this combined cycle arrangement. The topping cycle is used to power the bottom cycle. The purpose of the turbine in the topping cycle is solely to power the compressor, and the bottom cycle is responsible for producing the output power of the combined system. The bottom cycle begins with an expansion process, followed by constant pressure cooling and then isentropic compression processes that deliver the working fluid to the required stack condition. The inverse Brayton cycle is used to increase the power production by further expanding the gas turbine exhaust gasses beyond atmospheric conditions.

**Fig. 6.12** Schematic arrangement of combined Brayton and inverse Brayton cycle



Various researchers have carried out works related to the analysis and optimization of combined Brayton and inverse Brayton cycle optimization. Agnew et al. (2003) carried out the simulation and optimization of a combined Brayton and inverse Brayton cycle by varying both the upper cycle pressure ratio and the expansion pressure of the bottom cycle. They concluded that the optimum results could be obtained when the inlet pressure to the bottom cycle is above atmospheric pressure. Alabdoadaim et al. (2006) carried out the performance analysis of a combined Brayton and inverse Brayton cycle and identified the effect of the topping cycle compression ratio and the bottoming cycle expansion ratio on the performance of the cycle. Zhang et al. (2008) analyzed and optimized the power and efficiency of the open combined Brayton and two parallel inverse Brayton cycles by using finite-time thermodynamics. Zhang et al. (2009a, b) proposed a thermodynamic model for an open, combined Brayton and inverse Brayton cycle which considers the pressure drops of the working fluid. The author performed the optimization of the considered cycle by adjusting the compressor inlet pressure of the bottom cycle, the air mass flow rate, and the distribution of pressure losses along the flow path.

Besarati et al. (2010) carried out a multi-objective thermodynamic optimization of a combined Brayton and inverse Brayton cycle by adapting the genetic algorithm. The authors obtained the Pareto optimal solution between conflicting thermodynamic objectives. They also demonstrated the distribution of design variables corresponding to Pareto solutions. Zhang et al. (2012) carried out a performance analysis and parametric study of a combined Brayton and two parallel inverse Brayton cycles using the second law analysis. The authors derived the analytical

formulae of work output and exergy efficiency of the cycle. The authors also identified the impact of operating parameters on the exergy efficiency of the cycle. Chen et al. (2012) presented the thermodynamic modeling of an open, combined regenerative Brayton and inverse Brayton cycle with regeneration before the inverse cycle and analyzed the effect of different operating parameters on the cycle. Rao and Patel (2012) carried out the multi-objective optimization of a combined Brayton and inverse Brayton cycle by considering the maximization of thermal efficiency and specific work of the system as an objective function. The authors considered the optimization of the upper cycle pressure ratio and bottom cycle expansion ratio by adopting an artificial bee colony algorithm. The authors also validated the optimization results by comparing with those obtained using the genetic algorithm and the particle swarm optimization.

Zhang et al. (2007) carried out the second law-based optimization of a combined Brayton and inverse Brayton cycle and derived the analytical formula of optimal exergy efficiency and optimal expansion pressure of the bottom cycle. Then, authors such as Zhang et al. (2014) proposed a new cyclic model of a combined regenerative Brayton and inverse Brayton cycles, which recovers heat energy after the working fluid leaves the turbine of the inverse Brayton cycle. The authors concluded that the new combined cycle results in higher thermal efficiency and larger specific work in comparison with those of the original combined. Goodarzi et al. (2014) carried out the performance analysis of a modified regenerative Brayton and inverse Brayton cycle. The authors investigated the effect of the modification on the performance parameter of the cycle for different varieties of compressor pressure ratios and concluded that the proposed modification improved the performance parameters of the system, especially compared to the base cycle. Chen et al. (2016) performed an exergetic performance optimization of a combined, intercooled regenerative Brayton and inverse Brayton cycles. They concluded that the intercooling and regenerative processes increase exergy efficiency, especially when the total pressure ratio of the cycle varies over a certain range.

### 6.5.1 Thermal Model

In this part of the work, a combined Brayton and inverse Brayton cycle is considered for optimization. The schematic arrangement of the combined Brayton and inverse Brayton cycle is shown in Fig. 6.12. The thermal model of the combined Brayton and inverse Brayton cycle presented here is based on the previous work of Besarati et al. (2010) and Rao and Patel (2012).

The actual temperature of air ( $T_2$  in °C) after compression in the upper cycle is given by

$$T_2 = T_1 + \left( \frac{T'_2 - T_1}{\eta_c} \right) \quad (6.120)$$

where  $T_1$  is the temperature of the air supplied to the upper cycle compressor (in °C),  $\eta_c$  is the isentropic efficiency of the compressor, and  $T'_2$  is the temperature of the air after isentropic compression.  $T'_2$  is calculated with the following equation:

$$T'_2 = T_1 \times (P_r)^{\frac{\gamma-1}{\gamma}} \quad (6.121)$$

where  $P_r$  is the upper cycle compression ratio, and  $\gamma$  is the specific heat ratio.

Considering this temperature and the mechanical efficiency of turbomachinery ( $\eta_m$ ), the work required by the upper cycle compressor ( $w_{c1}$ ) is calculated as

$$w_{c1} = \frac{(h_2 - h_1)}{\eta_m} \quad (6.122)$$

where  $h$  is the specific enthalpy of air in kJ/kg and is obtained by

$$h = C_p(T_2 - T_1) \quad (6.123)$$

where  $C_p$  is the specific heat of air in kJ/kg °C.

The amount of heat added to the compressed air in the combustion chamber ( $q_{in}$ ) is given by

$$q_{in} = (h_3 - h_2) \quad (6.124)$$

The work developed in the upper cycle turbine ( $w_{t1}$ ) is just enough to run the upper cycle compressor and is calculated as

$$w_{t1} = (h_4 - h_3) \times \eta_m \quad (6.125)$$

Likewise, the work developed in the bottom cycle turbine ( $w_{t2}$  in kJ/kg) is given by

$$w_{t2} = (h_4 - h_3) \times \eta_m \quad (6.126)$$

Also, the temperature of the expanded gas ( $T_5$ ) after the bottom cycle turbine is calculated as

$$T_5 = T_4 - (T_4 - T'_5) \times \eta_t \quad (6.127)$$

Here  $\eta_t$  is the isentropic efficiency of the turbine and  $T'_5$  is the temperature of the air considering isentropic expansion and is obtained from the below equation:

$$T'_5 = T_4 \times \left( \frac{P_5}{P_4} \right)^{\frac{\gamma-1}{\gamma}} \quad (6.128)$$

where  $P_4$  and  $P_5$  are the topping cycle expansion pressure and bottom cycle expansion pressure, respectively.

The heat rejected by the expanded gas ( $q_{\text{out}}$ ) in the bottom cycle heat exchanger is calculated by

$$q_{\text{out}} = (h_5 - h_6) \quad (6.129)$$

The work required by the compressor in the bottom cycle ( $w_{c2}$ ) is obtained from the following equation.

$$w_{c2} = \frac{(h_7 - h_6)}{\eta_m} \quad (6.130)$$

Based on the above calculation, the specific work of the system ( $w_s$ ) is calculated as

$$w_s = w_{t2} - w_{c2} \quad (6.131)$$

Similarly, the thermal efficiency of the system ( $\eta_{\text{th}}$ ) is calculated as

$$\eta_{\text{th}} = \frac{w_s}{q_{\text{in}}} \quad (6.132)$$

Based on the above thermal model, the objective function for the present work is defined in the next section.

### 6.5.2 Case Study, Objective Function Description, and Constraints

A combined Brayton and inverse Brayton cycle needs to be designed and optimized for maximum thermal efficiency. The air in the study is supplied at a temperature of 15 °C, and the pressure in the upper cycle compressor is 1.013. The high-temperature gas is supplied at a constant temperature of 1300 °C to the upper cycle turbine after the addition of heat to the upper cycle heat exchanger. After rejecting heat in the bottom cycle heat exchanger for process heating, the low-pressurized, expanded gas enters the bottom cycle compressor at a temperature of 65 °C, and the pressure is 1.04 bar. The isentropic efficiencies of the compressors and turbines are taken as 0.85 and 0.9, respectively, while its mechanical efficiency is considered to be 99%. Two design variables such as the upper cycle pressure ratio ( $P_r$ ) and bottom cycle expansion pressure ( $P_5$ ) of the system are

**Table 6.18** Ranges of design variables for combined Brayton and inverse Brayton cycle optimization

Design variable	Lower bound	Upper bound
Upper cycle pressure ratio, ( $P_r$ )	8	25
Bottom cycle expansion pressure, ( $P_5$ ) bar	0.2	0.8

considered for the optimization problem. The upper and lower bounds of design variables are presented in Table 6.18.

As mentioned above, the maximization of the thermal efficiency ( $\eta_{th}$ ) of combined cycle is taken as an objective function in the present study. In addition, the operating parameters resulting in maximum thermal efficiency also satisfy the specific work ( $w_s$ ) constraints. So, considering all these aspects, the objective function of the combined Brayton and inverse Brayton cycle is formulated as below:

$$\left\{ \begin{array}{l} \text{Minimize } f(X) = \eta_{th}(X) + \sum_{j=1}^n G_1(g_j(X))^2 \\ X = [x_1, x_2, x_3, \dots, x_D], \quad x_{i,\text{minimum}} \leq x_i \leq x_{i,\text{maximum}} \quad i = 1, 2, 3, \dots, D \\ g_j(X) \leq 0, \quad j = 1, 2, 3, \dots, n \end{array} \right. \quad (6.133)$$

where  $X$  is the vector of design variables which is bounded between its minimum and maximum values.  $G_1$  is the penalty parameter. Note that the entire term takes into account the effects of the constraints violation, which for the combined Brayton and inverse Brayton cycle is shown below. This term comes into picture when the constraint violation takes place.  $g_j(X)$  indicates the constraints.

$$\text{Specific work, } (w_s) \geq 480 \text{ kJ/kg} \quad (6.134)$$

The next section describes the results and discussion of the case study.

### 6.5.3 Results and Discussion

The considered problem of the combined Brayton and inverse Brayton cycle is investigated using 11 different metaheuristic approaches to obtain maximum thermal efficiency. As all these methods are stochastic in their working, each algorithm is implemented 100 times on the considered problem to estimate the statistical variations of the algorithms. Each algorithm uses a population size of 50, and the termination criteria are set as 100,000 function evaluations. The results obtained using each algorithm are presented in the form of the best solution, the worst

solution, average solution, standard deviation, and the success rate (in the 100). These are presented in Table 6.19. Here, the solutions which are infeasible (i.e., affected by penalty) are eliminated. Then, the worst solution, average solution, standard deviation, and success rate (considering 0.1% variation from the global optimum value) are obtained.

It can be observed from the comparative results that the algorithms performed satisfactorily, producing identical maximum thermal efficiency for the combined Brayton and inverse Brayton cycle. In addition, the average performance of all the considered algorithms (except GA) is similar in obtaining the maximum thermal efficiency of the combined cycle. For success rate, the DE algorithm is the highest in obtaining the optimum value of thermal efficiency followed by the PSO and SOS algorithm. The success rate of GA is the lowest as compared to other algorithms. It can be observed from the results that it is difficult to judge the performance of the algorithm as all the algorithms have different variations for the results. So, the Friedman rank test is implemented to judge the best suitable algorithm for the combined Brayton and inverse Brayton cycle considering the capability to obtain the best, worst, and average solutions, and success rate. The results of the Friedman rank test are presented in Table 6.20, and its graphical representation is given in Fig. 6.13. The results are presented in the form of a Friedman value, where the normalized value with ‘1’ is the best performing algorithm. The rank is also shown. It can be observed from the results that DE has obtained the first rank followed by SOS and TLBO algorithms.

The optimized operating parameters of the combined Brayton and inverse Brayton cycle obtained using the DE algorithm are presented in Table 6.21. It can be noted from the results that the upper cycle pressure ratio and bottom cycle expansion pressure produced a conflicting effect on achieving the maximum thermal efficiency of the cycle. Furthermore, the specific work constraint is at a limiting value in the optimized operating condition of the combined Brayton and inverse Brayton cycle.

**Table 6.19** Comparative results of different algorithms for combined Brayton and inverse Brayton cycle optimization

Algorithms	Best	Worst	Average	SD	Success rate (%)
GA	0.48256	0.42142	0.47528	0.01524	60
PSO	0.48256	0.48256	0.48256	1.7E-06	97
DE	0.48256	0.48256	0.48256	1.7E-16	99
ABC	0.48256	0.48256	0.48256	1.7E-16	94
CSA	0.48256	0.48256	0.48256	1.1E-16	93
TLBO	0.48256	0.48256	0.48256	1.7E-16	95
SOS	0.48256	0.48256	0.48256	1.7E-16	96
WWO	0.48256	0.48236	0.48255	4.1E-05	91
HTS	0.48256	0.48256	0.48256	1.1E-16	91
PVS	0.48256	0.48256	0.48256	1.1E-16	94
SCA	0.48256	0.48251	0.48255	1.5E-05	91

**Table 6.20** Friedman rank test results for combined Brayton and inverse Brayton cycle optimization

Algorithms	Friedman value	Normalized value	Rank
GA	48	0.322917	11
PSO	27	0.574074	5
DE	15.5	1	1
ABC	20	0.775	4
CSA	31	0.5	7
TLBO	18.5	0.837838	3
SOS	17.5	0.885714	2
WWO	42	0.369048	9
HTS	35	0.442857	8
PVS	29.5	0.525424	6
SCA	46	0.336957	10

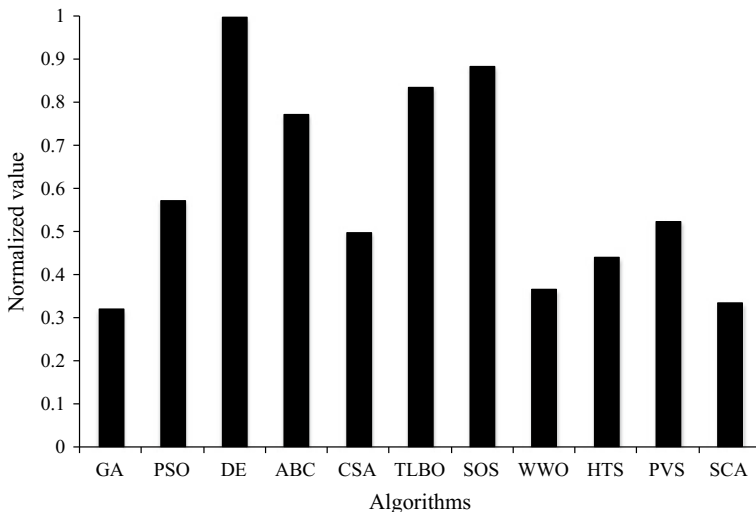


**Fig. 6.13** Graphical presentation of Friedman rank test for combined Brayton and inverse Brayton cycle optimization

**Table 6.21** The optimized operating condition of combined Brayton and inverse Brayton cycle

Operating parameters	Optimized value
<i>Operating variable</i>	
Upper cycle pressure ratio, ( $P_r$ )	18.28
Bottom cycle expansion pressure, ( $P_s$ ) bar	0.3834
<i>Constraint</i>	
Specific work, ( $w_s$ ), kJ/kg	480
<i>Objective function</i>	
Thermal efficiency ( $\eta_{th}$ )	0.48256

## 6.6 Atkinson Power Cycle Optimization

The Atkinson cycle is a type of air standard, internal combustion cycle designed to provide efficiency at the expense of power density. The thermodynamic presentation of the Atkinson cycle is shown in Fig. 6.14. It can be observed from the figure that the Atkinson cycle is composed of two isentropic processes, one a constant pressure process and the other a constant volume process. The atmospheric air is compressed with the help of a compressor (process 4–1). This process is isentropic in nature. In addition, the volume of air decreases from  $V_4$  to  $V_1$  and pressure increases from  $P_4$  to  $P_1$ . The temperature increases from  $T_4$  to  $T_1$  and heat is supplied to the compressed air at constant volume (process 1–2) with the help of a heat source. Due to the heat supplied, temperature of the air increases from  $T_1$  to  $T_2$  while its pressure increases from  $P_1$  to  $P_2$ . This high-pressure, high-temperature air further expands in the cylinder (process 2–3) during the expansion stroke. The expansion process is isentropic in nature. The expansion process reduces the pressure of air from  $P_2$  to  $P_3$  in the cycle. After expansion, the remaining heat of the air is rejected at constant pressure (i.e.,  $P_3 = P_4$ ) during the heat rejection process (process 3–4). Due to heat rejection, the volume and temperature of the air decrease to their initial value.

In the conventional Otto cycle, heat rejection takes place at constant pressure, which is three to four times higher than atmospheric pressure. Thus, there is loss in useful work that can be gained through power stroke if expansion is continued up to atmospheric pressure. In the Atkinson cycle, the expansion process extends up to atmospheric pressure and then heat rejection takes place at that pressure. Thus, the Atkinson cycle results in more power output compared to the conventional Otto cycle due to the extended expansion stroke. This further increases the efficiency of the cycle.

Earlier, researchers have carried out various works related to the analysis and optimization of the Atkinson power cycle. Chen et al. (1998) obtained the efficiency of the Atkinson cycle at maximum power density using finite-time thermodynamics

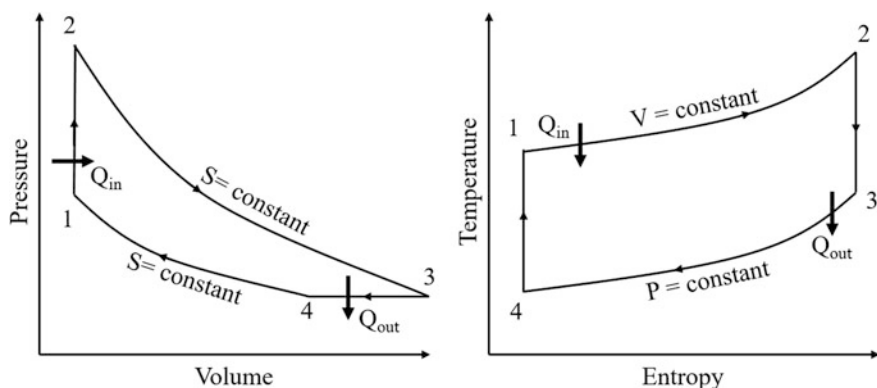


Fig. 6.14 Thermodynamic presentation of Atkinson cycle

and observed that the efficiency at maximum power density is always greater than that at maximum power. Wang and Hou (2005) carried out the performance analysis of an Atkinson cycle coupled to variable temperature heat reservoirs based on the maximum power and maximum power density conditions. Ge et al. (2006) analyzed the performance of an air standard Atkinson cycle with heat-transfer loss and variable specific heat of the working fluid based on finite-time thermodynamics. The relations between the power output and the compression ratio, between the thermal efficiency and the compression ratio, as well as the optimal relation between the power output and the efficiency of the cycle were all derived. Zhao and Chen (2006) carried out the performance analysis and parametric optimization of an Atkinson cycle. The authors derived the power output and efficiency of the cycle by introducing the pressure ratio as well as the compression and expansion efficiencies. The authors also identified the influences of various design parameters on the performance of the cycle. Hou (2007) analyzed the effects of heat transfer on the net output work and the indicated thermal efficiency of an air standard Atkinson cycle. The author demonstrated the performance comparisons of air standard Atkinson and Otto cycles and observed that an Atkinson cycle has a greater work output and a higher thermal efficiency than the Otto cycle at the same operating condition.

Sarkhii et al. (2008) presented the thermodynamic analysis of an ideal air-standard Atkinson cycle with temperature-dependent specific heat. The authors also investigated the effect of maximum power density on the performance of the cycle efficiency. Ust (2009) performed the thermodynamic optimization of an Atkinson cycle based on the maximum power (MP) and maximum power density (MPD) criteria. The authors compared the results at MPD conditions with those obtained using the MP and maximum thermal efficiency criteria and concluded that a design based on the MPD conditions is more advantageous. Zhao et al. (2012) carried out the optimization of a compression ratio and operating parameters of an Atkinson cycle by using the artificial neural network. The authors obtained the optimum value of the compression ratio for the maximization of a fuel economy for the cycle. Furthermore, they validated the optimization results by conducting the experiment on the actual cycle and observed the relationship between the numerical and experimental results. Zhao and Xu (2013) carried out the fuel economy optimization of an Atkinson cycle. The authors proposed a physical model-based optimization scheme by coupling the genetic algorithm and 1-D power simulation models of the Atkinson cycle engine.

Ahmadi et al. (2016a, b) carried out the multi-objective thermodynamic optimization of an Atkinson cycle. The authors considered the maximization of thermal efficiency and power output of the cycle as an objective function and used NSGA-II as an optimization method. Furthermore, a sensitivity analysis of the design variables is also performed to identify its effect on the objective function. The authors implemented decision-making techniques to select the best solution from the available Pareto points. Gonca and Sahin (2014) presented an ecological performance analysis and optimization of an air-standard irreversible Dual-Atkinson cycle based on the ecological coefficient of performance (ECOP) criterion. Furthermore, the authors compared the results obtained using the ECOP criterion

with those obtained using maximum power output conditions. Gonca (2016) carried out the performance analysis and optimization of an irreversible Dual-Atkinson cycle under nondimensional maximum power (MP), nondimensional maximum power density (MPD), and maximum thermal efficiency (MEF) conditions. The author also investigated the effects of the inlet temperature and heat transfer coefficient on the cycle performance.

### 6.6.1 Thermal Model

In this part of the work, an Atkinson cycle is considered for optimization. The thermodynamic presentation of the Atkinson cycle is shown in Fig. 6.14. The thermal model of the Atkinson cycle presented here is based on the previous work of Ahmadi et al. (2016a, b).

The heat input ( $Q_{\text{in}}$ ) to the Atkinson cycle can be given by the following equation:

$$Q_{\text{in}} = m \int_{T_2}^{T_3} C_p dT \quad (6.135)$$

where  $m$  is the mass flow rate of air,  $C_p$  is the specific heat of air at constant pressure. In addition, the heat rejected ( $Q_{\text{out}}$ ) during the Atkinson cycle can be given by the following equation.

$$Q_{\text{out}} = m \int_{T_1}^{T_4} C_p dT \quad (6.136)$$

The specific heat of the air is temperature dependent and can be obtained by the following equation:

$$C_p = a_1 + a_2 T \quad (6.137)$$

$$C_p - C_v = R \quad (6.138)$$

where  $a_1$  and  $a_2$  are the constants,  $C_v$  is the specific heat at constant volume, and  $R$  is the gas constant.

Replacing the temperature-dependent specific heat into the heat addition ( $Q_{\text{in}}$ ) and heat rejection ( $Q_{\text{out}}$ ) equations results in

$$Q_{\text{in}} = m \left( (a_1 - R)(T_3 - T_2) + \frac{a_2}{2} (T_3^2 - T_2^2) \right) \quad (6.139)$$

$$Q_{\text{out}} = m \left( a_1(T_4 - T_1) + \frac{a_2}{2} (T_4^2 - T_1^2) \right) \quad (6.140)$$

The following equation can give the power output ( $W$ ) of the Atkinson cycle:

$$W = m \left( (a_1 - R)(T_3 - T_2) + \frac{a_2}{2} (T_3^2 - T_2^2) - a_1(T_4 - T_1) - \frac{a_2}{2} (T_4^2 - T_1^2) \right) \quad (6.141)$$

where  $T_1$  to  $T_4$  are the temperatures of the air at different state points corresponding to Fig. 6.14. The relation between these temperatures is given by

$$\frac{T_4}{T_1} = \left( \frac{T_3}{T_2} \right)^{(1/k)} \quad (6.142)$$

where  $k$  is the ratio of specific heat and is given by

$$k = \frac{C_p}{C_v} \quad (6.143)$$

The following equation can give simplification power output ( $W$ ) of this cycle:

$$W = mT_1 \left( (a_1 - R)(\tau - \theta) + \frac{a_2 T_1}{2} (\tau^2 - \theta^2) - a_1 \left( \left( \frac{\tau}{\theta} \right)^{\frac{1}{k}} - 1 \right) - \frac{a_2 T_1}{2} \left( \left( \frac{\tau}{\theta} \right)^{\frac{2}{k}} - 1 \right) \right) \quad (6.144)$$

where  $\theta$  is the isentropic temperature ratio and  $\tau$  is the cycle temperature ratio and are given by

$$\theta = T_2/T_1 \quad (6.145)$$

$$\tau = T_3/T_1 \quad (6.146)$$

The following equation can give the efficiency ( $\eta$ ) of the Atkinson cycle.

$$\eta = 1 - \left( \frac{a_1 \left( (\tau/\theta)^{(1/k)} - 1 \right) + (a_2 T_1/2) \left( (\tau/\theta)^{(2/k)} - 1 \right)}{(a_1 - R)(\tau - \theta) + (a_2 T_1/2)(\tau^2 - \theta^2)} \right) \quad (6.147)$$

Based on the above thermal model, the objective function for the present work is defined in the next section.

### 6.6.2 Case Study, Objective Function Description, and Constraints

An air-standard Atkinson power cycle needs to be designed and optimized for maximum thermal efficiency. As air is used as a working fluid, the gas constant of air ( $R$ ) is taken as 0.287 kJ/kg K. The ratio of the specific heat ( $k$ ) is taken as 1.4 and the parameters used to obtain the temperature-dependent specific heat are as follows:  $a_1$  is 0.9521 kJ/kg K and  $a_2$  is 0.0002 kJ/kg K. Three design variables are considered for the optimization problem: the isentropic temperature ratio ( $\theta$ ), the cycle temperature ratio ( $\tau$ ), and the temperature of air at state point 1 ( $T_1$ ). Note that the upper and lower bounds of the design variables are presented in Table 6.22.

As mentioned above, the maximization of the thermal efficiency ( $\eta$ ) of the Atkinson cycle is taken as an objective function in the present study. For this section, the operating parameters which result in maximum thermal efficiency also satisfy the power output ( $W$ ) constraints. So, considering all the aspects, the objective function of the Atkinson cycle is formulated as below:

$$\begin{cases} \text{Minimize } f(X) = \eta(X) + \sum_{j=1}^n G_1(g_j(X))^2 \\ X = [x_1, x_2, x_3, \dots, x_D], \quad x_{i,\text{minimum}} \leq x_i \leq x_{i,\text{maximum}} \quad i = 1, 2, 3, \dots, D \\ g_j(X) \leq 0, \quad j = 1, 2, 3, \dots, n \end{cases} \quad (6.148)$$

where  $X$  is the vector of design variables and it has to be bounded between its minimum and maximum values, and  $G_1$  is the penalty parameter. The entire term takes into account the effect of constraints violation and is used when the constraint violation takes place. Here,  $g_j(X)$  indicates the constraints which for the Atkinson cycle are

$$\text{Power output}(W) \geq 417 \text{ W} \quad (6.149)$$

The next section describes the results and discussion of the case study.

**Table 6.22** Ranges of design variables for Atkinson power cycle optimization

Design variable	Lower bound	Upper bound
Isentropic temperature ratio, ( $\theta$ ),	0.1	2.1
Cycle temperature ratio, ( $\tau$ )	1	4
The temperature of the air at state point 1, ( $T_1$ )	1	380

### 6.6.3 Results and Discussion

The considered problem of the Atkinson cycle is investigated using 11 different metaheuristic approaches to obtain maximum thermal efficiency. As all these methods are stochastic in their working, each algorithm is run 100 times on the considered problem to estimate the statistical variations of the algorithms. Each algorithm is implemented with the population size of 50, and termination criteria are set as 100,000 function evaluations. The overall results from the 100 runs that were obtained using each algorithm are presented in the form of the best solution, the worst solution, average solution, standard deviation, and success rate. These results are illustrated in Table 6.23, where the infeasible solutions (i.e., affected by penalty) are eliminated. This is done while obtaining the worst solution, average solution, standard deviation, and success rate. Furthermore, the success rate of the algorithm is obtained by considering a 0.1% variation from the global optimum value.

It can be observed from the comparative results that tested algorithms performed equally good and produced nearly identical thermal efficiency of the Atkinson cycle. In addition, the average performance of the competitive algorithms (except GA) is similar. Not only that, but the success rate of DE, ABC, SOS, and the PVS algorithms is the highest in obtaining the optimum value while GA is the lowest. It can be observed from the results that it is difficult to judge the performance of the algorithm as all the algorithms have produced different results for the best, worst, and average results, and success rate. So, the Friedman rank test is implemented to judge the best suitable algorithm for the optimization of the Atkinson cycle considering the algorithms ability to obtain the best, worst, and average solutions, and its success rate. The results of the Friedman rank test are presented in Table 6.24, and its graphical representation is given in Fig. 6.15. The results are presented in the form of Friedman value, a normalized value with ‘1’ as the best performing

**Table 6.23** Comparative results of different algorithms for Atkinson power cycle optimization

Algorithms	Best	Worst	Average	SD	Success rate (%)
GA	0.59254	0.58197	0.59206	2.254E-3	84
PSO	0.59254	0.59254	0.59254	4.68E-07	88
DE	0.59254	0.59254	0.59254	2.27E-16	96
ABC	0.59254	0.59254	0.59254	2.27E-16	96
CSA	0.59254	0.59254	0.59254	3.41E-16	92
TLBO	0.59254	0.59254	0.59254	2.27E-16	92
SOS	0.59254	0.59254	0.59254	2.27E-16	96
WWO	0.59254	0.59254	0.59254	2.27E-16	88
HTS	0.59254	0.59254	0.59254	2.09E-06	92
PVS	0.59254	0.59254	0.59254	3.4E-16	96
SCA	0.59254	0.59248	0.59252	2.16E-05	92

**Table 6.24** Friedman rank test results for Atkinson power cycle optimization

Algorithms	Friedman value	Normalized value	Rank
GA	50	0.41	9
PSO	33.5	0.61194	7
DE	20.5	1	1
ABC	20.5	1	1
CSA	29.5	0.694915	4
TLBO	26.5	0.773585	3
SOS	20.5	1	1
WWO	30.5	0.672131	5
HTS	31.5	0.650794	6
PVS	24.5	0.836735	2
SCA	42.5	0.482353	8

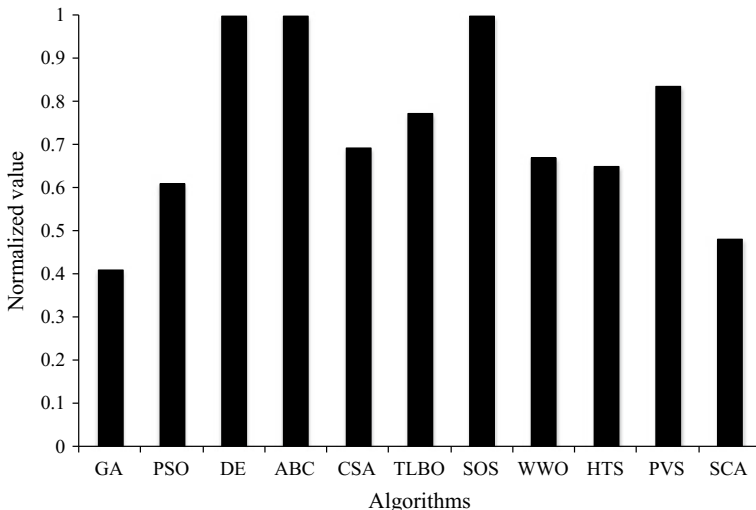


**Fig. 6.15** Graphical presentation of Friedman rank test for Atkinson power cycle optimization

algorithm and its rank. It can be observed from the results that DE, ABC, and SOS have obtained first rank followed by PVS and TLBO algorithms.

The optimized operating parameters of the Atkinson cycle obtained using the DE algorithm are presented in Table 6.25. It can be noted from the results that the Atkinson cycle with maximum cycle temperature ratio ( $\tau$ ) and having the temperature of the air at state point 1 ( $T_1$ ) results in the maximum thermal efficiency of the cycle. Isentropic temperature ratio of the cycle produced a conflicting effect on achieving the maximum thermal efficiency of the Atkinson cycle. Furthermore, in this cycle, the power output constraint is at the limiting value in the optimized operating condition of the Atkinson cycle.

**Table 6.25** The optimized operating condition of Atkinson power cycle

Operating parameters	Optimized value
<i>Operating variable</i>	
Isentropic temperature ratio, ( $\theta$ ),	1.845
Cycle temperature ratio, ( $\tau$ )	4
Temperature of air at state point 1, ( $T_1$ )	380
<i>Constraint</i>	
Power output (W)	417
<i>Objective function</i>	
Thermal efficiency ( $\eta$ )	0.59254

## References

- Açıklalp E. (2017) ‘Performance analysis of irreversible molten carbonate fuel cell–Braysson heat engine with ecological objective approach’, *Energy Conversion and Management*, vol. 132, pp. 432–437.
- Agnew B., Anderson A., Potts I., Frost T.H. and Alabdoadaaim M.A. (2003) ‘Simulation of combined Brayton and inverse Brayton cycles’, *Applied thermal engineering*, 23(8), pp. 953–963.
- Ahmadi M.H., Ahmadi M.A., Pourfayaz F., Bidi M. and Açıkkalp E. (2016a) ‘Multi-objective optimization and exergetic-sustainability of an irreversible nano scale Braysson cycle operating with Maxwell–Boltzmann gas’, *Alexandria Engineering Journal*, vol. 55(2), pp. 1785–1798.
- Ahmadi M.H., Ahmadi M.A., Shafaei A., Ashouri M. and Toghiani S. (2016b) ‘Thermodynamic analysis and optimization of the Atkinson engine by using NSGA-II’, *International Journal of Low-Carbon Technologies*, vol. 11(3), pp. 317–324.
- Ahmadi P. and Dincer I. (2011a) ‘Thermodynamic analysis and thermoeconomic optimization of a dual pressure combined cycle power plant with a supplementary firing unit’, *Energy Conversion and Management*, vol. 52(5), pp. 2296–2308.
- Ahmadi P. and Dincer I. (2011b) ‘Thermodynamic and exergoenvironmental analyses, and multi-objective optimization of a gas turbine power plant’, *Applied Thermal Engineering*, vol. 31(14–15), pp. 2529–2540.
- Alabdoadaaim M.A., Agnew B. and Potts I. (2006) ‘Performance analysis of combined Brayton and inverse Brayton cycles and developed configurations’, *Applied thermal engineering*, vol. 26 (14–15), pp. 1448–1454.
- Aljundi I.H. (2009) ‘Energy and exergy analysis of a steam power plant in Jordan’, *Applied Thermal Engineering*, vol. 29(2–3), pp. 324–328.
- Al-Sarkhi A., Akash B., Abu-Nada E. and Al-Hinti I. (2008) ‘Efficiency of Atkinson engine at maximum power density using temperature dependent specific heats’, *Jordan Journal of Mechanical and Industrial Engineering*, vol. 2(2).
- Ameri M., Ahmadi P. and Hamidi A. (2009) ‘Energy, exergy and exergoeconomic analysis of a steam power plant: a case study’, *International Journal of Energy Research*, vol. 33(5), pp. 499–512.
- Amin M. Elsafi (2015) ‘Exergy and exergoeconomic analysis of sustainable direct steam generation solar power plants’, *Energy Conversion and Management*, vol. 103, 338–347.
- Arslan O. (2011) ‘Power generation from medium temperature geothermal resources: ANN-based optimization of Kalina cycle system-34’, *Energy*, vol. 36(5), pp. 2528–2534.
- Ashouri M., Vandani A.M.K., Mehrpooya M., Ahmadi M.H. and Abdollahpour A. (2015) ‘Techno-economic assessment of a Kalina cycle driven by a parabolic Trough solar collector’, *Energy Conversion and Management*, vol. 105, pp. 1328–1339.

- Ataei A. and Yoo C. (2010) 'Combined pinch and exergy analysis for energy efficiency optimization in a steam power plant', *International Journal of Physical Sciences*, vol. 5(7), pp. 1110–1123.
- Barzegar Avval H., Ahmadi P., Ghaffarizadeh A.R. and Saidi M.H. (2011) 'Thermo-economic-environmental multiobjective optimization of a gas turbine power plant with preheater using evolutionary algorithm', *International Journal of Energy Research*, vol. 35(5), pp. 389–403.
- Bekdemir S., Öztürk R. and Yumurtac Z. (2003) 'Condenser optimization in steam power plant', *Journal of Thermal Science*, vol. 12(2), pp. 176–178.
- Besarati S.M., Atashkari K., Jamali A., Hajiloo A. and Nariman-Zadeh N. (2010) 'Multi-objective thermodynamic optimization of combined Brayton and inverse Brayton cycles using genetic algorithms', *Energy Conversion and Management*, vol. 51(1), pp. 212–217.
- Bombarda P., Invernizzi C.M. and Pietra C. (2010) 'Heat recovery from Diesel engines: A thermodynamic comparison between Kalina and ORC cycles', *Applied Thermal Engineering*, vol. 30 (2–3), pp. 212–219.
- Boyaghchi F.A. and Sabaghian M. (2016) 'Multi objective optimisation of a Kalina power cycle integrated with parabolic trough solar collectors based on exergy and exergoeconomic concept', *International Journal of Energy Technology and Policy*, Vol. 12, No. 2, pp. 154–180.
- Cheddie D.F. (2011) 'Thermo-economic optimization of an indirectly coupled solid oxide fuel cell/gas turbine hybrid power plant', *International Journal of Hydrogen Energy*, vol. 36(2), pp. 1702–1709.
- Chen L., Lin J., Sun F. and Wu C. (1998) 'Efficiency of an Atkinson engine at maximum power density', *Energy Conversion and Management*, vol. 39(3–4), pp. 337–341.
- Chen L., Ni D., Zhang Z. and Sun F. (2016) Exergetic performance optimization for new combined intercooled regenerative Brayton and inverse Brayton cycles. *Applied Thermal Engineering*, vol. 102, pp. 447–453.
- Chen L., Zhang Z. and Sun F. (2012) 'Thermodynamic modeling for open combined regenerative Brayton and inverse Brayton cycles with regeneration before the inverse cycle', *Entropy*, vol. 14(1), pp. 58–73.
- Dincer I. and Al-Muslim H. (2001) 'Thermodynamic analysis of reheat cycle steam power plants', *International Journal of Energy Research*, vol. 25(8), pp. 727–739.
- Dincer I., Rosen M.A. and Ahmadi P. (2017) 'Modeling and Optimization of Power Plants', *Optimization of Energy Systems*, pp. 275–316.
- Hajabdollahi, Z. Hajabdollahi, H. Hajabdollahi (2012) 'Soft computing based multi objective optimization of steam cycle power plant using NSGA-II and ANN', *Applied Soft Computing*, vol. 12, 3648–3655.
- Fallah M., Mahmoudi S.M.S., Yari M. and Ghiasi R.A. (2016) 'Advanced exergy analysis of the Kalina cycle applied for low temperature enhanced geothermal system', *Energy conversion and management*, vol. 108, pp. 190–201.
- Frost T.H., Anderson A. and Agnew B. (1997) 'A hybrid gas turbine cycle (Brayton/Ericsson): an alternative to conventional combined gas and steam turbine power plant', *Proceedings of the Institution of Mechanical Engineers, Part A: Journal of Power and Energy*, vol. 211(2), pp. 121–131.
- Ganjehkaviri A., Jaafar M.M. and Hosseini S.E. (2015) 'Optimization and the effect of steam turbine outlet quality on the output power of a combined cycle power plant', *Energy Conversion and Management*, vol. 89, pp. 231–243.
- Ge Y., Chen L., Sun F. and Wu C. (2006) 'Performance of an Atkinson cycle with heat transfer, friction and variable specific-heats of the working fluid', *Applied Energy*, vol. 83(11), pp. 1210–1221.
- Ghamami M., Fayazi Barjin A. and Behbahani S. (2016) 'Performance Optimization of a Gas Turbine Power Plant Based on Energy and Exergy Analysis', *Mechanics, Materials Science & Engineering Journal*, p. 29.
- Gonca G. and Sahin B. (2014) 'Performance optimization of an air-standard irreversible Dual-Atkinson cycle engine based on the ecological coefficient of performance criterion' *The Scientific World Journal*.

- Gonca G. (2016) 'Performance analysis and optimization of irreversible Dual-Atkinson cycle engine (DACE) with heat transfer effects under maximum power and maximum power density conditions', *Applied Mathematical Modelling*, vol. 40(13–14), pp. 6725–6736.
- Goodarzi M., Kiasat M. and Khalilidehkordi E. (2014) 'Performance analysis of a modified regenerative Brayton and inverse Brayton cycle', *Energy*, vol. 72, pp. 35–43.
- Hajabdollahi H., Ahmadi P. and Dincer I. (2011) 'An exergy-based multi-objective optimization of a heat recovery steam generator (HRSG) in a combined cycle power plant (CCPP) using evolutionary algorithm', *International Journal of Green Energy*, vol. 8(1), pp. 44–64.
- Hajabdollahi F., Hajabdollahi Z. and Hajabdollahi H. (2012b) 'Soft computing based multi-objective optimization of steam cycle power plant using NSGA-II and ANN', *Applied Soft Computing*, vol. 12(11), pp. 3648–3655.
- Haseli Y. (2013) 'Optimization of a regenerative Brayton cycle by maximization of a newly defined second law efficiency', *Energy conversion and management*, vol. 68, pp. 133–140.
- Hou S.S. (2007) 'Comparison of performances of air standard Atkinson and Otto cycles with heat transfer considerations', *Energy Conversion and Management*, vol. 48(5), pp. 1683–1690.
- Kalina Alexander I. (2003) 'New Binary Geothermal Power System', *International Geothermal Workshop*, Geothermal Energy Society, Sochi, Russia.
- Kaviri A.G., Jaafar M.N.M., Lazim T.M. and Barzegaravval H. (2013) 'Exergoenvironmental optimization of heat recovery steam generators in combined cycle power plant through energy and exergy analysis', *Energy conversion and management*, vol. 67, pp. 27–33.
- Kumar R., Kaushik S.C., Kumar R. and Hans R. (2016) 'Multi-objective thermodynamic optimization of an irreversible regenerative Brayton cycle using evolutionary algorithm and decision making', *Ain Shams Engineering Journal*, vol. 7(2), pp. 741–753.
- Li Y., Liao S. and Liu G. 2015. Thermo-economic multi-objective optimization for a solar-dish Brayton system using NSGA-II and decision making. *International Journal of Electrical Power & Energy Systems*, 64, pp. 167–175.
- Luo X., Zhang B., Chen Y. and Mo S. (2013) 'Operational planning optimization of steam power plants considering equipment failure in petrochemical complex', *Applied energy*, vol. 112, pp. 1247–1264.
- M. Topel, R. Guédez, B. Laumert (2015) 'Impact of Increasing Steam Turbine Flexibility on the Annual Performance of a Direct Steam Generation Tower Power Plant', *Energy Procedia*, vol. 69, 1171–1180.
- Modi A. and Haglind F. (2015) 'Thermodynamic optimisation and analysis of four Kalina cycle layouts for high temperature applications', *Applied Thermal Engineering*, vol. 76, pp. 196–205.
- Modi A., Kærn M.R., Andreasen J.G. and Haglind F. (2016) 'Thermoeconomic optimization of a Kalina cycle for a central receiver concentrating solar power plant', *Energy Conversion and Management*, vol. 115, pp. 276–287.
- Radcenco V., Vargas J.V.C. and Bejan A. (1998) 'Thermodynamic optimization of a gas turbine power plant with pressure drop irreversibilities', *Journal of energy resources technology*, vol. 120(3), pp. 233–240.
- Rao RV. and Patel V. (2012) 'Multi-objective optimization of combined Brayton and inverse Brayton cycles using advanced optimization algorithms', *Engineering Optimization*, vol. 44(8), pp. 965–983.
- S. K. Abadi, M. H. Khoshgoftar Manesh, M. A. Rosen, M. Amidpour, M. H. Hamed (2014) 'Integration of a Gas Fired Steam Power Plant with a Total Site Utility Using a New Cogeneration Targeting Procedure', *Chinese Journal of Chemical Engineering*, vol. 22, 455–468.
- Sadatsakkak S.A., Ahmadi M.H., Bayat R., Pourkiae S.M. and Feidt M. (2015) 'Optimization density power and thermal efficiency of an endoreversible Braysson cycle by using non-dominated sorting genetic algorithm', *Energy Conversion and Management*, vol. 93, pp. 31–39.

- Saffari H., Sadeghi S., Khoshzat M. and Mehregan P., (2016) 'Thermodynamic analysis and optimization of a geothermal Kalina cycle system using Artificial Bee Colony algorithm' *Renewable Energy*, vol. 89, pp. 154–167.
- Seyyedi S.M., Ajam H. and Farahat S. (2010) 'A new approach for optimization of thermal power plant based on the exergoeconomic analysis and structural optimization method: Application to the CGAM problem', *Energy Conversion and Management*, vol. 51(11), pp. 2202–2211.
- Singh O.K. and Kaushik S.C. (2013) 'Energy and exergy analysis and optimization of Kalina cycle coupled with a coal fired steam power plant', *Applied thermal engineering*, vol. 51(1–2), pp. 787–800.
- Sun F., Zhou W., Ikegami Y., Nakagami K. and Su X., (2014) 'Energy–exergy analysis and optimization of the solar-boosted Kalina cycle system 11 (KCS-11)', *Renewable Energy*, vol. 66, pp. 268–279.
- T. Richert, K. Riffelmann, P. Nava (2015) 'The Influence of Solar Field Inlet and Outlet Temperature on the Cost of Electricity in a Molten Salt Parabolic Trough Power Plant', *Energy Procedia*, vol. 69, 1143–1151.
- Tangwe S., Simon M. and Meyer E. (2015) 'An innovative optimization technique on performance efficiency verification in a coal thermal power plant unit', In *Industrial and Commercial Use of Energy (ICUE)* pp. 325–331.
- Tyagi S.K., Zhou Y. and Chen J. (2004) 'Optimum criteria on the performance of an irreversible Braysson heat engine based on the new thermoeconomic approach', *Entropy*, vol. 6(2), pp. 244–256.
- Üst Y. and Yilmaz T. (2005) 'Performance analysis of an endoreversible Braysson cycle based on the ecological criterion' *Turkish Journal of Engineering and Environmental Sciences*, vol. 29 (5), pp. 271–278.
- Ust Y., (2009) 'A comparative performance analysis and optimization of the irreversible Atkinson cycle under maximum power density and maximum power conditions', *International Journal of Thermophysics*, vol. 30(3), pp. 1001–1013.
- Usvika R., Rifaldi M. and Noor A. (2009) 'Energy and exergy analysis of kalina cycle system (KCS) 34 with mass fraction ammonia-water mixture variation', *Journal of mechanical science and technology*, vol. 23(7), pp. 1871–1876.
- Valdés M., Durán M.D. and Rovira A. (2003) 'Thermoeconomic optimization of combined cycle gas turbine power plants using genetic algorithms', *Applied Thermal Engineering*, vol. 23(17), pp. 2169–2182.
- Wang J., Yan Z., Zhou E. and Dai Y. (2013) 'Parametric analysis and optimization of a Kalina cycle driven by solar energy', *Applied Thermal Engineering*, vol. 50(1), pp. 408–415.
- Wang P.Y. and Hou S.S. (2005) 'Performance analysis and comparison of an Atkinson cycle coupled to variable temperature heat reservoirs under maximum power and maximum power density conditions', *Energy Conversion and Management*, vol. 46(15–16), pp. 2637–2655.
- Wu L., Lin G. and Chen J. (2010) 'Parametric optimization of a solar-driven Braysson heat engine with variable heat capacity of the working fluid and radiation–convection heat losses', *Renewable Energy*, vol. 35(1), pp. 95–100.
- X. Wu, J. Shen, Y. Li, K. Y. Lee (2015) 'Fuzzy modelling and predictive control of super heater steam temperature for power plant', *ISA Transactions*, vol. 56, 241–251.
- Zhang W., Chen L. and Sun F. (2008) 'Power and efficiency optimization for combined Brayton and two parallel inverse Brayton cycles. Part 2: performance optimization', *Proceedings of the Institution of Mechanical Engineers, Part C: Journal of Mechanical Engineering Science*, vol. 222(3), pp. 405–413.
- Zhang W., Chen L. and Sun F. (2009) 'Power and efficiency optimization for combined Brayton and inverse Brayton cycles', *Applied Thermal Engineering*, vol. 29(14–15), pp. 2885–2894.
- Zhang W., Chen L., Sun F. and Wu C. (2007) 'Second-law analysis and optimisation for combined Brayton and inverse Brayton cycles', *International Journal of Ambient Energy*, vol. 28(1), pp. 15–26.

- Zhang W., Chen L., Sun F. and Wu C. (2009) ‘Second law analysis and parametric study for combined Brayton and two parallel inverse Brayton cycles’, *International Journal of Ambient Energy*, vol. 30(4), pp. 179–192.
- Zhang Z., Chen L., and Sun F. (2012) Energy performance optimization of combined Brayton and two parallel inverse Brayton cycles with regeneration before the inverse cycles. *Scientia Iranica*, vol. 19(5), pp. 1279–1287.
- Zhang Z., Chen L. and Sun F. (2014) ‘Performance optimisation for two classes of combined regenerative Brayton and inverse Brayton cycles’, *International Journal of Sustainable Energy*, vol. 33(4), pp. 723–741.
- Zhao J. and Xu M. (2013) ‘Fuel economy optimization of an Atkinson cycle engine using genetic algorithm’, *Applied Energy*, vol. 105, pp. 335–348.
- Zhao J., Xu M., Li M., Wang B. and Liu S., (2012) ‘Design and optimization of an Atkinson cycle engine with the Artificial Neural Network Method’, *Applied energy*, vol. 92, pp. 492–502.
- Zhao Y. and Chen J. (2006) ‘Performance analysis and parametric optimum criteria of an irreversible Atkinson heat-engine’, *Applied Energy*, vol. 83(8), pp. 789–800.
- Zheng J., Chen L., Sun F. and Wu C. (2002a) ‘Powers and efficiency performance of an endoreversible Braysson cycle’, *International journal of thermal sciences*, vol. 41(2), pp. 201–205.
- Zheng J., Sun F., Chen L. and Wu C. (2001) ‘Exergy analysis for a Braysson cycle’, *Exergy, an International journal*, vol. 1(1), pp. 41–45.
- Zheng S., Chen J. and Lin G. (2005) ‘Performance characteristics of an irreversible solar-driven Braysson heat engine at maximum efficiency’, *Renewable Energy*, vol. 30(4), pp. 601–610.
- Zheng T., Chen L., Sun F. and Wu C. (2002b) ‘Power, power density and efficiency optimization of an endoreversible Braysson cycle’, *Exergy, an International Journal*, vol. 2(4), pp. 380–386.
- Zhou Y., Tyagi S.K. and Chen J. (2004) ‘Performance analysis and optimum criteria of an irreversible Braysson heat engine’, *International journal of thermal sciences*, vol. 43(11).

# Chapter 7

## Thermal Design and Optimization of Few Miscellaneous Systems



**Abstract** There are a few thermal components which can play an important role in power-generating systems, refrigeration systems, or any such system. Similarly, there are few thermal systems which can be operated with solar energy. In this chapter, thermal modeling of few such systems like the cooling tower, heat pipe, micro-channel heat sink, solar air heater, solar water heater, solar chimney, and other systems of such type is presented. The objective function for each of these systems is derived from the thermal model. The optimization of a derived objective is performed by implementing 11 different metaheuristic algorithms for each system, and then the comparative results are tabulated and discussed.

In this chapter, a thermal modeling of components which can play an important role in systems such as the power-generating system and refrigerating system is carried out. Apart from the conventional system, the thermal modeling of few solar-assisted systems is also performed in this chapter. The objective function of each component/system is derived based on the thermal modeling and optimization of the derived objective (which is carried out by implementing different metaheuristic algorithms).

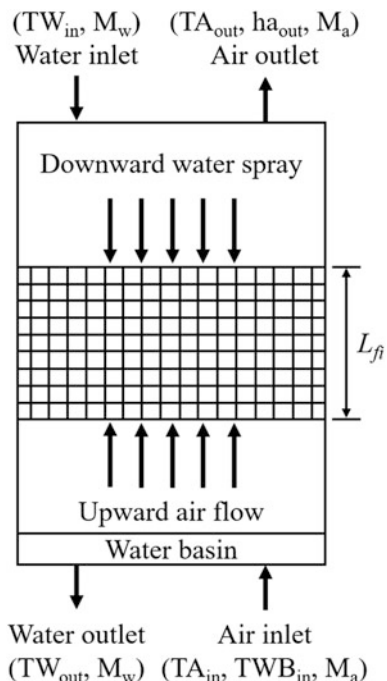
### 7.1 Cooling Tower

A cooling tower is a device used in thermal power plant refrigeration plants, air conditioning plants, and chemical and petrochemical industries to dissipate processed heat. The large quantities of processed heat must be removed to maintain standard operating parameters. The cooling tower works based on a combination of heat and mass transfers to cool water by direct contact between air and water. The water to be cooled is distributed in the tower by spray nozzles, fills, and splash bars in such a way that it exposes a large quantity of surface water to atmospheric air (Kröger 2004). The movement of the air is accomplished by fans, natural draft, or the induction effect from the water sprays. A portion of the water is evaporated

because the moisture content of the air is less than the saturated air at that specific temperature of water. Since this process of evaporation requires energy to change the water from liquid to vapor, the water is cooled (Rao and Patel 2011).

Cooling towers are distinguished from each other by different criteria. One of the important criteria is the movement of air through the cooling tower. If the circulation of air through the cooling tower is due to a natural convection current, then this type of cooling tower is known as the natural draft cooling tower. If the circulation of air takes place with the help of a fan, then that type of cooling tower is known as a forced draft cooling tower. Furthermore, based on the location of the fan, the forced draft cooling tower may either be of an induced draft (fan is installed at the top of cooling tower) or a forced draft (fan is installed at the bottom of cooling tower). Likewise, there are two flow types which are based on the flow direction of cooling tower: counter-flow type and cross-flow type. In any of the cooling towers, water to be cooled is entered from the top of the tower and flows downward while air flows either upward (counter-flow) or horizontally (cross-flow). After cooling, the cooled water is then collected in a cold water basin below the fill from which it is returned to the processed network. During cooling, some water is lost due to blowdown, evaporation, and drift. The lost water is replaced with fresh make-up water. In the present work, a mechanical draft counter-flow cooling tower is considered for optimization. Figure 7.1 shows the schematic arrangement of a mechanical draft counter-flow cooling tower.

**Fig. 7.1** Schematic arrangement of mechanical draft counter-flow cooling tower



Earlier, researchers have carried out various works related to the analysis and optimization of different types of cooling tower. Walker et al. (1923) proposed the basic theory of a cooling tower, but the practical use of the mathematical design was first presented by Merkel (1925). He combined the equations governing heat and mass transfer between water droplets and the air in the tower. Kintner-Meyer and Emery (1994, 1995) described a method for the optimum sizing of the cooling tower, which included the cost-optimal selection of the cooling tower range and approach. Mohiuddin and Kant (1996a, b) described a detailed procedure for the thermal design of wet cooling towers. Dessouky et al. (1997) carried out the performance analysis for the steady state counter-flow wet cooling tower with new definitions of the tower's effectiveness and the number of transfer units. Castro et al. (2000) developed an optimization model of a cooling water system. The model considered the thermal and hydraulic interactions in the optimization process. The author had considered the minimization of the total operating cost of the system as an objective function. Söylemez (2001) used the  $P_1-P_2$  method for the thermo economic optimization of the cooling tower. In the work, the author had also considered the optimization of the heat and mass transfer area of the cooling tower as an objective function, thus resulting in a minimum total cost.

Also, Söylemez (2004) presented a thermal-hydraulic model of the mechanical draft counter-flow wet cooling. This was based on the effectiveness-NTU method. Based on the model, the author obtained the optimum value of the ratio of the mass flow rate of water to dry air for the tower. In another work, Kloppers and Kröger (2004) carried out the optimization of the geometrical dimensions of a counter-flow natural draft wet cooling tower to obtain the minimum capital and operating costs. The authors concluded that the inlet height of the cooling tower is a critical parameter which influenced its total operational and capital cost. In addition, Zhai and Fu (2006) investigated the performance improvement of the cooling tower by using wind-break methods both in and around the towers. The authors employed numerical and experimental approaches to optimize the wind-break measures. The authors had also analyzed the relationship between the cooling efficiency recovery and the size of the wind-break walls. Smrekar et al. (2006) considered the optimization of the water to air mass flow rate ratio for minimizing exergy loss and maximizing the efficiency of the natural draft cooling tower. In 2007, Jin et al. proposed a thermal model of the mechanical cooling tower which was based on Merkel's theory and the effectiveness-NTU method. The authors developed the model by balancing energy and heat, and mass transfer analysis. The authors also validated the proposed model by using real operating data from the cooling towers of a heating, ventilating, and air conditioning system of a commercial hotel. Cortinovis et al. (2009) developed an optimization model for the cooling water system which included a cooling tower and its network of pipelines and heat exchangers. The model accounted for all hydraulic and thermal interactions of the system and had the objective of minimizing its operating cost. Ponce-Ortega et al. (2010) used the GAMS software environment, using the DICOPT solver and presented optimization model for re-circulating cooling water system used in the cooling tower. The authors had considered the minimization of the total annual cost

as an objective function. Three example problems are presented to show the application of the proposed approach.

Serna-González et al. (2010) formulated mixed-integer nonlinear programming (MINP) to obtain the minimum total annual cost design of the mechanical draft counter-flow cooling tower. The authors used the GAMS software environment with the DICOPT solver for the mixed-integer nonlinear programming optimization of the wet cooling towers. The author also considered six examples of different cooling towers to demonstrate the effectiveness of the optimization method. Rubio-Castro et al. (2011) presented an optimal design algorithm for the mechanical draft counter-flow wet cooling towers based on the Poppe model and mixed-integer nonlinear programming. The authors considered the minimization of the total annual cost of the cooling tower as an objective function and solved the MINP problem using GAMS software. The authors also compared the optimization results obtained using the Poppe method with those using the Merkel method. Rao and Patel (2011) carried out the multi-objective optimization of the mechanical draft counter-flow wet cooling tower by using the artificial bee colony algorithm. The authors considered the minimization of total cost of the cooling tower as an objective function and compared the results obtained using the artificial bee colony algorithm with those obtained using the GAAMS optimization package. Gu et al. (2016) adopted a computational fluid dynamics method to simulate the heat transfer performance of an indirect air-cooling tower with four different wind-break structures. The authors concluded that the wind-break wall is the most optimal structure for the improvement of heat transferring in cooling towers. However, its performance is strictly influenced by the direction and velocity of the wind.

### 7.1.1 Thermal Model

In this part of the work, a mechanical draft counter-flow wet cooling tower is considered for optimization. The schematic arrangement of the considered cooling tower is shown in Fig. 7.1. In addition, the following assumptions are considered in order to simplify the thermal model of the cooling tower.

- Constant thermodynamic properties of air and water across any horizontal section of the tower.
- The cooling tower operates under adiabatic conditions, and the cross-section area of the tower is uniform.
- The bulk temperature of the water is used to identify thermal properties of air at any section.
- Water waste due to drifting and blowdown is negligible, and the mass flow rate of water through the tower is constant.
- The exit air from the tower is saturated with water vapor.
- The Lewis number is constant throughout the tower.

The thermal model of the cooling tower presented here is based on the previous works of Serna-González et al. (2010) and Rao and Patel (2011).

The amount of heat removed from water to air stream is determined from

$$Q = C_{pw}m_w(TW_{in} - TW_{out}) = m_a(ha_{out} - ha_{in}) \quad (7.1)$$

where  $TW_{in}$  and  $TW_{out}$  are the inlet and outlet water temperatures from the cooling tower.

The cooling tower approach is the temperature difference between the water outlet temperature ( $TW_{out}$ ) and the wet bulb temperature of the entering air ( $TWB_{in}$ ). This approach is given by

$$\text{Approch} = TW_{out} - TWB_{in} \quad (7.2)$$

By considering heat and mass balance for the cooling tower, the Merkel's equation is represented as

$$Me = \int_{TW_{out}}^{TW_{in}} \frac{C_{pw}dTW}{hsa - ha} \quad (7.3)$$

where  $ha$  and  $hsa$  are the enthalpy of air and saturated air at any section of the tower, respectively, and  $Me$  is the required Merkel number for the cooling tower design.

The integral form of the required Merkel number can be converted into algebraic form by applying the four-point Chebyshev's integration technique. The required Merkel number, after applying the four-point Chebyshev's method, can be given by

$$Me = \int_{TW_{out}}^{TW_{in}} \frac{C_{pw}dTW}{hsa - ha} = 0.25C_{pw}(TW_{in} - TW_{out}) \sum_{i=1}^{i=4} \frac{1}{\Delta h_i} \quad (7.4)$$

where  $C_{pw}$  is the specific heat of water,  $TW_{in}$  is the inlet water temperature, and  $\Delta h_i$  is the local enthalpy difference which is given by

$$\Delta h_i = hsa_i - ha_i \quad i = 1, 2, \dots, 4 \quad (7.5)$$

The water temperature and air enthalpies corresponding to each Chebyshev point are

$$TW_i = TW_{out} + i(TW_{in} - TW_{out}) \quad i = 1, 2, \dots, 4 \quad (7.6)$$

$$\Delta ha_i = \Delta ha_i + \frac{C_{pw}m_w}{m_a}(TW_{in} - TW_{out}) \quad i = 1, 2, \dots, 4 \quad (7.7)$$

where  $m_w$  and  $m_a$  are the mass flow rates of water and air.  $TCH_i$  is a constant that represents the four points of Chebyshev's technique. Its values are  $TCH_1 = 0.1$ ,  $TCH_1 = 0.4$ ,  $TCH_3 = 0.6$ , and  $TCH_4 = 0.9$ .

Here, the enthalpy of the saturated air is calculated by the following correlation:

$$\begin{aligned} h_{sa_i} &= -6.38887667 + 0.865817 TW_i + 15.715367 \exp(0.05439 TW_i) \\ i &= 1, 2, \dots, 4 \end{aligned} \quad (7.8)$$

The value of the Merkel number determined without using the properties of the air and water at the inlet and exit from the cooling tower is known as the available Merkel number. The available Merkel number is calculated by using the following equation:

$$Me = \frac{h_d a_{fi} A_{fr} L_{fi}}{m_w} \quad (7.9)$$

where  $a_{fi}$  is the surface area per unit volume,  $A_{fr}$  is the fill area of the cooling tower,  $h_d$  is the mass transfer coefficient, and  $L_{fi}$  is the fill height. The available Merkel number is correlated with the measured transfer coefficients for a particular fill type and is given by

$$Me = c_1 \left( \frac{m_w}{A_{fr}} \right)^{c_2} \left( \frac{m_a}{A_{fr}} \right)^{c_3} (L_{fi})^{1+c_4} (TW_{in})^{c_5} \quad (7.10)$$

This empirical correlation of the available Merkel number provides a better fit to experimental data, especially in comparison with the traditional correlation mentioned previously. The values of the coefficients  $c_1$  to  $c_5$  for each packing under consideration are given in Table 7.1.

Another important parameter which is used to describe the tower fill performance is the loss coefficient per meter depth of fill. For the splash, trickle, and film type fills, the loss coefficient correlations are given by

$$K_{fi} = \left[ d_1 \left( \frac{m_w}{A_{fr}} \right)^{d_2} \left( \frac{m_a}{A_{fr}} \right)^{d_3} + d_4 \left( \frac{m_w}{A_{fr}} \right)^{d_5} \left( \frac{m_a}{A_{fr}} \right)^{d_6} \right] L_{fi} \quad (7.11)$$

**Table 7.1** Coefficient in the correlation of available Merkel number

$j$	$c_j^k$	$k = 1$ (splash fill)	$k = 2$ (trickle fill)	$k = 3$ (film fill)
1	0.249013	1.930306	1.019766	
2	-0.464089	-0.56823	-0.432896	
3	0.653578	0.6414	0.782744	
4	0	-0.352377	-0.29287	
5	0	-0.17867	0	

For the considered tower fill, the values of coefficient  $d_1$  to  $d_6$  are given in Table 7.2.

In the mechanical draft cooling tower, the pressure drop through the fill matrix is given by

$$\Delta P_{\text{fi}} = K_{\text{fi}} L_{\text{fi}} \frac{\text{mav}_m^2}{2\rho_m A_{\text{fr}}^2} \quad (7.12)$$

where  $\text{mav}_m$  is the arithmetic mean air-vapor flow rate through the fill and is given by

$$\text{mav}_m = \frac{\text{mav}_{\text{in}} + \text{mav}_{\text{out}}}{2} \quad (7.13)$$

The air-vapor flow at the fill inlet and outlet is calculated by

$$\text{mav}_{\text{in}} = m_a + w_{\text{in}} m_a \quad (7.14)$$

$$\text{mav}_{\text{out}} = m_a + w_{\text{out}} m_a \quad (7.15)$$

where  $w_{\text{in}}$  and  $w_{\text{out}}$  are the humidity of the inlet and outlet air, respectively, and are calculated by

$$w_{\text{in}} = \left( \frac{2501.6 - 2.3263 \text{ TWB}_{\text{in}}}{2506 + 1.8577 \text{ TA}_{\text{in}} - 4.184 \text{ TWB}_{\text{in}}} \right) \left( \frac{0.62509 \text{ PV}_{\text{wbin}}}{P_{\text{tot}} - 1.005 \text{ PV}_{\text{wbin}}} \right) - \left( \frac{1.00416(\text{TA}_{\text{in}} - \text{TWB}_{\text{in}})}{2506 + 1.8577 \text{ TA}_{\text{in}} - 4.184 \text{ TWB}_{\text{in}}} \right) \quad (7.16)$$

$$w_{\text{out}} = \frac{0.62509 \text{ PV}_{\text{out}}}{P_{\text{tot}} - 1.005 \text{ PV}_{\text{out}}} \quad (7.17)$$

where  $\text{PV}_{\text{out}}$  is the vapor pressure of water.

The vapor pressure of water at any specified temperature is calculated from the correlation and can be calculated by

**Table 7.2** Parameters for loss coefficient correlation

$j$	$c_j^k$		
	$k = 1$ (splash fill)	$k = 2$ (trickle fill)	$k = 3$ (film fill)
1	3.179688	7.047319	3.89783
2	1.083916	0.812454	0.777271
3	-1.965418	-1.143846	-2.114727
4	0.639088	2.677231	15.327472
5	0.684936	0.294827	0.215975
6	0.642767	1.018498	0.079696

$$\ln(PV) = \sum_{n=1}^{n=3} c_n T^n + 6.5459673 \ln(T) \quad (7.18)$$

where temperature  $T$  is in Kelvin, and values of the constants are:

$$\begin{aligned} c_{-1} &= 5800.22, c_0 = 1.3914, c_1 = -4.864 \times 10^{-3}, \\ c_2 &= -4.1764768 \times 10^{-5}, c_3 = -1.445209 \times 10^{-7} \end{aligned} \quad (7.19)$$

The inlet and outlet densities of the air-water vapor mixtures are calculated by using the ideal gas law, i.e.,

$$\rho_{\text{in}} = \frac{P_{\text{tot}}}{287.08 \text{ TA}_{\text{in}}} \left[ 1 - \frac{w_{\text{in}}}{w_{\text{in}} + 0.621198} \right] [1 + w_{\text{in}}] \quad (7.20)$$

$$\rho_{\text{out}} = \frac{P_{\text{tot}}}{287.08 \text{ TA}_{\text{out}}} \left[ 1 - \frac{w_{\text{out}}}{w_{\text{out}} + 0.621198} \right] [1 + w_{\text{out}}] \quad (7.21)$$

The miscellaneous pressure losses, such as those due to drift eliminators, air inlet, water distributing piping, and column support, are calculated by

$$\Delta P_{\text{mcl}} = K_{\text{mcl}} \frac{\rho_{\text{mcl}} v_{\text{mcl}}^2}{2} \quad (7.22)$$

where  $K_{\text{mcl}}$  is the component loss coefficient.

In the absence of the component loss coefficient data, the miscellaneous pressure losses of the cooling tower are expressed by total miscellaneous pressure losses in terms of the miscellaneous loss coefficient:

$$\Delta P_{\text{mix}} = K_{\text{misc}} \frac{\rho_m v_m^2}{2} \quad (7.23)$$

where  $K_{\text{misc}}$  is total miscellaneous loss coefficient ( $K_{\text{misc}} = K_{\text{drift}} + K_{\text{air inlet}} + K_{\text{piping}} + \dots$ ). For the mechanical draft cooling tower, an estimated value of 6.5 is used for  $K_{\text{misc}}$ . In addition,  $v_m$  is the mean velocity of air.

The sum of the pressure losses through the fill matrix and the miscellaneous pressure losses is known as the static pressure losses. The limiting value of the velocity pressure drop ( $\Delta P_{\text{vp}}$ ) is 2/3 of the static pressure drop.

$$\Delta P_{\text{vp}} = 2/3(\Delta P_{\text{fi}} + \Delta P_{\text{mix}}) \quad (7.24)$$

The total pressure drop in the mechanical draft cooling towers is the sum of the static and the velocity pressure drop and is expressed by

$$\Delta P_t = 1.667(\Delta P_{fi} + \Delta P_{misc}) \quad (7.25)$$

The power required to overcome the total pressure drop along the air path is calculated as

$$P = \frac{mav_{in}\Delta P_t}{\rho_{in}\eta_f} \quad (7.26)$$

The rate of water evaporated into the air stream is calculated by

$$m_{wev} = m_a(w_{out} - w_{in}) \quad (7.27)$$

A portion of the circulating water is removed from the system. This is known as blowdown and is calculated by

$$m_{bw} = \frac{m_{mw}}{\eta_{cycles}} - m_{wd} \quad (7.28)$$

where  $\eta_{cycle}$  is the number of cycles of concentration required to limit scale formation in cooling equipment. Usually, an average value between 2 and 4 is considered for the  $\eta_{cycle}$ .

Note that the drift loss should not be more than 0.2% of the total circulating water.

$$m_{wd} = 0.002m_w \quad (7.29)$$

The quantity of make-up water added in the cooling tower is calculated by

$$m_{wd} = \frac{\eta_{cycles}m_{wev}}{\eta_{cycles} - 1} \quad (7.30)$$

The total annual cost is the sum of the annualized capital cost and the annual operating cost of the cooling tower. It's given by

$$TAC = K_f C_{cap} + C_{op} \quad (7.31)$$

where  $K_f$  is the annualized factor of capital cost,  $C_{cap}$  is the installed capital cost of the cooling tower, and  $C_{op}$  is the annual operating cost of the cooling tower.

The capital cost of the cooling tower is calculated from the following formula:

$$C_{cap} = C_{CTF} + C_{CTV}A_{fr}L_{fi} + C_{CTMA}m_a \quad (7.32)$$

where  $C_{CTF}$  is the fixed cooling tower cost,  $C_{CTV}$  is the incremental cooling tower cost based on the fill volume, and  $C_{CTMA}$  is the air mass flow rate, respectively.

The cost coefficient  $C_{CTV}$  depends on types of packing. For splash fill, trickle fill, and film fill, its values are 2006.6, 1812.25, and 1606.15, respectively.

The annual operating cost is given by

$$C_{\text{op}} = H_Y c_w m_{\text{mw}} + H_y c_e P \quad (7.33)$$

where  $H_y$  is the yearly operating time,  $c_w$  is the unit operating cost of make-up water,  $c_e$  is the unit operating cost of electricity, and  $P$  is the electric power.

Based on the above thermal model, the objective function for the present work is defined in the next section.

### 7.1.2 Case Study, Objective Function Description, and Constraints

There is a need for a mechanical draft counter-flow wet cooling tower to be designed and optimized for the minimum total annual cost (TAC). The dry bulb temperature of the inlet air ( $TA_{\text{in}}$ ) is taken to be 22 °C, the wet bulb temperature of the inlet air ( $TWB_{\text{in}}$ ) is 12 °C, the minimum process inlet (TMPI) and outlet (TMPO) temperatures are 65 22 °C and 30 22 °C, respectively, and the lowest allowable temperature difference ( $\Delta T_{\text{min}}$ ) is 10 °C. Three design variables including the water-to-air mass ratio ( $m_w/m_a$ ), the mass velocity of air ( $m_a/A_{\text{fr}}$ ), and mass velocity of water ( $m_w/A_{\text{fr}}$ ) are considered for the optimization problem. The upper and lower bounds of the design variables are presented in Table 7.3.

As mentioned above, the minimization of the total annual cost (TAC) of the cooling tower is taken as an objective function in the present study. Fortunately, the operating parameters which result in the maximum thermal efficiency also satisfy the water and air temperature constraints. As such, the objective function of the mechanical draft counter-flow wet cooling tower is formulated as below:

$$\left\{ \begin{array}{l} \text{Minimize } f(X) = TAC(X) + \sum_{j=1}^n G_1(g_j(X))^2 \\ X = [x_1, x_2, x_3, \dots, x_D], \quad x_{i,\text{minimum}} \leq x_i \leq x_{i,\text{maximum}}, \quad i = 1, 2, 3, \dots, D \\ g_j(X) \leq 0, \quad j = 1, 2, 3, \dots, n \end{array} \right. \quad (7.34)$$

**Table 7.3** Ranges of design variables for cooling tower optimization

Design variable	Lower bound	Upper bound
Water-to-air mass ratio ( $m_w/m_a$ )	0.5	2.5
Mass velocity of air ( $m_a/A_{\text{fr}}$ )	1.2	4.25
Mass velocity of water ( $m_w/A_{\text{fr}}$ )	2.9	5.96

where  $X$  is the vector of design variables, bounded between its minimum and maximum values, and  $G_1$  is the penalty parameter. Here, the term takes into account the effect of the constraints violation and is used when the constraint violation takes place ( $g_j(X)$  indicates the constraints). The following constraints are considered for the cooling tower operation.

$$\text{TW}_{\text{out}} - \text{TWB}_{\text{in}} \geq 2.8 \quad (7.35)$$

$$\text{TW}_{\text{in}} \leq 323 \text{ K} \quad (7.36)$$

$$\text{TW}_{\text{in}} - \text{TW}_{\text{out}} \geq 0 \quad (7.37)$$

$$\text{TA}_{\text{out}} - \text{TA}_{\text{in}} \geq 0 \quad (7.38)$$

The next section describes the results and discussion of the case study.

### 7.1.3 Results and Discussion

The considered problem of the cooling tower is investigated using 11 different metaheuristic approaches to obtain a minimum total annual cost. As all these methods are stochastic in their method, each algorithm is implemented 100 times on the considered problem to estimate the statistical variations of the algorithms. Each algorithm is implemented with a population size of 50, and the termination criteria are set as 100,000 function evaluations. The results obtained using each algorithm are presented in Table 7.4 in the form of the best solution, the worst solution, average solution, standard deviation, and the success rate (over 100 runs). The infeasible solutions (i.e., affected by penalty) are eliminated, and the worst solution, average solution, standard deviation, and success rate are obtained. In addition, the success rate of the algorithm is obtained by considering a 0.1% variation from the global optimum value.

It can be observed from the results that the algorithm performed equally well, producing nearly identical minimum total annual costs (TAC). Additionally, the average performance of the TLBO, DE, and CSA is almost identical, being better than the remaining competitive algorithms. The success rate of the CSA and DE algorithms in obtaining the optimum value is the highest followed by the TLBO algorithm. The WWO and SOS algorithms exhibit the least success rate in obtaining the global optimum value. Since it is difficult to judge the performance of the algorithm as all the algorithms have performed differently in obtaining the best, worst, and average results, and success rate, the Friedman rank test is implemented to judge the best suitable algorithm for cooling tower optimization. The test considers the algorithms' capability to obtain the best, worst, and average solutions,

**Table 7.4** Comparative results of different algorithms for cooling tower optimization

Algorithms	Best	Worst	Average	SD	Success rate (%)
GA	59572.2	93234.6	72213.4	1.26E+04	16
PSO	59572.2	80948.5	70071.9	1.10E+04	12
DE	59572.2	59579.3	59572.5	1.52E+00	88
ABC	59572.2	80948.5	74357.9	9.10E+03	12
CSA	59572.2	59597.6	59573.3	5.43E+00	88
TLBO	59572.2	59577.6	59572.4	1.19E+00	84
SOS	59572.2	80948.5	78777.8	5.79E+03	4
WWO	59572.2	98634.6	78605.5	1.12E+04	4
HTS	59572.2	80946.9	60971.8	4.60E+03	76
PVS	59572.2	81060.8	70287.9	1.15E+04	16
SCA	59572.2	98634.6	71259.5	1.48E+04	16

**Table 7.5** Friedman rank test results for cooling tower optimization

Algorithms	Friedman value	Normalized value	Rank
GA	36.5	0.383562	7
PSO	30	0.466667	5
DE	14.5	0.965517	2
ABC	39	0.358974	9
CSA	14	1	1
TLBO	15.5	0.903226	3
SOS	42	0.333333	10
WWO	48.5	0.28866	11
HTS	19.5	0.717949	4
PVS	32.5	0.430769	6
SCA	38	0.368421	8

and success rate. The results of the Friedman rank test are presented in Table 7.5, and its graphical representation is given in Fig. 7.2. The results are presented in the form of a Friedman value, a normalized value with ‘1’ being the best, and its rank. It is observed from the results that CSA has obtained the first rank followed by DE and TLBO algorithms.

The optimized operating parameters of the cooling tower obtained using the CSA algorithm are presented in Table 7.6. It can be noted from the results that the cooling tower with the highest mass velocity of air and the lowest mass velocity of water results in the minimum total annual cost. The water-to-air mass ratio produced a conflicting effect on achieving the minimum total annual cost of the cooling tower. In this case, the water inlet temperature constraint is at the limiting value while the remaining constraints are above the limiting value. This occurs in the optimized operating conditions of the cooling tower.

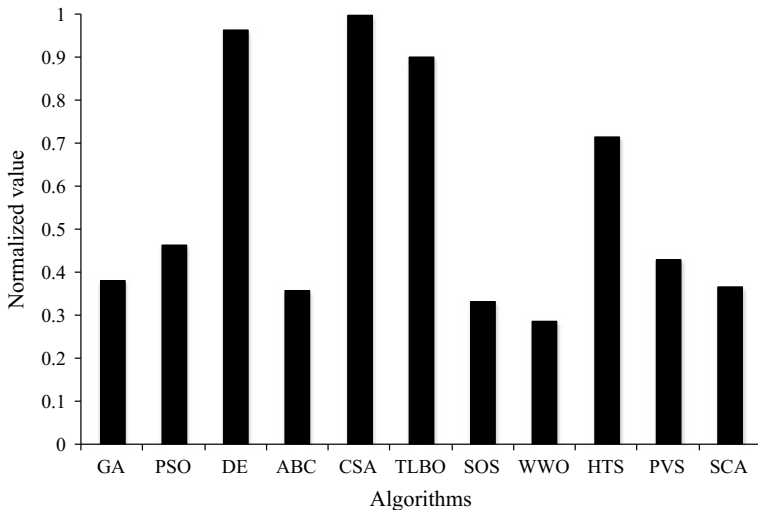


**Fig. 7.2** Graphical presentation of Friedman rank test for cooling tower optimization

**Table 7.6** The optimized operating condition of the cooling tower

Operating parameters <i>Operating variable</i>	Optimized value
Water-to-air mass ratio ( $m_w/m_a$ )	0.6367
Mass velocity of air ( $m_a/A_{fr}$ )	4.25
Mass velocity of water ( $m_w/A_{fr}$ )	2.9
<i>Constrain</i>	
$TW_{out} - TW_{B_{in}}$	8
$TW_{in}$	323
$TW_{in} - TW_{out}$	30
$TA_{out} - TA_{in}$	2.1
<i>Objective function</i>	
Total annual cost, US \$/yr	59,572.2

## 7.2 Heat Pipe → Work on this installation.

Heat pipes are an efficient heat exchange device which can transmit high heat with a relatively small temperature gradient. The working of heat pipes combines the principles of phase change and thermal conductivity (Faghri 1995). The other noticeable advantages of the heat pipes are as follows: it can transmit heat over a considerable distance without any external power requirement, is simply designed and simple to manufacture, it has low maintenance cost, is highly reliable, its light weight, and it can operate over a wide range of temperatures. As such, the heat pipes are used for cooling purposes in many applications like satellite, spacecraft, computer systems, and solar thermal systems (Dunn and Reay 1976).

A heat pipe is a hollow, sealed container with a wick structure and working fluid. Figure 7.3 shows the schematic arrangement of the heat pipe. From the construction viewpoint, a heat pipe is composed of three sections: the evaporator section, the adiabatic section, and the condenser section. The working fluid of the heat pipe is vaporized at the evaporator section by extracting heat from the heat source. After that, the vapor moves toward the condenser section via the adiabatic section. This movement of vapor from the evaporator section to the condenser section takes place through the core of the heat pipe. At the condenser section, the working fluid is converted into a liquid state by rejecting some of its heat to the surroundings. Then, the working fluid again moves toward the evaporator section through the periphery of the heat pipe by using capillary action provided by the wick structure (Reay and Kew 2006).

Earlier, researchers have carried out various analytical and experimental works related to the effect of the working fluid, the wick structure, and other operating parameters on the performance of the heat pipe. Recently, various works have explored the optimization of a heat pipe. For example, Wu et al. (2003) presented some modeling and analysis to determine the optimum length of the evaporator section to the condenser section of cylindrical heat pipes in the horizontal position. Kim et al. (2003) developed a mathematical model for the miniature heat pipe. Based on the developed model, the authors performed numerical optimization to enhance its thermal performance. In addition, Sousa et al. (2004) used a generalized external optimization to optimize the mass of a heat pipe used for space application. The authors investigated different working fluids like methanol, ammonia, and ethanol in their study. Sousa et al. (2004) performed the optimization of a heat pipe for different heat loads and heat sinks temperatures. The authors investigated different working fluid and used a generalized external optimization as an optimization tool in their study. Vlassov et al. (2006) performed the geometric optimization of a heat pipe used for space application and for the minimization of the mass of the heat pipe. Shi et al. (2006) carried out a performance evaluation and optimization of a

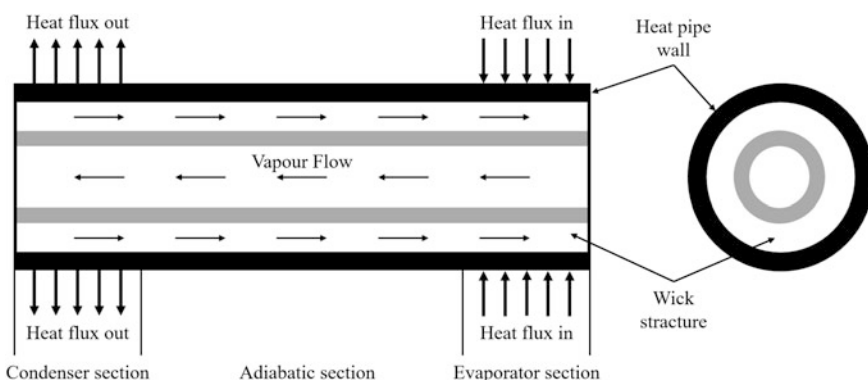


**Fig. 7.3** Schematic diagram of the heat pipe

miniature heat pipe through numerical analysis. The authors were able to identify the effect of groove depth, width, and vapor space on the heat transfer capacity of the miniature heat pipe. Jeong et al. (2007) performed the optimization of a satellite heat pipe with thermal conductance. He had made the total mass of the heat pipe as an objective function. The authors used the genetic algorithm as an optimization tool in their investigation.

Zhang et al. (2009) carried out the optimization of a heat pipe for the minimization of total thermal resistance. The authors considered the structural parameters of the heat pipe as decision variables and used the genetic algorithm as an optimization tool. Kiseev et al. (2010) carried out the optimization of geometric parameters of the capillary structure. They performed the optimization through extensive experimentation on different capillary structure material and working fluid. Kiseev et al. (2010) investigated the influence of the capillary structure characteristics on the performance of a heat pipe. The authors developed the theoretical formulation of the heat pipe and compared the analytical results with the experimental. Liang and Hung (2010) carried out an experimental investigation to obtain an optimum ratio for minimum thermal resistance of the evaporator section length to the condenser section length of the U-shape heat pipe. Roper (2010) performed a multi-objective optimization of a sandwich panel heat pipe. The author obtained the Pareto optimal solution for different working fluids and core materials. Tang et al. (2010) developed a novel loop heat pipe with a vapor separator to separate the evaporator into boiling and suction chambers. The authors investigated the effects of power inputs and refrigerants on the dynamic performances of the loop heat pipe. Maheshkumar and Muraleedharan (2011) performed the second-law-based optimization of a flat heat pipe. The authors obtained an optimum value of design variables for the minimization of the entropy generation of a flat heat pipe. Wan et al. (2012) performed the condenser section optimization of a loop heat pipe through the finite element method. The author obtained optimized structure parameters to enhance the condensation heat transfer of heat pipe.

Yang et al. (2014) presented a simplified mathematical model for estimating key parameters of a pulsating heat pipe from a limited number of measurements. The authors further solved the model numerically and compared the results with the experimental data drawn from the literature. Rao and More (2015) adapted a teaching–learning-based optimization algorithm for the optimization of thermal resistance and the total mass of the heat pipe. Esarte et al. (2016) investigated the influence of heat pipe length, wick thickness, and condensing temperature on the optimized performance of a loop heat pipe. Jokar et al. (2016) presented the simulation and optimization of a pulsating heat pipe to identify its optimized operating point by the simultaneous adaption of the artificial neural network and the genetic algorithm. Jalilian et al. (2016) employed the genetic algorithm for the optimization of a pulsating heat pipe used for efficiency improvement of a flat plate solar collector. Song et al. (2017) presented the thermodynamic analysis and optimization of a heat pipe to provide theoretical guidance for the structural design of the heat pipe used in a space power system. Du (2017) performed an experimental investigation on a nano-coated heat pipe plate used for solar cell cooling. The author observed

that the heat pipe plate provided sufficient cooling to the solar cells under various solar irradiances. Tiari et al. (2017) investigated the thermal performance of a heat pipe network used in the latent heat thermal energy storage system. The authors conducted an experimental study to demonstrate the functionality of the heat pipe network. Sun et al. (2018) carried out the numerical and experimental investigation of the gravity-assisted heat pipe (GAHP) used for the performance improvement of a thermo-electric cooler. The authors observed an augmentation in the cooling capacity of the thermo-electric cooler by using GAHP. Patel (2018) carried out a comparative analysis through the multi-objective optimization of the ammonia and methanol heat pipe used for satellite application. The author also used the multi-objective heat transfer search algorithm for the simultaneous optimization of thermal resistance and the total mass of the heat pipe.

### 7.2.1 Thermal Model

In this part of the work, an ammonia heat pipe used for satellite application is considered for optimization. The schematic arrangement of the considered heat pipe is shown in Fig. 7.3. The thermal model of the heat pipe presented here is based on the previous work of Patel (2018).

The thermal resistance of the heat pipe wall at the condenser section ( $R_{ct}$ ) is given by

$$R_{ct} = \frac{\ln\left(\frac{d_o}{d_i}\right)}{2\pi L_c k_t} \quad (7.39)$$

where  $d_o$  and  $d_i$  are the heat pipe's outer diameter and the internal diameter, respectively,  $L_c$  is the condenser section's length and  $k_t$  is the thermal conductivity of the heat pipe wall.

The thermal resistance of the heat pipe wall at the evaporator section ( $R_{et}$ ) is given by

$$R_{et} = \frac{\ln\left(\frac{d_o}{d_i}\right)}{2\pi L_e k_t} \quad (7.40)$$

where  $L_e$  is the evaporator section length.

The thermal resistance of the heat pipe wick at the condenser section ( $R_{cv}$ ) is given by

$$R_{cv} = \frac{\ln\left(\frac{d_i}{d_v}\right)}{2\pi L_c k_{eq}} \quad (7.41)$$

where  $d_v$  is the vapor core diameter, and  $k_{eq}$  is the effective thermal conductivity of the wick.

The thermal resistance of the heat pipe wick at the evaporator section ( $R_{ev}$ ) is given by

$$R_{ev} = \frac{\ln\left(\frac{d_i}{d_v}\right)}{2\pi L_e k_{eq}} \quad (7.42)$$

Here, the effective thermal conductivity of wick structure ( $k_{eq}$ ) is given by

$$k_{eq} = \frac{k_l[(k_l + k_w) - (1 - \varepsilon)(k_l - k_w)]}{[(k_l + k_w) + (1 - \varepsilon)(k_l - k_w)]} \quad (7.43)$$

where  $k_w$  is the thermal conductivity of the wick material,  $k_l$  is the thermal conductivity of the liquid, and  $\varepsilon$  is the porosity of the wick material and is given by the following equation:

$$\varepsilon = 1 - \frac{1.05\pi N d}{4} \quad (7.44)$$

where  $d$  is the wick wire diameter and  $N$  is the wick's mesh number.

The capillary limit of the heat pipe is given by

$$Q_c = P_c + P_g / (F_l + F_v) L_{eff} \quad (7.45)$$

where  $F_l$  is the liquid frictional coefficient and  $F_v$  is the vapor frictional coefficient. In addition,  $L_{eff}$  is the effective length of the heat pipe,  $P_c$  is the capillary pressure, and  $P_g$  is the hydrostatic pressure and is given by

$$P_c = \frac{2\sigma}{r_c} \quad (7.46)$$

$$P_g = \rho_1 g \{L_{total} \sin \alpha - d_v \cos \alpha\} \quad (7.47)$$

where  $\sigma$  is the surface tension,  $L_{total}$  is the total length of the heat pipe, and  $r_c$  is the capillary radius which is given by

$$r_c = \frac{1}{2N} \quad (7.48)$$

The effective length of the heat pipe ( $L_{eff}$ ) is given by

$$L_{eff} = L_a + \frac{L_e + L_c}{2} \quad (7.49)$$

where  $L_a$  is the length of the adiabatic section.

The liquid frictional coefficient ( $F_l$ ) and the vapor frictional coefficient ( $F_v$ ) are given by

$$F_l = \frac{\mu_l}{K \rho_l \lambda \left( \pi \frac{d_i^2 - d_v^2}{4} \right)} \quad (7.50)$$

$$F_v = \frac{128 \mu_v}{\rho_v \pi \lambda d_v^4} \quad (7.51)$$

where  $\mu$  is the viscosity of the fluid,  $\lambda$  is the latent heat of vaporization, and  $K$  is the permeability and is given by

$$K = \frac{d^2 \varepsilon^3}{122(1 - \varepsilon)^2} \quad (7.52)$$

The boiling limit ( $Q_b$ ) of the heat pipe is given by

$$Q_b = \frac{2\pi L_c k_{eq} T_v}{\lambda \rho_v \ln \left( \frac{d_i}{d_v} \right)} \left( \frac{2\sigma}{r_n} - P_c \right) \quad (7.53)$$

where  $r_n$  is the nucleation radius, and  $T_v$  is the vapor temperature.

The entrainment limit of the heat pipe is given by

$$Q_e = \frac{\pi d_v^2}{4} \lambda \left( \frac{\sigma \rho_v}{2r_{h,s}} \right)^{0.5} \quad (7.54)$$

where  $r_{h,s}$  is the hydraulic radius of the wick structure and is given by

$$r_{h,s} = \frac{1}{2N} - \frac{d}{2} \quad (7.55)$$

The viscous limit of the heat pipe is given by

$$Q_v = \frac{\pi \rho_v P_v \lambda d_v^4}{256 \mu_v L_{eff}} \quad (7.56)$$

Below, Reynolds number and the Mach number at the vapor core are shown:

$$Re_v = \frac{4Q}{\pi \lambda d_v \mu_v} \quad (7.57)$$

$$M_v = \frac{8Q}{\sqrt{\gamma_v R_v T_v} \pi \lambda d_v^3} \quad (7.58)$$

where  $R_v$  is the gas constant for vapor and  $Q$  is the heat load of the heat pipe.

The outside surface temperature of the evaporator section is given by

$$T_{so} = RQ + T_{si} \quad (7.59)$$

where  $T_{si}$  is the outside surface temperature of the condenser section.

The mass of the container of the heat pipe is given by

$$m_{cont} = \pi t_t (d_i + t_t) L_{total} \rho_t \quad (7.60)$$

where  $t_t$  is the heat pipe's tube thickness

The mass of the dry wick is given by

$$m_{wd} = \pi t_w (d_v + t_w) (1 - \varepsilon) L_{total} \rho_w \quad (7.61)$$

where  $t_w$  is the heat pipe's wick material thickness.

The mass of the liquid in the wick material is given by

$$m_{wl} = \pi t_w (d_v + t_w) \varepsilon L_{total} \rho_l \quad (7.62)$$

And the mass of the fluid vapor is given by

$$m_{vapor} = \frac{\pi d_v^2}{4} L_{total} \rho_v \quad (7.63)$$

Under steady state conditions, the total thermal resistance of the heat pipe is calculated using the following equation:

$$R = R_{et} + R_{ct} + R_{ew} + R_{cw} \quad (7.64)$$

where  $R_{et}$ ,  $R_{ct}$ ,  $R_{ew}$ , and  $R_{cw}$  are the thermal resistance of the heat pipe wall and heat pipe wick at the evaporator, and condenser, respectively.

Similarly, the total mass of the heat pipe is given by

$$m_{total} = m_{cont} + m_{wd} + m_{wl} + m_{vapor} \quad (7.65)$$

where  $m_{cont}$ ,  $m_{wd}$ ,  $m_{wl}$ , and  $m_{vapor}$  are the mass of the heat pipe container, the dry wick, the liquid in the wick, and the fluid vapor, respectively.

Based on the above thermal model, the objective function for the present work is defined in the next section.

### 7.2.2 Case Study, Objective Function Description, and Constraints

There is a need for designing and optimizing ammonia heat pipes used for satellite application for minimum thermal resistance ( $R$ ). The heat pipes are fabricated from stainless steel (SS 304). Here, ammonia is considered as the working fluid for the investigation. Note that the temperature-dependent thermophysical properties values of both fluids are considered during the optimization procedure. Since the heat pipes are used for space application, gravitational forces are not considered. Furthermore, it is assumed that axial heat conduction along the length of a heat pipe is negligible and there is uniform heat flux distributed along the condenser and evaporator sections. In addition, both liquid and vapor are incompressible and laminar within the heat pipe. The heat load of the heat pipe is 100 W, the condenser section temperature is at 273 K, and the length of the adiabatic section is 0.5. Seven design variables including the length of the evaporator section ( $L_e$ ), the length of the condenser section ( $L_c$ ), the thickness of the tube wall ( $t_t$ ), the thickness of the wick ( $t_w$ ), the vapor core's diameter ( $d_v$ ), the mesh number of the wick ( $N$ ), and the diameter of the wick wire ( $d$ ) are considered for the optimization problem. The upper and lower bounds of design variables are presented in Table 7.7.

As mentioned above, the minimization of the total thermal resistance ( $R$ ) of the heat pipe is taken as an objective function in the present study. Furthermore, the operating parameters resulting in minimum thermal resistance also satisfy the various constraints. So, considering these aspects, the objective function of the heat pipe is formulated as below:

$$\left\{ \begin{array}{l} \text{Minimize } f(X) = R(X) + \sum_{j=1}^n G_1(g_j(X))^2 \\ X = [x_1, x_2, x_3, \dots, x_D], \quad x_{i,\text{minimum}} \leq x_i, \leq x_{i,\text{maximum}}, \quad i = 1, 2, 3, \dots, D \\ g_j(X) \leq 0, \quad j = 1, 2, 3, \dots, n \end{array} \right. \quad (7.66)$$

**Table 7.7** Ranges of design variables for heat pipe optimization

Design variable	Lower bound	Upper bound
Length of evaporator section ( $L_e$ ) (m)	0.05	0.4
Length of condenser section ( $L_c$ ) (m)	0.05	0.4
The thickness of the tube ( $t_t$ ) (mm)	0.3	3
The thickness of wick ( $t_w$ ) (mm)	0.05	10
The diameter of the vapor core ( $d_v$ ) (mm)	5	80
Mesh number of the wick ( $N$ ) ( $\text{m}^{-1}$ )	315	1500
The diameter of wick wire ( $d$ ) (mm)	0.025	1

where  $X$  is the vector of design variables, bounded between its minimum and maximum values.  $G_I$  is the penalty parameter and  $g_j(X)$  indicates the constraints. Additionally, the entire term takes into account the effect of the constraints violation and it comes into picture when the constraints violation takes place. The following constraints are considered for the heat pipe operation.

$$Q_c - Q \geq 0 \quad (7.67)$$

$$Q_b - Q \geq 0 \quad (7.68)$$

$$Q_e - Q \geq 0 \quad (7.69)$$

$$Q_v - Q \geq 0 \quad (7.70)$$

$$M_v \leq 0.2 \quad (7.71)$$

$$Re_v \leq 2300 \quad (7.72)$$

$$0.0001 \leq \varepsilon \leq 0.9999 \quad (7.73)$$

$$m_{\text{total}} \leq 0.5 \quad (7.74)$$

The next section describes the results and discussion of the case study.

### 7.2.3 Results and Discussion

The considered problem of the heat pipe is investigated using 11 different meta-heuristic approaches to obtain minimum total thermal resistance. As all these methods are stochastic in their operation, each algorithm is run 100 times on the considered problem to estimate the statistical variations of the algorithms. Each algorithm is implemented with a population size of 50, and the termination criteria are set as 100,000 function evaluations. Like the others, the results obtained using the different algorithms (in the 100 runs) is presented in the form of the best solution, the worst solution, average solution, standard deviation, and the success rate. The results are illustrated in Table 7.8. Here, the solutions which are infeasible (i.e., affected by penalty) are eliminated while obtaining the worst solution, average solution, standard deviation, and success rate. For this section, the success rate of an algorithm is obtained by considering a maximum of 0.1% variation from the global optimum value.

Overall, it can be observed from the comparative results that the algorithms performed well and produced almost identical minimum total thermal resistance of the heat pipe. Individually, the average performance of the CSA, DE, TLBO, SOS, HTS, and PVS is almost identical and is the best in comparison with the competitive algorithms. The CSA algorithm had the highest success rate in obtaining

**Table 7.8** Comparative results of different algorithms for heat pipe optimization

Algorithms	Best	Worst	Average	SD	Success rate (%)
GA	0.0042	0.16546	0.03542	4.89E-02	52
PSO	0.0042	0.01378	0.00633	3.62E-03	80
DE	0.0042	0.00438	0.00422	5.35E-05	84
ABC	0.0042	0.00518	0.00433	2.73E-04	68
CSA	0.0042	0.00422	0.0042	7.40E-06	92
TLBO	0.0042	0.0044	0.00422	4.83E-05	76
SOS	0.0042	0.00438	0.00421	4.57E-05	76
WWO	0.0042	0.01236	0.00584	1.94E-03	32
HTS	0.0042	0.00879	0.00442	1.00E-03	80
PVS	0.0042	0.00438	0.00421	4.34E-05	80
SCA	0.0042	0.00443	0.00428	6.75E-05	24

**Table 7.9** Friedman rank test results for heat pipe optimization

Algorithms	Friedman value	Normalized value	Rank
GA	48	0.208333	10
PSO	38	0.263158	8
DE	22.5	0.444444	4
ABC	35	0.285714	7
CSA	10	1	1
TLBO	25.5	0.392157	5
SOS	22	0.454545	3
WWO	43	0.232558	9
HTS	34.5	0.289855	6
PVS	16.5	0.606061	2
SCA	35	0.285714	7

the optimum value. This is followed by the DE algorithm while the SCA algorithm had the least success. In addition, since the overall performance was well, it is difficult to judge the performance of the best algorithm. So, the Friedman rank test is implemented to judge the best suitable algorithm for heat pipe optimization focusing on their capability to obtain the best, worst, and average solutions, and success rate. Final results of the Friedman rank test are presented in Table 7.9, and its graphical representation is given in Fig. 7.4. The results are presented in the form of a Friedman value, a normalized value with '1' being the best performing, and its rank. It can be observed from the results that CSA has obtained the first rank followed by PVS and SOS algorithms.

The optimized operating parameters of the heat pipe using the CSA algorithm are presented in Table 7.10. It can be noted from the results that the heat pipe with the maximum length of the condenser section, the evaporator section, the thickness of the tube, and with minimum thickness and diameter of the wick results in minimum total thermal resistance. The diameter of the vapor core and the mesh

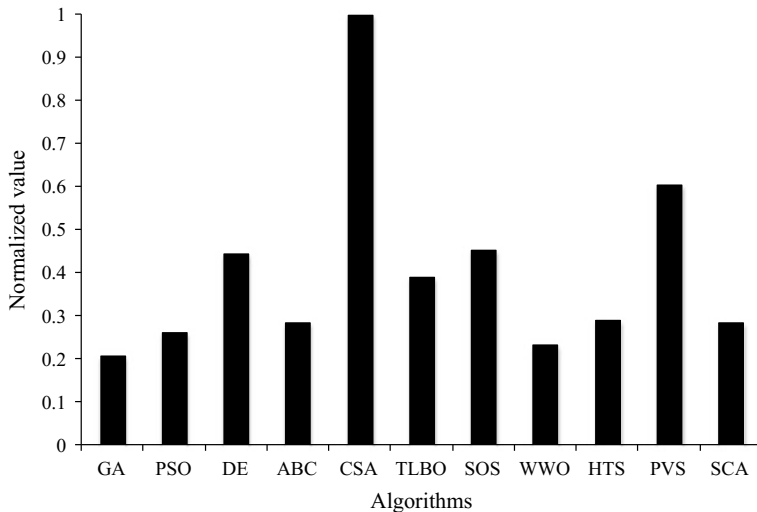


**Fig. 7.4** Graphical presentation of Friedman rank test for heat pipe optimization

**Table 7.10** The optimized operating condition of the heat pipe

Operating parameters	Optimized value
<i>Operating variable</i>	
Length of evaporator section ( $L_e$ ) (m)	0.4
Length of condenser section ( $L_c$ ) (m)	0.4
The thickness of the tube ( $t_t$ ) (mm)	0.3
The thickness of wick ( $t_w$ ) (mm)	0.06
The diameter of the vapor core ( $d_v$ ) (mm)	48.9
Mesh number of the wick ( $N$ ) ( $m^{-1}$ )	530.5
The diameter of wick wire ( $d$ ) (mm)	0.025
<i>Constrain</i>	
$Q_c - Q$	0.000738
$Q_b - Q$	4735.3
$Q_e - Q$	16481
$Q_v - Q$	1.41E+10
$M_v$	2.88E-05
$Re_v$	198
$\varepsilon$	0.989
$m_{total}$	0.5
<i>Objective function</i>	
Total thermal resistance ( $R$ ) (K/W)	0.0042

number of the wick produced a conflicting effect on achieving the minimum total thermal resistance of heat pipe. Furthermore, all the constraints here are above the limiting value in the optimized operating condition of the heat pipe.

### 7.3 Micro-channel Heat Sink

Generally, micro-channel heat sinks provide a powerful mean for dissipating high heat flux with a small range for temperature rise. Due to the relatively higher surface area and lower convective resistance at the solid/fluid interface, heat transfer is enhanced in micro-channels. These heat sinks can be applied in many important fields like microelectronics, aviation and aerospace, medical treatment, biological engineering, materials sciences, the cooling of high-temperature superconductors, thermal control of film deposition, and the cooling of powerful laser mirrors. The two essential characteristics of micro-channel heat sinks are the high heat transfer coefficients and the lower friction factors. Figure 7.5 shows the schematic arrangement of the micro-channel heat sink. The length of the heat sink is  $L$ , and the width is  $W$ . The top surface of the heat sink is insulated, and the bottom surface of the heat sink is uniformly heated. The coolant passes through several micro-channels and takes the heat away from the heat dissipating electronic component attached below.

Earlier, researchers have reported works related to the analysis and optimization of the micro-channel heat sink. Vafai and Zhu (1999) proposed a concept for a two-layered micro-channel heat sink with counter current flow arrangement for the cooling of the electronic components. The authors analyzed the thermal performance and temperature distribution for these types of micro-channels for the

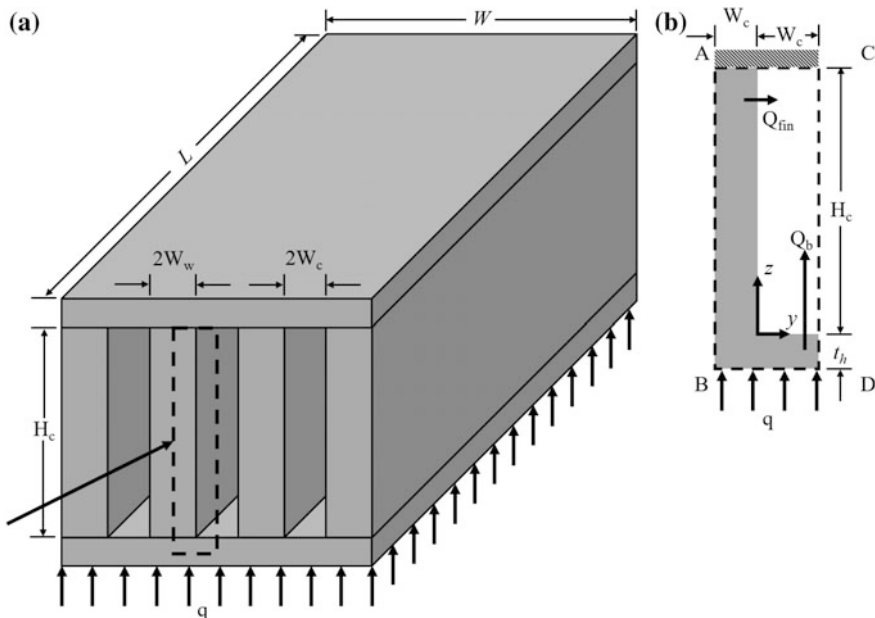


**Fig. 7.5** Schematic arrangement of the micro-channel heat sink with control volume

purpose of optimizing its geometrical design parameters. Qu and Mudawar (2002) investigated the pressure drop and heat transfer characteristics of a single-phase micro-channel heat sink. The authors performed the numerical investigation and validated it through experimentation. Wei and Joshi (2003) developed a thermal model to evaluate the overall thermal performance of a stacked micro-channel heat sink. He also performed the optimization of a developed model to obtain minimum overall thermal resistance using genetic algorithms. The authors considered the aspect ratio, the fin's thickness, and the ratio of the channel width to the fin's thickness as variables during the optimization. Liu and Garimella (2003) carried out the analyses and optimization of the thermal performance of a micro-channel heat sink through CFD analysis. Peles et al. (2005) investigated the heat transfer and pressure drop phenomena over a bank of the pin-fin micro heat sink. They (authors) derived a simplified expression for the total thermal resistance and validated it experimentally. Furthermore, the authors also identified the effects of geometrical and thermo-hydraulic parameters on the total thermal resistance.

Chein and Huang (2005) analyzed the heat transfer and hydraulic performance of a silicon micro-channel heat sink performance using nanofluids as coolants. The authors observed that the thermal performance of the heat sink was enhanced in the presence of the nanofluid while the pressure drop was not affected. This is a result of the particle's small size and its low volume fraction. Khan et al. (2006) carried out the optimization of micro-channel heat sinks using the entropy generation minimization method. The authors developed a general expression for the entropy generation rate of a micro-channel heat sink. Furthermore, the authors also performed a parametric study to identify the effects of different design variables on the overall performance of micro-channel heat sinks. Foli et al. (2006) adopted the multi-objective, genetic algorithm combined with CFD analysis to optimize the geometric parameters of the micro-channel heat sink. The authors considered the maximization of heat transfer and the minimization of the pressure drop of the heat sink simultaneously as an objective function. Li and Peterson (2007) developed a three-dimensional conjugate heat transfer model to simulate the heat transfer performance of silicon-based, parallel micro-channel heat sinks. The authors further optimized the geometric structure of these types of micro heat sinks. Another example is Husain and Kim (2008b) who carried out the numerical investigation of fluid flow and heat transfer in a rectangular micro-channel using water as a cooling fluid. The authors validated the obtained solutions with available analytical and experimental results and performed the shape optimization of a micro-channel using the surrogate method.

Husain and Kim (2008a) performed the multi-objective optimization of a micro-channel heat sink using the temperature-dependent thermophysical properties of the working fluid. The authors considered the minimization of thermal resistance and the pumping power of the heat sink as an objective function and applied NSGA-II as an optimization algorithm. Husain and Kim (2008c) investigated both the fin model and the porous medium model to minimize the thermal resistance of the micro-channel heat sink. The author obtained the optimized design variables and the corresponding thermal resistances by using the optimization methods for

both the models. Husain and Kim (2010) applied a hybrid multi-objective evolutionary algorithm coupled with surrogate models for the multi-objective optimization of a micro-channel heat sink. They considered the minimization of thermal resistance and the pumping power of heat sink as an objective function in their study. Wang et al. (2011) presented an inverse problem method to optimize the geometric design for micro-channel heat sinks. The authors adopted a multi-parameter optimization approach to minimize the overall thermal resistance of a micro-channel heat sink. In addition, Rahimi-Gorji et al. (2015) carried out the analytical investigation of heat transfer for the micro-channel heat sink, cooled by different nanofluids. They used the porous media approach and the Galerkin method. After, they compared the obtained results with a numerical procedure. Leng et al. (2015) performed a multi-parameter optimization of the flow and heat transfer for a double-layered micro-channel heat sink. Pourmehran et al. (2015) performed thermal and flow analysis of a fin-shaped micro-channel heat sink. The sink was cooled by different nanofluids using saturated porous mediums and the least square method. The authors also identified the effect of the nanoparticle's size and volume fraction on the thermal-hydraulic performance of the heat sink. Leng et al. (2015) employed a three-dimensional solid–fluid conjugate model coupled with a simplified conjugate-gradient method to optimize the performance of double-layered micro-channel heat sinks. Finally, Rao et al. (2016) performed a dimensional optimization of a micro-channel heat sink using the Jaya algorithm. The authors considered the thermal and hydraulic objective function of the heat sink and compared the obtained results with those obtained using other optimization algorithms.

### 7.3.1 Thermal Model

In this part of the work, a micro-channel heat sink is considered for optimization. The schematic arrangement of the considered micro-channel heat sink is shown in Fig. 7.5a. Furthermore, Fig. 5.1b shows the control volume used for the presentation of the thermal model. The control volume is selected in such a way, so that it gives the advantage of symmetry. There are  $N$  channels, and each channel has a height  $H_C$  and width  $2 W_C$ . The thickness of each fin is  $2 W_w$  whereas the thickness of the base is  $t_b$ . The temperature of the channel walls is assumed to be  $T_w$ . Moreover, the following assumptions are considered to simplify the thermal model of the micro-channel heat sink.

- The fin is made of an isotropic material with an adiabatic fin tip condition.
- The flow of the fluid through the micro-channel is steady, laminar, incompressible, and fully developed.
- The fin surface is smooth, and the heat flux on the surface of the fin is uniform.
- The axial conduction effect is negligible.

The thermal model of the micro-channel heat sink presented here is based on the previous work of Khan et al. (2009). Furthermore, the subscripts *in* and *out* indicate the inlet and outlet of the micro-channel in the other equation of the thermal model.

The total heat transferred from the bottom of the heat sink is given by

$$Q = \dot{m}(h_{\text{out}} - h_{\text{in}}) \quad (7.75)$$

where  $\dot{m}$  is the mass flow rate of the fluid going through the micro-channel heat sink, and  $h_{\text{out}} - h_{\text{in}}$  is the enthalpy difference of the air and is given by

$$h_{\text{out}} - h_{\text{in}} = T_a(s_{\text{out}} - s_{\text{in}}) + \frac{1}{\rho}(P_{\text{out}} - P_{\text{in}}) \quad (7.76)$$

where  $\rho$ ,  $s$ , and  $P$  are the density, specific entropy, and pressure of the air, respectively. Here,  $T_a$  is the ambient temperature.

In addition, the entropy generation rate for the micro-channel heat sink is given by

$$S_{\text{gen}} = \frac{QR_{\text{th}}}{T_a T_b} + \frac{\dot{m}\Delta P}{\rho T_a} \quad (7.77)$$

where  $R_{\text{th}}$  is the total thermal resistance and  $\Delta P$  is the total pressure drop across the channel. Note that if  $G$  is the volume flow rate, then the total mass flow rate can be written as

$$\dot{m} = \rho G \quad (7.78)$$

The average velocity in the channel is given by

$$U_{\text{av}} = \frac{\dot{m}}{N\rho(2w_c)h_c} \quad (7.79)$$

where  $w_c$  is half the channel's width, and  $N$  is the number of channels which is given by

$$N = \frac{W - w_w}{w_w + w_w} \quad (7.80)$$

where  $W$  is the width of the heat sink and  $w_w$  is half of the fins thickness

The total thermal resistance of the heat sink is defined as

$$R_{\text{th}} = \frac{T_b - T_f}{Q} + \frac{T_f - T_a}{Q} \quad (7.81)$$

where  $T_b$  is the heat sink's base temperature, and  $T_f$  is the bulk fluid's temperature. These temperatures are given by

$$T_b = T_a + QR_{th} \quad (7.82)$$

$$T_f = T_a + \frac{Q}{2\dot{m}C_p} \quad (7.83)$$

where  $C_p$  is the specific heat of air,  $A$  is the total heat transfer surface area and is given by

$$A = 2NL(w_c + H_c \eta_{fin}) \quad (7.84)$$

where  $H_c$  is the channel height,  $L$  is the length of the channel, and  $\eta_{fin}$  is the fin's efficiency and is given by

$$\eta_{fin} = \frac{\tan h(mH_c)}{mH_c} \quad (7.85)$$

where parameter  $m$  is defined as

$$m = \sqrt{\frac{2h_{av}}{kw_w}} \quad (7.86)$$

where  $k$  is the fin's material thermal conductivity and  $h_{av}$  is the average convective heat transfer coefficient and are obtained using the following correlation.

That the dimensionless heat transfer coefficient for a parallel plate micro-channel is given by

$$N_{uD_h} = \frac{h_{av}D_h}{k_f} = \frac{140}{17(1+\alpha_c)K_s} \quad (7.87)$$

where  $k_f$  is the thermal conductivity of the fluid,  $D_h$  is the hydraulic diameter,  $K_s$  the dimensionless parameter, and  $\alpha_c$  is the channel aspect ratio and is given by

$$K_s = 1 - \frac{6}{17} \left( \frac{U_s}{U_{av}} \right) + \frac{2}{51} \left( \frac{U_s}{U_{av}} \right)^2 - \frac{140}{17} \zeta_t \quad (7.88)$$

$$\alpha_c = \frac{2w_c}{H_c} \quad (7.89)$$

where  $\zeta_t$  is the temperature jump coefficient, and  $U_s/U_{av}$  is the velocity profile and is given by

$$\zeta_t = \left( \frac{2 - \sigma_t}{\sigma_t} \right) \cdot \frac{2\gamma}{\gamma + 1} \cdot \frac{Kn}{Pr} \quad (7.90)$$

$$\frac{U_s}{U_{av}} = \frac{6\alpha}{1+6\alpha} \quad (7.91)$$

where  $\sigma_t$  is the energy accommodation coefficient,  $Kn$  is the Knudsen number,  $Pr$  is the Prandtl number, and coefficient  $\alpha$  is given by

$$\alpha = \frac{2\zeta_u}{1+\alpha_c} \quad (7.92)$$

where  $\zeta_u$  is the slip velocity coefficient and is defined by

$$\zeta_u = \left( \frac{2-\sigma}{\sigma} \right) Kn \quad (7.93)$$

Based on the above correlation, the thermal resistance is simplified as below:

$$R_{th} = \frac{2C_3\alpha_{hs}}{k_f L C_1 C_2} \quad (7.94)$$

where the coefficient  $C_1$ ,  $C_2$ , and  $C_3$  are given below:

$$C_1 = N\alpha_{hs}(2\eta_{fin} + \alpha_c) \quad (7.95)$$

$$C_2 = \frac{(1+\alpha_c)}{\alpha_c} \quad (7.96)$$

$$C_3 = \frac{1}{Nu_{D_h}} + \frac{C_1}{Pe_{D_h}} \quad (7.97)$$

where  $\alpha_{hs}$  is the heat sink aspect ratio and is given by

$$\alpha_{hs} = \frac{L}{2w_c} \quad (7.98)$$

The pressure drop associated with the flow across the channel is given by

$$\Delta P = \frac{\rho U_{av}^2}{2} \left[ k_{ce} + \left( f \frac{L}{D_h} \right) \right] \quad (7.99)$$

where  $k_{ce}$  is the sum of the entrance and exit losses and  $f$  is the friction factor and is given by

$$f = \frac{24}{Re_{D_h}} \left( \frac{1}{1+6\alpha} \right) \left( \frac{1}{1+\alpha_c} \right) \quad (7.100)$$

$$K_{ce} = 1.79 - 2.32 \left( \frac{w_c}{w_c + w_w} \right) + 0.53 \left( \frac{w_c}{w_c + w_w} \right)^2 \quad (7.101)$$

Based on the above equation, the simplified form of the entropy generation rate is given by

$$S_{gen} = \frac{Q^2}{T_a T_b} \cdot \frac{2\alpha_{hs} C_3}{L k_f C_1 C_2} + \frac{\rho w_c H_c u_{av}^2}{T_a} C_4 = S_{gen,h} + S_{gen,f} \quad (7.102)$$

where  $S_{gen,h}$  and  $S_{gen,f}$  show the entropy generation rates due to heat transfer and fluid friction, respectively, and parameter  $C_4$  is given by

$$C_4 = \left[ k_{ce} + \left( f \frac{L}{D_h} \right) \right] \quad (7.103)$$

Based on the above thermal model, the objective function for the present work is defined in the next section.

### 7.3.2 Case Study, Objective Function Description, and Constraints

A micro-channel heat sink used for the electronic cooling application requires to be designed and optimized for minimum entropy generation rate ( $S_{gen}$ ). In this case, the air is used as a working fluid in the heat sink. The other input parameters considered for the case study are presented in Table 7.11. The two design variables considered are the channel aspect ratio ( $\alpha_c$ ) and the fin spacing ratio ( $\beta$ ). The upper and lower bounds of the design variables are presented in Table 7.12.

As mentioned above, the minimization of the entropy generation rate ( $S_{gen}$ ) of the micro-channel heat sink is taken as an objective function in the present study. Note that for this case, the operating parameters which resulted in minimum entropy generation rate also satisfy the flow constraint (i.e., Reynolds number constraint). So, considering these aspects, the objective function of the heat pipe is formulated as below:

$$\begin{cases} \text{Minimize } f(X) = S_{gen}(X) + \sum_{j=1}^n G_1(g_j(X))^2 \\ X = [x_1, x_2, x_3, \dots, x_D], \quad x_{i,\text{minimum}} \leq x_i \leq x_{i,\text{maximum}}, \quad i = 1, 2, 3, \dots, D \\ g_j(X) \leq 0, \quad j = 1, 2, 3, \dots, n \end{cases} \quad (7.104)$$

where  $X$  is the vector of design variables bounded between its minimum and maximum values, and  $G_1$  is the penalty parameter. The entire term considers the

**Table 7.11** Input parameters for micro-channel heat sink optimization

Design specification	Value
Channel Height $H_c$ (mm)	1.7
Channel Width $2w_c$ (mm)	0.25
Width of the heat sink, $W$ (mm)	51
Fin thickness, $2w_w$ (mm)	0.14
Channel or Heat sink length, $L$ (mm)	51
Thermal Conductivity of solid (W/m K)	148
Thermal Conductivity of air (W/m K)	0.0261
Density of air (kg/m <sup>3</sup> )	1.1614
Specific heat of air (J/kg.K)	1007
Heat flux (W/cm <sup>2</sup> )	15
Volume flow rate (m <sup>3</sup> /s)	0.007
Ambient Temperature (°C)	27
Kinematic Viscosity (m <sup>2</sup> /s)	$1.58 \times 10^{-5}$
Prandtl number (air)	0.71
Tangential Momentum accommodation coefficient	0.85
Thermal Energy Coefficient	0.85

**Table 7.12** Ranges of design variables for micro-channel heat sink optimization

Design variable	Lower bound	Upper bound
Channel aspect ratio ( $\alpha_c$ )	0.0001	10
Fin spacing ratio ( $\beta$ )	2	10

effects of the constraints violation and is used when the constraint violation take place.  $g_j(X)$  indicates the constraints. The following constraint is considered for the heat pipe operation.

$$Re_{dh} \leq 2300 \quad (7.105)$$

The next section describes the results and discussion of the case study.

### 7.3.3 Results and Discussion

Like other cases, the considered problem of the micro-channel heat sink is investigated using 11 different metaheuristic approaches to obtain minimum entropy generation rate. As all these methods are stochastic in their working, each algorithm is implemented 100 times on the considered problem to estimate the statistical variations of the algorithms. The population size considered was 50, and the termination criteria are set to 100,000 function evaluations. Below, in Table 7.13, the results obtained using each algorithm are presented in the form of the best solution,

**Table 7.13** Comparative results of different algorithms for micro-channel heat sink optimization

Algorithms	Best	Worst	Average	SD	Success rate (%)
GA	0.05414	0.16068	0.07675	3.35E-02	32
PSO	0.05414	0.07153	0.06368	7.52E-03	36
DE	0.05414	0.05416	0.05415	1.13E-05	48
ABC	0.05414	0.06751	0.05467	2.67E-03	96
CSA	0.05414	0.05416	0.05415	1.11E-05	80
TLBO	0.05414	0.07022	0.05564	4.24E-03	88
SOS	0.05414	0.05525	0.05425	3.12E-04	88
WWO	0.05414	0.21554	0.08655	4.83E-02	32
HTS	0.05414	0.09469	0.05652	8.79E-03	88
PVS	0.05414	0.06751	0.05521	3.70E-03	92
SCA	0.05414	0.07076	0.05597	5.08E-03	88

the worst solution, average solution, standard deviation, and success rate. The infeasible solutions (i.e., affected by penalty) are eliminated and the worst solution, the average solution, the standard deviation, and the success rate (maximum of 0.1% variation from the global optimum value) were obtained.

Based on the results, the algorithms performed equally well overall. They produced nearly identical minimum entropy generation rates for the micro-channel heat sink. For average performance, CSA and DE performed the best, though the success rate of the CSA algorithm in obtaining the optimum value was the highest. This is followed by the ABC and PVS algorithms and then ends with GA and WWO which produced the least success rate. Since it is difficult to judge the best algorithm, the Friedman rank test is implemented to judge the best suitable algorithm for micro-channel heat sink optimization. The rank test considers each algorithm's capability to obtain the best, worst, and average solutions, and its success rate. The results of the Friedman rank test are presented in Table 7.14, and its graphical representation is given in Fig. 7.6. The results are presented in the form of a Friedman value, a normalized value with '1' being the best performing algorithm,

**Table 7.14** Friedman rank test results for micro-channel heat sink optimization

Algorithms	Friedman value	Normalized value	Rank
GA	46.5	0.354839	8
PSO	40	0.4125	7
DE	19.5	0.846154	2
ABC	19.5	0.846154	2
CSA	16.5	1	1
TLBO	28.5	0.578947	4
SOS	19.5	0.846154	2
WWO	49.5	0.333333	9
HTS	36.5	0.452055	6
PVS	22.5	0.733333	3
SCA	31.5	0.52381	5

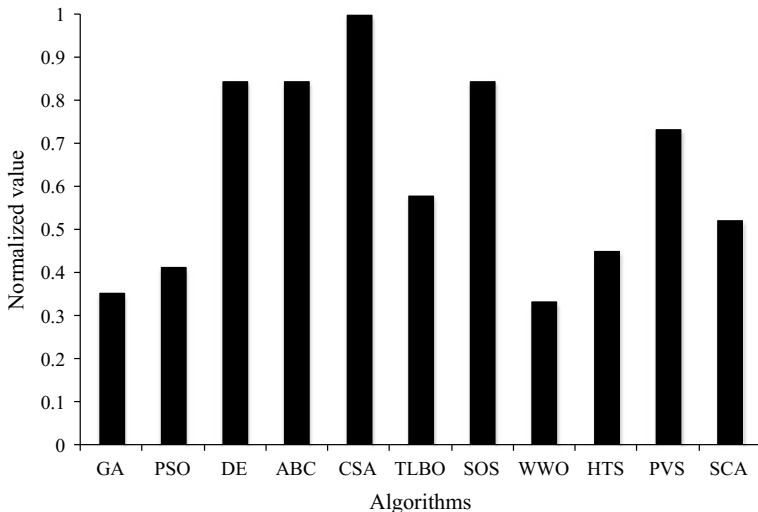


**Fig. 7.6** Graphical presentation of Friedman rank test for micro-channel heat sink optimization

**Table 7.15** The optimized operating condition of a micro-channel heat sink

Operating parameters	Optimized value
<i>Operating variable</i>	
Channel aspect ratio ( $\alpha_c$ )	0.0095
Fin spacing ratio ( $\beta$ )	2.35
<i>Constrain</i>	
Reynolds number ( $Re_{d_h}$ )	180.95
<i>Objective function</i>	
Entropy generation rate ( $S_{gen}$ ) (W/K)	0.054138

and its rank. As such, from the results, CSA has obtained the first rank followed by ABC, DE, and SOS algorithms.

The optimized operating parameters of the micro-channel heat sink obtained using the CSA algorithm are presented in Table 7.15. It can be noted from the results that the channel aspect ratio and fin spacing ratio produced a conflicting effect on achieving the minimum entropy generation rate of the micro-channel heat sink. In addition, the Reynolds number constraint is below the limiting value in the optimized operating condition of micro-channel.

## 7.4 Solar Air Heater

Solar air heating is a renewable energy heating technology which operates based on solar thermal conversion. Solar air heaters are in fact kinds of heat exchangers used to convert solar energy into useful heat for space heating, process heating, desalination, food drying, etc. A conventional solar air heater is essentially a flat plate collector with an absorber plate. It is equipped with a transparent cover system at the top and insulation at both the bottom and sides. The whole assembly is enclosed in a sheet metal container. Figure 7.7 shows the schematic diagram of the solar air heater. It can be observed from the figure that the arrangement of the solar air heater is always tilted to receive maximum solar radiation. The top surface of the solar air heater is provided with the transparent cover so that the maximum amount possible of solar energy is transmitted and enters the air heater. The transmitted solar radiation then falls on the absorber plate, which is placed below the transparent cover. When the absorber plate absorbs the solar radiation, its temperature increases. The remaining three sides (Bottom side and the two corners) are insulated to prevent heat loss. In the system, the air enters from the bottom side and passes parallel to the axis of the air heater. During this movement, the air absorbs heat from absorber plate, increasing its temperature. It then leaves from the other end of the air heater. Note that one can add a fin to the air flow's path to enhance the heat transfer from the absorber plate to the air (as shown in Fig. 7.7).

Earlier, researchers have reported various works related to the analysis and optimization of the solar air heater. Altfeld et al. (1988) modeled different types of solar air heaters to identify their thermal and pressure drop behavior. The authors also performed the second-law-based optimization of a solar air heater. Pottler et al.

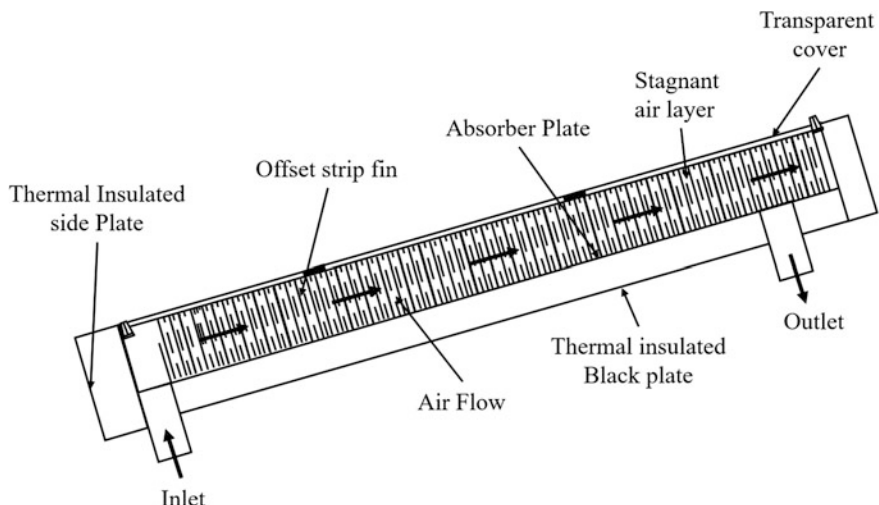


**Fig. 7.7** Schematic arrangement of the solar air heater

(1999) optimized the finned absorber geometries for the solar air heating collectors. The authors observed that the performance of the optimally spaced continuous fin was better than the offset strip fins due to the larger electrical power for this geometry. Naphon (2005) presented a mathematical model of the double-pass flat plate solar air heater with longitudinal fins to identify its heat transfer and entropy generation characteristics. The author also investigated the effects of the inlet condition of the working fluid and the dimensions of the solar air heater on its performance. Mittal and Varshney (2006) carried out the thermal-hydraulic investigations of a packed bed solar air heater. The author determined the performance of the thermal-hydraulic air heater in terms of its effective efficiency. Furthermore, the authors also developed a mathematical model to compute the effective efficiency of the solar air heater. Layek et al. (2007) performed a numerical study of the entropy generation of the duct of the solar air heater having repeated transverse chamfered rib-groove roughness on one broad wall. The authors also performed an entropy generation minimization and obtained reasonably optimized designs of roughness.

Gupta and Kaushik (2008) obtained the optimum aspect ratio and duct depth of a flat plate solar air heater for maximum exergy delivery. The authors also investigated the effects of the geometric parameters on the performance of the solar air heater. Varun Saini and Singal 2008 investigated the thermal performance of a solar air heater with a degree of roughness as a combination of inclined and transverse ribs on the absorber plate. Kumar and Saini (2009) analyzed the performance of a solar air heater duct equipped with an artificial roughness. They used computational fluid dynamics. The authors also investigated the effects of the roughness of the heater on the heat transfer coefficient, as well as the friction factor of the air heater. In another work, Nwosu (2010) employed exergy-optimized pin fins in the design of an absorber in a solar air heater. The author observed that the efficiency of the optimized fin improved the heat absorption and dissipation potential of a solar air heater. Karmare and Tikekar (2010) presented the fluid flow and heat transfer study in a solar air heater by using computational fluid dynamics. The authors carried out the experimental investigation to validate the CFD results and observed good relation between the experimental and CFD results. Akpinar and Koçyigit (2010) carried out an experimental investigation to identify the performance of a flat-plate solar air heater with and without obstacles. They determined the first and second laws of efficiency for the configuration of the solar air heater.

Varun and Siddharth (2010) adopted GA to optimize the operating parameters of the flat plate solar air heater. This resulted in the maximum thermal efficiency of the heater. In addition, Alta et al. (2010) carried out an experimental investigation of three different types of flat plate solar air heater. Based on the results, the authors concluded that the heater with the double glass that covers its fins is more effective. In addition, for the mentioned heater, the difference between the input and output air temperature is higher than of the others. Jeyadevi et al. (2012) carried out the optimization of the operating variables of the solar air heater for obtaining its maximum thermal efficiency. The authors adopted the differential evolution algorithm and compared the obtained results with the available ones obtained using both

the genetic algorithm and the particle swarm optimization algorithm. Yang et al. (2014) performed the optimization of a solar air heater with an offset strip fin by numerical modeling. The authors conducted a series of experiments to identify the thermal performance of an optimized air heater and observed that the optimized geometry resulted in a higher thermal efficiency in contrast to the conventional heater. Kumar and Kim (2014) carried out the optimization of the thermal and effective efficiency of the solar air heater. They presented a methodology, based on the heat transfer and friction factor correlation, that can be used for the prediction of the thermal and effective efficiency of the solar air heater. Yadav and Bhagoria (2014) carried out a CFD-based thermo-hydraulic performance analysis of an artificially roughened solar air heater that had equilateral triangular sectioned rib roughness on the absorber plate. The authors observed that the performance of the artificially roughened solar air heater is based heavily on the Reynolds number, the relative roughness pitch, and the relative roughness height. Prasad et al. (2015) performed the thermohydraulic optimization of solar air heaters, artificially roughened on three sides, and compared its performance parameter with a one-sided artificially roughened solar air heater.

#### 7.4.1 Thermal Model

In this part of the work, a solar air heater is considered for optimization. The schematic arrangement of the solar air heater is shown in Fig. 7.7. The thermal model of the solar air heater presented here is based on the previous work of Varun and Siddhartha (2010).

The top loss coefficient ( $U_T$ ) of the solar air heater is given by

$$U_T = \left[ \frac{N}{(349/t_p)[(t_p - t_a)/(N + \beta)]^{0.33}} + \frac{1}{h_w} \right]^{-1} + \frac{\sigma(t_p - t_a)(t_p^2 + t_a^2)}{[\varepsilon_p + 0.05N(1 - \varepsilon_p)]^{-1} + [(2N + \beta - 1)/\varepsilon_g] - N} \quad (7.106)$$

where  $t_p$  is the plate temperature,  $t_a$  is the air temperature,  $N$  is the number of glass covers,  $\varepsilon_p$  is the emittance of plate,  $\varepsilon_g$  is the emittance of the glass cover,  $\sigma$  is the Stefan Boltzmann constant,  $h_w$  is the wind convective coefficient, and  $\beta$  is the tilt angle of the solar air heater and is given by

$$\beta = (1 - 0.04 h_w + 0.005 h_w^2)(1 + 0.091N) \quad (7.107)$$

$$h_w = 5.7 + 3.8V_w \quad (7.108)$$

where  $V_w$  is the wind velocity. Using the top loss coefficient, the overall loss coefficient ( $U_L$ ) of the solar air heater can be determined from

$$U_L = U_T + \frac{k_i}{t} \quad (7.109)$$

where  $k_i$  and  $t$  are the thermal conductivity and thickness of the insulating material, respectively.

The following equation can obtain the heat removal factor ( $F_0$ ) of the solar air heater:

$$F_0 = \frac{GC_p}{U_L} [\text{Exp}(U_L F' / GC_p) - 1] \quad (7.110)$$

where  $C_p$  is the specific heat of air,  $G$  is the mass velocity, and  $F'$  is the collector efficiency factor and is described as

$$F' = \frac{h}{h + U_L} \quad (7.111)$$

where  $h$  is the convective heat transfer coefficient and is given by

$$h = 0.024 Re^{0.8} Pr^{0.4} \frac{k}{D} \quad (7.112)$$

where  $k$  is the thermal conductivity of air,  $Re$  is the Reynolds number,  $Pr$  is the Prandtl number, and  $D$  is the hydraulic diameter of the duct.

The net thermal energy gain ( $q_u$ ) by air is computed using the following equation:

$$q_u = A_c \{ \langle \tau \alpha \rangle I - U_L (t_p - t_a) \} \quad (7.113)$$

where  $A_c$  is the area of the absorber plate,  $\tau \alpha$  is the transmittance-absorptance product of the absorber plate, and  $t_p$  is the plate temperature and is given by

$$t_p = t_a - F_0 I (\tau \alpha) \left[ \frac{1 - F_0}{F_0 U_L} + \frac{t_o - t_i}{I (\tau \alpha)} \right] \quad (7.114)$$

where  $I$  is the irradiance and  $(t_o - t_i)$  is the temperature rise of the air and is given by the following equation:

$$(t_o - t_i) = \frac{q_u}{m C_p} \quad (7.115)$$

where  $m$  is the mass flow rate of air.

Finally, the thermal efficiency of the solar air heater is described as

$$\eta_{\text{th}} = F_0 \left[ (\tau\alpha) - U_L \left( \frac{t_o - t_i}{I} \right) \right] \quad (7.116)$$

Based on the above thermal model, the objective function for the present work is defined in the next section.

#### 7.4.2 Case Study, Objective Function Description, and Constraints

A solar air heater needs to be designed and optimized for maximum thermal efficiency ( $\eta_{\text{th}}$ ). For this case, the solar irradiance is considered as  $600 \text{ W/m}^2$ , and the number of glass cover is 3. In addition, the transmittance-absorptance product of the absorber plate ( $\tau\alpha$ ) is 0.85. The emittance of the glass cover ( $\varepsilon_g$ ) is taken as 0.88. The thickness of the insulating material ( $t$ ) is taken to be 0.1 m. The thermal conductivity of the insulation material ( $k_i$ ) is  $0.04 \text{ W/m}^2 \text{ K}$ . Finally, the temperature of the air is  $12^\circ\text{C}$ . The three design variables considered for the optimization problem are the velocity of air ( $V$ ), the tilt angle ( $\beta$ ), and the emittance of the plate ( $\varepsilon_p$ ). The upper and lower bounds of design variables are presented in Table 7.16.

As mentioned above, the maximum thermal efficiency ( $\eta_{\text{th}}$ ) of the solar air heater is taken as an objective function in the present study. Furthermore, the operating parameters resulting in the maximum thermal efficiency also satisfy the flow constraint (i.e., Reynolds number constraint). So, considering all these aspects, the objective function of solar air heater is formulated as below:

$$\begin{cases} \text{Minimize } f(X) = \eta_{\text{th}}(X) + \sum_{j=1}^n G_j(g_j(X))^2 \\ X = [x_1, x_2, x_3, \dots, x_D], \quad x_{i,\text{minimum}} \leq x_i \leq x_{i,\text{maximum}}, \quad i = 1, 2, 3, \dots, D \\ g_j(X) \leq 0, \quad j = 1, 2, 3, \dots, n \end{cases} \quad (7.117)$$

where  $X$  is a vector of design variables bounded between its minimum and maximum values. Above,  $G_j$  is the penalty parameter. Note that the entire term takes into account the effect of the constraint's violation. As such, this term comes into use when the constraint violation takes place.  $g_j(X)$  indicates the constraints. The following constraint is considered for the solar air heater.

**Table 7.16** Ranges of design variables for solar air heater optimization

Design variable	Lower bound	Upper bound
The velocity of air (V)	1	5
Tilt angle ( $\beta$ )	0	70
Emittance of the plate ( $\varepsilon_p$ )	0.85	0.95

$$Re_{dh} \leq 20,000 \quad (7.118)$$

The next section describes the results discussion of the case study.

### 7.4.3 Results and Discussion

The considered problem of the solar air heater is investigated using 11 different metaheuristic approaches. This is done to obtain the maximum thermal efficiency. As all these methods are stochastic in their working, each algorithm is implemented 100 times on the considered problem to estimate the statistical variations of the algorithms. Each algorithm is implemented with the population size of 50, and the termination criteria are set as 100,000 function evaluations. The results obtained using each algorithm are presented in Table 7.17 in the form of the best solution, the worst solution, average solution, standard deviation, and success rate. Here, the infeasible solutions (i.e., affected by penalty) are eliminated, and then the worst solution, average solution, standard deviation, and success rate are obtained. Note that the success rate of the algorithm is obtained by considering a 0.1% variation from the global optimum value.

It can be observed from the comparative results that only the DE, ABC, HTS, and PVS algorithms were able to obtain the maximum thermal efficiency of the solar air heater. In addition, DE had the highest average performance as well as the highest success rate in obtaining the optimum value. This is followed by PVS, HTS, and ABC algorithms. The remaining algorithms were not able to obtain the maximum thermal efficiency of the solar air heater and hence produced a zero success rate. Since the results vary so much, the Friedman rank test is implemented to judge the best suitable algorithm for solar air heater optimization. The test considers the

**Table 7.17** Comparative results of different algorithms for solar air heater optimization

Algorithms	Best	Worst	Average	SD	Success rate (%)
GA	0.77002	0.73592	0.75105	9.73E-03	00
PSO	0.76852	0.73304	0.7422	7.62E-03	00
DE	0.78135	0.73552	0.77124	1.69E-02	72
ABC	0.78086	0.75106	0.76741	7.77E-03	04
CSA	0.75421	0.73558	0.74421	4.97E-03	00
TLBO	0.77803	0.73552	0.74797	9.11E-03	00
SOS	0.75582	0.73621	0.74182	4.53E-03	00
WWO	0.76852	0.73525	0.74673	1.07E-02	00
HTS	0.78135	0.7448	0.75682	1.24E-02	08
PVS	0.78135	0.73698	0.7708	1.70E-02	12
SCA	0.73333	0.73264	0.73304	2.86E-04	00

**Table 7.18** Friedman rank test results for solar air heater optimization

Algorithms	Friedman value	Normalized value	Rank
GA	31	0.435484	5
PSO	38.5	0.350649	9
DE	13.5	1	1
ABC	24	0.5625	4
CSA	36	0.375	8
TLBO	32	0.421875	6
SOS	34	0.397059	7
WWO	38.5	0.350649	9
HTS	20.5	0.658537	3
PVS	20	0.675	2
SCA	42	0.321429	10

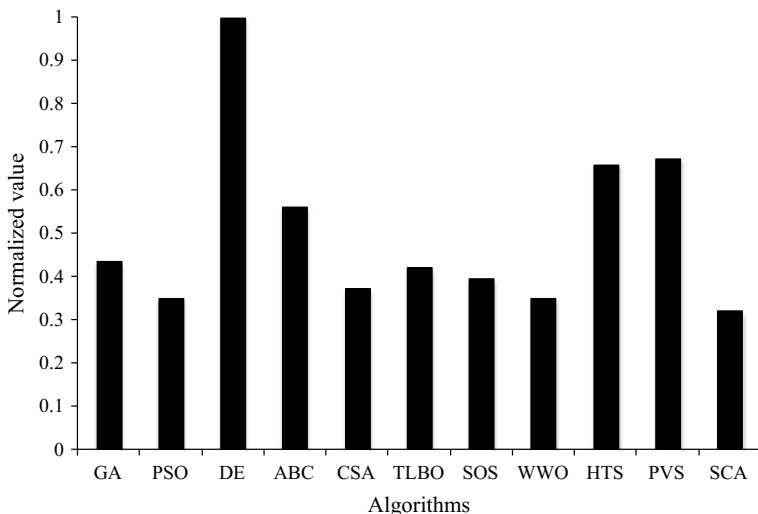


**Fig. 7.8** Graphical presentation of Friedman rank test for solar air heater optimization

capability of each algorithm to obtain the best, worst, and average solutions, and success rate. The results of the Friedman rank test are presented in Table 7.18, and its graphical representation is given in Fig. 7.8. The results are presented in the form of Friedman value, a normalized value with ‘1’ being the best performing algorithm, and its rank. It can be observed from the results that DE has obtained the first rank followed by PVS, HTS, and ABC algorithms.

The optimized operating parameters of the solar air heater obtained using the DE algorithm are presented in Table 7.19. It can be noted from the results that the solar air heater with a maximum tilt angle and minimum emittance of plate resulted in the maximum thermal efficiency, while the velocity of the air produced a conflicting

**Table 7.19** The optimized operating condition of the solar air heater

Operating parameters	Optimized value
<i>Operating variable</i>	
The velocity of air (V)	3.31
Tilt angle ( $\beta$ )	70
Emittance of the plate ( $\epsilon_p$ )	0.85
<i>Constraint</i>	
Reynolds number ( $Re$ )	20,000
<i>Objective function</i>	
Thermal efficiency ( $\eta_{th}$ )	0.78135

effect on achieving the maximum thermal efficiency for the heater. Note that the Reynolds number constraint is at the limiting value in the optimized operating condition of solar air heater.

## 7.5 Solar Water Heater

Solar water heaters are solar thermal technology. They convert solar energy into thermal energy which is used to heat water. A conventional solar water heater uses a flat plate collector. The solar water heater provides hot water for showers, kitchen use, washing clothes, etc. Figure 7.9 shows the schematic diagram of the solar air with a flat plate collector. It can be observed from the figure that the flat plate collector absorbs sunlight, hence increasing its temperature. The cold water is passed through the collector with the help of the pump. As it passes to the storage tank, the water gets heated. From the storage tank, the hot water is taken to a space where it is required.

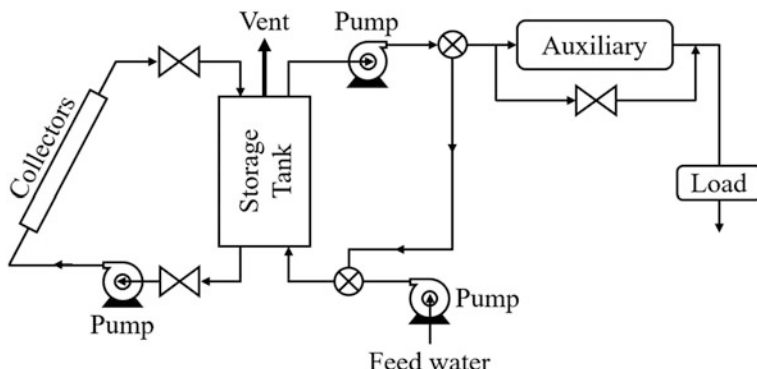


**Fig. 7.9** Schematic diagram of the solar water heater

Earlier, researchers have reported various works related to the analysis and optimization of the solar water heater. Shaariah and Löf (1996) analyzed the performance of a domestic solar water heating system through TRNSYS simulation. The authors also investigated the effect of the tank's height on the annual solar fraction of the system for different hot water load temperatures and storage tank volumes. Shariah and Shalabi (1997) obtained an optimized design parameter of a thermosyphon solar water heater. This gave it a maximum annual solar fraction of a system through TRNSYS simulation. Shariah et al. (2002) optimized the tilt angle of the solar collector of a thermosyphon solar water heater to maximize the performance of the system. Hussein (2003) investigated a natural circulation, two-phased closed thermosyphon flat plate solar water heater under actual field conditions. The author then concluded that both the storage tank volume to collector area ratio and the storage tank dimensions ratios have significant effects on the heater's performance. Esen and Esen (2005) carried out an experimental investigation to identify the effect of different refrigerants on the thermal performance of a two-phased thermosyphon solar collector used for water heating. The authors compared the experimental results with the results available in the literature and observed an agreement between them. Lima et al. (2006) developed an optimization model for the design parameters of water heating systems using a numerical simulation routine. The optimized design gave the slope and area of the flat plate collector, resulting in the minimum cost for the equipment life cycle. Kulkarni et al. (2007) proposed a methodology to determine the design space for the synthesis, analysis, and optimization of solar water heating systems. They observed a conflicting behavior between the storage volume and the collector area for a given fixed solar radiation. Furthermore, the authors performed the multi-objective optimization and obtained a Pareto solution between the storage volume and collector area.

Gunerhan and Hepbasli (2007) performed the exergy analysis of a solar water heater and presented an exergy efficiency curve for the system. The authors also investigated the effect of the water's inlet temperature on the exergy efficiencies of the system. Jaisankar et al. (2009) carried out an experimental investigation to identify the heat transfer and friction factor characteristics of the thermosyphon solar water heater system fitted with the spacer. Kulkarni et al. (2009) studied the effect of water replenishment on the system sizing. The authors proposed a novel strategy for water replenishment to improve the design and performance of solar water heating systems. Mohsen et al. (2009) carried out experimental studies on a compact solar water heater to evaluate the performance of the heater and determine the optimal depth of the storage tank. Hobbi and Siddiqui (2009) presented the modeling and simulation of an indirect forced circulation solar water heating systems using a flat-plate collector for domestic hot water requirements. Another example is Dagdougui et al. (2011) who carried out the thermal analysis and optimization of a flat plate collector used for solar water heating. The authors obtained the optimal water flow and collector area to achieve an ideal compromise between the collector's efficiency and the output water's temperature. Atia et al. (2012) used the genetic algorithm to optimize the life cycle cost of the solar water

heating system. In the work, the authors also carried out a parametric analysis to identify the effects of the solar fraction and collector area on the life cycle cost of the solar water heater.

Additionally, Chaabane et al. (2014) presented a numerical study of the thermal performance of an integrated collector storage solar water heater with phase-change materials. Elhabishi and Gryzgoridis (2016) carried out the performance comparison of a solar water heating system equipped with flat plate solar collector panels (that had numerically identical surface areas) of different geometric configurations. The authors concluded that the system's thermal efficiency was the best when the square collector was used. Hajabdollahi and Hajabdollahi (2017) performed a thermo-economic modeling and multi-objective optimization of a solar water heater. The authors considered the maximization of efficiency and minimization of total annual cost of the system as an objective function and adopted the Particle swarm optimization algorithm as an optimization tool to obtain the Pareto solutions between the conflicting objectives. Finally, Yaman and Arslan (2018) presented the optimum dimensions of a solar water heater. These were determined using the life cycle cost analysis constraint for the different regions of Turkey. The authors then applied the particle swarm optimization algorithm and obtained both the optimum number of solar collectors and the volume of the hot water storage tank of the solar water heater.

### 7.5.1 Thermal Model

In this part of the work, a solar water heater using flat plate collector is considered for optimization. The schematic arrangement of the solar water heater is shown in Fig. 7.9. The thermal model of a solar water heater presented here is based on the previous work of Hajabdollahi and Hajabdollahi (2017).

The amount of thermal energy (i.e., heat energy) gained by the water from the collector is given by

$$\dot{Q} = A_C F_R [S - U_L(T_i - T_a)] = (\dot{m} C_p \Delta T)_f \quad (7.119)$$

where  $A_C$  is the surface area of the collector,  $U_L$  is the overall loss coefficient of the collector,  $T_i$  is the water inlet temperature,  $T_a$  is the ambient temperature,  $\dot{m}$  is the mass flow rate of water,  $C_p$  is the specific heat of water,  $\Delta T$  is the temperature difference of water, and  $F_R$  is the heat removal factor which is defined as below:

$$F_R = \frac{\dot{m} C_p}{A_c U_L} \left[ 1 - \exp \left( -\frac{A_c U_L F'}{\dot{m} C_p} \right) \right] \quad (7.120)$$

where  $F'$  is the collector efficiency factor and is given by

$$F' = \frac{1/U_L}{W \left( \frac{1}{U_L [D_o + (W - D_o) \eta_F]} + \frac{1}{C_b} + \frac{1}{\pi D_i h_{fi}} \right)} \quad (7.121)$$

where  $D_i$  and  $D_o$  are the inner and outer tube diameters, respectively,  $W$  is the space between the tubes,  $1/C_b$  is the bond resistance,  $h_{fi}$  is the tube side convective heat transfer coefficient, and  $\eta_F$  is the fin efficiency.

In the present work, a straight fin with a rectangular profile was considered. The efficiency of such fins are given by

$$\eta_F = \frac{\tan h \left[ \sqrt{U_L / (k\delta)} (W - D_o) / 2 \right]}{\sqrt{U_L / (k\delta)} (W - D_o) / 2} \quad (7.122)$$

where  $k$  and  $\delta$  are the fins conductivity and thickness, respectively.

The tube side convective heat transfer coefficient ( $h_{fi}$ ) depends on the Reynolds number and is given by

$$h_{fi} = 4.36 \frac{k_f}{D_i} \quad \text{for } Re \leq 2300 \quad (7.123)$$

$$h_{fi} = \frac{k_f}{D_i} \left\{ \frac{\frac{f}{2} \times (Re - 1000).Pr}{1 + 12.7 \sqrt{\frac{f}{2} (Pr^{0.67} - 1)}} \right\} \quad \text{for } 2300 < Re \leq 10,000 \quad (7.124)$$

$$h_{fi} = \frac{k_f}{D_i} \left\{ \frac{\frac{f}{2} \times Re.Pr}{1.07 + \frac{900}{Re} - \frac{0.63}{1 + 10Pr} + 12.7 \sqrt{\frac{f}{2} (Pr^{0.67} - 1)}} \right\} \quad \text{for } Re > 10,000 \quad (7.125)$$

where  $k_f$  is the thermal conductivity of water and  $f$  is the friction factor which also depends on the Reynolds number and is given by

$$f = (1.58 \log(Re) - 3.28)^{-2} \quad \text{for } 2300 < Re \leq 10,000 \quad (7.126)$$

$$f = 0.00128 + 0.1143(Re)^{-0.311} \quad \text{for } Re > 10,000 \quad (7.127)$$

The Reynolds number for fluid flow is determined from the following equation:

$$Re = 4\dot{m}/(\pi D_i \mu N) \quad (7.128)$$

where  $\mu$  is the viscosity of water and  $N$  is the number of parallel tubes in the collector.

The following equation gives the overall loss coefficient of the collector ( $U_L$ ),

$$U_L = U_b + U_e + U_t \quad (7.129)$$

where  $U_b$  is the bottom loss coefficient,  $U_e$  is the edge loss coefficient, and  $U_t$  is the top loss coefficient of the collector. They are given by the following equations:

$$U_b = (k/t)_{\text{insulation},b} \quad (7.130)$$

$$U_e = (k/t)_{\text{insulation},e} (A_c/A_e) \quad (7.131)$$

$$U_t = 1/\left(R_1 + \sum_{i=1}^{N_c} R_{2,i}\right) \quad (7.132)$$

where  $k$  and  $t$  are the thermal conductivity and thickness of insulation.  $A_e$  is the edge heat transfer surface area, and  $N_c$  is the number of covers. The parameters  $R_1$  and  $R_2$  are defined as below:

$$R_1 = 1/(h_{r,ca} + h_{wind}) \quad (7.133)$$

$$R_2 = 1/(h_{r,pc} + h_{c,pc}) \quad (7.134)$$

where  $h_{r,ca}$  and  $h_{r,pc}$  are the radiation coefficients for the cover ambient and the plate cover, respectively, while  $h_{c,pc}$  is the convection heat transfer coefficient between the absorber plate and cover plate. They are given by the following equations:

$$h_{r,ca} = \varepsilon_c \sigma (T_c^2 - T_a^2) (T_c + T_a) \quad (7.135)$$

$$h_{r,pc} = \frac{\sigma (T_c^2 + T_p^2) (T_c + T_p)}{1/\varepsilon_p + \frac{1}{\varepsilon_c} - 1} \quad (7.136)$$

$$h_{c,pc} = \frac{Nu_a k_a}{t_{pc}} \quad (7.137)$$

where  $\varepsilon_c$  is the cover's emissivity,  $\varepsilon_p$  is the absorber plate's emissivity,  $\sigma$  is the Stefan Boltzmann constant,  $T_c$  is the cover's temperature,  $T_p$  is the absorber plate's temperature,  $k_a$  is the thermal conductivity of air,  $t_{pc}$  is the space between the plate and cover, and  $Nu_a$  is the Nusselt number. The following equation can estimate the collector's efficiency:

$$H_{\text{col}} = \frac{\dot{Q}}{I_t A_c} \quad (7.138)$$

where  $I_t$  is the total radiation on the tilt surface of the absorber and is given by the following equation:

$$S = (\tau\alpha)I_t \quad (7.139)$$

where  $S$  is the net absorbed radiation and  $\tau\alpha$  is the transmittance–absorptance product.

The pumping power required for a water heater is given by

$$\dot{W}_P = \frac{\dot{m}\Delta P}{\rho\eta_P} \quad (7.140)$$

where  $\rho$  is the density of water,  $\eta_P$  is the pump's efficiency, and  $\Delta P$  is the pressure drop which is estimated below:

$$\Delta P = \frac{2f(L_1/D_i)\rho V^2}{1000} \quad (7.141)$$

where  $V$  is the velocity in the tube and  $f$  is the friction factor.

Based on the above thermal model, the objective function for the present work is defined in the next section.

### 7.5.2 Case Study, Objective Function Description, and Constraints

A solar water heater with a flat plate is designed and optimized for the maximum thermal efficiency ( $\eta_{th}$ ). The solar irradiance is considered as  $250 \text{ W/m}^2$ . The water inlet temperature is considered as  $10^\circ\text{C}$ . The copper plate has thermal conductivity of  $385 \text{ W/mK}$  and an emissivity of 0.92 is used as the absorber plate. The transmittance–absorptance product of the absorber plate ( $\tau\alpha$ ) is 0.84. Other input parameters used in the case study are given in Table 7.20. For the optimization problem, five design variables including mass flow rate ( $\dot{m}$ ), tube diameter ( $D_i$ ), collector length ( $L_c$ ), collector width ( $W_c$ ), and insulator thickness ( $t$ ) are considered. The upper and lower bounds of the design variables are presented in Table 7.21.

**Table 7.20** Input parameters for solar water heater optimization

Input parameter	Value
Space between the cover and absorber plate (m)	0.025
Absorber emissivity	0.92
Cover emissivity	0.88
Insulator conductivity (W/m K)	0.045
Absorber plate thickness (m)	0.0005
Ambient temperature (°C)	10
Wind velocity (m/s)	5

**Table 7.21** Ranges of design variables for solar water heater optimization

Design variable	Lower bound	Upper bound
Mass flow rate ( $\dot{m}$ ) (kg/s)	0.2	2
Tube diameter ( $D_i$ ) (mm)	5	15
Collector length ( $L_c$ ) (m)	0.5	4
Collector width ( $W_c$ ) (m)	0.5	4
Insulator thickness ( $t$ ) (mm)	20	150

As mentioned above, the maximum thermal efficiency ( $\eta_{\text{th}}$ ) of the solar water heater is taken as an objective function in the present study. Furthermore, the operating parameters which result in the maximum thermal efficiency also satisfy the temperature rise of the water per circulation ( $\Delta T_{\text{circulation}}$ ) constraint. So, considering the mentioned aspects, the objective function of the solar water heater is formulated as below:

$$\left\{ \begin{array}{l} \text{Minimize } f(X) = \eta_{\text{th}}(X) + \sum_{j=1}^n G_1(g_j(X))^2 \\ X = [x_1, x_2, x_3, \dots, x_D], \quad x_{i,\text{minimum}} \leq x_i \leq x_{i,\text{maximum}}, \quad i = 1, 2, 3, \dots, D \\ g_j(X) \leq 0, \quad j = 1, 2, 3, \dots, n \end{array} \right. \quad (7.142)$$

where  $X$  is the vector of design variables, bounded between its minimum and maximum values.  $G_1$  is the penalty parameter. The term above considers the effect of the constraints violation and is used when the constraint violation takes place.  $g_j(X)$  indicates such constraints. The following constraint is considered for the solar air heater.

$$\Delta T_{\text{circulation}} \leq 0.25 \quad (7.143)$$

The next section describes the results and discussion of the case study.

### 7.5.3 Results and Discussion

The considered problem of the solar water heater is investigated using 11 different metaheuristic approaches to obtain the maximum thermal efficiency. As all these methods are stochastic in their working, each algorithm is implemented 100 times on the considered problem to estimate the statistical variations of the algorithms. Each algorithm is implemented with the population size of 50, and termination criteria are set as 100,000 function evaluations. The results obtained using each algorithm are presented in the form of the best solution, the worst solution, average solution, standard deviation, and success rate (Table 7.22). In this section, the

**Table 7.22** Comparative results of different algorithms for solar water heater optimization

Algorithms	Best	Worst	Average	SD	Success rate (%)
GA	0.7887	0.73627	0.76991	1.71E-02	28
PSO	0.7887	0.73559	0.77129	1.99E-02	36
DE	0.7887	0.73588	0.77492	1.83E-02	32
ABC	0.7887	0.75917	0.77938	8.78E-03	28
CSA	0.7887	0.7425	0.76991	1.89E-02	24
TLBO	0.7887	0.74178	0.76743	1.92E-02	28
SOS	0.7887	0.73855	0.76301	2.09E-02	20
WWO	0.7887	0.73631	0.76271	1.97E-02	12
HTS	0.7887	0.74931	0.77649	1.52E-02	32
PVS	0.7887	0.73789	0.77601	1.93E-02	40
SCA	0.7887	0.73405	0.76059	2.34E-02	24

infeasible solutions (i.e., affected by penalty) are eliminated. Afterward, the worst solution, average solution, standard deviation, and success rate (0.1% variation from the global optimum value) were obtained.

From the comparative results, it can be stated that the algorithm performed well and produced almost identical maximum thermal efficiency of the solar water heater. The average performance of the ABC algorithm was the highest, but the success rate of the PVS algorithm in obtaining the optimum value was the highest followed by the PSO algorithm. The WWO algorithm had the lowest success rate. The Friedman rank test is implemented to judge the best suitable algorithm for solar water heater optimization since it's difficult to judge which algorithm performed the best overall. This was done by considering each algorithm's capability to obtain the best, worst, and average solutions, and success rate. The results of the Friedman rank test are presented in Table 7.23, and its graphical representation is given in Fig. 7.10. The results are presented in the form of a Friedman value, a normalized

**Table 7.23** Friedman rank test results for solar water heater optimization

Algorithms	Friedman value	Normalized value	Rank
GA	29.5	0.338983	5
PSO	32.5	0.307692	8
DE	27	0.37037	4
ABC	10	1	1
CSA	30	0.333333	6
TLBO	30.5	0.327869	7
SOS	40.5	0.246914	9
WWO	42.5	0.235294	10
HTS	16	0.625	2
PVS	23.5	0.425532	3
SCA	48	0.208333	11

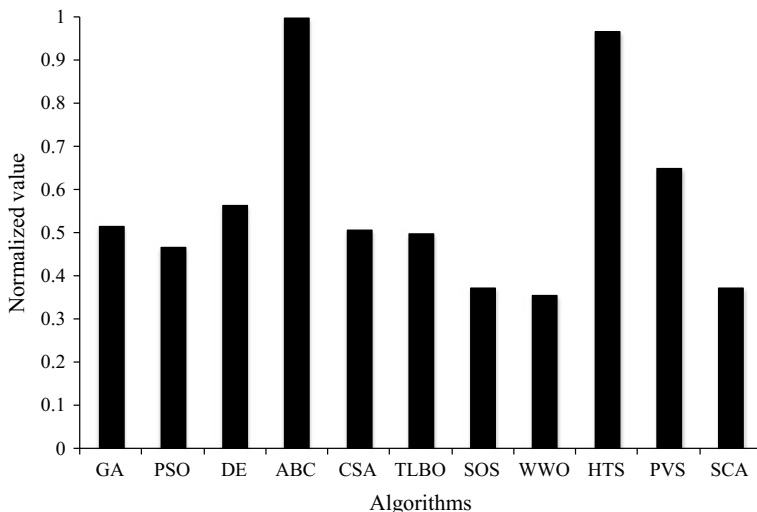


**Fig. 7.10** Graphical presentation of Friedman rank test for solar water heater optimization

**Table 7.24** The optimized operating condition of the solar water heater

Operating parameters	Optimized value
<i>Operating variable</i>	
Mass flow rate ( $\dot{m}$ ) (kg/s)	2
Tube diameter ( $D_i$ ) (mm)	5
Collector length ( $L_c$ ) (m)	0.5
Collector width ( $W_c$ ) (m)	3.2
Insulator thickness ( $t$ ) (mm)	150
<i>Constrain</i>	
The temperature rise of the water per circulation ( $\Delta T_{\text{circulation}}$ )	0.25
<i>Objective function</i>	
Thermal efficiency ( $\eta_{\text{th}}$ )	0.7887

value with ‘1’ being the best, and its rank. It can be observed from the results that ABC has obtained first rank followed by HTS and PVS algorithms.

The optimized operating parameters of the solar water heater obtained using the ABC algorithm are presented in Table 7.24. It can be noted from the results that the solar water heater with a maximum mass flow rate, insulation thickness, minimum tube diameter, and the lowest collector length results in the maximum thermal efficiency. On the other hand, collector width produced a conflicting effect on achieving the maximum thermal efficiency. Note that the temperature rise of the water per circulation is at the limiting value in the optimized operating condition of the solar water heater.

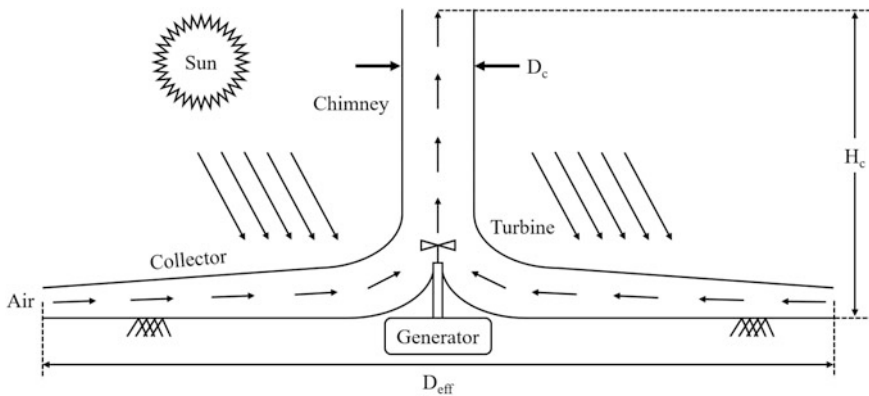


**Fig. 7.11** Schematic diagram of the solar chimney power plant

## 7.6 Solar Chimney Power Plant

A solar chimney power plant is a solar power-generating unit in which a solar air collector and central updraft tower are used to generate solar induced air flow. This drives the turbines to generate electricity. The solar chimney power plant belongs to solar thermal technology. A solar chimney power generator has three major components: a circular solar collector, a tall cylinder in the center of the solar collector (i.e., solar chimney), and a set of air turbines around the bottom of the solar chimney. A typical solar chimney power plant is shown in Fig. 7.11. It can be observed from the figure that the solar collector covers a large area. The air trapped into the collector is heated through solar energy. The air then tries to go up using the chimney. As it flows through the chimney, it drives the turbines situated at the chimney entrance, thus generating power.

Earlier, researchers have reported various works related to the analysis and optimization of solar chimney power plant. Pasumarthi and Sherif (1998) designed and developed the prototype of the solar chimney power plant to analyze its performance. Pretorius and Kröger (2006) evaluated the influence of a convective heat transfer equation, turbine inlet loss coefficient and the various types of soil on the performance of a large-scale solar chimney power plant. Pretorius and Kröger (2008) performed the thermo-economic optimization of a large-scale solar chimney power plant. The authors identified the effects of the collector's height, chimney height, and chimney diameter on the economic aspect of the power plant. Tingzhen et al. (2008) carried out numerical simulations of the solar chimney power plant systems coupled with the turbine. They developed the mathematical model of heat transfer and flow by dividing the whole system into three regions: the collector, the chimney, and the turbine. Fluri et al. (2009) developed an economic model to perform the cost analysis of a solar chimney power plant. The authors compared the

results obtained using their model with the other available model. They also investigated the impact of carbon credits on the leveled electricity cost.

Larbi et al. (2010) presented the performance analysis of a solar chimney power plant used to provide electric power in the villages located in the southwestern Algerian region. Xu et al. (2011) carried out the numerical simulations on airflow, heat transfer, and power output characteristics of a solar chimney power plant model with energy storage layer. The authors established a mathematical model to analyze the flow and heat transfer characteristics of the solar chimney power plant system. The authors also identified the impact of solar radiation and pressure drop across the turbine on the output power of the solar chimney power plant. Xu et al. (2011) carried out the energy and exergy analysis of the solar power tower system using molten salt as the heat transfer fluid. The authors analyzed the energy and exergy losses in each component of the system to identify the causes and locations of thermodynamic imperfection. The authors concluded that the maximum exergy loss occurs in the receiver system while the main energy loss occurs in the power cycle system. Hamdan (2011) performed the analysis of a solar chimney power plant for the Arabian Gulf region. The author developed an analytical model to predict the performance of the solar chimney power plant and compared the obtained results with the available experimental results. Najmi et al. (2012) carried out the feasibility study of a solar chimney power plant located at Kerman city in Iran. The authors performed the optimization of the affected parameters to maximize the power output. Furthermore, the economic analysis of the power plant is also presented and discussed.

Kasaeian et al. (2014) presented a mathematical model of a solar chimney power plant and performed its geometric optimization. Further, the authors validate numerical predictions through comparison with the experimental data of the solar chimney plant. Gholamalizadeh and Kim (2014) performed the multi-objective optimization of a solar chimney power plant using a multi-objective genetic algorithm. The authors considered maximization of efficiency, power output and minimization of a total expenditure of the power plant as an objective function. Further, the parametric study was also conducted to evaluate the effects of variation of design parameters on different objective functions. Dehghani and Mohammadi (2014) carried out the multi-objective optimization of a solar chimney power plant. The authors considered the maximization of power output and minimization of total cost of the system as an objective function and adopted NSGA-II as an optimization tool. Furthermore, the authors performed a sensitivity analysis to identify the effects of design variables on the optimized value of objective function. Shariatzadeh et al. (2015) carried out the modeling and optimization of a solar chimney cogeneration power plant combined with solid oxide electrolysis. Finally, Li et al. (2016) developed an unsteady comprehensive mechanism model and a streamlined unsteady mechanism model of a solar chimney power plant to analyze the energy conversion and transmission of the system. The authors observed that there exists a strong correlation between the chimney's height and the power quality factor, as well as a negative correlation between the solar collector radius and the power quality factor.

### 7.6.1 Thermal Model

In this part of the work, a solar chimney power plant is considered for the optimization. The schematic arrangement of the solar chimney power plant is shown in Fig. 7.11. The thermal model of a solar water heater presented here is based on the previous work of Dehghani and Mohammadi (2014).

The following equations give the collector efficiency of the solar chimney power plant:

$$\eta_{\text{coll}} = \frac{\dot{Q}}{A_{\text{coll}} \cdot G} = \frac{\dot{m} c_p \Delta T}{A_{\text{coll}} \cdot G} \quad (7.144)$$

where  $\dot{Q}$  is the heat received by air,  $G$  is the solar radiation,  $A_{\text{coll}}$  is the collector area,  $\dot{m}$  is the mass flow rate of air, and  $\Delta T$  is the temperature difference of the air between the collector's inlet ( $T_a$ ) and outlet ( $T_2$ ) and is given by

$$\dot{m} = \rho_2 V_2 A_{\text{ch}} \quad (7.145)$$

$$\Delta T = T_2 - T_a \quad (7.146)$$

where  $A_{\text{ch}}$  is the chimney area,  $V_2$  is the air's stream velocity at the collector outlet, and  $\rho$  is the air density.

On the other hand, the collector efficiency ( $\eta_{\text{coll}}$ ) is based on the effective absorption coefficient ( $\alpha$ ) and convective energy loss coefficient ( $\beta$ ) and is given by

$$\eta_{\text{coll}} = \alpha - \frac{\beta(T_{\text{pm}} - T_a)}{G} \quad (7.147)$$

where  $T_{\text{pm}}$  is the mean plate's temperature.

The air stream velocity at the collector outlet ( $V_2$ ) can be calculated as below:

$$V_2 = \frac{\alpha A_{\text{coll}} G - \beta A_{\text{coll}} (T_{\text{pm}} - T_a)}{\rho_2 A_{\text{ch}} C_p (T_2 - T_a)} \quad (7.148)$$

where  $C_p$  is the specific heat of air.

The mean air temperature ( $T_{\text{ma}}$ ) is obtained using the following equation:

$$T_{\text{ma}} = T_a + (1 - F_R) \frac{\rho_2 V_2 A_{\text{ch}} C_p (T_2 - T_a)}{\beta A_{\text{coll}} F_R} \quad (7.149)$$

where  $F_R$  denotes the collector's heat removal factor and is given by the following equation:

$$F_R = \frac{\dot{m}C_p}{\beta A_{\text{coll}}} \left( 1 - \exp\left(\frac{\beta A_{\text{coll}} F'}{\dot{m}C_p}\right) \right) \quad (7.150)$$

where  $F'$  is the collector flow factor. The relation between collector flow factor and heat removal factor is defined as

$$Z = \frac{F_R}{F'} \quad (7.151)$$

The relation between the collector flow factor and mean air temperature ( $T_{\text{ma}}$ ) is given as

$$T_{\text{ma}} = T_a + (1 + F') \frac{\rho_2 V_2 A_{\text{ch}} C_p (T_2 - T_a)}{\beta A_{\text{coll}} F_R} \quad (7.152)$$

Furthermore, the mean air temperature can be calculated by averaging mean plate temperature and collector inlet temperature as follows.

$$T_{\text{ma}} = \frac{T_{\text{pm}} + T_a}{2} \quad (7.153)$$

The chimney's efficiency  $\eta_{\text{ch}}$  of the solar chimney power plant can be given by

$$\eta_{\text{ch}} = \frac{g H_{\text{ch}}}{C T_a} \quad (7.154)$$

where  $g$  is the gravitational acceleration, and  $H_{\text{ch}}$  is the chimney's height.

The efficiency of the turbine used in the solar chimney power plant is given by

$$\eta_t = \frac{P_{\text{tc}} - P_{\text{cl}}}{P_{\text{tc}}} = 1 - \frac{V_2^2}{2 C_p \Delta T \eta_{\text{ch}}} \quad (7.155)$$

where  $P_{\text{tc}}$  is the power of the theoretical air cycle and  $P_{\text{cl}}$  is power loss due to exit kinetic energy.

Turbine power output  $P_o$  can be calculated as follows:

$$P_o = \dot{Q} \eta_p \eta_{\text{ge}} = A_{\text{coll}} G \eta_{\text{coll}} \eta_t \eta_{\text{ch}} \eta_{\text{ge}} \quad (7.156)$$

where  $\eta_{\text{ge}}$  is the combined blade, transmission, and generator efficiency and  $\eta_p$  is the plant efficiency and is given by the following equation.

$$\eta_p = \eta_{\text{coll}} \eta_t \eta_{\text{ch}} \quad (7.157)$$

Based on the above thermal model, the objective function for the present work is defined in the next section.

### 7.6.2 Case Study, Objective Function Description, and Constraints

A solar chimney power plant needs to be designed and optimized for the maximum power output ( $P_o$ ). The solar irradiance is considered as  $800 \text{ W/m}^2$ . The air inlet temperature to the collector ( $T_a$ ) is considered as  $25^\circ\text{C}$ . For this case, three design parameters—the collector diameter ( $D_{\text{coll}}$ ), the chimney diameter ( $D_{\text{ch}}$ ), and the chimney's height ( $H_{\text{ch}}$ )—are considered. The upper and lower bounds of the design variables are presented in Table 7.25.

As mentioned above, the maximum power output ( $P_o$ ) of the solar chimney power plant is taken as an objective function in the present study. The objective function of the solar chimney power plant is formulated as below:

$$\begin{cases} \text{Minimize } f(X) = P_o(X) \\ X = [x_1, x_2, x_3, \dots, x_D], \quad x_{i,\text{minimum}} \leq x_i \leq x_{i,\text{maximum}}, \quad i = 1, 2, 3, \dots, D \end{cases} \quad (7.158)$$

where  $X$  is the vector of design variables, bounded between its minimum and maximum values.

The next section describes the results and discussion of the case study.

### 7.6.3 Results and Discussion

The considered problem of a solar chimney power plant is investigated using 11 different metaheuristic approaches to obtain the maximum power output. As all these methods are stochastic in their working, each algorithm is implemented 100 times on the considered problem to estimate the statistical variations of the algorithms. Each algorithm is implemented with the population size of 50, and termination criteria are set as 100,000 function evaluations. The results obtained using each algorithm are presented in the form of the best solution, the worst solution, average solution, standard deviation, and success rate (obtained via 100 runs). These results are illustrated in Table 7.26. Here, the infeasible solutions (i.e., affected by penalty) are eliminated. Then, the worst solution, average solution, standard

**Table 7.25** Ranges of design variables for solar chimney power plant optimization

Design variable	Lower bound	Upper bound
Collector diameter ( $D_{\text{coll}}$ ) (m)	100	950
Chimney diameter ( $D_{\text{ch}}$ ) (m)	5	85
Chimney height ( $H_{\text{ch}}$ ) (m)	60	785

**Table 7.26** Comparative results of different algorithms for solar chimney power plant optimization

Algorithms	Best	Worst	Average	SD	Success rate (%)
GA	7989.3	7602.43	7872.2	1.41E+02	36
PSO	7982.23	7438.71	7802.58	1.92E+02	24
DE	7989.66	7428.9	7838.27	1.93E+02	32
ABC	7989.65	7665.1	7880.96	1.16E+02	32
CSA	7984.43	7425.01	7784.89	2.14E+02	24
TLBO	7987.17	7417.78	7792.69	2.49E+02	28
SOS	7983.13	7398.25	7783.08	2.27E+02	24
WWO	7981.83	7382.36	7736.27	2.45E+02	28
HTS	7989.53	7518.18	7906.14	1.32E+02	28
PVS	7987.2	7378.88	7774.73	2.24E+02	20
SCA	7987.15	7347.34	7741.02	2.71E+02	24

deviation, and success rate (which are obtained by considering a 0.1% variation from the global optimum value) are obtained.

It can be observed from the comparative results that the GA, DE, HTS, and SCA algorithm performed the best, producing almost identical maximum power output of the solar chimney power plant. That being said, the average performance of the HTS algorithm was the highest and the success rate of GA in obtaining the optimum value was the highest (PVS algorithm is the lowest). As such, it is difficult to judge the performance of the algorithm as all the algorithms have produced varying performances. So, the Friedman rank test is implemented to judge the best suitable algorithm for solar chimney power plant optimization considering its algorithms capability to obtain the best, worst, and average solutions, and success rate. The results of the Friedman rank test are presented in Table 7.27, and its graphical representation is given in Fig. 7.12. The results are presented in the form of

**Table 7.27** Friedman rank test results solar chimney power plant optimization

Algorithms	Friedman value	Normalized value	Rank
GA	13	0.961538	2
PSO	31.5	0.396825	5
DE	17.5	0.714286	4
ABC	12.5	1	1
CSA	35.5	0.352113	7
TLBO	35	0.357143	6
SOS	41.5	0.301205	8
WWO	45	0.277778	11
HTS	14	0.892857	3
PVS	42	0.297619	9
SCA	42.5	0.294118	10

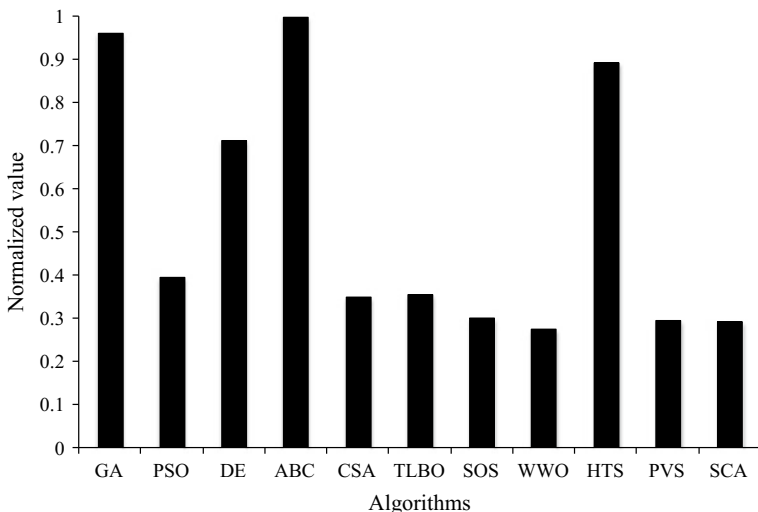


**Fig. 7.12** Graphical presentation of Friedman rank test solar chimney power plant optimization

**Table 7.28** The optimized operating condition of a solar chimney power plant

Operating parameters	Optimized value
<i>Operating variable</i>	
Collector diameter ( $D_{\text{coll}}$ ) (m)	950
Chimney diameter ( $D_{\text{ch}}$ ) (m)	33.2
Chimney height ( $H_{\text{ch}}$ ) (m)	784
<i>Objective function</i>	
Power output (Po) (kW)	7989.65

Friedman value, a normalized value with ‘1’ being the best performing algorithm, and its rank. It can be observed from the results that ABC has obtained the first rank followed by GA and HTS algorithms.

The optimized operating parameters of the solar chimney power plant obtained using the ABC algorithm are presented in Table 7.28. It can be noted from the results that the solar chimney power plant with the maximum collector diameter and chimney height results in the maximum power output.

## 7.7 Turbojet Engine

The turbojet engine is usually used in aircraft. It consists of a gas turbine with a propelling nozzle, compressor, and combustion chamber. The compressed air from the compressor is used for fuel combustion in the combustion chamber and then

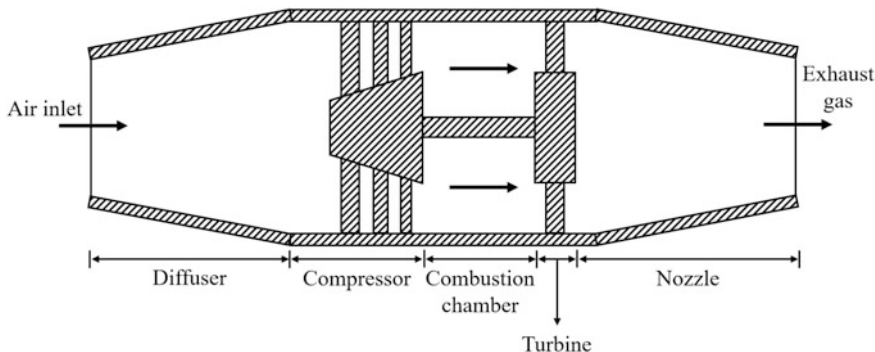


**Fig. 7.13** Schematic arrangement of the turbojet engine

allowed to expand through the turbine. The turbine exhaust is then expanded in the propelling nozzle, where it is accelerated to a high speed to provide thrust (Mattingly 1996). The performance parameters of the turbojet engine including specific thrust, thermal efficiency, propulsive efficiency, specific fuel consumptions, etc. are sensitive to different operating parameters like the compressor pressure ratio, the gas temperature at the inlet of a turbine, and the flight Mach number. Figure 7.13 shows the schematic arrangement of the turbojet engine.

Earlier, researchers have reported various works related to the analysis and optimization of the turbojet engine. By implementing the genetic algorithm, Atashkari et al. (2005) obtained a set of Pareto fronts between the conflicting thermodynamic objectives of the turbojet engine. Nariman-Zadeh et al. (2005) presented the inverse mapping of thermodynamically optimized ideal turbojet engines using neural networks and evolutionary algorithms. Benini et al. (2009) investigated the merits and drawbacks of the direct water/steam injection in a combustion chamber of a turbojet engine. The authors evaluated the effects of the water/steam injection on the NO/CO emission of the turbojet engine. Turan (2012) investigated the effects of the compressor pressure ratio and turbine inlet temperature on the exergetic performance of the small turbojet engine. The author concluded that the higher the turbine inlet's temperature, the lower the exergy efficiency of the small turbojet engine. Badami et al. (2013, 2014) reported numerical and experimental results regarding the influence of alternative fuels on the emission of a small scale turbojet engine. Guo et al. (2014) carried out the optimization of the centrifugal compressor of a mini turbojet engine. The authors considered the compressor's efficiency, the pressure ratio and the worked input to the compressor as objective functions.

Noori et al. (2015) carried out the multi-objective optimization of the turbojet engine using the genetic algorithm as an optimization tool. Tavakolpour-Saleh et al. (2015) presented both parametric and nonparametric models of a prototype turbojet engine based on the experimental observations as well by considering the fuel flow rate of the engine as the input and shaft speed as the output. Najjar and Balawneh (2015) focused on the gas turbine of a turbojet engine. The authors investigated the effects of the operating parameters of gas turbine on the performance parameter

(specific thrust and specific fuel consumption) of the turbojet engine. Balli (2017) presented the exergy analysis of a military aircraft turbojet engine. In the work, the author observed that there is a higher unavoidable exergy destruction rate compared to the avoidable rate. Finally, Patel et al. (2018) performed several objective thermodynamic optimization functions of a turbojet engine. The authors considered the maximization of thermal efficiency, propulsive efficiency, specific thrust, and minimization of specific fuel consumption of the turbojet engine as an objective function. They then adopted a multi-objective heat transfer search algorithm as an optimization tool. The authors also used the decision-making method to select the best solutions from the available Pareto points.

### 7.7.1 Thermal Model

In this part of the work, a turbojet engine is considered for the optimization. The schematic arrangement of the turbojet engine is shown in Fig. 7.13. The thermal model of turbojet engine presented here is based on the previous work of Atashkari et al. (2005) and Patel et al. (2018).

The total temperature ratio ( $T_i^0$ ) at the inlet of the engine is given by

$$T_i^0 = 1 + \frac{\gamma - 1}{2} M_a^2 \quad (7.159)$$

where  $M_a$  is the flight Mach number.  $\gamma$  is the ratio of specific heat and is estimated by

$$R = \frac{\gamma - 1}{\gamma} C_p \quad (7.160)$$

The total temperature ratio ( $T_{ch}^0$ ) at the combustion chamber is calculated as

$$T_{ch}^0 = 1 - \frac{T_i^0}{H_{ch}^0} (T_c^0 - 1) \quad (7.161)$$

where  $H_{ch}^0$  is the total enthalpy ratio at the combustion chamber and  $T_c^0$  is the total temperature ratio at the compressor. They are expressed by

$$H_{ch}^0 = \frac{T_c}{T_0} \quad (7.162)$$

$$T_c^0 = (p_r)^{\gamma-1/\gamma} \quad (7.163)$$

where  $T_0$  is the inlet temperature,  $T_c$  is the combustion chamber exit temperature, and  $p_r$  is the pressure ratio of the compressor.

The combustion gas velocity at the exit of the expansion nozzle is given by

$$V_o = a^0 \left( \frac{H_{ch}^0}{T_i^0 T_c^0} (T_i^0 T_{ch}^0 T_c^0 - 1) \frac{2}{\gamma - 1} \right)^{1/2} \quad (7.164)$$

where  $a^0$  is the sonic velocity at the flight's inlet and is given by

$$a^0 = (\gamma R T_o)^{1/2} \quad (7.165)$$

The specific fuel consumption of the engine is expressed as

$$SFC = \frac{fa}{ST} \quad (7.166)$$

where  $fa$  and  $ST$  are the fuel-air ratio and specific thrust, respectively, and are calculated by

$$fa = \frac{c_p T^0}{c_h} (H_{ch}^0 - T_i^0 T_c^0) \quad (7.167)$$

$$ST = a^0 \left( \frac{V^0}{a^0} - M_a \right)_o \quad (7.168)$$

where  $c_h$  is the heating value of the fuel. The thermal efficiency of the turbo jet engine is given by

$$\eta_t = 1 - \frac{1}{T_i^0 T_c^0} \quad (7.169)$$

Finally, the propulsive efficiency of the turbo jet engine is given by

$$\eta_p = 1 - \frac{2M_a}{\frac{V^0}{a^0} + M_a} \quad (7.170)$$

Based on the above thermal model, the objective function for the present work is defined in the next section.

### 7.7.2 Case Study, Objective Function Description, and Constraints

A turbojet engine operating in the surrounding air temperature of 216.6 K needs to be optimized for the maximum thermal efficiency ( $\eta_t$ ). In this case, two design variables

**Table 7.29** Ranges of design variables for turbojet engine optimization

Design variable	Lower bound	Upper bound
Compressor pressure ratio	1	40
Turbine inlet temperature (K)	1400	1666

—the compressor pressure ratio and the turbine inlet temperature—are considered. The upper and lower bounds of design variables are presented in Table 7.29.

As mentioned above, the maximization of the thermal efficiency of the turbojet engine is taken as an objective function in the present study. Note that the operating parameters resulting in the maximum thermal efficiency also satisfy the flight Mach number ( $M_a$ ), propulsive efficiency ( $\eta_p$ ), specific thrust (ST), and specific fuel consumption (SFC) constraints. As such, the objective function of the turbojet engine is formulated as below:

$$\left\{ \begin{array}{l} \text{Minimize } f(X) = \eta_t(X) + \sum_{j=1}^n G_1(g_j(X))^2 \\ X = [x_1, x_2, x_3, \dots, x_D], \quad x_{i,\text{minimum}} \leq x_i \leq x_{i,\text{maximum}}, \quad i = 1, 2, 3, \dots, D \\ g_j(X) \leq 0, \quad j = 1, 2, 3, \dots, n \end{array} \right. \quad (7.171)$$

where  $X$  is the vector of design variables, bounded between its minimum and maximum values, and  $G_1$  is the penalty parameter. The entire term takes into account the effects of constraints violation and is utilized when the constraint's violation takes place.  $g_j(X)$  indicates the constraints. The following constraints are considered for the turbojet engine.

$$\text{Flight Mach number, } (M_a) \leq 1 \quad (7.172)$$

$$\text{Propulsive efficiency, } (\eta_p) \geq 0.4 \quad (7.173)$$

$$\text{Specific thrust, } (\text{ST}) \geq 0.88 \text{ kN/kg/s} \quad (7.174)$$

$$\text{Specific fuel consumption(SFC)} \leq 0.0275 \text{ kg/s/kN} \quad (7.175)$$

The next section describes the results and discussion of the case study.

### 7.7.3 Results and Discussion

The considered problem of the turbojet engine is investigated using 11 different metaheuristic approaches to obtain the maximum thermal efficiency. As all these methods are stochastic in their working, each algorithm is implemented 100 times on the considered problem to estimate the statistical variations of the algorithms.

Each algorithm is implemented with the population size of 50, and termination criteria are set as 100,000 function evaluations. The results obtained using each algorithm are presented in the form of the best solution, the worst solution, average solution, standard deviation, and success rate. Table 7.30 presents the results. In addition, the infeasible solutions (i.e., affected by penalty) are eliminated. Finally, the worst solution, average solution, standard deviation, and success rate are obtained. Note that the success rate of the algorithm is obtained by considering a 0.1% variation from the global optimum value.

It can be observed from the comparative results that the algorithms performed well, producing almost identical maximum thermal efficiency of the turbojet engine. That being said, the average performance of the DE and CSA, which are almost identical, was better. In addition, the success rate of TLBO, HTS, and PVS algorithms in obtaining the optimum value was the highest while GA was the lowest. It can be observed from the results that it is difficult to judge the best performing as they all produced varying results in obtaining best, worst, and average results, and success rate. So, the Friedman rank test is implemented to judge the best suitable algorithm for turbojet engine optimization considering the above points. The results of the Friedman rank test are presented in Table 7.31, and its graphical representation is given in Fig. 7.14. The results are presented in the form of a Friedman value, a normalized value with ‘1’ being best performing algorithm, and the algorithm’s rank. It can be observed from the results that DE and CSA have obtained the first rank followed by TLBO and PVS algorithms.

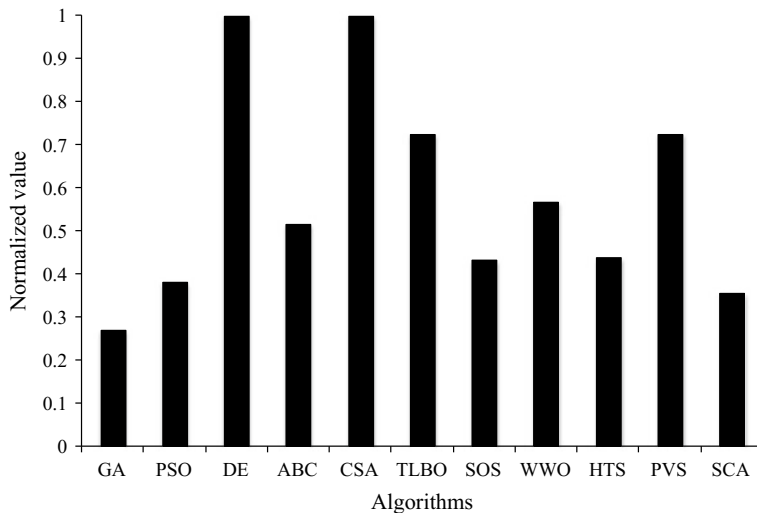
The optimized operating parameters of the turbojet engine obtained using the DE algorithm are presented in Table 7.32. It can be noted from the results that the maximum compressor pressure ratio results in the maximum thermal efficiency of the turbojet engine. On the other hand, the Turbine inlet temperature produced a conflicting effect on achieving the maximum thermal efficiency of the engine. In addition for this case, the flight Mach number, propulsive efficiency, and specific thrust constraints were all at the limit value while the specific fuel consumption constraint was below the limiting value.

**Table 7.30** Comparative results of different algorithms for turbojet engine optimization

Algorithms	Best	Worst	Average	SD	Success rate (%)
GA	0.70954	0.46153	0.67715	7.03E-02	56
PSO	0.70954	0.51739	0.69012	5.27E-02	73
DE	0.70954	0.67321	0.70519	9.77E-03	80
ABC	0.70954	0.51739	0.69085	5.28E-02	80
CSA	0.70954	0.67339	0.70523	9.71E-03	80
TLBO	0.70954	0.49456	0.69803	4.34E-02	84
SOS	0.70954	0.51739	0.68925	5.26E-02	74
WWO	0.70954	0.52852	0.6912	4.97E-02	76
HTS	0.70954	0.46153	0.69085	5.90E-02	84
PVS	0.70954	0.46153	0.69205	5.88E-02	84
SCA	0.70954	0.4703	0.68967	5.97E-02	76

**Table 7.31** Friedman rank test results for turbojet engine optimization

Algorithms	Friedman value	Normalized value	Rank
GA	53.5	0.271028	9
PSO	38	0.381579	7
DE	14.5	1	1
ABC	28	0.517857	4
CSA	14.5	1	1
TLBO	20	0.725	2
SOS	33.5	0.432836	6
WWO	25.5	0.568627	3
HTS	33	0.439394	5
PVS	20	0.725	2
SCA	40.5	0.358025	8

**Fig. 7.14** Graphical presentation of Friedman rank test for turbojet engine optimization**Table 7.32** The optimized operating condition of the turbojet engine

Operating parameters	Optimized value
<i>Operating variable</i>	
Compressor pressure ratio	40
Turbine inlet temperature (K)	1655.32
<i>Constrain</i>	
Flight Mach number ( $M_a$ )	1
Propulsive efficiency ( $\eta_p$ )	0.401
Specific thrust (ST) (kN/kg/s)	0.881
Specific fuel consumption (SFC) (kg/s/kN)	0.0216
<i>Objective function</i>	
Thermal efficiency ( $\eta_t$ )	0.70954

## References

- Akpınar E.K. and Koçyiğit F. (2010) 'Energy and exergy analysis of a new flat-plate solar air heater having different obstacles on absorber plates', *Applied Energy*, vol. 87(11), 3438–3450.
- Alta D., Bilgili E., Ertekin C. and Yaldız O. (2010) 'Experimental investigation of three different solar air heaters, energy and exergy analyses', *Applied Energy*, vol. 87(10), 2953–2973.
- Altfeld K., Leiner W. and Fiebig M. (1988) 'Second law optimization of flat plate solar air heaters Part I The concept of net exergy flow and the modeling of solar air heaters', *Solar Energy*, vol. 41(2), 127–132.
- Atashkari K., Nariman-Zadeh N., Pilechi A., Jamali A. and Yao X. (2005) 'Thermodynamic Pareto optimization of turbojet engines using multi-objective genetic algorithms', *International Journal of Thermal Sciences*, vol. 44(11), 1061–1071.
- Atia D.M., Fahmy F.H., Ahmed N.M. and Dorrah H.T., (2012) 'Optimal sizing of a solar water heating system based on a genetic algorithm for an aquaculture system', *Mathematical and Computer Modelling*', vol. 55(3–4), 1436–1449.
- Badami M., Nuccio P., Pastrone D. and Signoretto A. (2014) 'Performance of a small-scale turbojet engine fed with traditional and alternative fuels', *Energy Conversation and Management*', vol. 82, 219–228.
- Badami M., Nuccio P. and Signoretto A. (2013) 'Experimental and numerical analysis of a small scale turbojet engine', *Energy Conversation and Management*, vol. 76, 225–233.
- Balli O. (2017) 'Advanced exergy analyses to evaluate the performance of a military aircraft turbojet engine (TJE) with afterburner system, Splitting exergy destruction into unavoidable/ avoidable and endogenous/exogenous', *Applied Thermal Engineering* vol. 111, 152–169.
- Benini E., Pandolfo S. and Zoppellari S. (2009) 'Reduction of NO emissions in a turbojet combustor by direct water/steam injection, Numerical and experimental assessment', *Applied Thermal Engineering*, vol. 29, 3506–3510.
- Castro MM, Songa TW and Pinto JM. (2000) 'Minimization of operational costs in cooling water systems', *Chemical Engineering Research and Design*, vol. 78(2), 192–201.
- Chaabane M., Mhiri H. and Bournot, P. (2014) 'Thermal performance of an integrated collector storage solar water heater (ICSSWH) with phase change materials (PCM)', *Energy conversion and management*, vol. 78, 897–903.
- Chein R. and Huang G. (2005) 'Analysis of microchannel heat sink performance using nano fluids', *Applied thermal engineering*, vol. 25(17–18), 3104–3114.
- Cortinovis GF, Paiva JL, Song TW and Pinto JM. (2009) 'A systemic approach for optimal cooling tower operation', *Energy Conversation and Management*, vol. 50, 2200–2209.
- Dagdougui H., Ouammi A., Robba, M. and Sacile, R., (2011) 'Thermal analysis and performance optimization of a solar water heater flat plate collector, application to Tétouan (Morocco)', *Renewable and Sustainable Energy Reviews*, vol. 15(1), 630–638.
- Dehghani S. and Mohammadi A.H. (2014) 'Optimum dimension of geometric parameters of solar chimney power plants, A multi-objective optimization approach', *Solar Energy*, vol. 105, 603–612.
- Du Y., (2017) 'Advanced thermal management of a solar cell by a nano coated heat pipe plate A thermal assessment', *Energy Conservation Management*, vol. 134, 70–76.
- Dunn P, Reay D. (1976) *Heat Pipes*, Pergamon Press, New York.
- El-Dessouky HTA, Al-Haddad A and Al-Juwayhel F. (1997) 'A modified analysis of counter flow cooling towers', *ASME Journal of Heat Transfer*, vol. 119(3), 617–626.
- Elhabishi A. and Gryzgoridis J. (2016) 'Optimizing flat plate solar collector geometry for a solar water heating system', *Domestic Use of Energy (DUE), International Conference*, vol. 1(–6).
- Esarte J., Bernardini A., Blanco JM and Sancibrian R. (2016) 'Optimizing the design for a two phase cooling loop heat pipe, Part A, Numerical model, validation and application to a case study', *Applied Thermal Engineering*, vol. 99, 892–904.
- Esen M. and Esen H. (2005) 'Experimental investigation of a two-phase closed thermosyphon solar water heater', *Solar Energy*, vol. 79(5), 459–468.

- Faghri A, Taylor and Francis (1995) *Heat pipe science and technology*, Washington.
- Fluri T.P., Pretorius J.P., Van Dyk C., Von Backström T.W., Kröger D.G. and Van Zijl, G.P.A.G. (2009) 'Cost analysis of solar chimney power plants', *Solar Energy*, vol. 83(2), 246–256.
- Foli K., Okabe T., Olhofer M., Jin Y. and Sendhoff B. (2006) 'Optimization of micro heat exchanger, CFD, analytical approach and multi objective evolutionary algorithms', *International Journal of Heat and Mass Transfer*, vol. 49(5–6), 1090–1099.
- Gholamalizadeh E. and Kim M.H. (2014) 'Thermo-economic triple-objective optimization of a solar chimney power plant using genetic algorithms', *Energy*, vol. 70, 204–211.
- Gu H., Wang H., Gu Y. and Yao J. (2016) 'A numerical study on the mechanism and optimization of wind-break structures for indirect air-cooling towers', *Energy conversion and management*, vol. 108, 43–49.
- Gunerhan H. and Hepbasli A. (2007) 'Exergetic modeling and performance evaluation of solar water heating systems for building applications', *Energy and Buildings*, vol. 39(5), 509–516.
- Guo S., Duan F., Tang H., Lim SC and Yip MS. (2014) 'Multi-objective optimization for centrifugal compressor of mini turbojet engine', *Aerospace Science and Technology*, vol. 39, 414–425.
- Gupta M.K. and Kaushik S.C. (2008) 'Exergetic performance evaluation and parametric studies of solar air heater', *Energy*, vol. 33(11), 1691–1702.
- Hajabdollahi Z. and Hajabdollahi H. (2017) 'Thermo-economic modeling and multi objective optimization of solar water heater using flat plate collectors', *Solar Energy*, vol. 155, 191–202.
- Hamdan M.O. (2011). 'Analysis of a solar chimney power plant in the Arabian Gulf region', *Renewable Energy*, vol. 36(10), 2593–2598.
- Hobbi A. and Siddiqui K. (2009) 'Optimal design of a forced circulation solar water heating system for a residential unit in cold climate using TRNSYS', *Solar Energy*, vol. 83(5), 700–714.
- Husain A. and Kim K.Y. (2008a) 'Optimization of a microchannel heat sink with temperature dependent fluid properties', *Applied thermal engineering*, vol. 28 (8–9), 1101–1107.
- Husain A. and Kim K.Y. (2008b) 'Shape optimization of micro-channel heat sink for microelectronic cooling', *IEEE Transactions on Components and Packaging Technologies*, vol. 31(2), 322–330.
- Husain, A., & Kim, K. Y. (2008c). Multiobjective optimization of a microchannel heat sink using evolutionary algorithm. *Journal of Heat Transfer*, 130(11), 114505.
- Husain A. and Kim K.Y. (2010) 'Enhanced multi objective optimization of a microchannel heat sink through evolutionary algorithm coupled with multiple surrogate models', *Applied Thermal Engineering*, vol.30(13), 1683–1691.
- Hussein H.M.S. (2003) 'Optimization of a natural circulation two phase closed thermosyphon flat plate solar water heater', *Energy Conversion and Management*, vol. 44(14), 2341–2352.
- Jaisankar S., Radhakrishnan T.K. and Sheeba K.N. (2009) 'Experimental studies on heat transfer and friction factor characteristics of thermo siphon solar water heater system fitted with spacer at the trailing edge of twisted tapes', *Applied Thermal Engineering*, vol. 29(5–6), 1224–1231.
- Jalilian M., Kargarsharifabad H., Godarzi AA, Ghofrani A. and Shafii MB. (2016) 'Simulation and optimization of pulsating heat pipe flat plate solar collectors using neural networks and genetic algorithm, a semi-experimental investigation', *Clean Technology Environment*, vol. 18, 2251–2264.
- Jeong MJ, Kobayashi T and Yoshimura S. (2007), 'Multidimensional visualization and clustering for multi objective optimization of artificial satellite heat pipe design', *Journal of Mechanical Science and Technology*, vol. 21, 1964–1972.
- Jeyadevi S., Manikumar R., Gayathri P., Mahalakshmi B. and Seethalakshmi M. (2012), 'Optimization of solar air heater using differential evolution', *Third International Conference on Computing Communication & Networking Technologies (ICCCNT)*, vol. (1–7).
- Jin G.Y., Cai W.J., Lu L., Lee E.L. and Chiang A. (2007) 'A simplified modeling of mechanical cooling tower for control and optimization of HVAC systems', *Energy conversion and management*, vol. 48(2), 355–365.

- Jokar A, Godarzi AA, Saber M and Shafii MB (2016) ‘Simulation and optimization of a pulsating heat pipe using artificial neural network and genetic algorithm’, *Heat Mass Transfer*, vol. 52, 2437–2445.
- Karmare S.V. and Tikekar A.N. (2010) ‘Analysis of fluid flow and heat transfer in a rib grit roughened surface solar air heater using CFD’, *Solar Energy*, vol. 84(3), 409–417.
- Kasaeian A., Ghalamchi M. and Ghalamchi M. (2014) ‘Simulation and optimization of geometric parameters of a solar chimney in Tehran’, *Energy Conversion and Management*, vol. 83, 28–34.
- Khan W.A., Culham J.R., and Yovanovich M.M. (2009) ‘Optimization of microchannel heat sinks using entropy generation minimization method’, *IEEE Transactions on Components and Packaging Technologies*, vol. 32, 243–251.
- Khan, W. A., Yovanovich, M. M., & Culham, J. R. (2006, March). Optimization of microchannel heat sinks using entropy generation minimization method. In *Twenty-Second Annual IEEE Semiconductor Thermal Measurement and Management Symposium* (pp. 78–86). IEEE.
- Kim SJ, Seo JK, Do KH., (2003) ‘Analytical and experimental investigation on the operational characteristics and the thermal optimization of a miniature heat pipe with a grooved wick structure’, *International Journal of Heat and Mass Transfer*, vol. 46, 2051–2063.
- Kintner-Meyer M, Emery AF (1995) ‘Cost-optimal design for cooling towers’, *ASHRAE Journal*, vol. 37(4), 46–55.
- Kintner-Meyer M. and Emery AF. (1994) ‘Cost-optimal analysis of cooling towers’, *ASHRAE Transactions*, vol. 100, 92–101.
- Kiseev VM, Vlassov V and Muraoka I., (2010) ‘Experimental optimization of capillary structured for loop heat pipes and heat switches’, *Applied Thermal Engineering*, vol. 30, 1312–1319.
- Kiseev VM, Vlassov VV, Muraoka I. (2010) ‘Optimization of capillary structures for inverted meniscus evaporators of loop heat pipes and heat switches,’ *International Journal of Heat and Mass Transfer*, vol. 53, 2143–2148.
- Kloppers J.C. and Kröger D.G., (2004) ‘Cost optimization of cooling tower geometry’, *Engineering Optimization*, vol. 36(5), 575–584.
- Kröger, D. G. (2004). Air-cooled heat exchangers and cooling towers (Vol. 1). PennWell Books.
- Kulkarni G.N., Kedare S.B. and Bandyopadhyay S. (2007) ‘Determination of design space and optimization of solar water heating systems’, *Solar Energy*, vol. 81(8), 958–968.
- Kulkarni G.N., Kedare S.B. and Bandyopadhyay S. (2009) ‘Optimization of solar water heating systems through water replenishment’, *Energy Conversion and Management*, vol. 50(3), 837–846.
- Kumar S. and Saini R.P. (2009) ‘CFD based performance analysis of a solar air heater duct provided with artificial roughness’, *Renewable Energy*, vol. 34(5), 1285–1291.
- Kumar, A. and Kim M.H. (2014) ‘Numerical optimization of solar air heaters having different types of roughness shapes on the heated plate Technical note’, *Energy*, vol. 72, 731–738.
- Larbi S., Bouhdjar A. and Chergui T. (2010) ‘Performance analysis of a solar chimney power plant in the southwestern region of Algeria’, *Renewable and Sustainable Energy Reviews*, vol. 14(1), 470–477.
- Layek A., Saini J.S. and Solanki S.C. (2007) ‘Second law optimization of a solar air heater having chamfered rib groove roughness on absorber plate’, *Renewable Energy*, vol. 32(12), 1967–1980.
- Leng C., Wang X.D., Wang T.H. and Yan W.M. (2015) ‘Multi-parameter optimization of flow and heat transfer for a novel double-layered micro channel heat sink’, *International Journal of Heat and Mass Transfer*, vol. 84, 359–369.
- Li J. and Peterson G.P., (2007) ‘3-Dimensional numerical optimization of silicon based high performance parallel microchannel heat sink with liquid flow’, *International Journal of Heat and Mass Transfer*, vol. 50(15–16), 2895–2904.
- Li J., Guo H. and Huang S. (2016) ‘Power generation quality analysis and geometric optimization for solar chimney power plants’, *Solar Energy*, vol. 139, 228–237.

- Liang TS. and Hung YM. (2010) 'Experimental investigation of thermal performance and optimization of heat sink U-shape heat pipes', *Energy Conversation Management*, vol. 51, 2109–2116.
- Lima J.B.A., Prado R.T. and Taborianski V.M. (2006) 'Optimization of tank and flat-plate collector of solar water heating system for single-family households to assure economic efficiency through the TRNSYS program', *Renewable Energy*, vol. 31(10), 1581–1595.
- Liu D. and Garimella S.V. (2003) 'Analysis and optimization of the thermal performance of microchannel heat sinks', *International Electronic Packaging Technical Conference and Exhibition, ASME American Society of Mechanical Engineers*, vol. 557–565.
- Maheshkumar P. and Muraleedharan C. (2011) 'Minimization of entropy generation in flat heat pipe'. *International Journal of Heat and Mass Transfer*, vol. 54, 645–648.
- Mattingly JP. (1996) *Elements of Gas Turbine Propulsion*, McGraw-Hill, New York.
- Merkel F. Verdunstungshuhlung.(1925) 'Zeitschrift des Vereines Deutscher Ingenieure(VDI)', vol. 70, 123–128.
- Mittal M.K. and Varshney L. (2006) 'Optimal thermo hydraulic performance of a wire mesh packed solar air heater', *Solar Energy*, vol. 80(9), 1112–1120.
- Mohiuddin AKM, Kant /K. (1996a) 'Knowledge base for the systematic design of wet cooling towers part II, fill and other design parameters.' *International Journal of Refrigeration*, vol. 19 (1), 52–60.
- Mohiuddin AKM, Kant K. (1996b) 'Knowledge base for the systematic design of wet cooling towers part I, selection and tower characteristics', *International Journal of Refrigeration*, vol. 19(1), 43–51.
- Mohsen M.S., Al-Ghandoor A. and Al-Hinti I. (2009) 'Thermal analysis of compact solar water heater under local climatic conditions', *International Communications in Heat and Mass Transfer*, vol. 36(9), 962–968.
- Najjar YSH, Balawneh IAI. (2015) 'Optimization of gas turbines for sustainable turbojet propulsion' *Propulsion and Power Research*, vol. 4(2), 114–121.
- Najmi M., Nazari A., Mansouri H. and Zahedi G. (2012) 'Feasibility study on optimization of a typical solar chimney power plant', *Heat and Mass Transfer*, vol. 48(3), 475–485.
- Naphon P. (2005) 'On the performance and entropy generation of the double pass solar air heater with longitudinal fins', *Renewable Energy*, vol. 30(9), 1345–1357.
- Nariman-Zadeh N, Atashkari K, Jamali A, Pilechi A, Yao X. (2005) 'Inverse modelling of multi objective thermodynamically optimized turbojet engines using GMDH type neural networks and evolutionary algorithms', *Engineering Optimization*, vol. 37(5), 437–462.
- Noori F, Gorji M, Kazemi A, Nemati H. (2015) 'Thermodynamic optimization of ideal turbojet with afterburner engines using non-dominated sorting genetic algorithm', II - *Journal of Aerospace Engineering*, vol. 224, 1285–1296.
- Nwosu N.P. (2010) 'Employing exergy optimized pin fins in the design of an absorber in a solar air heater', *Energy*, vol. 35(2), 571–575.
- Pasumarthi N. and Sherif S.A. (1998) 'Experimental and theoretical performance of a demonstration solar chimney model Part II, experimental and theoretical results and economic analysis', *International Journal of Energy Research*, vol. 22(5), 443–461.
- Patel V.K. (2018) 'An efficient optimization and comparative analysis of ammonia and methanol heat pipe for satellite application', *Energy Conversion and Management*, vol. 165, 382–395.
- Patel VK, Savsani VJ, Mudgal A. (2018) 'Efficiency, thrust, and fuel consumption optimization of a subsonic/sonic turbojet engine', *Energy*, vol. 144, 992–1002.
- Peles Y., Koşar A., Mishra C., Kuo C.J. and Schneider B. (2005) 'Forced convective heat transfer across a pin fin micro heat sink', *International Journal of Heat and Mass Transfer*, vol. 48(17), 3615–3627.
- Ponce-Ortega JM, Serna-González M, Jiménez-Gutiérrez A (2010) 'Optimization model for re-circulating cooling water systems', *Computers and Chemical Engineering*, vol. 34, 177–195
- Pottler K., Sippel C.M., Beck A. and Fricke J. (1999) 'Optimized finned absorber geometries for solar air heating collectors', *Solar Energy*, vol. 67(1–3), 35–52.

- Pourmehran O., Rahimi-Gorji M., Hatami M., Sahebi S.A.R. and Domairry G. (2015) 'Numerical optimization of microchannel heat sink (MCHS) performance cooled by KKL based nano fluids in saturated porous medium', *Journal of the Taiwan Institute of Chemical Engineers*, vol. 55, 49–68.
- Prasad B.N., Kumar A. and Singh K.D.P. (2015) 'Optimization of thermo hydraulic performance in three sides artificially roughened solar air heaters', *Solar Energy*, vol. 111, 313–319.
- Pretorius J.P. and Kröger D.G. (2006) 'Critical evaluation of solar chimney power plant performance', *Solar Energy*, vol. 80(5), 535–544.
- Pretorius J.P. and Kröger D.G. (2008) 'Thermoeconomic optimization of a solar chimney power plant', *Journal of Solar Energy Engineering*, vol. 130(2), 021015.
- Qu W. and Mudawar I. (2002) 'Experimental and numerical study of pressure drop and heat transfer in a single phase microchannel heat sink', *International Journal of Heat and Mass Transfer*, vol. 45(12), 2549–2565.
- Rahimi Gorji M., Pourmehran O., Hatami M. and Ganji D.D. (2015) 'Statistical optimization of microchannel heat sink (MCHS) geometry cooled by different nano fluids using RSM analysis', *The European Physical Journal Plus*, vol. 130(2), 22.
- Rao R.V. and Patel V.K., (2011), 'Optimization of mechanical draft counter flow wet-cooling tower using artificial bee colony algorithm', *Energy Conversion and Management*, vol. 52(7), 2611–2622.
- Rao R.V., More K.C., Taler J. and Ocioń P. (2016) 'Dimensional optimization of a micro-channel heat sink using Jaya algorithm', *Applied Thermal Engineering*, vol. 103, 572–582.
- Rao RV, More KC. (2015) 'Optimal design of the heat pipe using TLBO (teaching-learning-based optimization) algorithm', *Energy*, vol. 80, 535–544.
- Reay D., Kew P., Butterwoth-Heinemann Oxford (2006) '*Heat pipes theory, design and applications*'.
- Roper CS. (2010) 'Multi-objective optimization for design of multifunctional sandwich panel heat pipes with micro-architected truss cores', *International journal of heat and fluid flow*, vol. 32, 239–248
- Rubio-Castro E., Serna-González M., Ponce-Ortega J.M. and Morales-Cabrera, M.A. (2011) 'Optimization of mechanical draft counter flow wet-cooling towers using a rigorous model', *Applied Thermal Engineering*, vol. 31(16), 3615–3628.
- Serna-González M., Ponce-Ortega J.M. and Jiménez-Gutiérrez A. (2010) 'MINLP optimization of mechanical draft counter flow wet-cooling towers', *Chemical Engineering Research and Design*, vol. 88(5–6), 614–625.
- Shariah A. and Shalabi B. (1997) 'Optimal design for a thermo siphon solar water heater.' *Renewable Energy*, vol. 11(3), 351–361.
- Shariah A., Al-Akhras M.A. and Al-Omari I.A. (2002) 'Optimizing the tilt angle of solar collectors', *Renewable Energy*, vol. 4, 587–598.
- Shariah A.M. and Löf G.O.G. (1996) 'The optimization of tank volume to collector-area ratio for a thermosyphon solar water heater', *Renewable Energy*, vol. 7(3), 289–300.
- Shariatzadeh O.J., Refahi A.H., Abolhassani S.S. and Rahmani M. (2015) 'Modeling and optimization of a novel solar chimney cogeneration power plant combined with solid oxide electrolysis/fuel cell', *Energy Conversion and Management*, vol. 105, 423–432.
- Shi PZ, Chua KM, Stephan CK, Wong YM, Tan YM. (2006) 'Design and performance optimization of miniature heat pipes in LTCC', *Journal of Physics*, vol. 34, 142–147.
- Smrekar J., Oman J., Sirok B. (2006) 'Improving the efficiency of natural draft cooling towers', *Energy Conversion and Management*, vol. 47, 1086–1100.
- Song JH, Zhang W, Li YQ, Yang ZW and Ming A. (2017) 'Exergy analysis and parameter optimization of heat pipe receiver with integrated latent heat thermal energy storage for space station in charging process', *Applied Thermal Engineering*, vol. 119, 304–311.
- Sousa FL, Vlassov VV and Ramos FM. (2004) 'Heat Pipe Design through generalized external optimization', *Heat Transfer Engineering*, vol. 25, 34–45.
- Söylemez M.S. (2001) 'On the optimum sizing of cooling towers', *Energy Conversion and Management*, vol. 42(7), 783–789.

- Söylemez M.S. (2004) 'On the optimum performance of forced draft counter flow cooling towers', *Energy Conversion and Management*, vol. 45(15–16), 2335–2341.
- Sun X, Ling L, Liao S, Chu Y, Fan S and Mo Y. (2018) 'A thermoelectric cooler coupled with a gravity assisted heat pipe. An analysis from heat pipe perspective', *Energy Conservation Management*, vol. 155, 230–242.
- Tang Y, Xiang JH, Wan ZP, Zhou W and Wu L. (2010) 'A novel miniaturized loop heat pipe', *Applied Thermal Engineering*, vol. 30, 1152–1158.
- Tavakolpour-Saleh AR, Nasib SAR, Sepasyan A and Hashemi SM. (2015) 'Parametric and nonparametric system identification of an experimental turbojet engine', *Aerospace Science and Technology*, vol. 43, 21–29.
- Tiari S, Mahdavi M, Qiu S. (2017) 'Experimental study of a latent heat thermal energy storage system assisted by a heat pipe network', *Energy Conversion and Management*, vol. 153, 362–373.
- Tingzhen M., Wei L., Guoling X., Yanbin X., Xuhu G. and Yuan P. (2008) 'Numerical simulation of the solar chimney power plant systems coupled with turbine', *Renewable Energy*, vol. 33(5), 897–905.
- Turan O. (2012) 'Exergetic effects of some design parameters on the small turbojet engine for unmanned air vehicle applications', *Energy*, vol. 46(1), 51–61.
- Vafai K. and Zhu L. (1999) 'Analysis of two-layered micro-channel heat sink concept in electronic cooling', *International Journal of Heat and Mass Transfer*, vol. 42(12), 2287–2297.
- Varun and Siddhartha (2010) 'Thermal performance optimization of a flat plate solar air heater using genetic algorithm', *Applied Energy*, vol. 87(5), 1793–1799.
- Varun Saini RP, Singal SK (2008) 'Investigation of thermal performance of solar air heater having roughness elements as a combination of inclined and transverse ribs on the absorber plate', *Renewable Energy*, vol. 33, 1398–405.
- Vlassov VV, Sousa FL and Takahashi WK (2006) 'Comprehensive optimization of a heat pipe radiator assembly filled with ammonia or acetone', *International Journal of Heat and Mass Transfer*, vol. 49, 4584–4595.
- Sousa FL, Vlassov VV and Ramos FM. (2004) 'Generalized external optimization: An application in heat pipe design', *Applied Mathematical Modelling*, vol. 28, 911–931.
- Walker WH, Lewis WK, McAdams WH and Gilliland ER. (1923) 'Principles of chemical engineering', Columbia, McGraw-Hill Inc.
- Wan Z, Wang X and Tang Y. (2012) 'Condenser design optimization and operation characteristics of a novel miniature loop heat pipe', *Energy Conversion and Management*, vol. 35, 35–42.
- Wang Z.H., Wang X.D., Yan W.M., Duan Y.Y., Lee D.J. and Xu J.L. (2011) 'Multi-parameters optimization for microchannel heat sink using inverse problem method', *International Journal of Heat and Mass Transfer*, vol. 54(13–14), 2811–2819.
- Wei X. and Joshi Y. (2003) 'Optimization study of stacked micro channel heat sinks for microelectronic cooling', *IEEE transactions on components and packaging technologies*, vol. 26(1), 55–61.
- Wu XP, Mochizuki M, Saito Y, Nguyen T, Wuttijumnong V and Wu D. (2003) 'Analyzing and modelling on optimized L-ratio of evaporator section to condenser section for micro heat pipe heat sinks', *Semiconductor Thermal Measurement and Management Symposium, IEEE Annual*, pp. 185–190.
- Xu C., Wang Z., Li X. and Sun F. (2011) 'Energy and exergy analysis of solar power tower plants', *Applied Thermal Engineering*, vol. 31(17–18), 3904–3913.
- Xu G., Ming T., Pan Y., Meng F. and Zhou C. (2011) 'Numerical analysis on the performance of solar chimney power plant system', *Energy Conversion and Management*, vol. 52(2), 876–883.
- Yadav, A.S. and Bhagoria, J.L., (2014) 'A CFD based thermo-hydraulic performance analysis of an artificially roughened solar air heater having equilateral triangular sectioned rib roughness on the absorber plate', *International Journal of Heat and Mass Transfer*, vol. 70, 1016–1039.
- Yaman K. and Arslan G. (2018) 'Modeling, simulation, and optimization of a solar water heating system in different climate regions', *Journal of Renewable and Sustainable Energy*, vol. 10(2), 023703.

- Yang M., Yang X., Li X., Wang Z. and Wang P. (2014) ‘Design and optimization of a solar air heater with offset strip fin absorber plate’, *Applied Energy*, vol. 113, 1349–1362.
- Yang X, Karamanoglu M, Luan T and Koziel S. (2014) ‘Mathematical modeling and parameter optimization of pulsating heat pipes’, *Journal of Computer Science and Technology*, vol. 5, 119–125.
- Zhai Z. and Fu S., (2006) ‘Improving cooling efficiency of dry-cooling towers under cross-wind conditions by using wind-break methods’, *Applied Thermal Engineering*, vol. 26(10), 1008–1017.
- Zhang C, Chen Y, Shi M and Peterson GP. (2009) ‘Optimization of heat pipe with axial “Ω”-shaped micro grooves based on a niched Pareto genetic algorithm (NPGA)’, *Applied Thermal Engineering*. vol. 29, 3340–3345.

# MATLAB Code of Optimization Algorithms

## 1. Genetic Algorithm (GA):

```
function GA()
run=1;
for i=1:run
    GA_Run(@F01);
end
%%%%%%%%%%%%%%%%%%%%%%%%%%%%%%%%%%%%%
function [OPTIONS, MinCost, AvgCost, InitFunction, CostFunction, FeasibleFunction, ...
    MaxParValue, MinParValue, Population, FeasibleFunction_1, CostFunction_1] =
Init(DisplayFlag, ProblemFunction, RandSeed)
OPTIONS.popsize = 50;
OPTIONS.Maxgen = 2000;
OPTIONS.numVar = 2;
if ~exist('RandSeed', 'var')
    RandSeed = round(sum(100*clock));
end
```

```
rand('state', RandSeed);
[InitFunction, CostFunction, FeasibleFunction,FeasibleFunction_1,CostFunction_1] =
ProblemFunction();
[MaxParValue, MinParValue, Population, OPTIONS] = InitFunction(OPTIONS);
Population = CostFunction(OPTIONS, Population);
Population = PopSort(Population);
AverageCost = ComputeAveCost(Population);
MinCost = [Population(1).cost];
AvgCost = [AverageCost];
return;
%%%%%%%%%%%%%%%
function [InitFunction, CostFunction, FeasibleFunction,FeasibleFunction_1,CostFunction_1] =
F01
InitFunction = @F01Init;
CostFunction = @F01Cost;
CostFunction_1 = @F01Cost_1;
FeasibleFunction = @F01Feasible;
FeasibleFunction_1 = @F01Feasible_1;
return;
function [MaxParValue, MinParValue, Population, OPTIONS] = F01Init(OPTIONS)
global MinParValue MaxParValue ll ul
ll=[13 0 ];
ul=[100 100];
MaxParValue = ul;
for popindex = 1 : OPTIONS.popsize
    for k = 1 : OPTIONS.numVar
        variable(k) =(ll(k)+(ul(k) - ll(k)) * rand);
    end
end
```

```
    Population(popindex).variable = variable;
end
return;
function [Population] = F01Cost(OPTIONS, Population)
global MinParValue MaxParValue
popsize = OPTIONS.popsize;
for popindex = 1 : popsize
    for k = 1 : OPTIONS.numVar
        x(k) = Population(popindex).variable(k);
    end
    Population(popindex).cost = objective(x);
end
return
function [Population_1] = F01Cost_1(OPTIONS, Population)
global MinParValue MaxParValue
popsize = size(Population,1);
Population_1 =[];
for popindex = 1 : popsize
    for k = 1 : OPTIONS.numVar
        x(k) = Population(popindex,k);
    end
    Population_1(popindex) = objective(x);
end
return
function [Population] = F01Feasible(OPTIONS, Population)
global MinParValue MaxParValue ll ul
for i = 1 : OPTIONS.popsize
    for k = 1 : OPTIONS.numVar
        Population(i).variable(k) = max(Population(i).variable(k), ll(k));
        Population(i).variable(k) = min(Population(i).variable(k), ul(k));
    end
end
return;
function [Population] = F01Feasible_1(OPTIONS, Population)
global MinParValue MaxParValue ll ul
for i = 1 : size(Population,1)
    for k = 1 : OPTIONS.numVar
        Population(i,k) = max(Population(i,k), ll(k));
        Population(i,k) = min(Population(i,k), ul(k));
    end
end
return;
%%%%%
function yy=objective(x)
p1=x(1);
p2=x(2);
```

```

z1=((p1-10)^3)+((p2-20)^3);
t1=-((p1-5)^2)-((p2-5)^2)+100;
t2=((p1-6)^2)+((p2-5)^2)-82.81;
nc=2;
    g1(1)=t1;
    g1(2)=t2;
    violate=0;
    for io=1:nc
        if g1(io)>0
            violate=violate+g1(io)^2;
        end
    end
yy=(z1)+(1e5*violate);
%%%%%%%
function GA_Run(ProblemFunction, DisplayFlag)
global ll ul
if ~exist('DisplayFlag', 'var')
    DisplayFlag = true;
end
[OPTIONS, MinCost, AvgCost, InitFunction, CostFunction, FeasibleFunction, ...
    MaxParValue, MinParValue, Population] = Init(DisplayFlag, ProblemFunction);
Xover_Type = 1;
OPTIONS.pcross = 0.8;
OPTIONS.pmutate = 0.05;
Keep = 1;
for GenIndex = 1 : OPTIONS.Maxgen
    for i = 1 : Keep
        variableKeep(i,:) = Population(i).variable;
        costKeep(i) = Population(i).cost;
    end
    InverseCost = [];
    for i = 1 : OPTIONS.popsize
        InverseCost = [InverseCost, 1 / (Population(i).cost+1e-20)];
    end
    for k = 1 : 2 : OPTIONS.popsize
        mate = [];
        for selParents = 1 : 2
            Random_Cost = rand * sum(InverseCost);
            Select_Cost = InverseCost(1);
            Select_index = 1;
            while Select_Cost < Random_Cost
                Select_index = Select_index + 1;
                if Select_index >= OPTIONS.popsize
                    break;
                end
                Select_Cost = Select_Cost + InverseCost(Select_index);
            end
        end
    end
end

```

```

    end
    mate = [mate Select_index];
end
Parent(1, :) = Population(mate(1)).variable;
Parent(2, :) = Population(mate(2)).variable;
switch Xover_Type
    case 1
        if OPTIONS.pcross > rand
            Xover_Pt = ceil(rand * OPTIONS.numVar);
            x = setdiff(Parent(1, Xover_Pt:OPTIONS.numVar), Parent(2,
Xover_Pt:OPTIONS.numVar));
            y = setdiff(Parent(2, Xover_Pt:OPTIONS.numVar), Parent(1,
Xover_Pt:OPTIONS.numVar));
            alpha=rand;
            child(k,:)=alpha*Parent(1,:)+(1-alpha)*Parent(2,:);
            child(k+1,:)=alpha*Parent(2,:)+(1-alpha)*Parent(2,:);
        else
            child(k, :) = Parent(1, :);
            child(k+1, :) = Parent(2, :);
        end
    case 2
        if OPTIONS.pcross > rand
            Xover_Pt1 = ceil(rand * OPTIONS.numVar);
            Xover_Pt2 = ceil(rand * OPTIONS.numVar);
            if Xover_Pt1 > Xover_Pt2
                temp = Xover_Pt2;
                Xover_Pt2 = Xover_Pt1;
                Xover_Pt1 = temp;
            end
            child(k-Keep, :) = [Parent(1, 1:Xover_Pt1) Parent(2, Xover_Pt1+1:Xover_Pt2)
Parent(1, Xover_Pt2+1:OPTIONS.numVar)];
            child(k-Keep+1, :) = [Parent(2, 1:Xover_Pt1) Parent(1, Xover_Pt1+1:Xover_Pt2)
Parent(2, Xover_Pt2+1:OPTIONS.numVar)];
        else
            child(k-Keep, :) = Parent(1, :);
            child(k-Keep+1, :) = Parent(2, :);
        end
    case 3
        for i = 1 : OPTIONS.numVar
            if OPTIONS.pcross > rand
                child(k-Keep, i) = Parent(1, i);
                child(k-Keep+1, i) = Parent(2, i);
            else
                child(k-Keep, i) = Parent(2, i);
                child(k-Keep+1, i) = Parent(1, i);
            end
        end
    end
end

```

```

        end
    end
end
for k = 1 : 2 : OPTIONS.popsize
    Population(k).variable = child(k, :);
    Population(k+1).variable = child(k+1, :);
end
for individual = 1 : OPTIONS.popsize
    for parnum = 1 : OPTIONS.numVar
        if OPTIONS.pmutate > rand
            Population(individual).variable(parnum) = (ll(parnum) + (ul(parnum) - ll(parnum)) *
rand);
        end
    end
end
Population = FeasibleFunction(OPTIONS, Population);
Population = CostFunction(OPTIONS, Population);
Population = PopSort(Population);
n = OPTIONS.popsize;
for i = 1 : Keep
    Population(n-i+1).variable = variableKeep(i,:);
    Population(n-i+1).cost = costKeep(i);
end
Population = PopSort(Population);
MinCost = [MinCost Population(1).cost];
if DisplayFlag
    disp([num2str(MinCost(end))]);
end
end
Variable =(Population(1).variable);
fprintf('\n %f',MinCost(end));
fprintf('\n %f,Variable);
%%%%%%%%%%%%%
function [Population, indices] = PopSort(Population)
popsize = length(Population);
Cost = zeros(1, popsize);
indices = zeros(1, popsize);
for i = 1 : popsize
    Cost(i) = Population(i).cost;
end
[Cost, indices] = sort(Cost, 2, 'ascend');
variables = zeros(popsize, length(Population(1).variable));
for i = 1 : popsize
    variables(i, :) = Population(indices(i)).variable;
end
for i = 1 : popsize

```

```

Population(i).variable = variables(i, :);
Population(i).cost = Cost(i);
end
%%%%%%%%%%%%%%%
function [AveCost, nLegal] = ComputeAveCost(Population)
Cost = [];
nLegal = 0;
for i = 1 : length(Population)
if Population(i).cost < inf
    Cost = [Cost Population(i).cost];
    nLegal = nLegal + 1;
end
end
AveCost = mean(Cost);
return;
%%%%%%%%%%%%%%%

```

## 2. Particle Swarm Optimization (PSO):

```

function PSO()
run=1;
for i=1:run
    PSO_Run(@F01);
end
%%%%%%%%%%%%%%
function [OPTIONS, MinCost, AvgCost, InitFunction, CostFunction, FeasibleFunction, ...
    MaxParValue, MinParValue, Population,FeasibleFunction_1,CostFunction_1] =
Init(DisplayFlag, ProblemFunction, RandSeed)
OPTIONS.popsize = 50;
OPTIONS.Maxgen = 2000;
OPTIONS.numVar =2;
if ~exist('RandSeed', 'var')
    RandSeed = round(sum(100*clock));
end
rand('state', RandSeed);
[InitFunction, CostFunction, FeasibleFunction,FeasibleFunction_1,CostFunction_1] =
ProblemFunction();
[MaxParValue, MinParValue, Population, OPTIONS] = InitFunction(OPTIONS);
Population = CostFunction(OPTIONS, Population);
Population = PopSort(Population);
AverageCost = ComputeAveCost(Population);
MinCost = [Population(1).cost];
AvgCost = [AverageCost];
return;
%%%%%%%%%%%%%%
function [InitFunction, CostFunction, FeasibleFunction,FeasibleFunction_1,CostFunction_1] =
F01

```

```

InitFunction = @F01Init;
CostFunction = @F01Cost;
CostFunction_1 = @F01Cost_1;
FeasibleFunction = @F01Feasible;
FeasibleFunction_1 = @F01Feasible_1;
return;
function [MaxParValue, MinParValue, Population, OPTIONS] = F01Init(OPTIONS)
global MinParValue MaxParValue ll ul
ll=[13 0 ];
ul=[100 100];
MaxParValue = ul;
for popindex = 1 : OPTIONS.popsize
    for k = 1 : OPTIONS.numVar
        variable(k) =(ll(k)+ (ul(k) - ll(k)) * rand);
    end
    Population(popindex).variable = variable;
end
return;
function [Population] = F01Cost(OPTIONS, Population)
global MinParValue MaxParValue
popsize = OPTIONS.popsize;
for popindex = 1 : popsize
    for k = 1 : OPTIONS.numVar
        x(k) = Population(popindex).variable(k);
    end
    Population(popindex).cost = objective(x);
end
return;
function [Population_1] = F01Cost_1(OPTIONS, Population)
global MinParValue MaxParValue
popsize = size(Population,1);
Population_1 =[];
for popindex = 1 : popsize
    for k = 1 : OPTIONS.numVar
        x(k) = Population(popindex,k);
    end
    Population_1(popindex) = objective(x);
end
return;
function [Population] = F01Feasible(OPTIONS, Population)
global MinParValue MaxParValue ll ul
for i = 1 : OPTIONS.popsize
    for k = 1 : OPTIONS.numVar
        Population(i).variable(k) = max(Population(i).variable(k), ll(k));
        Population(i).variable(k) = min(Population(i).variable(k), ul(k));
    end
end

```

```

end
return;
function [Population] = F01Feasible_1(OPTIONS, Population)
global MinParValue MaxParValue ll ul
for i = 1 : size(Population,1)
    for k = 1 : OPTIONS.numVar
        Population(i,k) = max(Population(i,k), ll(k));
        Population(i,k) = min(Population(i,k), ul(k));
    end
end
return;
%%%%%
function yy=objective(x)
p1=x(1);
p2=x(2);
z1=((p1-10)^3)+((p2-20)^3);
t1=-((p1-5)^2)-((p2-5)^2)+100;
t2=((p1-6)^2)+((p2-5)^2)-82.81;
nc=2;
    g1(1)=t1;
    g1(2)=t2;
    violate=0;
    for io=1:nc
        if g1(io)>0
            violate=violate+g1(io)^2;
        end
    end
yy=(z1)+(1e5*violate);
%%%%%
function PSO_Run(ProblemFunction, DisplayFlag, ProbFlag)
if ~exist('DisplayFlag', 'var')
    DisplayFlag = true;
end
if ~exist('ProbFlag', 'var')
    ProbFlag = true;
end
[OPTIONS, MinCost, AvgCost, InitFunction, CostFunction, FeasibleFunction, ...
    MaxParValue, MinParValue, Population, FeasibleFunction_1, CostFunction_1] =
Init(DisplayFlag, ProblemFunction);
Keep = 1;
w = 0.9;
c1 = 2;
c2 = 2;
vel = zeros(OPTIONS.popsize, OPTIONS.numVar);
pbest = Population;
max_vel=4;

```

```

maxv=max_vel*ones(OPTIONS.popsize, OPTIONS.numVar);
for GenIndex = 1 : OPTIONS.Maxgen
    for i = 1 : Keep
        variableKeep(i,:)=Population(i).variable;
        costKeep(i)=Population(i).cost;
    end
    if ProbFlag
        for i = 1 : 1 : length(Population)
            function_1(i,:)=Population(i).variable;
        end
    end
    function_1_cost=CostFunction_1(OPTIONS, function_1);
    [ii jj]=min(function_1_cost);
    gbest.cost=Population(jj).cost;
    gbest.variable=Population(jj).variable;
    for i = 1 : OPTIONS.popsize
        if Population(i).cost < pbest(i).cost
            pbest(i)=Population(i);
        end
    end
    for i = 1 : OPTIONS.popsize
        r = rand(2, OPTIONS.numVar);
        x = Population(i).variable;
        deltaVpersonal = c1 * r(1,:).* (pbest(i).variable - x);
        deltaVswarm = c2 * r(2,:).* (gbest.variable - x);
        vel(i,:)= w * vel(i,:)+deltaVpersonal + deltaVs swarm ;
        for j=1:OPTIONS.numVar
            if vel(i,j)>maxv(i,j)
                vel(i,j)=maxv(i,j);
            else if vel(i,j)<-maxv(i,j)
                vel(i,j)=-maxv(i,j);
            end
        end
    end
    Population(i).variable = ( x + vel(i,:));
end
Population = FeasibleFunction(OPTIONS, Population);
Population = CostFunction(OPTIONS, Population);
n = OPTIONS.popsize;
for i = 1 : Keep
    Population(n-i+1).variable = variableKeep(i,:);
    Population(n-i+1).cost = costKeep(i);
end
Population = PopSort(Population);
if ProbFlag
    for i = 1 : 1 : length(Population)

```

```

        function_1(i,:) = Population(i).variable;
    end
end
function_1_cost = CostFunction_1(OPTIONS, function_1);
[ii jj]=min(function_1_cost);
MinCost=ii;
[AverageCost, nLegal] = ComputeAveCost(Population);
AvgCost = [AvgCost AverageCost];
if DisplayFlag
    disp([num2str(MinCost(end))]);
end
Variable =(Population(1).variable);
fprintf("\n %f,MinCost(end));
fprintf("\n %f,Variable);
%%%%%%%%%%%%%%%
function [Population, indices] = PopSort(Population)
popsze = length(Population);
Cost = zeros(1, popsize);
indices = zeros(1, popsize);
for i = 1 : popsize
    Cost(i) = Population(i).cost;
end
[Cost, indices] = sort(Cost, 2, 'ascend');
variables = zeros(popsize, length(Population(1).variable));
for i = 1 : popsize
    variables(i, :) = Population(indices(i)).variable;
end
for i = 1 : popsize
    Population(i).variable = variables(i, :);
    Population(i).cost = Cost(i);
end
%%%%%%%%%%%%%%%
function [AveCost, nLegal] = ComputeAveCost(Population)
Cost = [];
nLegal = 0;
for i = 1 : length(Population)
    if Population(i).cost < inf
        Cost = [Cost Population(i).cost];
        nLegal = nLegal + 1;
    end
end
AveCost = mean(Cost);
return;
%%%%%%%%%%%%%%%

```

### 3. Differential Evolution (DE):

```

function DE()
run=1;
for i=1:run
    DE_Run(@F01);
end
%%%%%%%%%%%%%%%
function [OPTIONS, MinCost, AvgCost, InitFunction, CostFunction, FeasibleFunction, ...
    MaxParValue, MinParValue, Population, FeasibleFunction_1, CostFunction_1] =
Init(DisplayFlag, ProblemFunction, RandSeed)
OPTIONS.popsize = 50;
OPTIONS.Maxgen = 2000;
OPTIONS.numVar = 2;
if ~exist('RandSeed', 'var')
    RandSeed = round(sum(100*clock));
end
rand('state', RandSeed);
[InitFunction, CostFunction, FeasibleFunction, FeasibleFunction_1, CostFunction_1] =
ProblemFunction();
[MaxParValue, MinParValue, Population, OPTIONS] = InitFunction(OPTIONS);
Population = CostFunction(OPTIONS, Population);
Population = PopSort(Population);
AverageCost = ComputeAveCost(Population);
MinCost = [Population(1).cost];
AvgCost = [AverageCost];
return;
%%%%%%%%%%%%%%%
function [InitFunction, CostFunction, FeasibleFunction, FeasibleFunction_1, CostFunction_1] =
F01
InitFunction = @F01Init;
CostFunction = @F01Cost;
CostFunction_1 = @F01Cost_1;
FeasibleFunction = @F01Feasible;
FeasibleFunction_1 = @F01Feasible_1;
return;
function [MaxParValue, MinParValue, Population, OPTIONS] = F01Init(OPTIONS)
global MinParValue MaxParValue ll ul
ll=[13 0 ];
ul=[100 100];
MaxParValue = ul;
for popindex = 1 : OPTIONS.popsize
    for k = 1 : OPTIONS.numVar
        variable(k) =(ll(k)+ (ul(k) - ll(k)) * rand);
    end
    Population(popindex).variable = variable;
end

```

```
return;
function [Population] = F01Cost(OPTIONS, Population)
global MinParValue MaxParValue
popsize = OPTIONS.popsize;
for popindex = 1 : popsize
    for k = 1 : OPTIONS.numVar
        x(k) = Population(popindex).variable(k);
    end
    Population(popindex).cost = objective(x);
end
return
function [Population_1] = F01Cost_1(OPTIONS, Population)
global MinParValue MaxParValue
popsize = size(Population,1);
Population_1 = [];
for popindex = 1 : popsize
    for k = 1 : OPTIONS.numVar
        x(k) = Population(popindex,k);
    end
    Population_1(popindex) = objective(x);
end
return
function [Population] = F01Feasible(OPTIONS, Population)
global MinParValue MaxParValue ll ul
for i = 1 : OPTIONS.popsize
    for k = 1 : OPTIONS.numVar
        Population(i).variable(k) = max(Population(i).variable(k), ll(k));
        Population(i).variable(k) = min(Population(i).variable(k), ul(k));
    end
end
return;
function [Population] = F01Feasible_1(OPTIONS, Population)
global MinParValue MaxParValue ll ul
for i = 1 : size(Population,1)
    for k = 1 : OPTIONS.numVar
        Population(i,k) = max(Population(i,k), ll(k));
        Population(i,k) = min(Population(i,k), ul(k));
    end
end
return;
%%%%%%%%%%%%%
function yy=objective(x)
p1=x(1);
p2=x(2);
z1=((p1-10)^3)+((p2-20)^3);
t1=-((p1-5)^2)-((p2-5)^2)+100;
```

```

t2=((p1-6)^2)+((p2-5)^2)-82.81;
nc=2;
g1(1)=t1;
g1(2)=t2;
violate=0;
for io=1:nc
    if g1(io)>0
        violate=violate+g1(io)^2;
    end
end
yy=(z1)+(1e5*violate);
%%%%%%%%%%%%%%%%%%%%%%%%%%%%%%%%%%%%%
function DE_Run(ProblemFunction, DisplayFlag, ProbFlag)
if ~exist('DisplayFlag', 'var')
    DisplayFlag = true;
end
[OPTIONS, MinCost, AvgCost, InitFunction, CostFunction, FeasibleFunction, ...
    MaxParValue, MinParValue, Population] = Init(DisplayFlag, ProblemFunction);
F = 0.5;
CR = 0.8;
PopTest = Population(1:2);
for GenIndex = 1 : OPTIONS.Maxgen
    for k = 1 : OPTIONS.popsize
        r1 = round(OPTIONS.popsize * rand + 0.5);
        while true
            r2 = round(OPTIONS.popsize * rand + 0.5);
            if (r2 ~= r1),
                break,
            end
        end
        while true
            r3 = round(OPTIONS.popsize * rand + 0.5);
            if (r3 ~= r1) & (r3 ~= r2),
                break,
            end
        end
        v.variable = (Population(r1).variable + F * (Population(r2).variable -
Population(r3).variable));
        r4 = round(OPTIONS.popsize * rand + 0.5);
        for j = 1 : OPTIONS.numVar
            if rand < CR
                uvariable(j) = v.variable(j);
            else
                uvariable(j) = Population(r4).variable(j);
            end
        end
    end
end

```

```

PopTest(1).variable = uvariable;
PopTest(2) = Population(r4);
SavePopSize = OPTIONS.popsize;
OPTIONS.popsize = 2;
PopTest = FeasibleFunction(OPTIONS, PopTest);
PopTest = CostFunction(OPTIONS, PopTest);
OPTIONS.popsize = SavePopSize;
if PopTest(1).cost < Population(r4).cost
    Population(r4) = PopTest(1);
end
end
Population = PopSort(Population);
MinCost = [MinCost Population(1).cost];
if DisplayFlag
    disp([num2str(MinCost(end))]);
end
end
disp([num2str(MinCost(end))]);
Variable =(Population(1).variable);
fprintf("\n %f",MinCost(end));
fprintf("\n %f",Variable);
%%%%%%%%%%%%%%%
function [Population, indices] = PopSort(Population)
popsize = length(Population);
Cost = zeros(1, popsize);
indices = zeros(1, popsize);
for i = 1 : popsize
    Cost(i) = Population(i).cost;
end
[Cost, indices] = sort(Cost, 2, 'ascend');
variables = zeros(popsize, length(Population(1).variable));
for i = 1 : popsize
    variables(i, :) = Population(indices(i)).variable;
end
for i = 1 : popsize
    Population(i).variable = variables(i, :);
    Population(i).cost = Cost(i);
end
%%%%%%%%%%%%%%
function [AveCost, nLegal] = ComputeAveCost(Population)
Cost = [];
nLegal = 0;
for i = 1 : length(Population)
    if Population(i).cost < inf
        Cost = [Cost Population(i).cost];
        nLegal = nLegal + 1;
    end
end
AveCost = mean(Cost);
return;
%%%%%%%%%%%%%

```

#### 4. Artificial Bee Colony (ABC):

```

function ABC()
run=1;
for i=1:run
    ABC_Run(@F01);
end
%%%%%%%
function [OPTIONS, MinCost, AvgCost, InitFunction, CostFunction, FeasibleFunction, ...
    MaxParValue, MinParValue, Population, FeasibleFunction_1, CostFunction_1] =
Init(DisplayFlag, ProblemFunction, RandSeed)
OPTIONS.popsize = 50;
OPTIONS.Maxgen = 2000;
OPTIONS.numVar =2;
if ~exist('RandSeed', 'var')
    RandSeed = round(sum(100*clock));
end
rand('state', RandSeed);
[InitFunction, CostFunction, FeasibleFunction, FeasibleFunction_1, CostFunction_1] =
ProblemFunction();
[MaxParValue, MinParValue, Population, OPTIONS] = InitFunction(OPTIONS);
Population = CostFunction(OPTIONS, Population);
Population = PopSort(Population);
AverageCost = ComputeAveCost(Population);
MinCost = [Population(1).cost];
AvgCost = [AverageCost];
return;
%%%%%%%
function [InitFunction, CostFunction, FeasibleFunction, FeasibleFunction_1, CostFunction_1] =
F01
InitFunction = @F01Init;
CostFunction = @F01Cost;
CostFunction_1 = @F01Cost_1;
FeasibleFunction = @F01Feasible;
FeasibleFunction_1 = @F01Feasible_1;
return;
function [MaxParValue, MinParValue, Population, OPTIONS] = F01Init(OPTIONS)
global MinParValue MaxParValue ll ul
ll=[13 0 ];
ul=[100 100];
MaxParValue = ul;

```

```
for popindex = 1 : OPTIONS.popsize
    for k = 1 : OPTIONS.numVar
        variable(k) =(ll(k)+ (ul(k) - ll(k)) * rand);
    end
    Population(popindex).variable = variable;
end
return;

function [Population] = F01Cost(OPTIONS, Population)
global MinParValue MaxParValue
popsize = OPTIONS.popsize;
for popindex = 1 : popsize
    for k = 1 : OPTIONS.numVar
        x(k) = Population(popindex).variable(k);
    end
    Population(popindex).cost = objective(x);
end
return;

function [Population_1] = F01Cost_1(OPTIONS, Population)
global MinParValue MaxParValue
popsize = size(Population,1);
Population_1 =[];
for popindex = 1 : popsize
    for k = 1 : OPTIONS.numVar
        x(k) = Population(popindex,k);
    end
    Population_1(popindex) = objective(x);
end
return;

function [Population] = F01Feasible(OPTIONS, Population)
global MinParValue MaxParValue ll ul
for i = 1 : OPTIONS.popsize
    for k = 1 : OPTIONS.numVar
        Population(i).variable(k) = max(Population(i).variable(k), ll(k));
        Population(i).variable(k) = min(Population(i).variable(k), ul(k));
    end
end
return;

function [Population] = F01Feasible_1(OPTIONS, Population)
global MinParValue MaxParValue ll ul
for i = 1 : size(Population,1)
    for k = 1 : OPTIONS.numVar
        Population(i,k) = max(Population(i,k), ll(k));
        Population(i,k) = min(Population(i,k), ul(k));
    end
end
return;
```

```

%%%%%
function yy=objective(x)
p1=x(1);
p2=x(2);
z1=((p1-10)^3)+((p2-20)^3);
t1=-((p1-5)^2)-((p2-5)^2)+100;
t2=((p1-6)^2)+((p2-5)^2)-82.81;
nc=2;
    g1(1)=t1;
    g1(2)=t2;
    violate=0;
    for io=1:nc
        if g1(io)>0
            violate=violate+g1(io)^2;
        end
    end
yy=(z1)+(1e5*violate);
%%%%%
function ABC_Run(ProblemFunction, DisplayFlag, ProbFlag)
global ll ul
if ~exist('DisplayFlag', 'var')
    DisplayFlag = true;
end
[OPTIONS, MinCost, AvgCost, InitFunction, CostFunction, FeasibleFunction, ...
    MaxParValue, MinParValue, Population, FeasibleFunction_1, CostFunction_1] =
Init(DisplayFlag, ProblemFunction);
trial=zeros(1,OPTIONS.popsize);
limit=50;
Keep=1;
for GenIndex = 1 : OPTIONS.Maxgen
    for i = 1 : Keep
        variableKeep(i,:)=Population(i).variable;
        costKeep(i)=Population(i).cost;
    end
    for i=1:OPTIONS.popsize
        pp(i,:)=Population(i).variable;
        pp_cost(i)=Population(i).cost;
    end
    pp_new=pp;
    for i=1:OPTIONS.popsize
        ii=fix(rand*(OPTIONS.popsize))+1;
        while(ii==i)
            ii=fix(rand*(OPTIONS.popsize))+1;
        end;
        j=fix(rand*OPTIONS.numVar )+1;
    end
end

```

```

pp_new(i,j) = (Population(i).variable(j)+(-1+rand*(2))*(Population(i).variable(j)-
Population(ii).variable(j)));
pp_new1 = FeasibleFunction_1(OPTIONS, pp_new(i,:));
pp_new_cost1 = CostFunction_1(OPTIONS, pp_new1);
if pp_new_cost1<Population(i).cost
    Population(i).variable =pp_new1;
    Population(i).cost=pp_new_cost1;
    trial(i)=0;
else
    trial(i)=trial(i)+1;
end
end
for i=1:OPTIONS.popsize
    if Population(i).cost>=0
        xx(i)=1/(Population(i).cost+1);
    else
        xx(i)=1+abs(Population(i).cost);
    end
end
for j=1:OPTIONS.popsize
prob(i)=(0.9*xx(i)/max(xx))+0.1;
end
i=1;
t=0;
while(t<OPTIONS.popsize)
    if (rand<prob(i))
        t=t+1;
        ii=fix(rand*(OPTIONS.popsize))+1;
        while(ii==i)
            ii=fix(rand*(OPTIONS.popsize))+1;
        end;
        j=fix(rand*OPTIONS.numVar )+1;
        pp_new(i,j) = (Population(i).variable(j)+(-1+rand*(2))*(Population(i).variable(j)-
Population(ii).variable(j)));
        pp_new1 = FeasibleFunction_1(OPTIONS, pp_new(i,:));
        pp_new_cost1 = CostFunction_1(OPTIONS, pp_new1);
        if pp_new_cost1<Population(i).cost
            Population(i).variable =pp_new1;
            Population(i).cost=pp_new_cost1;
            trial(i)=0;
        else
            trial(i)=trial(i)+1;
        end
    end
    i=i+1;
    if (i==OPTIONS.popsize+1)

```

```

        i=1;
    end
end
for i=1:OPTIONS.popsize
pp1_cost(i)=Population(i).cost;
end
[minimum_sol min_num]=min(pp1_cost);
ind=find(trial==max(trial));
ind=ind(end);
if (trial(ind)>limit)
    Bas(ind)=0;
    sol=(ul-ll).*rand(1,OPTIONS.numVar)+ll;
    sol_cost = CostFunction_1(OPTIONS,sol);
    Population(ind).variable =sol;
    Population(ind).cost=sol_cost;
end;
Population(1).variable=Population(min_num).variable;
Population(1).cost=minimum_sol;
Population = PopSort(Population);
n = length(Population);
for i = 1 : Keep
    Population(n-i+1).variable = variableKeep(i,:);
    Population(n-i+1).cost = costKeep(i);
end
MinCost = [MinCost Population(1).cost];
if DisplayFlag
    disp([num2str(MinCost(end))]);
    end
end
disp([num2str(Population(1).variable)]);
Variable = (Population(1).variable);
fprintf("\n %f,MinCost(end));
fprintf("\n %f,Variable);
%%%%%%%%%%%%%
function [Population, indices] = PopSort(Population)
popsize = length(Population);
Cost = zeros(1, popsize);
indices = zeros(1, popsize);
for i = 1 : popsize
    Cost(i) = Population(i).cost;
end
[Cost, indices] = sort(Cost, 2, 'ascend');
variables = zeros(popsize, length(Population(1).variable));
for i = 1 : popsize
    variables(i, :) = Population(indices(i)).variable;
end

```

```

for i = 1 : popsize
    Population(i).variable = variables(i, :);
    Population(i).cost = Cost(i);
end
%%%%%
function [AveCost, nLegal] = ComputeAveCost(Population)
Cost = [];
nLegal = 0;
for i = 1 : length(Population)
    if Population(i).cost < inf
        Cost = [Cost Population(i).cost];
        nLegal = nLegal + 1;
    end
end
AveCost = mean(Cost);
return;
%%%%%

```

## 5. Cuckoo Search Optimization:

```

function CSA()
run=1;
for i=1:run
    CSA_Run(@F01);
end
%%%%%
function [OPTIONS, MinCost, AvgCost, InitFunction, CostFunction, FeasibleFunction, ...
    MaxParValue, MinParValue, Population,FeasibleFunction_1,CostFunction_1] =
Init(DisplayFlag, ProblemFunction, RandSeed)
OPTIONS.popsize = 50;
OPTIONS.Maxgen = 2000;
OPTIONS.numVar =2;
if ~exist('RandSeed', 'var')
    RandSeed = round(sum(100*clock));
end
rand('state', RandSeed);
[InitFunction, CostFunction, FeasibleFunction,FeasibleFunction_1,CostFunction_1] =
ProblemFunction();
[MaxParValue, MinParValue, Population, OPTIONS] = InitFunction(OPTIONS);
Population = CostFunction(OPTIONS, Population);
Population = PopSort(Population);
AverageCost = ComputeAveCost(Population);
MinCost = [Population(1).cost];
AvgCost = [AverageCost];
return;
%%%%%

```

```
function [InitFunction, CostFunction, FeasibleFunction,FeasibleFunction_1,CostFunction_1] = F01
InitFunction = @F01Init;
CostFunction = @F01Cost;
CostFunction_1 = @F01Cost_1;
FeasibleFunction = @F01Feasible;
FeasibleFunction_1 = @F01Feasible_1;
return;
function [MaxParValue, MinParValue, Population, OPTIONS] = F01Init(OPTIONS)
global MinParValue MaxParValue ll ul
ll=[13 0];
ul=[100 100];
MaxParValue = ul;
for popindex = 1 : OPTIONS.popsize
    for k = 1 : OPTIONS.numVar
        variable(k) =(ll(k)+ (ul(k) - ll(k)) * rand);
    end
    Population(popindex).variable = variable;
end
return;
function [Population] = F01Cost(OPTIONS, Population)
global MinParValue MaxParValue
popsize = OPTIONS.popsize;
for popindex = 1 : popsize
    for k = 1 : OPTIONS.numVar
        x(k) = Population(popindex).variable(k);
    end
    Population(popindex).cost = objective(x);
end
return;
function [Population_1] = F01Cost_1(OPTIONS, Population)
global MinParValue MaxParValue
popsize = size(Population,1);
Population_1 =[];
for popindex = 1 : popsize
    for k = 1 : OPTIONS.numVar
        x(k) = Population(popindex,k);
    end
    Population_1(popindex) = objective(x);
end
return;
function [Population] = F01Feasible(OPTIONS, Population)
global MinParValue MaxParValue ll ul
for i = 1 : OPTIONS.popsize
    for k = 1 : OPTIONS.numVar
        Population(i).variable(k) = max(Population(i).variable(k), ll(k));
    end
end
```

```

    Population(i).variable(k) = min(Population(i).variable(k), ul(k));
end
return;
function [Population] = F01Feasible_1(OPTIONS, Population)
global MinParValue MaxParValue ll ul
for i = 1 : size(Population,1)
    for k = 1 : OPTIONS.numVar
        Population(i,k) = max(Population(i,k), ll(k));
        Population(i,k) = min(Population(i,k), ul(k));
    end
end
return;
%%%%%
function yy=objective(x)
p1=x(1);
p2=x(2);
z1=((p1-10)^3)+((p2-20)^3);
t1=-((p1-5)^2)-((p2-5)^2)+100;
t2=((p1-6)^2)+((p2-5)^2)-82.81;
nc=2;
    g1(1)=t1;
    g1(2)=t2;
    violate=0;
    for io=1:nc
        if g1(io)>0
            violate=violate+g1(io)^2;
        end
    end
yy=(z1)+(1e5*violate);
%%%%%
function CSA_Run(ProblemFunction, DisplayFlag, ProbFlag)
global ll GenIndex ul
if ~exist('DisplayFlag', 'var')
    DisplayFlag = true;
end
[OPTIONS, MinCost, AvgCost, InitFunction, CostFunction, FeasibleFunction, ...
    MaxParValue, MinParValue, Population, FeasibleFunction_1, CostFunction_1] =
Init(DisplayFlag, ProblemFunction);
pa=0.25;
Keep=1;
for GenIndex = 1 : OPTIONS.Maxgen/2
    for i = 1 : Keep
        variableKeep(i,:)=Population(i).variable;
        costKeep(i)=Population(i).cost;
    end

```

```

for i = 1 : 1 : OPTIONS.popsize
    function_1(i,:)=Population(i).variable;
    fitness(i)=Population(i).cost;
end
[best best_X]=min(fitness);
Fbest=best;
Lbest=function_1(best_X,:);
new_nest=get_cuckoos(function_1,Lbest,ll,ul);
fitness_after_cukoo = CostFunction_1(OPTIONS, new_nest) ;
for i = 1 : OPTIONS.popsize
    if fitness_after_cukoo(i)<Population(i).cost
        Population(i).variable =new_nest(i,:);
        Population(i).cost=fitness_after_cukoo(i);
    end
end
for i = 1:OPTIONS.popsize
function_1(i,:)=Population(i).variable;
end
new_nest=empty_nests(function_1,ll,ul,pa) ;
new_nest = FeasibleFunction_1(OPTIONS, new_nest);
fitness_after_empty = CostFunction_1(OPTIONS, new_nest) ;
for i = 1 : OPTIONS.popsize
    if fitness_after_empty(i)<Population(i).cost
        Population(i).variable =new_nest(i,:);
        Population(i).cost=fitness_after_empty(i);
    end
end
n = length(Population);
for i = 1 : Keep
    Population(n-i+1).variable = variableKeep(i,:);
    Population(n-i+1).cost = costKeep(i);
end
Population = PopSort(Population);
MinCost = [MinCost Population(1).cost];
if DisplayFlag
    disp([num2str(MinCost(end))]);
end
Variable =(Population(1).variable);
fprintf("\n %f",MinCost(end));
fprintf("\n %f,Variable);
function nest=get_cuckoos(nest,best,Lb,Ub)
n=size(nest,1);
beta=3/2;
sigma=(gamma(1+beta)*sin(pi*beta/2)/(gamma((1+beta)/2)*beta*2^((beta-1)/2)))^(1/beta);
for j=1:n,

```

```

s=nest(j,:);
u=randn(size(s))*sigma;
v=randn(size(s));
step=u./abs(v).^(1/beta);
stepsize=0.01*step.*(s-best);
s=s+stepsize.*randn(size(s));
nest(j,:)=simplebounds(s,Lb,Ub);
end
return
function new_nest=empty_nests(nest,Lb,Ub,pa)
n=size(nest,1);
K=rand(size(nest))>pa;
stepsize=rand*(nest(randperm(n),:)-nest(randperm(n),:));
new_nest=nest+stepsize.*K;
return
function s=simplebounds(s,Lb,Ub)
ns_tmp=s;
I=ns_tmp<Lb;
ns_tmp(I)=Lb(I);
J=ns_tmp>Ub;
ns_tmp(J)=Ub(J);
s=ns_tmp;
%%%%%%%%%%%%%%%
function [Population, indices] = PopSort(Population)
popsize = length(Population);
Cost = zeros(1, popszie);
indices = zeros(1, popszie);
for i = 1 : popszie
    Cost(i) = Population(i).cost;
end
[Cost, indices] = sort(Cost, 2, 'ascend');
variables = zeros(popszie, length(Population(1).variable));
for i = 1 : popszie
    variables(i, :) = Population(indices(i)).variable;
end
for i = 1 : popszie
    Population(i).variable = variables(i, :);
    Population(i).cost = Cost(i);
end
%%%%%%%%%%%%%%%
function [AveCost, nLegal] = ComputeAveCost(Population)
Cost = [];
nLegal = 0;
for i = 1 : length(Population)
    if Population(i).cost < inf
        Cost = [Cost Population(i).cost];
    end
end
AveCost = sum(Cost)/length(Cost);
nLegal = sum(isfinite(Cost));

```

```

    nLegal = nLegal + 1;
end
end
AveCost = mean(Cost);
return;

%%%%%%%%%%%%%%%

```

## 6. Teaching-Learning-based Optimization (TLBO) :

```

function TLBO()
run=1;
for i=1:run
    TLBO_Run(@F01);
end
%%%%%%%%%%%%%%
function [OPTIONS, MinCost, AvgCost, InitFunction, CostFunction, FeasibleFunction, ...
    MaxParValue, MinParValue, Population,FeasibleFunction_1,CostFunction_1] =
Init(DisplayFlag, ProblemFunction, RandSeed)
OPTIONS.popsize = 50;
OPTIONS.Maxgen = 2000;
OPTIONS.numVar =2;
if ~exist('RandSeed', 'var')
    RandSeed = round(sum(100*clock));
end
rand('state', RandSeed);
[InitFunction, CostFunction, FeasibleFunction,FeasibleFunction_1,CostFunction_1] =
ProblemFunction();
[MaxParValue, MinParValue, Population, OPTIONS] = InitFunction(OPTIONS);
Population = CostFunction(OPTIONS, Population);
Population = PopSort(Population);
AverageCost = ComputeAveCost(Population);
MinCost = [Population(1).cost];
AvgCost = [AverageCost];
return;
%%%%%%%%%%%%%%
function [InitFunction, CostFunction, FeasibleFunction,FeasibleFunction_1,CostFunction_1] =
F01
InitFunction = @F01Init;
CostFunction = @F01Cost;
CostFunction_1 = @F01Cost_1;
FeasibleFunction = @F01Feasible;
FeasibleFunction_1 = @F01Feasible_1;
return;
function [MaxParValue, MinParValue, Population, OPTIONS] = F01Init(OPTIONS)
global MinParValue MaxParValue ll ul
ll=[13 0 ];

```

```
ul=[100 100];
MaxParValue = ul;
for popindex = 1 : OPTIONS.popsize
    for k = 1 : OPTIONS.numVar
        variable(k) =(ll(k)+ (ul(k) - ll(k)) * rand);
    end
    Population(popindex).variable = variable;
end
return;
function [Population] = F01Cost(OPTIONS, Population)
global MinParValue MaxParValue
popsize = OPTIONS.popsize;
for popindex = 1 : popsize
    for k = 1 : OPTIONS.numVar
        x(k) = Population(popindex).variable(k);
    end
    Population(popindex).cost = objective(x);
end
return
function [Population_1] = F01Cost_1(OPTIONS, Population)
global MinParValue MaxParValue
popsize = size(Population,1);
Population_1 =[];
for popindex = 1 : popsize
    for k = 1 : OPTIONS.numVar
        x(k) = Population(popindex,k);
    end
    Population_1(popindex) = objective(x);
end
return
function [Population] = F01Feasible(OPTIONS, Population)
global MinParValue MaxParValue ll ul
for i = 1 : OPTIONS.popsize
    for k = 1 : OPTIONS.numVar
        Population(i).variable(k) = max(Population(i).variable(k), ll(k));
        Population(i).variable(k) = min(Population(i).variable(k), ul(k));
    end
end
return;
function [Population] = F01Feasible_1(OPTIONS, Population)
global MinParValue MaxParValue ll ul
for i = 1 : size(Population,1)
    for k = 1 : OPTIONS.numVar
        Population(i,k) = max(Population(i,k), ll(k));
        Population(i,k) = min(Population(i,k), ul(k));
    end
end
```

```

end
return;
%%%%%
function yy=objective(x)
p1=x(1);
p2=x(2);
z1=((p1-10)^3)+((p2-20)^3);
t1=-((p1-5)^2)-((p2-5)^2)+100;
t2=((p1-6)^2)+((p2-5)^2)-82.81;
nc=2;
    g1(1)=t1;
    g1(2)=t2;
    violate=0;
    for io=1:nc
        if g1(io)>0
            violate=violate+g1(io)^2;
        end
    end
yy=(z1)+(1e5*violate);
%%%%%
function TLBO_Run(ProblemFunction, DisplayFlag, ProbFlag)
global ll ul
if ~exist('DisplayFlag', 'var')
    DisplayFlag = true;
end
[OPTIONS, MinCost, AvgCost, InitFunction, CostFunction, FeasibleFunction, ...
    MaxParValue, MinParValue, Population, FeasibleFunction_1, CostFunction_1] =
Init(DisplayFlag, ProblemFunction);
Keep=1;
for GenIndex = 1 : OPTIONS.Maxgen/
    for i = 1 : Keep
        variableKeep(i,:)=Population(i).variable;
        costKeep(i)=Population(i).cost;
    end
    for i=1:OPTIONS.popsize
        pp(i,:)=Population(i).variable;
        pp_cost(i)=Population(i).cost;
    end
    pp_new=pp;
    Mean_pop=mean(pp);
    TF=round(1+rand*(1));
    for i=1:size(pp,2)
        New_Mean(i)=((pp(1,i)));
        for j=1:size(pp,1)
            pp_new(j,i)=pp(j,i)+rand*(New_Mean(i)-TF*Mean_pop(i));
        end
    end
end

```

```

end
pp_new = FeasibleFunction_1(OPTIONS, pp_new);
pp_new_cost = CostFunction_1(OPTIONS, pp_new);
for i = 1 : OPTIONS.popsize
    if pp_new_cost(i)<Population(i).cost
        Population(i).variable = pp_new(i,:);
        Population(i).cost=pp_new_cost(i);
    end
end
for i = 1 : 1 : OPTIONS.popsize
    ii=ceil(rand*(OPTIONS.popsize));
    while ii==i
        ii=ceil(rand*(OPTIONS.popsize));
        end
    if Population(i).cost<Population(ii).cost
        function_1(i,:)= (Population(i).variable + rand*(Population(i).variable-
Population(ii).variable));
    else
        function_1(i,:)= (Population(i).variable+rand*(Population(ii).variable-
Population(i).variable));
    end
end
function_1 = FeasibleFunction_1(OPTIONS, function_1);
function_1_cost = CostFunction_1(OPTIONS, function_1);
for i = 1 : OPTIONS.popsize
    if function_1_cost(i)<Population(i).cost
        Population(i).variable =function_1(i,:);
        Population(i).cost=function_1_cost(i);
    end
end
Population = FeasibleFunction(OPTIONS, Population);
Population = CostFunction(OPTIONS, Population);
Population = PopSort(Population);
n = OPTIONS.popsize;
for i = 1 : Keep
    Population(n-i+1).variable = variableKeep(i,:);
    Population(n-i+1).cost = costKeep(i);
end
Population = PopSort(Population);
MinCost = [MinCost Population(1).cost];
if DisplayFlag
    disp([num2str(MinCost(end))]);
    end
end
disp([num2str(MinCost(end))]);
Variable =(Population(1).variable);

```

```

fprintf("\n %f",MinCost(end));
fprintf("\n %f",Variable);
%%%%%
function [Population, indices] = PopSort(Population)
popsize = length(Population);
Cost = zeros(1, popsize);
indices = zeros(1, popsize);
for i = 1 : popsize
    Cost(i) = Population(i).cost;
end
[Cost, indices] = sort(Cost, 2, 'ascend');
variables = zeros(popsize, length(Population(1).variable));
for i = 1 : popsize
    variables(i, :) = Population(indices(i)).variable;
end
for i = 1 : popsize
    Population(i).variable = variables(i, :);
    Population(i).cost = Cost(i);
end
%%%%%
function [AveCost, nLegal] = ComputeAveCost(Population)
Cost = [];
nLegal = 0;
for i = 1 : length(Population)
    if Population(i).cost < inf
        Cost = [Cost Population(i).cost];
        nLegal = nLegal + 1;
    end
end
AveCost = mean(Cost);
return;
%%%%%

```

## 7. Symbiotic Organism Search (SOS) :

```

function SOS()
run=1;
for i=1:run
    SOS_Run(@F01);
end
%%%%%
function [OPTIONS, MinCost, AvgCost, InitFunction, CostFunction, FeasibleFunction, ...
    MaxParValue, MinParValue, Population, FeasibleFunction_1, CostFunction_1] =
    Init(DisplayFlag, ProblemFunction, RandSeed)
OPTIONS.popsize = 50;
OPTIONS.Maxgen = 2000;
OPTIONS.numVar = 2;

```

```
if ~exist('RandSeed', 'var')
    RandSeed = round(sum(100*clock));
end
rand('state', RandSeed);
[InitFunction, CostFunction, FeasibleFunction, FeasibleFunction_1, CostFunction_1] =
ProblemFunction();
[MaxParValue, MinParValue, Population, OPTIONS] = InitFunction(OPTIONS);
Population = CostFunction(OPTIONS, Population);
Population = PopSort(Population);
AverageCost = ComputeAveCost(Population);
MinCost = [Population(1).cost];
AvgCost = [AverageCost];
return;
%%%%%
function [InitFunction, CostFunction, FeasibleFunction, FeasibleFunction_1, CostFunction_1] =
F01
InitFunction = @F01Init;
CostFunction = @F01Cost;
CostFunction_1 = @F01Cost_1;
FeasibleFunction = @F01Feasible;
FeasibleFunction_1 = @F01Feasible_1;
return;
function [MaxParValue, MinParValue, Population, OPTIONS] = F01Init(OPTIONS)
global MinParValue MaxParValue ll ul
ll=[13 0 ];
ul=[100 100];
MaxParValue = ul;
for popindex = 1 : OPTIONS.popsize
    for k = 1 : OPTIONS.numVar
        variable(k) =(ll(k)+ (ul(k) - ll(k)) * rand);
    end
    Population(popindex).variable = variable;
end
return;
function [Population] = F01Cost(OPTIONS, Population)
global MinParValue MaxParValue
popsize = OPTIONS.popsize;
for popindex = 1 : popsize
    for k = 1 : OPTIONS.numVar
        x(k) = Population(popindex).variable(k);
    end
    Population(popindex).cost = objective(x);
end
return;
function [Population_1] = F01Cost_1(OPTIONS, Population)
global MinParValue MaxParValue
```

```

popsize = size(Population,1);
Population_1 =[];
for popindex = 1 : popszie
    for k = 1 : OPTIONS.numVar
        x(k) = Population(popindex,k);
    end
    Population_1(popindex) = objective(x);
end
return
function [Population] = F01Feasible(OPTIONS, Population)
global MinParValue MaxParValue ll ul
for i = 1 : OPTIONS.popsize
    for k = 1 : OPTIONS.numVar
        Population(i).variable(k) = max(Population(i).variable(k), ll(k));
        Population(i).variable(k) = min(Population(i).variable(k), ul(k));
    end
end
return;
function [Population] = F01Feasible_1(OPTIONS, Population)
global MinParValue MaxParValue ll ul
for i = 1 : size(Population,1)
    for k = 1 : OPTIONS.numVar
        Population(i,k) = max(Population(i,k), ll(k));
        Population(i,k) = min(Population(i,k), ul(k));
    end
end
return;
%%%%%%%%%%%%%
function yy=objective(x)
p1=x(1);
p2=x(2);
z1=((p1-10)^3)+((p2-20)^3);
t1=-((p1-5)^2)-((p2-5)^2)+100;
t2=((p1-6)^2)+((p2-5)^2)-82.81;
nc=2;
g1(1)=t1;
g1(2)=t2;
violate=0;
for io=1:nc
    if g1(io)>0
        violate=violate+g1(io)^2;
    end
end
yy=(z1)+(1e5*violate);
%%%%%%%%%%%%%
function SOS_Run(ProblemFunction, DisplayFlag, ProbFlag)

```

```
global ll ul
if ~exist('DisplayFlag', 'var')
    DisplayFlag = true;
end
[OPTIONS, MinCost, AvgCost, InitFunction, CostFunction, FeasibleFunction, ...
    MaxParValue, MinParValue, Population, FeasibleFunction_1, CostFunction_1] =
Init(DisplayFlag, ProblemFunction);
Keep=1;
for GenIndex = 1 : OPTIONS.Maxgen/3
    for i = 1 : Keep
        variableKeep(i,:) = Population(i).variable;
        costKeep(i) = Population(i).cost;
    end
    for i=1:OPTIONS.popsize
        pp(i,:)=Population(i).variable;
        pp_cost(i)=Population(i).cost;
    end
    pp_new=pp;
    for i=1:OPTIONS.popsize
        k=i;
        while i==k
            seed=randperm(OPTIONS.popsize);
            k=seed(1);
        end
        mutualVector=mean([Population(i).variable;Population(k).variable]);
        BF1=round(1+rand);
        BF2=round(1+rand);
        pp_new1=Population(i).variable+rand(1,size(pp,2)).*(Population(1).variable-
BF1.*mutualVector);
        pp_new2=Population(k).variable+rand(1,size(pp,2)).*(Population(1).variable-
BF2.*mutualVector);
        pp_new1 = FeasibleFunction_1(OPTIONS, pp_new1);
        pp_new2 = FeasibleFunction_1(OPTIONS, pp_new2);
        pp_new_cost1 = CostFunction_1(OPTIONS, pp_new1);
        pp_new_cost2 = CostFunction_1(OPTIONS, pp_new2);
        if pp_new_cost1<Population(i).cost
            Population(i).variable =pp_new1;
            Population(i).cost=pp_new_cost1;
        end
        if pp_new_cost2<Population(k).cost
            Population(k).variable =pp_new2;
            Population(k).cost=pp_new_cost2;
        end
        k=i;
        while i==k
            seed=randperm(length(Population));
```

```

k=seed(1);
end
pp_new1=Population(i).variable+(rand(1,size(pp,2))*2-1).*(Population(1).variable-
Population(k).variable);
pp_new1 = FeasibleFunction_1(OPTIONS, pp_new1);
pp_new_cost1 = CostFunction_1(OPTIONS, pp_new1);
if pp_new_cost1<Population(i).cost
    Population(i).variable =pp_new1;
    Population(i).cost=pp_new_cost1;
end
k=i;
while i==k
    seed=randperm(length(Population));
    k=seed(1);
end
parasiteVector=Population(i).variable;
seed=randperm(size(pp,2));
pick=ceil(rand*size(pp,2)));
parasiteVector(:,pick)=rand(1,length(pick)).*(ul(pick)-ll(pick))+ll(pick);
parasiteVector_cost = CostFunction_1(OPTIONS, parasiteVector);
if parasiteVector_cost<Population(k).cost
    Population(k).variable =parasiteVector;
    Population(k).cost=parasiteVector_cost;
end
Population = PopSort(Population);
n = OPTIONS.popsize;
for i = 1 : Keep
    Population(n-i+1).variable = variableKeep(i,:);
    Population(n-i+1).cost = costKeep(i);
end
Population = PopSort(Population);
MinCost = [MinCost Population(1).cost];
if DisplayFlag
    disp([num2str(MinCost(end))]);
end
Variable =(Population(1).variable);
fprintf("\n %f",MinCost(end));
fprintf("\n %f",Variable);
%%%%%%%%%%%%%
function [Population, indices] = PopSort(Population)
popsize = length(Population);
Cost = zeros(1, popsize);
indices = zeros(1, popsize);
for i = 1 : popsize

```

```

    Cost(i) = Population(i).cost;
end
[Cost, indices] = sort(Cost, 2, 'ascend');
variables = zeros(popsize, length(Population(1).variable));
for i = 1 : popsize
    variables(i, :) = Population(indices(i)).variable;
end
for i = 1 : popsize
    Population(i).variable = variables(i, :);
    Population(i).cost = Cost(i);
end
%%%%%
function [AveCost, nLegal] = ComputeAveCost(Population)
Cost = [];
nLegal = 0;
for i = 1 : length(Population)
    if Population(i).cost < inf
        Cost = [Cost Population(i).cost];
        nLegal = nLegal + 1;
    end
end
AveCost = mean(Cost);
return;
%%%%%

```

## 8. Water Wave Optimization (WWO) :

```

function WWO()
run=1;
for i=1:run
    WWO_Run(@F01);
end
%%%%%
function [OPTIONS, MinCost, AvgCost, InitFunction, CostFunction, FeasibleFunction, ...
    MaxParValue, MinParValue, Population,FeasibleFunction_1,CostFunction_1] =
Init(DisplayFlag, ProblemFunction, RandSeed)
OPTIONS.popsize = 50;
OPTIONS.Maxgen = 2000;
OPTIONS.numVar =2;
if ~exist('RandSeed', 'var')
    RandSeed = round(sum(100*clock));
end
rand('state', RandSeed);
[InitFunction, CostFunction, FeasibleFunction,FeasibleFunction_1,CostFunction_1] =
ProblemFunction();
[MaxParValue, MinParValue, Population, OPTIONS] = InitFunction(OPTIONS);
Population = CostFunction(OPTIONS, Population);

```

```

Population = PopSort(Population);
AverageCost = ComputeAveCost(Population);
MinCost = [Population(1).cost];
AvgCost = [AverageCost];
return;
%%%%%%%%%%%%%
function [InitFunction, CostFunction, FeasibleFunction,FeasibleFunction_1,CostFunction_1] =
F01
InitFunction = @F01Init;
CostFunction = @F01Cost;
CostFunction_1 = @F01Cost_1;
FeasibleFunction = @F01Feasible;
FeasibleFunction_1 = @F01Feasible_1;
return;
function [MaxParValue, MinParValue, Population, OPTIONS] = F01Init(OPTIONS)
global MinParValue MaxParValue ll ul
ll=[13 0 ];
ul=[100 100];
MaxParValue = ul;
for popindex = 1 : OPTIONS.popsize
    for k = 1 : OPTIONS.numVar
        variable(k) =(ll(k)+ (ul(k) - ll(k)) * rand);
    end
    Population(popindex).variable = variable;
end
return;
function [Population] = F01Cost(OPTIONS, Population)
global MinParValue MaxParValue
popsize = OPTIONS.popsize;
for popindex = 1 : popsize
    for k = 1 : OPTIONS.numVar
        x(k) = Population(popindex).variable(k);
    end
    Population(popindex).cost = objective(x);
end
return
function [Population_1] = F01Cost_1(OPTIONS, Population)
global MinParValue MaxParValue
popsize = size(Population,1);
Population_1 =[];
for popindex = 1 : popsize
    for k = 1 : OPTIONS.numVar
        x(k) = Population(popindex,k);
    end
    Population_1(popindex) = objective(x);
end

```

```

return
function [Population] = F01Feasible(OPTIONS, Population)
global MinParValue MaxParValue ll ul
for i = 1 : OPTIONS.popsize
    for k = 1 : OPTIONS.numVar
        Population(i).variable(k) = max(Population(i).variable(k), ll(k));
        Population(i).variable(k) = min(Population(i).variable(k), ul(k));
    end
end
return;
function [Population] = F01Feasible_1(OPTIONS, Population)
global MinParValue MaxParValue ll ul
for i = 1 : size(Population,1)
    for k = 1 : OPTIONS.numVar
        Population(i,k) = max(Population(i,k), ll(k));
        Population(i,k) = min(Population(i,k), ul(k));
    end
end
return;
%%%%%%%%%%%%%%%%%%%%%%%%%%%%%%%%%%%%%
function yy=objective(x)
p1=x(1);
p2=x(2);
z1=((p1-10)^3)+((p2-20)^3);
t1=-((p1-5)^2)-((p2-5)^2)+100;
t2=((p1-6)^2)+((p2-5)^2)-82.81;
nc=2;
    g1(1)=t1;
    g1(2)=t2;
    violate=0;
    for io=1:nc
        if g1(io)>0
            violate=violate+g1(io)^2;
        end
    end
yy=(z1)+(1e5*violate);

%%%%%%%%%%%%%%%%%%%%%%%%%%%%%%%%%%%%%
function WWO_Run(ProblemFunction, DisplayFlag, ProbFlag)
global ll ul
if ~exist('DisplayFlag', 'var')
    DisplayFlag = true;
end
% if ~exist('ProbFlag', 'var')
%     ProbFlag = true;
% end

```

```

[OPTIONS, MinCost, AvgCost, InitFunction, CostFunction, FeasibleFunction, ...
MaxParValue, MinParValue, Population, FeasibleFunction_1, CostFunction_1] =
Init(DisplayFlag, ProblemFunction);
lambda(1:OPTIONS.popsize)=0.5;
Keep=1;
epsilon=0.0000001;
hMax=12;
alpha=1.0026;
betaMax=0.25;
betaMin=0.001;
beta=betaMax;
kmax=min(12,OPTIONS.numVar/2);
h(1:OPTIONS.popsize)=hMax;
optValue=Population(1).cost;
% Begin the optimization loop
for GenIndex = 1 : OPTIONS.Maxgen
    [minIndex,maxIndex] = MinIndexMaxIndex(Population);
    for i = 1 : Keep
        variableKeep(i,:)=Population(minIndex).variable;
        costKeep(i)=Population(minIndex).cost;
    end
    for i=1:OPTIONS.popsize
        pp(i,:)=Population(i).variable;
        pp_cost(i)=Population(i).cost;
    end
    pp_new=pp;
    pp;
    Mean_pop=mean(pp);
    Stdev_pop=std(pp);
    for i=1:OPTIONS.popsize
        pp_new1=Population(i).variable+(unifrnd(-1,1,1,size(pp,2))).*lambda(i).*(ul-l);
        pp_new1 = FeasibleFunction_1(OPTIONS, pp_new1);
        pp_new_cost1 = CostFunction_1(OPTIONS, pp_new1);
        if pp_new_cost1<Population(i).cost
            Population(i).variable =pp_new1;
            Population(i).cost=pp_new_cost1;
            h(i)=hMax;
            [minIndex,maxIndex] = MinIndexMaxIndex(Population);
            if pp_new_cost1<optValue && i~= minIndex
                optValue = pp_new_cost1;
                k=kmax;
                temp = randperm(size(pp,2));
                for l=1:k
                    tempX = pp_new1;
                    d=temp(l);
                    pp_temp=Population(i).variable ;

```

```

tempX(d) = pp_temp(d)+normrnd(0,1)*beta*(ul(d)-ll(d));
pp_new_temp = FeasibleFunction_1(OPTIONS, tempX);
pp_new_temp_cost1 = CostFunction_1(OPTIONS, pp_new_temp);
if pp_new_temp_cost1 < pp_new_cost1
    Population(i).variable =pp_new_temp;
    lambda(i)=lambda(i)*pp_new_temp_cost1/Population(i).cost;
    Population(i).cost=pp_new_temp_cost1;
    pp_new_cost1=pp_new_temp_cost1;
    if pp_new_temp_cost1 < optValue
        optValue = pp_new_temp_cost1;
        optVector = Population(i).variable;
    end
end
end
else
    h(i)=h(i)-1;
    if h(i)==0
        pp_temp=Population(i).variable;
        for d=1:size(pp,2)
            pp_new1(d) = normrnd((optVector(d)+pp_temp(d))/2,abs(optVector(d)-
pp_temp(d))/2);
        end
        pp_new_temp = FeasibleFunction_1(OPTIONS, pp_new1);
        oldValue = Population(i).cost;
        Population(i).variable = pp_new1;
        Population(i).cost = CostFunction_1(OPTIONS, pp_new_temp);
        h(i)=hMax;
        lambda(i) = lambda(i)*Population(i).cost/oldValue;
    end
end
end
[minIndex,maxIndex] = MinIndexMaxIndex(Population);
worstValue= Population(maxIndex).cost;
optValue= Population(minIndex).cost ;
optVector=Population(minIndex).variable;
den=(worstValue-optValue+epsilon);
for i=1:OPTIONS.popsize
    lambda(i)=lambda(i)*power(alpha, -(worstValue-Population(i).cost+epsilon) / den);
end
beta = betaMax - (betaMax - betaMin) * GenIndex / OPTIONS.Maxgen;
n = OPTIONS.popsize;
for i = 1 : Keep
    Population(maxIndex).variable = variableKeep(i,:);
    Population(maxIndex).cost = costKeep(i);
end

```

```
[AverageCost, nLegal] = ComputeAveCost(Population);
[minIndex,maxIndex] = MinIndexMaxIndex(Population);
MinCost = [MinCost Population(minIndex).cost];
AvgCost = [AvgCost AverageCost];
if DisplayFlag
    disp([num2str(MinCost(end))]);
end
end
[minIndex,maxIndex] = MinIndexMaxIndex(Population);
Variable = (Population(minIndex).variable);
fprintf("\n %f",MinCost(end));
fprintf("\n %f",Variable);
function [minIndex,maxIndex] = MinIndexMaxIndex(Population) %Get the indicies of best and
worst solutions of the population
minIndex = 1;
maxIndex = 1;
bestValue = Population(1).cost;
worstValue = bestValue;
for i=2:length(Population)
    if Population(i).cost<bestValue
        minIndex = i;
        bestValue = Population(i).cost;
    elseif Population(i).cost>worstValue
        maxIndex = i;
        worstValue = Population(i).cost;
    end
end
%%%%%%%%%%%%%
function [Population, indices] = PopSort(Population)
popszie = length(Population);
Cost = zeros(1, popszie);
indices = zeros(1, popszie);
for i = 1 : popszie
    Cost(i) = Population(i).cost;
end
[Cost, indices] = sort(Cost, 2, 'ascend');
variables = zeros(popszie, length(Population(1).variable));
for i = 1 : popszie
    variables(i, :) = Population(indices(i)).variable;
end
for i = 1 : popszie
    Population(i).variable = variables(i, :);
    Population(i).cost = Cost(i);
end
%%%%%%%%%%%%%
function [AveCost, nLegal] = ComputeAveCost(Population)
```

```

Cost = [];
nLegal = 0;
for i = 1 : length(Population)
    if Population(i).cost < inf
        Cost = [Cost Population(i).cost];
        nLegal = nLegal + 1;
    end
end
AveCost = mean(Cost);
return;
%%%%%%%%%%%%%%%

```

## 9. Heat Transfer Search (HTS):

```

function HTS()
run=1;
for i=1:run
    HTS_Run(@F01);
end
%%%%%%%%%%%%%%%
function [OPTIONS, MinCost, AvgCost, InitFunction, CostFunction, FeasibleFunction, ...]
    MaxParValue, MinParValue, Population,FeasibleFunction_1,CostFunction_1] =
Init(DisplayFlag, ProblemFunction, RandSeed)
OPTIONS.popsize = 50;
OPTIONS.Maxgen = 2000;
OPTIONS.numVar =2;
if ~exist('RandSeed', 'var')
    RandSeed = round(sum(100*clock));
end
rand('state', RandSeed);
[InitFunction, CostFunction, FeasibleFunction,FeasibleFunction_1,CostFunction_1] =
ProblemFunction();
[MaxParValue, MinParValue, Population, OPTIONS] = InitFunction(OPTIONS);
Population = CostFunction(OPTIONS, Population);
Population = PopSort(Population);
AverageCost = ComputeAveCost(Population);
MinCost = [Population(1).cost];
AvgCost = [AverageCost];
return;
%%%%%%%%%%%%%%%
function [InitFunction, CostFunction, FeasibleFunction,FeasibleFunction_1,CostFunction_1] =
F01
InitFunction = @F01Init;
CostFunction = @F01Cost;
CostFunction_1 = @F01Cost_1;
FeasibleFunction = @F01Feasible;
FeasibleFunction_1 = @F01Feasible_1;

```

```

return;
function [MaxParValue, MinParValue, Population, OPTIONS] = F01Init(OPTIONS)
global MinParValue MaxParValue ll ul
ll=[13 0];
ul=[100 100];
MaxParValue = ul;
for popindex = 1 : OPTIONS.popsize
    for k = 1 : OPTIONS.numVar
        variable(k) =(ll(k)+ (ul(k) - ll(k)) * rand);
    end
    Population(popindex).variable = variable;
end
return;
function [Population] = F01Cost(OPTIONS, Population)
global MinParValue MaxParValue
popsize = OPTIONS.popsize;
for popindex = 1 : popsize
    for k = 1 : OPTIONS.numVar
        x(k) = Population(popindex).variable(k);
    end
    Population(popindex).cost = objective(x);
end
return
function [Population_1] = F01Cost_1(OPTIONS, Population)
global MinParValue MaxParValue
popsize = size(Population,1);
Population_1 =[];
for popindex = 1 : popsize
    for k = 1 : OPTIONS.numVar
        x(k) = Population(popindex,k);
    end
    Population_1(popindex) = objective(x);
end
return
function [Population] = F01Feasible(OPTIONS, Population)
global MinParValue MaxParValue ll ul
for i = 1 : OPTIONS.popsize
    for k = 1 : OPTIONS.numVar
        Population(i).variable(k) = max(Population(i).variable(k), ll(k));
        Population(i).variable(k) = min(Population(i).variable(k), ul(k));
    end
end
return;
function [Population] = F01Feasible_1(OPTIONS, Population)
global MinParValue MaxParValue ll ul
for i = 1 : size(Population,1)

```

```

for k = 1 : OPTIONS.numVar
    Population(i,k) = max(Population(i,k), ll(k));
    Population(i,k) = min(Population(i,k), ul(k));
end
end
return;
%%%%%
function yy=objective(x)
p1=x(1);
p2=x(2);
z1=((p1-10)^3)+((p2-20)^3);
t1=-((p1-5)^2)-((p2-5)^2)+100;
t2=((p1-6)^2)+((p2-5)^2)-82.81;
nc=2;
    g1(1)=t1;
    g1(2)=t2;
    violate=0;
    for io=1:nc
        if g1(io)>0
            violate=violate+g1(io)^2;
        end
    end
yy=(z1)+(1e5*violate);
%%%%%
function HTS_Run(ProblemFunction, DisplayFlag, ProbFlag)
global ll
global ul
CDF=2;
COF=10;
RDF=2;
if ~exist('DisplayFlag', 'var')
    DisplayFlag = true;
end
Population.variable=[];
Population.cost=[];
[OPTIONS, MinCost, AvgCost, InitFunction, CostFunction, FeasibleFunction, ...
    MaxParValue, MinParValue, Population, FeasibleFunction_1, CostFunction_1] =
Init(DisplayFlag, ProblemFunction);
Keep=1;
for GenIndex = 1 : OPTIONS.Maxgen
    for i = 1 : Keep
        variableKeep(i,:)=Population(i).variable;
        costKeep(i)=Population(i).cost;
    end
    for i=1:OPTIONS.popsize
        pp(i,:)=Population(i).variable;
    end
end

```

```

pp_cost(i)=Population(i).cost;
end
pp1=pp;
Mean_pop=mean(pp);
R=rand;
for i = 1 : 1 : OPTIONS.popsize
if R<=0.3333
    ii=ceil(rand*(OPTIONS.popsize));
    while ii==i
        ii=ceil(rand*(OPTIONS.popsize));
    end
    if Population(i).cost<Population(ii).cost
        for jj = 1:OPTIONS.numVar
            if GenIndex < (OPTIONS.Maxgen /CDF)
                pp1(i,jj) = (1-R^2)*pp(i,jj);
            else
                pp1(i,jj) = (1-rand)*pp(i,jj);
            end
            end
            pp_new = FeasibleFunction_1(OPTIONS, pp1(ii,:));
            pp_new_cost = CostFunction_1(OPTIONS, pp_new);
            if pp_new_cost<Population(ii).cost
                Population(ii).variable =pp_new;
                Population(ii).cost=pp_new_cost;
            end
        else
            for jj = 1:OPTIONS.numVar
                if GenIndex < (OPTIONS.Maxgen /CDF)
                    pp1(i,jj) = (1-R^2)*pp(ii,jj);
                else
                    pp1(i,jj) = (1-rand)*pp(ii,jj);
                end
                end
                pp_new = FeasibleFunction_1(OPTIONS, pp1(i,:));
                pp_new_cost = CostFunction_1(OPTIONS, pp_new);
                if pp_new_cost<Population(i).cost
                    Population(i).variable =pp_new;
                    Population(i).cost=pp_new_cost;
                end
            end
        elseif 0.3333< R && R <=0.6666
            ii=ceil(rand*(OPTIONS.popsize));
            while ii==i
                ii=ceil(rand*(OPTIONS.popsize));
            end
            if Population(i).cost<Population(ii).cost

```

```

for j=1:OPTIONS.numVar
if GenIndex < (OPTIONS.Maxgen /RDF)
pp1(i,j) = pp(i,j)+ (R)*(pp(i,j)-pp(ii,j));
else
pp1(i,j) = pp(i,j)+ (rand)*(pp(i,j)-pp(ii,j));
end
end
else
for j=1:OPTIONS.numVar
if GenIndex < (OPTIONS.Maxgen/RDF)
pp1(i,j) = pp(i,j)+ (R)*(pp(ii,j)-pp(i,j));
else
pp1(i,j) = pp(i,j)+ (rand)*(pp(ii,j)-pp(i,j));
end
end
end
fesible_1 = FeasibleFunction_1(OPTIONS, pp1(i,:));
fesible_1_cost = CostFunction_1(OPTIONS, fesible_1);
if fesible_1_cost<Population(i).cost
Population(i).variable =fesible_1;
Population(i).cost=fesible_1_cost;
end
else
for j=1:OPTIONS.numVar
if GenIndex < round(OPTIONS.Maxgen /COF)
pp1(i,j) = pp(i,j)+ (R)*(pp(1,j)- Mean_pop(j)*abs(R-rand));
else
pp1(i,j) = pp(i,j)+ (R)*(pp(1,j)- Mean_pop(j)*round(1+rand));
end
end
end
fesible_1 = FeasibleFunction_1(OPTIONS, pp1(i,:));
fesible_1_cost = CostFunction_1(OPTIONS, fesible_1);
if fesible_1_cost<Population(i).cost
Population(i).variable =fesible_1;
Population(i).cost=fesible_1_cost;
end
end
Population = FeasibleFunction(OPTIONS, Population);
Population = CostFunction(OPTIONS, Population);
Population = PopSort(Population);
n = length(Population);
for i = 1 : Keep
Population(n-i+1).variable = variableKeep(i,:);
Population(n-i+1).cost = costKeep(i);
end

```

```

Population = PopSort(Population);
MinCost = [MinCost Population(1).cost];
if DisplayFlag
    disp([num2str(MinCost(end))]);
end
end
disp([num2str(MinCost(end))]);
Variable =(Population(1).variable);
fprintf("\n %f",MinCost(end));
fprintf("\n %f",Variable);
%%%%%%%%%%%%%%%
function [Population, indices] = PopSort(Population)
popsize = length(Population);
Cost = zeros(1, popsize);
indices = zeros(1, popsize);
for i = 1 : popsize
    Cost(i) = Population(i).cost;
end
[Cost, indices] = sort(Cost, 2, 'ascend');
variables = zeros(popsize, length(Population(1).variable));
for i = 1 : popsize
    variables(i, :) = Population(indices(i)).variable;
end
for i = 1 : popsize
    Population(i).variable = variables(i, :);
    Population(i).cost = Cost(i);
end
%%%%%%%%%%%%%%
function [AveCost, nLegal] = ComputeAveCost(Population)
Cost = [];
nLegal = 0;
for i = 1 : length(Population)
    if Population(i).cost < inf
        Cost = [Cost Population(i).cost];
        nLegal = nLegal + 1;
    end
end
AveCost = mean(Cost);
return;
%%%%%%%%%%%%%

```

## 10. Passing Vehicle Search (PVS):

```

function PVS()
run=1;
for i=1:run
    PVS_Run(@F01);

```

```

end
%%%%%%%
function [OPTIONS, MinCost, AvgCost, InitFunction, CostFunction, FeasibleFunction, ...
    MaxParValue, MinParValue, Population, FeasibleFunction_1, CostFunction_1] =
Init(DisplayFlag, ProblemFunction, RandSeed)
OPTIONS.popsize = 50;
OPTIONS.Maxgen = 2000;
OPTIONS.numVar = 2;
if ~exist('RandSeed', 'var')
    RandSeed = round(sum(100*clock));
end
rand('state', RandSeed);
[InitFunction, CostFunction, FeasibleFunction, FeasibleFunction_1, CostFunction_1] =
ProblemFunction();
[MaxParValue, MinParValue, Population, OPTIONS] = InitFunction(OPTIONS);
Population = CostFunction(OPTIONS, Population);
Population = PopSort(Population);
AverageCost = ComputeAveCost(Population);
MinCost = [Population(1).cost];
AvgCost = [AverageCost];
return;
%%%%%%%
function [InitFunction, CostFunction, FeasibleFunction, FeasibleFunction_1, CostFunction_1] =
F01
InitFunction = @F01Init;
CostFunction = @F01Cost;
CostFunction_1 = @F01Cost_1;
FeasibleFunction = @F01Feasible;
FeasibleFunction_1 = @F01Feasible_1;
return;
function [MaxParValue, MinParValue, Population, OPTIONS] = F01Init(OPTIONS)
global MinParValue MaxParValue ll ul
ll=[13 0 ];
ul=[100 100];
MaxParValue = ul;
for popindex = 1 : OPTIONS.popsize
    for k = 1 : OPTIONS.numVar
        variable(k) =(ll(k)+ (ul(k) - ll(k)) * rand);
    end
    Population(popindex).variable = variable;
end
return;
function [Population] = F01Cost(OPTIONS, Population)
global MinParValue MaxParValue
popsize = OPTIONS.popsize;
for popindex = 1 : popsize

```

```

for k = 1 : OPTIONS.numVar
    x(k) = Population(popindex).variable(k);
end
Population(popindex).cost = objective(x);
end
return
function [Population_1] = F01Cost_1(OPTIONS, Population)
global MinParValue MaxParValue
popsize = size(Population,1);
Population_1 = [];
for popindex = 1 : popsize
    for k = 1 : OPTIONS.numVar
        x(k) = Population(popindex,k);
    end
    Population_1(popindex) = objective(x);
end
return
function [Population] = F01Feasible(OPTIONS, Population)
global MinParValue MaxParValue ll ul
for i = 1 : OPTIONS.popsize
    for k = 1 : OPTIONS.numVar
        Population(i).variable(k) = max(Population(i).variable(k), ll(k));
        Population(i).variable(k) = min(Population(i).variable(k), ul(k));
    end
end
return;
function [Population] = F01Feasible_1(OPTIONS, Population)
global MinParValue MaxParValue ll ul
for i = 1 : size(Population,1)
    for k = 1 : OPTIONS.numVar
        Population(i,k) = max(Population(i,k), ll(k));
        Population(i,k) = min(Population(i,k), ul(k));
    end
end
return;
%%%%%%%%%%%%%
function yy=objective(x)
p1=x(1);
p2=x(2);
z1=((p1-10)^3)+((p2-20)^3);
t1=-((p1-5)^2)-((p2-5)^2)+100;
t2=((p1-6)^2)+((p2-5)^2)-82.81;
nc=2;
    g1(1)=t1;
    g1(2)=t2;
    violate=0;

```

```

for io=1:nc
    if g1(io)>0
        violate=violate+g1(io)^2;
    end
end
yy=(z1)+(1e5*violate);
%%%%%%%%%%%%%%%%%%%%%%%%%%%%%%%%%%%%%%%%%%%%%%%%%%%%%%%%%%%%%%%%%%%%%%%%%%%%%%%%
function PVS_Run(ProblemFunction, DisplayFlag, ProbFlag)
global ll ul
if ~exist('DisplayFlag', 'var');DisplayFlag = true;
end
Population.variable=[];
Population.cost=[];
[OPTIONS, MinCost, AvgCost, InitFunction, CostFunction, FeasibleFunction, ...
MaxParValue, MinParValue, Population,FeasibleFunction_1,CostFunction_1] =
Init(DisplayFlag,ProblemFunction);
Keep=1;
norm_factor=1;
VF=1;
for GenIndex = 1 : OPTIONS.Maxgen
    for i = 1 : Keep
        variableKeep(i,:)=Population(i).variable;
        costKeep(i)=Population(i).cost;
    end
    for i=1:OPTIONS.popsize
        temp_1(i,:)=Population(i).variable;
        temp_1_cost(i)=Population(i).cost;
    end
    Pop_size=OPTIONS.popsize;
    for k = 1 : OPTIONS.popsize
        r=[]; v=[];
        r(1) = k;
        while true;
            r(2) = round(OPTIONS.popsize * rand + 0.5);
            if (r(2) ~= r(1)),
                break,
            end
        end
        while true
            r(3) = round(OPTIONS.popsize* rand + 0.5);
            if (r(3) ~= r(1)) && (r(3) ~= r(2)),
                break,
            end
        end
        r2=r;
        r=(norm_factor/Pop_size)*r;
    end
end

```

```

r1=r;
v1=(rand(1,3)).*(VF-r1);
y=abs(r1(3)-r1(2));
x=abs(r1(3)-r1(1));
x1=(x*v1(3))/(v1(1)-v1(3));
y1=(x*v1(2))/(v1(1)-v1(3));
if v1(1)>v1(3)
    if(y-y1)>x1;
    con1=v1(1)/(v1(1)-v1(3));
    temp_1_new= Population(r2(1)).variable+
con1*rand(1,OPTIONS.numVar).*(Population(r2(1)).variable-Population(r2(3)).variable);
else
    temp_1_new= Population(r2(1)).variable+
rand(1,OPTIONS.numVar).*(Population(r2(1)).variable-Population(r2(2)).variable);
end
else
    temp_1_new = Population(r2(1)).variable+
rand(1,OPTIONS.numVar).*(Population(r2(3)).variable-Population(r2(1)).variable);
end
temp_1_new = FeasibleFunction_1(OPTIONS, temp_1_new);
temp_1_new_cost = CostFunction_1(OPTIONS, temp_1_new);
if temp_1_new_cost<Population(k).cost
    Population(k).variable =temp_1_new;
    Population(k).cost=temp_1_new_cost;
end
Population = PopSort(Population);
n = length(Population);
for i = 1 : Keep
    Population(n-i+1).variable = variableKeep(i,:);
    Population(n-i+1).cost = costKeep(i);
end
Population = PopSort(Population);
MinCost = [MinCost Population(1).cost];
if DisplayFlag
    disp([num2str(MinCost(end))]);
end
end
disp([num2str(MinCost(end))]);
Variable =(Population(1).variable);
fprintf("\n %f,MinCost(end));
fprintf("\n %f,Variable);
%%%%%%%%%%%%%%%
function [Population, indices] = PopSort(Population)
popsiz = length(Population);
Cost = zeros(1, popsiz);

```

```

indices = zeros(1, popsize);
for i = 1 : popsize
    Cost(i) = Population(i).cost;
end
[Cost, indices] = sort(Cost, 2, 'ascend');
variables = zeros(popsize, length(Population(1).variable));
for i = 1 : popsize
    variables(i, :) = Population(indices(i)).variable;
end
for i = 1 : popsize
    Population(i).variable = variables(i, :);
    Population(i).cost = Cost(i);
end
%%%%%%%%%%%%%%%%%%%%%%%%%%%%%%%%%%%%%
function [AveCost, nLegal] = ComputeAveCost(Population)
Cost = [];
nLegal = 0;
for i = 1 : length(Population)
    if Population(i).cost < inf
        Cost = [Cost Population(i).cost];
        nLegal = nLegal + 1;
    end
end
AveCost = mean(Cost);
return;
%%%%%%%%%%%%%%%%%%%%%%%%%%%%%%%%%%%%%

```

## 11. Sine-Cosine Algorithm (SCA):

```

function SCA()
run=1;
for i=1:run
    SCA_Run(@F01);
end
%%%%%%%%%%%%%%%%%%%%%%%%%%%%%%%%%%%%%
function [OPTIONS, MinCost, AvgCost, InitFunction, CostFunction, FeasibleFunction, ...
    MaxParValue, MinParValue, Population,FeasibleFunction_1,CostFunction_1] =
Init(DisplayFlag, ProblemFunction, RandSeed)
OPTIONS.popsize = 50;
OPTIONS.Maxgen = 2000;
OPTIONS.numVar =2;
if ~exist('RandSeed', 'var')
    RandSeed = round(sum(100*clock));
end
rand('state', RandSeed);
[InitFunction, CostFunction, FeasibleFunction,FeasibleFunction_1,CostFunction_1] =
ProblemFunction();

```

```

[MaxParValue, MinParValue, Population, OPTIONS] = InitFunction(OPTIONS);
Population = CostFunction(OPTIONS, Population);
Population = PopSort(Population);
AverageCost = ComputeAveCost(Population);
MinCost = [Population(1).cost];
AvgCost = [AverageCost];
return;
%%%%%%%%%%%%%%%%%%%%%%%%%%%%%%%%%%%%%
function [InitFunction, CostFunction, FeasibleFunction,FeasibleFunction_1,CostFunction_1] =
F01
InitFunction = @F01Init;
CostFunction = @F01Cost;
CostFunction_1 = @F01Cost_1;
FeasibleFunction = @F01Feasible;
FeasibleFunction_1 = @F01Feasible_1;
return;
function [MaxParValue, MinParValue, Population, OPTIONS] = F01Init(OPTIONS)
global MinParValue MaxParValue ll ul
ll=[13 0 ];
ul=[100 100];
MaxParValue = ul;
for popindex = 1 : OPTIONS.popsize
    for k = 1 : OPTIONS.numVar
        variable(k) =(ll(k)+ (ul(k) - ll(k)) * rand);
    end
    Population(popindex).variable = variable;
end
return;
function [Population] = F01Cost(OPTIONS, Population)
global MinParValue MaxParValue
popsize = OPTIONS.popsize;
for popindex = 1 : popszie
    for k = 1 : OPTIONS.numVar
        x(k) = Population(popindex).variable(k);
    end
    Population(popindex).cost = objective(x);
end
return;
function [Population_1] = F01Cost_1(OPTIONS, Population)
global MinParValue MaxParValue
popszie = size(Population,1);
Population_1 =[];
for popindex = 1 : popszie
    for k = 1 : OPTIONS.numVar
        x(k) = Population(popindex,k);
    end

```

```

    Population_1(popindex) = objective(x);
end
return
function [Population] = F01Feasible(OPTIONS, Population)
global MinParValue MaxParValue ll ul
for i = 1 : OPTIONS.popsize
    for k = 1 : OPTIONS.numVar
        Population(i).variable(k) = max(Population(i).variable(k), ll(k));
        Population(i).variable(k) = min(Population(i).variable(k), ul(k));
    end
end
return;
function [Population] = F01Feasible_1(OPTIONS, Population)
global MinParValue MaxParValue ll ul
for i = 1 : size(Population,1)
    for k = 1 : OPTIONS.numVar
        Population(i,k) = max(Population(i,k), ll(k));
        Population(i,k) = min(Population(i,k), ul(k));
    end
end
return;
%%%%%%%%%%%%%
function yy=objective(x)
p1=x(1);
p2=x(2);
z1=((p1-10)^3)+((p2-20)^3);
t1=-((p1-5)^2)-((p2-5)^2)+100;
t2=((p1-6)^2)+((p2-5)^2)-82.81;
nc=2;
    g1(1)=t1;
    g1(2)=t2;
    violate=0;
    for io=1:nc
        if g1(io)>0
            violate=violate+g1(io)^2;
        end
    end
yy=(z1)+(1e5*violate);
%%%%%%%%%%%%%
function SCA_Run(ProblemFunction, DisplayFlag, ProbFlag)
global ll ul
if ~exist('DisplayFlag', 'var')
    DisplayFlag = true;
end
Population.variable=[];
Population.cost=[];

```

```
[OPTIONS, MinCost, AvgCost, InitFunction, CostFunction, FeasibleFunction, ...
    MaxParValue, MinParValue, Population, FeasibleFunction_1, CostFunction_1] =
Init(DisplayFlag, ProblemFunction);
Keep=1;
a=1;
for GenIndex = 1 : OPTIONS.Maxgen
    for i = 1 : Keep
        variableKeep(i,:) = Population(i).variable;
        costKeep(i) = Population(i).cost;
    end
    for i=1:OPTIONS.popsize
        pp(i,:)=Population(i).variable;
        pp_cost(i)=Population(i).cost;
    end
    best_sol=pp(1,:);
    r1=a-(a*GenIndex/OPTIONS.Maxgen);
    for i = 1 : 1 : OPTIONS.popsize
        for j=1:OPTIONS.numVar
            r4=rand;
            r2=(2*pi)*rand;
            r3=2*rand;
            if r4<0.5
                pp1(j)= Population(i).variable(j) +(r1*sin(r2)*abs(r3*best_sol(j)-
Population(i).variable(j)));
            else
                pp1(j)= Population(i).variable(j) +(r1*cos(r2)*abs(r3*best_sol(j)-
Population(i).variable(j)));
            end
        end
        function_1 = FeasibleFunction_1(OPTIONS, pp1);
        function_1_cost = CostFunction_1(OPTIONS, function_1);
        Population(i).variable =function_1;
        Population(i).cost=function_1_cost;
    end
    Population = PopSort(Population);
    n = length(Population);
    for i = 1 : Keep
        Population(n-i+1).variable = variableKeep(i,:);
        Population(n-i+1).cost = costKeep(i);
    end
    Population = PopSort(Population);
    MinCost = [MinCost Population(1).cost];
    if DisplayFlag
        disp([num2str(MinCost(end))]);
    end
end
```

```
Variable =(Population(1).variable);
fprintf("\n %f",MinCost(end));
fprintf("\n %f",Variable);
%%%%%%%%%%%%%%%
function [Population, indices] = PopSort(Population)
popsize = length(Population);
Cost = zeros(1, popsize);
indices = zeros(1, popsize);
for i = 1 : popsize
    Cost(i) = Population(i).cost;
end
[Cost, indices] = sort(Cost, 2, 'ascend');
variables = zeros(popsize, length(Population(1).variable));
for i = 1 : popsize
    variables(i, :) = Population(indices(i)).variable;
end
for i = 1 : popsize
    Population(i).variable = variables(i, :);
    Population(i).cost = Cost(i);
end
%%%%%%%%%%%%%%
function [AveCost, nLegal] = ComputeAveCost(Population)
Cost = [];
nLegal = 0;
for i = 1 : length(Population)
    if Population(i).cost < inf
        Cost = [Cost Population(i).cost];
        nLegal = nLegal + 1;
    end
end
AveCost = mean(Cost);
return;
%%%%%%%%%%%%%
```

# Index

## A

- Absorber plate, 378–382, 389, 390  
Absorber temperature, 216–219  
Absorption heat pump, 182–191  
Ambient temperature, 135, 144, 153, 179, 188, 214, 216, 225, 226, 249, 252, 267, 276, 277, 371, 375, 387, 390  
Artificial bee colony (ABC), 7, 14, 15, 31, 36, 47, 48, 59, 60, 70, 71, 74, 80, 81, 90, 91, 107, 108, 116, 126, 127, 137, 138, 145, 146, 154–156, 162, 163, 171, 172, 180, 181, 189, 190, 208, 209, 218, 228, 229, 240, 250, 251, 259, 260, 269, 270, 278, 279, 297, 298, 306, 307, 314, 315, 324, 331, 332, 338, 339, 356, 366, 376, 377, 383, 384, 392, 393, 399, 400, 405, 406, 430  
Atkinson power cycle, 333, 337–340  
Average temperature, 185, 188, 267, 317

## B

- Braysson power cycle, 308–310, 313–316  
Brayton cycle, 128, 130, 131, 174–176, 179–182, 191, 287, 299, 301–306, 308, 309, 325  
Brayton heat engine, 128–131, 135–139  
Brayton power cycle, 299–302, 304–308, 325

## C

- Capacitance rate, 104, 145, 179, 267–269, 271, 277, 279, 280, 311  
Capital cost, 36, 44, 56, 60, 62, 72, 236, 294, 295, 347, 353  
Carnot cycle, 100, 101, 103, 111, 120, 156, 158, 200, 203

- Carnot heat engine, 99–109, 156–158, 161, 162, 203  
Carnot refrigerator, 199–204, 207–210  
Cascade refrigerator, 229–231, 233, 237–241, 244  
Case study, 37, 45–47, 57–59, 68–70, 78, 79, 89, 90, 105, 106, 114, 115, 124, 125, 135, 136, 144, 145, 153, 154, 161, 170, 171, 179, 180, 188, 189, 207, 208, 216, 217, 226, 227, 237, 239, 249, 257, 258, 267, 268, 277, 278, 290, 294, 296, 305, 306, 313, 314, 318, 322, 323, 329, 330, 337, 354, 355, 364, 365, 374, 375, 382, 383, 390, 391, 398, 403, 404  
Coefficient of performance (COP), 99, 166, 173, 179, 180, 182, 184, 187–191, 200, 202, 210, 215, 216, 219, 221, 226, 227, 232, 233, 244, 249, 252–254, 257, 263, 264, 272, 277, 280  
Cold-side heat exchange, 267–269, 271, 277, 279, 280  
Cold stage, 252, 255–258, 260, 261  
Collector efficiency, 319, 381, 387, 396  
Combustion chamber, 128, 129, 133, 147–149, 299, 328, 400–402  
Comparative results, 33, 47, 48, 59, 60, 70, 80, 90, 99, 107, 115, 116, 126, 137, 145, 146, 154, 162, 171, 172, 180, 189, 199, 208, 209, 217, 218, 228, 239, 240, 250, 259, 269, 278, 279, 287, 297, 306, 307, 314, 315, 323, 324, 331, 338, 345, 356, 365, 366, 376, 383, 392, 399, 405  
Compression process, 128, 148, 299  
Compressor, 57, 58, 68, 78, 128, 132, 135, 139, 141, 164, 165, 176, 177, 179, 182,

- 200, 229–231, 234, 235, 261, 262, 270, 271, 299, 300, 309, 325–329, 333, 400–402, 404–406
- Condenser, 36, 109, 110, 174, 184–186, 188, 191, 203, 204, 207, 210–217, 219, 220, 223–232, 234, 235, 237, 238, 242, 244, 249, 252, 288–293, 295, 308, 317, 318, 321, 358–360, 363, 364, 366, 367
- Condenser temperature, 216, 218, 219, 237–240, 251
- Constant pressure process, 109, 128, 139, 150, 174, 231, 309, 333
- Constant volume process, 119, 150, 333
- Constraints, 1, 2, 45–48, 50, 51, 57, 58, 60, 61, 68, 69, 72, 74, 78, 79, 81–83, 89, 92, 105–107, 109, 114, 115, 124, 125, 135, 136, 144, 145, 147, 153, 161, 164, 170, 171, 173, 179, 182, 188, 189, 191, 207, 208, 210, 216–219, 226–228, 230, 237–240, 249, 252, 257, 258, 261, 267, 268, 271, 277–280, 294, 296, 298, 305, 313, 314, 322, 323, 329, 330, 337, 354–356, 364, 365, 367, 374, 375, 382, 390, 391, 398, 403–405
- Convective heat transfer coefficient, 54, 123, 303, 305, 372, 381, 388
- Cooling load, 202, 203, 207, 209, 210, 221, 225, 233, 253, 254, 263, 266, 267, 270–272, 275–280
- Cooling tower, 289, 345–357
- Correction factor, 39–41, 44, 45, 77
- Cost estimation, 44, 45, 56, 57, 67
- Counter-flow, 49, 84, 346–348, 354
- Cross-flow, 49, 346
- Cryogenic refrigerator, 199, 261–263, 271, 272
- Cuckoo search algorithm (CSA), 8, 16, 47, 48, 59, 60, 70–72, 80, 81, 90, 91, 107, 108, 116, 126, 127, 137, 138, 145, 146, 154, 155, 162, 163, 171, 172, 180–182, 189, 190, 208–210, 218, 228, 229, 240, 250, 251, 259, 260, 269, 270, 278, 279, 297, 298, 306, 307, 315, 323, 324, 331, 332, 338, 339, 355, 356, 365, 366, 376, 377, 383, 384, 392, 399, 405, 406
- D**
- Design specification, 1, 46, 375
- Design variables, 1, 13, 14, 17, 18, 21, 24, 25, 35–37, 45, 47, 50, 52, 57, 58, 61, 63, 68, 69, 72, 78, 79, 82, 89, 105, 106, 110, 114, 115, 124, 125, 135, 136, 144, 145, 153, 161, 170, 171, 179, 188, 207, 208, 216, 217, 226, 227, 237, 238, 244, 249, 258, 267, 268, 277, 294, 296, 305, 313, 314, 322, 323, 326, 329, 330, 334, 337, 354, 355, 359, 364, 365, 369, 374, 382, 390, 391, 395, 398, 403, 404
- Diesel cycle, 147, 150, 151
- Diesel heat engine, 147, 149, 150, 152–156
- Differential evolution (DE), 7, 12, 13, 30, 35, 47, 48, 59, 60, 70, 71, 80, 81, 90, 91, 107, 108, 116, 126, 127, 137, 138, 145, 146, 154–156, 162, 163, 171, 172, 180, 181, 189, 190, 208–210, 218, 228, 229, 239, 240, 250, 251, 259, 260, 269, 270, 278, 279, 297, 298, 307, 314, 315, 324, 331, 332, 338, 339, 355, 356, 365, 366, 376, 377, 383, 384, 392, 399, 405, 406, 426
- Dimensionless power, 136, 139, 144, 147, 152, 153, 156, 158, 160, 161, 164, 310, 312, 313, 315, 316
- E**
- Ecological coefficient of performance (ECOP), 130, 131, 135–139, 179, 182, 188, 206, 207, 210, 334
- Ecological function, 102, 104, 105, 109, 120, 124, 128, 130, 135, 144, 147, 158, 160, 161, 164, 166, 170, 173, 176, 178, 179, 182, 184, 222, 225, 227, 230, 264, 272, 276, 277, 280
- Effectiveness, 1, 4, 7, 33, 34, 36, 37, 49, 51–53, 61, 63, 73, 74, 76–80, 82–84, 131, 135, 141, 142, 144–147, 170, 172, 173, 176, 179, 182, 204, 205, 207, 210, 216, 267–269, 271, 274, 277, 279, 280, 301, 302, 305, 307, 308, 311, 347, 348
- Effective thermal conductivity, 361
- Efficiency, 45, 52, 57, 58, 62, 68, 69, 101–103, 110, 111, 118–122, 124, 130, 131, 140, 141, 143, 149, 150, 152, 157, 175–179, 203, 213, 214, 216, 231–234, 236, 243, 244, 248, 249, 264, 272, 288, 290, 291, 293, 301, 309–312, 317, 318, 321–329, 333, 334, 336, 347, 359, 372, 379, 380, 386–390, 395, 397, 401
- Ejector refrigerator, 241, 242, 244, 249–252
- Emittance, 380, 382, 384, 385
- Energy balance, 213, 214, 222, 248, 293, 320, 321
- Enthalpy, 111, 213, 247, 248, 320, 328, 349, 350, 371, 402
- Entropy generation, 35, 37, 51, 52, 63, 74, 103, 104, 119, 120, 124, 130, 134, 139, 144, 157, 160, 177, 187, 206, 214, 267, 268, 270, 271, 276, 288, 309, 359, 369, 371, 374–377, 379

- Ericsson cryogenic refrigerator, 199, 270–272  
Ericsson heat engines, 99, 139–141, 144–147  
Evaporator, 174, 184–186, 188, 191, 205–207, 210–216, 221, 223–231, 233, 234, 237, 242, 244, 248, 249, 252, 317, 320, 358–361, 363, 364, 366, 367  
Evaporator temperature, 186, 188, 216, 218, 219, 230, 251  
Evolutionary algorithms, 2, 36, 401  
Exergetic efficiency, 36, 124, 128, 175, 178, 179, 182, 213, 215–219, 221, 227, 233, 243, 249–252, 267, 270, 271, 288  
Exergetic performance criterion (EPC), 206, 233  
Exergy balance, 214  
Exergy destruction, 178, 234–240, 290, 310, 402  
Exergy input, 178, 203, 206, 207, 210, 235  
Expansion process, 109, 139, 148, 183, 211, 231, 289, 303, 325, 333  
Expansion valve, 183, 184, 211, 214, 231, 242
- F**  
Fin and tube heat exchanger (FTHE), 62–64, 67–72  
Fin height, 54, 57, 58, 61  
Fin pitch, 63, 65, 68, 69, 72  
Fin thickness, 54, 57, 58, 61, 64, 237, 375  
Friedman rank test results, 48, 60, 71, 81, 91, 108, 116, 127, 138, 146, 155, 163, 172, 181, 190, 209, 218, 229, 240, 251, 260, 270, 279, 298, 307, 315, 324, 332, 339, 356, 366, 376, 384, 392, 399, 406
- G**  
Generator temperature, 186, 188, 216, 218, 219, 221  
Genetic algorithm (GA), 7–9, 12, 30, 35–37, 47, 48, 51–53, 59, 60, 63, 70, 71, 74, 80, 81, 84, 90, 91, 107, 108, 116, 126, 127, 137, 138, 145, 146, 154, 155, 162, 163, 171, 172, 180, 181, 189, 190, 208, 209, 218, 228, 229, 239, 240, 244, 250, 251, 253, 259, 260, 269, 270, 278, 279, 297, 298, 306, 307, 314, 315, 323, 324, 331, 332, 338, 339, 356, 366, 376, 379, 383, 384, 392, 399, 400, 405, 406  
Glass cover, 380, 382  
Graphical presentation of Friedman rank test, 49, 61, 71, 81, 91, 108, 117, 127, 138, 147, 155, 163, 173, 181, 190, 209, 219, 229, 241, 251, 260, 270, 280, 298, 308, 316, 325, 332, 339, 357, 367, 377, 384, 393, 400, 406
- H**  
Heat absorbed, 141, 143, 200, 203, 224, 248, 273, 274, 302, 304, 311  
Heat capacitance, 114, 115, 117, 130, 141, 144, 146, 147, 167, 170, 173, 264, 273  
Heat conductance, 114, 115, 117, 176, 202, 206, 313, 315, 316  
Heat conductance ratio, 102, 313  
Heat conduction rate, 207, 210  
Heat duty, 34, 35, 41, 57, 63, 69, 79, 89, 92, 235  
Heat engines, 4, 99, 100, 102, 103, 119, 157  
Heat exchangers, 4, 33, 34, 43, 49, 51–53, 62, 63, 82–84, 102, 141, 174, 184, 200, 212, 292, 302, 309, 313, 347, 378  
Heat flux, 252, 364, 368, 370, 375  
Heat input, 221–224, 335  
Heat loss, 84, 121, 139, 142, 150–152, 167, 186, 263, 292, 378  
Heat output, 222, 223  
Heat pipe, 345, 357–367, 374, 375  
Heat pumps, 4, 99, 100, 174, 175, 184  
Heat rejected, 99, 131, 150, 185, 224, 255, 257, 273, 274, 302, 329, 335  
Heat removal factor, 319, 381, 387, 396, 397  
Heat sink, 103, 105–107, 109, 111, 112, 117, 118, 120, 121, 124, 125, 127–129, 131, 132, 134–136, 138, 139, 141, 144, 158, 161, 164, 166, 170, 173, 174, 176, 177, 179, 222, 267–269, 271, 275, 277, 279, 280, 287, 302, 305, 309, 311, 345, 368–371, 373–377  
Heat sink temperature difference, 114, 115, 117  
Heat source, 103, 105–109, 111, 112, 115, 117, 118, 120, 121, 124, 125, 127, 128, 131, 132, 134–136, 138, 139, 141, 144, 158, 161, 164, 166, 170, 173, 174, 176, 182, 183, 187, 221, 222, 244, 252, 267–269, 271, 275, 277, 279, 280, 302, 305, 309–311, 316, 333, 358  
Heat source temperature difference, 114, 115, 117  
Heat source temperature ratio, 105–107, 109  
Heat transfer, 1, 4, 24–26, 33, 36–42, 44, 49, 51–55, 62–67, 75–77, 82–85, 89, 102–107, 109, 112, 120–122, 139, 141–143, 156–158, 161, 162, 167, 176, 177, 184, 186, 202–206, 215, 221, 222, 224–226, 229, 230, 244, 248, 253, 254,

- 262, 263, 271, 273, 275, 293, 311, 334, 335, 348, 359, 360, 368–370, 372, 374, 378–380, 386, 389, 394, 395, 402
- Heat transfer area, 35, 51–53, 55, 72, 75, 84, 85, 87, 142, 158, 167, 169, 184, 186, 203, 205, 223–228, 230, 290
- Heat transfer search (HTS), 8, 24–26, 31, 37, 47, 48, 59, 60, 70, 71, 80, 81, 90–92, 107, 108, 115–117, 126, 127, 137, 138, 145, 146, 154, 155, 162, 163, 171, 172, 180, 181, 189–191, 208, 209, 218, 228, 229, 240, 250, 251, 259, 260, 269, 270, 278, 279, 297, 298, 307, 315, 324, 331, 332, 338, 339, 356, 365, 366, 376, 383, 384, 392, 393, 399, 400, 405, 406, 455
- Hot-side heat exchanger, 144, 145, 147, 267–269, 271, 277, 279, 280, 302, 305, 307, 308, 311
- Hot stage, 252, 255–258, 260, 261
- I**
- Initial cost, 35, 48, 50, 67, 83
- Internal irreversibility, 103, 130, 144, 159, 161, 163, 164, 166, 184, 188, 202, 205, 207, 212, 214, 272
- Inverse Brayton cycle, 325–327, 329–332
- Irreversible process, 102, 103, 130, 139, 141, 149, 152, 153, 156, 157, 164, 166, 175, 184, 202, 221, 222, 262, 263, 266, 272, 309, 310, 334
- Isentropic compression, 130, 148, 200, 231, 303, 325, 328
- Isentropic efficiency, 129, 135, 148, 151, 153, 245, 249, 292–294, 320, 322, 328
- Isentropic expansion, 133, 148, 200, 245, 328
- Isentropic process, 112
- Isobaric process, 310
- Isothermal compression, 101, 118, 200, 261, 262, 271
- Isothermal expansion, 101, 119, 139, 201, 271
- Isothermal process, 141, 309
- K**
- Kalina power cycle, 316–319, 322–325
- L**
- Log mean temperature difference, 205, 273
- Loss coefficient, 150–152, 319, 350–352, 380, 381, 387–389, 394, 396
- M**
- Mach number, 245, 247, 248, 362, 401, 402, 404–406
- Mass flow rate, 41, 57, 58, 60, 76, 78, 85, 89, 112, 213, 232, 234, 244, 246, 293, 312, 319–321, 326, 335, 347, 348, 350, 353, 371, 381, 387, 390, 391, 393, 396
- Mean effective pressure, 122, 124, 125, 127, 128
- Merkel number, 349, 350
- Metaheuristic methods, 4
- Microchannel heat sink, 345, 368–371, 374–377
- Multi-temperature vapor absorption refrigerator, 219
- N**
- Network, 51, 119, 205, 221, 244, 318, 322, 334, 346, 347, 359, 360, 401
- Nozzle, 242, 245, 400, 401, 403
- Number of transfer unit, 142
- Number of tube passes, 45, 46
- Number of tubes, 35, 38, 39, 50, 65, 238, 319
- O**
- Objective function, 1, 2, 14, 16, 25, 33, 37, 45, 46, 50–52, 57, 62, 63, 68, 72, 74, 78, 79, 82, 88, 89, 92, 99, 102, 105, 106, 109, 110, 114, 117, 119, 124, 125, 128, 135, 136, 139, 141, 144, 147, 150, 153, 156, 160, 161, 164, 166, 170, 173, 175, 178, 179, 182, 184, 185, 188, 191, 199, 202, 207, 210, 212, 213, 216, 217, 219, 221, 222, 226, 227, 230, 232, 233, 237, 238, 240, 243, 244, 248–250, 252, 254, 257, 258, 261, 267, 268, 271, 276, 277, 280, 287, 290, 294, 299, 301, 304, 305, 308, 310, 313, 316, 318, 322, 325, 327, 329, 330, 332, 334, 336, 337, 340, 345, 347, 348, 354, 357, 359, 363, 364, 367, 369, 370, 374, 377, 382, 385, 387, 390, 391, 393, 395, 397, 398, 400, 402–404, 406
- Operating cost, 35, 36, 44, 45, 48, 50, 56, 57, 60, 62, 67, 68, 72, 213, 347, 353, 354
- Operating variables, 166, 272, 290, 379
- Optimization, 1–4, 7, 8, 10, 11, 14, 16–18, 20, 24, 25, 30–33, 35–37, 46–49, 51–53, 58–61, 63, 64, 68–71, 74, 78–81, 83, 84, 89–91, 99, 100, 102, 103, 105–108, 110, 111, 114–117, 119, 120, 124–127, 130, 131, 136–138, 140, 141, 144–147, 149, 150, 153–155, 157, 158, 161–163, 166, 167, 170–173, 175, 176, 179–181, 184, 185, 188–190, 199, 201–203, 207–209, 212, 213, 216, 218–222, 226–229, 232, 233, 237, 238, 240, 241, 243, 244, 249–254, 258–260, 262–264,

- 267–270, 272, 273, 277–280, 287–292, 294, 296–298, 300, 301, 305–310, 313, 314, 318, 319, 322–324, 326, 327, 330–335, 337–339, 345–348, 354–360, 364, 366–370, 375–380, 382–384, 386, 387, 390–396, 398–402, 404–406, 440
- Optimized design geometry, 82, 92, 230, 252, 271
- Overall heat transfer coefficient, 41, 43, 54, 66, 67, 85, 92, 112, 132, 158, 188, 203, 205, 264, 273, 320
- P**
- Parallel flow, 62, 221, 222
- Particle swarm optimization (PSO), 7, 10, 11, 13, 30, 36, 47, 48, 51–53, 59, 60, 70, 71, 80, 81, 90, 91, 107, 108, 116, 126, 127, 137, 138, 145, 146, 154, 155, 162, 163, 171, 172, 180, 181, 189, 190, 208, 209, 217, 218, 228, 229, 240, 244, 250, 251, 259, 260, 269, 270, 278, 279, 297, 298, 306, 307, 314, 315, 324, 331, 332, 338, 339, 356, 366, 376, 383, 384, 392, 399, 405, 406, 421
- Passing vehicle search (PVS), 8, 27, 28, 31, 47, 48, 59, 60, 70, 71, 80, 81, 90, 91, 107, 108, 116, 126, 127, 137, 138, 145, 146, 154, 155, 162, 163, 171, 172, 180–182, 189–191, 208–210, 218, 228, 229, 240, 250, 251, 259, 260, 269, 270, 278, 279, 297, 298, 306, 307, 315, 323, 324, 331, 332, 338, 339, 356, 365, 366, 376, 383, 384, 392, 393, 399, 405, 406, 460
- Plate-fin heat exchanger (PFHE), 49, 51–53, 56–61
- Plate heat exchanger (PHE), 82–84, 87, 89–91
- Power cycle, 287, 300–302, 317, 395
- Power density, 102, 130, 157, 158, 175, 309, 310, 312, 313, 315, 316, 333–335
- Power input, 166, 168, 170–173, 263, 265, 272, 275, 277, 280
- Power output, 99, 102–105, 109, 110, 117, 119, 120, 124–128, 130, 131, 134, 136, 139, 141, 143, 144, 147, 149, 152, 153, 156, 157, 161, 164, 175, 268, 288, 300, 301, 304, 305, 307–312, 318, 321, 322, 333–337, 339, 340, 395, 397–400
- Prandtl number, 38, 55, 58, 66, 76, 86, 124, 373, 375, 381
- Pressure drop, 1, 33–35, 37, 38, 42, 43, 46, 48, 50–53, 56, 57, 60–63, 67–69, 72–74, 77–79, 81–84, 87–90, 92, 99, 120–124, 141, 234, 264, 292, 294, 351–353, 369, 371, 373, 378, 390, 395
- Pressure ratio, 151, 153, 156, 175, 177, 179, 182, 273, 277, 300, 301, 326, 327, 329–332, 334, 401, 402, 404–406
- Propulsive efficiency, 401–406
- Pseudocode, 7, 10, 11, 13, 15, 17, 19, 21, 23, 26, 28, 29
- Pump, 69, 99, 100, 109, 147, 149, 166–170, 174–177, 179–185, 187, 188, 190, 191, 211, 212, 214, 216, 232, 242, 243, 253, 263, 272, 288–290, 292, 293, 295, 321, 322, 385, 390
- R**
- Radiative-type heat engine, 156, 157
- Ranges of design variables, 46, 69, 79, 89, 106, 115, 125, 136, 145, 153, 161, 170, 179, 188, 207, 216, 227, 238, 249, 258, 268, 277, 296, 305, 313, 322, 330, 337, 354, 364, 375, 382, 391, 398, 404
- Rankine cycle, 108, 110, 111, 113, 174, 287–291, 294, 318
- Rankine heat engine, 99, 108–112, 114–117
- Rankine power cycle, 110, 288, 296–298
- Refrigeration cycle, 183, 221, 233, 243, 244, 262, 263, 271, 272, 276
- Regenerative heat exchanger (rotary regenerator), 72
- Regenerative time, 265, 274
- Regenerator diameter, 124, 125, 127, 128, 264
- Regenerator effectiveness, 74, 79–81, 136, 138, 139, 166, 168, 265, 305, 308
- Regenerator heat loss, 265, 274
- Regenerator length, 124, 125, 127, 128, 264
- Results and discussion, 47, 59, 70, 79, 90, 106, 115, 125, 136, 145, 154, 161, 162, 171, 180, 189, 208, 217, 227, 239, 249, 250, 258, 268, 278, 296, 306, 314, 323, 330, 337, 338, 355, 365, 375, 383, 391, 398, 404
- Reversed Brayton cycle, 175, 179, 182
- Reversible process, 100, 130, 164, 187, 200, 225
- Reynolds number, 38, 40, 41, 55, 65, 66, 76, 86–88, 362, 374, 377, 380–382, 385, 388
- S**
- Shell and tube heat exchanger (STHE), 33–37, 46–49
- Shell diameter, 35, 37, 42, 45, 46, 50, 238

- Sine cosine algorithm (SCA), 8, 29, 31, 47, 48, 59, 60, 70–72, 80, 81, 90, 91, 107, 108, 116, 126, 127, 137, 138, 145, 146, 154, 155, 162, 163, 171, 172, 180, 181, 189, 190, 208, 209, 218, 228, 229, 239, 240, 250, 251, 259, 260, 269, 270, 278, 279, 297, 298, 306, 307, 314, 315, 323, 324, 331, 332, 338, 339, 356, 366, 376, 383, 384, 392, 399, 405, 406, 465
- Single-effect vapor absorption refrigerator, 210
- Solar air heater, 345, 378–385, 391
- Solar chimney, 345, 394–400
- Solar water heater, 345, 385–387, 390–393, 396
- Specific fuel consumption, 149, 150, 402–406
- Specific heat, 39, 58, 66, 76, 77, 85, 112, 121, 124, 131, 142, 150, 152, 153, 168, 170, 176, 191, 203, 205, 265, 267, 274, 277, 312, 313, 319, 322, 328, 334–337, 349, 372, 375, 381, 387, 396, 402
- Specific thrust, 401–406
- Specific work, 103, 327, 329–332
- Stirling cryogenic refrigerator, 199, 261–264, 271
- Stirling cycle, 118, 120, 164, 167, 261, 262, 264
- Stirling heat engine, 118, 120, 124–128
- Stirling heat pump, 99, 164–167, 169–174
- Swarm intelligence based on algorithms, 2
- Symbiotic organism search (SOS), 8, 19, 20, 31, 47, 48, 59, 60, 70, 71, 80, 81, 90, 91, 107, 108, 116, 126, 127, 137, 138, 145, 146, 154, 155, 162, 163, 171, 172, 180, 181, 189, 190, 208, 209, 217, 218, 228, 229, 239, 240, 250, 251, 259, 260, 269, 270, 278, 279, 297, 298, 306, 307, 314, 315, 323, 324, 331, 332, 338, 339, 355, 356, 365, 366, 376, 377, 383, 384, 392, 399, 405, 406, 444
- T**
- Teaching–learning-based optimization (TLBO), 8, 17–19, 31, 36, 47, 48, 52, 59, 60, 70, 71, 74, 80, 81, 90, 91, 107, 108, 116, 126, 127, 137, 138, 145, 146, 154–156, 162, 163, 171, 172, 180–182, 189–191, 208–210, 218, 228, 229, 240, 250, 251, 259, 260, 269, 270, 278, 279, 297, 298, 306, 307, 315, 324, 331, 332, 338, 339, 355, 356, 365, 366, 376, 383, 384, 392, 399, 405, 406, 440
- Temperature, 1, 24–26, 33, 34, 40, 41, 44–46, 57, 58, 62, 63, 67, 68, 73, 77, 78, 83, 89, 99–107, 109, 111–113, 115, 117–119, 121, 124, 125, 127–129, 131–136, 139–144, 151–153, 156, 158, 161, 163–167, 170, 173–177, 179, 183–186, 188, 191, 199–201, 203–205, 207, 210, 211, 215, 216, 219–224, 226–234, 237–240, 244–247, 249, 252, 253, 255, 257, 261–264, 267–271, 273, 277, 279, 280, 288, 289, 291, 293, 294, 299, 302, 303, 305, 307–311, 316–320, 322, 324, 325, 327–329, 333–337, 339, 340, 346, 348, 349, 351, 352, 354, 356, 357, 359, 362–364, 368–372, 378–382, 385–387, 389–391, 393, 396–398, 401–406
- Temperature of the heat sink, 112, 114, 115, 117, 124, 125, 128, 205, 207
- Temperature of the heat source, 112, 114, 124, 125, 128, 204, 207
- Temperature ratio, 102, 105–107, 109, 122, 132, 135, 136, 138, 139, 144–147, 159, 161, 164, 170, 173, 177, 179, 182, 206, 210, 223, 224, 226–228, 230, 267–269, 271, 277, 279, 280, 300, 301, 309, 310, 312, 313, 315, 316, 336, 337, 339, 340, 402
- Thermal conductivity, 1, 38, 49, 55, 66, 69, 85, 237, 238, 255–257, 357, 360, 361, 372, 375, 381, 382, 388–390
- Thermal design and optimization, 4, 33, 99, 287
- Thermal efficiency, 99, 104–107, 109, 110, 114, 115, 117, 119, 120, 124, 128, 130, 136, 141, 143–147, 153, 154, 156–158, 160–164, 208, 288, 290, 293, 294, 301, 304–308, 310, 313–316, 318, 327, 329–332, 334, 335, 337–340, 354, 379–385, 387, 390–393, 401–406
- Thermal model, 33, 37, 53, 64, 68, 74, 78, 84, 88, 99, 101, 103, 105, 111, 114, 119, 120, 124, 131, 135, 141, 144, 150, 153, 158, 160, 167, 170, 176, 178, 185, 188, 199, 203, 207, 213, 216, 222, 226, 233, 237, 244, 248, 254, 257, 264, 267, 273, 276, 287, 291, 294, 301, 302, 304, 310, 311, 313, 319, 322, 327, 329, 335, 336, 345, 347–349, 354, 360, 363, 369–371, 374, 380, 382, 387, 390, 396, 397, 402, 403
- Thermal resistance, 101, 201, 255, 257, 359–361, 363–367, 369–371, 373
- Thermal systems, 1, 7, 30, 32, 345, 357
- Thermodynamic cycle, 100, 118, 119, 129, 140, 149, 156, 164, 165, 174, 182, 183, 199–201, 231, 242, 287, 299

- Thermodynamic presentation, 101, 103, 109–111, 120, 128, 129, 131, 139, 141, 148, 150, 157, 158, 167, 174, 176, 185, 203, 233, 241, 244, 262, 264, 271, 273, 290, 300, 301, 309, 310, 333, 335
- Thermo-electric modules, 252–258, 260, 261
- Thermo-electric refrigerator, 254
- Throat, 242–245, 249
- Total cost, 1, 35–37, 44–46, 50–52, 56, 57, 62, 64, 68, 84, 166, 202, 233, 236, 238–240, 290, 293, 294, 296, 297, 301, 310, 347, 348, 395
- Total weight, 51, 61, 63, 72
- Traditional optimization techniques, 2, 3, 8
- Tube diameter, 35–37, 40, 64, 68, 69, 72, 319, 388, 390, 391, 393
- Tube layout, 35, 46, 50
- Tube length, 36, 50, 63
- Tube pitch, 35, 40, 42, 45, 46, 50, 63, 64, 68, 72
- Turbine, 73, 135, 141, 288–295, 298–301, 308, 309, 316–318, 320–322, 324, 325, 327–329, 394, 395, 397, 400, 401, 404–406
- Turbojet engine, 400–406
- V**
- Vapor absorption refrigerator, 199, 213, 216, 218, 219, 229
- W**
- Water wave optimization (WWO), 8, 22, 23, 31, 47, 48, 59, 60, 70–72, 80, 81, 90, 91, 107, 108, 116, 126, 127, 137, 138, 145, 146, 154, 155, 162, 163, 171, 172, 180, 181, 189, 190, 208, 209, 218, 228, 229, 240, 250, 251, 259, 260, 269, 270, 278, 279, 297, 298, 306, 307, 315, 323, 324, 331, 332, 338, 339, 355, 356, 366, 376, 383, 384, 392, 399, 405, 406, 449, 68